

Copyright is owned by the Author of the thesis. Permission is given for a copy to be downloaded by an individual for the purpose of research and private study only. The thesis may not be reproduced elsewhere without the permission of the Author.

**The role of the G protein and cAMP/PKA
signalling pathway in establishment and
maintenance of the mutualistic *Epichloë
festucae* – ryegrass association**

A thesis presented in partial fulfilment of the
requirements for the degree of

Doctor of Philosophy

in Genetics

at



MASSEY UNIVERSITY

Palmerston North, New Zealand

Alexander Bisson

2017

“Never Give Up, Never Surrender!”

Jason Nesmith

(Galaxy Quest)

ABSTRACT

Growth of the fungal endophyte *Epichloë festucae* in mutualistic symbiotic association with *Lolium perenne* (perennial ryegrass) is highly regulated and synchronised with the growth of the host plant leaf. To maintain this pattern of fungal growth *in planta*, specific signalling between symbiont and its host grass is required. To sense the extracellular environment and respond to changes, filamentous fungi rely on G protein-coupled receptors (GPCRs), which transmit signals predominantly via heterotrimeric G proteins to downstream pathways such as the cAMP/Protein Kinase A (PKA) and MAP kinase signalling pathways. In phytopathogenic fungi, G protein signalling and the associated cAMP/PKA pathways are often essential for a normal host interaction. Signal transduction using the second messenger cAMP to activate the PKA activity is finely balanced through a regulatory feedback loop for signal attenuation regulated by 3'-5'-cyclic nucleotide phosphodiesterases (PDE).

Using a blast-based bioinformatic approach, a total of 40 genes encoding putative GPCRs were identified in the genome of *E. festucae*, grouping into 13 of 14 classes of the recent classification system for fungal GPCRs. Among genes encoding components of the G protein signalling cascade, nine of these GPCRs including the two cAMP receptor-like GPCRs, Gpr1b and Gpr2, show significant transcriptional up-regulation in association with the host compared to the respective expression level when grown in axenic culture. A reverse genetics approach was used to functionally characterise the identified cAMP receptor-like GPCRs (Gpr1a, Gpr1b and Gpr2). While deletion of *gpr1a* was unsuccessful, plants infected with an *E. festucae* Δ *gpr1b* mutant showed a severe breakdown of the *E. festucae*-ryegrass association, whilst no effects were observed for Δ *gpr2*-inoculated plants. Among numerous other genes putatively involved in G-protein and cAMP/PKA signalling, two putative PDEs involved in regulation of the cAMP-mediated signal were also identified. Deletion of *pdeH* (Δ *pdeH*), a gene encoding a PDE with high affinity towards cAMP, had a dramatic effect on the endophyte-plant association. In contrast, deletion of *pdeL* (Δ *pdeL*), a gene encoding a PDE with low affinity towards cAMP, had no effect on the host interaction phenotype, while primarily modulating the intracellular cAMP level during nutrient-induced activation of the cAMP/PKA

signalling pathway in axenic culture. Finely balanced cAMP levels are crucial for various cellular processes including hyphal growth, cellular differentiation of asexual development and conidiogenesis.

This research identified Gpr1b as an important receptor involved in maintenance of the highly restricted endophytic growth pattern of *E. festucae* in association with the host, potentially regulated by plant-derived molecules. These signals are mediated by the cAMP/PKA signalling pathway for an appropriate alteration in gene expression and subsequent cellular adaptation. Intracellular cAMP levels triggering these concentration-dependent processes are regulated by PdeH, which specifically acts *in planta*. This study shows that G-protein and cAMP/PKA signalling play an important role in regulating environmental signalling for establishment and maintenance of the mutualistic association between *E. festucae* and *L. perenne*.

ACKNOWLEDGEMENTS

An erster Stelle will ich Mich bei meinen Eltern und meiner Familie für deren Unterstützung über die langen Jahre meines Studiums und speziell während der Dissertation im weit entfernten Neuseeland bedanken. Danke, dass ihr immer an mich und meine Fähigkeiten geglaubt habt, daran dass ich diese Hürde meistern werde und dass ich diesen Weg gehen konnte. Danke für den stetigen Kontakt, der mir die Abwesenheit von euch wesentlich vereinfachte und danke für jedes aufbauende Wort und finanzielle Unterstützung in der Not. Auch wenn ich viel verpasst habe, war ich doch immer irgendwie dabei. Ohne euch wäre ich nicht da, wo ich jetzt bin!

First and foremost, I want to thank my parents and family without who this thesis would not have been possible. For their unconditional love and support through out the years of study, especially during my journey to complete my PhD thesis in a country far away from home. Thank you for encouraging me to pursue this track. I am grateful for your constant belief in my abilities and me.

A warm thank you to my primary supervisor Prof. Barry Scott for the opportunity to conduct this research project leading to the thesis and his support and guidance throughout the many ups and downs during its progress. Also, thank you to my co-supervisor Dr. Carla Eaton for her input and help during the course of the research. Dr. Dave Wheeler and Dr. Pierre-Yves Dupont – your timely advice is appreciated.

Thank you to the members of the Scottbase lab for their cooperative help and friendship, espceially to Arvina Ram, who never said “no” when I needed help. I also want to thank the team of the MMIC for their help, guidance and friendship.

A special thanks to Ivana, who was tremendously helpful throughout the thesis and particularly during the hard times while writing up. Thanks to all my friends, back home in Germany and those I made during my time in New Zealand for their support and friendship.

I would also like to acknowledge the BioProtection Research Centre for funding this PhD project.

I am grateful for all the experience I gained, during this journey in a professional and private manner, all the people I have met, shared adventures, laughter and pain with.

TABLE OF CONTENTS

Chapter 1 Introduction	1
1.1 <i>Epichloë festucae</i> forms a mutualistic association with perennial ryegrass	2
1.1.1 Mutual benefits of symbiotic interaction	2
1.1.2 The lifecycle of <i>E. festucae</i> includes both asexual and sexual stages	3
1.1.3 <i>E. festucae</i> shows a host-synchronised growth pattern in association with perennial ryegrass.....	6
1.2 Specific signalling is necessary for symbiosis between fungus and host.....	9
1.2.1 G protein signalling pathways transduce extracellular signals to downstream pathways.....	9
1.2.2 The mitogen-activated protein kinase pathway	13
1.2.3 The G protein cyclic AMP/PKA signalling pathway	16
1.2.4 G protein coupled receptors sense environmental changes and transduce signals for cellular response.....	19
1.2.5 Role of fungal GPCRs in pathogenicity through activating the cAMP-dependent PKA signalling cascade.....	22
1.2.6 cAMP-phosphodiesterases terminate cAMP/PKA signalling	24
1.3 Aims	27
Chapter 2 Materials and Methods.....	29
2.1 Bioinformatics.....	30
2.1.1 Nucleotide and protein sequences	30
2.1.2 tBLASTn analysis.....	30
2.1.3 Multiple sequence alignment	30
2.1.4 Phylogenetic analysis	31
2.1.5 Protein prediction	31
2.1.6 GC profile	31
2.2 Molecular and biological material.....	31
2.3 Growth conditions and media	40
2.3.1 <i>Escherichia coli</i>	40
2.3.1.1 Luria-Bertani growth (LB) medium	40
2.3.1.2 SOC medium.....	40
2.3.2 <i>Saccharomyces cerevisiae</i>	40
2.3.2.1 Yeast Peptone Dextrose (YPD) medium	41

2.3.2.2	SD uracil dropout (SD ura ⁻) medium	41
2.3.3	<i>Epichloë festucae</i>	41
2.3.3.1	Potato dextrose (PD) medium	41
2.3.3.2	Regeneration (RG) medium	41
2.3.3.3	Water (H ₂ O) medium	42
2.3.3.4	Modified Czapek Dox (CDGN) medium.....	42
2.3.3.5	Czapek Dox salts (CD) medium	42
2.3.3.6	Czapek Dox (CZ) medium	42
2.3.3.7	Modified Blankenship medium.....	42
2.4	Colony growth in axenic culture	46
2.4.1	Analysis of hyphal growth.....	46
2.4.1.1	Non-transfer experiment.....	46
2.4.1.2	Transfer experiment	47
2.4.2	Determination of hyphal growth rate	47
2.4.2.1	Hyphal growth rate for non-transfer experiment.....	47
2.4.2.2	Hyphal growth rate for transfer experiment	48
2.4.3	Fungal growth under stress conditions	48
2.4.4	Fungal growth in presence of plant-derived molecules	49
2.4.5	Chemical treatment of fungal colonies	50
2.5	Molecular techniques.....	51
2.5.1	DNA isolation	51
2.5.1.1	Plasmid DNA isolation from <i>E. coli</i>	51
2.5.1.2	Cosmid DNA isolation from <i>E. coli</i>	51
2.5.1.3	Plasmid DNA isolation from <i>S. cerevisiae</i>	51
2.5.1.4	Genomic DNA from <i>E. festucae</i>	52
2.5.1.5	Crude genomic DNA from <i>E. festucae</i>	53
2.5.2	DNA purification	53
2.5.3	Restriction enzyme (RE) digestions	53
2.5.4	Ethanol precipitation	54
2.5.5	Gel electrophoresis.....	54
2.5.6	DNA quantification	54
2.5.7	Polymerase chain reaction (PCR).....	55
2.5.7.1	Standard PCR	55
2.5.7.2	High-Fidelity PCR.....	55
2.5.7.3	PCR for GC-rich DNA sequences	56
2.5.8	TOPO-cloning.....	57
2.5.9	DNA sequencing.....	57
2.5.10	Preparation of constructs	58

2.5.10.1	<i>E. festucae gpr1a</i> gene replacement construct	58
2.5.10.2	<i>E. festucae gpr1b</i> gene replacement construct	58
2.5.10.3	<i>E. festucae gpr2</i> gene replacement construct	58
2.5.10.4	<i>E. festucae pdeH</i> gene replacement construct	59
2.5.10.5	<i>E. festucae pdeL</i> gene replacement construct	59
2.5.10.6	<i>E. festucae gpr1b</i> complementation construct.....	59
2.5.10.7	<i>E. festucae pdeH</i> complementation construct.....	59
2.5.10.8	<i>E. festucae pdeL</i> complementation construct.....	60
2.5.10.9	Yeast recombinational cloning (YRC)	60
2.5.10.10	Gibson assembly (GA)	61
2.5.11	Bacterial Transformation	61
2.5.11.1	Transformation of electrocompetent <i>E. coli</i> cells	61
2.5.11.2	Transformation of chemically competent <i>E. coli</i> cells.....	62
2.5.11.3	<i>E. coli</i> - transformation plasmid screen (CloneChecker™)	62
2.5.12	Fungal transformation	63
2.5.12.1	Preparation of fungal protoplasts	63
2.5.12.2	Transformation of fungal protoplasts	63
2.5.13	Single spore isolation	64
2.5.14	Southern blotting	64
2.5.14.1	DNA probe-labelling.....	65
2.5.14.2	Hybridisation and detection.....	66
2.5.15	Identification of cosmids from <i>E. festucae</i> cosmid library	67
2.6	Quantification of intracellular cAMP.....	67
2.6.1	Growth and harvest of fungal mycelia and extraction of cAMP.....	67
2.6.2	Quantification of cAMP by ELISA assay.....	68
2.7	Plant methods.....	68
2.7.1	Seed sterilisation	68
2.7.2	Seedlings growth conditions	69
2.7.3	Plant inoculation	69
2.7.4	Standard plant growth conditions	69
2.7.5	Axenic culture plant growth conditions.....	69
2.7.5.1	Murashige and Skoog (MSO) medium	70
2.7.6	Detection of endophyte infected plants	70
2.7.7	Extraction of apoplastic fluid (APF) from <i>L. perenne</i> plants.....	70
2.8	Microscopic analysis.....	71
2.8.1	In culture analysis.....	71
2.8.1.1	Determination of hyphal fusion frequency	71
2.8.2	<i>In planta</i> analysis.....	71

2.8.2.1	Confocal laser scanning microscopy (CLSM).....	71
2.8.2.2	Transmission electron microscopy (TEM).....	72
2.9	Statistical analyses	72
2.9.1	Carbon sources	73
2.9.2	Amino acids.....	73
2.9.3	Environmental pH stress.....	73
2.9.4	Plant-derived molecules	74
Chapter 3	Bioinformatic analysis of the cAMP G protein-coupled receptors and phosphodiesterases in the <i>E. festucae</i> genome.....	75
3.1	Identification of G protein-coupled receptors in <i>E. festucae</i> genome	76
3.2	Bioinformatic approach to characterize cAMP-receptor like GPCRs in <i>Epichloë</i> spp.	84
3.3	Cyclic nucleotide AMP phosphodiesterases (PDEs) in the <i>E. festucae</i> genome	100
3.4	Transcriptional difference of <i>E. festucae</i> wild-type growth in culture and in association with the host	110
Chapter 4	Functional analysis of cAMP receptor-like G protein-coupled receptors.....	115
4.1	Functional analysis of the Gpr1a.....	116
4.1.1	Attempted deletion of the <i>E. festucae gpr1a</i> gene	116
4.2	Functional analysis of the Gpr1b.....	122
4.2.1	Deletion of the <i>E. festucae gpr1b</i> gene	122
4.2.2	Deletion of <i>gpr1b</i> does not alter fungal development in axenic culture	124
4.2.3	Deletion of <i>gpr1b</i> caused a dramatic breakdown of the symbiotic interaction	126
4.2.3.1	Symbiotic interaction phenotype of $\Delta gpr1b$ strains.....	126
4.2.3.2	Microscopic analysis reveals unrestricted growth and increase of fungal biomass <i>in planta</i>	130
4.2.3.3	$\Delta gpr1b$ strains display an increased number of epiphyllous hyphae	135
4.3	Functional analysis of the Gpr2.....	136
4.3.1	Deletion of the <i>E. festucae gpr2</i> gene	136
4.3.2	Deletion of <i>gpr2</i> had no effect on fungal development in axenic culture	138
4.3.3	Gpr2 does not show a functional role in the plant symbiotic interaction....	140
4.3.3.1	Symbiotic interaction phenotype of $\Delta gpr2$ strains.....	140

4.3.3.2	Microscopic analysis of $\Delta gpr2$ revealed wild-type like fungal colonisation of host tissue	142
4.4	Analysis of hyphal growth for $\Delta gpr1b$ and $\Delta gpr2$ mutant strains.....	147
4.4.1	<i>E. festucae</i> cAMP-receptor like GPCRs are not directly involved in nutrient sensing.....	148
4.4.2	Gpr1b or Gpr2 may have an accessory role in sensing specific amino acids	151
4.4.3	Deletion of <i>gpr1b</i> may increase sensitivity of <i>E. festucae</i> to oxidative stress	155
4.4.4	<i>E. festucae</i> Gpr1b is potentially involved in sensing of an unknown component in apoplastic fluid.....	157
4.4.5	Gpr1b and Gpr2 are not directly involved in any processes in culture potentially mediated by the cAMP signalling pathway.....	160
4.4.6	Nutrient rich medium triggers increase in intracellular cAMP levels, but Gpr1b or Gpr2 are not directly responsible	162
Chapter 5	Functional analysis of cAMP-phosphodiesterases	165
5.1	Functional analysis of PdeH	166
5.1.1	Deletion of the <i>E. festucae pdeH</i> gene.....	166
5.1.2	Deletion of <i>pdeH</i> does not alter fungal development in axenic culture	168
5.1.3	Deletion of <i>pdeH</i> caused a dramatic breakdown of the symbiotic interaction.....	170
5.1.3.1	Symbiotic interaction phenotype of $\Delta pdeH$ strains	170
5.1.3.2	Microscopic analysis reveals unrestricted growth and increase of fungal biomass	174
5.1.3.3	Microscopic analysis of $\Delta pdeH$ revealed wild-type like fungal colonisation of host tissue	179
5.2	Functional analysis of PdeL.....	180
5.2.1	Deletion of the <i>E. festucae pdeL</i> gene	180
5.2.2	Deletion of <i>pdeL</i> resulted in a significant reduction in hyphal growth in axenic culture	182
5.2.3	PdeL does not show a functional role in the plant symbiotic interaction	187
5.2.3.1	Symbiotic interaction phenotype of the $\Delta pdeL$ strain	187
5.2.3.2	Microscopic analysis of $\Delta pdeL$ revealed wild-type like fungal colonisation of host tissue	189
5.3	Analysis of hyphal growth for the $\Delta pdeH$ and $\Delta pdeL$ mutant strains	191

5.3.1	<i>E. festucae</i> low affinity phosphodiesterase is important for hyphal growth especially on nutrient-rich media.....	191
5.3.2	Hyphal growth is negatively affected by the presence of various amino acids when PdeH or PdeL are absent	195
5.3.3	Cell-wall stress and oxidative stress masks the hyphal growth defect of the $\Delta pdeL$ mutant strain in culture	199
5.3.4	Plant derived molecules have no obvious effect on the hyphal growth for the mutant strains, $\Delta pdeH$ and $\Delta pdeL$, in axenic culture	201
5.3.5	Chemical alteration of activity for key-enzymes of the cAMP signalling pathway in the PDE mutants	203
5.3.6	Nutrient-dependent increase of intracellular cAMP levels in culture is regulated mainly by the low affinity phosphodiesterase in culture.....	206
Chapter 6 Summary discussion and conclusions with recommendations for future work.....		209
6.1	Fungal GPCRs and the role of cAMP receptor-like GPCRs in the mutualistic <i>E. festucae</i> – <i>L. perenne</i> association.....	210
6.1.1	Phylogenetic diversity of cAMP receptor-like GPCRs	212
6.1.2	Role of class V GPCRs in <i>E. festucae</i> and other fungi.....	213
6.1.3	Role of cAMP receptor-like GPCRs in nutrient and amino acid sensing.	216
6.1.4	Role in association with the host.....	217
6.2	The role of the cAMP-phosphodiesterases in <i>E. festucae</i>	229
6.2.1	PDEs in <i>E. festucae</i>	230
6.2.2	The potential role of cAMP signalling in expressoria development.....	239
6.3	Conclusion	241
Chapter 7 Appendices.....		247
Chapter 8 Supplementary data files in accompanying digital media		277
Chapter 9 References.....		283

LIST OF FIGURES

Figure 1-1 Lifecycle of <i>Epichloë</i> endophyte.....	5
Figure 1-2 <i>E. festucae</i> shows a synchronised growth <i>in planta</i>	8
Figure 1-3. The heterotrimeric G-protein cycle.....	11
Figure 1-4 The G-protein cAMP/PKA signalling pathway.....	18
Figure 1-5 Structure of G-protein coupled receptors.....	20
Figure 1-6 cAMP synthesis and hydrolysis.....	25
Figure 3-1 Classification of fungal G protein-coupled receptors.....	82
Figure 3-2 Multiple sequence alignment of <i>E. festucae</i> Gpr1a homologues.....	84
Figure 3-3 Multiple sequence alignment of <i>E. festucae</i> Gpr1b homologues.....	87
Figure 3-4 Multiple sequence alignment of <i>E. festucae</i> Gpr2 homologues.....	88
Figure 3-5 Phylogenetic analysis of fungal class V cAMP receptor-like GPCRs.....	91
Figure 3-6 Phylogenetic analysis of class V GPCRs within the <i>Epichloë</i> species.....	92
Figure 3-7 Organisation of the <i>E. festucae gpr1a</i> gene and predicted polypeptide.....	94
Figure 3-8 Organisation of <i>E. festucae gpr1b</i> gene and predicted polypeptide.....	96
Figure 3-9 Organisation of <i>E. festucae gpr2</i> gene and predicted polypeptide.....	98
Figure 3-10 Multiple sequence alignment of fungal PdeH homologues.....	102
Figure 3-11 Multiple sequence alignment of fungal PdeL homologues.....	103
Figure 3-12 Maximum-likelihood dendrogram of fungal 3'-5' cyclic phosphodiesterases.....	104
Figure 3-13 Organisation of the <i>E. festucae pdeH</i> gene and predicted polypeptide.....	106
Figure 3-14 Organisation of the <i>E. festucae pdeL</i> gene and predicted polypeptide.....	108
Figure 3-15 Gene expression change of GPCR encoding genes of <i>E. festucae</i> wild-type in association with the host plant.....	110
Figure 3-16 Transcriptional change of genes encoding components of the G protein and cAMP/PKA signalling pathway of the <i>E. festucae</i> wild-type in association with the host plant.....	113
Figure 4-1 Strategy for deletion of <i>E. festucae gpr1a</i>	117
Figure 4-2 DNA GC content of <i>gpr1a</i> locus.....	118
Figure 4-3 Molecular analysis of <i>E. festucae gpr1a</i> -containing cosmids.....	120

Figure 4-4 Physical map of <i>E. festucae gpr1a</i> locus and PCR amplification of non-specific products	121
Figure 4-5 Strategy for deletion of <i>gpr1b</i> and identification of $\Delta gpr1b$ mutant strains	122
Figure 4-6 Culture phenotype analysis of the $\Delta gpr1b$ mutant strain	125
Figure 4-7 Hyphal fusion event in $\Delta gpr1b$ mutant strains.....	125
Figure 4-8 Symbiosis phenotype of <i>Lolium perenne</i> infected with $\Delta gpr1b$ mutant strain.....	127
Figure 4-9 Complementation of $\Delta gpr1b$ mutant strain.....	128
Figure 4-10 Light microscopy of the $\Delta gpr1b$ mutant strain <i>in planta</i>	131
Figure 4-11 Transmission electron microscopy of the $\Delta gpr1b$ mutant strain <i>in planta</i>	132
Figure 4-12 Hyphae per intercellular space of $\Delta gpr1b$ mutant strain	133
Figure 4-13 Confocal laser-scanning microscopy of the $\Delta gpr1b$ mutant strain <i>in planta</i>	135
Figure 4-14 Strategy for deletion of and identification of $\Delta gpr2$ mutant strains ..	136
Figure 4-15 Culture phenotype analysis of $\Delta gpr2$ mutant strain.....	139
Figure 4-16 Hyphal fusion event in $\Delta gpr2$ mutant strains	140
Figure 4-17 Symbiosis phenotype of <i>Lolium perenne</i> infected with $\Delta gpr2$ mutant strain.....	141
Figure 4-18 Light microscopy of the $\Delta gpr2$ mutant strain <i>in planta</i>	143
Figure 4-19 Transmission electron microscopy of the $\Delta gpr2$ mutant strain <i>in planta</i>	144
Figure 4-20 Hyphae per intercellular space of $\Delta gpr2$ mutant strain.....	145
Figure 4-21 Confocal laser-scanning microscopy of the $\Delta gpr2$ mutant strain <i>in planta</i>	147
Figure 4-22 Colony morphology of the GPCR mutant strains in response to nutrient limitation.....	149
Figure 4-23 Variation in hyphal growth rate of the GPCR mutant strains in response to nutrient starvation and to growth on various carbon sources.....	151
Figure 4-24 Variation in hyphal growth-rate of the GPCR mutant strains in response to amino acids	152
Figure 4-25 Variation in colony growth of the GPCR mutant strains under various stress conditions	157

Figure 4-26 Variation in hyphal growth rate of the GPCR mutants in response to plant extracts	158
Figure 4-27 Effect of inhibition/activation of key enzymes in the cAMP signalling pathway on growth of wild-type and GPCR mutants	161
Figure 4-28 Quantification of the intracellular cAMP levels in the <i>Δgpr1b</i> and <i>Δgpr2</i> mutants under nutrient limitation	163
Figure 5-1 Strategy for deletion of <i>pdeH</i> and identification of <i>ΔpdeH</i> mutant strains	166
Figure 5-2 Culture phenotype analysis of <i>ΔpdeH</i> mutant strain	169
Figure 5-3 Hyphal fusion event in <i>ΔpdeH</i> mutant strains	170
Figure 5-4 Symbiosis phenotype of <i>Lolium perenne</i> infected with <i>ΔpdeH</i> mutant strain	171
Figure 5-5 Complementation of <i>ΔpdeH</i> mutant strain	172
Figure 5-6 Light microscopy of the <i>ΔpdeH</i> mutant strain <i>in planta</i>	175
Figure 5-7 Transmission electron microscopy of the <i>ΔpdeH</i> mutant strain <i>in planta</i>	176
Figure 5-8 Hyphae per intercellular space of <i>ΔpdeH</i> mutant and complementation strains	177
Figure 5-9 Confocal laser-scanning microscopy of the <i>ΔpdeH</i> mutant strain <i>in planta</i>	179
Figure 5-10 Strategy for deletion of and identification of <i>ΔpdeL</i> mutant strains ..	180
Figure 5-11 Culture phenotype analysis of <i>ΔpdeL</i> mutant strain	183
Figure 5-12 Hyphal fusion event in <i>ΔpdeL</i> mutant strains	184
Figure 5-13 Sporulation assay for the <i>ΔpdeL</i> mutant strains	184
Figure 5-14 Complementation of <i>ΔpdeL</i> mutant strain	187
Figure 5-15 Symbiosis phenotype of <i>Lolium perenne</i> infected with <i>ΔpdeL</i> mutant strain	188
Figure 5-16 Confocal laser-scanning microscopy of the <i>ΔpdeL</i> mutant strain <i>in planta</i>	191
Figure 5-17 Colony morphology of the PDE mutant strains in response to nutrient limitation	193
Figure 5-18 Variation in hyphal growth rate of the PDE mutant strains in response to nutrient starvation and to growth on various carbon sources	195

Figure 5-19 Variation in hyphal growth-rate of the PDE mutant strains in response to amino acids	196
Figure 5-20 Variation in colony growth of the PDE mutant strains under various stress conditions	200
Figure 5-21 Variation in hyphal growth rate of the PDE mutants in response to plant extracts	203
Figure 5-22 Effect of inhibition/activation of key enzymes in the cAMP signalling pathway on growth of wild-type and GPCR mutants	204
Figure 5-23 Quantification of intracellular cAMP concentration in $\Delta pdeH$ and $\Delta pdeL$ mutants under nutrient limitation.....	207
Figure 6-1 The fungal G protein and cAMP pathway in association with the host.....	244

LIST OF TABLES

Table 2-1	Organisms and plasmids used.....	32
Table 2-2	List of primers used.....	35
Table 2-3	Table of growth media and supplements.....	43
Table 2-4	Table of growth media and amino acid supplements	45
Table 3-1	Table of putative <i>Epichloë</i> GPCRs.....	76
Table 3-2	<i>Epichloë</i> Class XIV - Pth11-like GPCRs.....	81
Table 3-3	<i>Epichloë</i> PDEs.....	100
Table 3-4	Components of G-protein and cAMP/PKA signalling pathway	112

LIST OF APPENDICES

Appendix 1: Table of genes used in this study	248
Appendix 2: Plasmid map of pRS426.....	257
Appendix 3: Plasmid map of pSF15.15.....	258
Appendix 4: Plasmid map of pSF16.17.....	259
Appendix 5: Plasmid map of pAB01	260
Appendix 6: Plasmid map of pAB02	261
Appendix 7: Plasmid map of pAB03	262
Appendix 8: Plasmid map of pAB04.....	263
Appendix 9: Plasmid map of pAB05.....	264
Appendix 10: Plasmid map of pAB06	265
Appendix 11: Plasmid map of pAB08	266
Appendix 12: Plasmid map of pCR2.1-TOPO®	267
Appendix 13: Non-transfer experiment design (A) and measurement (B)	268
Appendix 14: Transfer experiment design (A) and measurement (B).....	269
Appendix 15: Table of <i>E. festucae</i> GPCR homologues.....	2670
Appendix 16: Rooted phylogenetic dendrogram of class V GPCRs among <i>Epichloë</i> species	272
Appendix 17: Table of <i>E. festucae</i> homologues for components of the G protein and cAMP/PKA signalling pathway.....	2673
Appendix 18: Table of transcriptional difference of <i>E. festucae</i> wild-type growth in culture and in association with the host.....	2674

LIST OF SUPPLEMENTARY FILES

Supplementary 1: Multiple sequence alignment of <i>E. festucae</i> Pre2 homologues	278
Supplementary 2: Predicted protein topology of <i>E. festucae</i> Pre2.....	278
Supplementary 3: Multiple sequence alignment of <i>E. festucae</i> Pre1 homologues	278
Supplementary 4: Predicted protein topology of <i>E. festucae</i> Pre1.....	278
Supplementary 5: Multiple sequence alignment of <i>E. festucae</i> Gpr4 homologues	278
Supplementary 6: Predicted protein topology of <i>E. festucae</i> Gpr4	278
Supplementary 7: Multiple sequence alignment of <i>E. festucae</i> Gpr5 homologues	278
Supplementary 8: Predicted protein topology of <i>E. festucae</i> Gpr5	278
Supplementary 9: Multiple sequence alignment of <i>E. festucae</i> Gpr6 homologues	278
Supplementary 10: Predicted protein topology of <i>E. festucae</i> Gpr6.....	278
Supplementary 11: Multiple sequence alignment of <i>E. festucae</i> Gpr7a homologues	278
Supplementary 12: Predicted protein topology of <i>E. festucae</i> Gpr7a	278
Supplementary 13: Multiple sequence alignment of <i>E. festucae</i> Gpr7b homologues	278
Supplementary 14: Predicted protein topology of <i>E. festucae</i> Gpr7b	279
Supplementary 15: Multiple sequence alignment of <i>E. festucae</i> Gpr7c homologues	279
Supplementary 16: Predicted protein topology of <i>E. festucae</i> Gpr7c.....	279
Supplementary 17: Multiple sequence alignment of <i>E. festucae</i> Gpr8 homologues	279
Supplementary 18: Predicted protein topology of <i>E. festucae</i> Gpr8.....	279
Supplementary 19: Multiple sequence alignment of <i>E. festucae</i> Gpr9 homologues	279
Supplementary 20: Predicted protein topology of <i>E. festucae</i> Gpr9.....	279
Supplementary 21: Multiple sequence alignment of <i>E. festucae</i> Gpr10 homologues	279
Supplementary 22: Predicted protein topology of <i>E. festucae</i> Gpr10	279
Supplementary 23: Multiple sequence alignment of <i>E. festucae</i> Gpr10b homologues	279
Supplementary 24: Predicted protein topology of <i>E. festucae</i> Gpr10b.....	279

Supplementary 25: Multiple sequence alignment of <i>E. festucae</i> Gpr9b homologues	279
Supplementary 26: Predicted protein topology of <i>E. festucae</i> Gpr9b.....	279
Supplementary 27: Multiple sequence alignment of <i>E. festucae</i> Ops1 homologues	280
Supplementary 28: Predicted protein topology of <i>E. festucae</i> Ops1.....	280
Supplementary 29: Multiple sequence alignment of <i>E. festucae</i> Gpr11 homologues	280
Supplementary 30: Predicted protein topology of <i>E. festucae</i> Gpr11.....	280
Supplementary 31: Multiple sequence alignment of <i>E. festucae</i> Gpr13 homologues	280
Supplementary 32: Predicted protein topology of <i>E. festucae</i> Gpr13.....	280
Supplementary 33: Multiple sequence alignment of <i>E. festucae</i> Gpr14a homologues	280
Supplementary 34: Predicted protein topology of <i>E. festucae</i> Gpr14a.....	280
Supplementary 35: Multiple sequence alignment of <i>E. festucae</i> Gpr14b homologues	280
Supplementary 36: Predicted protein topology of <i>E. festucae</i> Gpr14b.....	280
Supplementary 37: Predicted protein topology of <i>E. festucae</i> Pth11-1.....	280
Supplementary 38: Predicted protein topology of <i>E. festucae</i> Pth11-2.....	280
Supplementary 39: Predicted protein topology of <i>E. festucae</i> Pth11-3.....	280
Supplementary 40: Predicted protein topology of <i>E. festucae</i> Pth11-4.....	280
Supplementary 41: Predicted protein topology of <i>E. festucae</i> Pth11-5.....	281
Supplementary 42: Predicted protein topology of <i>E. festucae</i> Pth11-6.....	281
Supplementary 43: Predicted protein topology of <i>E. festucae</i> Pth11-7.....	281
Supplementary 44: Predicted protein topology of <i>E. festucae</i> Pth11-8.....	281
Supplementary 45: Predicted protein topology of <i>E. festucae</i> Pth11-9.....	281
Supplementary 46: Predicted protein topology of <i>E. festucae</i> Pth11-10.....	281
Supplementary 47: Predicted protein topology of <i>E. festucae</i> Pth11-11.....	281
Supplementary 48: Predicted protein topology of <i>E. festucae</i> Pth11-12.....	281
Supplementary 49: Predicted protein topology of <i>E. festucae</i> Pth11-13.....	281
Supplementary 50: Predicted protein topology of <i>E. festucae</i> Pth11-14.....	281
Supplementary 51: Predicted protein topology of <i>E. festucae</i> Pth11-15.....	281
Supplementary 52: Predicted protein topology of <i>E. festucae</i> Pth11-16.....	281

Supplementary 53: Predicted protein topology of <i>E. festucae</i> Pth11-17.....	281
Supplementary 54: Predicted protein topology of <i>E. festucae</i> Pth11-18.....	281
Supplementary 55: Predicted protein topology of <i>E. festucae</i> Pth11-19.....	281
Supplementary 56: Multiple sequence alignment of <i>E. festucae</i> Gpa1 homologues	281
Supplementary 57: Multiple sequence alignment of <i>E. festucae</i> Gpa2 homologues	282
Supplementary 58: Multiple sequence alignment of <i>E. festucae</i> Gpa3 homologues	282
Supplementary 59: Multiple sequence alignment of <i>E. festucae</i> Gpb1 homologues	282
Supplementary 60: Multiple sequence alignment of <i>E. festucae</i> Gpg1 homologues	282
Supplementary 61: Multiple sequence alignment of <i>E. festucae</i> Ric8 homologues	282
Supplementary 62: Multiple sequence alignment of <i>E. festucae</i> AcyA homologues	282
Supplementary 63: Multiple sequence alignment of <i>E. festucae</i> Pkac1 homologues	282
Supplementary 64: Multiple sequence alignment of <i>E. festucae</i> Pkar1 homologues	282

ABBREVIATIONS

aa, AA	amino acid(s)
AC	adenylate cyclase
Amp	Ampicillin
AMP	Adenosine monophosphate
AmpR	Ampicillin resistance
APF	Apoplastic fluid
APS	Apoplastic space
ADP	Adenosine diphosphate
ATP	Adenosine triphosphate
BLAST	Basic local alignment search tool
BLASTn	BLAST search against a nucleotide sequence database with a nucleotide sequence query
BLASTp	BLAST search against a protein sequence database with a protein sequence query
bp	Base pairs
C	Plant cuticle
C-terminus	carboxyl terminal sequence (COOH-terminus)
cAMP	cyclic adenosine monophosphate
cGMP	cyclic guanosine monophosphate
COOH	Carboxy terminal sequence
CD	Czapek Dox salts medium
CDGN	Czapek Dox salts medium, modified
cDNA	Complementary DNA
CDS	Coding sequence
CLSM	Confocal laser-scanning (fluorescence) microscopy
cm	Centimeter
conc.	Concentration
CR	Congo Red
CRISPR	Clustered regularly-interspaced short palindromic repeats
CFW	Calcofluor white
CWI	Cell wall integrity

CZ	Czapek Dox medium
cPKA/Pkac	Protein kinase A catalytic subunit
DAB	3,3'-Diaminobenzidine
DIC	Differential interference contrast
DIG	Digoxigenin
DMSO	Dimethyl sulfoxide
DNA	Deoxyribonucleic acid
dNTP	deoxyribose nucleoside triphosphate
ECL	Extracellular loop
EDTA	Ethylene diamine tetra-acetic acid
Epi	Epiphyllous/Epiphytic (hyphae)
<i>E</i> value	Expect value
Exp	Expressoria structure (hyphae)
FRET	Förster resonance energy transfer
g	Gram
x g	Acceleration due to gravity on Earth (9.8 m s ²)
gDNA	Genomic DNA
Gen	Geneticin
Gen ^R	Geneticin resistance
GPCR	G protein-coupled receptor
G protein	Guanine nucleotide-binding protein
G α	Guanine nucleotide-binding protein alpha (α) subunit
G β	Guanine nucleotide-binding protein beta (β) subunit
G γ	Guanine nucleotide-binding protein gamma (γ) subunit
GEF	Guanine nucleotide exchange factor
GAP	GTPase-activating proteins
GTP	guanosine triphosphate
GDP	guanosine diphosphate
GTPase	hydrolase enzymes that bind and hydrolyze guanosine triphosphate (GTP)
GMP	Guanosine monophosphate
h	Hour(s) or hyphae according to context
His	Histamine
<i>hph</i>	Hygromycin resistance-conferring gene

Hyg	Hygromycin
Hyg ^R	Hygromycin resistance
ICS	Intracellular space
ICL	Intracellular loop
IMBX	3-iso-1-methylxanthine
Kb	kilobase
LA	Linoleic acid
LB	Luria-Bertani
l	Litre
M	Molar (Moles per liter)
MAPK	Mitogen-activated protein kinases
MAPKK	Mitogen-activated protein kinases kinases
MAPKKK	Mitogen-activated protein kinases kinases kinases
mRNA	Messenger RNA
mg	Milligram
min	Minute(s)
mm	Millimeter
mM	millimole
ml	millilitre
NADPH	Nicotinamide adenine dinucleotide phosphate
NCBI	National Center for Biotechnology Information
NCM	Nitrocellulose membrane
ng	Nanograms
N-terminus	Amino terminal sequence (NH ₂ -terminus)
<i>nptII</i>	Geneticin resistance-conferring gene
°C	Degrees Celsius
ORF	Open reading frame
PC	Plant cell
PCR	Polymerase chain reaction
PCW	Plant cell wall
PD	Potato dextrose
PEG	Polyethylene glycol
PKA	Protein kinase A
Ppi	Pyrophosphate

PR	pheromone response pathway
PDE	phosphodiesterase
PAQR	progesterin adipoQ Receptor
qPCR	Quantitative polymerase chain reaction
Qui	Quinine
RE	Restriction enzyme
RG	Regeneration (medium)
RGS	Regulator of G protein signalling
RNA	Ribonucleic acid
RNAseq	RNA sequencing
Rnase	Ribonuclease
ROS	reactive oxygen species
RPM	Revolution per minute
RPKM	Reads Per Kilobase Million
RT	Room temperature
RT-PCR	Reverse transcription polymerase chain reaction
RT-qPCR	Reverse transcription quantitative polymerase chain reaction
rPKA/Pkar	Protein kinase A regulatory subunit
s	Second(s)
SAM	Shoot apical meristem
SDS	Sodium dodecyl sulfate
SM	Secondary metabolism OR secondary metabolite
SD	Standard deviation
SE	Standard error
Sub	Sub-cuticular (hyphae)
TBE	Tris-boric acid-EDTA
tBLASTn	BLAST search against a translated nucleotide sequence database with a protein sequence query
TE	Trace elements
TF	Transcription factor
TM	Transmembrane
Tm	Melting temperature
V	vacuole
v/v	Volume:volume ratio

w/v	Weight:volume ratio
WGA	Wheat germ agglutinin
WT	Wild type
μg	microgram
μl	microliters
μm	micrometer
μM	micromolar

Chapter 1 Introduction

1.1 *Epichloë festucae* forms a mutualistic association with perennial ryegrass

The genus of *Epichloë* endophytes belong to the fungal family of *Clavicipitaceae* (Phylum Ascomycota; Order Hypocreales) and are characterised by mutualistic association with cool-season grasses of the genera *Lolium* and *Festuca* (Family *Poaceae*) (Schardl et al. 1994, Clay and Schardl 2002). In contrast to pathogenic fungi, *Epichloë* spp. mostly form asymptomatic symbioses with their host plants, and there is benefit for both partners. The *Epichloë* spp. comprises strictly asexual anamorphic species, formerly known as *Neotyphodium* spp., and teleomorphic species, with the latter able to switch between sexual and asexual lifecycles (Leuchtman et al. 2014). The asexual form usually result from interspecific hybridisation as well as sexual intraspecific hybridisation (Schardl et al. 1994, Schardl 1996, Moon et al. 2004). *Epichloë festucae*, as well as its asexual derivative *Epichloë festucae* var. *lolii* (formerly *Neotyphodium lolii*), are biotrophic endophytes forming mutualistic associations with perennial ryegrass (*Lolium perenne*), however the former can switch to an antagonistic interaction during sexual reproduction (Christensen et al. 1997, Tanaka et al. 2012). In contrast to the natural symbiont of *L. perenne*, *E. festucae* var. *lolii*, which is intractable to genetic modification, *E. festucae* is an ideal experimental model organism to study the molecular and cellular mechanisms of symbiotic endophyte-grass associations (Schardl et al. 1997, Scott et al. 2007). *E. festucae* forms a stable interaction with *L. perenne* under natural and laboratory conditions, is amenable to a broad range of molecular manipulation methods including transformation for homologous or non-homologous recombination (Tanaka et al. 2005, Young et al. 2005) and has an available genome sequence for strains E2368 and E894 F11 (Scott et al. 2012).

1.1.1 Mutual benefits of symbiotic interaction

The association of *E. festucae* and *L. perenne* is usually beneficial to both the plant and the fungus. The advantages for the fungal symbiont are access to nutrients from the plant apoplast, protection and transmission and dispersal through colonisation of the host seed. Vice versa, the host grass benefits by increased tolerance to abiotic and biotic stresses like drought and herbivory (reviewed in

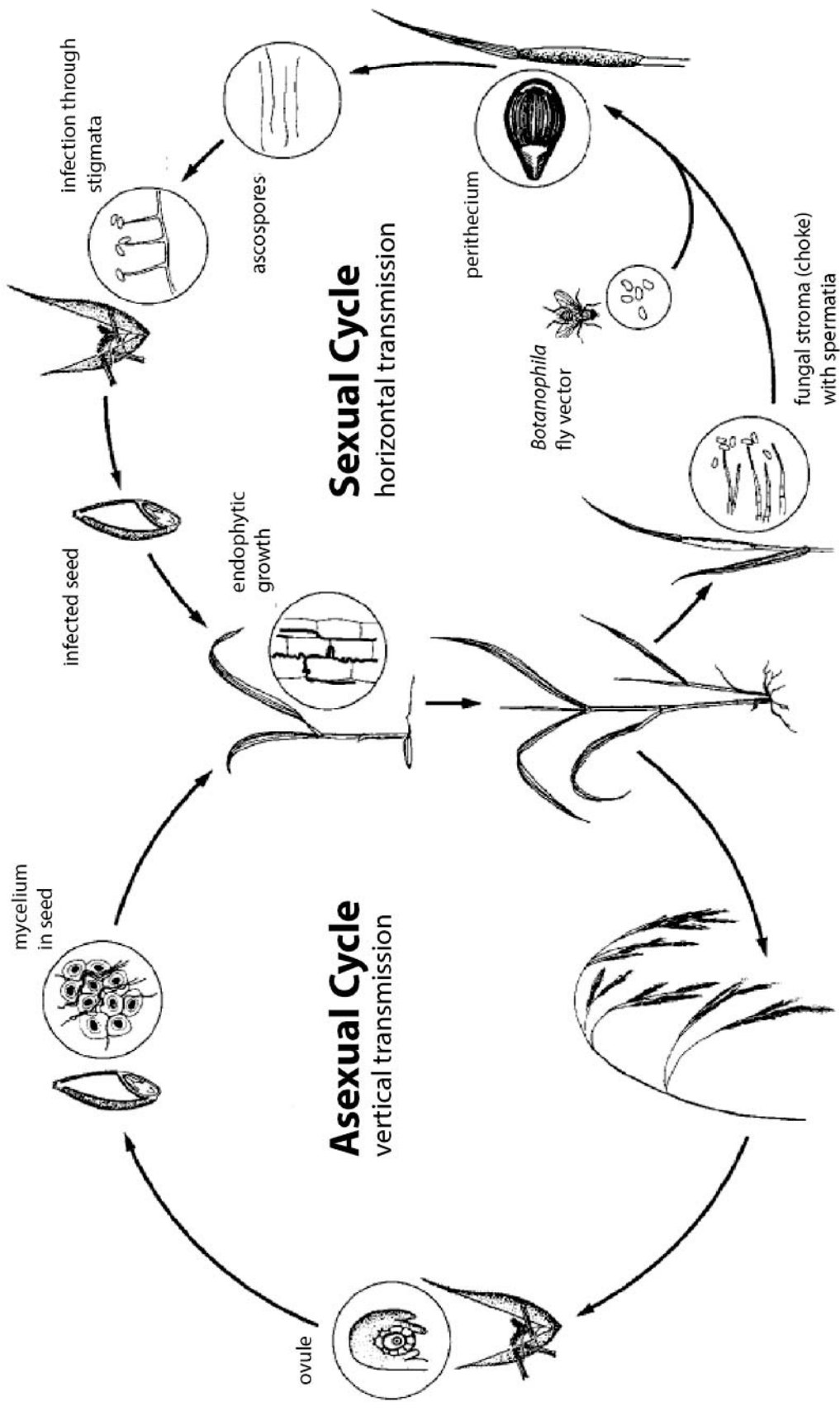
Johnson et al. 2013), leading to an overall increased host fitness and plant growth. The endophyte induces changes in host metabolism and produces bio-protective secondary metabolites, which protect the host from insects and mammalian herbivores (Kuldau and Bacon 2008, Rasmussen et al. 2008, Zhang et al. 2009). *Epichloë* endophytes synthesise four main classes of bioprotective secondary metabolites: peramine, indole diterpenes, ergot alkaloids and lolines, and any one strain has the genetic capability for synthesis of up to three of these components (Schardl et al. 2012). *Epichloë* spp. range from exclusively mutualistic to marginally antagonistic species, dependent on production of specific secondary metabolites and the form of transmission (Schardl et al. 2004, Schardl et al. 2013). With the exception of stromata formation by some *Epichloë* endophyte species; which inhibit host flowering and cause "choke" disease, the endophyte-plant association remains asymptomatic.

1.1.2 The lifecycle of *E. festucae* includes both asexual and sexual stages

During endophytic colonisation of the host aerial tissues, *E. festucae* has the capacity to switch between asexual and sexual development. The fungal lifecycle is normally highly restricted within the host, and fungal reproduction is synchronized with the host flowering process. This developmental alteration is initiated when the plant changes from vegetative to reproductive growth. During its asexual lifecycle, *E. festucae* can maintain its restrictive endophytic growth and infect the ovules of inflorescence primordia subsequently leading to colonisation of the seeds (vertical transmission) (Philipson and Christey 1986, reviewed in Johnson et al. 2013). However, the hyphae can alternatively switch to proliferative growth for antagonistic sexual development, leading to horizontal transmission (Scott and Schardl 1993). In this case, the fungus emerges on the leaf surface through penetration of the flag leaf sheath and forms a compact mycelial structure (stromata) enveloping the developing inflorescence by epiphyllous growth (White and Chambless 1991, White et al. 1997). Formation of these external reproduction structures from where conidia (or spermatia) arise, suppress host inflorescence development and cause the so called "choke" disease (Schardl et al. 2004). In stromata, mating of transferred spermatia takes place, but also continuous

anamorph conidiogenesis with resulting conidia that serve as spermatia (Tadych et al. 2014). Sexual development, involves horizontal transfer of spermatia from unfertilized stromata, to stromata of opposite mating type by the symbiotic anthomyiid fly vector (*Botanophila* spp.), that are attracted by fungal-produced volatile organic compounds (Chung and Schardl 1997, Bultman et al. 1998, Steinebrunner et al. 2008, Li et al. 2014). A heterothallic mating system regulates sexual cell fusion of two species with opposite mating types (Chung and Schardl 1997, Oberhofer and Leuchtman 2012). After meiosis, perithecia (fruiting bodies) are formed followed by asci and finally ascospores, which are released and transferred horizontally to the new uninfected host (Rodriguez et al. 2009, Schardl 2010). When ascospores land on new host stigma, they germinate, immediately undergo microcycle conidiogenesis to produce large numbers of conidia, which then germinate and infect the developing ovules, colonise the developing embryo and subsequently the grass seeds (Bacon and Hinton 1991, Chung and Schardl 1997, Rodriguez et al. 2009, Tadych et al. 2014). Once grass seeds germinate the systemic fungal colonisation of the host starts in the meristematic tissue and asexual endophytic infection starts over again (reviewed in (Johnson et al. 2013)).

Figure 1-1 Lifecycle of *Epichloë* endophytes: Schematic lifecycle of *Epichloë* endophytes showing sexual and asexual stages in association with their host grass. *Epichloë* species comprise strictly asexual species (Type I), strictly sexual species (Type III) and endophytes that show both sexual and asexual stages (Type II) such as *E. festucae*. The asexual cycle is characterised by vertical transmission of fungal hyphae through host seed colonisation. In the sexual cycle, hyphae proliferate over the developing host inflorescence forming a mycelial structure known as a stroma, which prevents host inflorescent emergence, a process known as “choke”. The endophyte produces spermatia on the surface of the stroma, which are transferred to a stroma of opposite mating type via *Botanophila* flies (horizontally transmission). Perithecia then develop on the stroma where ascospores mature and get ejected on new host plant. Germinating ascospores on grass surfaces undergo microconidiogenesis with resulting conidia grow into the ovule to colonise the host seed (adapted from Schardl et., 2004)



An incomplete sexual cycle occurs when conidia from stromata are horizontally transferred directly to stigma of a new host inflorescence (Tadych et al. 2014). *E. festucae*, as a type II endophyte, is capable of reproducing sexually (horizontal transmission) and asexually (vertical transmission) in the same host on different tillers, although asymptomatic inflorescence dominate (Scharndl et al. 2004). While sexual development only occurs in some native hosts such as *Festuca rubra* (*Poaceae*), choke formation has not been observed in the synthetic association with perennial ryegrass *L. perenne* (Scharndl et al. 2004).

1.1.3 *E. festucae* shows a host-synchronised growth pattern in association with perennial ryegrass

To establish and maintain a stable symbiotic interaction, the development as well as the endophytic growth of *E. festucae* has to be regulated within the host. A tightly synchronised and distinct growth pattern has evolved. From the shoot apical meristem (SAM), the leaf primordia develop by rapid cell division and give rise to new leaves and sequentially the leaf sheath and blade through by displacing older cells upwards and cell expansion from the meristematic center, while the axillary bud gives rise to new tillers. The origin of endophytic plant colonisation is the SAM and it starts at the embryo, through the vegetative meristematic tissues of leaf primordia, axillary buds, sheaths and blades to the inflorescence tillers (Christensen et al. 2008). The hyphae generate a mycelial network by frequent branching and fusion with nearby hyphae, but nevertheless retain a low overall biomass. With the exception of the root apical meristem (RAM), the fungus does not grow through the root tissue (Christensen et al. 2008, Voisey 2010). During systemic colonisation, the endophyte elongates among the dividing cells of the leaf sheath and blades with usually a single hypha parallel to the leaf axis, which appears to be firmly attached to the mesophyll cell wall a situation ideal for nutrient and signal exchange (Christensen et al. 2008). In the meristematic zones, where plant cell division takes place, the hyphae grow by apical proliferation. However, when plant cells undergo rapid elongation followed by expansion the fungal hyphae stay attached to the plant cells. The hyphal growth is synchronised with host leaf expansion to avoid shearing forces caused by host cell division. To do this, the hyphae follow morphological differentiation and switch to intercalary division and extension (Christensen et al.

2001, Christensen et al. 2008), which allows simultaneous growth with the rapidly expanding and largely extending leaf tissue by the attached fungal hyphae (Christensen et al. 2008, Voisey 2010, Eaton et al. 2011). During this rapid hyphal-expansion, the stretched sub-apical hyphae undergo septation and form multiple compartments including nuclear division, to divide the stretched hyphae (intercalary growth) (Christensen et al. 2008, Voisey 2010, Ariyawansa 2015). The exact mechanism that triggers intercalary growth is not fully understood but mechanical stretching of the fungal cell wall, caused by the plant cell expansion, is reported to promote intercalary extension and compartmentalization, which is regulated by the mechano-stress activated calcium channel MidA that triggers calcium signalling and sequential cell wall biosynthesis (Ariyawansa 2015). In addition to the proposed model for the mechanical regulation of intercalary growth, further signalling pathways such as the stress-activated MAP kinase pathway as well as other unknown factors are involved in cellular processes and morphological changes leading to intercalary extension and the highly restricted growth *in planta* (Brand and Gow 2009, Eaton et al. 2011). While hyphae in the meristematic tissue grow by apical proliferation, hyphal growth in other tissues is highly restricted and are rarely colonise the vascular bundle tissue (Christensen et al., 2001). The exact trigger that coordinates the restricted and synchronized endophytic growth including the switch to intercalary extension in sub-apical hyphae has yet to be identified. However, the regulation of the necessary cellular processes that alter fungal growth and differentiation, including the avoidance of the plant-defense system, requires the exchange of signals between the endophyte and the host and therefore recognition of host-derived or tissue-specific molecules (inter-species communication).

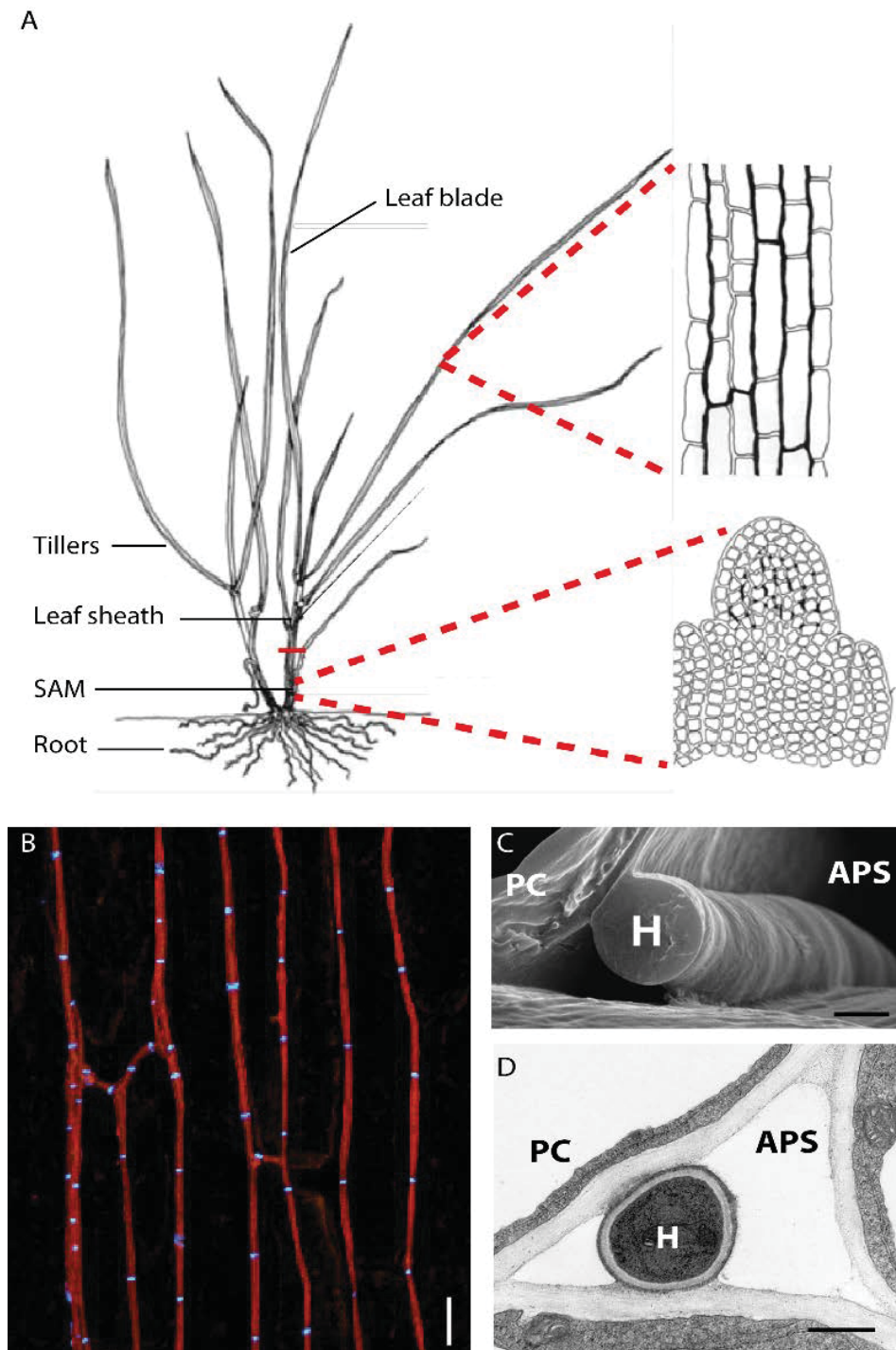


Figure 1-2 *E. festucae* shows a synchronised growth *in planta*: (A) Schematic representation of fungal colonisation of perennial ryegrass (*Lolium perenne*) with magnified longitudinal section of vegetative tillers and shoot apical meristem (SAM). *E. festucae* colonisation between plant cells is indicated by dark lines (adapted from May et al., 2008). (B) Longitudinal section of pseudostem tissue infected with *E. festucae* using confocal laser-scanning microscopy (CLSM). Sample stained with aniline blue (red) and WGA-AlexaFluor488 (blue), staining fungal chitin in cell walls and septa respectively. Bar = 10 μ m. (C and D) Restricted growth of single hyphae (H) between plant cells (PC) in apoplastic space (aps) with attachment of hyphae to plant cell wall. (C) Frozen fractured SEM micrograph of *Epichloë coenophialum* in tall fescue leaf (adapted from Christensen et al., 2008). (D) TEM micrograph of pseudostem tissue cross-section showing *L. perenne* infected with *E. festucae* and hyphal growth in host apoplast. Bar = 1 μ m (C and D).

1.2 Specific signalling is necessary for symbiosis between fungus and host

To sense the extracellular environment and be able to respond to changes, a highly versatile and largely conserved signal transduction system has evolved in filamentous fungi. Cells contain multiple pathways to recognise external and internal signals and transduce them from the cell surface to the nucleus in order to transform environmental changes into alterations of gene expression. Among a battery of various cell surface receptors, G protein-coupled receptors (GPCRs) are frequently responsible for sensing the extracellular environment for more specific signals. The protein family of GPCRs transmits changes predominantly to the heterotrimeric G proteins, which transduce these signals to downstream pathways (Xue et al. 2008). Two of the most important downstream signalling pathways are the MAP kinase cascade and the second messenger cAMP/PKA-signalling pathway (Banuett 1998, Kronstad et al. 1998). The interconnection and direct involvement of these pathways in controlling developmental changes, metabolic processes, sexual development, starvation and stress response, filamentous growth and pathogenesis has been extensively reviewed (Christianson et al. 1992, Rispaill and Di Pietro 2009, Kronstad et al. 2011, Cullen and Sprague 2012).

1.2.1 G protein signalling pathways transduce extracellular signals to downstream pathways

The G protein signalling pathway is one of the most important signal transduction pathways in filamentous fungi (reviewed in Li et al. 2007). It is involved in a broad range of cellular processes in response to extracellular signals and environmental changes. The components of the pathway are the membrane bound G protein-coupled receptors (GPCRs), heterotrimeric G proteins and the subsequently activated downstream pathways (e.g. MAP kinase-, cAMP or Ca²⁺ signalling pathway). The cell surface-located G protein coupled receptors transduce extracellular signals to intracellular bound heterotrimeric guanine nucleotide-binding proteins (G proteins) and activates them (Neer 1995, Li et al. 2007). The heterotrimeric G proteins consist of three subunits G α , G β and G γ and represent the major proteins for signal transmission of the G protein signalling pathway. When an agonist binds to the GPCR, a conformational change in the GPCR triggers the G

protein α subunit to release its bound GDP, which is immediately replaced with GTP. This is promoted by the guanine nucleotide exchange factor (GEF)-function of the GPCR or cytosolic GEFs like RIC8 in *N. crassa* (Wright et al. 2011). This induces the release of the heterotrimeric subunits and the activation of the signal transduction pathway. The trimer dissociates into a GTP-bound $G\alpha$ subunit and a $G\beta/\gamma$ -dimer, both of which can interact and activate different downstream effectors and initiate pathways such as various MAPK pathways, the phosphatidylinositol signalling pathways or the cAMP-signalling cascade that activates the protein kinase A (cAMP/PKA signalling pathway). After the release of the heterotrimeric G protein, the receptor is able to activate the next G protein. Along with the GTP-binding domain, the $G\alpha$ subunit also contains an autoregulatory GTPase domain, which deactivates the protein at a certain threshold. To enhance this process, regulatory proteins, known as GTPase-activating proteins (GAPs), bind to the $G\alpha$ subunit and hydrolyse the GTP to stimulate the re-association of the heterotrimer at the plasma membrane. GAPs, also known as the regulator of G protein signalling proteins (RGS), have a crucial role in controlling the G protein signalling cascade and signal intensity. The G protein signalling cascade is inactivated by hydrolysis of the GTP bound $G\alpha$ subunit into GDP, which results in the re-association with the $G\beta/\gamma$ -dimer and the GPCR at the membrane (Neer 1995, Li et al. 2007).

Heterotrimeric G protein signalling has most commonly been investigated in *Neurospora crassa*, the first filamentous fungus in which this pathway was identified (Turner and Borkovich 1993, Li et al. 2007). The activation of downstream signalling pathways like the MAPK and cAMP/PKA signalling pathways by the heterotrimeric G protein signalling, and the G protein pathway itself have been shown to play an essential role in vegetative growth, carbon sensing, asexual conidiogenesis, sexual development and stress resistance and virulence of various phytopathogens (Li et al. 2007, Eaton et al. 2011), but its role in mutualism is still unclear. *E. festucae* encodes genes for all essential components of the heterotrimeric G protein signalling pathway. Most filamentous fungi, including *E. festucae*, possess three genes for the $G\alpha$ subunit (termed Group I, Group II, Group III), which allows for diverse functions and affects variable targets in the cell (Li et al. 2007, Eaton et al. 2011, Won et al. 2012). Despite their essential role in signal transduction, little is known about the role these proteins play in phytopathogenicity or mutualism.

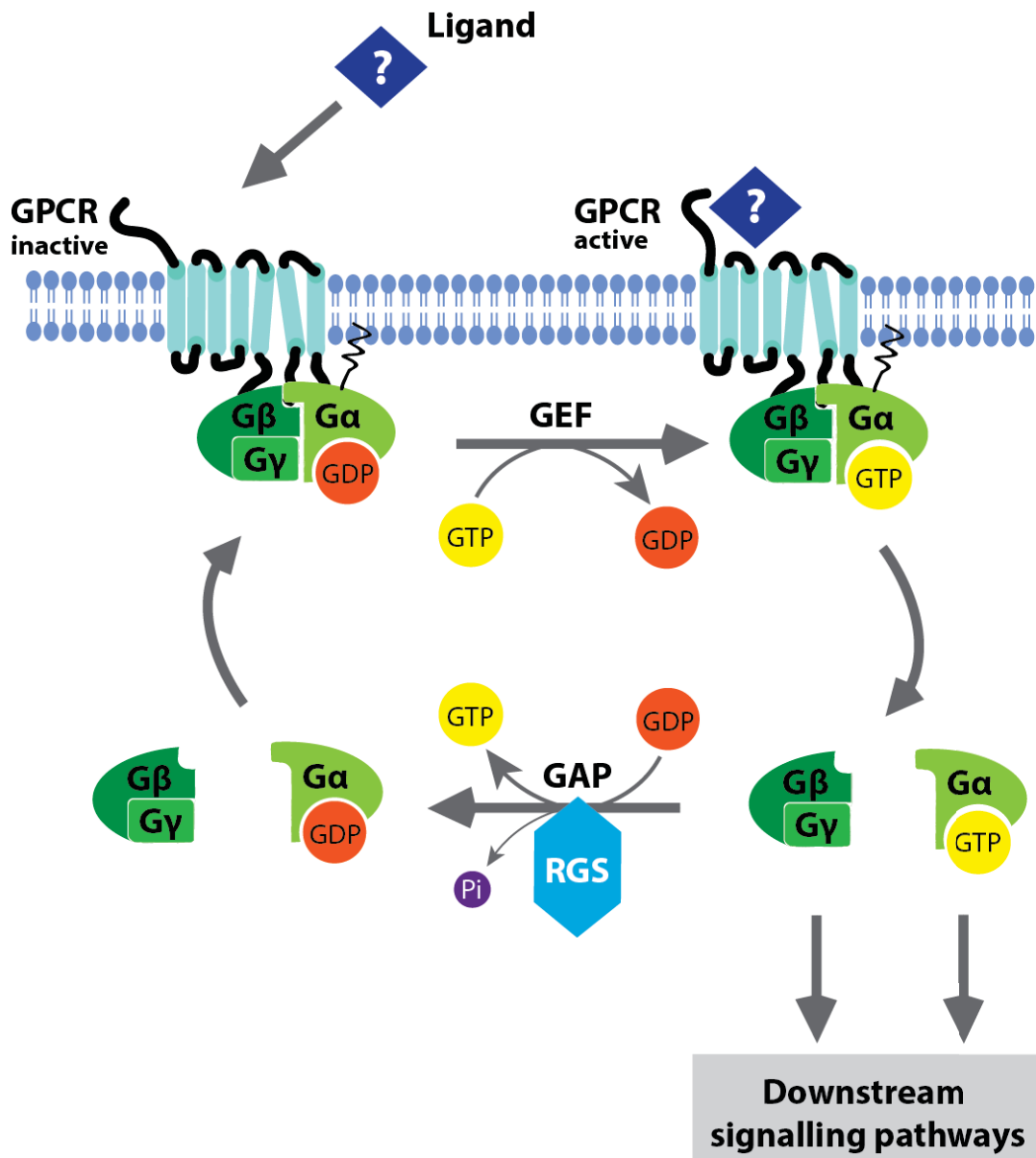


Figure 1-3. The heterotrimeric G-protein cycle: The heterotrimeric G-protein consists of three subunits, $G\alpha$, $G\beta$, $G\gamma$, which interact intracellularly with the C-terminus of the G protein coupled receptor (GPCR). When the GPCR binds a ligand, a conformational change occurs and it functions as a guanine nucleotide exchange factor (GEF), inducing release of GDP by the $G\alpha$ subunit, which is quickly replaced with GTP. GTP binding activates the $G\alpha$ subunit and it dissociates from $G\beta$ and $G\gamma$, which then stay as a dimer and both can activate downstream pathways. Regulator of G protein signalling (RGS) proteins which act as GTPase-activating proteins (GAPs) and induce hydrolysis of GTP to GDP, trigger the reassociation of the heterotrimeric G-protein subunits, which stay in an inactive form until again activated by a GPCR.

In phytopathogenic fungi, like *Magnaporthe oryzae* (*magA*, *magB*, *mgb1*) (Liu and Dean 1997), *Fusarium oxysporum* (*fga1*, *fga2*, *fgb1*) and other *Fusarium* spp.

(Jain et al. 2002), *Botrytis cinerea* (*bcg1*, *bcg2*, *bcg3*) (Gronover et al. 2001), *Ustilago maydis* (*gpa3*) (Regenfelder et al. 1997) and *Trichoderma atroviride* (*tga3*) (Zeilinger et al. 2005), it has been shown that at least one component of the heterotrimeric G proteins is required for virulence and host penetration. In *N. crassa*, the G α subunits are essentially involved in vegetative growth, carbon sensing, sexual (perithecia formation) and asexual (conidiogenesis) development, each to a different extent (reviewed in Won et al. 2012). In the dimorphic phytopathogen *Mycosphaarella graminicola*, the G proteins (*MgGpa1*, *MgGpa3*, *MgGprb1*) are involved in morphogenic differentiation, essential for the pathogenic development and mutant strain analysis revealed similar defects in hyphal growth and sexual and asexual development that were observed for the *N. crassa* G proteins (Mehrabi et al. 2009, Won et al. 2012). While the G β -subunit also regulates the pheromone response pathway in *M. graminicola*, *MgGpa3* and *MgGprb1* positively regulate the cAMP/PKA signalling pathway (Mehrabi et al. 2009). Pathogenicity and asexual sporulation was compromised in the wheat pathogen *Stagonospora nodorum* when *Gna1* (G α subunit Group I) was deleted (Solomon et al. 2004). The disruption of the heterotrimeric G protein signalling pathway by deletion of one of the *E. festucae* G α subunits, leads to breakdown of the mutualistic endophyte-plant association and a severe phenotype in culture (Takemoto, pers. com.). However, the likely role of the heterotrimeric G protein signalling pathway, especially of the G α subunits, in transducing host-derived signals needs further investigation. The genes for the G β - and G γ -subunits are in single copy and are highly conserved within most filamentous fungi, including *E. festucae* (Li et al. 2007, Eaton et al. 2011). Although it is unclear what role G γ plays in virulence, the G β and G γ gene products are proposed to have distinct roles in phytopathogenicity (Li et al. 2007). The G β subunit (*mgb1*) is essential for normal pathogenic response in *M. oryzae* as it functions in activating the pheromone response pathway (Nishimura et al. 2003), whereas gene deletion of *F. oxysporum fgb1* (Jain et al. 2003) resulted in reduced virulence but not complete loss of pathogenicity. In *S. nodorum*, deletion of either *Gba1* (G β -subunit) or *Gga1* (G γ -subunit) resulted in a similar phenotype to that described for the G α subunit *Gna1* (Gummer et al. 2012). In *N. crassa*, mutants of the G β -subunit (*Gnb-1*) and G γ -subunit (*Gng-1*) have defects in asexual sporulation and form sterile female fruiting bodies, identical for both mutant strains, in a double deletion mutant and similar to the phenotype observed for the G α subunit *Gna-3*

(Yang 2002, Krystofova and Borkovich 2005, Won et al. 2012). This indicates that the G β - and G γ - subunit function as a dimer and form a heterodimer with Gna-3, while Gna-1 functions independent of the G β /G γ -dimer (Yang and Borkovich 1999). It is possible that the G β /G γ -dimer, or just the G β subunit, is also important for symbiotic maintenance in *E. festucae*, in a similar fashion than in *M. oryzae* by regulating the pheromone response pathway. All of the individual heterotrimeric G proteins in *E. festucae*, were identified by their particularly high homology to the *N. crassa* homologues, and are currently being functionally characterised (Takemoto, pers. com.).

1.2.2 The mitogen-activated protein kinase pathway

The components of the mitogen-activated protein kinase (MAPK) pathway are evolutionarily highly conserved in all eukaryotes and responsible for transduction of multiple signals to downstream effectors in response to external stimuli (Banuett 1998). The signalling process functions by a phosphorylation chain of the three core protein kinases. The MAPKKK (MAP kinase kinase kinase) phosphorylates the MAPKK which in turn phosphorylates the MAPK (Banuett 1998). In filamentous fungi, three different MAPK cascades (pheromone response pathway, cell wall integrity pathway, stress response pathway) are responsible for the response to extracellular changes, depending on their particular external stimulus.

The pheromone response pathway is activated by heterotrimeric G protein signalling when extracellular chemoattractants such as pheromones bind to the responsible GPCR localised on the cell surface e.g. pheromone receptor. The MAPK cascade transfers the signal to specific target proteins, which induce changes in gene expression (Risipail and Di Pietro 2009). The pathway triggers filamentation and polarised growth and initiates the mating process in yeast (Cullen 2012). In the phytopathogen *U. maydis*, pheromone stimulation initiates the developmental switch from yeast-like to filamentous growth, followed by sexual cell fusion, dikaryon formation and the infection of the host plant (Brefort et al. 2009). The pheromone response is the essential trigger for sexual development which is required for pathogenicity and virulence in many fungi, particularly phytopathogens (Kahmann et al. 1995, Kahmann et al. 1999, Brefort et al. 2009,

Rispail et al. 2009). This is illustrated for example in the phytopathogenic fungi *F. oxysporum* and *F. graminearum* (Rispail and Di Pietro 2009, Rispail and Di Pietro 2010), *M. oryzae* (Xu and Hamer 1996) and the rye pathogen *Claviceps purpurea* (Mey et al. 2002). In the phytopathogens *M. oryzae*, *B. cinerea* or in the mycoparasitic fungus *Trichoderma atroviride* the pheromone response pathway is involved in signalling host-specific chemo-attractants enabling initiation of pathogenic development and host penetration (Wilson and Talbot 2009, Zhang et al. 2011, Gruber and Zeilinger 2014, Lichius and Lord 2014). Based on the close phylogenetic relationship of *E. festucae* to *C. purpurea*, this pathway may also be required for the symbiotic endophyte-host interaction in *E. festucae*, whose genome contains homologues of the pheromone response pathway (Eaton et al. 2011).

Physical stresses on the cell surface trigger the cell wall integrity (CWI) pathway to induce different remodeling processes (Levin 2005, Levin 2011). In a similar manner to the pheromone response pathway, the CWI pathway is also important for phytopathogenic virulence as well as for symbiotic establishment (reviewed in Turra et al., 2014; Hamel et al., 2012; Becker et al., 2015). Plants infected by mutant strains with deletions of the MAPKK MkkA and downstream MAPK MpkA of the CWI pathway showed a stunted phenotype with increased tillering and proliferative fungal growth *in planta*, signifying a breakdown of the symbiotic association (Becker et al. 2015). Similar to *C. purpurea*, the CWI signalling pathway is required for a normal host interaction between *E. festucae* and *L. perenne*, showing a conserved function within the close taxonomic relationship between *C. purpurea* and *E. festucae*.

The stress response MAP kinase pathway is initiated when the cell has to manage environmental changes, like osmolarity or oxidative stresses. Hyperosmolarity activates the stress-activated high osmolarity glycerol MAPK pathway (Hog1), a response best characterised in *S. cerevisiae* (Brewster et al. 1993, Banuett 1998, Rispail et al. 2009). The homologous protein Sty1/Spc1 (Suppressor of tyrosine phosphatase/suppressor of phosphatase 2C) in the fission yeast *Schizosaccharomyces pombe* and the homologous proteins in filamentous fungi and human, p38 MAPK, are functionally similar to the Hog1, but also respond to additional stresses such as oxidative and temperature stresses (Rispail et al. 2009). The stress-activated MAPK (SakA) pathway also plays a crucial role in the establishment and maintenance of the mutualistic *E. festucae*-*L. perenne*-

association. Gene deletion of *sakA* causes a drastic developmental change in both the endophyte and host plant, resulting in a complete breakdown of the interaction, with the fungus switching to pathogenic-like growth, but with reduced infection rate. Host plants infected by *E. festucae* Δ *sakA* mutants have a stunted phenotype with swollen tiller bases, increased tillering and reduced root development, which indicates a loss of apical dominance. The Δ *sakA* mutant hyphae lost their ability for systemic growth *in planta*, resulting in an increased biomass production, poorly aligned hyperbranching hyphae, colonisation of host vascular cells and hyphae with large vacuoles. In addition, considerable differences in gene expression by the fungus and the plant host were detected by high-throughput mRNA sequencing. Furthermore, disruption of the *sakA* pathway triggered host defense. These findings highlight the significance of the *sakA* pathway for maintenance of the mutualistic endophyte-grass interaction and the correct epiphytic growth pattern (Eaton et al. 2010). This adaptive stress response is not always essential for virulence but generally enhances pathogenicity, as phytopathogens often have to face high concentrations of reactive oxygen species (ROS) produced by the host defence response (Eaton et al. 2011).

In *Epichloë* endophytes, fungal produced ROS plays an important role for the symbiotic growth *in planta* during host colonisation (Tanaka et al. 2006, Tanaka et al. 2008, Scott et al., 2012, Kayano et al., 2013, Becker et al., 2016). In filamentous fungi, the production of reactive ROS as signalling molecules by the Nox complex is essential for polarised growth and hyphal orientation (Scott et al. 2007, Semighini and Harris 2008, Eaton et al. 2010, Martín and Di Pietro 2012). Deletion of components of the Nox complex including NoxA, NoxB, NoxR, RacA, BemA, leads to unrestricted endophytic growth, breakdown of the symbiosis and frequently to host mortality, similar to the mutants of the CWI MAPK or stress-response MAPK (Eaton et al. 2011, Kayano et al. 2013, Becker et al. 2015). However, it is not clear whether these mutants are impaired in switching from prolific to restricted growth or if they switch to unrestricted apical polarization in response to environmental changes. The mutants of the Nox complex share the cellular phenotype of defective hyphal fusion and are therefore impaired in generation of an interconnected hyphal network *in planta*. The establishment of these hyphal networks for nutrient and signal distribution, is essential for the mutualistic *E. festucae* – *L. perenne* association. Lack of ProA, encoding a C6 zinc finger transcription factor, which is

essential for fruiting body formation during sexual development in other fungi such as *Sordaria macrospora*, *Aspergillus nidulans* and *N. crassa* exhibited similar phenotypes including hyphal fusion (Masloff et al. 1999, Colot et al. 2006, Vienken and Fischer 2006, Tanaka et al. 2013). Deletions of the *E. festucae* genes *soft (so)*, $\Delta mkkA$ and $\Delta mpkA$, genes encoding components of the cell wall integrity (CWI) MAPK pathway, and *mobC*, encoding the kinase activator of the STRIPAK (striatin-interacting phosphatase and kinase) complex that regulates hyphal anastomosis in *S. macrospora* and *N. crassa*, had cellular phenotypes defective in hyphal fusion (Charlton et al. 2012, Teichert et al. 2014, Becker et al. 2015, Green et al. 2016). Based on this common phenotype, not only ROS but also hyphal fusion was identified as putative key factors for establishment the symbiotic interaction, regulated by the proposed formation of an interconnected signalling complex including ROS, CWI, and STRIPAK signalling (Green et al. 2016).

1.2.3 The G protein cyclic AMP/PKA signalling pathway

In response to extracellular signals, G protein-coupled receptors (GPCR) and members of the heterotrimeric G protein family can activate the cAMP/protein kinase A (PKA) signalling pathway to mediate gene expression changes. The stimulated G protein α subunit activates the catalytic functions of the membrane bound adenylate cyclase (Alspaugh et al. 2002, Kronstad et al. 2011). Adenylate cyclase (AC), which catalyses intracellular adenosine triphosphate (ATP) into cyclic adenosine monophosphate (cAMP), is a conserved integral membrane protein with twelve transmembrane domains and two cytosolic domains that can interact with different proteins (Jeraj et al. 2005, Pinto et al. 2008, Pinto et al. 2009, Wang et al. 2013). The second messenger cAMP is a small molecule, regulating a wide range of intracellular developmental and metabolic processes, and is crucial for fungal pathogenicity (D'Souza et al. 2001, Kronstad et al. 2011). After synthesis by the AC, the intracellular concentration of cAMP increases, leading to activation of the downstream effector enzyme protein kinase A (PKA), also known as cAMP-dependent protein kinase A. The PKA is a tetrameric holoenzyme consisting of two regulatory and two catalytic subunits. When cAMP binds to the regulatory subunits of the PKA, both catalytic subunits dissociate from the original complex and from each other and interact with various transcription factors, initiating changes in gene

expression via phosphorylation. The level of cAMP synthesis and the intracellular concentration is downregulated by cAMP phosphodiesterases (PDE), that degrade cAMP into 5'-AMP, terminating signal transduction. The phosphodiesterase activity is triggered by phosphorylation through the catalytic PKA subunit, which acts as a feedback regulator. Additionally, the generation of cAMP stops when the G α subunit dissociates from the AC, a response also triggered by PDE and GTPases, after inactivation of G protein signalling (Alspaugh et al. 2002, Li et al. 2007, Xue et al. 2008). The components of the cAMP/PKA signalling pathway are highly conserved (D'Souza and Heitman 2001) and have a key role in fungal development, especially in filamentous growth and pathogenicity processes (Eaton et al. 2011, Kronstad et al. 2011). The genomes of *E. festucae* Fl1 and E2368 contain homologues of the cAMP/PKA signalling pathway components, identified by their homology to the closely related *M. graminicola* genome (Kulkarni et al. 2005, Eaton et al. 2008, Mehrabi et al. 2009). It has been shown, that deletion of the *E. festucae* *acyA* (adenylate cyclase) resulted in a comparable, but less severe phenotype of reduced infection rate and hyperbranching (Voisey et al. 2007), as has been shown for Δ *noxA* and Δ *sakA* (Eaton et al. 2010). Although infected plants were not stunted, the phenotype might indicate an interconnection between the cAMP/PKA pathway and other pathways. Nevertheless, the cAMP-dependent signalling might be crucial in establishing the mutualistic endophyte-plant association, as has been shown for the stress-activated or cell wall integrity MAPK pathway (Eaton et al. 2008, Scott and Eaton 2008, Eaton et al. 2010, Scott et al. 2012).

A key unanswered question is which endogenous signals (small secreted molecules, host derived-molecules or host metabolites) and which fungal receptors and signalling pathways are responsible for establishing and maintaining the mutualistic association between endophyte and grass host. The G protein signalling pathway including the G protein coupled receptors, the heterotrimeric G protein signalling cascade and the cAMP/PKA signalling pathways are ideal candidates for this role.

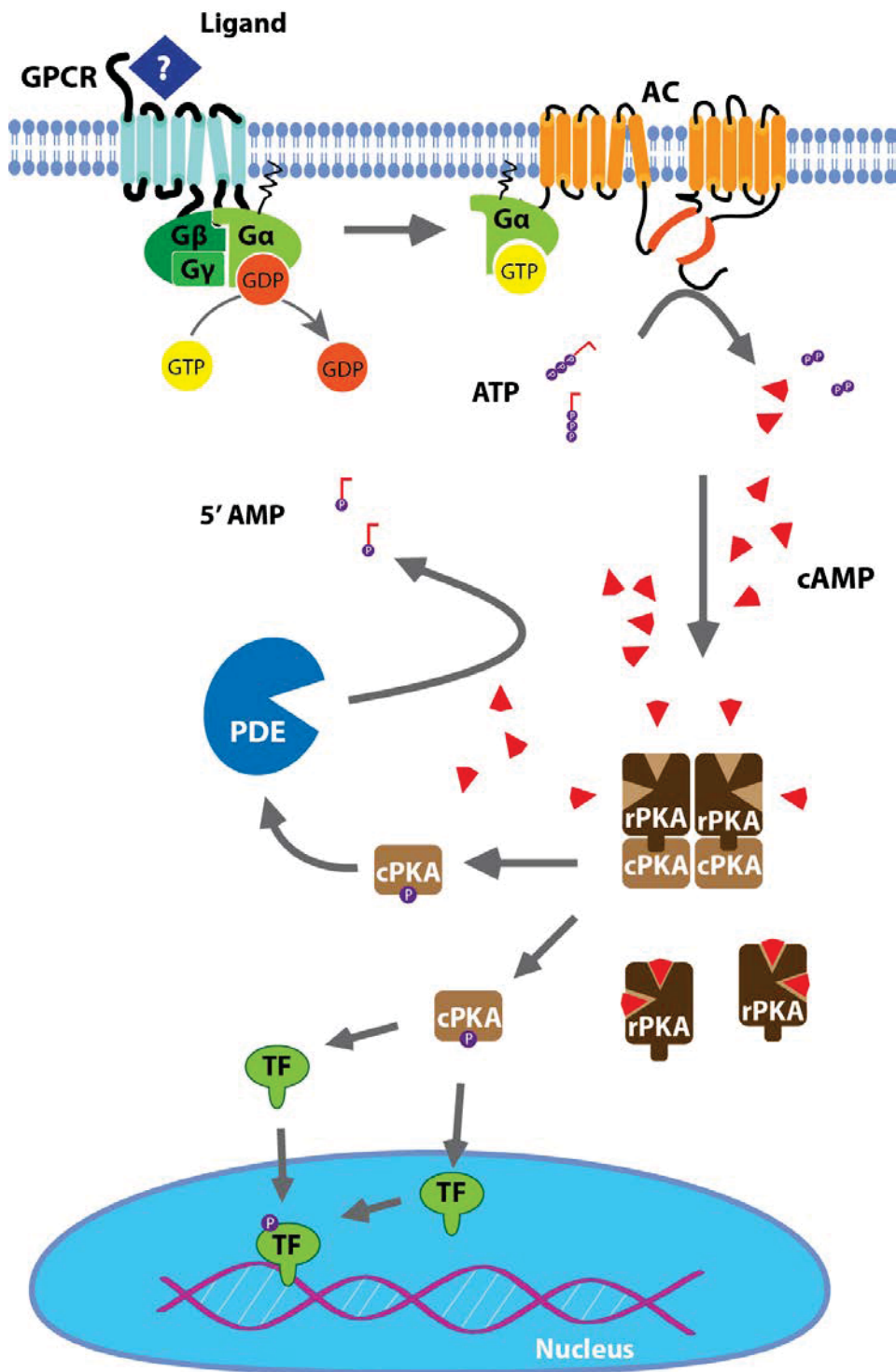


Figure 1-4 The G-protein cAMP/PKA signalling pathway: The cAMP/PKA signalling pathway is a key downstream effector of GPCR and G-protein signalling. The $G\alpha$ -GTP subunit activates adenylate cyclase (AC), which generates cyclic AMP from ATP. The Second messenger cAMP binds to the regulatory subunits (rPKA) of protein kinase A (PKA) and induces dissociation of the tetrameric holoenzyme. The catalytic subunits (cPKA) can activate several downstream transcription factors (TF) which alter gene expression, as well as phosphodiesterases (PDEs) which hydrolyse cAMP into 5'-AMP.

1.2.4 G protein coupled receptors sense environmental changes and transduce signals for cellular response

The G protein coupled receptors (GPCRs), one of the largest protein families in eukaryotes, are localised in the plasma membrane and are characterised by the presence of seven membrane-spanning α -helices of hydrophobic amino acids (7-TM), which are connected to each other by extra- and intra-cellular loops. An extracellular amino-terminal tail senses environmental signals (ligands) and a cytosolic carboxy-terminal sequence interacts with components inside of the cell and mediates the signalling (Dohlman et al. 1991, Li et al. 2007, Tuteja 2009). GPCRs sense a broad range of environmental changes and transfer these endogenous signals including photons, pheromones, carbon and nutrient sources, amino acids or fatty acids into the cell (Xue et al. 2008, Chattopadhyay 2014). Based on sequence homology and functional similarity GPCRs in mammalian systems are separated into six classes including the rhodopsin-like superfamily (class A), the secretin receptor family (class B), the metabotropic glutamate/pheromone receptors (class C), fungal mating pheromone receptors (class D), cyclic AMP receptors (class E) and the frizzled/smoothened receptors (class F) (Attwood and Findlay 1994, Krishnan et al. 2012). However, no uniform classification system has been established leading to alternative categorization into families comprising similar separation, such as the rhodopsin family, the secretin family, the adhesion family, the glutamate family and the frizzled/taste family (Fredriksson et al. 2003, Zhang et al. 2015). In line with the fact that fungal receptors are functionally and structurally different from mammalian GPCRs, a separate classification system for fungal GPCRs has been developed. In recent years, through advances in genome sequencing techniques and improved bioinformatics analysis, a large number of putative GPCRs in a variety of different fungal species were identified, that share the common 7-TM domain (DeZwaan et al. 1999, Kulkarni et al. 2005, Lafon et al. 2006, Li et al. 2007, Brunner et al. 2008, Zheng et al. 2010, Amselem et al. 2011, Brakhage 2013, Gruber et al. 2013, Affeldt et al. 2014, Cabrera et al. 2015).

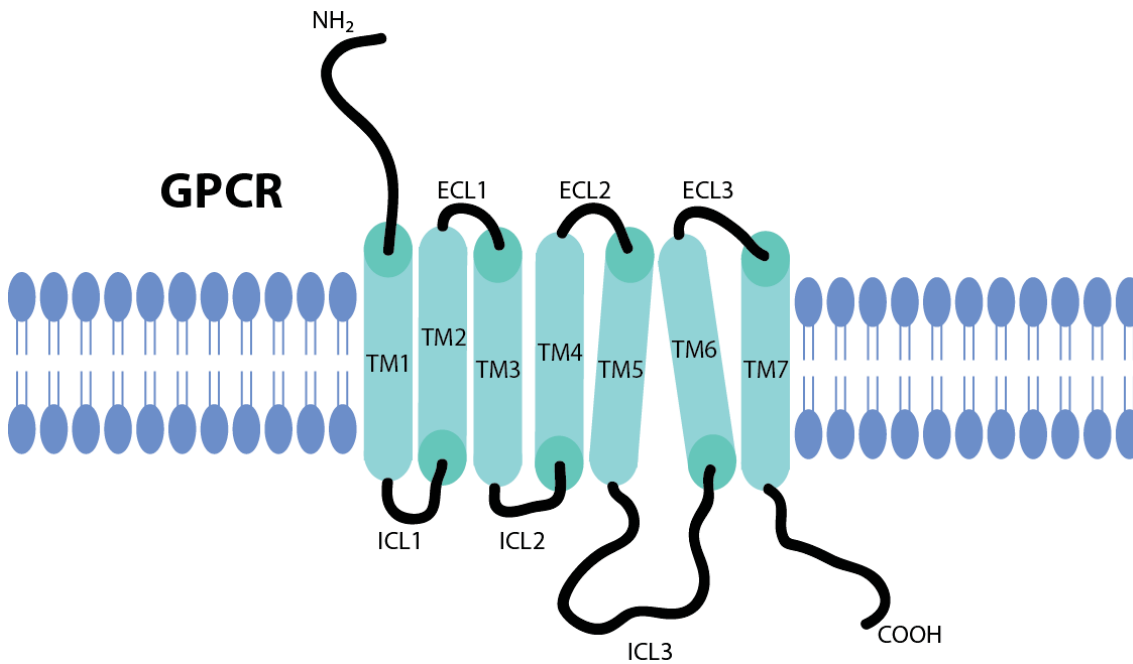


Figure 1-5 Structure of G-protein coupled receptors: G-protein coupled receptor proteins consist of seven transmembrane alpha-helices (TM) connected by three extracellular (ECL) and three intracellular (ICL) loops of varying length. An extracellular N-terminal amino-group (NH₂) and a cytoplasmic C-terminal carboxyl-group (COOH) interact with ligands at the cell surface and intracellular proteins like the heterotrimeric G-protein, respectively.

These studies revealed a high diversity among fungal GPCRs with classes highly conserved in number and structure within individual classes and between fungal species, while other classes comprise a greater variety among all fungal species (Gruber et al. 2013). A high diversity of GPCRs, suggests a role in species-specific functions in adaptation to a particular life style by individual species. Based on the latest research in *N. crassa* and *Trichoderma* spp., GPCRs in fungi can be categorized into the 14 classes of fungal pheromone receptors (class I and II), putative carbon and nitrogen sensors (class III and IV respectively), cAMP receptor-like proteins (class V), GPCR-RGS fusion protein (class VI), mammalian rat growth hormone-releasing factor-like receptor (class VII), PAQR-GPCRs (class VIII), microbial opsin receptors (class IX), the putative PTM1-like GPCRs (class X), ABA/GPR89A GPCRs (class XI), family-C-like GPCRs (class XII), PsGPR11-like (class XIII) and the large and unique protein family of PTH11-related proteins (class XIV) (Gruber et al. 2013, Cabrera et al. 2015).

During signal transduction, the GPCRs function as guanine nucleotide exchange factors (GEFs) promoting the catalytic exchange of guanosine diphosphate (GDP) to guanosine triphosphate (GTP) on the G α subunit of the heterotrimeric G proteins (Li et al. 2007). Ligand binding causes a conformational change in the GPCR that activates the respective signalling pathway. The conformational change of the receptor is a highly dynamic feature that depends on multiple factors including the individual structural components like the flexible intra- and extra-cellular loops as well as the lipid-composition of the cell membrane the receptor is embedded in. Interaction with extracellular ligands varies in binding intensity, which also influences the conformational change and therefore the signal transduction. These dynamic properties make GPCRs highly adaptable (Deupi and Kobilka 2010). Details about how GPCRs perceive ligands and activate the heterotrimeric G protein are based on the solved crystal structure analysis of predominantly human GPCRs, which are likely to only capture a portion of the protein dynamic (Rasmussen et al. 2011, reviewed in Zhang et al. 2015). Ligand specificity and function of fungal GPCRs are based on *in vivo* analysis of deletion mutant strains.

Due to the variety of extracellular signals, organisms have developed numerous types of GPCRs linked to several downstream signalling pathways. Classically, the GPCR interacts with the heterotrimeric G proteins for signal transduction. However, there is growing evidence for multiple G protein independent GPCR activity. The diversity of extracellular signals and the number of different GPCRs in the cell, which interact with only a small number of G proteins, the ligand specificity requires various signal mediators. In mammalian cells, functional interaction between GPCRs and other intracellular proteins, including arrestins, GPCR kinases, small GTP-binding proteins and many more (Bhattacharya et al. 2008, Oldham and Hamm 2008, Chattopadhyay 2014). GPCRs are highly diverse proteins functionally and structurally distinct among themselves, despite the common seven trans-membrane domains. With the increasing numbers of GPCRs identified in various fungal species, G protein-independent functions might be possible.

To increase ligand specificity and effectiveness, GPCRs can form homo- or hetero-oligomers (reviewed in Xue et al. 2008, Borroto-Escuela et al. 2014). Due to technical limitations for receptor-ligand analysis in fungi, GPCR dimerization has only been identified in rare cases using fluorescence-based detection methods

(Gehret et al. 2006). The pheromone receptors Ste2 in *S. cerevisiae* or Mam2 in *S. pombe* form GPCR homo-oligomers that are necessary for signal-transduction (Ladds et al. 2005, Gehret et al. 2006). Interaction of intracellular domains of the putative carbon receptor Gpr4 in the human pathogen *Cryptococcus neoformans* in a yeast-2-hybrid screen is indicative for GPCR oligomerization (Xue et al. 2006). In the phytopathogen *Aspergillus flavus*, hetero-dimerization of the class III GPCRs GprC and GprD during carbon sensing was proposed, for full functionality (Affeldt et al. 2014). Absolute essential functions for host-fungus interaction have not been assigned to specific receptors in *A. flavus*, based on single mutation of all GPCRs (Affeldt et al. 2014). In *A. nidulans*, functional heter-oligomerization has been proposed between the class III GPCR GprD and the class V GPCR GprH during carbon and amino acid sensing (Brown et al. 2015). However, a conserved or specific role for GPCR oligomerization has not been identified and requires further analysis such as fluorophore-based protein-interaction analysis.

GPCRs play an essential role in recognition of environmental changes through various cellular mechanisms and a range of intracellular response pathways like pheromone response, cAMP response and carbon sensing, but the specific role in phytopathogenic or mutualistic systems remains mostly unclear. They may be important for extracellular detection and transmission of host derived molecules that trigger a species-specific cellular response, important for pathogenicity or mutualism.

1.2.5 Role of fungal GPCRs in pathogenicity through activating the cAMP-dependent PKA signalling cascade

The essential role of GPCRs of the pheromone receptor class and the relationship between mating, polarized growth and virulence has been extensively shown in the human pathogen *C. neoformans* and the phytopathogen *U. maydis*. (Xue et al. 2006, Xue et al. 2008) Also, the connection between hyphal morphogenesis and virulence are dependent on the glucose receptors (GprC, GprD) as regulators for filamentous growth and pathogenicity in *A. fumigatus* and in other *Asperillus* spp., demonstrating the essential role of GPCRs for fungal pathogenicity (Gehrke et al. 2010). Involvement of GPCRs in chemotropic response is not limited to pheromones; but also fatty acids, oxylipins, or specific plant-derived serve as

chemoattractant. In *F. oxysporum*, the pheromone receptor Ste2 regulates hyphal orientation towards the host root system and invasive growth after penetration (Turrà et al. 2015). While Ste2 mediates host specific chemotropism through the CWI MAPK pathway, the pheromone receptor pathway regulates invasive and directed hyphal growth towards available nutrients and amino acids and is ironically not involved in response to the α -pheromone of the opposite mating type. Ste2 regulates chemotropism interlinking these two MAPK pathways. However, deletion of the G α -subunit *fga1* resulted in avirulence indicative for involvement of the cAMP/PKA signalling pathway in this processes as well (Jain et al. 2002). Involvement of the pheromone response pathway and the cAMP/PKA signalling pathway in chemotropism and pathogenic development has been shown in multiple pathogenic fungi, with altered mechanism, according to the respective lifestyle. In *B. cinerea*, the pheromone response pathway and the cAMP/PKA signalling pathway are equally essential for host recognition and pathogenic development, however the receptor mediating this processes has not been identified yet while in *M. oryzae* a member of the novel Pth11-like class, initiates these processes (Schumacher et al. 2008, Wilson and Talbot 2009). Sensing of fatty acids and oxylipins derived from the host is governed by GPCRs of different classes in *Aspergillus* spp., which also are involved in carbon source and amino acid sensing (Affeldt et al. 2012, Grice et al. 2013, Affeldt et al. 2014, Brown et al. 2015). In the mycoparasite *Trichoderma atroviride*, which attaches to and attacks its host fungus, it has been shown that the recognition of fungal hyphae is dependent on the GPCR Gpr1 of the cAMP receptor-like protein family (Brunner et al. 2008, Omann and Zeilinger 2010, Omann et al. 2012). The *gpr1*-silenced mutants display an avirulent phenotype and are unable to recognise living host hyphae and initiate production and secretion of hydrolytic and cell-wall-degrading enzymes. It has been hypothesised that the expression of chitinase- and protease enzymes is triggered by the Gpr1 receptor (Omann et al. 2012). The impaired recognition of host by the silenced *gpr1*-mutant could be restored by exogenous cAMP however mycoparasitic overgrowth, invasive growth or the induction of hydrolytic enzyme expression remained impaired. Similar phenotypes were shown for mutants for the pheromone response pathway, indicative of regulation by Gpr1 (Schumacher et al. 2008). These results highlight the essential sensing role of host-derived molecules by GPCRs of the cAMP-receptor-like class, and the activation of multiple downstream pathways. To establish and

maintain the mutualistic endophyte-grass association in *E. festucae*, signalling by host derived molecules or small-secreted molecules must occur, and the fungus must sense and mediate responses to these signals to enable the highly restricted endophytic growth and synchronized development with the host.

1.2.6 cAMP-phosphodiesterases terminate cAMP/PKA signalling

The control of cellular levels of the second messenger cyclic AMP play an important role in regulation of PKA-mediated responses. The intracellular cAMP level is not only regulated by the controlled catalytic production by adenylate cyclase (AC), but also by cyclic nucleotide phosphodiesterases (PDEs), which hydrolyse cAMP (Fig. 1.6). The activation of PKA, the target protein of the cAMP signalling cascade, results in phosphorylation of many different downstream proteins like transcription factors for alteration in gene expression, as well as the cAMP phosphodiesterases for feedback control (Hicks et al. 2005). PDEs hydrolyse the phosphodiester bond of cyclic nucleotides like cAMP or cGMP and convert them into monophosphates (e.g. 5'-AMP, 5'-GMP). Some PDEs show a high affinity towards cyclic nucleotides which function as regulatory elements for cellular concentration-dependent gradients of cAMP and play an important role in regulating the specificity and temporal duration of cAMP signalling. Therefore they are responsible for a rapid turnover in the cellular level of cAMP (Conti and Beavo 2007).

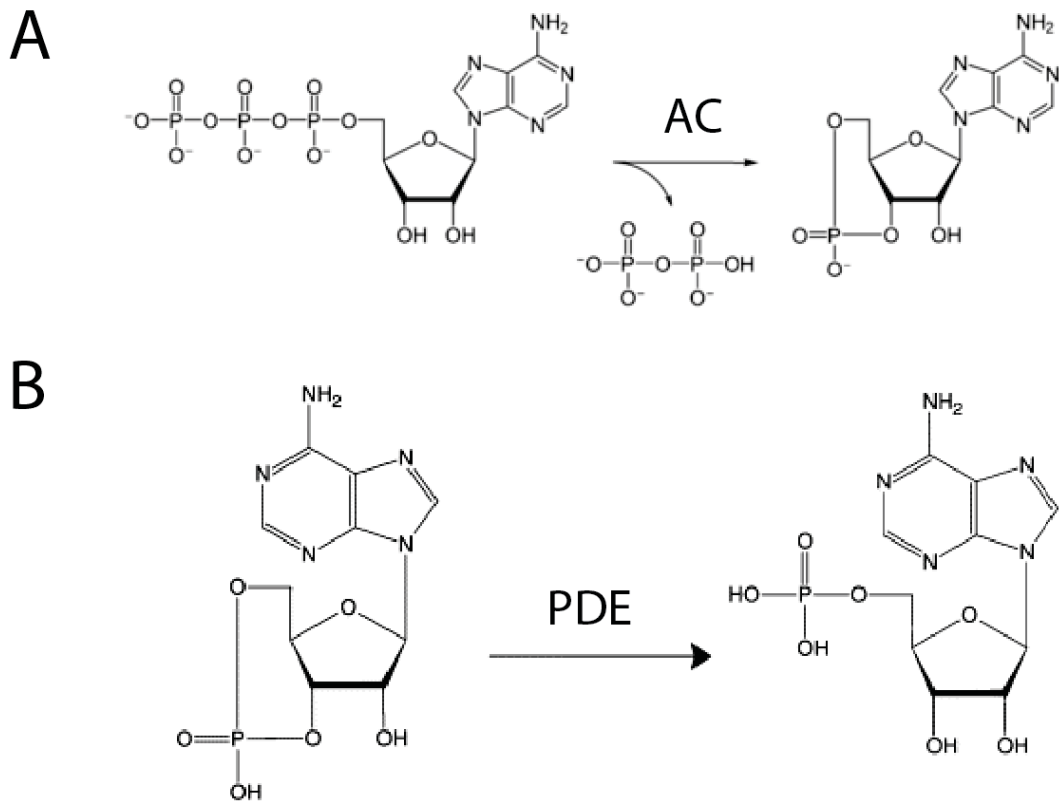


Figure 1-6 cAMP synthesis and hydrolysis: (A) The catalytic subunit of adenylate cyclase (AC) produces cyclic adenosine monophosphate (cAMP) from intracellular adenosine triphosphate (ATP) and monophosphate. (B) Phosphodiesterases (PDE) hydrolyse the phosphodiester bond of cAMP, converting it into 5' monophosphate (5'AMP).

PDEs are highly conserved but vary in number and activity. The human genome possesses eleven PDE families, while fungi typically have two (Ramanujam and Naqvi 2010). Fungal PDEs are divided into Class I and Class II PDEs, showing low-affinity towards cAMP (high K_m) and high affinity towards cAMP (low K_m), respectively. *S. cerevisiae* possesses a low-affinity phosphodiesterase, Pde1, used for glucose stimulation or intracellular acidification, and a high-affinity phosphodiesterase, Pde2, with regulatory function for a steady state level of cAMP. While cell growth is not dependent on PDE activity, it seems to be necessary for stress response and to overcome starvation (Park et al. 2005). For example, the *C. albicans* Pde2 mutant shows high sensitivity to exogenous stress stimuli like heat shock as well as antifungal agents and is avirulent. However, the general function of Pde1 and Pde2 in fungi is not uniform. In the human pathogen *C. neoformans* Pde1

regulates the basal level of cellular cAMP and its activity is regulated through the catalytic subunit of PKA, activated by cAMP dependent phosphorylation. While the deletion of *pde2*, encoding a low affinity PDE, showed a mild phenotype, the $\Delta pde1$ mutant strains displayed severe defects in different virulence factors (Hicks et al. 2005).

Indeed, the fungal PDEs appear to play an important role in pathogenicity. In the phytopathogenic fungi *U. maydis*, *B. cinerea* and *M. oryzae* deletion of the high affinity PDE *umpde1*, *bcpde2* and *pdeH* respectively, showed reduced pathogenicity (Agarwal et al. 2010, Ramanujam and Naqvi 2010, Harren et al. 2013). These mutants showed defects in appressorium formation under conditions that initiates differentiation of this infectious structure for host penetration, indicative for impaired host sensing. In *M. oryzae* and *B. cinerea* cAMP signalling was shown to be required for production of the asexual spores (conidia). The cAMP/PKA signalling triggers this sensing and response to plant derived molecules as well as the initiation of appressorium formation. A disruption of the regulator of cellular steady-state cAMP level by deletion of $\Delta pdeH$ or $\Delta bcpde2$, resulted in an avirulent phenotype, with impaired appressoria formation (Zhang et al. 2011), similar to deletion of MAC1 or BAC (AC) (Choi and Dean 1997). Moreover, both mutants of the high affinity PDE seemed to be impaired in responding to plant-derived stimuli (Ramanujam and Naqvi 2010, Zhang et al. 2011). Further characterisation of the high affinity PDE PdeH and the low affinity PDE PdeL showed that the avirulent phenotype of $\Delta pdeH$ could not be completely overcome by PdeL. While $\Delta pdeL$ strains only showed a minor reduction in virulence, the $\Delta pdeH\Delta pdeL$ double deletion mutant was similar to the $\Delta pdeH$ mutant (Zhang et al. 2011). This result suggests a conserved function in phytopathogenic fungi, that the high affinity PDE regulates the cAMP-dependent signalling and is required for pathogenicity and virulence, supported by the low affinity PDE (Zhang et al. 2011).

1.3 Aims

The aim of the research presented in this thesis was to determine the role of cAMP-dependent signalling in establishing and maintaining the mutualistic *E. festucae-L. perenne* association by focusing on the cell surface receptors acting upstream and the regulatory proteins that terminate the signal. To achieve this, the focus was to identify putative G protein-coupled receptors in the genome of *E. festucae* and functionally characterise the G protein coupled receptors of the cAMP receptor-like class to determine their role in the interaction between *E. festucae* and the host plant. This was done by reverse genetic approach and phenotype analysis of the resulting gene deletion mutants. To fully understand the *E. festucae-L.perenne* association, it is important to clarify the signalling cascades involved and this research gives insight into which receptors (GPCRs) play a role as sensors of extracellular signals and as activators of intracellular signalling pathways in response to environmental changes. While the endophyte induces alteration in gene expression in the plant, it is important to determine which signalling pathway is involved in transducing plant-specific signals and if these host-derived molecules, such as specific plant secreted peptides or small fungal secreted molecules, are required to maintain the mutualistic association. Another aim of this thesis was to functionally characterise the phosphodiesterases in *E. festucae*, which included identification of putative PDEs, gene deletion and analysis of the resulting phenotype in culture and *in planta*. While various important cellular processes depend on intracellular levels of cAMP, the regulatory elements of the cAMP/PKA signalling pathway are crucial for maintaining cAMP homeostasis. This thesis provides an overview of GPCRs in *E. festucae*, highlights particular interests and gives insights into the importance of the cAMP/PKA signalling pathway and its regulation.

Chapter 2 Materials and Methods

2.1 Bioinformatics

2.1.1 Nucleotide and protein sequences

Nucleotide and protein sequences from different *Epichloë* and other fungal species within the *Clavicipitaceae* (Schardl et al. 2013) were obtained from the genome database (<http://www.endophyte.uky.edu>) curated by C. L. Schardl at the University of Kentucky. The proposed gene models were validated based on HMM-based gene structure prediction by FGENESH (<http://www.softberry.com>). Other nucleotide and protein sequences were obtained from the Broad institute (<https://www.broadinstitute.org>) and NCBI GenBank database (<https://www.ncbi.nlm.nih.gov/genbank/>) (Appendix 1).

2.1.2 tBLASTn analysis

Genes in the *E. festucae* F11 (E894) genome were identified by tBLASTn analysis using protein sequences from *N. crassa* for *E. festucae* genes encoding G-protein coupled receptor proteins and from *M. oryzae* for *E. festucae* genes encoding phosphodiesterases, obtained from the Broad Institute. Blast analysis was conducted against the *E. festucae* genome (F11), using the *E. festucae* database (<http://csbio-l.csr.uky.edu/ef894-2011/blast/blast.html>) and reciprocal tblastn against the NCBI non-redundant database (<https://blast.ncbi.nlm.nih.gov/Blast.cgi>) to confirm the *E. festucae* homologues using respective *E. festucae* amino acid sequences. Identity and similarity scores were calculated using MAFFT (v7.017) pairwise alignment performed in Geneious (v7.1.5). Figures for multiple sequence alignments were generated MacVector (v12.0.5) using ClustalW (Thompson et al. 1994), which generated similar identity and similarity scores to those obtained from using MAFFT (v7.017).

2.1.3 Multiple sequence alignment

Alignments of nucleotide sequences were performed using the ClustalW algorithm (Larkin et al. 2007) provided with MacVector 14.5 (MacVector, Inc.) using default parameters. Alignments of protein sequences were performed using the MAFFT (v7.017) algorithm (Katoh et al. 2002, Katoh and Standley 2013), provided as a plug in tool in Geneious (7.1.5).

2.1.4 Phylogenetic analysis

Phylogenetic reconstruction was performed using the maximum likelihood method utilised by PhyML (v20120412) (Guindon et al. 2010) in Geneious 7.1.5. The bootstrap method with 500 replicates was used to test all phylogenies.

2.1.5 Protein prediction

Protein domain analysis was performed using InterProScan (v. 5) (Zdobnov and Apweiler 2001, Quevillon et al. 2005), InterProScan lookup service (v. 43.1), phobius (v. 1.01) (Kall et al. 2004), SignalP (v. 4.1) and TMHMM (v. 2.0c) plus all software given by default with InterProScan (BlastProDom, FprintScan, HMMPiR, HMMPfam, HMMSmart, HMMTigr, ProfileScan, HAMAP, PatternScan, SuperFamily, Gene3D); ExPasy Prosite; Smart interphase (Schultz et al. 1998, Letunic et al. 2015). Transmembrane domains were identified using TMHMM (Server v2.0) (Sonnhammer et al. 1998, Krogh et al. 2001); phobius (v1.01) (Kall et al. 2004); TMPred (Hofmann and Stoffel 1993); TMMTOP (v2.0) (Tusnady and Simon 2001) and CCTOP (Dobson et al. 2015). Transmembrane domain-containing proteins were visualised using Protter v1.0 (Omasits et al. 2014), using manual annotation, based on TMHMM prediction. 3D Protein structure modelling and homology comparison was performed by Phyre2 (v2.0) (Kelley et al. 2015).

2.1.6 GC profile

Analysis of the DNA GC content was performed using GC-Profile (<http://tubic.tju.edu.cn/GC-Profile/>) (Gao and Zhang 2006).

2.2 Molecular and biological material

Organisms and plasmids (Table 2.1) and primers (Table 2.2) that were used are listed as follows:

Table 2-1 Organisms and plasmids used

Strain	Relevant characteristic(s)	Source or reference
<u>Fungal strains</u>		
<i>Epichloë festucae</i>		
PN2278	Wild-type Fl1	Young et al., 2005
PN3036 ($\Delta gpr2\#2$)	Fl1/ $\Delta gpr2::PtrpC-hph$; Hyg ^R	This study
PN3037 ($\Delta gpr2\#40$)	Fl1/ $\Delta gpr2::PtrpC-hph$; Hyg ^R	This study
PN3038 ($\Delta gpr2\#41$)	Fl1/ $\Delta gpr2::PtrpC-hph$; Hyg ^R	This study
PN3038 ($\Delta gpr2\#42$)	Fl1/ $\Delta gpr2::PtrpC-hph$; Hyg ^R	This study
PN3054 ($\Delta gpr1b\#24$)	Fl1/ $\Delta gpr1b::PtrpC-nptII$; Gen ^R	This study
PN3055 ($\Delta gpr1b\#222$)	Fl1/ $\Delta gpr1b::PtrpC-nptII$; Gen ^R	This study
PN3056 ($\Delta pdeH\#21$)	Fl1/ $\Delta pdeH::PtrpC-hph$; Hyg ^R	This study
PN3057 ($\Delta pdeH\#74$)	Fl1/ $\Delta pdeH::PtrpC-hph$; Hyg ^R	This study
PN3058 ($\Delta pdeH\#114$)	Fl1/ $\Delta pdeH::PtrpC-hph$; Hyg ^R	This study
PN3059 ($\Delta pdeH\#141$)	Fl1/ $\Delta pdeH::PtrpC-hph$; Hyg ^R	This study
PN3060 ($\Delta pdeL\#13-1$)	Fl1/ $\Delta pdeL::PtrpC-nptII$; Gen ^R	This study
PN3061 ($\Delta pdeL\#13-3$)	Fl1/ $\Delta pdeL::PtrpC-nptII$; Gen ^R	This study
AB-1 (<i>gpr1b24C-4</i>)	$\Delta gpr1b\#24/Pgpr1b-gpr1b-Tgpr1bC$ (pAB06); Gen ^R , Hyg ^R	This study
AB-2 (<i>gpr1b24C-5</i>)	$\Delta gpr1b\#24/Pgpr1b-gpr1b-Tgpr1bC$ (pAB06); Gen ^R , Hyg ^R	This study
AB-3 (<i>gpr1b24C-6</i>)	$\Delta gpr1b\#24/Pgpr1b-gpr1b-Tgpr1bC$ (pAB06); Gen ^R , Hyg ^R	This study
AB-4 (<i>gpr1b24C-10</i>)	$\Delta gpr1b\#24/Pgpr1b-gpr1b-Tgpr1bC$ (pAB06); Gen ^R , Hyg ^R	This study
AB-5 (<i>gpr1b222C-4</i>)	$\Delta gpr1b\#222/Pgpr1b-gpr1b-$ <i>Tgpr1bC</i> (pAB06); Gen ^R , Hyg ^R	This study
AB-6 (<i>gpr1b222C-5</i>)	$\Delta gpr1b\#222/Pgpr1b-gpr1b-$ <i>Tgpr1bC</i> (pAB06); Gen ^R , Hyg ^R	This study
AB-7 (<i>gpr1b222C-6</i>)	$\Delta gpr1b\#222/Pgpr1b-gpr1b-$ <i>Tgpr1bC</i> (pAB06); Gen ^R , Hyg ^R	This study
AB-8 (<i>gpr1b222C-13</i>)	$\Delta gpr1b\#222/Pgpr1b-gpr1b-$ <i>Tgpr1bC</i> (pAB06); Gen ^R , Hyg ^R	This study

Strain	Relevant characteristic(s)	Source or reference
AB-9 (<i>pdeH21C-1</i>)	$\Delta pdeH\#21/PpdeH-pdeH-TpdeHC$ (pAB07); Gen ^R , Hyg ^R	This study
AB-10 (<i>pdeH21C-2</i>)	$\Delta pdeH\#21/PpdeH-pdeH-TpdeHC$ (pAB07); Gen ^R , Hyg ^R	This study
AB-11 (<i>pdeH21C-3</i>)	$\Delta pdeH\#21/PpdeH-pdeH-TpdeHC$ (pAB07); Gen ^R , Hyg ^R	This study
AB-12 (<i>pdeH21C-4</i>)	$\Delta pdeH\#21/PpdeH-pdeH-TpdeHC$ (pAB07); Gen ^R , Hyg ^R	This study
AB-13 (<i>pdeH114C-1</i>)	$\Delta pdeH\#114/PpdeH-pdeH-TpdeHC$; Gen ^R , Hyg ^R	This study
AB-14 (<i>pdeH114C-2</i>)	$\Delta pdeH\#114/PpdeH-pdeH-TpdeHC$; Gen ^R , Hyg ^R	This study
AB-15 (<i>pdeH114C-3</i>)	$\Delta pdeH\#114/PpdeH-pdeH-TpdeHC$; Gen ^R , Hyg ^R	This study
AB-16 (<i>pdeH114C-4</i>)	$\Delta pdeH\#114/PpdeH-pdeH-TpdeHC$; Gen ^R , Hyg ^R	This study
AB-17 (<i>pdeH114C-7</i>)	$\Delta pdeH\#114/PpdeH-pdeH-TpdeHC$; Gen ^R , Hyg ^R	This study
AB-18 (<i>pdeLC-4</i>)	$\Delta pdeL\#13/PpdeL-pdeL-TpdeLC$ (pAB08); Gen ^R , Hyg ^R	This study
AB-19 (<i>pdeLC-5</i>)	$\Delta pdeL\#13/PpdeL-pdeL-TpdeLC$ (pAB08); Gen ^R , Hyg ^R	This study
AB-20 (<i>pdeLC-6</i>)	$\Delta pdeL\#13/PpdeL-pdeL-TpdeLC$ (pAB08); Gen ^R , Hyg ^R	This study
AB-21 (<i>pdeLC-22</i>)	$\Delta pdeL\#13/PpdeL-pdeL-TpdeLC$ (pAB08); Gen ^R , Hyg ^R	This study
AB-22 (<i>pdeLC-23</i>)	$\Delta pdeL\#13/PpdeL-pdeL-TpdeLC$ (pAB08); Gen ^R , Hyg ^R	This study

Yeast strains

Saccharomyces

cerevisiae

PN2806 (FY834) *MATa his3Δ200 ura3-52 leu2Δ1 lys2Δ202 trp1Δ63* Winston et al, 1995

Strain	Relevant characteristic(s)	Source or reference
<u>Bacterial strains</u>		
<i>Escherichia coli</i>		
PN4138	DH5 α /pRS426	Christianson et al., 1992
PN4254	DH5 α /pAB02	This study
PN4255	DH5 α /pAB03	This study
PN4256	DH5 α /pAB04	This study
PN4257	DH5 α /pAB05	This study
PN4292	DH5 α /pAB06	This study
PN4293	DH5 α /pAB08	This study
<u>Plasmids</u>		
pRS426	Amp ^R ; URA3	Christianson et al., 1992 (Appendix 2)
pSF15.15	Amp ^R ; Hyg ^R	S. Foster (Appendix 3)
pSF16.17	Amp ^R ; Gen ^R	S. Foster (Appendix 4)
pAB02	pRS426 containing 5' <i>gpr1b</i> -PtrpC- <i>nptII</i> -TtrpC-3' <i>gpr1b</i> ; Amp ^R /Gen ^R	This study (Appendix 6)
pAB03	pRS426 containing 5' <i>gpr2</i> -PtrpC- <i>hph</i> -3' <i>gpr2</i> ; Amp ^R /Hyg ^R	This study (Appendix 7)
pAB04	pRS426 containing 5' <i>pdeH</i> -PtrpC- <i>hph</i> -3' <i>pdeH</i> ; Amp ^R /Hyg ^R	This study (Appendix 8)
pAB05	pRS426 containing 5' <i>pdeL</i> -PtrpC- <i>nptII</i> -TtrpC-3' <i>pdeL</i> ; Amp ^R /Gen ^R	This study (Appendix 9)
pAB06	pRS426 containing <i>Pgpr1bC-gpr1b-Tgpr1b</i> ; Amp ^R /Gen ^R	This study (Appendix 10)
pAB08	pCR2.1-TOPO® containing <i>PpdeL-pdL-TpdeL</i> ; Amp ^R /Gen ^R	This study (Appendix 11)
pCR2.1-TOPO®	Amp ^R ; Neo ^R Kan ^R	Invitrogen (Appendix 12)

Table 2-2 List of primers used

Name	Primer sequence (5' - 3')	Target sequence
hph-F	AGCTTGGAAGTATATTGAAG	selectable marker cassette <i>hph</i>
hph-R	CTATTCCTTTGCCCTCGGACG	selectable marker cassette <i>hph</i>
hph screen_for	GTACTTCTACACAGCCATCG	selectable marker cassette <i>hph</i> internal fragment
hph screen_rev	TCAAGCAAGGTAAGTGGACG	selectable marker cassette <i>hph</i> internal fragment
nptII-F	GATATTGAAGGAGCACTTTTT G	selectable marker cassette <i>nptII</i>
nptII-R	CTACCCATCTTAGTAGGAATG	selectable marker cassette <i>nptII</i>
nptII screen_for	AGCTGACATCGACACCAACG	selectable marker cassette <i>nptII</i> internal fragment
nptII screen_rev	AGGCAACTGGTCAGATCAGC	selectable marker cassette <i>nptII</i> internal fragment
pRS426_F	GCTGTTTCCTGTGTGAAATTG	pRS426 vector for Gibson assembly
pRS426_R	GTCGTGACTGGGAAAACCC	pRS426 vector for Gibson assembly
TC44	CGAAGCTGAAAGCACGAGATT CTTC	<i>PtpC</i> rev
TC45	TCCAACAATGTCCTGACGGAC AATG	<i>hph</i> for
gpr1a 1	GTAACGCCAGGGTTTTCCCAG TCACGACGTGCAGCTTGTAGA CGAGG	5' <i>gpr1a</i> replacement construct
gpr1a 2	CCAGCACTCGTCCGAGGGCAA AGGAATAGGTTGAACTTGGCA GGAGATG	5' <i>gpr1a</i> replacement construct
gpr1a 3	AAATGCTCCTTCAATATCAGT TCCAAGCTCTATCCACCTTGAT GTGTAGC	3' <i>gpr1a</i> replacement construct
gpr1a 4	GCGGATAACAATTTACACAG GAAACAGCGTGGTCATCATTC ACAGCAG	3' <i>gpr1a</i> replacement construct

Name	Primer sequence (5' - 3')	Target sequence
gpr1a 5	CGTGCAGCTTGTAGACGAGG	<i>gpr1a</i> gene replacement construct (pAB01)
gpr1a 6	CCAGCACTCGTCCGAGGGCA	<i>gpr1a</i> gene replacement construct (pAB01)
gpr1a 7	TGCACAGAGCTTCGCAAGAC	³² P- <i>gpr1a</i> probe
gpr1a 8	ATCCAGACGCCTCAACTTC	³² P- <i>gpr1a</i> probe
gpr1b 1	GTAACGCCAGGGTTTTCCCAG TCACGACGAGTCAACAAGACC AGCATTC	5' <i>gpr1b</i> replacement construct
gpr1b 2	CTCGAAAATCATTCTACTAA GATGGGTAAGAATCTCGTAGT CCCAGC	5' <i>gpr1b</i> replacement construct
gpr1b 3	CCAAGCCCCAAAAGTGCTCCT TCAATATCCACCACCCTTTGTC CCATAC	3' <i>gpr1b</i> replacement construct
gpr1b 4	GCGGATAACAATTTACACAG GAAACAGCTGTTCTTGGATTC GTCATCG	3' <i>gpr1b</i> replacement construct
gpr1b 5	GAGTCAACAAGACCAGCATTC	<i>gpr1b</i> gene replacement construct (pAB02)
gpr1b 6	TGTTCTTGGATTTCGTCATCG	<i>gpr1b</i> gene replacement construct (pAB02)
gpr1b 13	CAGTGGCTGTTATGTGGCTC	1 st PCR screen for Δ <i>gpr1b</i>
gpr1b 14	GATTGGTTGTGCTTCCGAGC	1 st PCR screen for Δ <i>gpr1b</i>
gpr1b 15	CTGGGTCATCAGTTGCTTCT	2 nd PCR screen for Δ <i>gpr1b</i>
gpr1b 16	GCTGATAGCAAGCACAAACC	2 nd PCR screen for Δ <i>gpr1b</i>
gpr1b 17	CTCGTGCTTTACGGTATCG	PCR screen outside pII 99 <i>nptII</i> - <i>TtrpC</i>
gpr1b 18	CATAGCCGAATAGCCTCTC	PCR screen outside pII 99 <i>PtrpC</i> - <i>nptII</i>
gpr1b_19	GAAGAAGATGAGCGAGTTCC	³² P- <i>gpr1b</i> probe
gpr1b_20	GCAGCACAGTACTTCTCTAC	³² P- <i>gpr1b</i> probe
gpr1b screen_for	AGATGAGCGAGTTCCACAGC	<i>gpr1b</i> internal fragment
gpr1b screen_rev	AATGTACGTCATCCTGTCTGC	<i>gpr1b</i> internal fragment

Name	Primer sequence (5' - 3')	Target sequence
gpr1b screen_rev	AATGTACGTCATCCTGTCTGC	<i>gpr1b</i> internal fragment
Tgpr1b_for	CAGGGTTTTCCCAGTCACGAC GATGAGGATGATAGGATACG	<i>gpr1b</i> complementation construct (pAB06)
Pgpr1b_rev	CAATTCACACAGGAAACAGC CAACATGATGACGGATGACG	<i>gpr1b</i> complementation construct (pAB06)
gpr2 1	GTAACGCCAGGGTTTTCCCAG TCACGACGTCAATGGCACAAT GAATGTC	5' <i>gpr2</i> replacement construct
gpr2 2	CCAGCACTCGTCCGAGGGCAA AGGAATAGGTTCCCTGGAGAAT CACACTC	5' <i>gpr2</i> replacement construct
gpr2 3	AAATGCTCCTTCAATATCAGT TCCAAGCTGAATCTTCAGCCT GTTCCCTC	3' <i>gpr2</i> replacement construct
gpr2 4	GCGGATAACAATTTACACAG GAAACAGCTCACTTGGCAGGC TGGATTG	3' <i>gpr2</i> replacement construct
gpr2 5	GTCAATGGCACAATGAATGTC	<i>gpr2</i> gene replacement construct (pAB03)
gpr2 6	TCACTTGGCAGGCTGGATTG	<i>gpr2</i> gene replacement construct (pAB03)
gpr2 7	AGAGCGAAGCAACGGTGAAG	1 st PCR screening for Δ <i>gpr2</i>
gpr2 8	ACCAGTTGTTGACCTTGTGG	1 st PCR screening for Δ <i>gpr2</i>
gpr2 9	AACGTGGACCGGATCAAGAG	2 nd PCR screening for Δ <i>gpr2</i>
gpr2 10	TGGTCCGTATGTACATGCAG	2 nd PCR screening for Δ <i>gpr2</i>
pdeH 1	GTAACGCCAGGGTTTTCCCAG TCACGACGAATTCCAATGGTG TGATGGGATTTG	5' <i>pdeH</i> replacement construct
pdeH 2	CCAGCACTCGTCCGAGGGCAA AGGAATAGCTGAATGGGTGGT CATTCGA	5' <i>pdeH</i> replacement construct

Name	Primer sequence (5' - 3')	Target sequence
pdeH 3	AAATGCTCCTTCAATATCAGT TCCAAGCTCCACGACAATGAA CTCAACG	3' <i>pdeH</i> replacement construct
pdeH 4	GCGGATAACAATTTTCACACAG GAAACAGCGAATTCGCAAGTC AGCAAGTCAGCAA	3' <i>pdeH</i> replacement construct
pdeH 5	GAATTCCCAATGGTGTGATGG GATTTG	<i>pdeH</i> gene replacement construct (pAB04)
pdeH 6	GCAAGTCAGCAAGTCAGCAA	<i>pdeH</i> gene replacement construct (pAB04)
pdeH 7	CTGGTGCGTATCCGATTTCG	1 st PCR screen for $\Delta pdeH$
pdeH 8	CATGAGCCCTTCATAGTCG	1 st PCR screen for $\Delta pdeH$
pdeH 9	CTGCCAGACGATTTTCATCAC	2 nd PCR screen for $\Delta pdeH$
pdeH 10	CTGGTCACATCCATTGATGG	2 nd PCR screen for $\Delta pdeH$
pdeH_11	GCATTGCTGAGTCCGTTTGAG	³² P- <i>pdeH</i> probe
pdeH_12	CGTTCTTGAGCATCACCGAG	³² P- <i>pdeH</i> probe
pdeH_screen_for	TCCATTTCGATGATCAGCTGC	<i>pdeH</i> internal fragment
pdeH_screen_rev	TTTCTTCCACGACTCCTTCG	<i>pdeH</i> internal fragment
PpdeH_for	CAGGGTTTTCCCAGTCACGAC TGATGGGATTTGCTACTCCG	<i>pdeH</i> complementation construct (pAB07)
TpdeH_rev	CTGGGAAAACCCTGGCGTTAC AGCAGAGGGAAACAACATCG	<i>pdeH</i> complementation construct (pAB07)
pdeH_split_rev	GGTGATGAGATATTGCCAGC	<i>pdeH</i> complementation construct screen
pdeH_split_for	GCTGGCAATATCTCATCACC	<i>pdeH</i> complementation construct screen
pdeL 1	GTAACGCCAGGGTTTTCCCAG TCACGACGAATTCACCAGTCAA GTTCTGGTAGG	5' <i>pdeL</i> replacement construct
pdeL 2	CTCGAAAATCATTCCTACTAA GATGGGTACGTCACCTTGTTG TTGGTCT	5' <i>pdeL</i> replacement construct

Name	Primer sequence (5' - 3')	Target sequence
pdeL 3	CCAAGCCCAAAAAGTGCTCCT TCAATATCCGAAGTATGACTG GATGACAG	3' <i>pdeL</i> replacement construct
pdeL 4	GCGGATAACAATTTACACACAG GAAACAGCGAATTCCGTCCTAC GGAGTACATTTCA	3' <i>pdeL</i> replacement construct
pdeL 5	ACCAGTCAAGTTCTGGTAGG	<i>pdeL</i> gene replacement construct (pAB05)
pdeL 6	CGTCCTACGGAGTACATTTCA	<i>pdeL</i> gene replacement construct (pAB05)
pdeL 7	GTCCGTGATTGATCCAACCTC	1 st PCR screen for $\Delta pdeL$
pdeL 8	GAAGTCTGGGAATGGAATGGA	1 st PCR screen for $\Delta pdeL$
pdeL 9	GAGGTCAGACATCAACTTGAG	2 nd PCR screen for $\Delta pdeL$
pdeL 10	CAGTCTTGACAAGTAGCGTGC	2 nd PCR screen for $\Delta pdeL$
pdeL screen_for	TGGTCTACCCATTCCACAGC	<i>pdeL</i> internal fragment
pdeL screen_rev	CTGAGAGTCGTCGTAACCTGC	<i>pdeL</i> internal fragment
pdeL_probe _for	TCAAGACTTGGAGCGTCAGC	<i>pdeL</i> internal fragment
pdeL_probe _rev	TGAAGATGGCTGCCAATGTGC	<i>pdeL</i> internal fragment
PpdeL_for	CAGGGTTTTCCAGTCACGAC ATCACCTGGCTATCACCTGC	<i>pdeL</i> complementation construct (pAB08)
TpdeL_rev1	CTGGGAAAACCTGGCGTTAC GAACGAATGAAGGCTTTGAGC	<i>pdeL</i> complementation construct (pAB08)
pdeL_split_re v	GCAAGATTAGCTTTCACGTCG	<i>pdeL</i> complementation construct screen
pdeL_split_for	CGACGTGAAAGCTAATCTTGC	<i>pdeL</i> complementation construct screen

2.3 Growth conditions and media

All media were prepared using deionized water (Milli-Q) using the Barnstead NANOpure ultrapure water purification system (Thermo Scientific™ Barnstead™) and sterilised by autoclaving at 121°C for 20 min, unless specified otherwise.

2.3.1 *Escherichia coli*

E. coli cultures (Table 2.2.1) were grown either on solid plates or in 3-5 ml liquid LB (2.3.3.1) medium with shaking (200 rpm), at 37°C for approx. 18 h (overnight culture) (Miller 1972). For antibiotic selection LB medium contained a final concentration of 100 µg/ml ampicillin, added after autoclaving. Cultures were stored short-term at 4°C and long-term (cryopreservation) in 1.8 ml cryotubes in 50% (v/v) glycerol at -80°C.

2.3.1.1 Luria-Bertani broth (LB) medium

LB medium contained 1% (w/v) tryptone, 0.5% (w/v) yeast extract, 86 mM NaCl, adjusted to pH of 7.0-7.5, as previously described (Miller 1972). For solid medium plates (LB agar), 1.5% (w/v) agar was added before autoclaving.

2.3.1.2 SOC medium

SOC medium contained 2% (w/v) tryptone, 0.5% (w/v) yeast extract, 10 mM NaCl, 2.5 mM KCl, 10 mM MgCl₂, 10 mM MgSO₄·7H₂O and 20 mM glucose as previously described (Dower et al. 1988). Sterilised glucose was added after autoclaving.

2.3.2 *Saccharomyces cerevisiae*

S. cerevisiae cultures (Table 2.1) were grown either on solid plates or in 3-5 ml liquid YPD medium (2.3.2.1) with shaking (200 rpm) at 30°C for three days. Cultures were stored short-term at 4°C and long-term (cryopreservation) in 1.8 ml cryotubes in 20% (v/v) glycerol at -80°C.

2.3.2.1 Yeast Peptone Dextrose (YPD) medium

YPD medium contained 2% (w/v) mycological peptone (Difco) and 1% (w/v) yeast extract, adjusted to pH of 5.8. 50 ml of sterile 40% (w/v) glucose was added to 950 ml prepared medium after autoclaving, as previously described (Bergman 2001). For solid medium plates (YPD agar), 1.5% (w/v) Noble agar (Difco) was added before autoclaving.

2.3.2.2 SD uracil dropout (SD ura⁻) medium

SD ura⁻ medium contained 18% (w/v) sorbitol, 0.67% (w/v) yeast nitrogen base without amino acids (Sigma-Aldrich), 0.077% (w/v) uracil dropout supplement (Clontech), adjusted to pH of 5.8. 50ml of sterile 40% (w/v) glucose was added to 950 ml medium after autoclaving. For solid medium, 2% agar (w/v) was added before autoclaving.

2.3.3 *Epichloë festucae*

E. festucae cultures were grown on either solid PD (2.3.3.1) medium (plates) at 22°C for 7 days, or in liquid PD medium at 22°C for 4-5 days with shaking (150 rpm). Mycelial plugs (4 mm² in diameter) from the edge of 6-7 day old cultures, previously grown on solid PD medium, were used for inoculation. For antibiotic selection hygromycin B at a final concentration of 150 µg/ml or geneticin at a final concentration of 200 µg/ml was added after autoclaving, respectively. *E. festucae* protoplasts were regenerated in soft RG medium on solid RG agar (2.3.3.2) and overlaid with soft RG medium containing antibiotic where selection was required. *E. festucae* cultures, were stored at 4°C short term or long term in 15% (v/v) glycerol at -80°C.

2.3.3.1 Potato dextrose (PD) medium

PD medium contained 2.4% (w/v) potato dextrose broth (Difco), adjusted to pH of 6.5. For solid PD medium 1.5% (w/v) agar was added before autoclaving.

2.3.3.2 Regeneration (RG) medium

RG medium (modified from Oliver et al., 1987; Cartwright et al., 2014) contained 2.4% (w/v) potato dextrose broth (Difco), 0.8 M sucrose, adjusted to pH

of 6.5. For soft overlay medium, 0.8% (w/v) agar and for solid RG medium 1.5% (w/v) agar was added before autoclaving.

2.3.3.3 Water (H₂O) medium

Water medium contained Milli-Q water and 3% (w/v) agar was added before autoclaving.

2.3.3.4 Modified Czapek Dox (CDGN) medium

CDGN medium (Fleetwood et al. 2007) contained 4.4 mM K₂HPO₄·3H₂O, 2 mM MgSO₄·7H₂O, 6.7 mM KCl, 36 μM Fe₂SO₄·7H₂O, adjusted to pH of 6.8. Glucose and (NH₄)₂SO₄ were added after autoclaving to a final concentrations of 100 mM and 10 mM, respectively. For solid medium 1.5% (w/v) agar was added before autoclaving.

2.3.3.5 Czapek Dox salts (CD) medium

CD salts medium (Young et al., 2005) contained 4.4 mM K₂HPO₄·3H₂O; 2 mM MgSO₄·7H₂O; 6.7 mM KCl; 36 μM Fe₂SO₄·7H₂O, adjusted to a pH of 6.8. For solid CD medium 1.5% (w/v) agar was added before autoclaving.

2.3.3.6 Czapek Dox (CZ) medium

Czapek Dox medium contained 3.3% (w/v) Czapek Dox liquid medium (Oxoid); consisting of 2 mM sodium nitrate, 0.5 mM potassium chloride, 0.5 mM magnesium glycerophosphate, 0.01 mM ferrous sulphate, 0.35 potassium sulphate, 30 mM sucrose; adjusted to pH of 6.8 and 1.5% (w/v) agar added before autoclaving for solid medium.

2.3.3.7 Modified Blankenship medium

Modified Blankenship medium (MSM3 defined medium) contained 3.67 mM KH₂PO₄, 3.44 mM K₂HPO₄, 15 mM sucrose, 5 mM glutamine, 2 mM MgSO₄, 0.6 μM thiamine and trace elements: 3.6 μM H₃BO₄, 1 μM CuSO₄, 0.7 μM KI, 0.8 μM FeNa-ethylenediaminetetraacetic acid, 1 μM MnSO₄, 0.5 μM NaMoO₄ and 0.4 μM ZnSO₄ (Blankenship et al. 2001). For solid medium 2% (w/v) agar was added before autoclaving.

Table 2-3 Table of growth media and supplements

Medium (abbrev.)	Content (in final conc.)	Purpose
PD	Potato Dextrose Agar;	Standard growth media
RG	1.5 % Regeneration Media Agar	Sucrose-rich osmotic media
Blankenship (MSM3)	Blankenship et al., 2005 (modified)	defined growth media
CZ	Czapek Dox (Oxoid) + Agar	defined growth media
H ₂ O	Mili-Q water + 3% agar	Nutrient starvation
CD	Czapek Dox salts	Nutrient starvation
CDGN	CD salts + 100mM Glucose + 10 mM (NH ₄) ₂ SO ₄	defined growth media
CDGNn	CD salts + 100 mM Glucose + 20 mM NaNO ₃	Alternative C - and N-source (defined growth media)
CD+ManNn	CD salts + 100 mM Mannitol + 20 mM NaNO ₃	Alternative C - and N-source (defined growth media)
CD+GlyNn	CD salts + 100 mM Glycerol + 20 mM NaNO ₃	Alternative C - and N-source (defined growth media)
CD+SucN	CD salts + 100 mM Sucrose + 10 mM (NH ₄) ₂ SO ₄	Alternative C - and N-source (defined growth media)
CD+SucNn	CD salts + 100 mM Sucrose + 20 mM NaNO ₃	Alternative C - and N-source (defined growth media)

Medium (abbrev.)	Content (in final conc.)	Purpose
CD+Glu	CD salts + 100 mM Glucose	Alternative C – source
CD+Glu	CD salts + 10 mM Glucose	Alternative C – source
CD+Suc	CD salts + 100 mM Sucrose	Alternative C - source
	CD salts + 10 mM Sucrose	Alternative C - source
CD+Glut	CD salts + 100 mM Glutamate	Alternative C - source
	CD salts + 10 mM Glutamate	Alternative C - source
CD+Xyl	CD salts + 100 mM Xylan	Alternative C - source
CD+Man	CD salts + 100 mM Mannitol	Alternative C - source
CD+Gly	CD salts + 100 mM Glycerol	Alternative C-/N - source
CD+N	CD salts + 10 mM (NH ₄) ₂ SO ₄	Alternative N - source
CD+Nn	CD salts + 20 mM NaNO ₃	Alternative N - source
CD+ NH ₄ NO ₃	CD salts + 20 mM NOH ₃	Alternative N - source
	CD salts + 10 mM NOH ₃	Alternative N - source
CD+NH ₄ CL	CD salts + 20 mM NH ₄ Cl	Alternative N - source
	CD salts + 10 mM NH ₄ Cl	Alternative N - source
CD+MSG	CD salts + 100 mM Monosodium glutamate	Alternative N - source
	CD salts + 50 mM Monosodium glutamate	Alternative N - source

Table 2-4 Table of growth media and amino acid supplements

Medium	Amino acids	Final concentration
CD + Ala	alanine	10 mM
		1 mM
CD + Arg	arginine	10 mM
		1 mM
CD + Asn	asparagine	10 mM
		1 mM
CD + Asp	aspartic acid	10 mM
		1 mM
CD + Cys	cysteine	10 mM
		1 mM
CD + Glu	glutamic acid	10 mM
		1 mM
CD + Gln	glutamine	10 mM
		1 mM
CD + Gly	glycine	10 mM
		1 mM
CD + His	histidine	10 mM
		1 mM
CD + Ile	isoleucine	10 mM
		1 mM
CD + Leu	leucine	10 mM
		1 mM
CD + Lys	lysine	10 mM
		1 mM
CD + Met	methionine	10 mM
		1 mM
CD + Phe	phenylalanine	10 mM
		1 mM
CD + Pro	proline	10 mM
		1 mM

Medium	Amino acids	Final concentration
CD + Ser	serine	10 mM
		1 mM
CD + Thr	threonine	10 mM
		1 mM
CD + Trp	tryptophan	10 mM
		1 mM
CD + Tyr	tyrosine	10 mM
		1 mM
CD + Val	valine	10 mM
		1 mM

2.4 Colony growth in axenic culture

2.4.1 Analysis of hyphal growth

E. festucae cultures to be analysed for hyphal growth were grown under standard conditions (2.3.3) and analysis was conducted using either non-transfer (2.4.1.1) or transfer experimental (2.4.1.2) conditions. Generally, mycelia were inoculated on either solid PD medium (2.3.3.1) or solid CD medium (2.3.3.2), supplemented with various C- and/or N- sources (Table 2.3.3.8). Overall colony growth of the wild-type strain and the mutant strains were compared. Each experiment was conducted in two independent biological replicates and measurements were taken at two - three different positions for each colony as specified below (2.4.2).

2.4.1.1 Non-transfer experiment

The non-transfer experiment was conducted as a preliminary screen to identify mutant strains that show significantly altered hyphal growth-rates from that of the wild-type strain, grown solely on selective media for 7 days at 22°C. Conditions that triggered altered hyphal growth (putatively trigger cAMP signalling) for mutant strains were then selected for further quantification of intracellular cAMP (2.6) to analyse the potential involvement of the cAMP signalling under these conditions. *E. festucae* mycelial plugs (2.3.3) from freshly grown culture on PD medium (2.3.3.1) were used to inoculate either solid PD medium (2.3.3.1) or

solid CD medium (2.3.3.5), supplemented with various C- and/or N-sources (Table 2.3), amino acids (Table 2.4) or applied stress conditions and hyphal growth-rate was determined after 7 days (2.4.2.1)(Appendix 13 A). Non-transfer conditions were identical to standard growth conditions for *E. festucae* cultures, but have been listed to distinguish from the transfer experiment (2.4.1.2).

2.4.1.2 Transfer experiment

The transfer experiment (modified from Girard et al., 2004) was conducted as preliminary screen to identify mutant strains that show significantly altered hyphal growth-rates (2.4.2.1) from that of the wild-type strain, when transferred from nutrient rich onto selective media. Conditions that triggered altered hyphal growth rates (putatively trigger cAMP signalling) for mutant strains after short term exposure on selective media, were then selected for further quantification of intracellular cAMP (2.6) to identify putative involvement of cAMP signalling under these selective conditions. *E. festucae* mycelial plugs (2.3.3) from freshly grown culture on PD medium (2.3.3.1) were used to inoculate sterilised cellophane overlays of PD medium (2.3.3.1), for 4 days at 22°C. Cellophane discs with attached colonies were then transferred onto solid CD medium (2.3.3.5), supplemented with various C- and/or N-sources (Table 2.3), amino acids (Table 2.4) or applied stress conditions, then further incubated for 3 days at 22°C and hyphal growth-rate was determined (2.4.2.2) (Appendix 14 A). In contrast to the non-transfer experiment, the transfer experiment, hypothetically mimics environmental changes and identified putative restrictions in the fungus ability to adjust to the above conditions.

2.4.2 Determination of hyphal growth rate

2.4.2.1 Hyphal growth rate for non-transfer experiment

Using the non-transfer experimental conditions (2.4.1.1), hyphal radial growth was determined by measuring the overall colony growth in diameter and the initial inoculum (in diameter) at a minimum of two different positions using a vernier scale caliper (Appendix 13 B). Each measurement of the overall colony growth and the inoculum (mycelial plug) were then subtracted from each other and divided by two. In addition, the distance from the edge of the colony to the edge of

the original plug was measured at three different positions using a vernier caliper and compared to the primary measurement value, for independent verification. The hyphal growth rate per day was determined by dividing the radial growth (per 7 days inoculation) by the days of inoculation on the specific medium (e.g. CD + supplement). Each experiment was conducted twice in biological replicates with the respective measurements for each strain on each medium.

2.4.2.2 Hyphal growth rate for transfer experiment

Using the transfer experiment conditions (2.4.1.2), hyphal radial growth was determined by measuring the overall colony growth in diameter and the colony growth of the inoculum after 4 days on PD medium in diameter at minimum of two different positions using a vernier scale caliper (Appendix 14 B). Each measurement of overall colony growth and 4 day-inoculum were then subtracted from each other and divided by two. In addition, the distance from the edge of the colony to the edge of the 4 day-inoculum was measured at three different positions using a vernier caliper and compared to the primary measurement values, for independent verification. The hyphal growth rate per day was determined by dividing the radial growth by the days of inoculation on the specific medium (e.g. CD + supplement). Each experiment was conducted twice in biological replicates with the respective measurements for each strain on each medium.

2.4.3 Fungal growth under stress conditions

E. festucae cultures to be analysed were grown on either solid PD medium (2.3.3.1) or solid CD medium (2.3.3.5), under a particular stress treatment for 7 days at 22°C. Overall colony growth of the wild-type strain and the mutant strains were compared. Each experiment was carried out in three independent experiments (technical replicate) using three biological replicates for each experiment. Concentration of additives represents the final concentration in the respective medium.

Temperature stress was induced by incubation at 30°C for 7 days. Osmotic stress was induced by addition of NaCl (0.3 mM, 0.5 mM, 0.1 M, 0.3 M, 0.5 M, 1 M), KCl (0.7 mM, 0.7 M, 1 M) or sorbitol (0.7 mM, 0.7 M, 1 M). Oxidative stress was induced by addition of hydrogen peroxide (7 mM, 14 mM H₂O₂) and menadione (40

µM). Cell wall stress was induced by addition of SDS (0.01% (w/v)), Calcofluor white (100 µg/ml; CFW), congo red (25 µg/ml; CR) or caffeine (0.5 mM, 1 mM, 3 mM, 5 mM and 10 mM; caff). Calcofluor white and Congo red were added to PD medium buffered with 50 mM HEPES (pH 6.5). Plates containing hydrogen peroxide, Calcofluor white or Congo red were stored and incubated in the dark to prevent breakdown of the additives. Extracellular pH under nutrient starvation conditions was induced by using solid CD medium (2.3.3.5) with an adjusted pH to 4, 6.8, 8.5 and 10 in a non-transfer (2.4.1.1) and transfer (2.4.1.2) experiment and the hyphal growth rate per day was determined (2.4.2).

2.4.4 Fungal growth in presence of plant-derived molecules

E. festucae cultures to be analysed were grown on either solid PD (2.3.3.1) or solid defined medium containing CD salts (2.3.3.5) and apoplastic fluid or linoleic acid (LA), for 7 days at 22°C. Colony growth of the wild-type strain and the mutant strains were compared, using non-transfer (2.4.1.1) and transfer (2.4.1.2) experimental conditions and the hyphal growth rate per day was determined (2.4.2). Each experiment was carried out in three independent experiments (technical replicates) using two biological replicates. Concentration of additive represents the final concentration in the respective medium. To each medium plate (approx. 25 ml), 200 µl sterilised apoplastic fluid, extracted from uninfected (APF) or *E. festucae* wild-type infected (APF WT) *L. perenne* plants (2.7.7), was added after autoclaving at approx. 50°C or spread onto medium plates and air-dried. Linoleic acid (0.1 mM, 0.3 mM, 0.5 mM, 1 mM, 2 mM, 5 mM, 10 mM; Sigma-Aldrich), ethanol (0.1% (v/v), 1% (v/v), 10% (v/v)) or 1% (v/v) Dimethyl sulfoxide (DMSO), was added to medium after autoclaving. Linoleic acid was dissolved in 10% ethanol to a 100 mM stock solution or in DMSO to a 10 mM stock solution. Solid PD medium was supplemented with linoleic acid (0.01 mM, 0.1 mM, 1 mM, 2 mM, 5 mM; Sigma-Aldrich); ethanol (1% (v/v), 10% (v/v); EtOH) or Dimethyl sulfoxide (DMSO). Solid CD medium was supplemented with linoleic acid (0.1 mM, 0.3 mM, 0.5 mM, 1 mM, 2 mM, 5 mM, 10 mM; Sigma-Aldrich); ethanol (0.1% (v/v), 1% (v/v), 10% (v/v); EtOH), Dimethyl sulfoxide (DMSO), apoplastic fluid extracted (2.7.7) from *Lolium perenne* plants uninfected or infected with *E. festucae* wild-type strain.

2.4.5 Chemical treatment of fungal colonies

E. festucae cultures to be analysed were grown on either solid PD medium (2.3.3.1) or solid CD medium (2.3.3.5), supplemented with the particular chemical additive, for 7 days at 22°C. Overall colony growth and morphology of the mutant strains were compared to the wild-type strain. Each experiment was carried out in three independent experiments (technical replicates) using three biological replicates for each experiment. Concentration of additive represents the final concentration in the respective medium.

Solid PD medium (2.3.3.1) was supplemented with caffeine (0.3 mM, 0.5 mM, 1 mM, 3 mM, 5 mM, 10 mM; caff); theobromine (0.5 mM, 1 mM, 3 mM, , 5 mM; Theo, Sigma-Aldrich); 3-isobutyl-1-methylxanthine (0.1 mM, 0.3 mM, 0.5 mM, 1 mM; IMBX, Sigma-Aldrich); histamine (0.3 mM, 0.5mM, 1 mM, 3 mM 5mM; Sigma-Aldrich); quinine (0.3 mM, 0.5 mM, 1 mM, 3 mM; Sigma-Aldrich) or Dimethyl sulfoxide (DMSO). Solid CD medium (2.3.3.5) was supplemented with 3-isobutyl-1-methylxanthine (0.5 mM, 1 mM; IMBX) or Dimethyl sulfoxide (DMSO).

2.5 Molecular techniques

2.5.1 DNA isolation

2.5.1.1 Plasmid DNA isolation from *E. coli*

Pure *E. coli* overnight cultures, grown in liquid LB (2.3.1.1) medium, were pelleted by centrifugation (17,000 x g, 2 min) and high quality plasmid DNA was isolated using the Wizard® Plus SV Miniprep system (Promega), following the manufacturer's instruction.

2.5.1.2 Cosmid DNA isolation from *E. coli*

For isolation of cosmids from the *E. festucae* cosmid library, pure *E. coli* overnight cultures, grown in liquid LB (2.3.1.1) medium, were pelleted by centrifugation (17,000 x g, 2 min). Cells were resuspended in 200 µl of Solution I (50 mM glucose, 25 mM Tris-HCL, 10 mM EDTA; pH 8), then lysed by adding lysozyme (0.5 mg) and incubated at room temperature for 5 min. 300 µl of fresh Solution II (0.4 M NaOH, 2% (w/v) SDS) was added and cells were incubated on ice for 5 min, then neutralised by adding 300 µl ice cold Solution III (3 M potassium acetate, 11.5% (v/v) glacial acetic acid), incubated on ice for 5 min and pelleted by centrifugation (17,000 x g, 10 min). Contaminating RNAs were removed by adding RNaseA at a final concentration of 20 µg/ml (Sigma-Aldrich) to the supernatant and incubated at 37°C for 20 min, followed by two consecutive purification rounds using chloroform extraction. An equal volume of isopropanol was added to the aqueous phase to precipitate the DNA, which was then pelleted by centrifugation (17,000 x g, 10 min), washed with 70% ethanol, air-dried and resuspended in 32 µl Milli-Q water. For high quality preparations, DNA was further purified and precipitated by addition of NaCl (to 0.4 M) and 6.5% (w/v) PEG 8000 and incubated on ice for 20 min. The DNA was pelleted by centrifugation (17,000 x g, 15 min, 4°C), washed with 70% ethanol, air-dried and resuspended in 50 µl Milli-Q water.

2.5.1.3 Plasmid DNA isolation from *S. cerevisiae*

S. cerevisiae (FY834) cultures were grown on solid YPD medium (2.3.2.1) and cells were harvested by addition of two times 1 ml YPD medium and repeated

scrubbing with a sterile glass spreader. The resulting yeast suspension was transferred into a 2 ml microcentrifuge tube, pelleted by centrifugation (17,000 x g for 15 s) and the cells lysed using a mixture containing approx. 100 µl glass beads, 100 µl phenol, 100 µl chloroform and 100 µl lysis buffer (2% (v/v) Triton X-100, 1% (w/v) SDS, 100 mM NaCl, 10 mM Tris (pH 8) and 1 mM EDTA) and mixed by vortexing for 2 min. The lysate was pelleted by centrifugation (17,000 x g, 10 min) and 100 µl aliquots of the DNA-containing supernatant was transferred to new microcentrifuge tubes. The DNA was precipitated using 10 µl 3 M NaAc and 250 µl isopropanol or 95% (v/v) ethanol, incubated at room temperature for 10 min, pelleted by centrifugation (17,000 x g, 10 min), washed using 70% (v/v) ethanol, air-dried and resuspended in 50 µl sterile Milli-Q water.

2.5.1.4 Genomic DNA from *E. festucae*

High molecular weight genomic DNA from *E. festucae* was isolated following a previously described and adapted method from (Byrd et al. 1990). *E. festucae* mycelia, grown in liquid PD medium (2.3.3.1) for four days, were harvested using filtration through a nappy-liner filter, freeze-dried and ground to a fine power under liquid nitrogen (N₂) using a mortar and pestle. Approx. 20 mg of ground mycelia was resuspended in 800 µl of extraction buffer (150 mM EDTA, 50 mM Tris-HCl and 1% (w/v) SDS, adjusted to pH 8) and incubated at room temperature for 1 min, followed by addition of proteinase K to a final concentration of 2 mg/ml and incubation at 37°C for 20 min. The cell debris was pelleted by centrifugation (17,000 x g, 10 min) and the supernatant was transferred into a fresh 2 ml microcentrifuge tube. The genomic DNA was then purified by three repeated extractions using equal volumes (400 µl each) of phenol and chloroform and one extraction using one volume (800 µl) of chloroform. In each step, the lysate-mixture was thoroughly mixed by vortexing and separated by centrifugation (17,000 x g, 10 min), followed by isolation and transfer of the DNA-containing aqueous upper phase by pipetting into a new tube. The genomic DNA was then precipitated using 1 volume (800 µl) isopropanol, incubated at room temperature for 20 min or at -20°C, overnight. DNA was then pelleted by centrifugation (17,000 x g, 10 min), washed using 70% (v/v) ethanol (17,000 x g, 5 min), air-dried and resuspended in 100 µl sterile Milli-Q water. Genomic DNA samples were stored at 4°C.

2.5.1.5 Crude genomic DNA from *E. festucae*

Fungal DNA from *E. festucae*, grown on solid PD medium (2.3.3.1), was isolated by removing an approx. 1 cm² mycelial blocks from the outer edge of the colony using a sterile tooth pick. Mycelia was transferred into a 1.5 ml microcentrifuge tube, chopped up and lysed using 200 µl lysis buffer (150 mM EDTA, 50 mM Tris-HCl, 1% (w/v) SDS) and incubated at 70°C for 0.5 - 2 hours. The lysate was neutralised by adding 1 volume (200 µl) of 5 M potassium acetate, incubated on ice for 10 minutes and the cells pelleted by centrifugation (17,000 x g, 20 min). The supernatant was transferred to a new microcentrifuge tube containing 0.7 volumes (140 µl) chilled isopropanol for DNA precipitation and incubated at room temperature for 2 hours or at 4°C, overnight. The DNA was pelleted by centrifugation (17,000 x g, 20 min), washed using 70% (v/v) ethanol (17,000 x g, 5 min), air-dried and resuspended in 20 µl sterile Milli-Q water. Crude genomic DNA samples were stored at 4°C and used for PCR screening.

2.5.2 DNA purification

DNA from PCR reactions or from agarose blocks containing fragments separated by gel electrophoresis (2.5.5) was purified using the Wizard® SV Gel and PCR Clean-up System (Promega), following the manufacturer's instructions.

2.5.3 Restriction enzyme (RE) digestions

Restriction endonucleases were used to digest plasmid, cosmid or fungal genomic DNA to identify particular DNA fragments of interest and fragment sizes checked against the *in silico* maps. The enzymatic digests were performed using enzymes from Roche® or New England Biolabs™ and according to the appropriate enzyme properties using a thermocycler or water bath for incubation. Generally, enzymatic digests were performed using 100ng DNA in a total volume of 10 µl using 2 U restriction enzyme. For Southern analysis, 1.2 µg genomic DNA was digested in a total volume of 100 µl overnight using 30 U of restriction enzyme and appropriate buffer (10 µl). When DNA was not sufficiently digested, an additional 10 U of enzyme was added to the sample and incubated for a further 4 hours. Double digests were performed using equal amounts of the enzymes according to the total volume of the

reaction and an appropriate buffer suitable for both enzymes. Digest reactions were stopped by addition of SDS loading dye.

2.5.4 Ethanol precipitation

To increase the concentration of DNA in a solution, nucleic acids were precipitated using 0.1 volume 3 M sodium acetate and 2.5 volumes of 95% (v/v) ethanol, added to a 1.5 ml microcentrifuge tube containing the DNA. Samples were mixed by inversion, incubated at room temperature for 20 min, pelleted by centrifugation (17,000 x g, 10 min), washed using 1 ml 70% (v/v) ethanol (centrifuged at 17,000 x g, 5 min), air-dried and resuspended in a desired volume of sterile Milli-Q water.

2.5.5 Gel electrophoresis

DNA fragments were separated according to their molecular size using gels of 0.8% -1% (w/v) agarose in 1x TBE (89 mM Tris, 89 mM boric acid, 2 mM Na₂EDTA) buffer. For larger DNA fragments and Southern analysis, 0.7% (w/v) agarose gels were used. DNA samples were mixed with 6x loading dye (20% sucrose (w/v), 5 mM EDTA, 1% (w/v) SDS and 0.2% (w/v) bromophenol blue) and loaded into the wells of the solidified agarose gels alongside a 1 kb⁺ reference size marker (Invitrogen). The Gels were run in 1x TBE buffer, stained afterwards with ethidium bromide (1 µg/ml) in 1x TBE buffer, destained using tap water for photography or Milli-Q water for gel purification and Southern blotting. Marker and DNA fragments were visualised using a UV transilluminator Gel Documentation System (Bio-rad).

2.5.6 DNA quantification

The DNA concentration of PCR fragments, plasmids and cosmids was determined using a NanoPhotometer™ (Implen) as per the manufacturer's instruction. Fungal genomic DNA concentration was quantified using a DyNA Quant 200 Fluorometer (Hoefer), as per the manufacturer's instructions.

2.5.7 Polymerase chain reaction (PCR)

2.5.7.1 Standard PCR

Standard PCR amplifications were performed using *Taq* DNA polymerase (Roche®) or *OneTaq*® DNA polymerase (New England Biolabs, Inc.) in a total volume of 25 µl or 50 µl using a thermocycler (Mastercycler™ Nexus Thermal Cycler, Eppendorf™).

Using *Taq* DNA polymerase, the reaction mixture in a total volume of 50 µl contained 5 µl 10x Standard *Taq* Reaction buffer, 1 µl of each primer (10 µM), 1 µl dNTPs (10 mM), 1 µl template DNA (1ng/µl plasmid DNA; 10 ng/µl genomic DNA) and 0.25 µl of *Taq* polymerase (1 U). The PCR-conditions were set as followed: Initial cycle at 95°C for 2 min; 35 cycles at 95°C for 40 s, 45-68°C for 30 s and 72°C for 1.5 min per kb; final extension cycle at 72°C for 10 min.

Using *OneTaq*® DNA polymerase, the reaction mixture in a total volume of 50 µl contained 10 µl 5x *OneTaq* Reaction buffer, 1 µl dNTPs (10 mM), 1 µl of each primer (10 µM), 1 µl template DNA (1ng/µl plasmid DNA; 10 ng/µl genomic DNA) and 0.25 µl of *Taq* polymerase (1 U). The PCR-conditions were set as followed: Initial cycle at 94°C for 30 sec; 35 cycles at 94°C for 20 s, 45-68°C for 30 s and 68°C for 1 min per kb; final extension cycle at 68°C for 10 min.

2.5.7.2 High-Fidelity PCR

When proof reading activity was required, High-Fidelity PCR amplification was performed using Phusion® DNA polymerase (ThermoFisher Scientific), Q5® DNA polymerase (New England Biolabs, Inc.) or Expand™ High Fidelity *Taq* DNA polymerase (Sigma-Aldrich®) in a total volume of 50 µl using a thermocycler (Mastercycler™ Nexus Thermal Cycler, Eppendorf™). PCR was further processed or stored at 4°C until used.

Using Phusion® DNA polymerase, the reaction mixture in a total volume of 50 µl contained 10 µl 5x Phusion HF Reaction buffer, 1 µl dNTPs (10 µM), 2.5 µl of each primer (10 µM), 1 µl template DNA (1ng/µl plasmid DNA; 10 ng/µl genomic DNA), 1.5 µl optional DMSO and 0.5 µl of *Taq* polymerase (1 U). The PCR-conditions

were set as followed: Initial cycle at 98°C for 30 s; 10 cycles at 98°C for 10 s, 55°C for 30 s and 72°C for 15 s per kb; 20 cycles at 98°C for 10 s and 72°C for 20 s per kb; final extension cycle at 72°C for 10 min.

Using Q5® DNA polymerase, the reaction mixture in a total volume of 50 µl contained 10 µl 5x Q5 Reaction buffer, 1 µl dNTPs (10 mM), 2.5 µl of each primer (10 µM), 1 µl template DNA (1ng/µl plasmid DNA; 10 ng/µl genomic DNA) and 0.5 µl of Q5 High-Fidelity DNA polymerase (1 U). The PCR-conditions were set as followed: Initial cycle at 98°C for 30 s; 10 cycles at 98°C for 10 s, 52-72°C for 30 s and 72°C for 20 s per kb; 20 cycles at 98°C for 10 s and 72°C for 15 s per kb; final extension cycle at 72°C for 2 min.

Using Expand™ High Fidelity *Taq* DNA polymerase, the reaction mixture in a total volume of 50 µl contained 5 µl 10x Expand High Fidelity Buffer, 1 µl of each primer (10 µM), 1 µl dNTPs (10 mM), 1 µl template DNA (1ng/µl plasmid DNA; 10 ng/µl genomic DNA) and 0.75 µl of *Taq* polymerase (2.6 U). The PCR-conditions were set as followed: Initial cycle at 94°C for 2 min; 35 cycles at 94°C for 30 s, 45-68°C for 30 s and 72°C for 1 min per kb, final extension cycle at 72°C for 10 min.

2.5.7.3 PCR for GC-rich DNA sequences

To amplify GC rich DNA sequences, multiple conditions were tested as follows: alterations of primer annealing temperature using gradient PCR, addition of DMSO (2-5% (v/v)), using alternative solutions such as the 5x One*Taq* GC Reaction buffer (10 µl) and High GC Enhancer (10 µl), 5x Phusion GC Reaction buffer (10 µl), 5x Q5 Reaction buffer (10 µl) and 5x Q5 High GC Enhancer (10 µl) or 10x Expand High Fidelity Buffer (5 µl) and GC Enhancer (5 µl) with the respective DNA polymerase and PCR conditions (2.5.7.2). KAPA High-fidelity™ GC-rich PCR kit (KAPA Biosystems) using either the KAPA HiFi™ GC Buffer or the KAPA HiFi™ Buffer (KAPA Biosystems). Hot start PCR was performed using the KAPA HiFi™ HotStart ReadyMix PCR Kit (KAPA Biosystems). The reaction conditions were followed as per manufacturer's instructions in a total volume of 25 - 50 µl using a thermocycler (Mastercycler™ Nexus Thermal Cycler, Eppendorf™). PCR was further processed or stored at 4°C until used.

Using KAPA High-fidelity™ GC-rich PCR kit, the reaction mixture in a total volume of 50 µl contained 10 µl 5x KAPA HiFi Buffer (Fidelity or GC), 1.5 µl KAPA dNTP Mix (10 mM), 1.5 µl of each primer (10 µM), 1µl template DNA (1ng/µl plasmid DNA; 10 ng/µl genomic DNA) and 1 µl of *Taq* polymerase (1 U). The PCR-conditions were set as followed: Initial cycle at 95°C for 3 min; 35 cycles at 98°C for 20 s, 65°C for 15 s and 72°C for 15 s per kb; final extension cycle at 72°C for 5 min.

Using KAPA HiFi™ HotStart ReadyMix PCR kit, the reaction mixture in a total volume of 25 µl containing 12.5 µl (2x) KAPA HiFi™ HotStart Ready mix, 0.75 µl of each primers (10 µM), 1.5 µl DMSO (5%), 1µl template DNA (1ng/µl plasmid DNA; 10 ng/µl genomic DNA). The PCR-conditions were set as followed: Initial cycle at 95°C for 5 min; 35 cycles at 98°C for 20 s, 65°C for 15 s and 72°C for 1 min per kb; final extension cycle at 72°C for 5 min.

2.5.8 TOPO-cloning

TOPO® TA cloning was used to sub-clone PCR products into an *E. coli* plasmid vector using the TOPO® TA Cloning kit (Invitrogen), following the manufacturer's instructions. PCR fragments were A-tailed using *Taq* DNA polymerase to facilitate integration into the pCR2.1-TOPO® vector (Invitrogene; Appendix 12), containing the complementary 3'-thymidine (T) overhangs. A-tailing was performed by incubating the PCR product in a reaction mixture of 10 µl containing 5 U DNA polymerase, 1 µl *Taq* Reaction buffer and 200 nM dATP at 72°C. A-tailed PCR products were ligated into pCR2.1-TOPO® vector (10 ng) by incubating in a reaction mixture of 10 µl containing 20 mM NaCl, 6 mM MgCl₂ at room temperature for 30 min.

2.5.9 DNA sequencing

DNA sequencing of PCR products and plasmids was carried out by the Massey Genome Service using a 3730 DNA Analyser (applied Biosystems) with BigDye™ Terminator Version 3.1 chemistry (Applied Biosystems).

2.5.10 Preparation of constructs

2.5.10.1 *E. festucae gpr1a* gene replacement construct

In an attempt to generate the *gpr1a* replacement construct (referred to as pAB01), the *gpr1a* 5' flanking region was amplified from wild-type *E. festucae* genomic DNA (2.5.1.4) and the hygromycin selectable marker was amplified from pSF15.15 (Appendix 3) using Phusion High-Fidelity™ DNA Polymerase (2.5.7.2) and the primers *gpr1a_1/gpr1a_2*, *gpr1a_3/gpr1a_4* and *hph_f/hph_rev*, respectively (Appendix 5). Attempts were made to amplify the *gpr1a* 3' flanking region from wild-type *E. festucae* genomic DNA (2.5.1.4) or from cosmid DNA (2.5.1.2) from a cosmid library of *E. festucae* F11 genomic DNA (2.5.15) using different PCR methodologies (2.5.7.3). However, PCR amplification of the 1322 bp *gpr1a* 3' flank was unsuccessful.

2.5.10.2 *E. festucae gpr1b* gene replacement construct

To generate the *gpr1b* replacement construct (pAB02), the flanking regions 5' and 3' of *gpr1b* were amplified from wild-type *E. festucae* genomic DNA (2.5.1.4) and the geneticin selectable marker was amplified from pSF16.17 (Appendix 4) using Phusion High-Fidelity™ DNA Polymerase (2.5.7.2) and the primers *gpr1b_1/gpr1b_2*, *gpr1b_3/gpr1b_4* and *nptII_f/nptII_rev*, respectively (Appendix 6). The fragments (1159 bp *gpr1b* 5' flank, 1390 bp *gpr1b* 3' flank, 1741 bp *nptII* cassette) were purified and assembled in pRS426 (Appendix 2) using yeast recombinational cloning (2.5.10.8).

2.5.10.3 *E. festucae gpr2* gene replacement construct

To generate the *gpr2* replacement construct (pAB03), the flanking regions 5' and 3' of *gpr2* were amplified from wild-type *E. festucae* genomic DNA (2.5.1.4) and the hygromycin selectable marker was amplified from pSF15.15 (Appendix 3) using Phusion High-Fidelity™ DNA Polymerase (2.5.7.2) and the primers *gpr2_1/gpr2_2*, *gpr2_3/gpr2_4* and *hph_f/hph_rev*, respectively (Appendix 7). PCR-amplified fragments (1319 bp *gpr2* 5' flank, 1268 bp *gpr2* 3' flank, 1394 bp *hph* cassette) were purified and assembled in pRS426 (Appendix 2) using yeast recombinational cloning (2.5.10.8).

2.5.10.4 *E. festucae pdeH* gene replacement construct

To generate the *pdeH* replacement construct (pAB04), the flanking regions 5' and 3' of *pdeH* were amplified from wild-type *E. festucae* genomic DNA (2.5.1.4) and the hygromycin selectable marker was amplified from pSF15.15 (Appendix 3) using Phusion High-Fidelity™ DNA Polymerase (2.5.7.2) and the primers *pdeH_1/pdeH_2*, *pdeH_3/pdeH_4* and *hph_for/hph_rev*, respectively (Appendix 8). PCR-amplified fragments (1374 bp *pdeH* 5' flank, 1296 bp *pdeH* 3' flank, 1394 bp *hph* cassette) were purified and assembled in pRS426 (Appendix 2) using yeast recombinational cloning (2.5.10.8).

2.5.10.5 *E. festucae pdeL* gene replacement construct

To generate the *pdeL* replacement construct (pAB05), the flanking regions 5' and 3' of *pdeL* were amplified from wild-type *E. festucae* genomic DNA (2.5.1.4) and the geneticin selectable marker was amplified from pSF16.17 (Appendix 4) using Phusion High-Fidelity™ DNA Polymerase (2.5.7.2) and the primers *pdeL_1/pdeL_2*, *pdeL_3/pdeL_4* and *nptII_f/nptII_rev*, respectively (Appendix 9). PCR-amplified fragments (1946 bp *pdeL* 5' flank, 2333 bp *pdeL* 3' flank, 1741 bp *nptII* cassette) were purified (2.5.2) and assembled in pRS426 (Appendix 2) using yeast recombinational cloning (2.5.10.8).

2.5.10.6 *E. festucae gpr1b* complementation construct

To generate the Δ *gpr1b* complementation construct (pAB06; Appendix 10), a 2860 bp fragment containing a wild-type copy of *gpr1b* and the native promoter (941bp) and terminator (269 bp) sequence was PCR-amplified from wild-type genomic DNA using Q5®-DNA polymerase (NEB) and the primers *Tgpr1b_for/Pgpr1b_rev*. The PCR fragment was purified (2.5.2) and assembled in pRS426 (Appendix 2) using Gibson assembly (2.5.10.9). Error-free gene sequence was verified by DNA sequencing (2.5.9).

2.5.10.7 *E. festucae pdeH* complementation construct

To generate the Δ *pdeH* complementation construct (referred to as pAB07), a 5193 bp fragment containing a wild-type copy of *pdeH* (3058 bp) and the native

promoter (1608 bp) and terminator (527 bp) sequence was PCR-amplified from wild-type genomic DNA using Q5®-DNA polymerase (NEB) and the primers PpdeH_for/TpdeH_rev. The PCR fragment was purified (2.5.2) and verified to be error-free by DNA sequencing (2.5.9). For unknown reasons, assembly in pRS426 using Yeast recombinational cloning (2.5.10.8) or Gibson assembly (2.5.10.9) or assembly in pCR2.1-TOPO using TOPO-cloning (2.5.8), was unsuccessful. The linear *ΔpdeH* complementation fragment was co-transformed with pSF16.17 into *ΔpdeH* protoplasts (2.5.12.2).

2.5.10.8 *E. festucae pdeL* complementation construct

To generate the *ΔpdeL* complementation construct (pAB08; Appendix 11), a 3503 bp fragment containing a wild-type copy of *pdeL* (1708 bp) and the native promoter (1429 bp) and terminator (366 bp) sequence was PCR-amplified from wild-type genomic DNA using Q5®-DNA polymerase (NEB) and the primers PpdeL_for/TpdeL_rev. The PCR fragment was purified (2.5.2) and assembled into pCR2.1-TOPO (Appendix 12) using TOPO-cloning (2.5.8). Error-free gene sequence was verified by DNA sequencing (2.5.9).

2.5.10.9 Yeast recombinational cloning (YRC)

Yeast recombinational cloning was used to generate gene replacement constructs using the highly efficient recombination machinery of *S. cerevisiae* (Colot et al. 2006). One ml of a *S. cerevisiae* FY834 culture, grown overnight (2.3.2), was used to inoculate 50 ml liquid YPD in sterile 125 ml conical flask and incubated at 30°C until an OD of 0.4 – 0.5 (approx. for 4-5 h) with shaking at 200 rpm. Yeast cells were harvested in sterile 50 ml Falcon tubes, pelleted by centrifugation (2500 x rpm, 5 min), washed with 25 ml sterile Milli-Q water, pelleted by centrifugation (2500 x rpm, 5 min) and resuspended in 1 ml 100 mM lithium acetate (LiAc) and pelleted by centrifugation (17,000 x g, 15 s). The cell suspension was resuspended in 400 µl of 100 mM LiAc and divided into 50 µl aliquots, which were then pelleted by centrifugation (17,000 x g, 15 s). A total of 34 µl of the construct DNA-mix containing 300 ng of each DNA fragment was added to the transformation master mix (240 µl 50% PEG 4000, 36 µl 1 M LiAc, 10 µl of 2 mg/ml single-stranded (boiled) carrier DNA (salmon sperm DNA or herring sperm DNA). The cell suspension was mixed by

gentle vortexing, incubated at 30°C for 30 min, mixed by inversion and further incubated at 42°C for 30 min. Cells were then repeatedly washed in 1 ml sterile Milli-Q water, pelleted by centrifugation (17,000 x g; 15 s) and resuspended in 50 µl sterile Milli-Q water. The transformed yeast cells were then spread onto SD plates lacking uracil (2.3.2.2) in equal aliquots and incubated at 30°C for 3-4 days. Once the yeast colonies had grown up, plasmid DNA was isolated using the yeast 'smash and grab' method (2.5.1.3). Isolated plasmids were then transformed into electrocompetent *E. coli* cells (2.5.11.1).

2.5.10.10 Gibson assembly (GA)

The Gibson assembly (GA) master mix (2x concentration) was prepared on ice in a final volume of 250 µl using 100 µl of 5x isothermal buffer (25% (w/v) PEG-8000, 500 mM Tris-HCl (from 1 M pH 7.5 stock solution), 50 mM MgCl₂, 50 mM 1,4-dithiothreitol, 5 mM NAD and 1 mM dNTPs), 2 µl T5 exonuclease (10 U/µl; New England Biolabs, Inc.), 6.25 µl Phusion DNA polymerase (2 U/µl; ThermoFisher Scientific), 50 µl *Taq* ligase (40 U/µl; New England Biolabs, Inc.) and 91.75 µl of Milli-Q water. The GA master mix was then divided into 10 µl aliquots (25 x 10 µl) into PCR tubes and stored at -20°C. Primers used to amplify the DNA fragments were designed to contain 15-25 bp overlapping sequence with the fragments to be joined with a T_m > 50°C and no additional sequences. In order to assemble the PCR-amplified fragments with the vector, the purified DNA fragments were mixed in a 3:1 ratio of relative molar concentration to the pRS426 vector DNA of 50-150 ng in a final volume of 10 µl. The assembly was facilitated by combining the DNA fragment mix with an equal volume of GA 2x master mix (10 µl aliquots) and incubated at 50°C for 1 hour in a thermocycler. The resulting reaction mixture, presumably containing the construct, was then used for transformation into chemically competent *E. coli* cells (2.5.11.2).

2.5.11 Bacterial Transformation

2.5.11.1 Transformation of electrocompetent *E. coli* cells

Electro-competent DH5α *E. coli* cells (Invitrogen) were thawed on ice (50 µl aliquots) and gently mixed with 100-200 ng/µl (1 µl) of isolated plasmid DNA and

incubated on ice for 1 min. Cells were transferred into a pre-chilled 2 mm cuvette and transformation was facilitated by electroporation (electric pulse) using a Gene Pulser (Bio-Rad; settings of 25 mF, 2.5 kV, 200 Ω). SOC medium (2.3.1.2) was added and the samples were incubated at 37°C for 1 h with shaking at 200 rpm. Aliquots (100 μ l) were spread and plated on solid LB medium (2.3.1.1) containing 100 μ g/ml antibiotics using a sterile glass spreader, then incubated at 37°C, overnight.

2.5.11.2 Transformation of chemically competent *E. coli* cells

Chemically competent DH5 α *E. coli* cells (Invitrogen) were thawed on ice (50 μ l aliquots) and gently mixed with 100-200 ng/ μ l (1 μ l) isolated plasmid DNA or Gibson assembly reaction and incubation on ice for 20-30 min. Cells were then heat shocked and incubated at 42°C for 30-60 s and placed on ice for 2-5 min. SOC medium (2.3.1.2) was added and the samples were incubated at 37°C for 1 h with shaking at 200 rpm. Aliquots (300 μ l) were spread and plated on solid LB medium (2.3.1.1) containing 100 μ g/ml ampicillin (2.3.1) using a sterile glass spreader, then incubated at 37°C overnight.

2.5.11.3 *E. coli*- transformation plasmid screen (CloneChecker™)

Putative positive transformants derived from *E. coli* transformation (2.5.11), grown on solid LB medium (2.3.1.1), were analysed using the CloneChecker™ System (ThermoFisher Scientific), following the manufacturer's instruction. Colonies were picked using sterile 20 μ l pipette tips, transferred in parallel onto a solid LB medium (2.3.1.1) plate (backup plate) and into 0.2 ml PCR tubes containing either 8 μ l lysis solution or 6 μ l of LB medium (2.3.1.1) for optional overnight incubation (2.3.1). The cells were lysed in 8 μ l of lysis solution (0.1 M NaCl, 10 mM Tris-HCl, 1 mM EDTA, 0.5% Triton X-100, pH 8) and incubated at 99°C for 30 s using a thermocycler. Once cooled to room temperature, 2 μ l of RE mixture (1-5 U of RE, 1 μ l of the corresponding 10x reaction buffer) was added and incubated for 37°C for 30 min. DNA fragments of digested plasmid were separated by gel electrophoresis (2.5.5). *E. coli* colonies containing the correct plasmid, as determined by reference to the *in silico* map, were used to inoculate 5 ml liquid LB medium (2.3.1, 2.3.1.1) for isolation of plasmid DNA (2.5.1.1). Remaining *E. coli* colonies from the backup plate or liquid overnight culture were stored at 4°C for subsequent experiments.

2.5.12 Fungal transformation

2.5.12.1 Preparation of fungal protoplasts

Protoplasts of *E. festucae* were prepared as previously described (Yelton et al. 1984). *E. festucae* mycelia, grown in liquid PD medium (2.3.3, 2.3.3.1) for four days, were harvested under sterile conditions by filtration through a nappy-liner filter, followed by repeated washing with sterile Milli-Q water and finally with OM buffer (1.2 M MgSO₄, 10 mM NaHPO₄, pH to 5.8 using NaH₂PO₄). Mycelia (~4 g) was then lysed using filter-sterilised lysing enzymes from *Trichoderma harzianum* (40 ml of 10 mg/ml stock in OM buffer; Sigma-Aldrich) by incubating at 22°C for 18 h while shaking at 80 rpm or until the cells were sufficiently lysed (examined by microscopy). Lysed cells were filtered through a nappy-liner filter and divided into 5 ml aliquots into universal 15 ml tubes (Falcon/Greiner). Protoplasts were isolated by overlaying the filtrate with 2 ml ST buffer (0.6 M sorbitol, 100 mM Tris, pH 8.0), followed by centrifugation (2375 x g, 5 min, 4 °C) and transferred from the interphase into a new tubes using a sterile 1 ml pipette-filter tip. The protoplasts were then repeatedly washed by sequential pelleting and resuspension in 5 ml of STC buffer (1 M sorbitol, 50 mM Tris, 50 mM CaCl₂, pH 8.0), gentle mixing and centrifugation (2375 x g, 15 min, 4°C). After each step, samples were combined until the protoplasts were contained within a single tube and resuspended in 500 µl STC buffer. The concentration was estimated by counting cells using a haemocytometer and diluted in STC buffer if necessary to a final concentration of 1.25 x 10⁸ protoplasts/ml. The protoplasts suspension was then divided into 80-100 µl aliquots, 20 µl of 40% (v/v) polyethylene glycol added and stored at -80°C until use.

2.5.12.2 Transformation of fungal protoplasts

Transformation of *E. festucae* protoplasts was carried out as per the method of (Oliver et al. 1987). Previously prepared *E. festucae* protoplasts (2.5.12.1) from storage (-80°C) were thawed by incubating on ice for 10-15 min and 2 µl spermidine (50 mM; filter-sterilised), 5 µl heparin (5 mg/ml; filter-sterilised) and 5 µg target DNA (e.g. plasmid DNA, linearised DNA fragments, etc.) or positive-control plasmid DNA was subsequently added to each aliquot and incubated on ice for 30 min. Then,

900 µl of cold 40% (v/v) polyethylene glycol were gently mixed into each tube and aliquots of 50 – 100 µl transformed protoplasts or 100 – 300 µl positive-control transformed protoplasts were mixed into 3.5 ml prewarmed (50°C) molten 0.8 % soft RG (2.3.3.2) medium, spread onto solid 1.5 % RG (2.3.3.2) medium and incubated at 22°C, overnight. The plates were overlaid using 5 ml pre-warmed (50°C) molten 0.8 % soft RG medium, supplemented with antibiotic (150 µg/ml hygromycin B or 200 µg/ml geneticin) for selection according to the final plate volume (approx. 24.5 ml) or without antibiotics for negative and viability control. Plates were incubated at 22°C for 10-14 days until colonies emerged through the overlay. Approximately 200 putative transformants were transferred onto PD medium plates (2.3.3.1) containing the respective antibiotic, using sterile toothpicks and further incubated at 22°C for 7 days. For nuclear purification, putative transformants were sub-cultured three times on selective PD medium plates containing the respective antibiotics (Young et al. 2005), followed by an optional additional step of single-spore isolation (2.5.13). Co-transformation of *E. festucae* protoplasts with two or more plasmids at the same time was carried out as described above. Plasmids to be transformed were added in equal molar mass.

2.5.13 Single spore isolation

Four to five *E. festucae* colonies of the same strain, grown on the same plate of solid PD medium (2.3.3.1) for 10 d at 22°C, were used to harvest fungal spores. Plates were flooded with 2 ml liquid PD medium (2.3.3.1) or sterile Milli-Q water, then colonies were scrubbed multiple times to release the spores using a sterilised glass spreader. The resulting suspension was then filtered twice through sterile glass wool, loosely placed in 1 ml pipette tips. The spore suspension was captured in a sterile 1.5 ml microcentrifuge tube and aliquots of 200 – 500 µl plated onto PD medium and incubated at 22°C for 10 d. This method was used to generate homokaryons from heterokaryons.

2.5.14 Southern blotting

To verify fungal gene deletion strains, 1.2 µg digested (2.5.2.1) high-quality genomic DNA (2.5.1.4) was transferred to a positively charged nylon membrane (Roche) by capillary transfer (Southern 1975). DNA was separated by agarose (0.7

- 0.8% (w/v)) gel electrophoresis (2.5.5). The gel was stained with ethidium bromide for 30 min by agitation, destained in Milli-Q water for 30 min and the gel photographed with a ruler for subsequent size estimation. The gels were depurinated in solution I (0.25 M HCl) for 15 min, denatured in solution II (0.5 M NaOH, 0.5 M NaCl) for 40 min, neutralized in solution III (0.5 M Tris, pH 7.4, 2 M NaCl) for 40 min and then washed in 2x SSC (0.3 M NaCl, 30 mM sodium citrate) for 2 min. The gel was then placed on the blotting apparatus and assembled as follows: A double layer of 3MM Whatman sheets ("wick") soaked in 20x SSC (3 M NaCl, 0.3 M sodium citrate), which were submerged in 20x SSC-reservoirs; the gel placed on top, followed by a positively charged nylon transfer membrane, fitted to the size of the gel and soaked in 2x SSC, two sheets of 3MM sheets soaked in 2x SSC and two dry 3MM sheets of the same size. To prevent liquid bypass of the gel, high-salt solution (reservoirs and wick) was covered with cling-film with precise cutting for the gel. Multiple layers of dry paper towels and an evenly positioned weight were placed on. Transfer of the DNA to the membrane occurred overnight. The membrane was washed in 2x SSC for 5-10 min and the DNA was then cross-linked to the nylon membrane by UV irradiation for 2 min using a CEX-800 UV cross-linker (120 mJ/cm², 254 nm; Ultralum, Inc.).

2.5.14.1 DNA probe-labelling

DNA fragments consisting of a target sequence or the linear gene replacement construct were PCR amplified (2.5.7.1), purified (2.5.2) and were used for hybridisation probes, which were labelled by incorporation of radioactive isotope [α -³²P] dCTP or DIG Digoxigenin-11-dUTP.

Single-stranded DNA (30 ng) were radioactively labelled with [α -³²P] dCTP (3,000 Ci/mmol; Amersham Biosciences) by random priming using the Klenow DNA polymerase in the High Prime kit (Roche Diagnostics), following the manufacturer's instruction. Unincorporated isotope was removed from labelled probes using a Probe Quant G50 Micro Column (Amersham) and a MSE centrifuge (2050 rpm, 1 min). The labelled probe was then transferred into a microcentrifuge tube, 50 μ l TES buffer were added and the sample was stored in sealed perspex box at -20°C until use.

Digoxigenin-11-dUTP (DIG-11-dUTP) was incorporated into the DNA probe by random primer labelling using the PCR DIG probe synthesis kit (Roche) by incubation at 37°C for 18-20h, as per manufacturer's instructions. The reaction was stopped by adding 2 µl 200 mM EDTA buffer (pH 8), and a suitable concentration of DIG-labelled probe for hybridisation was determined using the manufacturer's concentration detection system.

2.5.14.2 Hybridisation and detection

Using radioactive-labelled DNA probes, the membrane was prehybridised in approx. 30 ml 10x Denhardt's solution (0.4 M HEPES buffer (pH 7.0), 3 x SSC, 0.02 mg/ml *E. coli* tRNA, 0.1% SDS, 0.2% (w/v) Ficoll, 0.2% (w/v) bovine serum albumin, 0.2% (w/v) polyvinylpyrrolidone 18 mg/L (w/v) phenol-extracted herring DNA) using PYREX™ hybridisation tubes (Fisher Scientific) and incubated at 65°C for 2 h with slow rotation. The ³²P-labelled probes were denatured by boiling and added to the pre-hybridised membrane in hybridisation tubes and incubated at 65°C, overnight with agitation. The hybridised membrane was then repeatedly washed in pre-incubated (50°C) 2x SSC containing 0.1% (v/v) SDS for up to two hours, semi-dried and exposed to X-ray film (Fuji) at -80°C. X-ray film was developed using a 100Plus™ automatic X-ray processor (All-Pro Imaging Corp.).

Using DIG-labelled DNA probes, The membrane was prehybridised in 20 ml hybridisation buffer (5x SSC, 50% (v/v) deionized formide, 0.1% (w/v) sodium lauroylsarcosine, 0.02% (w/v) SDS, 2% Blocking reagent) using PYREX™ hybridisation tubes (Fisher Scientific) and incubated at 42°C for 2 h with slow agitation. The DIG-labelled DNA probe was denatured by boiling for 10 min and added to a corresponding volume of pre-warmed (42°C) hybridisation buffer. Prehybridisation buffer was exchanged with probe and hybridisation buffer mixture, added to the membrane into the hybridisation tube and incubated at approx. 42°C (calculated optimal hybridisation temperature for probe), overnight with agitation. The hybridised membrane was repeatedly washed in 2x SSC, 0.1% SDS, incubated at room temperature for 2 min. The membrane was then repeatedly washed in 0.5x SSC, 0.1% SDS and incubated at 68°C for 15 min. The hybridised DNA

on the membrane was detected using NBT/BCIP colour detection (DIG-labelled probes), following the manufacturer's instruction.

2.5.15 Identification of cosmids from *E. festucae* cosmid library

A cosmid library of *E. festucae* F11 genomic DNA (Tanaka et al. 2005) was screened using previously prepared microtitre plates and corresponding filter (F11 Cosmid library Array, Australian Genome Research Facility (AGRF); stored at -80°C). The filter was screened using a [³²P]-labelled DNA probe (2.5.14.1). The filters were pre-hybridised in 30-40 ml of pre-incubated (65°C) buffer solution (0.36 M Na₂HPO₄ (51.1g/L), 50 mM NaH₂PO₄ (7.8 g/L), 243 mM SDS (70g/L), BSA (10 g/L), 0.25 M (w/v) EDTA pH8) and incubated at 65–68°C for 2-3 h. For the hybridisation, the [³²P]-labelled probe was denatured by boiling, added to the solution and incubated at 65–68°C, overnight. The hybridised filter was repeatedly washed in pre-warmed (65°C) wash solution (0.1 M SSC, 0.1% SDS) and incubated at 65°C for 30-60 min. The filter was wrapped in glad-wrap, exposed to X-ray film and incubated at -80°C for 6-8 h. X-ray film was developed using a 100Plus™ automatic X-ray processor (All-Pro Imaging Corp.). Once, the hybridised DNA-filter was visualised, the resulting film was aligned to a reference grid and the coordinates were used to identify the *E. coli* colonies containing the corresponding cosmids. Cosmid DNA was isolated (2.5.1.2) for further analysis and verified by PCR (2.5.7.1) and restriction enzyme digestion (2.5.3). DNA isolated (2.5.1.2) from the positive clones 30C2 and 33E10 were digested with appropriate enzymes (EcoRI and BamHI), fragments were separated by agarose gel electrophoresis and aligned to an *in silico* map.

2.6 Quantification of intracellular cAMP

2.6.1 Growth and harvest of fungal mycelia and extraction of cAMP

A total of 4-6 *E. festucae* cultures of the same strain were inoculated on solid PD medium (2.3.3.1), overlaid with a sterilised cellophane disc, for 4 days at 22°C. Cellophane disc with attached mycelia were then transferred onto the medium to be analysed and incubated for further 3 days at 22°C. Media tested for putative changes in intracellular cAMP were PD medium (2.3.3.1) and 3% water (H₂O) medium

(2.3.3.3) for nutrient starvation. Cultures were harvested, the initial inoculum was cut from the mycelia using a scalpel and the mycelia was transferred into a mortar and pestle, flash frozen and ground to a fine power under liquid nitrogen (N₂). Ground homogenized mycelia was lysed by treatment with 10 volumes of 0.1 M HCl and incubated at room temperature for 10 min, pelleted by centrifugation ($\geq 600 \times g$, 10 min) and the resulting supernatant was transferred into a fresh microcentrifuge tube. Supernatant was used immediately for analysis or stored at -80°C.

2.6.2 Quantification of cAMP by ELISA assay

Intracellular concentration of 3',5'-cyclic adenosine monophosphate (cAMP) was quantified using the direct cyclic AMP Enzyme-linked Immunosorbent Assay kit (Enzo Life sciences) and the non-acetylated assay, following the manufacturer's instructions. In the competition-based assay, the optical density was read at 405 nm to determine the cAMP concentration using a microplate reader (Polarstar Omega microplate reader (BMG LABTECH)). The results were calculated from the standard curve and data were analysed using a 4 parameter logistic (4PL) curve fitting program (Polar Omega Lab). The results were expressed as pmol cAMP per ml of total protein. Protein content was normalised by dividing the resulting picomole per ml determinations (pmol/ml) by the total protein concentration (mg/ml) in each sample. This is expressed as pmol cAMP per mg of total protein.

2.7 Plant methods

2.7.1 Seed sterilisation

Endophyte-free *L. perenne* seeds ('Samson'; AgResearch) were surface sterilized by soaking in 50% (v/v) H₂SO₄ for 30 min, repeatedly rinsing using tap water, followed by soaking in 50% (v/v) chlorine bleach for 30 min and repeatedly rinsing using sterile Milli-Q water. Surface-sterilized seeds were air-dried under sterile condition using ethanol-sterilised filter paper in a laminar flow cabinet. Seeds were stored at 4°C in sealed sterile petri dishes.

2.7.2 Seedlings growth conditions

Surface-sterilised seeds (2.7.1) were placed on 3% solid water medium (2.3.3.3) for germination and incubated at 22°C for 7 days in the dark in a vertical position. About 12 (round petri dish) to 20 (square petri dish) seeds were aligned in the lower quarter of the plate with the coleoptile germination point (Awn) facing upwards. After inoculation (2.7.3), plant seedlings were further incubated for 5-7 days in the dark, followed by incubation for 7 days in the light. Grown seedlings were planted in the Plant Growth Facility (Scottbase; Massey University).

2.7.3 Plant inoculation

Germinated 7 day-old *L. perenne* seedlings (2.7.2) were inoculated with freshly grown mycelia of *E. festucae* (2.3.3) under sterile conditions (Latch and Christensen 1985). A 1-2 mm block of freshly grown fungal mycelia was inserted into a shallow longitudinal cut (2-3 mm) between the mesocotyl and coleoptile, using a sterile scalpel under a dissecting microscope.

2.7.4 Standard plant growth conditions

L. perenne plants were grown in an environmentally controlled Plant Growth Facility (Massey University), at 22°C under artificial illumination with a day – night cycle (16 h light – 8 h dark; approximately 100 $\mu\text{E}/\text{m}^2/\text{s}$). Seedlings (2.7.2) were planted in root trainers filled with fungicide-free potting mix (AgResearch) and incubated for 10-12 weeks. Plants were watered with tap water as required.

2.7.5 Axenic culture plant growth conditions

For growth of *L. perenne* plants in association with *E. festucae* in axenic culture, inoculated *L. perenne* plants were planted into sterilised plastic containers, containing 50 ml MSO-Phytoagar (2.7.5.1) under sterile conditions. Plant-growth containers were covered with the appropriate lid, sealed using UV-surface sterilized parafilm to prevent anaerobic conditions and incubated at 22°C for 10-12 weeks under standard conditions (2.7.4).

2.7.5.1 Murashige and Skoog (MSO) medium

MSO-medium contained 0.43% (w/v) MSO and 0.75% (w/v) phytoagar, autoclaved and filled (approx. 50 ml) into autoclaved plant growth containers for axenic cultures.

2.7.6 Detection of endophyte infected plants

Endophyte-infected *L. perenne* plants (2.7.3) were identified by immunoblotting. A single tiller per plant was cut close to the base and pressed onto a nitrocellulose membrane (NCM). The membrane was then incubated in blocking solution (20 mM Tris, 50 mM NaCl, 0.5% (w/v) non-fat milk powder) for 2 h, rinsed and further incubated overnight at 4 °C, in blocking solution, supplemented with primary antibody (5 µl AB/5ml blocking solution; polyclonal rabbit antibody raised against homogenised mycelium of *Epichloë festucae* var. *lolii* (Christensen et al. 1993). The NCM was rinsed using blocking solution and incubated in an appropriate volume of blocking solution supplemented with the secondary antibody (2.5 µl AB/5ml blocking solution; goat anti-rabbit antibody with an alkaline phosphatase conjugate, Sigma) for 2 h. The NCM was rinsed using blocking solution and the presence of the endophyte was determined by incubation in the development solution (SIGMAFAST™ Fast Red TR/Naphthol AS-MX tablets (per 10 ml Milli-Q water)) for 15-30 min. The reaction was stopped by rinsing the NCM in Milli-Q water. Endophyte infection was identified by a strong red color reaction.

2.7.7 Extraction of apoplastic fluid (APF) from *L. perenne* plants

Apoplastic fluid from endophyte-infected or uninfected (uninoculated) *L. perenne* plants (2.7.4) was extracted as previously described (van Hove et al. 2002). Plant pseudostem tissue (approx. 5 cm) was cut and used to fill a 50 ml syringe barrel, which was sealed using a modified filter disk as stopper lid. Plant leaf material was covered with sterile Milli-Q water and vacuum was applied by pressure using consecutive pushing and pulling motion in 30 sec intervals. Once plant tissue was saturated with water, leaf tissue was removed from the syringe and gently dry-blotted using paper towel to remove the excess water on the outside of the leaf material. The plant material was then placed into prepared white 5 ml tips (tip cut to suitable length), placed in 15 ml Falcon tubes and incubated on ice. The

apoplastic fluid was collected by centrifugation (4300 rpm, 20 min, 4°C), transferred into a sterile 1.5 ml microcentrifuge tube and filter sterilized using 0.2 µm filter disks. The extracted apoplastic fluid was used immediately or stored at -80°C.

2.8 Microscopic analysis

2.8.1 In culture analysis

E. festucae cultures were grown on medium plates, consisting of approx. 15 ml solid PD (2.3.3.1) or water (2.3.3.3) medium with a sterilised microscope slide place on top and overlaid by a thin layer (approx. 5 ml) of water agar (1.5%) medium. Mycelial plugs (2.3.3), from freshly grown cultures, were inoculated at the edge of this overlaid-microscope slide and incubate for 7 – 10 days at 22°C. The microscopy slide was carefully cut out off the medium, including the covering overlay and attached grown mycelium. Hyphae were transferred to new microscope slide, stained with Calcofluor white (3 mg/ml) (Fluorescent Brighter 28; Sigma), which stains cellulose and chitin in the fungal cell wall and septa, and examined and imaged using the inverted fluorescence microscope (Olympus IX71) and U-MWU2 ultraviolet excitation cube (wideband) with filter set for differential interference contrast (DIC) and Calcofluor white staining.

2.8.1.1 Determination of hyphal fusion frequency

Hyphal fusion frequency was quantified by counting hyphal fusion events at 10 microscopic sites at similar areas of the fungal colony for eight biological replicates of each strain at 400x magnification.

2.8.2 In planta analysis

2.8.2.1 Confocal laser scanning microscopy (CLSM)

For microscopic examination of hyphal growth *in planta*, pseudostem tissue of infected ryegrass tillers (10-12 week post inoculation; 2.7.4, 2.7.6) were cut close to the tiller base into two longitudinal sections (1.5-2 cm). Isolated tissue was soaked in 95% (v/v) ethanol (and incubated at 4°C, overnight or up to 7 days), using 1.5 ml microcentrifuge tube, then soaked in 10% (w/v) potassium hydroxide and

incubated at room temperature for 3 -4 h. Plant tissue was repeatedly washed in PBS (pH 7.4) and finally soaked in PBS (pH 7.4) overnight at 4°C. Sample staining was achieved by pre-incubation at room temperature for 10 min and subsequent vacuum infiltration of the staining solution (0.02% (w/v) aniline blue (Sigma), 0.001% (w/v) WGA-AF488 (10 ng/ml; Wheat Germ Agglutinin-AlexaFluor®488; Invitrogen/Molecular Probes), 0.02% (v/v) Tween 20 in PBS (pH 7.4)) for 20–30 min. Hyphal growth *in planta* was then determined and imaged by CLSM using a Leica SP5 DM6000B confocal microscope (488 nm argon and 561 nm DPSS laser, x40 oil immersion objective, NA = 1.3) (Leica Microsystems). If not indicated otherwise, images are displayed as stack of 10 confocal images (z-section) using maximum intensity, with a sample depth of 5 – 10 µm and a step size of 0.5 - 1 µm, respectively.

2.8.2.2 Transmission electron microscopy (TEM)

For microscopic examination of hyphal ultrastructure *in planta* and host-tissue colonisation, pseudostem tissue from close to the base of infected ryegrass tillers (10-12 week post-inoculation; 2.7.4, 2.7.6) were cut into small sections (0.5 mm thickness). Tissue samples were fixed (3% glutaraldehyde, 2% formaldehyde in 0.1 M phosphate buffer (pH 7.2)); and incubated at room temperature for 1 h and small sections for light microscopy were stained using toluidine blue (Spiers and Hopcroft 1993, Christensen et al. 2002). Transverse sections of stained tissue samples were examined for TEM-preselection using light microscopy. Fixed samples were examined using TEM (Philips CM10 transelectron microscope) and imaged using an SIS Morada digital camera.

2.9 Statistical analyses

Alterations in fungal growth was quantified by determination of hyphal growth rate per day (2.4.2) using non-transfer (2.4.1.1) and transfer (2.4.1.2) experimental conditions in replicates of each experiment. The data was recorded in triplicate, for each biological replicate, for each strain on the respective growth medium. Statistical analyses were conducted in the SYSTAT statistical suite (version 13) (Wilkinson 2010). All data was tested for normal distribution using the

Kolmogorov Smirnov-Lilliefors Test (KSL) and transformed if necessary using Johnson's algorithm to render them amenable to parametric analysis. A level of significance of $p < 0.05$ was considered significant.

2.9.1 Carbon sources

Data from the transfer experiment was normally distributed (KSL), whereas from the non-transfer experiment required transformation by Johnson's algorithm $(-0.57+0.82*\ln((X-0.16)/(1.47-X)))$ ($n = 275$, all strains grown on each carbon source). For both experiments the differences between the wild-type and each of the mutant strains grown on each carbon source was assessed by the *Student's t test*. A paired t test was also used to assess significant differences for each of the strains grown on the various carbon sources in comparison to the control CD medium (2.3.3.5). Differences between two concentrations of respective carbon source, i.e. 100 mM and 10 mM, on the radial growth, for each stain, was further assessed by doubly repeat measure ANOVA and the *Student's t test*.

2.9.2 Amino acids

Data from the transfer experiment were normally distributed (KSL) while data from the non-transfer experiment required transformation ($n = 765$, all strains grown on each amino acid source) using Johnson's algorithm $(0.12+0.75*\ln((X+0.001)/(1.48-X)))$. For each experiment, the differences between the WTF11 and each of the mutant strains grown on each amino acid source was assessed by *Student's t test*. The paired t test was also used to assess significant differences for each of the strains grown on the various CD supplemented amino acid sources in comparison to the control CD media (2.3.3.5).

2.9.3 Environmental pH stress

Data for both the transfer and the non-transfer experiments were normally distributed (KSL). Significant differences between the wild-type and each of the mutant strains grown on each media was assessed by *Student's t test*. Differences for

each of the strains grown on the various media in comparison to the control CD medium (2.3.3.5) were also determined using the *Student's t test*.

2.9.4 Plant-derived molecules

Data for both the transfer and the non-transfer experiments were normally distributed (KSL). Significant differences between the wild-type and each of the mutant strains grown on each media was assessed by *Student's t test*. Differences for each of the strains grown on the various media in comparison to the control CD medium (2.3.3.5) were assessed by paired t test. Again, significant differences between the ethanol media with those of the two concentrations of the ethanol and linoleic acid media were also determined using the *Student's t test*.

Chapter 3 Bioinformatic analysis of the cAMP G protein-coupled receptors and phosphodiesterases in the *E. festucae* genome

3.1 Identification of G protein-coupled receptors in *E. festucae* genome

To identify the *E. festucae* genes encoding putative G-protein coupled receptors, the identified and partially characterised *N. crassa* GPCR sequences (Li et al. 2007, Cabrera et al. 2015) were used as queries for amino acid sequence blast (tblastn) against *E. festucae* genome (F11) using the *E. festucae* database (2.1.1; 2.1.2) (Table 3.1). To confirm that the *E. festucae* genes identified are indeed homologues a reciprocal tblastn was done, using the *E. festucae* amino acid sequences against the NCBI non-redundant database (2.1.2). Homologues for the closely related fungal species *M. oryzae*, *F. graminearum*, *T. atroviride* and *N. crassa* were also identified (Appendix 15). The *N. crassa* query blast and the reciprocal blast identified a total of 40 putative GPCR homologues in *E. festucae* (F11), including members in 13 out of 14 GPCR classes (Gruber et al. 2013, Cabrera et al. 2015). The putative GPCRs in *E. festucae* were analysed for typical GPCR-like topology and characteristic seven transmembrane domains using InterProScan, TMHMM 2.0, TMPred, Phobius, SMART and ExPASy Prosite independently (2.1.5), which was predicted by at least two programmes.

Table 3-1 Table of putative *Epichloë* GPCRs

Class	<i>E. festucae</i>		<i>N. crassa</i>		Identity (%)	<i>E</i> value	Description (signature domain)
	Name	Locus (EfM3.)	Name	Locus (NCU)			
I	<i>pre2</i>	072620	<i>pre-2</i>	05758	23.8	6e ⁻³³	Pheromone (STE2-type)
II	<i>pre1</i>	016320	<i>pre-1</i>	00138	26.7	e ⁻⁵⁰	Pheromone (STE3-type)
III	<i>gpr4</i>	044840	<i>gpr-4</i>	06312	20.1	6e ⁻³⁸	carbon sensory (Git3-domain)
IV	<i>gpr5</i>	042760	<i>gpr-5</i>	00300	35.7	e ⁻⁴¹	nitrogen sensors (Stm-1 like)
	<i>gpr6</i>	019030	<i>gpr-6</i>	09195	52.8	4e ⁻⁴⁹	(PQ-loops)

Class	<i>E. festucae</i>		<i>N. crassa</i>		Identity (%)	<i>E</i> value	Description (characteristics)
	Name	Locus (EfM3.)	Name	Locus (NCU)			
V	<i>gpr1a</i>	049190	<i>gpr-1</i>	00786	31	6e ⁻⁵³	cAMP receptor- like
	<i>gpr1b</i>	080640			30	7e ⁻⁴⁰	(Dicty_CAR domain)
	<i>gpr2</i>	066920	<i>gpr-2</i>	04626	41.4	5e ⁻⁹³	(secretin-like; gpcr-2 family)
			<i>gpr-3</i>	09427	37.7	2e ⁻⁸⁵	
VI	<i>gpr7a</i>	007810	<i>gpr-7</i>	09883	43.3	e ⁻¹³⁶	gprK-like
	<i>gpr7b</i>	040610	<i>gpr-7</i>	09883	44.8	e ⁻¹²⁷	(RGS domain)
	<i>gpr7c</i>	059600	<i>gpr-7</i>	09883	34.7	4e ⁻⁶²	
VII	<i>gpr8</i>	118420	<i>gpr-8</i>	03253	53	e ⁻¹²⁸	rat growth hormone releasing factor
VIII	<i>gpr9</i>	063600	<i>gpr-9</i>	03238	60.7	e ⁻¹⁷⁰	mPR-like (PAQR)
	<i>gpr10</i>	029580	<i>gpr-10</i>	04986	56.8	e ⁻¹⁰³	(HlyIII-superfamily)
	<i>gpr10b</i>	021530		04987	32.4	5e ⁻³⁷	
IX	<i>ops1</i>	031650	<i>orp-1</i>	01735	34.9	2e ⁻³⁸	Microbial opsin
			<i>nop-1</i>	10055	30.3	6e ⁻³²	(BAC_rhodopsin)
X	<i>gpr11</i>	071470	<i>gpr-11</i>	00182	60.8	e ⁻¹⁵⁹	PTM1 (Lung7_TM superfamily)
XI			<i>gpr-12</i>	00005			GPCR89/ ABA -GPCR domain)
XII	<i>gpr13</i>	38560	<i>gpr-13</i>	06629	23.7	6e ⁻²³	Family C-like
XIII	<i>gpr14a</i>	040570	<i>gpr-14</i>	06987	44	e ⁻¹²⁸	GPR11 (DUF300 superfamily)
	<i>gpr14b</i>	021230			17	4e ⁻²⁶	
IV	19 members*		25 members				Pth-11-like
	(* see Table 3.2)						

The *E. festucae* genome possesses two genes encoding putative homologues of the fungal pheromone receptors Pre1 (EfM3.016320; Supplementary 1 and 2) and Pre2 (EfM3.072620; Supplementary 3 and 4), which contain the typical STE2 (pfam02116) and STE3 (pfam02076) protein domain of the fungal GPCR classes I and II, respectively.

One gene encoding the Git3-domain containing (pfam11710; IPR023041) putative carbon sensor of class III GPCRs, Gpr4 (EfM3.044840; Supplementary 5 and 6), and the two putative class IV Stm1-like nitrogen sensors Gpr5 (EfM3.042760;

Supplementary 7 and 8) and Gpr6 (EfM3.019030; Supplementary 9 and 10), containing two PQ-loop repeats (pfam04193; IPR006603), were identified.

The genome of *E. festucae* possess three genes encoding class V cAMP receptor-like GPCRs, *gpr1a* (EfM3.049190), *gpr1b* (EfM3.080640) and *gpr2* (EfM3.066920), harbouring a Dicty_CAR domain (pfam05462) based on structural relationship to the four cAMP receptors of *Dictyostelium discoideum* (Lafon et al. 2006, Li et al. 2007). While Gpr1a and Gpr1b were characterised as secretin-like GPCRs, all three GPCRs contain the mammalian family-2 GPCRs domain (IPR000832, IPR017981), described as acting upstream of the cAMP/PKA signalling pathway. Interestingly, the gene for the cAMP receptor-like protein GPR-2 (NCU04626) of *N. crassa* shows high homology to the *E. festucae* gene *gpr2* (EfM3.066920), while a GPR-3 (NCU09427) homolog appears to be absent in the *E. festucae* genome. The two genes *gpr1a* (EfM3.049190) and *gpr1b* (EfM3.080640) in *E. festucae* show high homology to GPR-1 (NCU00786) of the cAMP receptor-like protein class in *N. crassa*. Interestingly, the reciprocal blast of *E. festucae* *gpr1a* and *gpr1b* identified a previously unidentified class V receptor of *M. oryzae* (MGG_11962).

Unlike most filamentous fungi, which possess a single gene encoding a class VI GPCR that contains a cytoplasmic regulator of G protein signalling (RGS) domain (pfam00615; IPR016137) in addition to the seven-transmembrane domains, the *E. festucae* genome contains three. The *Trichoderma* spp., *T. atroviride*, *T. virens* and *T. reesi*, also possess three class VI GPCRs, respectively (Gruber et al. 2013). The predicted *E. festucae* homologues to the single Gpr7 in *N. crassa* (NCU09883), Gpr7a (EfM3.007810; Supplementary 11 and 12), Gpr7b (EfM3.040610; Supplementary 13 and 14) and Gpr7c (EfM3.059600; Supplementary 15 and 16) share sequence similarity to the *T. atroviride* receptors, TaGpr7a, TaGpr7b and TaGpr7c, respectively (Gruber et al. 2013, Cabrera et al. 2015).

The *E. festucae* Gpr8 (Ef.M3.118420; Supplementary 17 and 18) and *N. crassa* homolog Gpr-8 (NCU03253) represent the class VII GPCRs, that share similarity to the mammalian rat growth hormone-releasing factor receptor, initially identified and described in *M. oryzae* (Kulkarni et al. 2005). The Gpr8 homolog in *E. festucae* contains a GPCR family 2-like domain (IPR017981) and was initially identified during the reciprocal blast of the *E. festucae* class V GPCR Gpr2 against the NCBI database of *N. crassa*.

Four genes of the *E. festucae* genome grouping into the PAQR-GPCR class VIII, which contains receptors responding to hormones like progesterone and adiponectin therefore classified as progestin-adipoQ receptors (PAQR) (Tang et al. 2005). The predicted polypeptide of *E. festucae* Gpr9 (EfM3.063600; Supplementary 19 and 20), Gpr10 (EfM3.029580; Supplementary 21 and 22), Gpr10b (EfM3.021530; Supplementary 23 and 24) and Gpr9b (EfM3.064650; Supplementary 25 and 26) share sequence identity with the *N. crassa* Gpr-9 (NCU03238) and Gpr-10 (NCU04987), and contain a long N-terminal tail and a AdipoR/Haemolysin-III-related domain (IPR004254; pfam03006; HlyIII-superfamily) (Narasimhan et al. 2005, Gruber et al. 2013, Cabrera et al. 2015). The *E. festucae* Gpr9b predicted protein exhibits a GPCR-atypical topology with nine transmembrane domains, a long cytoplasmic N-terminal and extracellular C-terminal sequence. Despite the non-classical GPCR structure, homologues of this protein were categorised as class VIII GPCRs in fungal species like *N. crassa* (NCU08283), *S. cerevisiae* (Izh2) and *Trichoderma* spp. (Narasimhan et al. 2005, Tang et al. 2005, Gruber et al. 2013). However, there is no evidence that these proteins have classic GPCR functions. Due to the lack of evidence, the *E. festucae* Gpr9b and its homolog in *M. oryzae* (MGG_01538) were not classified as canonical GPCRs and grouped into the class of Pth11-like receptors which contain members with atypical GPCR topology (Table 3.2).

The *E. festucae* genome also contains the class IX opsin receptor Ops1 (EfM3.031650; Supplementary 27 and 28), which shares higher sequence homology to the *N. crassa* bacteriorhodopsin-like domain-containing protein NCU01735 (e value $2e^{-38}$) than to the characterised opsin receptor NOP-1 (NCU10055; $6e^{-32}$), suggesting *E. festucae* may only have one gene encoding an opsin receptor.

The *E. festucae* Gpr11 (EfM3.071470; Supplementary 29 and 30) was identified as homolog for the *N. crassa* Gpr-11 (NCU00182) of the putative PTM1-like GPCRs of class X, which contains a Lung_7-TM_R domain (pfam06814) and shares similarity to the putative tumor necrosis factor receptor-like GPCR PTM1 of *S. cerevisiae*. In addition to *N. crassa*, this receptor was also described for *Trichoderma* spp. and *Verticillium* spp. and homologues were identified in *A. nidulans* and *M. oryzae* (Zheng et al. 2010, Gruber et al. 2013).

No homolog for the *N. crassa* Gpr-12 (NCU00005) receptor, a member of the class XI GPCRs, was identified in the genome of *E. festucae*. This class contains putative receptors related to human GPR89A receptors (ABA_GPCR domain; pfam12430) and was identified in various filamentous fungi incl. *N. crassa* and *Trichoderma* spp. (Gruber et al. 2013, Cabrera et al. 2015).

With similarity to mammalian metabotropic glutamate/pheromone receptors (family-C), *E. festucae* possess a member (Gpr13; EfM3.38560; Supplementary 31 and 32) of the class XII family-C like GPCRs that contains a DUF3112 domain of unknown function (pfam11309; IPR021460), a long extracellular N-terminal and cytoplasmic C-terminal sequence. Homologues of this putative fungal receptor were described in *N. crassa* (Gpr-13; NCU06629), *Trichoderma* spp. as well as *Verticillium* spp. and also identified in *A. nidulans* and *M. oryzae* (Zheng et al. 2010, Gruber et al. 2013, Cabrera et al. 2015).

The putative receptor protein Gpr14a (EfM3.040570; Supplementary 33 and 34) in *E. festucae*, homologous to the *N. crassa* Gpr-14 (NCU06987), represents the member of the recently identified GPCR class XIII (Gruber et al. 2013, Cabrera et al. 2015). Based on sequence identity to the putative DUF300 domain-containing GPCR in *Phytophthora sojae* (GPR11), homologues were identified in various filamentous fungi including *Trichoderma* spp., *M. oryzae* and *A. fumigatus* (Wang et al. 2010, Gruber et al. 2013). Similar to *M. oryzae* (MGG_15321), *E. festucae* possess a second orthologous, Gpr14b (EfM3.021230; Supplementary 35 and 36). However, a DUF300 domain (pfam03619) was not predicted for the *E. festucae* proteins using InterProScan, SMART or ExpASy Prosite.

Using the *N. crassa* and the *M. oryzae* amino acid sequences of the described GPCRs of the PTH11-like proteins as query, a total of 19 putative GPCRs of the highly diverse class XIV were identified in the genome of *E. festucae* (Table 3.2). Only a subset of six PTH11-like receptors was predicted to contain the fungal-specific cysteine-rich extracellular CFEM domain (pfam05730) as found in *M. oryzae* Pth11 (Kulkarni et al. 2005, Gruber et al. 2013, Cabrera et al. 2015). Interestingly, no direct *E. festucae* homolog of the *M. oryzae* Pth11 receptor was identified. Pth11-6 was predicted to only contain five transmembrane domains, while Pth11-19 contains nine, representing GPCR atypical topology such as Gpr9. Also similar to Gpr9, Pth11-18 has an intracellular N-terminal and extracellular C-terminal sequence. The

PTH11-like proteins comprises the highest number of GPCRs within the individual fungal species, while also displaying the highest variety in number and structural differences among filamentous fungi, including *N. crassa* (25 members), *M. oryzae* (61 members), *F. graminearum* (106 members), *T. atroviride* (38 members), *T. reesei* (35 members), *T. virens* (52 members), *A. nidulans* and *A. flavus* with 56 and 55 members, respectively (Kulkarni et al. 2005, Gruber et al. 2013, Affeldt et al. 2014, Cabrera et al. 2015). Based on their sequence homology to the *N. crassa* GPCRs, the identified *E. festucae* GPCRs were classified into the same 14 classes.

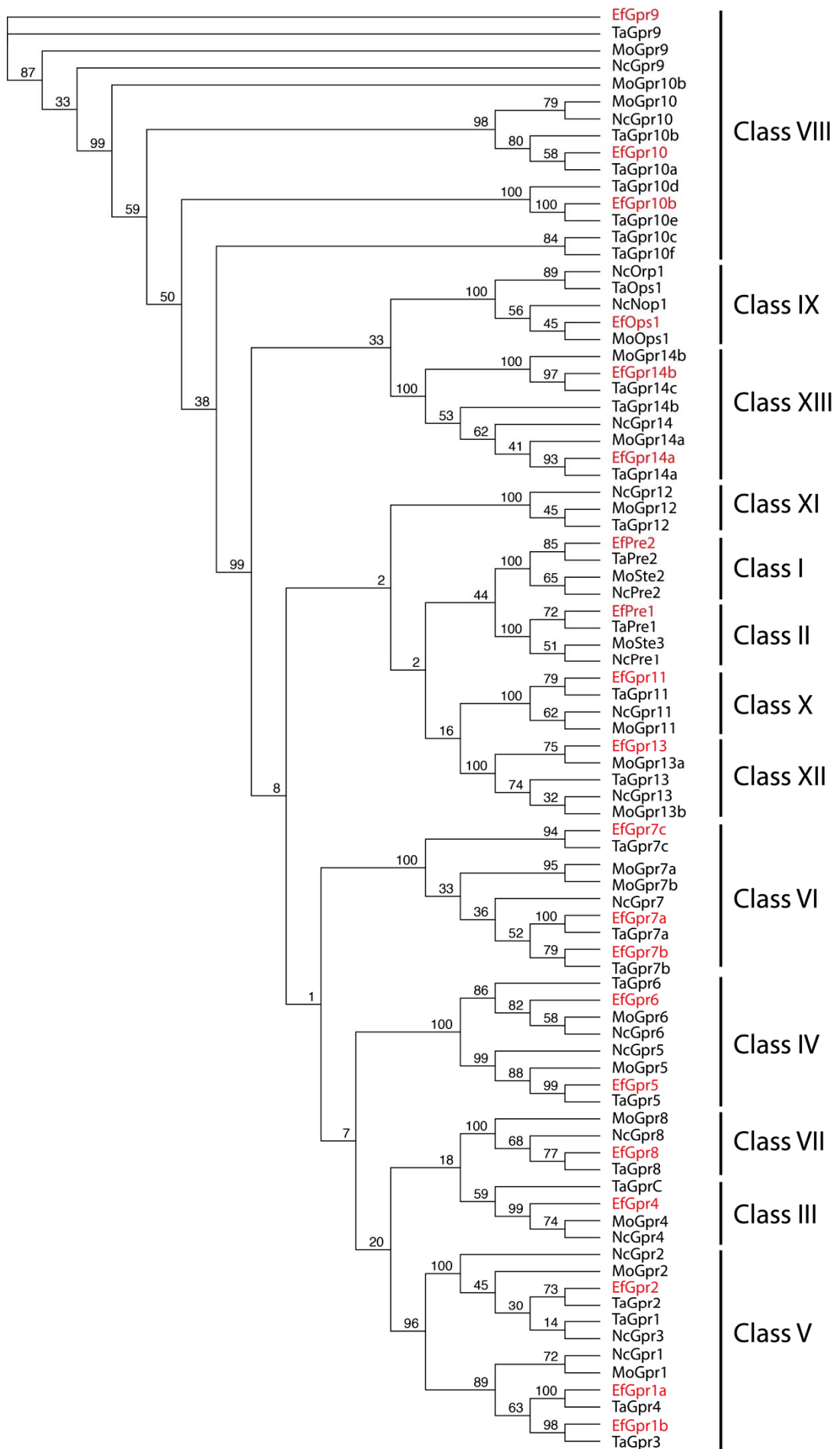
A phylogenetic analysis was carried out to test the distribution of the putative GPCRs of *E. festucae* into the different classes alongside the fungal species *N. crassa*, *M. oryzae* and *T. atroviridae* (Fig. 3.1). Because of the high diversity and structural differences among the Pth11-like GPCRs, the members of the class XIV were not included in this phylogenetic analysis.

Table 3-2 *Epichloë* Class XIV - Pth11-like GPCRs

Name	Locus	Comments	Reference
<i>pth11-1</i>	EfM3.055430	Signal peptide- and CFEM-domain	Supplementary 37
<i>pth11-2</i>	EfM3.012710	Signal peptide- and CFEM-domain	Supplementary 38
<i>pth11-3</i>	EfM3.031700	Signal peptide- and CFEM-domain	Supplementary 39
<i>pth11-4</i>	EfM3.041190	CFEM-domain	Supplementary 40
<i>pth11-5</i>	EfM3.079370	CFEM-domain	Supplementary 41
<i>pth11-6</i>	EfM3.008620	CFEM-domain; 5 TM	Supplementary 42
<i>pth11-7</i>	EfM3.056870	Signal peptide-domain	Supplementary 43
<i>pth11-8</i>	EfM3.042570		Supplementary 44
<i>pth11-9</i>	EfM3.028870		Supplementary 45
<i>pth11-10</i>	EfM3.008360		Supplementary 46
<i>pth11-11</i>	EfM3.001250		Supplementary 47
<i>pth11-12</i>	EfM3.048960		Supplementary 48
<i>pth11-13</i>	EfM3.032250		Supplementary 49
<i>pth11-14</i>	EfM3.012500		Supplementary 50
<i>pth11-15</i>	EfM3.025720		Supplementary 51
<i>pth11-16</i>	EfM3.047160		Supplementary 52

<i>pth11-17</i>	EfM3.062190		Supplementary 53
<i>pth11-18</i>	EfM3.000460	Reverse GPCR topology	Supplementary 54
<i>pth11-19</i>	EfM3.159360	9 TM	Supplementary 55
<i>gpr9b</i>	EfM3.064650	9 TM; Reverse GPCR topology	Supplementary 26

Figure 3-1 Classification of fungal G protein-coupled receptors: Maximum-likelihood dendrogram showing phylogenetic classification for fungal G protein-coupled receptors based on the classification system used for *N. crassa* [Cabrera et al., 2015]. Fungal GPCR classification and fungal species with used Gene names and identifier as following: Class I of Ste2-like pheromone receptors *Neurospora crassa* NcPre1 (NCU00138), *Magnaporthe oryzae* MoSte3 (MGG_06452), *Trichoderma atroviride* TaPre1 (ID_147894), *Epichloë festucae* EfPre1 (EfM3.016320); Class II of Ste3-like pheromone receptors NcPre2 (NCU0575), MoSte2 (MGG_04711), TaPre2 (ID_36032), EfPre2 (EfM3.072620); Class III of Git3 domain-containing putative carbon sensor NcGpr4 (NCU06312), MoGpr4 (MGG_08803), TaGprC (ID_246916), EfGpr4 (EfM3.044840); Class IV of PQ loop repeat containing Stm1-like nitrogen sensors with respective homologues NcGpr5 (NCU00300) and NcGpr6 (NCU09195), MoGpr5 (MGG_04698) and MoGpr6 (MGG_02855), TaGpr5 (ID_238619) and TaGpr6 (ID_300620), EfGpr5 (EfM3.042760) and EfGpr6 (EfM3.019030); Class V of cAMP receptor-like GPCRs NcGpr1 (NCU00786), NcGpr2 (NCU04626), NcGpr3 (NCU09427), MoGpr1 (MGG_11962), MoGpr2 (MGG_06738), TaGpr1 (ID_160995), TaGpr2 (ID_50902), TaGpr3 (ID_83166), TaGpr4 (ID_81233), EfGpr1a (EfM3.049190), EfGpr1b (EfM3.080640) and Ef_Gpr2 (EfM3.066920); Class VI of RGS-containing gprK-like GPCRs NcGpr7 (NCU09883), MoGpr7a (MGG_13926), MoGpr7b (MGG_11693), TaGpr7a (ID_293686), TaGpr7b (ID_40423), TaGpr7c (ID_210761), EfGpr7a (EfM3.007810), EfGpr7b (EfM3.040610) and EfGpr7c (EfM3.059600); Class VII of GPCRs with similarity to the rat growth hormone releasing factor receptor NcGpr-8 (NCU03253), MoGpr8 (MGG_00532), TaGpr8 (ID_133045), EfGpr8 (EfM3.118420); Class VIII of mPR-like GPCRs (PAQR) NcGpr9 (NCU03238) and NcGpr10 (NCU04987), MoGpr9 (MGG_04679), MoGpr10 (MGG_16855) and MoGpr10b (MGG_09091), TaGpr9 (ID_136196), TaGpr10a (ID_290047), TaGpr10b (ID_210209), TaGpr10c (ID_142943), TaGpr10d (ID_46847), TaGpr10e (ID_142946), TaGpr10f (ID_152366), EfGpr9 (EfM3.063600), EfGpr10 (EfM3.029580) and Ef_Gpr10b (EfM3.021530); Class IX of microbial opsin receptors NcNop1 (NCU10055), NcOrp1 (NCU01735), MoOps1 (MGG_09015), TaOps1 (ID_210598), EfOps1 (EfM3.031650); Class X of GPCRs containing the Lung_7TM_R domain NcGpr11 (NCU00182), MoGpr11 (MGG_06418), TaGpr11 (ID_210445), EfGpr11 (EfM3.071470); Class XI of GPCR89/ABA NcGpr12 (NCU00005), MoGpr12 (MGG_05269), TaGpr12 (ID_93659); Class XII of Family C-like GPCRs NcGpr13 (NCU06629), MoGpr13a (MGG_07414), MoGpr13b (MGG06103), TaGpr13 (ID_130836), EfGpr13 (EfM3.038560); Class XIII of GPCRs with similarity to *Phytophthora sojae* GPR11 NcGpr14 (NCU06987), MoGpr14a (MGG_01467), MoGpr14b (MGG_15321), TaGpr14a (ID_152316), TaGpr14b (ID_296436), EfGpr14a (EfM3.040570), EfGpr14b (EfM3.021230). Values above branches indicate bootstrap values based on 100 replicates.



3.2 Bioinformatic approach to characterize cAMP-receptor like GPCRs in *Epichloë* spp.

The class V GPCRs are predicted to act upstream of the cAMP/PKA signalling pathway. To characterise the predicted cAMP receptor-like GPCRs Gpr1a, Gpr1b and Gpr2 in *E. festucae*, their predicted amino acid sequences were aligned to the appropriate homologues from *N. crassa*, *F. graminearum*, *M. oryzae*, *T. atroviride* closely related *Metharizium acridum*. Based on the tblastn result, the *E. festucae* Gpr1a and Gpr1b, both hit *N. crassa* Gpr-1. Hence both were compared to the corresponding Gpr-1 sequences by multiple sequence alignment using MAFFT (v7.017).

E. festucae Gpr1a (EfM3.049190) shows 28% amino acid identity to the Gpr-1 protein from *N. crassa* (NCU00786), 44.4% identity to the *F. graminearum* homologue Gpr1 (FGSG_09693), 30% identity to the *M. oryzae* homologue (MGG_11962) and 57% identity to the *T. atroviride* TaGpr4 (TRIATDRAFT_81233), while *E. festucae* Gpr1b (EfM3.080640) shows 26.3% amino acid ID to *N. crassa* Gpr-1, 49.1% identity to the *F. graminearum* Gpr2 (FGSG_05239) homologue and 28% identity to the *M. oryzae* homologue and 53.8% identity to the *T. atroviride* (TaGpr3 (TRIATDRAFT_83166)). The amino acid sequence alignment show, high similarity along the characteristic seven transmembrane domains as well as the typical low similarity along the variable sequence covering the third intracellular loop (ICL3) and the intracellular carboxy-terminal domain for Gpr1a (Fig. 3.2) and Gpr1b (Fig. 3.3).

Figure 3-2 Multiple sequence alignment of *E. festucae* Gpr1a homologues: The predicted amino acid sequence of *E. festucae* Gpr1a (Ef_Gpr1a) is aligned with the corresponding homologues *N. crassa* Nc_Gpr1 (NCU00786), *F. graminearum* Fg_Gpr1 (FGSG_09693) and Fg_Gpr2 (FGSG_05239), *M. oryzae* Mo_Gpr1 (MGG_11962), *T. atroviride* Ta_Gpr4 (TRIATDRAFT_81233) and *M. acridum* Mac_Gpr1a (MAC_03969). *E. festucae* Gpr1a displays 30% amino acid identity to *N. crassa* Gpr-1, 44% identity to the *F. graminearum* homologue, 30% identity to the *M. oryzae* homologue, 67% to the *M. acridum* homologue and to and 58% identity to the *T. atroviride* homologue. ClustalW was used to align GPCR sequences, with conserved residues are shaded in grey. Red bars above the sequence mark the predicted seven transmembrane domains (TM I – TM VII).

TM I **TM II**

Ef_Gpr1a 10 20 30 40 50 60 70 80
 Mac_Gpr1a - MESS - - DDGS L STEHTNT I I T I E R T G A G L S M A I L L T V I S Y L A F A K L R K T P N L F L V F A S I A N A G A
 Ta_Gpr4 - M H P P P H D T S G S E L S A T Q I E I L I T I E R T G A G L S M V A I T L L S F L L F A R L R K T P N L F L V F A S I A N A G A
 Fg_Gpr1
 Fg_Gpr2 - M S H K Y I S G R D P D V L D E G E R S I T V L F E R I G G S T S L L A V L L F I A Y A L V P V K R N V Q N T F F I F A S I A N V G A
 Mo_Gpr1 - M E V R N S I S G Q R E T A A D S T I M A F D P D Q R Y I L S T L E R V G G A L S L V G V S M I F V T F Y A S K R I R T V P N T F I L F A S I A N V G A
 Nc_Gpr1 **M D D E I G T T Q A Q V E Q P P V E Y S Q G Y M N L T Q T Q R N T I E H V E R I G A S L S L L G V F L I F I A Y G L F A R V R T V P N T F I L F A S I A N V G A**

TM III **TM IV**

Ef_Gpr1a 90 100 110 120 130 140 150 160
 Mac_Gpr1a S I A S N M G Y D G L R M G Y N S A L C Q A Q G F I F E W F M Q A D P P W S F A M A V N V F L V F F N N A D P S L F R K Y T W Y C I I C F G G P M V P A V Y L
 Ta_Gpr4 S I A S N M I G Y D G L D R G E S T L C Q A Q G F I F E W F M Q A D P P W S F A M A F N V F L V F F N N A N P S M F Q K Y K W Y C V I C F G G P L L P A V Y L
 Fg_Gpr1 S I A S N M I G Y D G L D R G E S T L C Q A Q G F I F E W F M Q S D P P W S F A M A F N V F L V F F C N A D P R M F R S A W Y C I I C F G G P L I P A V Y L
 Fg_Gpr2 S C A S I T A M D G L E L G Y A S L C Q A Q S F M F H M F M Q S D P P W S L A M A F N V F L V F F F R A S P D S F R K R W W Y C I I C F G G P F A I A I A L
 Mo_Gpr1 C V A S L I A L E G I E G E T S P L C Q T Q A F L F E M F M Q S D P P W S F A M A I N V F L V F F W S T N P T S F R K R L W Y C A I C F G G P A V P A F I C
 Nc_Gpr1 S T A C F I G Y A G I V A G E N S A L C H T Q A F L L E M F M Q S D P P W S L A M A I N V F L V F F F A L N P N A F R D Y L W Y C L V C Y G L P S V P A I Y L

TM V

Ef_Gpr1a 170 180 190 200 210 220 230 240
 Mac_Gpr1a V A L Q G D P K G P V I G D A A L W C W I S P S W S I V R L Y A Y I P I W I C I L L S I I Y I A V G C Y V F R R R N Q L R N F T I P E L I R G R V N V S L S
 Ta_Gpr4 V S I R D E E K G P V F G D A A L W C W I R P E W S I V R L Y A Y I P I W I C I L L S I F I Y I A V G Y H V F R S R N Q L R N L T F Q H P T S N W R N G S L T
 Fg_Gpr1 I S I R N S P R G L M F G D A T L W C W I G T D W S L V R L Y A Y I P I W I F S F L S I M I Y I A V G Y H V F H A R N M L R D L V D G M K V G R S D S I P Y
 Fg_Gpr2 L L V R N P N R G L V P G Q A I I W C W V Y R D W E G I R I I T Y Y M L I W V C I A G S L L F Y F M V G Y H V F R S R N R L K S L S A S K S R E P A A D P S Q
 Mo_Gpr1 L F Y A P P G G - A Y I G D A I L W C W I D N N F N L R I W T Y Y L P I W V C I F L S A V I Y V A V G Y Q V F H Q R N Q L R N L T L S N P G K E T S T S D V R
 Nc_Gpr1 L A H S P A T - T R Y Y G N A T L W C W I A D T W N P L R I Y T Y Y L P I W T C I F L S G L V Y L A V G Y Q V F H Q R N Q L R N L T F S N Q G K N Y S G S E H I

Ef_Gpr1a 250 260 270 280 290 300 310 320
 Mac_Gpr1a G S E N R I S G E G S F A R P N E W Y G L A Y T E V H I T T D Y P
 Ta_Gpr4 D S E N R I S G E A N P T R T N V C Y G L A I T E V Q V T I N F P
 Fg_Gpr1 A S D A G D S A E E S L T R K I D H Y G T A T T E V Q V T S I T P
 Fg_Gpr2 S S S E H R G S S E A V A P P H D I S E S G D T D S Y P Q N L I G R Q E F Y G T A Y T E V Q I R E E P
 Mo_Gpr1 T Q G L P R V D L L T V P Q D C F Y G T I Y V D I Q V V H S T A
 Nc_Gpr1 D S A E K N L T R H G S Y Y G T V Y T E V Q V T T M D H Q C D A H T T H S T P P P T P P N N W N S N S N T T L
 Ef_Gpr1a 330 340 350 360 370 380 390 400
 Mac_Gpr1a E L G E K H S Y G I S A G R D S P C P T V I P M D L S N H P G C Y G T V Y T Q V E V N I S D N - T D F Q P M T P L S P A P S I T E
 Ta_Gpr4 G F D S Q E A I A S P T A A H S A E
 Fg_Gpr1 G F V D E H V P V L P A A V H R T P
 Fg_Gpr2 E N D Y P G L P A I P P A I Y A H G P T
 Mo_Gpr1 R Q A T H H G L A Q P A T A H A G S N
 Nc_Gpr1 S S N H L P E P R P A Y
 Ef_Gpr1a 410 420 430 440 450 460 470 480
 Mac_Gpr1a T P P P C Y H P W V S T A T F P F D L E A C N G S G P S Q T N F N A G I N Q D S F A Q P P L P R P L S P C G N P N C H Y A N I P N A I F P I P P P A S
 Ta_Gpr4 V P L A T H P P G Q N N S I H P W D S N Y S S S S S S E D H I V P P A A V Y A G S S S P P F G V H V H H A T N E T T H N G V P K S S L K K T T T Y I S Q G D R
 Fg_Gpr1 S R M C G G - - L S H N D S Q A E F R A R P T Q Q F E T T C S S - - - - G G R H T N R T I L S G R F G T L T S T A S M K L R R L D P V K M A Y L R T S F I
 Mac_Gpr1a S R M R G R S W L D S H N D S D S E - R V V P T Q L F E T T C S S - - - - G G R Y T N N N S L V G R F G A L K S T A S M K L R R L D P V K M A Y L R T S G I
 Ta_Gpr4 I V S R G S S W V P V H G L G Y S P E A F G N T P Q R Y A T I T - - - - A R Q P E Q S T F F S L R H I V R S N A S L K L R L D P V K M A Y L R T S F I
 Fg_Gpr1 P P R I Q S W V L P G S F E Q L E R T T S G R A Q R F E T V C T S S - - - - D S T P Q P S T L I T L R A I K S N A S L K L R L D P V K M A Y L R T S F I
 Fg_Gpr2 T T R S S S P Q V S F D E P S T G F P N S S H Y F S T S I S P G - - - - V V A Q T S S E S P L R R M T S A T S R T V S K F K V D D P I R A Y L R T S F I
 Mo_Gpr1 P T T K R Q A T A S A A A T H - R S S P P P Q P Q T F S I T S V I T A A P R P K R R S T S R P S V L T R V Q S S G H R I T A K L R H M D P V K L A Y L R T S F I
 Nc_Gpr1 P Y H H P F G Y G H T Y S S Y N R T S N T T T G T H Q V H A S S C G H Q S A S H Q T R S H T L S L S L R R P P F R K F W A K L H R L D P T M L A Y L R T S F I

TM VI

Ef_Gpr1a 490 500 510 520 530 540 550 560
 Mac_Gpr1a F G I S Y L I T W I P S S Y N R L Y S L A N E G Q V S Y S L S I A S G C V L P L Q G V W N A I I F F T T S W S A V R A P A T
 Ta_Gpr4 F G F A T I T W I P S S Y N R L Y S L T Y H G R V N F Q L S Y A S G C V L P L Q G V W N A L I Y F T T S
 Fg_Gpr1 F G F A T I T W I P S S Y N R L Y S L T H G D R I S F S L S V A S G C V L P L Q G F W N T L I Y F T T S W K V F R E E V R
 Fg_Gpr2 F A L S Y L V T W I P S S L N R I H S W L F G - K S P F E F H V A T A A V L P L Q G L W N A V I F F V T S W K P L K E W Y R N
 Mo_Gpr1 F A I S Y L V T W I P S S I N R V Y N L V Y P E Q A S Y G L N L A S A A V L P L Q G V W N A V I Y F S T S H K I L R E E L E V A S S R R P V L R R
 Nc_Gpr1 F A I S T A V T W I P S S I N R V H S L L Y P K D T S Y P L N L A S A V L P L Q G V W N A V I F A A T W V V L R E E V D G L W K R S S L G A W W E R R G R K

TM VII

Ef_Gpr1a 570 580 590 600 610 620 630 640
 Mac_Gpr1a A V K A R F G Y G - H R E Y P R G T T R L D S R L G L S S T D T S D D F G E S Q V P G K K W C G
 Ta_Gpr4 T L K A R L G Y G V C E Y P R - S T A L E S R L G I S S V E T Y D S F N E S Q C H A T R R C R
 Fg_Gpr1 T A K A E W F K R P E E C T D G I R L N S R L G I F K G D Y R D T L E R T R P V R A G S T E
 Fg_Gpr2 I G E P T H Q D R E M I Q T R D E H D E H V G R S G E S F L D D T D S G S D V E L R R M G
 Mo_Gpr1 V L W L R M I D P S S H L V G V D G G S L D R A R - S A G V Y S G S V C H G G P S G A V P P A V A S P A F E R T T T R - - - - G G R
 Nc_Gpr1 **G R G R G R G R G T T T T T S E A R T A V N M M M M G G G G G H G H G Q R G V R L G S D G L P R P S P P P P P F S T T T A A A T T T T T S G A G G R K**

Ef_Gpr1a 650 660 670 680 690 700 710
 Mac_Gpr1a C S R C C G G D E T E I Y E H E K
 Ta_Gpr4 C D K F V G - E A V R L E D W D G C A S P S P S N S S A G R R R Q T M R R V
 Fg_Gpr1 D A E K S V T E
 Fg_Gpr2 E A P G K R S S S L
 Mo_Gpr1 L S R H Y S S D A V E M N - - - - T R N P R I G - - - - S N V R V Q R G K G Q L D I S L
 Nc_Gpr1 **P T T Q G Y K A W R N G X G G S Y N G Y G V H S T V M K D D D F L E T R S H C S G A G G G G K K S G K R G P M D P N R L G T V R V I R D G S L**

Figure 3-3 Multiple sequence alignment of *E. festucae* Gpr1b homologues: The predicted amino acid sequence of *E. festucae* Gpr1b (Ef_Gpr1b, EfM3.080640) is aligned with the corresponding homologues *N. crassa* Nc_Gpr1 (NCU00786), *F. graminearum* Fg_Gpr2 (FGSG_05239) and *M. oryzae* Mo_Gpr1 (MGG_11962). *T. atroviride* Ta_Gpr3 (TRIATDRAFT_83166), *M. acridum* Mac_Gpr1b (MAC_01277). *E. festucae* Gpr1b displays 30% amino acid identity to *N. crassa* Gpr-1, 50% identity to the *F. graminearum* homologue, 30% identity to the *M. oryzae* homologue, 55% to the *M. acridum* homologue and to and 54% identity to the *T. atroviride* homologue. ClustalW was used to align GPCR sequences, with conserved residues are shaded in grey. Red bars above the sequence mark the predicted seven transmembrane domains (TM I – TM VII).

The *E. festucae* Gpr2 homologue (EfM3.066920) shows 39.6% amino acid identity (ID) to the Gpr-2 protein from *N. crassa* (NCU04626), 59.4% identity to the *F. graminearum* homologue Gpr3 (FGSG_1861), 45.2% identity to the *M. oryzae* homologue (MGG_06738) and 54.7% to the *T. atroviride* TaGpr2 (TRIATDRAFT_50902). The *E. festucae* Gpr2 further shares 37.8% sequence identity with the distantly related *A. nidulans* GprH (AN8262). Likewise to Gpr1b, the amino acid sequence alignment of Gpr2 displays high similarity especially along the transmembrane domains as well as the typical low similarity along the variable sequence covering the third intracellular loop (ICL3) and the intracellular carboxy-terminal sequence typical for GPCRs (Fig. 3.4). Interestingly, with 34.9% identity, the *E. festucae* Gpr2 homologue (EfM3.066920) also shows a high sequence identity to the *N. crassa* Gpr3 (NCU09427), despite the absence of a Gpr3 homolog in the *E. festucae* genome.

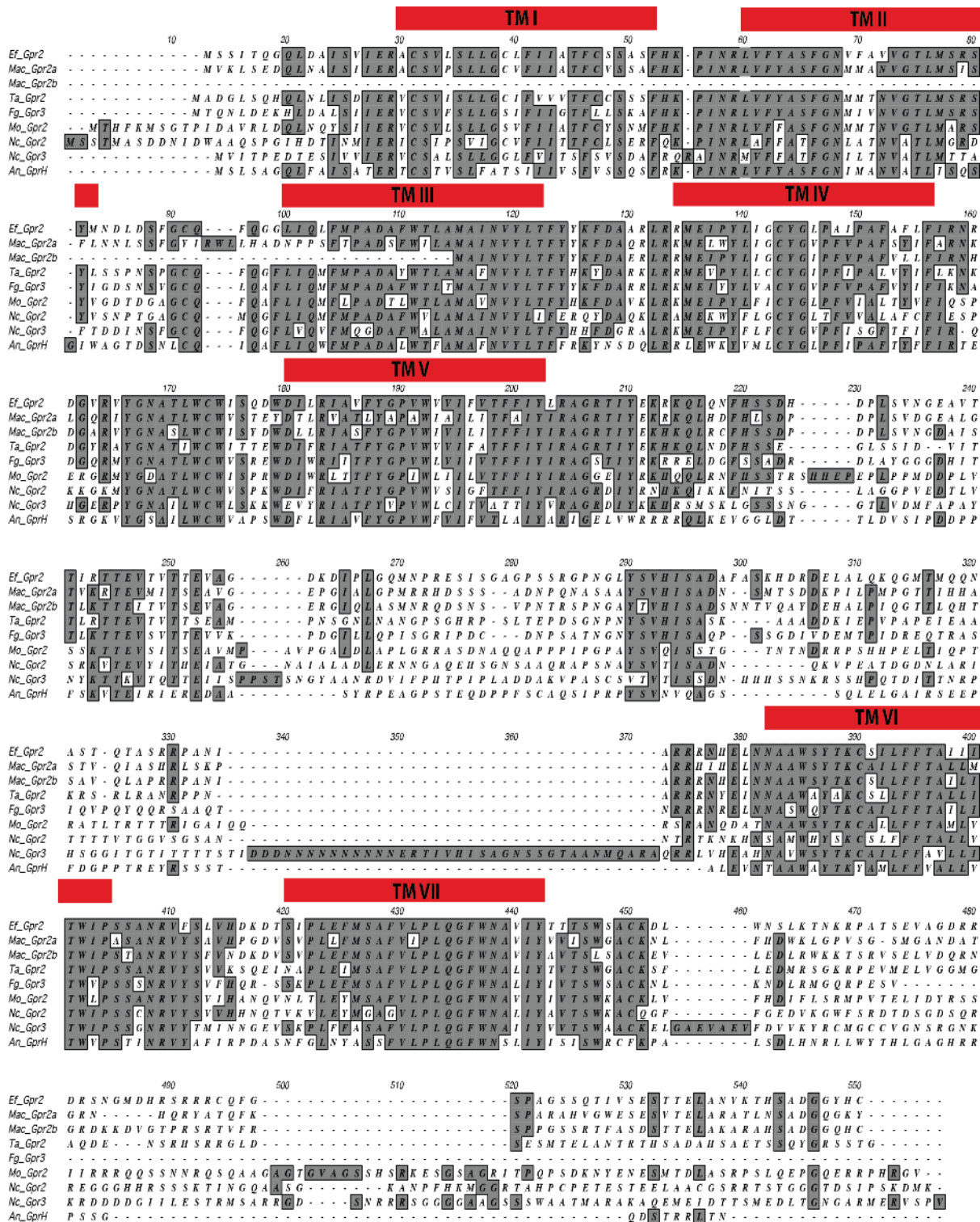


Figure 3-4 Multiple sequence alignment of *E. festucae* Gpr2 homologues: The predicted amino acid sequence of *E. festucae* Gpr2 Ef_Gpr2 (EfM3.066920) is aligned with corresponding homologues from *N. crassa* Nc_Gpr2 (NCU04626), *F. graminearum* Fg_Gpr3 (FGSG_01861), *M. oryzae* Mo_Gpr2 (MGG_06738), *T. atroviride* Ta_Gpr2 (TRIATDRAFT_50902), *M. acridum* Mac_Gpr2a (MAC_08590) and *A. nidulans* An_GprH (AN8262). Furthermore *E. festucae* Gpr2 is aligned with *N. crassa* Nc_Gpr3 (NCU09427) and Mac_Gpr2b (MAC_02892) to visualise high sequence identity. *E. festucae* Gpr2 displays 40% amino acid identity to *N. crassa* Gpr-2 and , 59.4% identity to the *F. graminearum* homologue, 44% identity to the *M. oryzae* homologue, 39% identity to *A. nidulans* GprH, 68% to the

M. acridum homologue Mac_Gpr2a and 55.5% identity to TaGpr2 of *T. atroviride*. *E. festucae* Gpr2 shares 35% amino acid identity to *N. crassa* Gpr-3 and 55% identity to *M. acridum* Mac_Gpr2b. ClustalW was used to align GPCR sequences, with conserved residues are shaded in grey. Red bars above the sequence mark the predicted seven transmembrane domains (TM I – TM VII).

For further characterisation and to clarify the relationship between the *E. festucae* cAMP receptor-like GPCRs and their corresponding homologues in *N. crassa*, *M. oryzae* and *F. graminearum*, a phylogenetic analysis was conducted. The unrooted Maximum likelihood dendrogram shows that the presence of the two *N. crassa* Gpr1 homologues in the *E. festucae* genome, *gpr1a* and *gpr1b* (*Efgpr1a* and *Efgpr1b*), supports the hypothesis that both arose from a gene duplication event (Fig. 3.4). This gene duplication event is present in the genome of various species within the *Clavicipitaceae* family (*Epichloë* spp., *Metarhizium* spp. and some *Claviceps* spp. (*C. paspali* but not *C. purpurea*)). Multiple class V GPCRs were also identified in *F. graminearum*, which genome encodes at least five. The *gpr1a* and *gpr1b* gene duplication is present throughout the analysed *Epichloë* spp., available from the endophyte genome database. The presence of this gene duplication within the analysed *Epichloë* spp., some *Claviceps* spp. and the *Trichoderma* spp. supports the hypothesis that this duplication arose within the Order of *Hypocreales*, that include the *Clavicipitaceae*.

The generated phylogenetic tree also indicates that *N. crassa* Gpr3 was evolutionarily derived from Gpr2, which would explain the similar sequence identity of *E. festucae* Gpr2 to both, *N. crassa* Gpr2 and Gpr3. While the genome of *M. oryzae* contains multiple genes encoding class V GPCRs, only MGG_11962 (*gpr1*) and MGG_06738 (*gpr2*) were identified as homologues for the *E. festucae* GPCRs by tblastn. A high variety in number in this class indicates multiple gene duplication events, which also occurred in *F. graminearum* whose genome contains the highest number of genes encoding GPCRs overall. Using the more distantly related *A. nidulans* class V GPCR homologue, *gprH* (AN8262), which represents the only cAMP-receptor-like GPCR in the organism; the phylogenetic tree was artificially rooted to better visualise the genetic lineage (Fig. 3.5).

Figure 3-5 Phylogenetic analysis of fungal class V cAMP receptor-like GPCRs: Maximum-likelihood dendrogram visualises phylogenetic relationship between the fungal cAMP receptor-like GPCRs including following species: *Aspergillus nidulans* AnGprH (AN8262); *Neurospora crassa* NcGpr1 (NCU00786), NcGpr2 (NCU04626), NcGpr3 (NCU09427); *Magnaporthe oryzae* MoGpr1 (MGG_11962), MoGpr2 (MGG_06738); *Fusarium graminearum* FgGpr1 (FGSG_09693), Fg_gpr2 (FGSG_05239), FgGpr3 (FGSG_01861), FgGpr4 (FGSG_07716), FgGpr5 (FGSG_03023); *Trichoderma atroviride* TaGpr1 (TRIATDRAFT_160995), TaGpr2 (TRIATDRAFT_50902), TaGpr3 (TRIATDRAFT_83166), TaGpr4 (TRIATDRAFT_81233), *Metarhizium acridum* MacGpr1a (MAC_03969), MacGpr1b (MAC_01277), MacGpr2a (MAC_08590), MacGpr2b (MAC_02892), MacGpr3 (MAC_08966); *Metarhizium robertsii* MrobGpr1a (MAA_07004), MrobGpr1b (MAA_06299), MrobGpr2a (MAA_10964), MrobGpr2b (MAA_01664), MrobGpr3 (MAA_09921); *Claviceps paspali* CpasGpr1a (EfP3.049190), CpasGpr1b (EfP3.080640), CpasGpr2 (EfP3.066920); *Claviceps purpurea* CpurGpr2 (EfP3.049190); *Epichloë festucae* EfGpr1a (EfM3.049190), EfGpr1b (EfM3.080640), EfGpr2 (EfM3.066920). Gene names (Gene IDs); values above branches indicate bootstrap values based on 500 replicates.

Based on two independent blast approaches (tblastn) against the available genomes of the closely related *Claviceps* species *C. purpurea*, *C. fusiformis* and *C. paspali* (<http://www.endophyte.uky.edu/>), multiple gene duplication events were identified, using either the protein sequences of *E. festucae gpr1a*, *gpr1b* and *gpr 2* or *N. crassa gpr-1*, *gpr-2*, *gpr-3* as a query. While *Claviceps purpurea* appears to have only a single GPCR of the cAMP receptor-like protein class, Cpur_gpr2 (EfP3.049190) grouping within the *E. festucae gpr2* clade, *C. fusiformis* contains two genes encoding class V GPCRs, Cfus_gpr1a (EfP3.049190) and Cfus_gpr2 (066920) have high sequence identity to *E. festucae gpr1a/N. crassa gpr-1* and *E. festucae gpr2/N. crassa gpr-2* respectively. Similar to *E. festucae*, *C. paspalli* contains three genes encoding class V GPCRs: Cpas_gpr1a (Cpas_049190; EfM3.049190), Cpas_gpr1b (Cpas_080640; EfM3.060840) and Cpas_gpr2 (Cpas_066920; EfM3.066920) with high sequence identity to the *E. festucae* homologues *gpr1a*, *gpr1b* and *gpr2*, respectively. Additionally the *Claviceps* species also lack a *N. crassa gpr3* homolog. The presence of the *gpr1a-gpr1b* gene duplication event as well as the absence of an *N. crassa Gpr3* homolog is consistent among the *Epichloë* species (Fig. 3.6; Appendix 16).

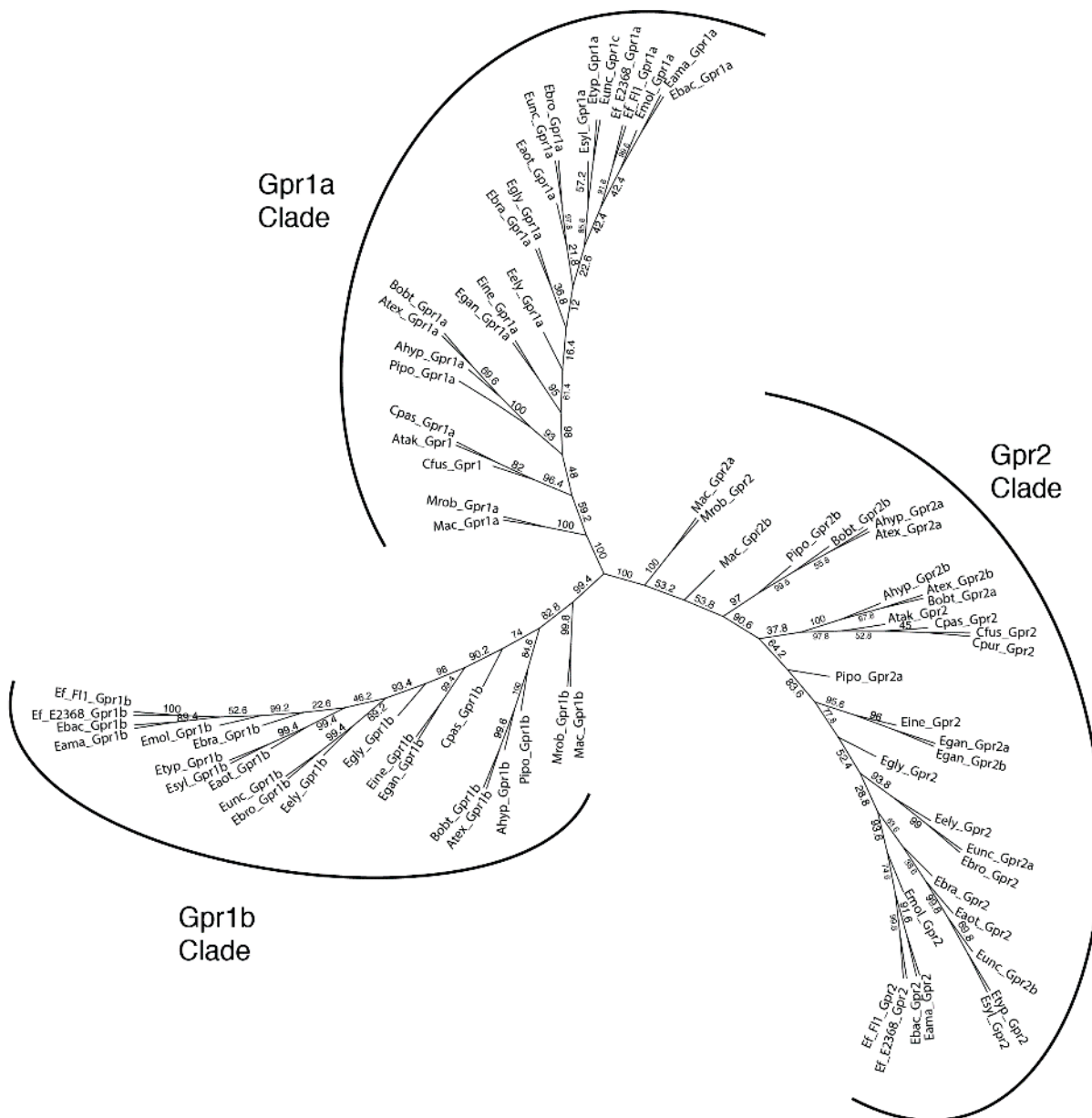


Figure 3-6 Phylogenetic analysis of class V GPCRs within the *Epichloë* species: Maximum-likelihood dendrogram showing the phylogenetic relationship of cAMP receptor-like GPCRs within the *Epichloë* species and closely related species in unrooted tree layout (rooted tree: Appendix 16) as follows: *Aciculosporium take* Atak_gpr1 (EfP3.049190), Atak_gpr2 (EfP3.080640); *Atkinsonella hypoxylon* Ahyp_gpr1a (EfP3.049190), Ahyp_gpr1b (EfP3.080640), Ahyp_gpr2a (EfP3.066920a), Ahyp_gpr2b (EfP3.066920b); *A. texensis* Atex_gpr1a (EfP3.049190), Atex_gpr1b (EfP3.080640), Atex_gpr2a (EfP3.066920a), Atex_gpr2b (EfP3.066920b); *Balansia obtecta* Bobt_gpr1a (EfP3.049190), Bobt_gpr1b (EfP3.080640), Bobt_gpr2a (EfP3.066920a), Bobt_gpr2b (EfP3.066920b); *Claviceps fusiformis* Cfus_gpr1 (EfP3.049190), Cfus_gpr2 (EfP3.066920); *C. paspali* Cpas_gpr1a (EfP3.049190), Cpas_gpr1b (EfP3.080640), Cpas_gpr2 (EfP3.066920); *C. purpurea* Cpur_gpr2 (EfP3.049190); *Epichloë amarillans* Eama_gpr1a (EfP3.049190), Eama_gpr1b (EfP3.080640), Eama_gpr2 (EfP3.066920); *E. aotearoae* Eaot_gpr1a (EfP3.049190), Eaot_gpr1b (EfP3.080640), Eaot_gpr2 (EfP3.066920); *E. baconii* Ebac_gpr1a (EfP3.049190), Ebac_gpr1b (EfP3.080640), Ebac_gpr2 (EfP3.066920); *E. brachyelytri* Ebra_gpr1a (EfP3.049190), Ebra_gpr1b (EfP3.080640), Ebra_gpr2 (EfP3.066920); *E. bromicola* Ebro_gpr1a (EfP3.049190), Ebro_gpr1b

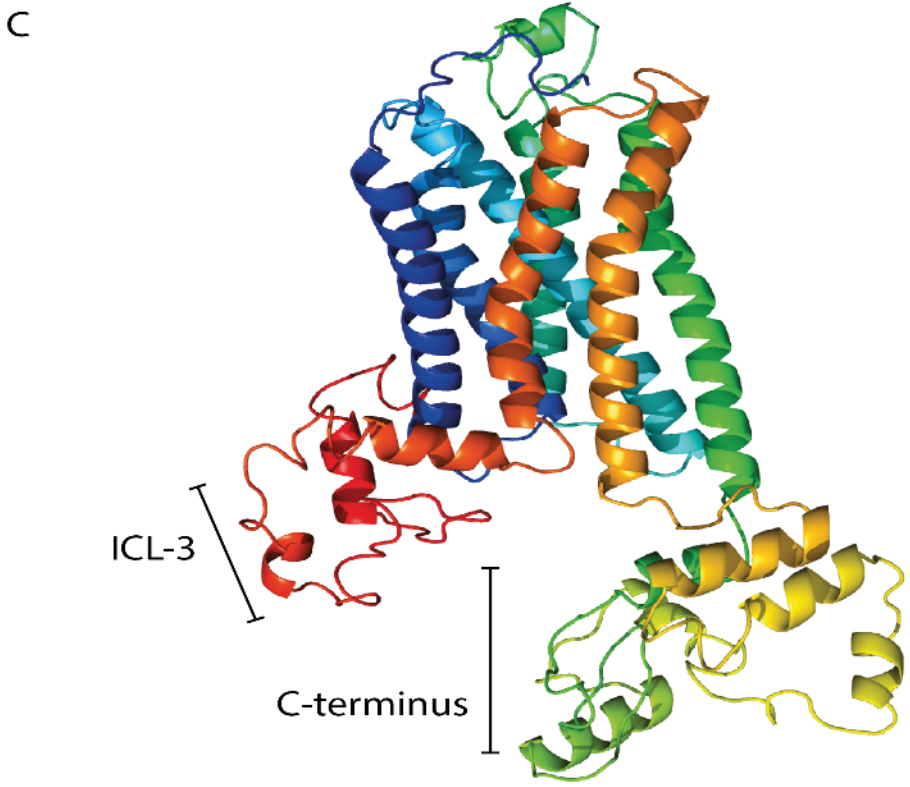
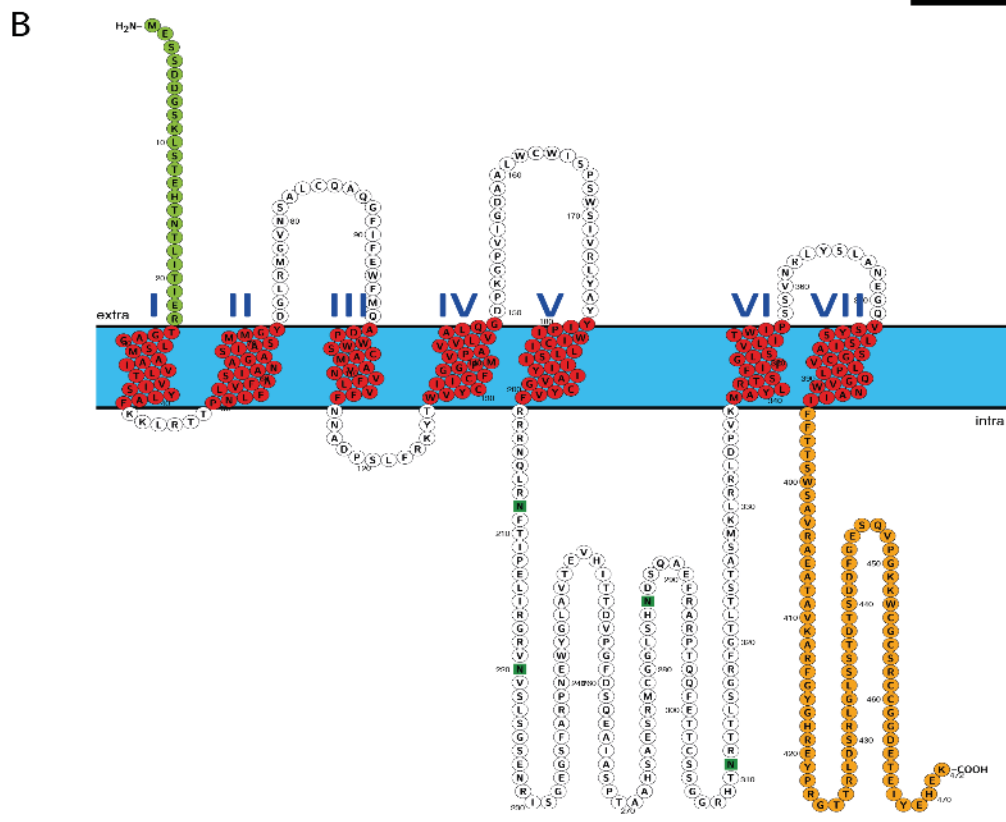
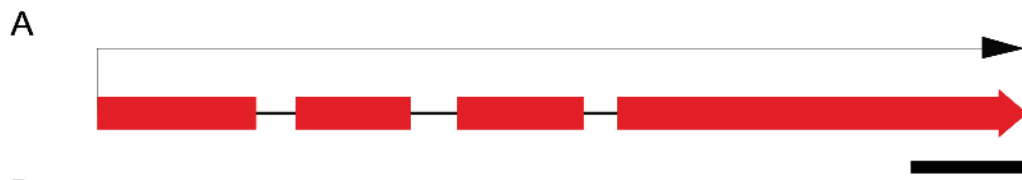
(EfP3.080640), Ebro_gpr2 (EfP3.066920); *E. elymi* Eely_gpr1a (EfP3.049190), Eely_gpr1b (EfP3.080640), Eely_gpr2 (EfP3.066920); *E. festucae* E2368 EfesE2368_gpr1a (EfM3.049190), EfesE2368_gpr1b (EfM3.080640), EfesE2368_gpr2 (EfM3.066920); *E. festucae* F11 EfF11_gpr1a (EfM3.049190), EfF11_gpr1b (EfM3.080640), EfF11_gpr2 (EfM3.066920); *E. gansuensis* Egan_gpr1a (EfP3.049190), Egan_gpr1b (EfP3.080640), Egan_gpr2a (EfP3.066920a), Egan_gpr2b (EfP3.066920b); *E. glyceriae* Egly_gpr1a (EfP3.049190), Eama_gpr1b (EfP3.080640), Eama_gpr2 (EfP3.066920); *E. inebrians* Eine_gpr1a (EfP3.049190), Eine_gpr1b (EfP3.080640), Eine_gpr2 (EfP3.066920); *E. mollis* Emol_gpr1a (EfP3.049190), Emol_gpr1b (EfP3.080640), Emol_gpr2 (EfP3.066920); *E. sylvatica* Esyl_gpr1a (EfP3.049190), Esyl_gpr1b (EfP3.080640), Esyl_gpr2 (EfP3.066920); *E. typhina* Etyp_gpr1a (EfP3.049190), Etyp_gpr1b (EfP3.080640), Etyp_gpr2 (EfP3.066920); *E. uncinata* Eunc_gpr1a (EfP3.049190), Eunc_gpr1b (EfP3.080640), Eunc_gpr2a (EfP3.066920a), Eunc_gprb (EfP3.066920b); *Metarhizium acridum* Mac_gpr1a (EfP3.049190; MAC_03969*), Mac_gpr1b (EfP3.080640; MAC_01277*), Mac_gpr2a (EfP3.066920a; MAC_08590*), Mac_gpr2b (EfP3.066920b; MAC_02892*); *M. robertsii* Mrob_gpr1a (EfP3.049190; MAA_06299*), Mrob_gpr1b (EfP3.080640; MAA_01664*), Mrob_gpr2 (EfP3.066920, MAA_10964*); *Periglandula ipomeae* Pipo_gpr1a (EfP3.049190), Pipo_gpr1b (EfP3.080640a), Pipo_gpr1c (EfP3.080640b), Pipo_gpr2a (EfP3.066920a), Pipo_gpr2b (EfP3.066920b). Gene names and corresponding identification number from Genome project UKY (Endophyte genome database); values above branches indicate bootstrap values based on 500 replicates; * = respective NCBI GenBank identifier

Analysis of the polypeptide structure of Gpr1a, Gpr1b and Gpr2 predicted the characteristic seven transmembrane (TM) domains of G protein-coupled receptors for all three proteins. With the typical topology of class V cAMP receptor-like GPCRs, all three proteins exhibit five transmembranes at the N-terminal part, a long sequence of the third intracellular loop sequence and two C-terminal transmembrane domains (Lafon et al. 2006). Characteristic for G protein coupled receptors, the proteins contain a highly variable amino-terminal sequence for interaction with extracellular ligands and a carboxy-terminal sequence for intracellular protein-protein interaction. The individual transmembrane domains are connected by extracellular (ECL) and intracellular loop (ICL) sequences, which are highly variable in length and amino acid sequence composition. As the topological prediction for positioning of the transmembrane domains were inconsistent among the different prediction tools, the domains were manually mapped based on the TMHMM (v2.0) results and visualised using Protter (v.1.0). Based on solved crystal structures of known GPCRs, three-dimensional (3D) structure models were predicted using the protein sequence and the Phyre2 server. The formation of a disulfide bond between cysteines in extracellular loop regions are common among GPCRs and appear to be a conserved feature, however not always necessary for receptor functionality (Strader et al., 1994, Naranjo et al.,

2015). Disulfide bonds were not predicted reliably for Gpr1a, Gpr1b or Gpr2 using a variety of bioinformatic prediction tools and therefore not included in the predicted models.

E. festucae gpr1a is 1626 bp nucleotide sequence, located on contig 01170 of the *E. festucae* F11 genome and contains four exons, that encodes a predicted 473 amino acid polypeptide, as predicted by FGENESH. The predicted Gpr1a polypeptide contains seven transmembrane domains, which are connected by three ICL (ICL 1-3) and three ECL (ECL 1-3). Two regions showing low complexity (LCR) with unknown function located in the highly variable third intracellular loop (ICL 3) and the C-terminus were also predicted for Gpr1a (Fig. 3.7).

Figure 3-7 Organisation of the *E. festucae gpr1a* gene and predicted polypeptide: (A) The *gpr1a* gene is 1626 bp and contains four exons (represented by red boxes). Scale bar = 200 bp. (B) The predicted Gpr1a polypeptide is 473 amino acids in length and is predicted to contain seven transmembrane domains (TM), an amino-terminal domain (NH) for interaction with extracellular ligand and a carboxy-terminal domain (COOH) for intracellular protein-protein interaction as well as intracellular (ICL) and extracellular loop domains (ECL). Topology was predicted by TMHMM v2.0 and visualised using Protter v1.0; predicted transmembrane helices (red), N-terminal sequence (green) and C-terminal sequence (orange). (C) 3-dimensional structure model, predicted using the Phyre2 server.



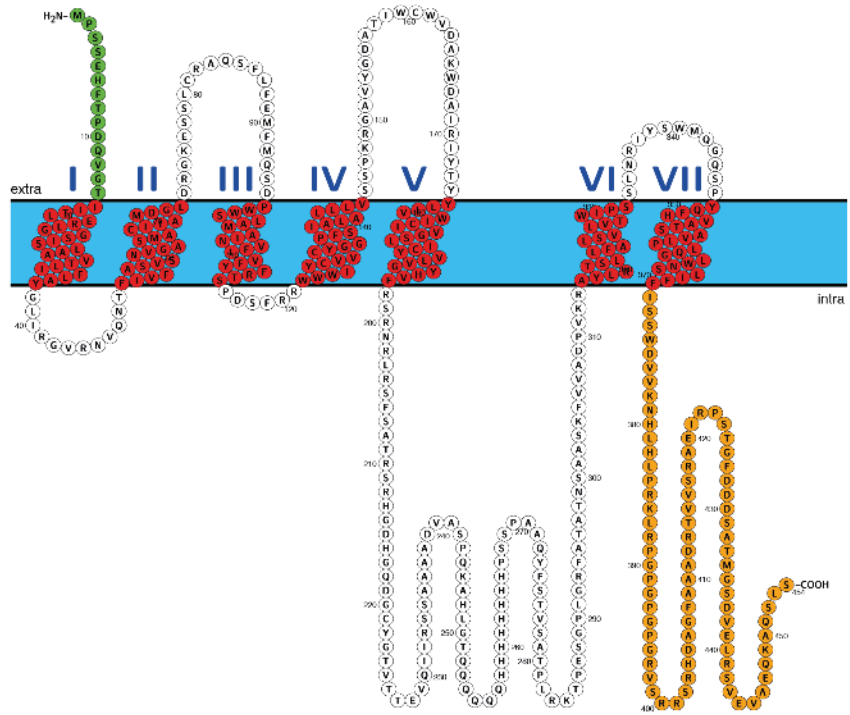
E. festucae gpr1b is 1630 bp nucleotide sequence, located on contig 00545 of the *E. festucae* Fl1 genome, contains three exons separated by two introns and encodes a 454 amino acid polypeptide, as predicted by FGENESH. The predicted Gpr1b polypeptide contains seven transmembrane domains, which are connected by three ICL (ICL 1-3) and three ECL (ECL 1-3). Two regions showing low complexity (LCR) with unknown function located in the highly variable third intracellular loop (ICL 3) and the C-terminus were also predicted for Gpr1b (Fig 3.8).

Figure 3-8 Organisation of *E. festucae gpr1b* gene and predicted polypeptide: (A) The *gpr1b* gene is 1365 bp and contains three exons (represented by red boxes). Scale bar = 200 bp. (B) The predicted Gpr1b polypeptide is 454 amino acids in length and is predicted to contain seven transmembrane domains (TM) an amino-terminal domain (NH) for interaction with extracellular ligand and a carboxy-terminal domain (COOH) for intracellular protein-protein interaction. Topology was predicted by TMHMM v2.0 and visualised using Protter v1.0; predicted transmembrane helices (red), N-terminal sequence (green) and C-terminal sequence (orange). (C) 3-dimensional structure model, predicted using the Phyre2 server.

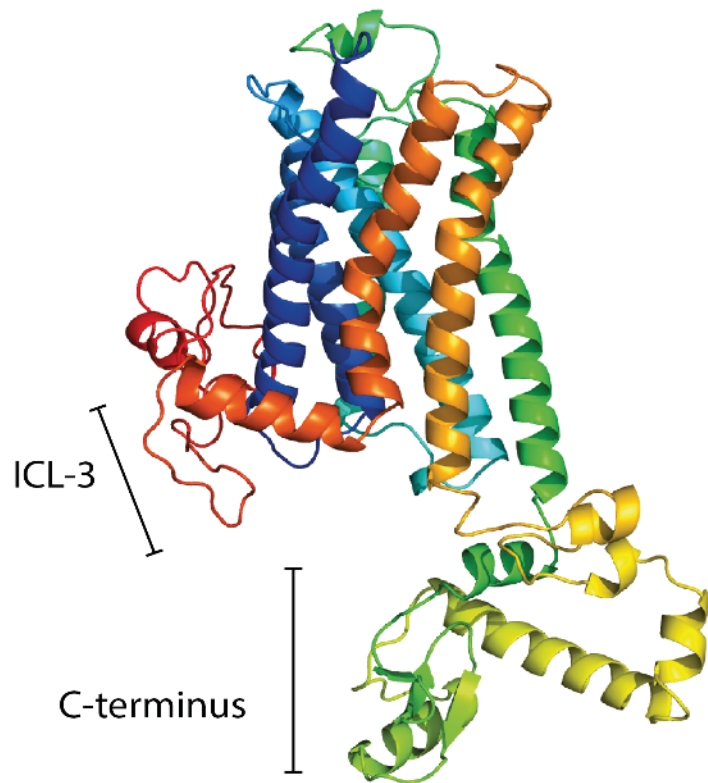
A



B

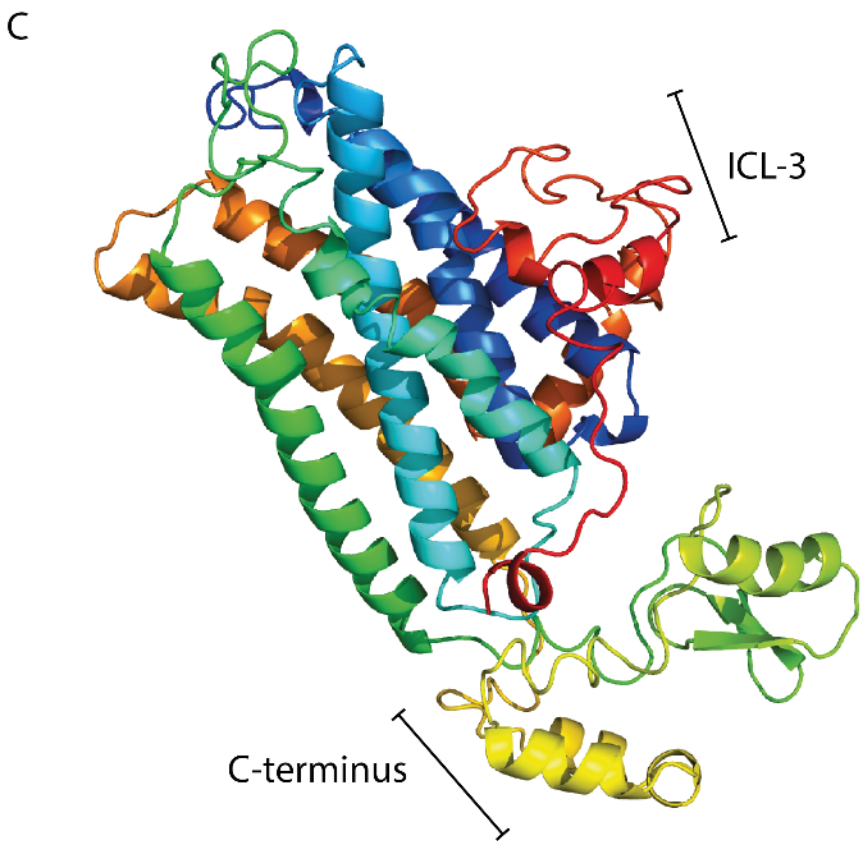
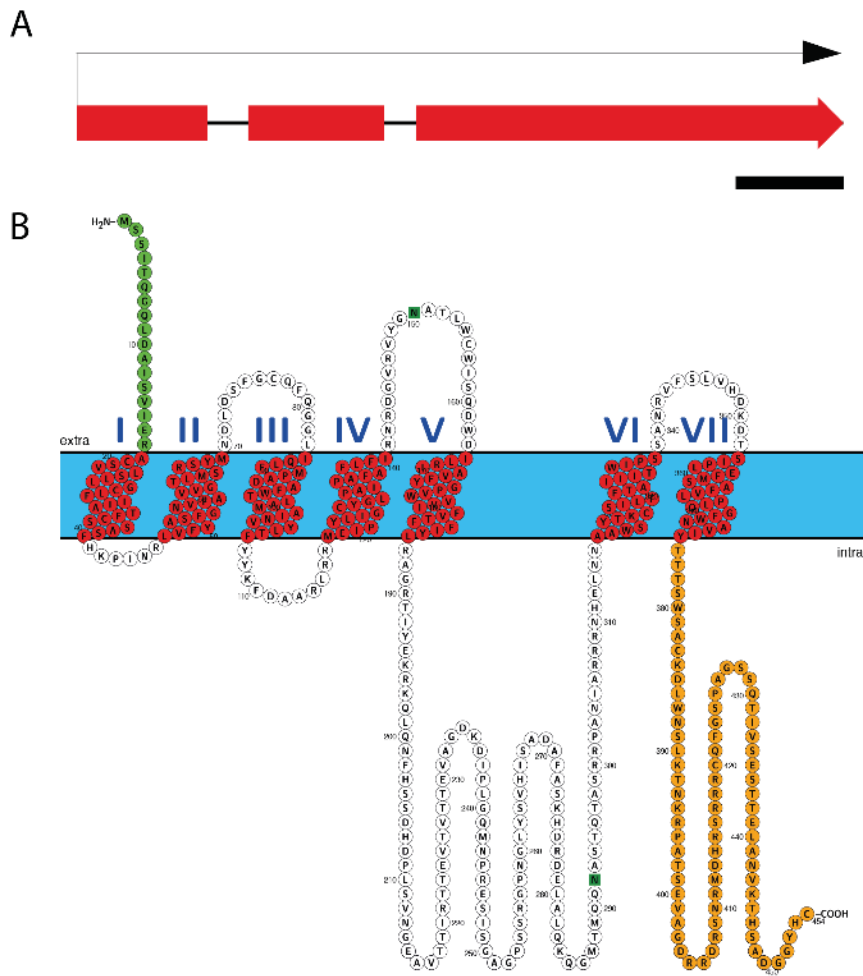


C



The *gpr2* gene is 1508 bp in length located on contig00247 of the *E. festucae* Fl1 genome, contains three exons and encodes a 454 amino acid polypeptide, as predicted by FGENESH. The Gpr2 polypeptide was analysed and seven transmembrane domains as well as two regions showing low complexity (LCR) were predicted. Gpr2 also contains three ICL and three ECL connecting the transmembrane domains. Similar to Gpr1b, two regions with low sequence complexity (LCR) are located in the highly variable third intracellular loop (ICL 3) and the C-terminus (Fig. 3.9).

Figure 3-9 Organisation of *E. festucae gpr2* gene and predicted polypeptide : (A) The *gpr2* gene is 1458 bp and contains three exons (represented by red boxes). Scale bar = 100 bp. (B) The predicted Gpr2 polypeptide is 454 amino acids in length and is predicted to contain seven transmembrane domains (TM), an amino-terminal domain (NH) for interaction with extracellular ligand and a carboxy-terminal domain (COOH) for intracellular protein-protein interaction as well as intracellular (ICL) and extracellular loop domains (ECL). Topology was predicted by TMHMM v2.0 and visualised using Protter v1.0; predicted transmembrane helices (red), N-terminal sequence (green) and C-terminal sequence (orange). (C) 3-dimensional structure model, predicted using the Phyre2 server.



3.3 Cyclic nucleotide AMP phosphodiesterases (PDEs) in the *E. festucae* genome

Using the characterised *M. oryzae* amino acid sequences of the cAMP phosphodiesterases PdeH and PdeL (Ramanujam and Naqvi 2010) for tblastn against the fungal non-redundant NCBI database, homologues for the closely related fungal species *N. crassa* and *F. graminearum*. Using the *E. festucae* database (<http://csbio-l.csr.uky.edu/ef894-2011/blast/blast.html>), homologues of the PDEs showing high and low affinity towards cAMP in the *E. festucae* genome (Fl1), were identified using the corresponding *M. oryzae* amino acid sequences (Table 3.3; Appendix 15). To confirm that the *E. festucae* genes identified were indeed the homologues a reciprocal tblastn against the NCBI non-redundant NCBI database was done, using the *E. festucae* amino acid sequences. The *M. oryzae* query blast and the reciprocal blast show that the *E. festucae* genes EfM3.026670 (*pdeH*) and EfM3.002980 (*pdeL*) are true homologues of the *M. oryzae* *pdeH* and *pdeL* respectively. The predicted amino acid sequences of the putative high affinity PDE (PdeH) and low affinity PDE (PdeL) in *E. festucae* were aligned to the appropriate homologues from *N. crassa*, *F. graminearum* and *M. oryzae* using ClustalW and MAFFT (2.1.3).

Table 3-3 *Epichloë* PDEs

<i>E. festucae</i>		<i>M. oryzae</i>				Description
Name	Locus (EfM3.)	Name	Locus (MGG)	Identity (%)	<i>E</i> value	
<i>pdeH</i>	026670	PdeH	05664	50	e ⁻¹⁵⁵	high affinity cAMP phosphodiesterase
<i>pdeL</i>	002980	PdeL	07707	77	e ⁻¹⁴¹	low affinity cAMP phosphodiesterase

The *E. festucae* PdeH homologue (EfM3.026670) shows 49.6% amino acid identity to the *M. oryzae* PdeH (MGG_05664), 60.5% identity to the *F. graminearum* homologue (FGSG_06914) and 35.3% identity to the *N. crassa* homologue Pde2 (NCU00478). The amino acid sequence alignment also shows a highly conserved sequence primarily along the PDE Class I consensus sequence [H-D-(LIVMFY)-H-x-(AG)-x₂-(NQ)-x-(LIVMFY)], indicative of a cAMP high affinity phosphodiesterase (Fig. 3.13 c) (Charbonneau et al. 1986). Homology of *E. festucae* PdeH to the characterised homologues in *S. cerevisiae* Pde2 and *M. oryzae* PdeH was further predicted by 3-dimensional protein structure models using Phyre2 (Kelley et al. 2015) (Fig. 3.10).

The *E. festucae* PdeL homologue (EfM3.002980) shows 49.2% amino acid identity to the PdeL protein from *M. oryzae* (MGG_07707), 64.2% identity to the *F. graminearum* homologue (FGSG_06633) and 39.6% identity to the *N. crassa* homologue (NCU00237). The amino acid sequence alignment also identified the PDE Class II consensus sequence (H-x-H-L-D-H-(LIVM)-x-(GS)-(LIVMA)-(LIVM)₂-x-S-(AP)), indicative of a cAMP low affinity phosphodiesterase (Fig. 3.14 c) (Ma et al. 1999, Hicks et al. 2005). Homology of *E. festucae* PdeL to the characterised homologues in *S. cerevisiae* Pde1 and *M. oryzae* PdeL was further predicted by 3-dimensional protein structure models using Phyre2 (Kelley et al. 2015) (Fig. 3.11).

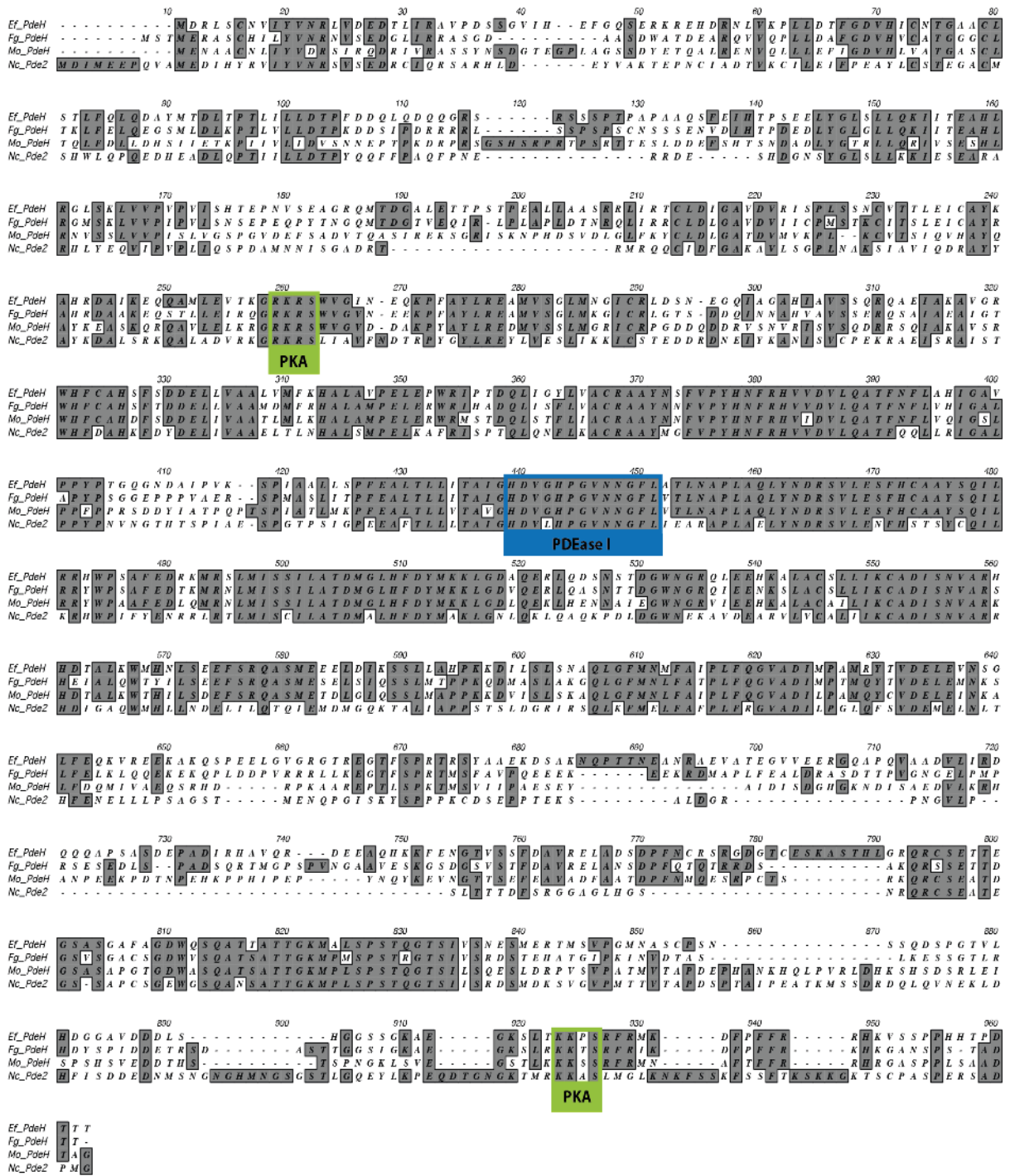


Figure 3-10 Multiple sequence alignment of funga PdeH homologues: The predicted amino acid sequences of the *E. festucae* high affinity cAMP phosphodiesterase PdeH (Ef, EfM3.026670) is aligned with PdeH homologues from *M. oryzae* MoPdeH (MGG_05664), *N. crassa* NcPde2 (NCU00478) and *F. graminearum* FgPdeH (FGSG_06914). *E. festucae* PdeH displays 50% identity to characterised *M. oryzae* MoPdeH, 35% amino acid identity to the *N. crassa* homologue Pde2 and 61% identity to the *F. graminearum* homologue. ClustalW was used to align the PDE sequences, with conserved residues are shaded in grey. The highly conserved cAMP-phosphodiesterase class I consensus sequence (H-D-(LIVMFY)-H-x-(AG)-x2-(NQ)-x-(LIVMFY)) is marked by a blue box and the predicted PKA phosphorylation sites are marked by green boxes.

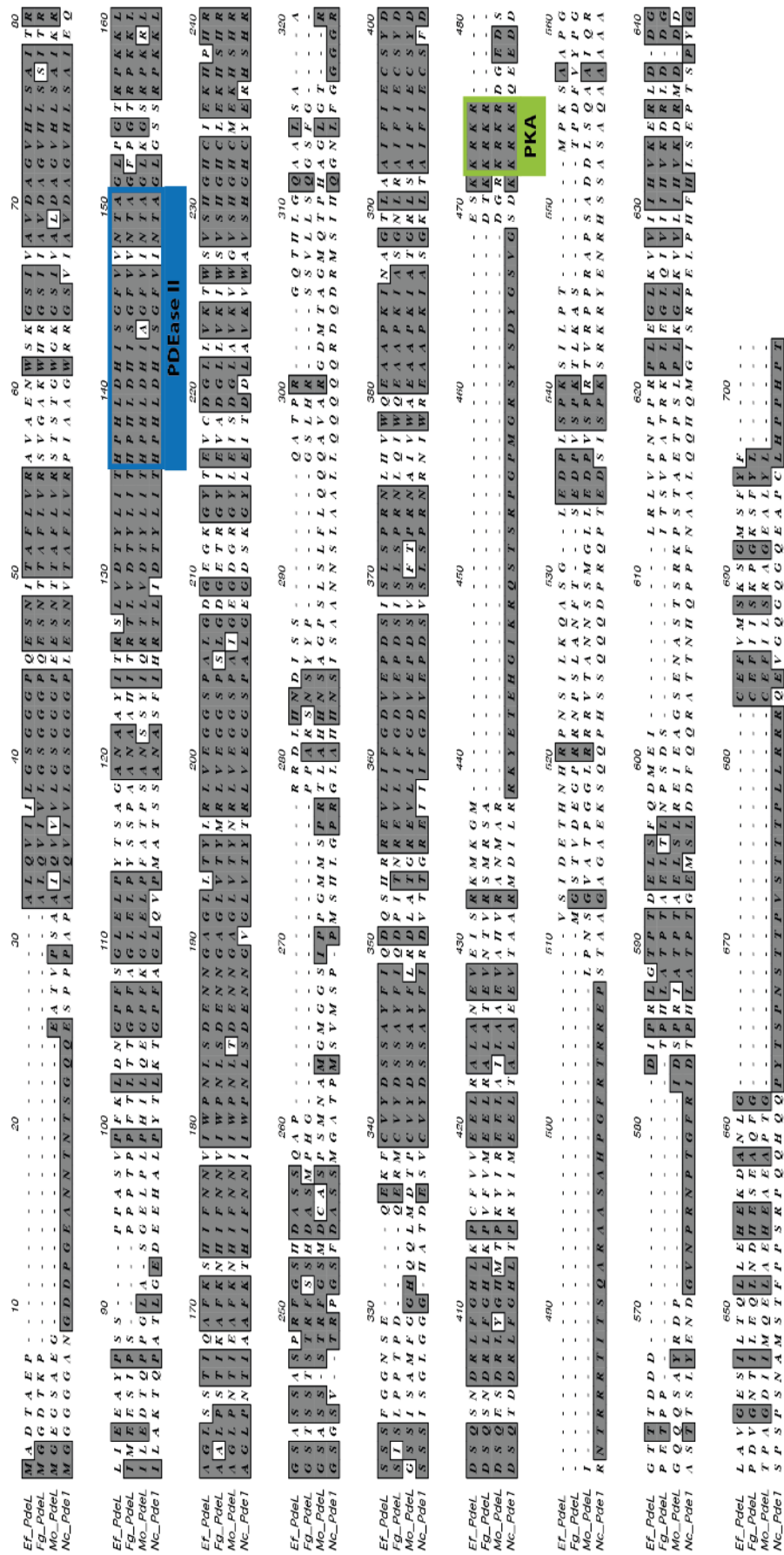
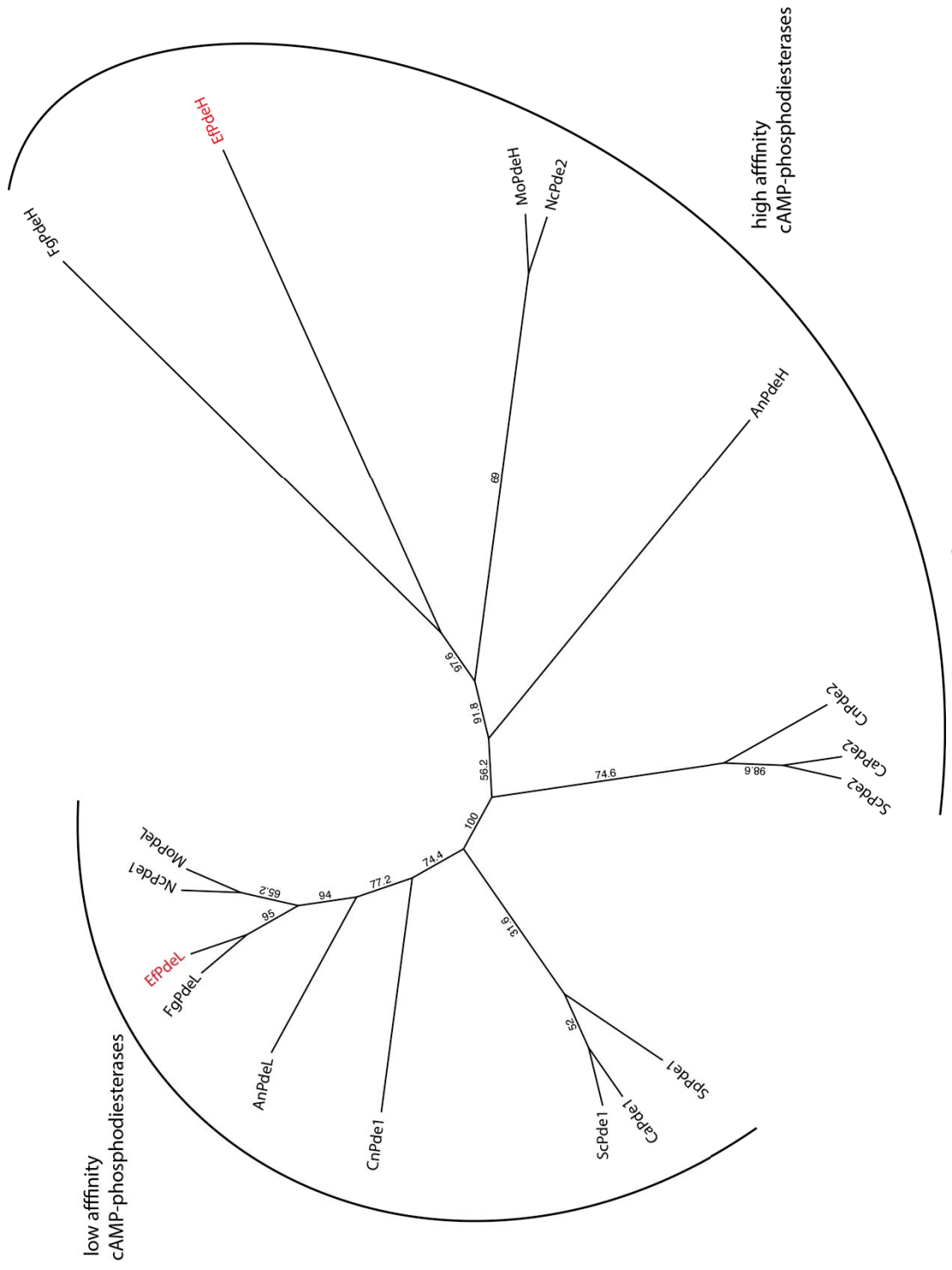


Figure 3-11 Multiple sequence alignment of fungal PdeL homologues: The predicted amino acid sequences of the *E. festucae* low affinity cAMP phosphodiesterase PdeL (Ef, EfM3.002980) is aligned with PdeL homologues from *M. oryzae* MoPdeL (MGG.0770), *N. crassa* NcPde1 (NCU00237) and *F. graminearum* FgPdeL (FGSG_0663). *E. festucae* PdeL displays 49% identity to the *M. oryzae* pdeL, 40% amino acid identity to the *N. crassa* homologue NcPde1 and 64% identity to the *F. graminearum* homologue Clusta1W was used to align the PDE sequences, with conserved residues are shaded in grey. The highly conserved cAMP-phosphodiesterase class II consensus sequence (H-x-H-L-D-H-(LIVM)-x-(GS)-(LIVMA)-(LIVM)₂-x-S-(AP)) is marked by a blue box and the predicted PKA phosphorylation site is marked by a green box.

Phylogenetic analysis clearly divides the two *E. festuace* PDEs (3'-5' cAMP-phosphodiesterases) into separate clades and groups them with the corresponding homologues in *M. oryzae*, *F. graminearum*, *N. crassa*, *A. nidulans*, *S. cerevisiae*, *S. pombe*, *C. neoformans* and in case of the low affinity PDE with *S. pombe*, which does not possess a homolog of the high affinity PDE (Fig. 3.12).

Figure 3-12 Maximum-likelihood dendrogram of fungal 3'-5' cyclic phosphodiesterases:

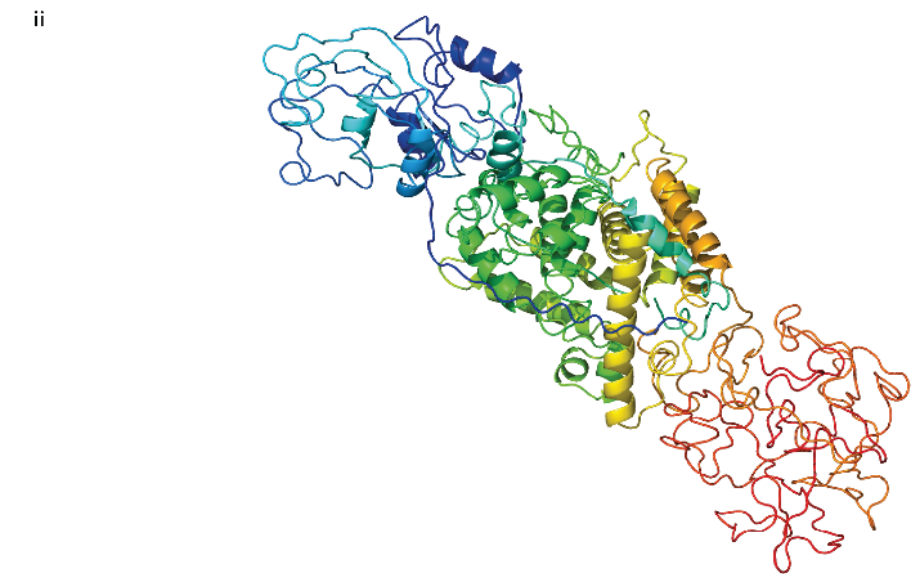
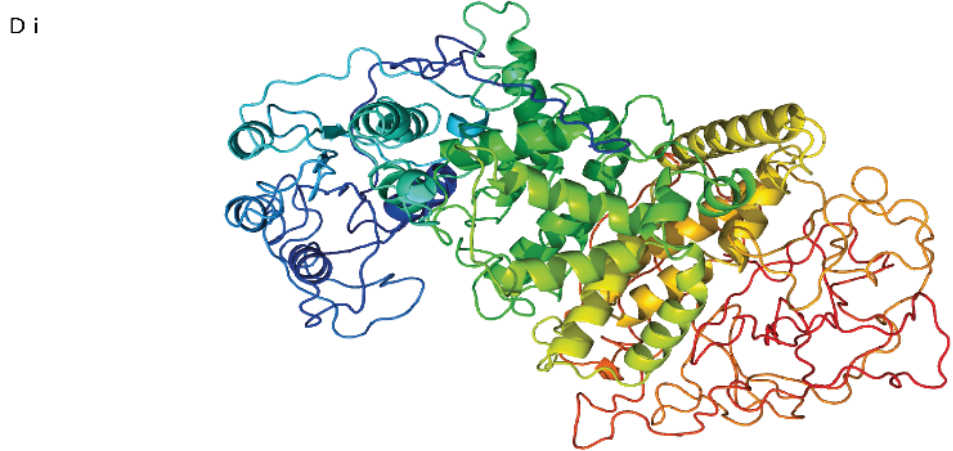
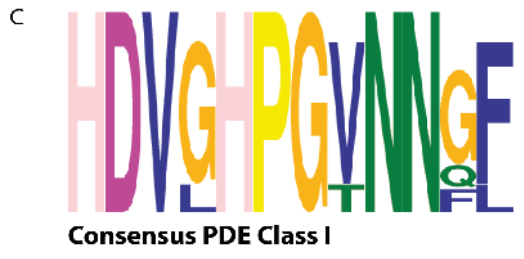
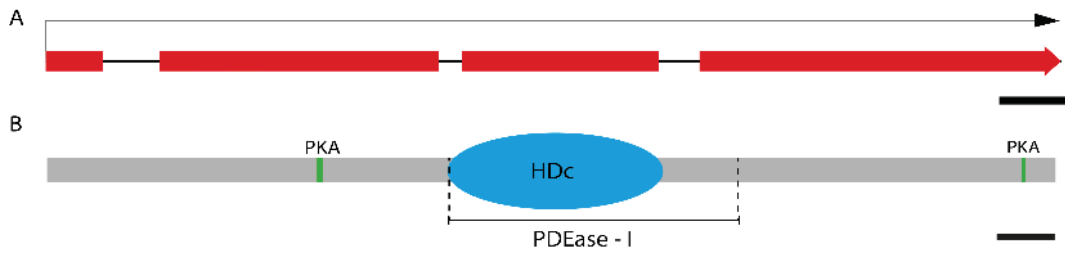
Maximum-likelihood dendrogram showing the phylogenetic relationship of cyclic PDEs among their corresponding homologues and dividing those into two clades characterised as high (PdeH) and low (PdeL) affinity towards cAMP respectively. Sequences are as follows: *Saccharomyces cerevisiae* ScPde2 (PDE2p) and ScPde1 (PDE1p), *Schizosacchomyces pombe* SpPde1 (PDE1), *Candida albicans* CaPde2 (PDE2) and CaPde1 (PDE1), *Cryptococcus neoformans* CnPde2 (PDE2) and CnPde1 (PDE1), *Magnaporthe oryzae* MoPdeH (MGG_05664) and MoPdeL (MGG_07707), *Neurospora crassa* NcPde2 (NCU00478) and NcPde1 (NCU00237), *Fusarium graminearum* FgPdeH (FGSG_06914) and FgPdeL (FGSG_06633), *Aspergillus nidulans* AnPdeH (AN2740) and AnPdeL (AN0829), *Epichloë festucae* EfPdeH (EfM3.026670) and EfPdeL (EfM3.002980). Values above branches indicate bootstrap values based on 500 replicates.



To analyse the polypeptide structure of *E. festucae* PdeH and PdeL, their predicted amino acid sequences were used for domain prediction using ExPASy PROSITEscan, InterProScan and SMART, independently.

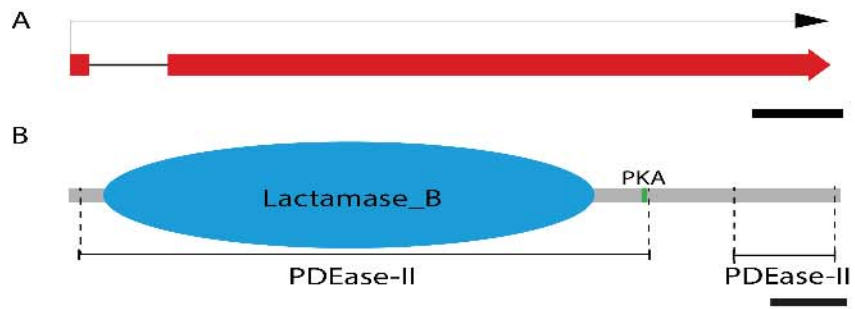
The *E. festucae pdeH* gene is 3058 bp in length, located on contig 00124 in the *E. festucae* Fl1 genome, contains three exons, and encodes a 898 amino acid polypeptide, predicted by FGENESH. The predicted PdeH polypeptide was found to contain a central 3'5'-cyclic nucleotide phosphodiesterase domain (IPR002073) with the cAMP phosphodiesterase class I signature motif (Pfam:PDEase-I, PF02333) and a HD metal dependent phosphohydrolase domain (IPR003607) as catalytic centre. MEME analysis (Multiple Em for motif Elicitation software Meme suite 4.11.1; <http://meme-suite.org/tools/meme>) was then used to characterise the consensus sequence of the conserved cAMP-phosphodiesterase class I using polypeptide sequences of the homologues in *S. cerevisiae* (Pde2), *C. albicans* (Pde2), *A. nidulans* (AN2740), *N. crassa* Pde2 (NCU00478), *F. graminearum* (FGSG_06914), *M. oryzae* (PdeH) and *E. festucae* PdeH. Using ExPASy PROSITE and a high sensitivity scan that includes motifs with a high probability of occurrence, two cAMP- and cGMP-dependent protein kinase phosphorylation sites (RKrS and KKpS) at the residue 241-244 (RKrS) and 867-870 (KKpS) were predicted, that exhibit the consensus PKA phosphorylation site motif [(K/R)-(K/R)-(X)-(S/T)] (Fig. 3.13) (Hicks et al. 2005).

Figure 3-13 Organisation of the *E. festucae pdeH* gene and predicted polypeptide: (A) The *pdeH* gene is 3058 bp and contains four exons (represented by red boxes). Scale bar = 200 bp. (B) The predicted PdeH polypeptide is 897 amino acids in length and contains a metal dependent phosphohydrolase domain (HDc) as catalytic centre with the consensus domain of class I cAMP-phosphodiesterases (PDEaseI). Scale bar = 50 aa. (C) Motif sequence showing highly conserved cAMP-phosphodiesterase class I consensus sequence (H-D-(LIVMFY)-H-x-(AG)-x₂-(NQ)-x-(LIVMFY)) using polypeptide sequences of *S. cerevisiae* (Sc_Pde2, PDE2p), *C. albicans* (Ca_Pde2, PDE2), *A. nidulans* (An_PdeH, AN2740), *N. crassa* (Nc_Pde2, NCU00478), *M. oryzae* (Mo_PdeH, MGG_05664), *F. graminearum* (Fg_PdeH, FGSG_06914) and *E. festucae* (Ef_PdeH, EfM3.026670). (D) 3-dimensional structure model of (i) *E. festucae* PdeH and (ii) *M. oryzae* PdeH, predicted using the Phyre2 server.



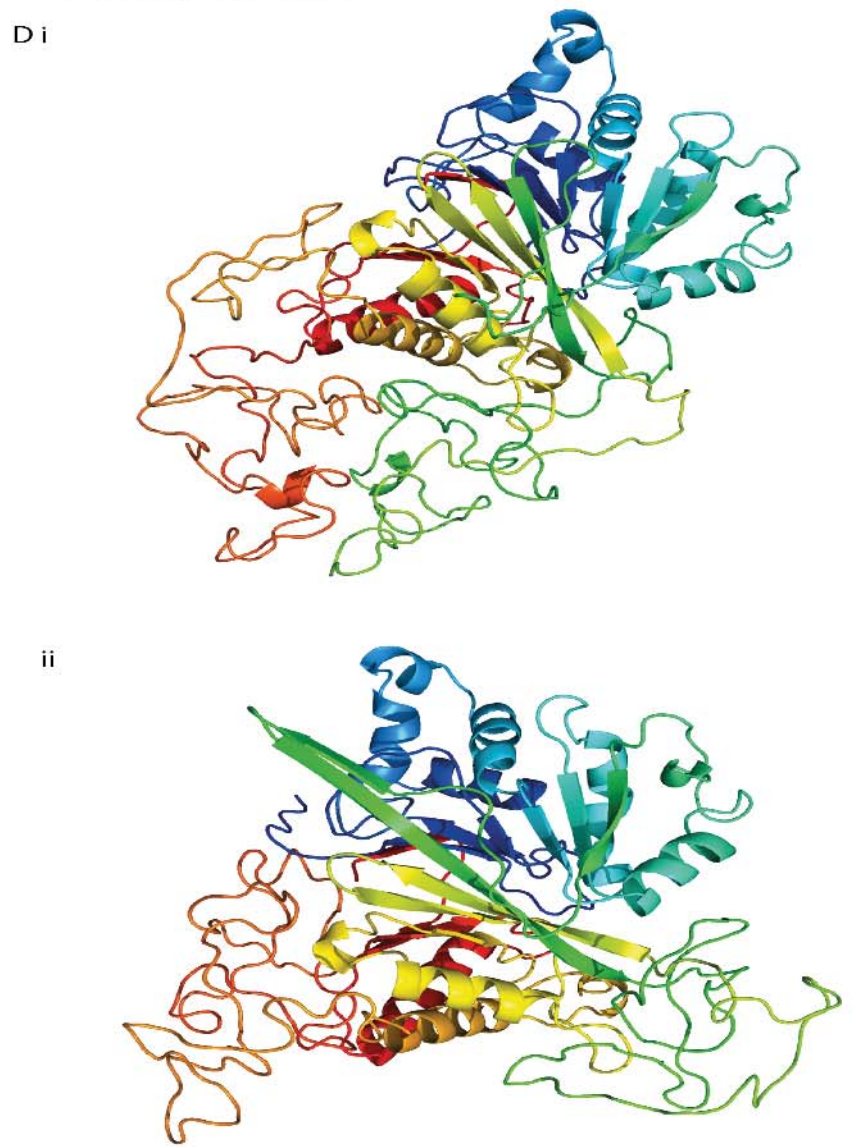
The *E. festucae pdeL* gene is 1708 bp in length, located on contig 00011 in the *E. festucae* F11 genome, contains two exons separated by a single intron and encodes a 509 amino acid polypeptide, predicted by FGENESH. The predicted PdeL polypeptide contains a cAMP phosphodiesterase class II domain (IPR000396) that contains the cAMP phosphodiesterase class II signature motif (Pfam: Pdease-2, PF02112) and a metallo- β -lactamase domain (IPR001279) as catalytic centre. The MEME motif sequence prediction identified a highly conserved cAMP-phosphodiesterase class II consensus sequence using polypeptide sequences of the homologue proteins of *S. cerevisiae* Pde1, *S. pombe* PDE1, *C. albicans* Pde1, *A. nidulans* AN0829, *N. crassa* NCU00237, *F. graminearum* FGSG_06633, *M. oryzae* PdeL and *E. festucae* PdeL (EfM3.002980). Using ExPASy PROSITE and a high sensitivity scan that includes motifs with a high probability of occurrence, one cAMP- and cGMP-dependent protein kinase phosphorylation site (RKvS) at residues 378-381 with the consensus PKA phosphorylation site-motif [(K/R)-(K/R)-(X)-(S/T)] was predicted (Fig. 3.14) (Hicks et al. 2005).

Figure 3-14 Organisation of the *E. festucae pdeL* gene and predicted polypeptide: (A) The *pdeL* gene is 1708 bp and contains two exons (represented by red boxes) separated by a single intron. Scale bar = 200 bp. (B) The predicted PdeL polypeptide is 509 amino acids in length and is predicted to contain three class-II cAMP-phosphodiesterase domains (PDEaseII) and Beta-lactamase like-protein domain (LACTBL). Scale bar = 50 aa. (C) Motif sequence showing the highly conserved cAMP-phosphodiesterase class II consensus sequence (H-x-H-L-D-H-(LIVM)-x-(GS)-(LIVMA)-(LIVM)₂-x-S-(AP)) using polypeptide sequences of *S. cerevisiae* (Sc_Pde1, PDE1p), *C. albicans* (Ca_Pde1, PDE1), *A. nidulans* (An_PdeL, AN0829), *N. crassa* (Nc_Pde1, NCU00237), *M. oryzae* (Mo_PdeL, MGG_07707), *F. graminearum* (Fg_PdeL, FGSG_06633) and *E. festucae* (Ef_PdeL, EfM3.002980). (D) 3-dimensional structure model of (i) *E. festucae* PdeL and (ii) *M. oryzae* PdeL, predicted using the Phyre2 server.



H P H L D H I S G E V I N T A
 V A A A M I P

Consensus PDE Class II

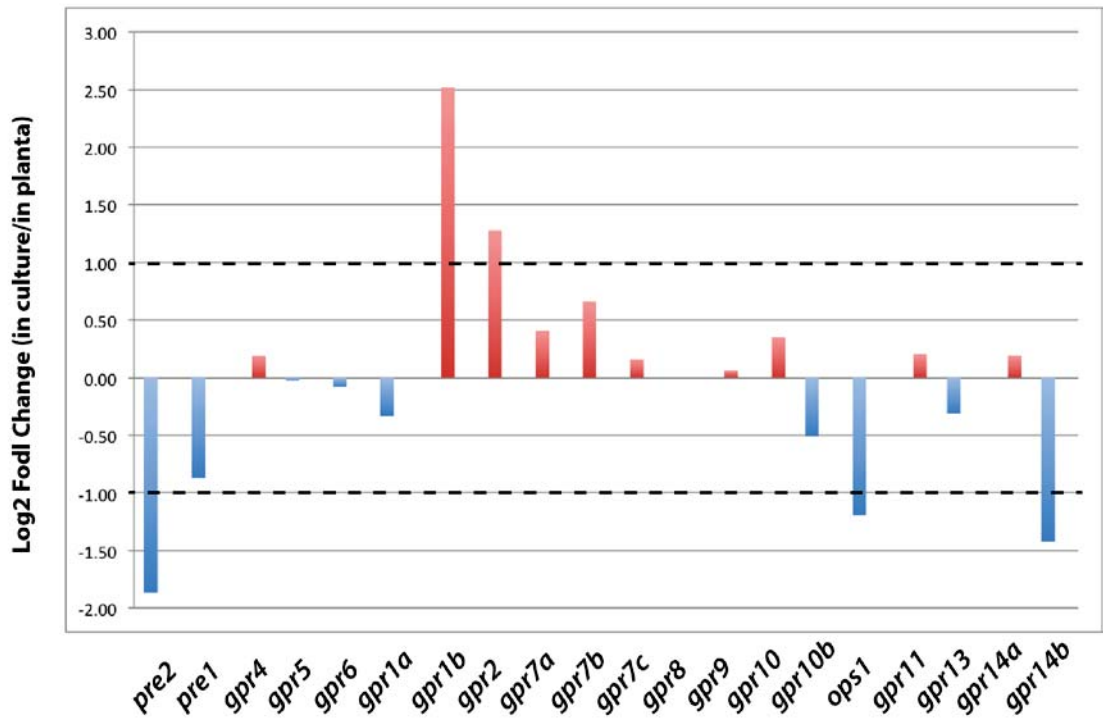


3.4 Transcriptional difference of *E. festucae* wild-type growth in culture and in association with the host

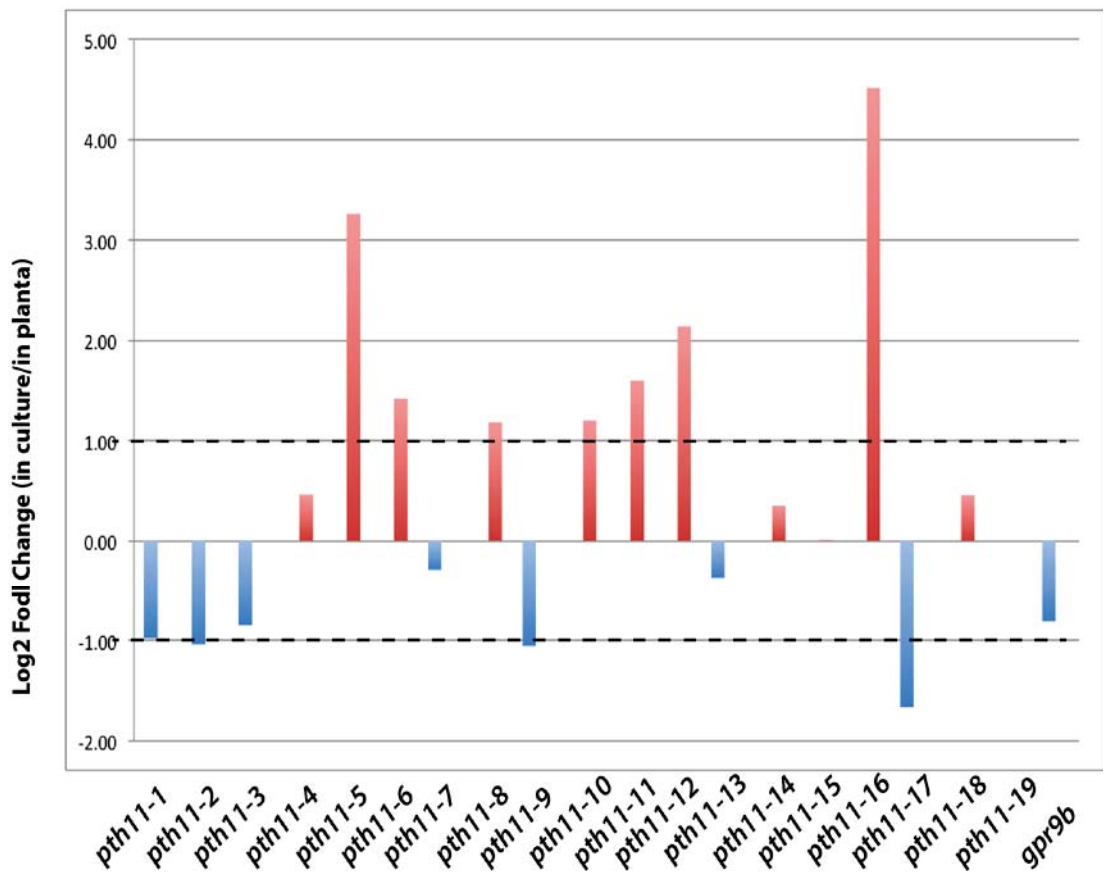
By comparing the transcriptome of the *E. festucae* wild-type isolated from culture growing on defined media (Blankenship) under laboratory growth conditions and from association with the host plant, differential expression patterns of various genes were identified (Appendix 16) [Chujo et al., unpublished]. In association with the host fungal growth significantly changes, so does signal perception shown in up-regulation of genes encoding GPCRs. A total of nine genes encoding GPCRs are significantly up-regulated *in planta* compared to growth in culture, above the expression fold-difference cut off of 2 for statistical significance. Among those, two genes encoding the class V cAMP receptor-like GPCRs (*gpr1b* and *gpr2*) and seven members of the Pth11-like receptors. In particular, Gpr1b shows a 5.74-fold up-regulation and Gpr2 is 2.43-fold up-regulated in association with the host (Fig. 3.15 A). In contrast, the gene encoding Gpr1a is 1.26-fold transcriptional down-regulated compared to its expression in culture. Some genes encoding Pth11-like proteins exhibit significant differential expression *in planta*, including *pth11-5* and *pth11-16* showing 9.55 fold and 22.84 fold up-regulation *in planta*, respectively (Fig. 3.15 B). In contrast, multiple GPCRs are down-regulated including genes encoding the pheromone receptors *pre1* (3.64 fold) and *pre2* (1.83 fold) or the microbial opsin receptor *ops1* (2.28 fold). Significantly increased gene expression *in planta* for members of the class V and class XIV GPCRs, indicates that these receptors, including Gpr1b and Gpr2, may play important roles in the *E. festucae* - *L. perenne* association.

Figure 3-15 Gene expression change of GPCR encoding genes of *E. festucae* wild-type in association with the host plant: Graphs showing expression fold-difference (\log_2) for differentially expressed genes of *E. festucae* in association with the host compared to growth on defined medium. Transcriptionally up-regulated (red) and down-regulated (blue) genes *in planta* encoding *E. festucae* GPCRs of (A) class I to XIII and (B) Pth11-like GPCRs as listed in Table 3.1 and Table 3.2, respectively. The class V GPCRs Gpr1b and Gpr2 (A) and seven Pth11-like GPCRs (B) show significant up-regulation. Cut-off for statistical significance indicated by black dashed line.

A



B



The components of the heterotrimeric G protein and the cAMP/PKA signalling pathway were identified by blast using the respective characterised *N. crassa* sequences as query against the *E. festucae* genome database (Table 3.4) (2.1.1; 2.1.2) (Li et al. 2007). The *E. festucae* homologues were confirmed by reciprocal blast against the NCBI non-redundant database using the amino acid query sequence, which also identified the homologues in *T. atroviride*, *F. graminearum* and *M. oryzae* (Appendix 17; Supplementary 56 – 64).

Table 3-4 Components of G-protein and cAMP/PKA signalling pathway

<i>E. festucae</i>		<i>N. crassa</i>				Description
Name	Locus (EfM3.)	Name	Locus (NCU)	Identity (%)	<i>E</i> value	
<i>gpa1</i>	62630	<i>gna-1</i>	06493	98.9	e ⁻¹⁵⁷	Gα-subunit type 1
<i>gpa2</i>	45200	<i>gna-2</i>	06729	87.9	e ⁻¹³⁴	Gα-subunit type 2
<i>gpa3</i>	73950	<i>gna-3</i>	05206	91.6	3.e ⁻⁸¹	Gα-subunit type 3
<i>gpb1</i>	13730	<i>gnb-1</i>	00440	98.9	e ⁻¹⁶⁵	Gβ-subunit type 1
<i>gpg1</i>	15250	<i>gng-1</i>	00041	93.5	2.e ⁻²⁴	Gγ-subunit type 1
<i>ric8</i>	64840	<i>ric8</i>	02788	71.4	0.0	GEF Ric8
<i>acyA</i>	22460	<i>cr-1</i>	08377	65.8	e ⁻¹²⁸	Adenylate cyclase
<i>pkac1</i>	15410	<i>pkac-1</i>	06240	73.9	e ⁻¹⁶³	PKA catalytic subunit 1
<i>pkar1</i>	71930	<i>mcb</i>	01166	77.0	e ⁻¹³¹	PKA regulatory subunit

Most components of the G-protein signalling cascade and the cAMP/PKA signalling pathway are transcriptionally up-regulated in association with the grass host, however not all genes show a significant expression fold-difference above the cut off of 2 (Fig. 3.16; Appendix 18). Expression of the genes encoding the G α-subunits *gpa1* and *gpa3*, the G β-subunit *gpb1* and the G γ-subunit *gpg1*, exhibit significant up-regulation *in planta*. While *acyA* and *pkar1*, encoding the adenylate cyclase and the putative regulatory PKA subunit in *E. festucae*, are higher expressed, the catalytic PKA subunit *pkac1* is down-regulated *in planta*, although not significantly. Interestingly, the genes encoding the two cAMP phosphodiesterases show opposing expression in association with the host. Although not significant, the

PdeH-encoding gene is 1.5 fold up-regulated *in planta*, while the *pdeL* is significantly down-regulated (2.82 fold) compared to the gene expression in culture (Fig. 3.16). This is a strong indicator that the role of PdeL is more important for fungal growth in culture than *in planta*.

The results of the comparative transcriptome analysis of the *E. festucae* wild-type strain indicate important roles for several GPCRs including Gpr1b and Gpr2 and the heterotrimeric G protein in the mutualistic *E. festucae* – ryegrass association.

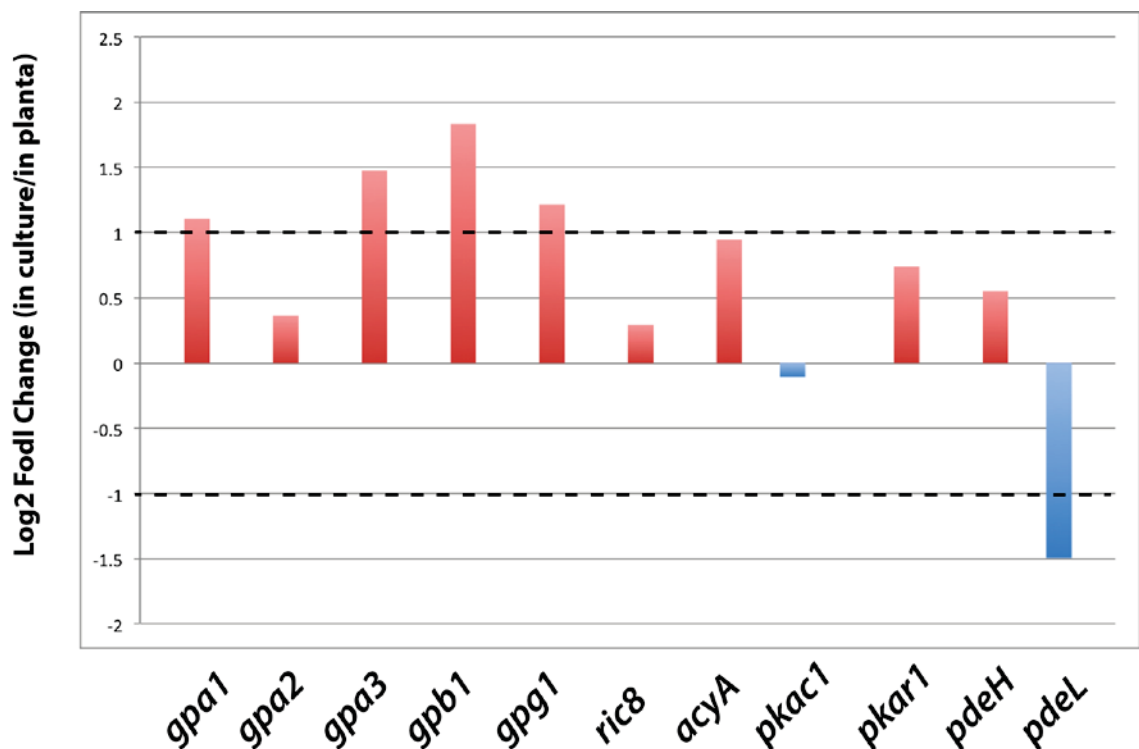


Figure 3-16 Transcriptional change of genes encoding components of the G protein and cAMP/PKA signalling pathway of the *E. festucae* wild-type in association with the host plant: Graphs showing expression-fold difference (\log_2) for differentially expressed genes of *E. festucae* in association with the host compared to growth on defined medium. Transcriptionally up-regulated (red) and down-regulated (blue) *in planta* of genes encoding components of the G protein and cAMP/PKA signalling pathway as listed in Table 3.4 and the low and high affinity cAMP phosphodiesterase, PdeL and PdeH (Table 3.3; Appendix 16). Cut-off for statistical significance of up- or down-regulated genes is indicated by black dashed line.

Chapter 4 Functional analysis of cAMP receptor-like G protein-coupled receptors

To investigate the role of cAMP-receptor like GPCRs in *E. festucae*, a reverse genetic approach was taken to delete genes encoding Gpr1a, Gpr1b and Gpr2 and to determine their function in hyphal growth, fungal development and effect on the host *L. perenne*.

4.1 Functional analysis of the Gpr1a

4.1.1 Attempted deletion of the *E. festucae gpr1a* gene

To examine the function of Gpr1a, a gene replacement construct (pAB01) was designed *in silico* (Fig. 4.1; Appendix 5), followed by *in vitro* amplification of fragments for construct assembly (2.5.10.1). While the 1413 bp 5' flanking fragment of the construct was successfully amplified using the primers gpr1a_1/gpr1a_2, initial attempts to amplify the 1322 bp 3' flank using the primers gpr1a_3/gpr1a_4 from wild-type genomic DNA as template were unsuccessful.

The GBrowse display of the *E. festucae* genome database and GC-Profile was used to analyse the GC/AT content of the *gpr1a* 3' flanking region at the wild-type genomic locus. This showed an enriched GC content (Fig. 4.2), which possibly could have resulted in mis-priming or DNA polymerase slippage, due to secondary structures such as hairpin loops, known to be formed in GC rich sequences (Mamedov et al. 2008). To try to overcome this problem, several alternative PCR methodologies, adapted to GC-rich DNA sequences (2.5.7.3) were applied, but the amplification of the *gpr1a* 3' flanking region remained unsuccessful. To remedy the problem, a cosmid library of *E. festucae* Fl1 genomic DNA (Tanaka et al. 2005) was screened to isolate cosmids containing the *gpr1a* locus to be used as an alternative DNA template for PCR. A radioactive isotope [³²P]-labelled *gpr1a* probe (2.5.14.1) was generated by PCR using the primers gpr1a_7 and gpr1a_8 (Fig. 1), which amplified a 307 bp product exclusively in the *gpr1a* gene sequence. Two clones, 30C2 and 33E10, were identified that hybridised with the probe (2.5.15) and were isolated (2.5.1.2). To test whether the *gpr1a* coding sequence and required 5' and 3' sequences were present, the two positive clones were analysed by restriction enzyme digestion using *EcoRI* and *BamHI* (2.5.3).

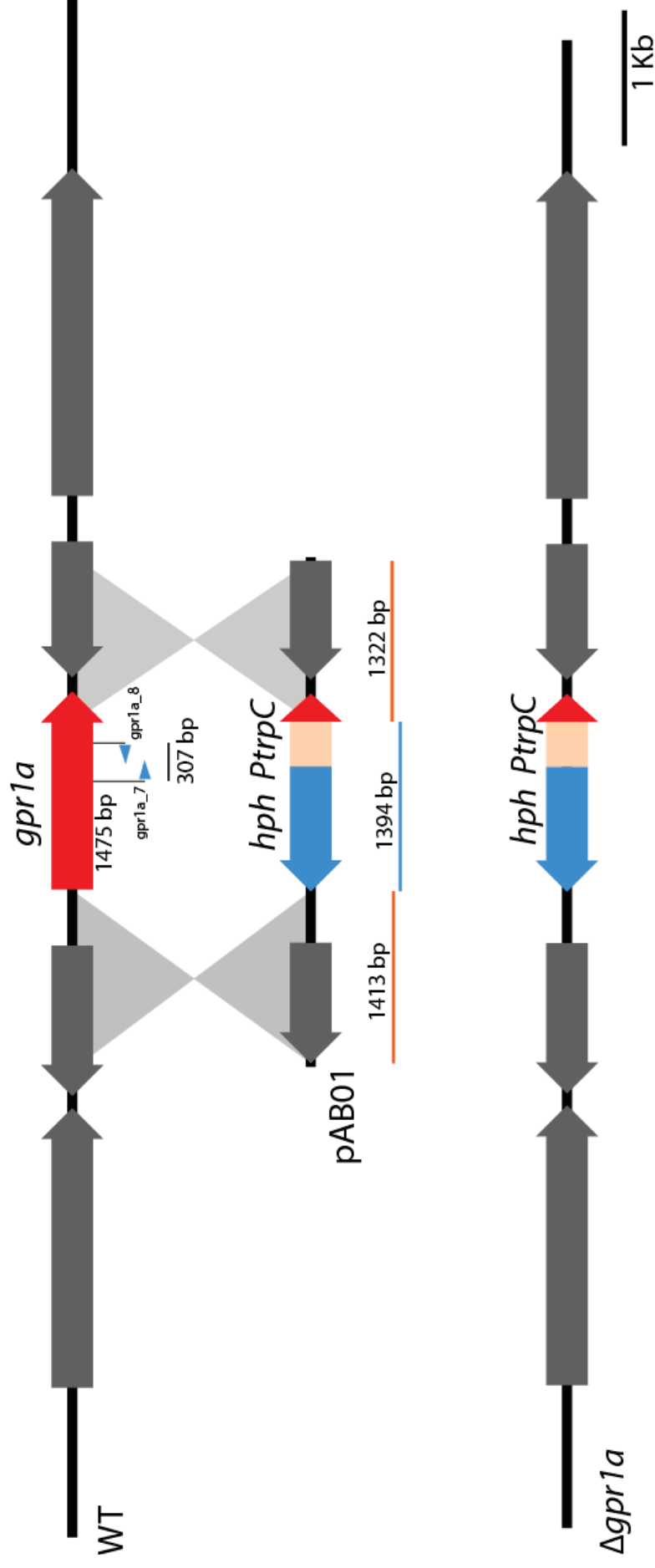


Figure 4-1 Strategy for deletion of *E. festucae gpr1a*: Physical map of the *gpr1a* genomic locus, linear insert of *gpr1a* replacement construct pAB01 and $\Delta gpr1a$ mutant locus. Primers *gpr1a_7* and *gpr1a_8* were used to amplify a fragment of *gpr1a* as a probe to screen an *E. festucae* cosmid library to identify clones containing *gpr1a*.

Showing 5 kbp from Supercontig66, positions 33,272 to 38,271

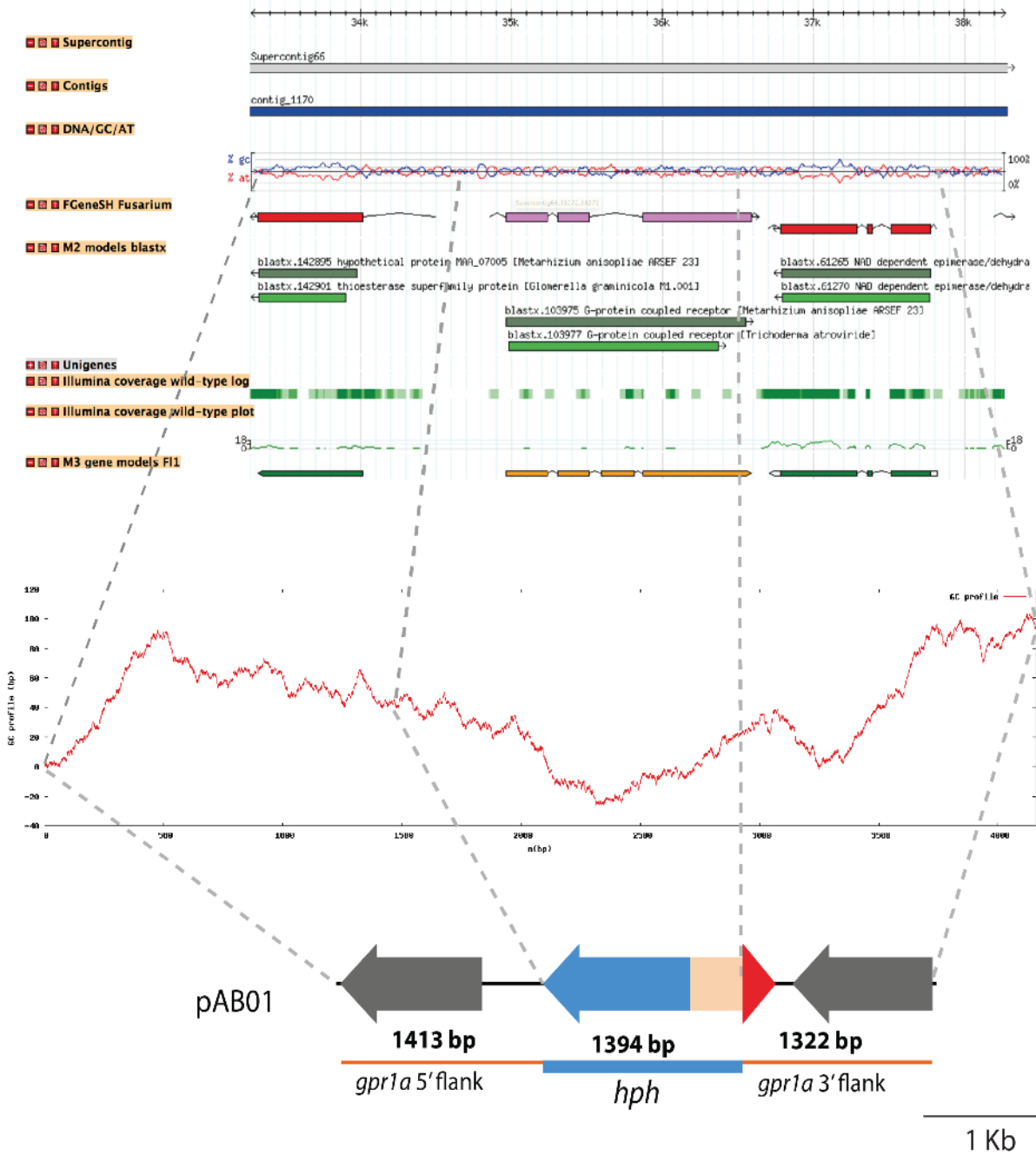


Figure 4-2 DNA GC content of *gpr1a* locus: Physical map of *gpr1a* genomic locus reproduced from GBrowse display (<http://csbio-l.csr.uky.edu/ef894-2011/gbrowse/ef/>) highlighting high GC content of adjacent sequence at this locus, the GC-profile (<http://tubic.tju.edu.cn/GC-Profile/>) of the native *gpr1a* locus and the adjacent 5' and 3' flanking region, aligned with the linear insert of the *gpr1a* replacement construct.

Both clones gave the expected restriction enzyme digest pattern predicted from the genome sequence (Fig. 4.3). Despite using cosmid DNA as the PCR template, only a low yield of the correct 1322 bp *gpr1a* 3' flanking fragment was amplified. This was gel purified and mixed with the purified *gpr1a* 5' flanking fragment and the *hph* selectable marker cassette to generate the *gpr1a* gene replacement construct (pAB01) using yeast recombinational cloning (2.5.10.9) or Gibson assembly (2.5.10.10) alternatively. However, no clones were identified with a restriction enzyme pattern consistent with the predicted map of pAB01.

Besides the correct 1322 bp fragment a non-specific 2900 bp fragment was strongly amplified (Fig. 4.4) using the 30C2 and 33E10 cosmid template-DNA and *gpr1a* 3' flanking primers (*gpr1a_3/gpr1a_4*) as well as using the *gpr1a* 5' flanking primers (*gpr1a_1/gpr1a_2*). The DNA sequence of the respective regions could not be matched to the *in silico* reference sequence that was initially designed. Conversely, a successful PCR amplification of the *gpr1a* 5' fragment (1413 bp) was achieved using the wild-type genomic DNA but not using cosmid DNA. Hence it was concluded that the strong amplification of the non-specific product could have occurred due to mis-priming or due to the formation of secondary structures in the GC rich region (Fig. 4.2).

The time required for modifying the method or alternative methods to generate the Δ *gpr1a* mutant strain exceeded the timeframe set for completion of the experiment and with no suitable available alternatives at that time point it was decided that no further attempts would be made to generate this construct.

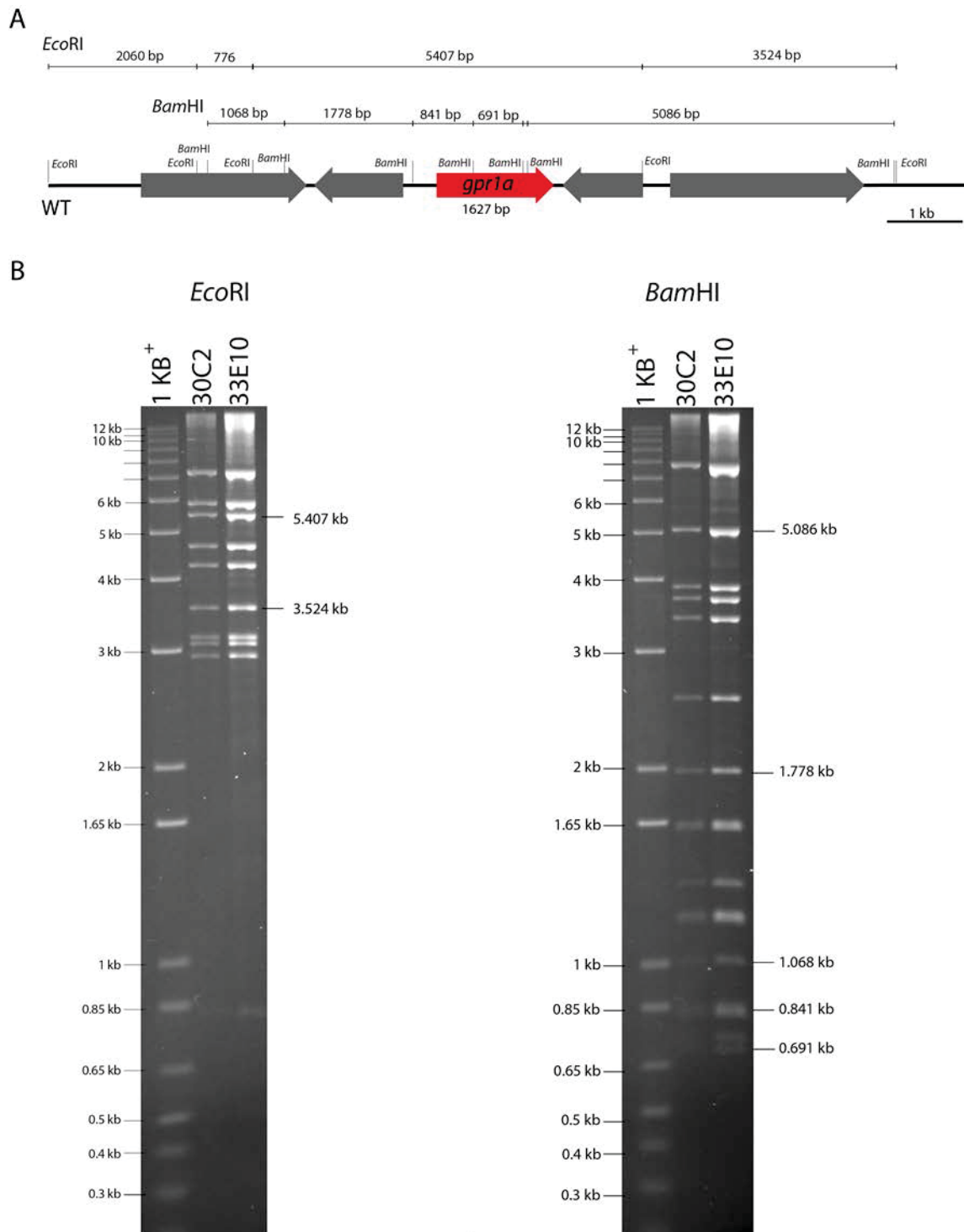


Figure 4-3 Molecular analysis of *E. festucae* *gpr1a*-containing cosmids: (A) Physical map of two *gpr1a*-containing cosmids showing their location in the *E. festucae* F11 genome. (B) Restriction enzyme digests of cosmids 30C2 and 33E10 separated by agarose gel electrophoresis alongside 1 kb⁺ DNA ladder standard. Sizes of fragments are shown in kilobase (kb).

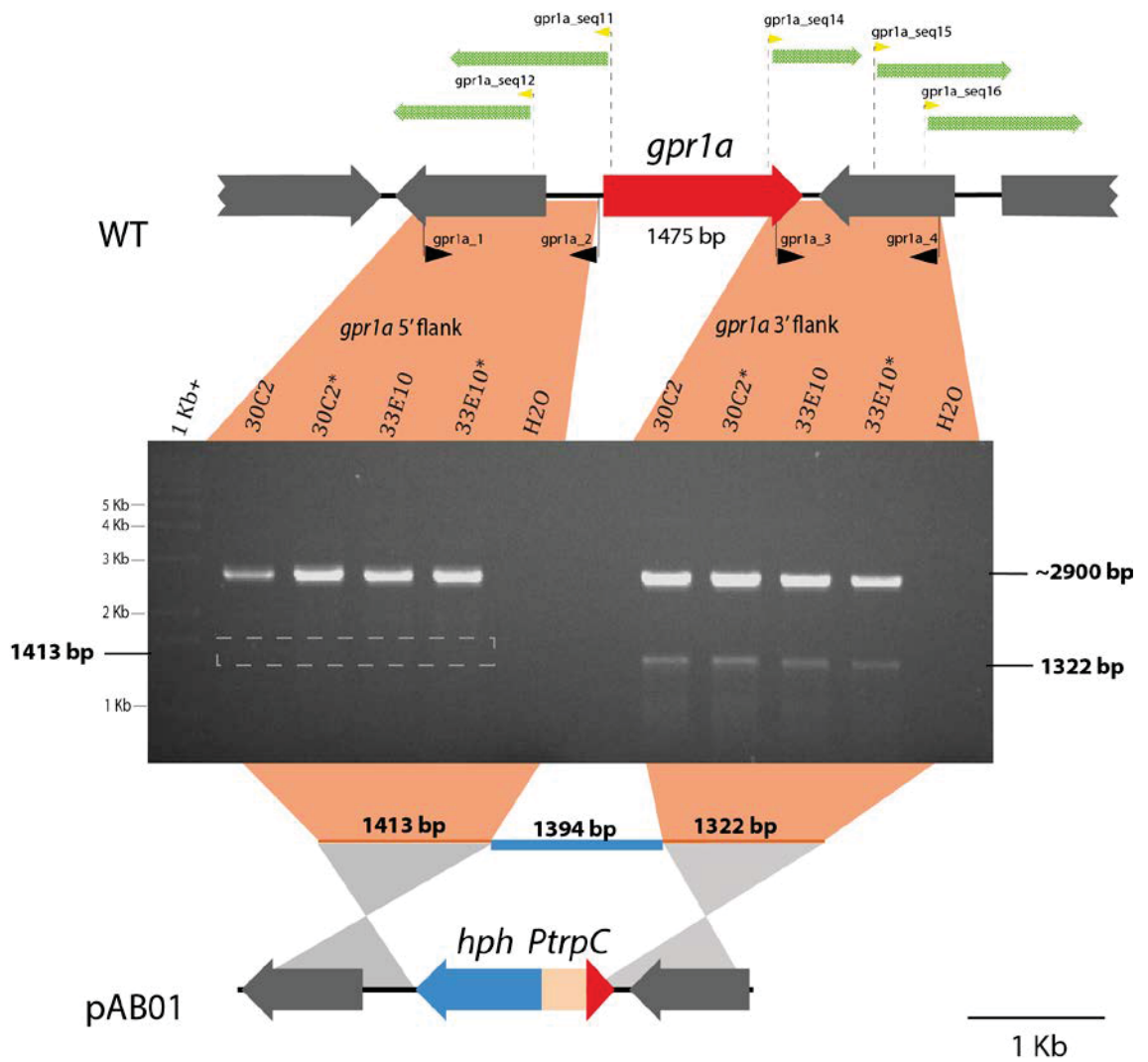


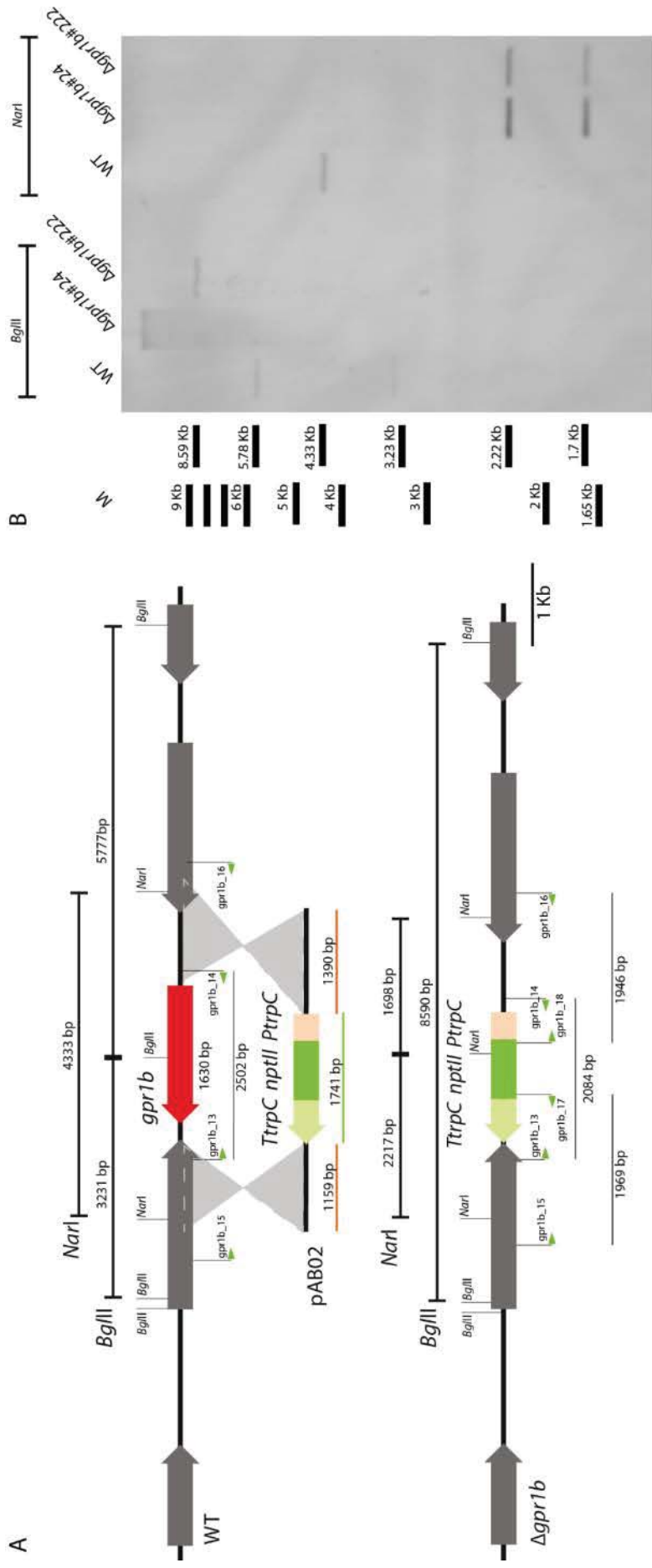
Figure 4-4 Physical map of *E. festucae gpr1a* locus and PCR amplification of non-specific products: Physical map of the *gpr1a* genomic locus, linearised *gpr1a* replacement construct pAB01 and $\Delta gpr1a$ mutant locus with overlay of PCR products amplified from 30C2 and 33E10 cosmid DNA using primers *gpr1a*_1 and *gpr1a*_2 to amplify the 5'- and *gpr1a*_3 and *gpr1a*_4 to amplify the 3'-flank of *gpr1a*. Also shown are the regions sequenced from cosmid 30C2 (green arrows) using primers indicated.

4.2 Functional analysis of the Gpr1b

4.2.1 Deletion of the *E. festucae* *gpr1b* gene

To functionally analyse the symbiotic role of Gpr1b in *E. festucae*, a gene deletion mutant of *gpr1b* was generated by replacing the *gpr1b* gene with the neomycin phosphotransferase (*nptII*) cassette using homologous recombination with the construct pAB02 (Fig. 4.5; Appendix 6; 2.5.10.2). A linear fragment containing the *nptII* cassette and *gpr1b* flanking regions was PCR-amplified from pAB02 plasmid DNA (2.5.7.2), purified (2.5.2), transformed into protoplasts of wild-type *E. festucae* (2.5.12), and screened for antibiotic resistance by growth on PD medium (2.3.3.1) containing geneticin. PCR screening of an arbitrary selection of these transformants identified three putative $\Delta gpr1b$ (#24, #190, #222) mutants, where two (#24, #222) of these candidates were confirmed as clean 'knock-outs' by genomic DNA digest and Southern blot (2.5.14) analysis (Fig. 4.5B).

Figure 4-5 Strategy for deletion of *gpr1b* and identification of $\Delta gpr1b$ mutant strains: (A) Physical map of the *gpr1b* genomic locus in wild-type *E. festucae* (WT), linear insert of the *gpr1b* replacement construct (pAB02) and $\Delta gpr1b$ mutant locus. Also shown are primers used to screen for *gpr1b* replacement mutants (gpr1b_13/gpr1b_14, gpr1b_15/gpr1b_17, gpr1b_16/gpr1b_18) and restriction enzyme cutting sites for *NaeI* and *BglII*. Digestion with *NarI*, followed by probing with pAB02 will produce a diagnostic single fragment of 4333 bp for the wild-type strain and fragments of 1698 bp and 2217 bp for $\Delta gpr1b$. Digestion with *BglII*, followed by probing with pAB02 will produce diagnostic fragments of 5777 bp and 3231 bp for wild-type strains and a single fragment of 8590 bp for $\Delta gpr1b$. (B) Autoradiograph of Southern blot of *BglII* and *NarI* genomic digest (1 μ g) of wild-type and $\Delta gpr1b$ strains probed with DIG-labelled linear insert of the *gpr1b* replacement construct (pAB02). Approximate fragment sizes in kilobase (kb).



4.2.2 Deletion of *gpr1b* does not alter fungal development in axenic culture

In axenic culture, the colony size and morphology of the $\Delta gpr1b$ strains were indistinguishable from wild-type (Fig. 4.6 A). Microscopic examination (2.8.1) of hyphal development and morphology was conducted in detail by bright field (BF) and inverted light microscopy (iLM) of stained hyphae (Fig. 4.6 B and 4.6 C), using Calcofluor white (CFW), which binds to fungal chitin in the cell wall and septa.

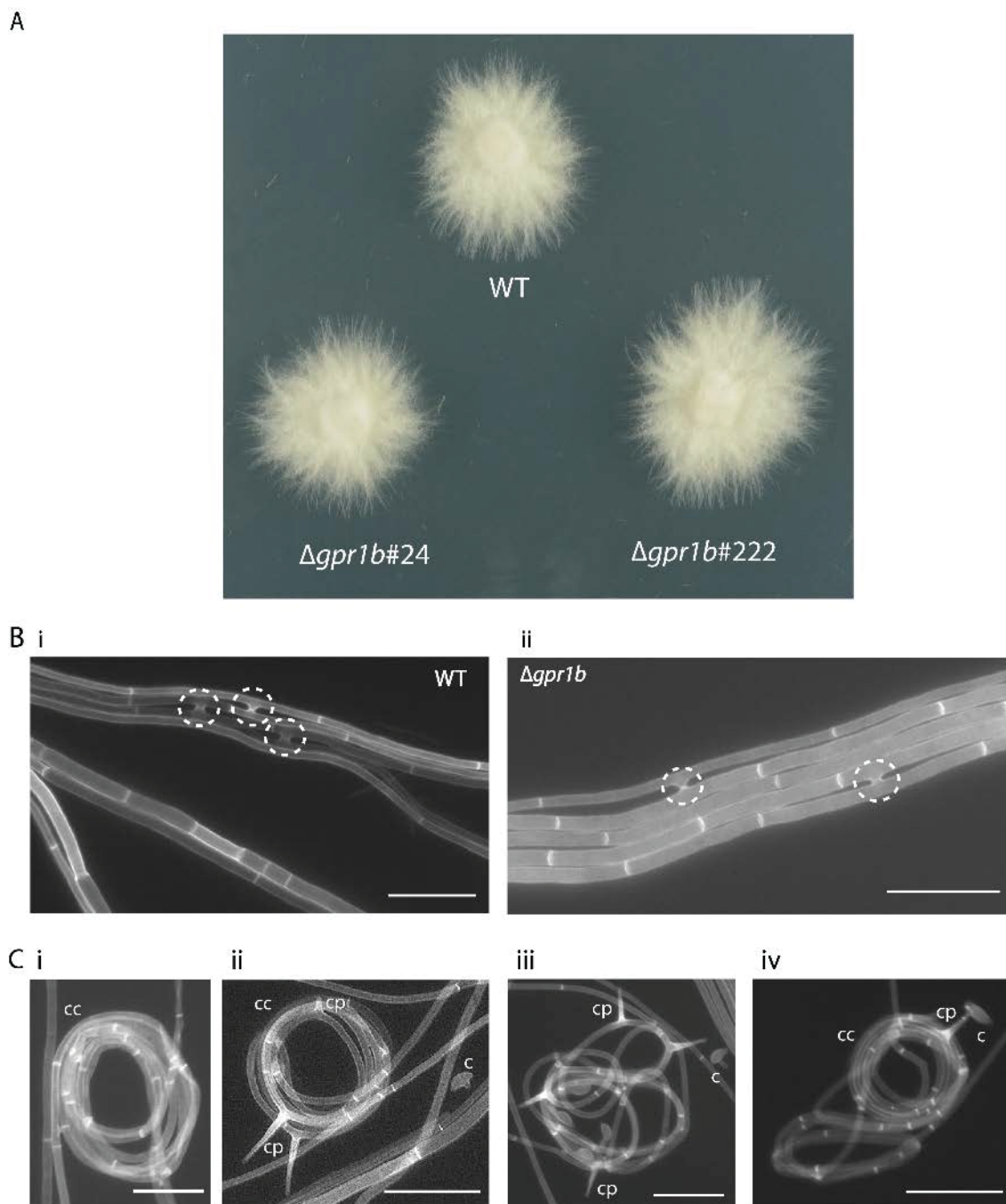


Figure 4-6 Culture phenotype analysis of the $\Delta gpr1b$ mutant strain: Phenotype analysis of the *E. festucae* $\Delta gpr1b$ mutant compared to the wild-type strain in axenic culture. (A) Growth on PD agar for 7 days. (B + C) Bright field (BF) light microscopy images of *E. festucae* $\Delta gpr1b$ mutant and wild-type (WT) strains grown on 3% H₂O agar for 10 days. Hyphal cell wall and septa stained with Calcofluor white (CFW). (B) Hyphal growth of the $\Delta gpr1b$ mutant strain with frequent hyphal fusion (circles). (C) Hyphae growing in coils (cc) to form conidiophores (cp) and conidiospores (c). Bar = 20 μ m.

The microscopic examination showed, that wild-type and $\Delta gpr1b$ mutant strains similarly form bundles of hyphae (Fig. 4.6 B), undergo hyphal fusion (Fig. 4.6 B, Fig. 4.7) and grow in coils of hyphae from which conidiophores arise (Fig. 4.6C). Conidia formation and conidiophore development, indirectly quantified by the number of colonies that arose from single spore isolation (2.5.13), of the $\Delta gpr1b$ mutant strain was similar to that observed for the wild-type strain.

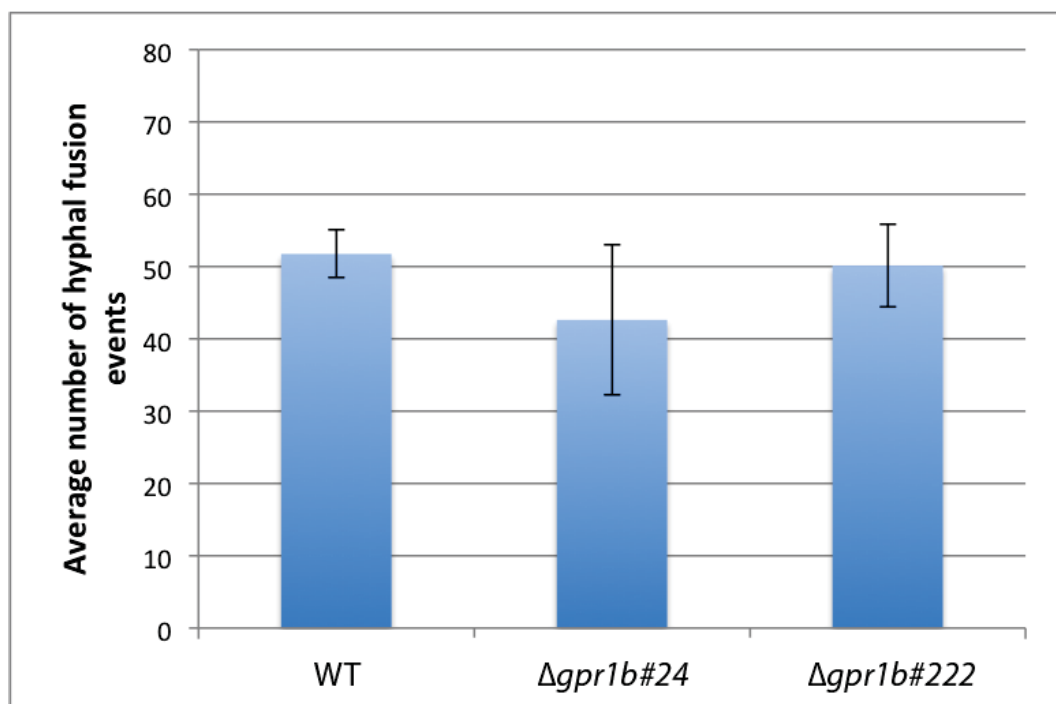


Figure 4-7 Hyphal fusion event in $\Delta gpr1b$ mutant strains: Graph showing no significant differences (*Student's t-test*) in the average number of hyphal fusion events of the wild-type (WT) and the $\Delta gpr1b$ mutant strains ($\Delta gpr1b\#24$, $\Delta gpr1b\#222$) in axenic culture, grown on 3% water agar (H₂O) for 10 days at 22°C. Hyphal fusion events were counted at 10 microscopic sites per strain in eight independent repeats. (Mean \pm SD)

Colony growth and morphology was further tested on different media including Blankenship (2.3.3.7), modified Czapek-DOX (2.3.3.6), CDGN (2.3.3.4), media facilitating nutrient starvation (CD (2.3.3.5), H₂O (2.3.3.3)) and defined media containing CD salts and various carbon and/or nitrogen sources as listed in Table 2.3. No noticeable differences in growth of $\Delta gpr1b$ mutant strains compared to the wild-type strain was observed on all media that were tested.

4.2.3 Deletion of *gpr1b* caused a dramatic breakdown of the symbiotic interaction

4.2.3.1 Symbiotic interaction phenotype of $\Delta gpr1b$ strains

To determine whether Gpr1b was required for establishment and maintenance of a mutualistic symbiotic interaction, seedlings of *L. perenne* were inoculated (2.7.3) with wild-type and the $\Delta gpr1b$ mutant strains. In contrast to wild-type, $\Delta gpr1b$ infected plants showed a high mortality about 3-5 weeks post inoculation. From those plants that survived, single tillers were immunoblotted (2.7.6) at 10-12 weeks post inoculation, to identify which plants were infected. Plants infected with $\Delta gpr1b$ were severely stunted with only one or two remaining tillers, exhibited premature senescence and had poorly developed root systems, compared to plants infected with wild-type (Fig. 4.8). Infected plants were subsequently analysed by microscopy (2.8.2).



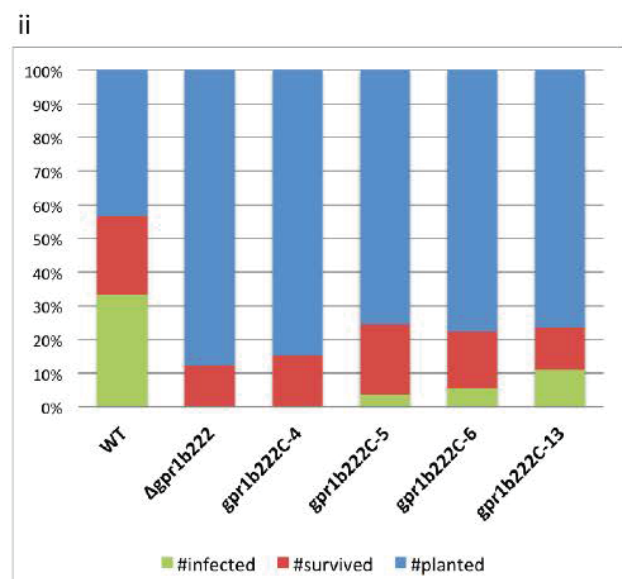
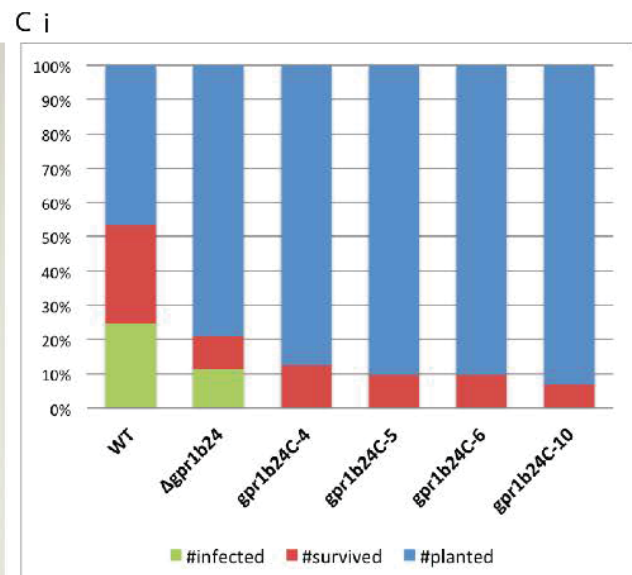
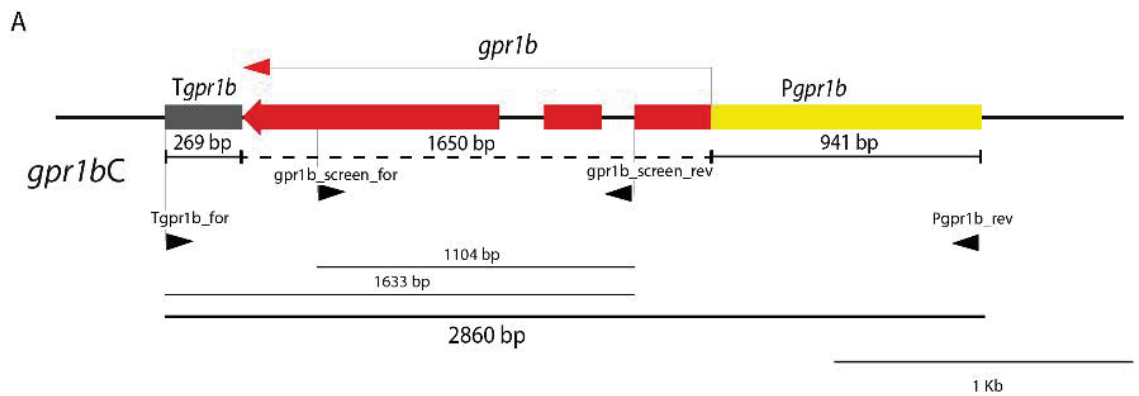
Figure 4-8 Symbiosis phenotype of *Lolium perenne* infected with $\Delta gpr1b$ mutant strain: Phenotype of perennial ryegrass plants infected with *Epichloë festucae* wild-type (WT) and the two independent $\Delta gpr1b$ mutant strains $\Delta gpr1b\#24$ and $\Delta gpr1b\#222$. Dead leaves were removed for imaging. Photographs were taken 12 weeks post-inoculation.

To confirm the phenotype observed was due to deletion of *gpr1b*, a construct containing a wild-type copy of *gpr1b* (a linear 2860 bp fragment amplified by PCR using Tgpr1b_for/Pgpr1b_rev) was prepared (pAB06; Appendix 10) (2.5.10.6). For selective screening, the pAB06 plasmid was co-transformed (2.5.12.2) with pSF15.15 (Appendix 3) into the $\Delta gpr1b$ mutant background to facilitate resistance against hygromycin in addition to the geneticin resistance of the $\Delta gpr1b$ mutant strain. The resulting transformants were screened for antibiotic resistance by growth on PD medium (2.3.3.1) containing hygromycin and an arbitrary selection of transformants were screened by PCR (Fig. 4.9A).

As expected, PCR using primers gpr1b_screen_for/gpr1b_screen_rev, Tgpr1b_for/gpr1b_screen_rev, gpr1bC_seq5/Pgpr1b_rev and Tgpr1b_for/Pgpr1b_rev produced bands of 1104 bp, 1633 bp, 1445 bp and 2860 bp, respectively that identified integrity of ectopically integrated construct. Four of the positive identified strains of each mutant background, $\Delta gpr1b\#24$ (*gpr1b\#24C-4*, *gpr1b\#24C-5*, *gpr1b\#24C-6*, *gpr1b\#24C-10*) and $\Delta gpr1b\#222$ (*gpr1b\#222C-4*, *gpr1b\#222C-5*, *gpr1b\#222C-6*, *gpr1b\#222C-13*), were inoculated into *L. perenne* plants for further analysis (2.7.3). Introduction by ectopic integration of a *gpr1b* wild-type copy did not restore the wild-type interaction phenotype (Fig. 4.9B). Plants infected with these strains had a mortality rate similar to plants infected with $\Delta gpr1b\#222$ mutant strains (Fig. 4.9C). Unfortunately, time and financial restraints did not allow further experiments, including the quantification of gene expression of the ectopically integrated complementation constructs, ectopic integration of the complementation construct under a stronger promoter or re-insertion of the construct into the native locus by homologous recombination. However due to the two independent mutants $\Delta gpr1b\#24$ and $\Delta gpr1b\#222$, which exhibited a similar plant interaction phenotype as described above, it is highly likely that the deletion of *gpr1b* is causing the observed phenotype.

Figure 4-9 Complementation of $\Delta gpr1b$ mutant strain: (A) Physical map of the *gpr1b* complementation (pAB06), containing 941 bp of the promoter sequence (yellow), the wild-type copy of *gpr1b* (red) and 269 bp of the terminator sequence (grey). Also shown are primers used for PCR amplification (Tgpr1b_for/Pgpr1b_rev) and screening for integration of *gpr1b* in the $\Delta gpr1b\#222$ mutant background (gpr1b_screen_for/gpr1b_screen_rev, gpr1bC_seq5/Pgpr1b_rev,

Tgpr1b_for/gpr1b_screen_rev) and PCR product sizes. (B) Phenotype of perennial ryegrass plants infected with *E. festucae* wild-type (WT) and complementation strains *gpr1b222C-6* and *gpr1b222C-13*. Dead leaves were removed for imaging. Photographs were taken 12 weeks post-inoculation. (C) Graphs showing the proportion of plants, inoculated with the respective fungal strains in the (i) $\Delta gpr1b\#24$ and (ii) $\Delta gpr1b\#222$ mutant background, that were planted (blue), survived (red) and were infected (green), superimposed onto each other.



4.2.3.2 Microscopic analysis reveals unrestricted growth and increase of fungal biomass *in planta*

To examine the cellular phenotype, plants infected with the *Δgpr1b* mutant were harvested and pseudostem tissue was analysed using transmission electron microscopy (TEM; 2.8.2.2) and confocal laser scanning microscopy (CLSM; 2.8.2.1).

Wild-type infected plants typically showed one to three electron dense hyphae per intercellular space and no colonisation of the vascular bundles (Fig. 4.10 B; Fig. 4.11 A, B, E). In contrast, plants infected with *Δgpr1b* displayed an unrestricted pattern of fungal growth (Fig. 4.10 D; Fig. 4.11 C, D, F), resulting in increased fungal biomass. Multiple hyphae of *Δgpr1b* were observed in intercellular spaces (Fig. 4.11 C and D; Fig. 4.12) and extensive colonisation of the plant vascular bundles was observed (Fig. 4.10; Fig. 4.11 F). While hyphae in the vascular bundle tissue appeared to be more electron-dense, presumably reflecting the abundant supply of nutrients, hyphae in other tissue were highly vacuolated and frequently formed intrahyphal hyphae especially underneath the cuticle layer (Fig. 4.11 I, K), suggestive of nutrient starvation and stress. The wild-type strains exhibited an electron dense darkly stained layer surrounding the hyphae (Fig. 4.11 A, B), which was not observed around hyphal bundles consisting of large numbers of hyphae or subcuticular hyphae of the *Δgpr1b* mutant strains (Fig. 4.11 D, I, K). This suggests a potential alteration of the cell-wall composition of *Δgpr1b* mutants when hyphae were accumulated into bundles or exposed to nutrient-deficit stress.

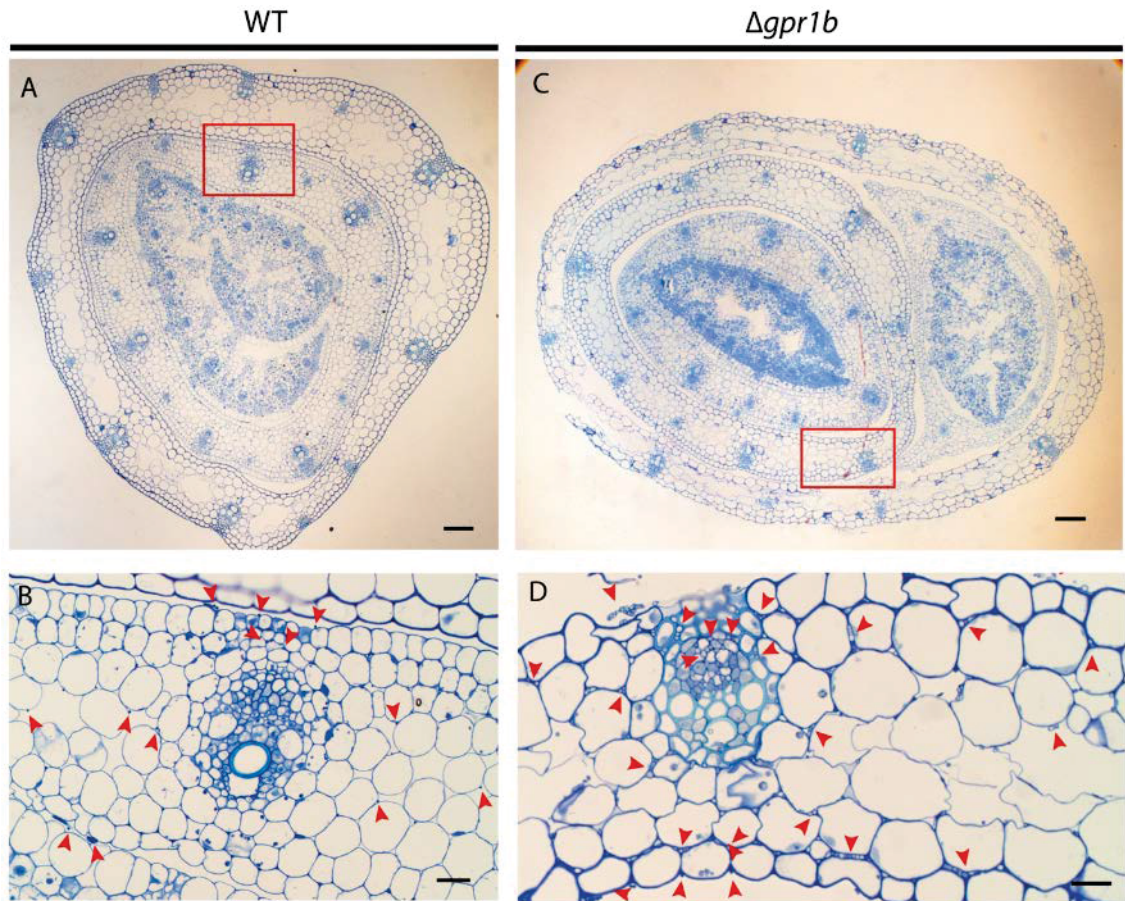


Figure 4-10 Light microscopy of the $\Delta gpr1b$ mutant strain *in planta*: Microscopic analysis of ryegrass pseudostem tissue infected with the wild-type and $\Delta gpr1b$ mutant strain using light microscopy (LM). Transverse sections of ryegrass pseudostem tissue infected with wild-type (A + B) and $\Delta gpr1b$ mutant strain (C + D), stained with toluidine blue. Light micrograph shows increased fungal colonisation including colonisation of the host vascular bundles and epiphyllous hyphae for $\Delta gpr1b$ (D). Arrow indicates hyphae position. Red box in A and C indicates the magnified area in B and D, respectively. Bar = 100 mm (A + C) and 20 mm (B + D).

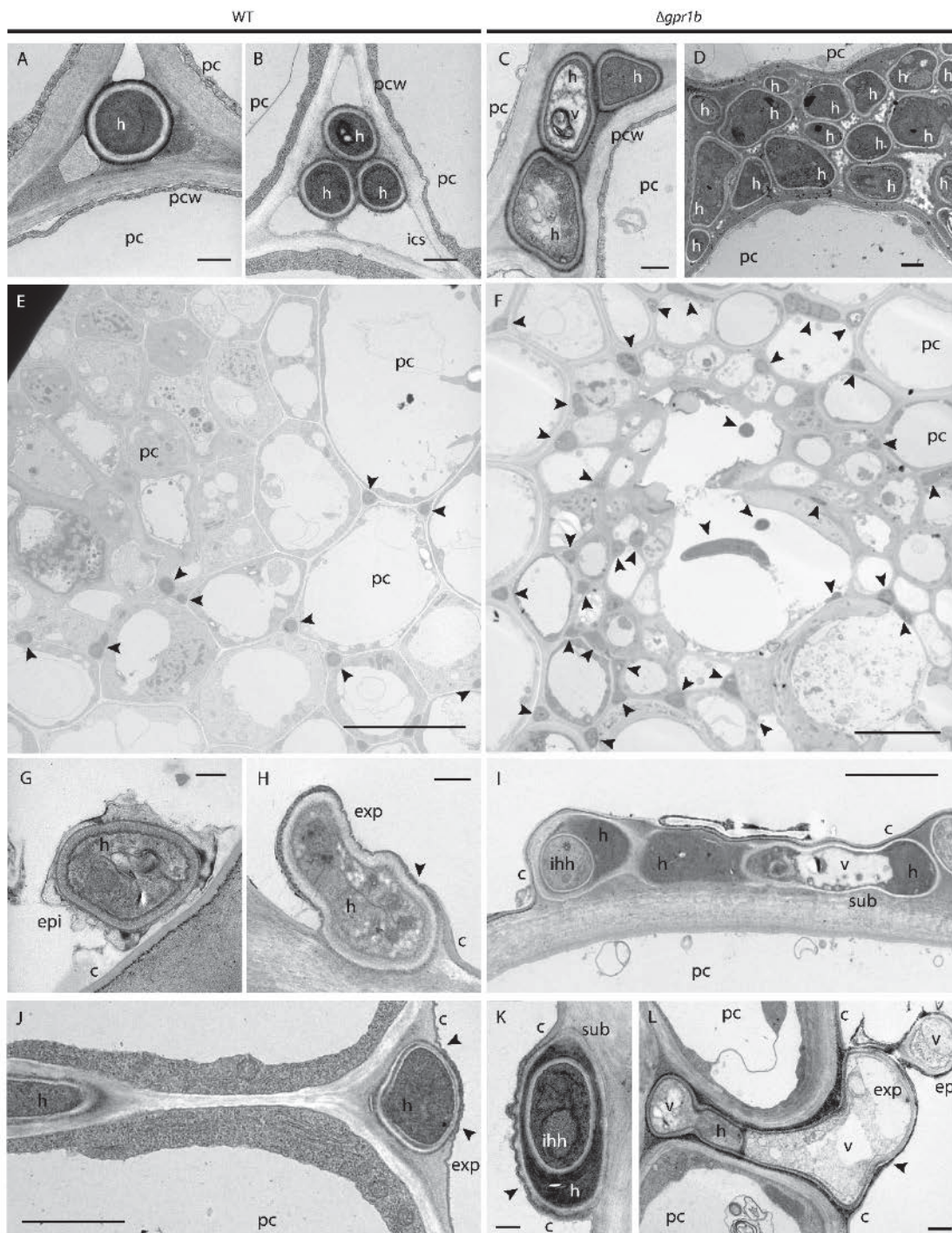


Figure 4-11 Transmission electron microscopy of the *Δgpr1b* mutant strain *in planta*: Microscopic analysis of ryegrass pseudostem tissue infected with the wild-type and *Δgpr1b* mutant strain using transmission electron microscopy (TEM). Micrographs of cross-sections show hyphal growth in host apoplast with multiple hyphae per intercellular space (C, D); colonisation of vascular bundles (F), highly vacuolated hyphae (C, I, L), intrahyphal hyphae (ihh) formed by *Δgpr1b* mutant strains especially in hyphae underneath the plant cuticle (c), referred to as sub-cuticular hyphae (sub) (I, K). Epiphyllous hyphae (epi) and expressoria-like structure (exp) (L) formed. Arrow indicates fungal hyphae in E and F, Arrows indicates hyphal breaching through plant cuticle in H, J - L. Bar = 500nm (A -D, G, H, K, L), 10 μ m (E, F), 2 μ m (I, J).

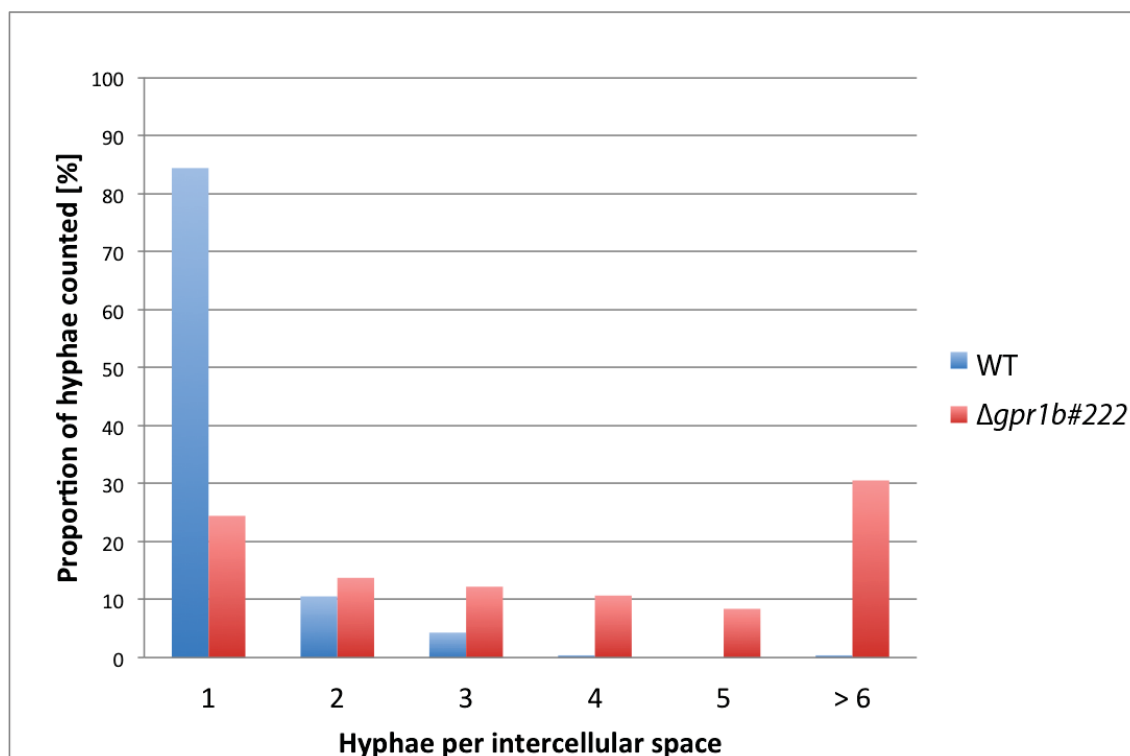
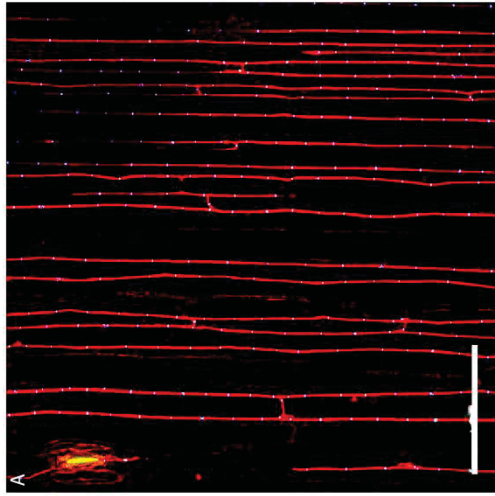


Figure 4-12 Hyphae per intercellular space of $\Delta gpr1b$ mutant strain: Graph showing the proportion of hyphae per intercellular space in *L. perenne* tissue, infected with the wild-type (WT) and the $\Delta gpr1b\#222$ mutant strain.

The prolific growth of the $\Delta gpr1b$ mutants in leaf tissue compared to the more restrictive growth of the wild-type infected plants was also evident using CLSM (Fig. 4.13). Longitudinal sections of pseudostem were stained (2.8.2.1) with aniline blue (red pseudocolour) and WGA-AlexaFlour488 (blue pseudocolour), which stain the fungal β -glucan and fungal chitin in cell walls and septa respectively (Ram and Klis 2006). Beside the increased number of fungal hyphae, no altered hyphal morphology or irregular growth patterns were observed for $\Delta gpr1b$. Frequent hyphal fusion from lateral branching was not impaired in $\Delta gpr1b$ mutants (Fig. 4.13), unlike in mutants with a similar prolific cellular phenotype *in planta* such as $\Delta proA$, Δnox , $\Delta saka$, $\Delta mpkA$, $\Delta mkkA$, $\Delta symB$ or $\Delta symC$ (Takemoto et al. 2006, Tanaka et al. 2006, Eaton et al. 2008, Becker et al. 2015, Green et al. 2016).

WT



$\Delta gpr1b$

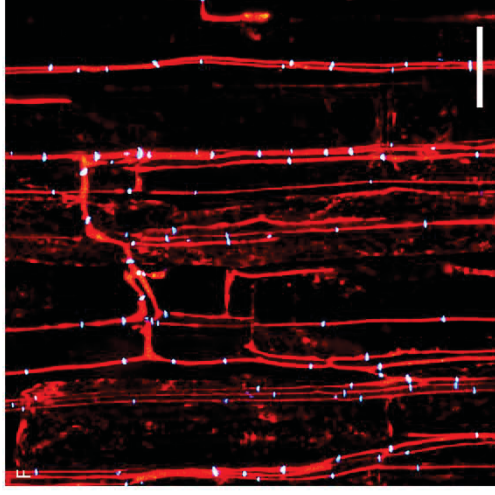
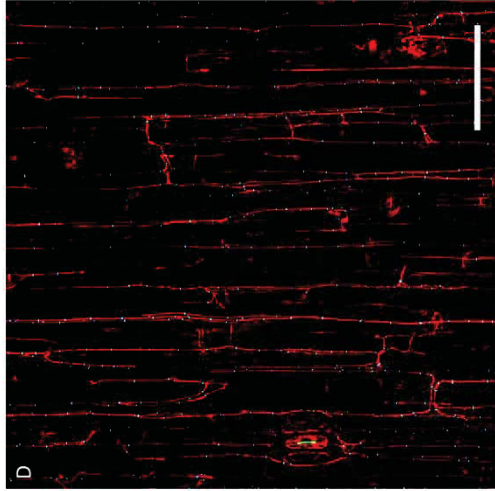
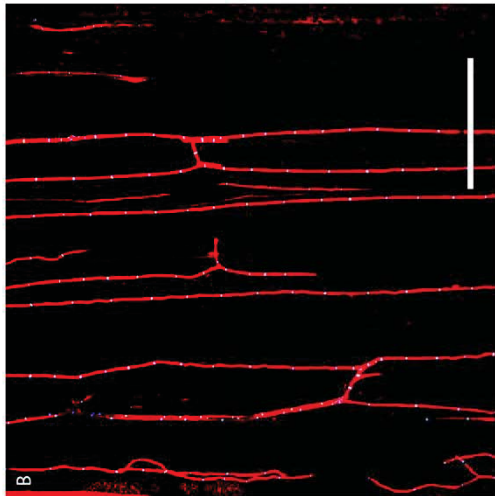
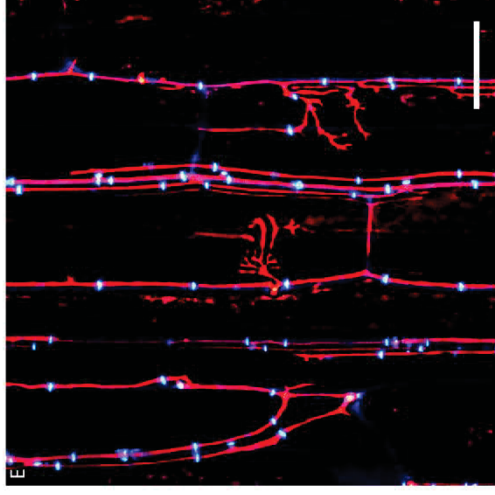
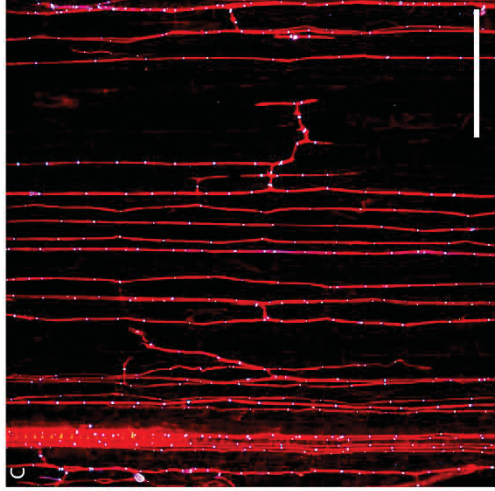


Figure 4-13 Confocal laser-scanning microscopy of the *Δgpr1b* mutant strain *in planta*: Microscopic analysis of ryegrass pseudostem tissue infected with the wild-type (WT) and *Δgpr1b* mutant strains using confocal laser-scanning microscopy (CLSM) showing longitudinal section with hyphal growth parallel to the leaf axis. The *Δgpr1b* mutant strain (C-F) with increased fungal biomass compared to wild-type (A-B) infected plants. Plant tissue stained using aniline blue (red pseudocolour) and WGA-AlexaFluor488 (blue pseudocolour). Frequent hyphal fusion occurs in WT and *Δgpr1b* mutant strain. Confocal depth series images generated by maximum intensity projection of 10 x 1 μm confocal Z-stacks. Bar = 100 μm A, C, D; Bar = 20 μm B, E, F.

4.2.3.3 *Δgpr1b* strains display an increased number of epiphyllous hyphae

Analysis by TEM also revealed an increased number of epiphyllous hyphae, emerging on the surface of leaf sheaths and blades (Fig. 4.10 d). Hyphae exiting the plant by formation of expressoria structures were connected with the endophytic network (Becker et al. 2016). In *Δgpr1b*-infected plants, epiphyllous hyphae were highly vacuolated and frequently showed intrahyphal hyphae. Due to the severe plant interaction phenotype and the high mortality rate of potentially infected plants growing under sterile conditions (2.7.5), expressoria and epiphyllous growth could not be analysed using scanning electron microscopy (SEM). Expressoria structures, allowing *E. festucae* hyphae to emerge from the host plant, seemed to be impaired in penetration of the plant cuticle (Fig. 4.11 I, K, L). Thinning of the cuticle, as found for expressoria structures formed in wild-type (Becker et al. 2016), was not observed for *Δgpr1b*, resulting in hyphae unable to exit the plant. As a result, large numbers of subcuticular hyphae and hyphal bundles were formed (Fig. 4.11 I). Eventually these hyphae rupture the cuticle possibly by increased pressure, through increased fungal biomass, and/or by degradation of the cuticle (Fig. 4.11 L). To date it is not clear whether cellular differentiation for expressorium formation or any other unknown factors was impaired at the point of physical contact between the hyphal tip and the plant cuticle layer.

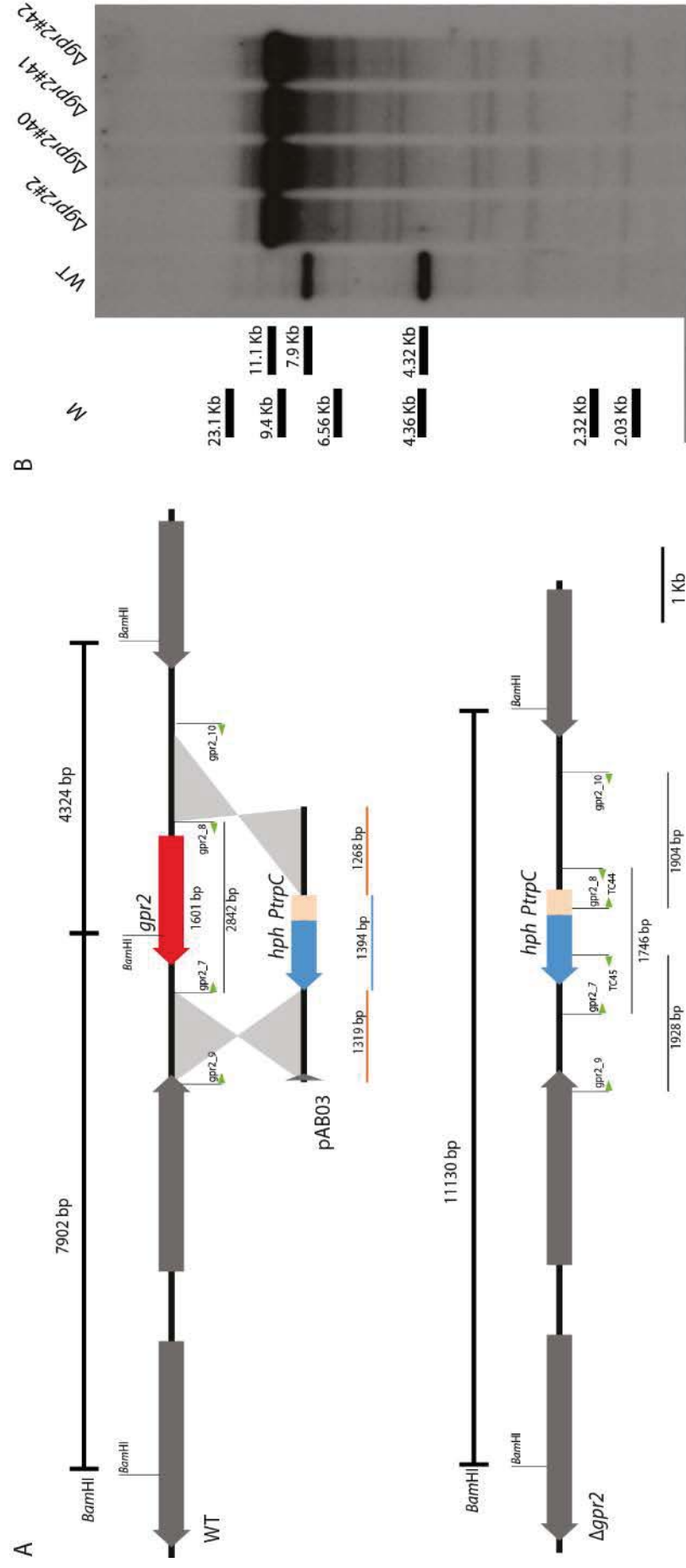
In summary, the strong symbiotic interaction phenotype, with increased fungal biomass and unrestricted fungal growth shows that the disruption of *Gpr1b* highly affects restricted growth of *E. festucae in planta*.

4.3 Functional analysis of the Gpr2

4.3.1 Deletion of the *E. festucae* *gpr2* gene

To functionally analyse the symbiotic role of Gpr2 in *E. festucae*, a gene deletion mutant of *gpr2* was generated by replacing the *gpr2* gene with the hygromycin B phosphotransferase (*hph*) cassette using homologous recombination with the construct pAB03 (Fig. 4.14 A; Appendix 7; 2.5.10.3). A linear fragment containing the *hph* cassette and *gpr2* flanking regions was PCR-amplified from pAB03 plasmid DNA (2.5.7.2), purified (2.5.2), transformed into protoplasts of wild-type *E. festucae* (2.5.12), and screened for antibiotic resistance by growth on PD medium (2.3.3.1) containing hygromycin. PCR screening of an arbitrary selection of these transformants identified four putative for $\Delta gpr2$ mutants (#2, #40, #41, #42) which were then confirmed as clean 'knock-outs' by genomic DNA digest and Southern blot (2.5.14) analysis (Fig. 4.14 B).

Figure 4-14 Strategy for deletion of and identification of $\Delta gpr2$ mutant strains: (A) Physical map of the *gpr2* genomic locus in wild-type *E. festucae* (WT), linearised *gpr2* replacement fragment construct (pAB03) and $\Delta gpr2$ mutant locus. Also shown are primers used to screen for *gpr2* replacement mutants (*gpr2_7/gpr2_8*, *gpr2_9/TC45*, *TC44/gpr2_10*) and restriction enzyme cutting sites for *Bam*HI. Digestion with *Bam*HI, followed by probing with pAB03 will produce diagnostic fragments of 7902 bp and 4324 bp for wild-type strains and a single fragment of 11130 bp for $\Delta gpr2$. (B) Autoradiograph of Southern blot of *Bam*HI genomic digest (1 μ g) of wild-type and $\Delta gpr2$ strains probed with [³²P]-labelled linear insert of the *gpr2* replacement construct (pAB03). Approximate fragment sizes in kilobase (kb).



4.3.2 Deletion of *gpr2* had no effect on fungal development in axenic culture

In axenic culture, the colony size and morphology of $\Delta gpr2$ strains were indistinguishable from wild-type (Fig. 4.15 A). Microscopic examination (2.8.1) of hyphal development and morphology was conducted using bright field (BF) and inverted light microscopy (iLM) of stained hyphae (Fig. 4.15 B, C), using Calcofluor white (CFW) (2.8.1). Given all four *gpr2* mutant had an identical culture phenotype just the mutant strains $\Delta gpr2\#2$ and $\Delta gpr2\#41$ were used for all subsequent phenotype analysis unless stated otherwise.

Microscopic analysis showed, that the wild-type and the $\Delta gpr2$ mutant strains form hyphal bundles (Fig. 4.15 B), undergo hyphal fusion at a similar frequency to wild-type (Fig. 4.15 B; Fig. 4.16) and form coils of hyphae from which conidiophores arise. Conidia formation and conidiophore development of the $\Delta gpr2$ mutant strain was similar to that observed for the wild-type strain. Conidia formation was quantified by counting colonies that arose from single-spore isolation (Section 5.2.2) (2.5.13).

Colony growth and morphology was further tested on different media including Blankenship (2.3.3.7), modified Czapek-DOX (2.3.3.6), CDGN (2.3.3.4), media facilitating nutrient starvation (CD (2.3.3.5), H₂O (2.3.3.3)) and defined media containing CD salts and various different carbon and/or nitrogen supplements as listed in Table 2.3. No noticeable differences in growth of the $\Delta gpr2$ mutants compared to the wild-type strain was observed.

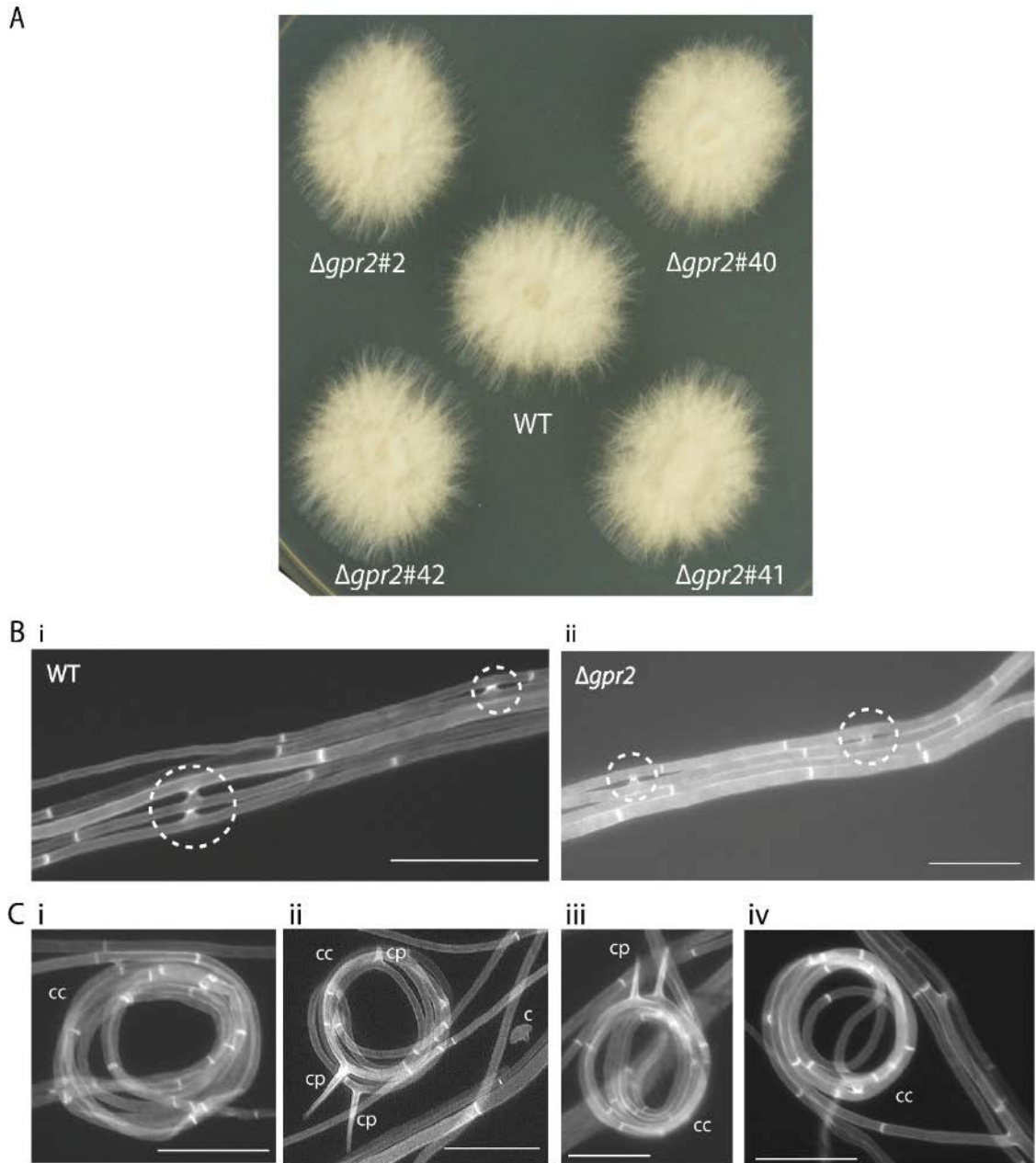


Figure 4-15 Culture phenotype analysis of $\Delta gpr2$ mutant strain: Phenotype analysis of the *E. festucae* $\Delta gpr2$ mutant compared to the wild-type strain in axenic culture. (A) Growth on PD agar for 7 days. (B) Bright field (BF) light microscopy images of *E. festucae* $\Delta gpr2$ mutant and wild-type (WT) strains grown on 3% H₂O agar for 10 days. Hyphal cell wall and septa stained with Calcofluor white (CFW); hyphal growth of $\Delta gpr2$ mutant strain with frequent hyphal fusions (circles); (C) hyphae growing in coils (cc) to form conidophores (cp) and conidiospores (c). Bar = 20 μ m.

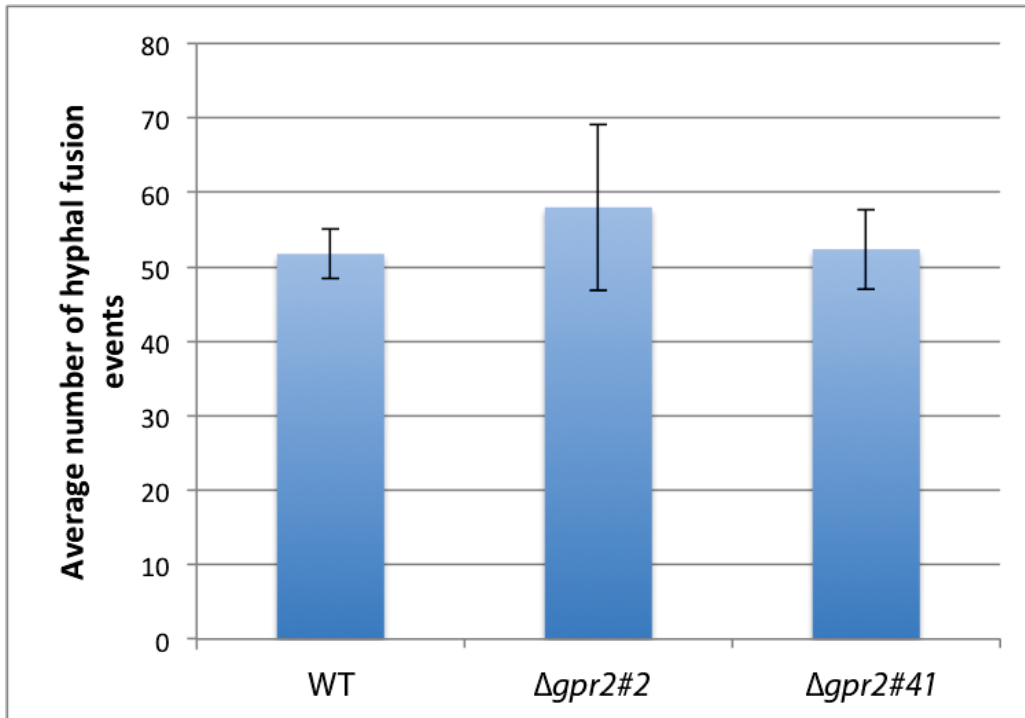


Figure 4-16 Hyphal fusion event in $\Delta gpr2$ mutant strains: Graph showing no significant differences (*Student's t-test*) in the average number of hyphal fusion events of the wild-type (WT) and the $\Delta gpr2$ mutant strains ($\Delta gpr2\#2$, $\Delta gpr2\#41$) in axenic culture, grown on 3% water agar (H₂O) for 10 days at 22°C. Hyphal fusion events were counted at 10 microscopic sites per strain in eight independent repeats. (Mean ± SD).

4.3.3 Gpr2 does not show a functional role in the plant symbiotic interaction

4.3.3.1 Symbiotic interaction phenotype of $\Delta gpr2$ strains

To determine whether Gpr2 was required for establishment and maintenance of a mutualistic symbiotic interaction, seedlings of *L. perenne* were inoculated (2.7.3) with wild-type and all four $\Delta gpr2$ mutant strains individually. After 10-12 weeks post inoculation, single tillers were immunoblotted (2.7.6) to identify which plants were infected. The symbiosis phenotype of wild-type and $\Delta gpr2$ infected plants were indistinguishable (Fig. 4.17). Infected plants were subsequently analysed by microscopy (2.8.2). Because there was no observable culture or plant phenotype for $\Delta gpr2$ no complementation test was carried out.



Figure 4-17 Symbiosis phenotype of *Lolium perenne* infected with $\Delta gpr2$ mutant strain: Phenotype of perennial ryegrass plants infected with *Epichloë festucae* wild-type (WT) and four independent $\Delta gpr2$ mutant strains $\Delta gpr2\#2$, $\Delta gpr2\#40$, $\Delta gpr2\#41$ and $\Delta gpr2\#42$. Dead leaves were removed for imaging. Photographs were taken 12 weeks post-inoculation.

4.3.3.2 Microscopic analysis of $\Delta gpr2$ revealed wild-type like fungal colonisation of host tissue

To examine the cellular phenotype, plants infected with the fungal $\Delta gpr2$ mutant strains were sampled and pseudostem tissue was analysed using transmission electron microscopy (TEM; 2.8.2.2) and confocal laser scanning microscopy (CLSM; 2.8.2.1).

Plants infected with the wild-type or $\Delta gpr2$ showed identical plant phenotypes with the typical restricted pattern of growth, systemic colonisation of one-two electron dense hyphae per intercellular space and an absence of hyphae in the vascular bundles (Fig. 4.18; Fig. 4.19 A-C and D-E; Fig. 4.20). Epiphyllous hyphae and expressoria formation were similarly observed in $\Delta gpr2$ and wild-type strain (Fig. 4.19 F-K).

The indistinguishable cellular phenotype of wild-type and $\Delta gpr2$ infected plant tissue was also evident using CLSM (Fig. 4.21). CLSM analysis was performed as for the $\Delta gpr1b$ mutant strain (2.8.2.1). Aligned hyphal growth along the leaf axis, hyphal branching and fusion and overall fungal biomass was indistinguishable from the wild-type strain.

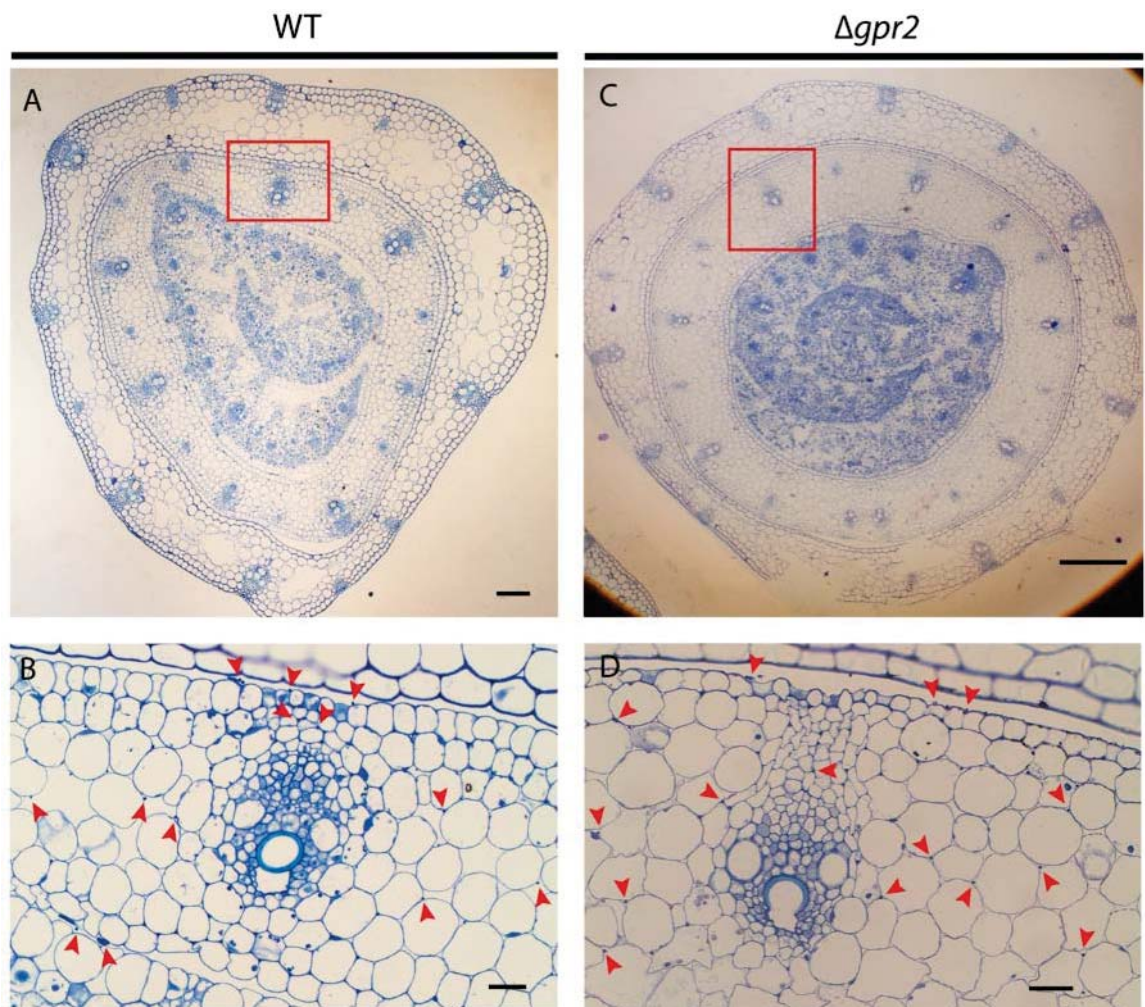


Figure 4-18 Light microscopy of the $\Delta gpr2$ mutant strain *in planta*: Microscopic analysis of ryegrass pseudostem tissue infected with the wild-type and $\Delta gpr2$ mutant strain using light microscopy (LM). Transverse sections of ryegrass pseudostem tissue infected with wild-type (A + B) and $\Delta gpr2$ mutant strain (C + D), stained with toluidine blue. Light micrograph shows fungal colonisation of the host tissue is indistinguishable between WT and $\Delta gpr2$. Arrows indicate position of hyphae. Red box in A and C indicates the magnified area in B and D, respectively. Bar = 100 μ m (A + C) and 20 μ m (B+D).

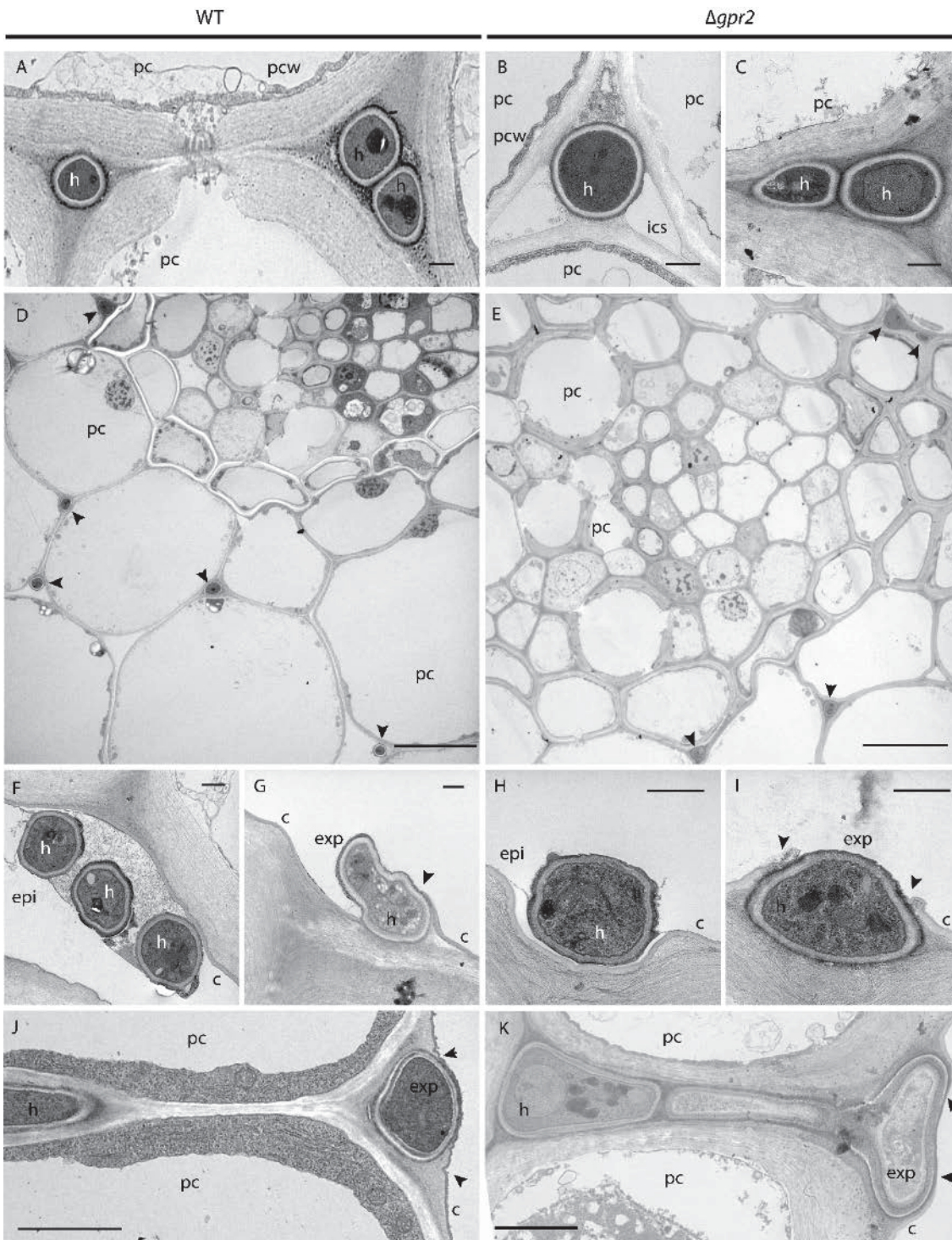


Figure 4-19 Transmission electron microscopy of the $\Delta gpr2$ mutant strain *in planta*: Microscopic analysis of ryegrass leaf pseudostem tissue infected with wild-type and $\Delta gpr2$ mutant strain using transmission electron microscopy (TEM). Cross-section micrograph shows hyphal growth in host apoplast with single or two hyphae per intercellular space (A - C), absence of hyphae in host vascular bundles (D, E), electron dense hyphae in wild-type (WT) and $\Delta gpr2$ mutant strains. Formation of epiphyllous hyphae (F, H) and expressoria (exp) similar for wild-type (G, J) and $\Delta gpr2$ (I, K). Arrows in D and E indicate location of fungal hyphae. Arrows in G, I, J and K indicate hyphal breaching through plant cuticle (c) (G, I) or cuticle thinning (J, K) from expressoria. Bar = 500 nm (A -D, G, H, K, L), 10 μ m (E, F), 2 μ m (I, J)

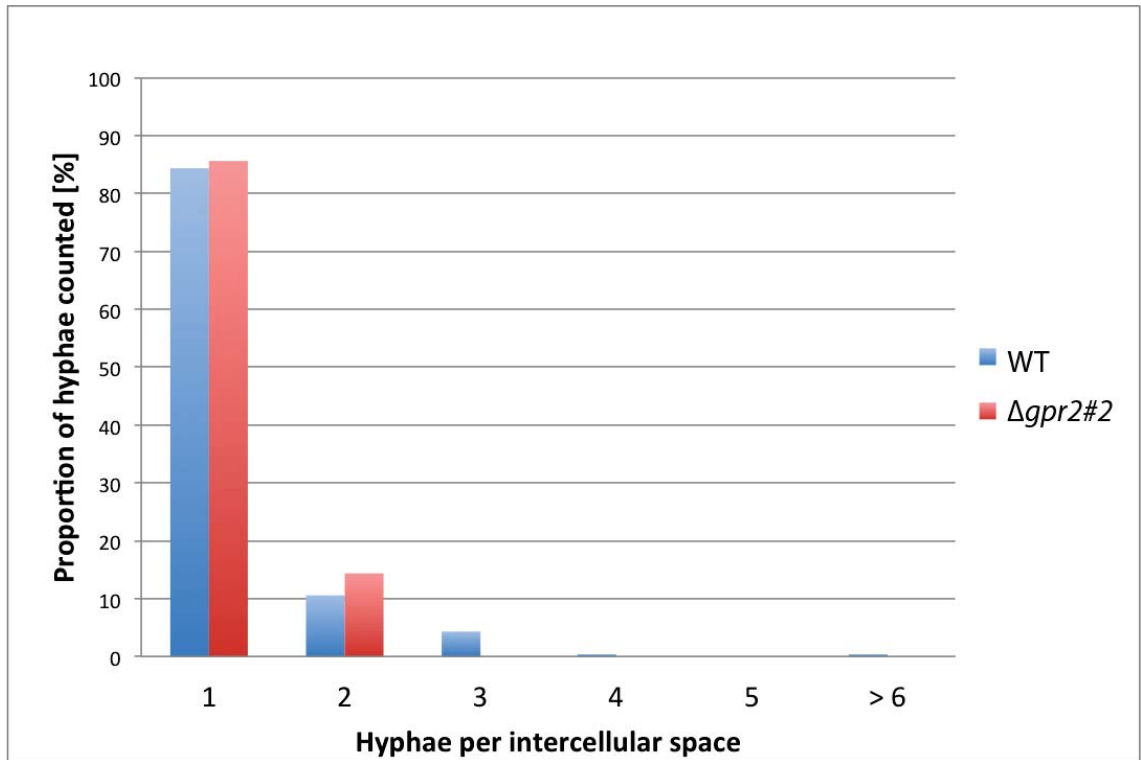
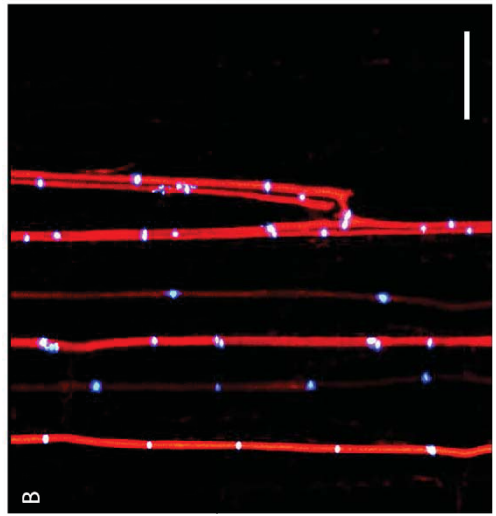
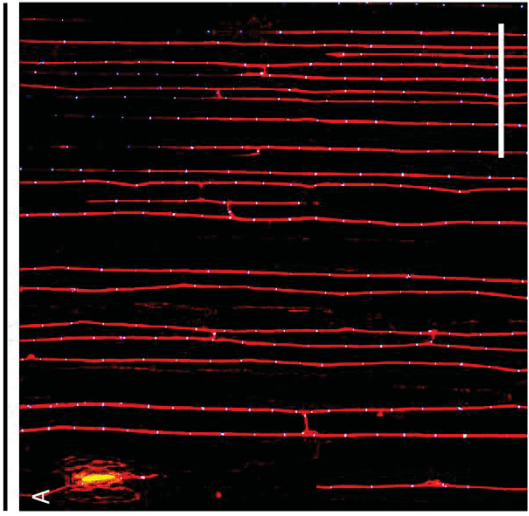


Figure 4-20 Hyphae per intercellular space of $\Delta gpr2$ mutant strain: Graph showing the proportion of hyphae per intercellular space in *L. perenne* tissue, infected with the wild-type (WT) and the $\Delta gpr2\#2$ mutant strain.

WT



$\Delta gpr2$

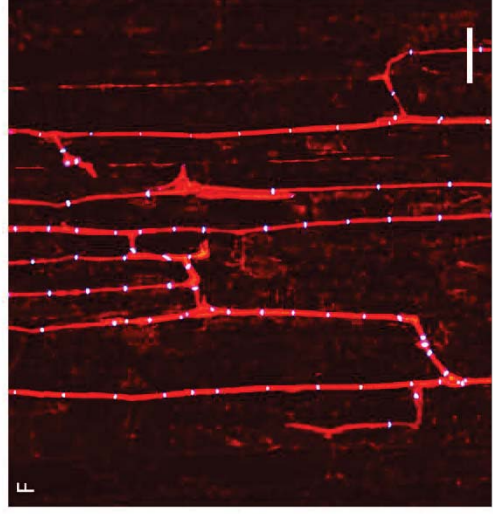
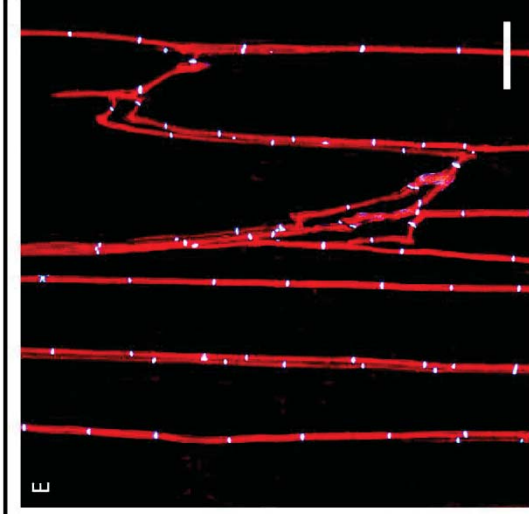
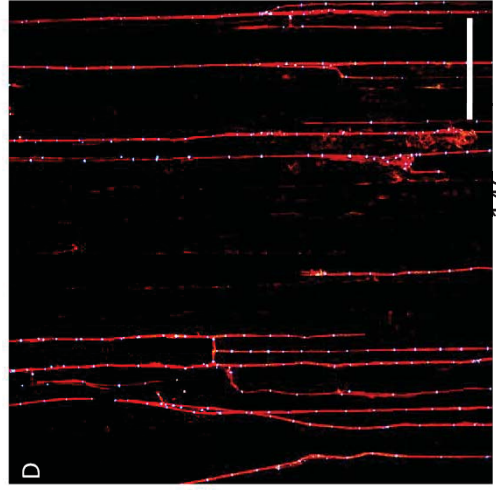
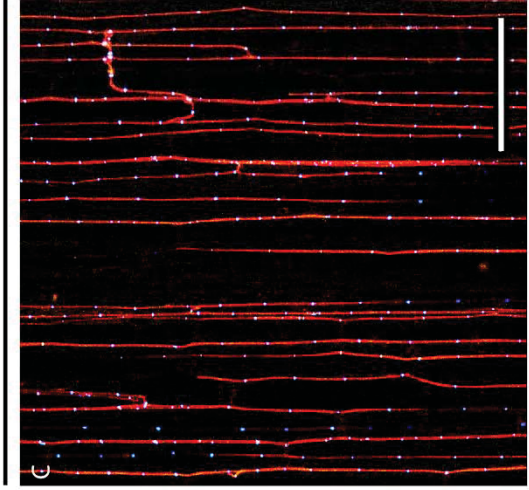


Figure 4-21 Confocal laser-scanning microscopy of the *Δgpr2* mutant strain in planta: Microscopic analysis of ryegrass pseudostem tissue biomass with the wild-type (WT) and *Δgpr2* (*Δgpr2#2*) mutant strains using confocal laser-scanning microscopy (CLSM) showing longitudinal section with hyphal growth parallel to the leaf axis. The *Δgpr2* mutant strain (C-F) with similar number and distribution of hyphae as wild-type (A-B) infected plants. Plant tissue was stained using aniline blue (red pseudocolour) and WGA-AlexaFluor488 (blue pseudocolour). Frequent hyphal fusion occurs in WT and *Δgpr2* mutant strain. Confocal depth series images generated by maximum intensity projection of 10 x 1 μm confocal Z-stacks. Bar = 100 μm A, C and D; Bar = 20 μm B, E and F.

4.4 Analysis of hyphal growth for *Δgpr1b* and *Δgpr2* mutant strains

Hyphal growth and colony morphology are cellular processes linked with the cAMP signalling pathway, especially for morphological differentiation (Cullen et al., 2012, Regenfeller et al., 2009, Adachi et al., 1998, Ramanujam and Naqvi 2010, Choi et al., 1997, Terenzi et al., 1979). Despite no direct evidence for involvement of cAMP signalling in polarised growth, alteration in levels of intracellular cAMP indirectly affects the hyphal growth-rate and apical dominance. In *E. festucae*, the deletion of the cAMP synthesising adenylate cyclase (*acyA*) resulted in strongly reduced hyphal growth, increased lateral branching and highly compact colonies (Voisey et al., 2007). To investigate whether a certain receptor (*Gpr1b* or *Gpr2*) is responsible for sensing specific ligands, which potentially trigger an alteration of intracellular cAMP levels and sequentially alter the hyphal growth-rate, a series of preliminary analyses were conducted in two independent growth experiments. Firstly, colonies were grown on various selective growth media for 7 days followed by the determination of the hyphal growth rate (referred to as non-transfer experiment 2.4.1.1). In a second experiment, colonies were grown on nutrient-rich medium for 4 days to gain sufficient biomass and were then transferred to various selective growth media for 3 days before hyphal growth-rate was determined (referred to as transfer experiment 2.4.1.2). In contrast to the non-transfer experiment, which is reflective of long-term exposure on growth medium, the transfer experiment was conducted to show potential direct influence of specific ligands present in the growth media on hyphal growth-rate following short-term exposure. Further, these analyses were designed to identify ligands that potentially trigger the cAMP signalling pathway for

subsequent quantification of the intracellular cAMP concentration under these selected conditions.

4.4.1 *E. festucae* cAMP-receptor like GPCRs are not directly involved in nutrient sensing

To investigate whether Gpr1b or Gpr2 were involved in sensing nutrients or specific carbon sources, hyphal growth was analysed on various growth media including complex, nutrient poor and defined media containing CD salts (CD) and a number of different C- sources in the latter. Some of these media contain sufficient nutrients for comparable growth to that observed on PD medium (e.g. CZ, CDGN), whereas other media were nutrient limiting (e.g. H₂O, CD). The growth on nutrient rich medium showed that the wild-type strain and the $\Delta gpr1b$ and $\Delta gpr2$ mutant strains grew in fluffy colonies with a solid fungal biomass (Fig. 4.22 A), similarly on all complex media tested. In comparison, growth on nutrient poor medium exhibited a reduction in biomass with the absence of aerial hyphae (Fig. 4.22 B), although colony size and hyphal radial growth-rate remained similar to that determined on nutrient rich medium (Fig. 4.23) for all strains tested, respectively. The radial growth of the $\Delta gpr1b$ and $\Delta gpr2$ mutant strains was measured and the determined hyphal growth-rate per day compared to that of the wild-type strain (2.4.1; 2.4.2) (Fig. 4.23), which showed no obvious difference when grown on nutrient rich, nutrient poor or in the presence of any specific carbon sources apart of individual cases (Fig. 4.22 and 4.23). The $\Delta gpr2$ mutant strain grew with an increased hyphal growth-rate on CDGN medium and in the presence of galactose (Gal), whereas the $\Delta gpr1b$ mutant showed significantly reduced growth on medium containing sucrose ($p < 0.05$) (Fig. 23). When xylan was available as only carbon source, both the $\Delta gpr1b$ and $\Delta gpr2$ mutant strains exhibited significantly reduced growth compared to the wild-type strain ($p < 0.05$). In the presence of galactose as sole carbon source, the hyphal growth rate-per day was significantly reduced compared to that on PD medium in all strains (Fig. 4.23).

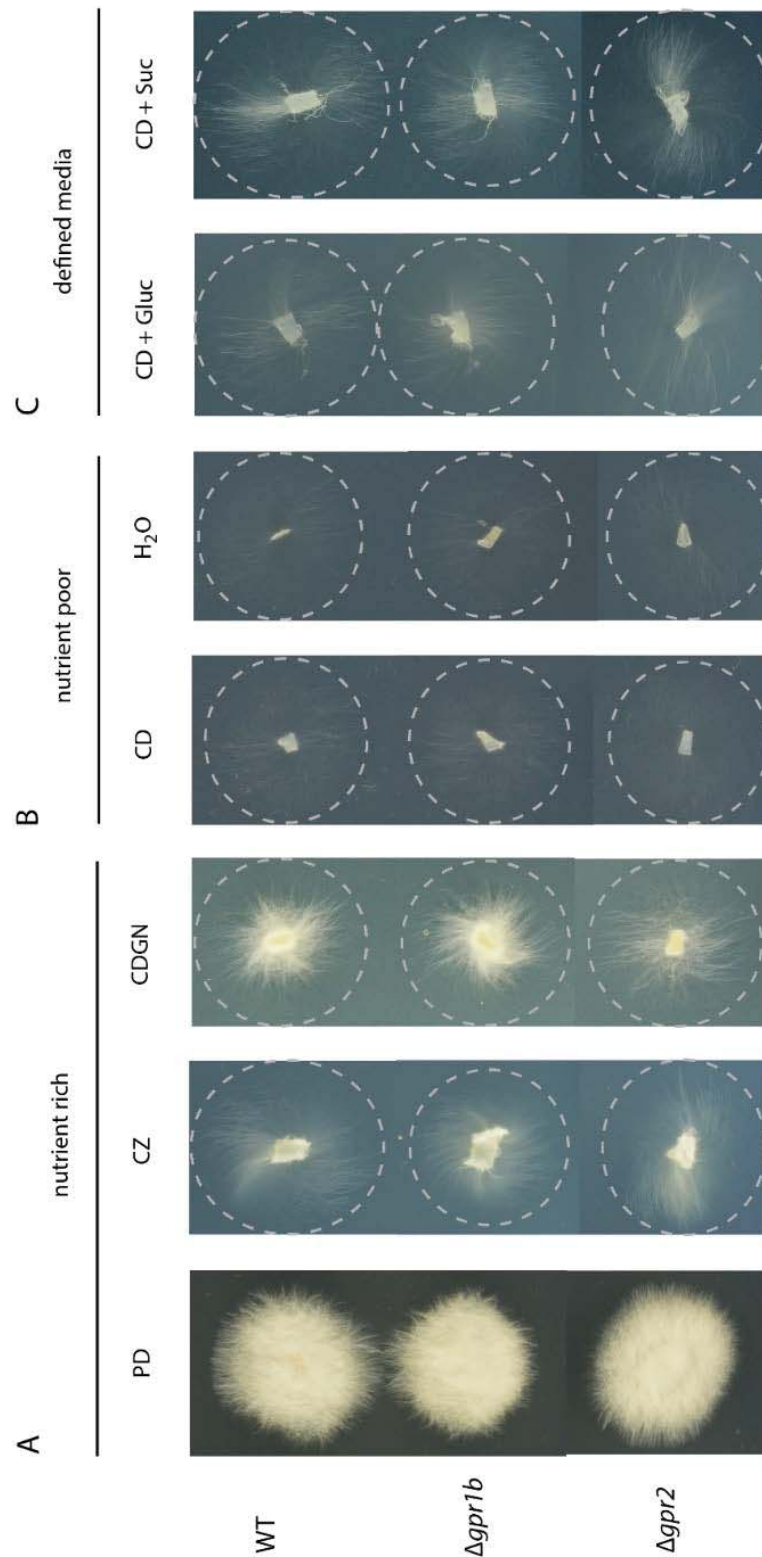


Figure 4-22 Colony morphology of the GPCR mutant strains in response to nutrient limitation: *E. festucae* hyphal growth and colony morphology in axenic culture for wild-type (WT), $\Delta gpr1b$ and $\Delta gpr2$ mutant strains on nutrient rich and nutrient poor medium after 7 days at 22°C. Fungal growth on (A) nutrient rich media, PD agar, Czapek-Dox (CZ) and defined media containing CD salts (CD) supplemented with glucose and (NH₄)₂SO₄ (CDGN), (B) on nutrient poor medium, 3% water (H₂O) agar and defined medium containing CD salts (CD) for nutrient starvation conditions and (C) on defined medium containing CD salts and 100 mM glucose (CD + Gluc) or 100 mM sucrose and (CD + Suc). Dashed circle indicates colony edge.

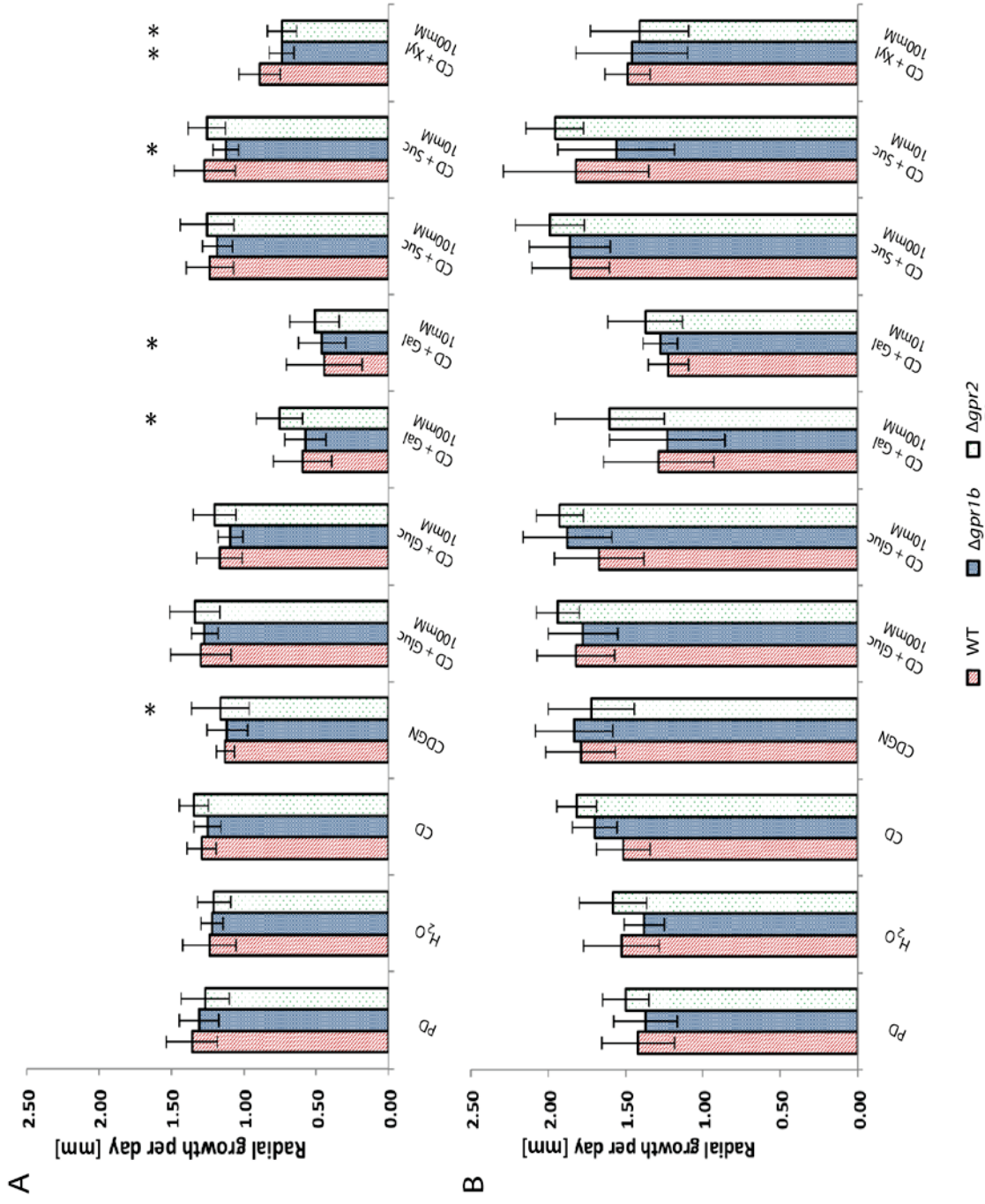


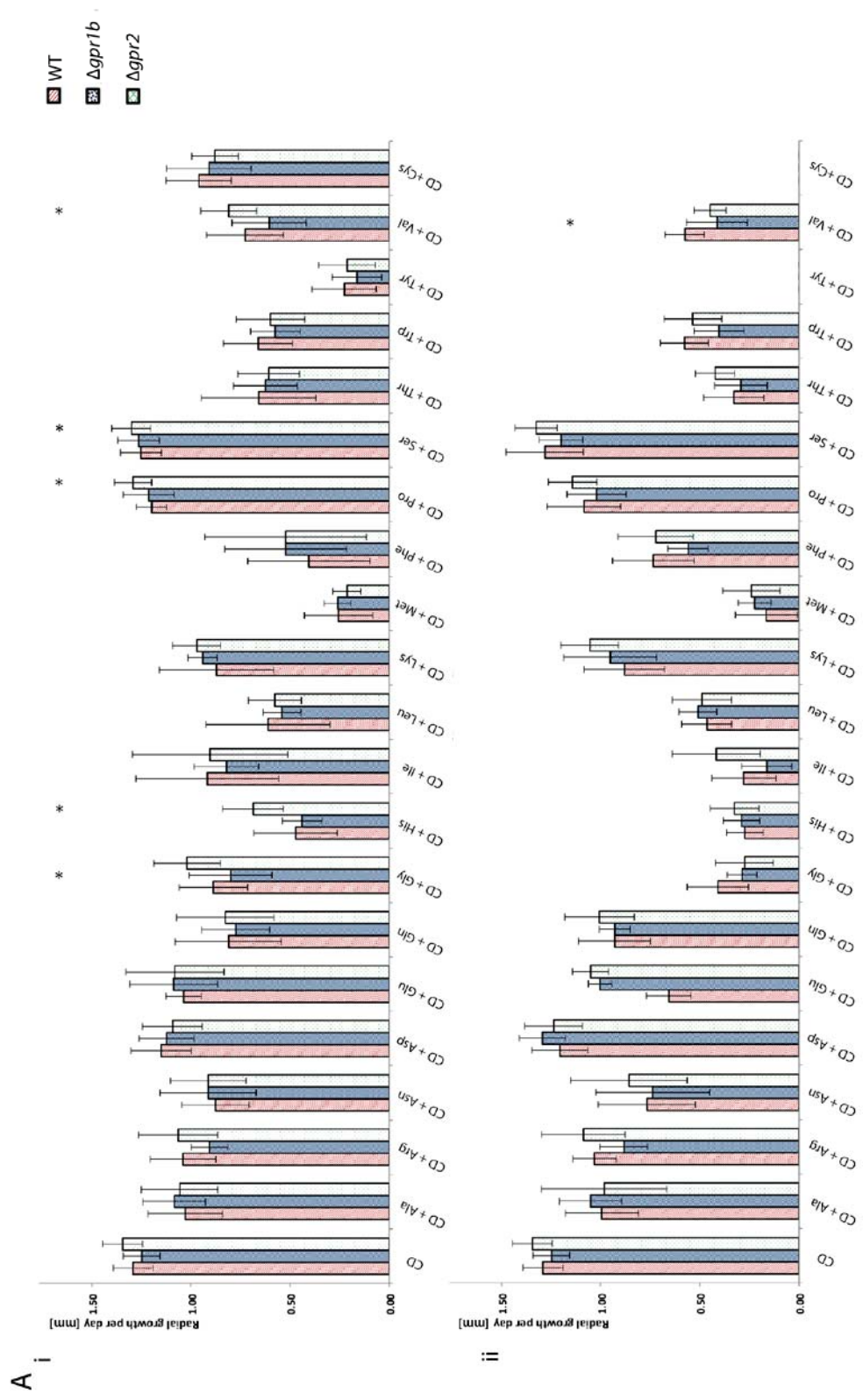
Figure 4-23 Variation in hyphal growth rate of the GPCR mutant strains in response to nutrient starvation and to growth on various carbon sources: *E. festucae* colony growth in axenic culture of the wild-type (WT), $\Delta gpr1b$ and $\Delta gpr2$ mutant strains in response to nutrient starvation or to various carbon sources, (A) following a non-transfer experiment and (B) a transfer experiment. Radial growth on nutrient rich media (PD and CDGN), nutrient poor media (H₂O and CD) and on defined media containing CD salts, supplemented with the particular carbon sources in two concentrations, 100 mM and 10 mM, was measured after 7 days at 22°C and the hyphal growth-rate per day was determined. Data are represented as the Mean \pm SD. Significant differences in hyphal growth rate between the WT and the respective mutant strain, $\Delta gpr1b$ and $\Delta gpr2$ on each growth medium are denoted * $p < 0.05$ (*Student's t test*; $n = 4$ non-transfer experiment, $n = 5$ transfer experiment). Media contained 1.5% agar. PD = Potato Dextrose, CD = Czapek Dox salts media, CDGN = CD + 100 mM glucose + 10 mM (NH₄)₂SO₄, CD salts supplemented with individual carbon sources: Glu = glucose, Suc = sucrose, Gal = galactose, Xyl = xylan.

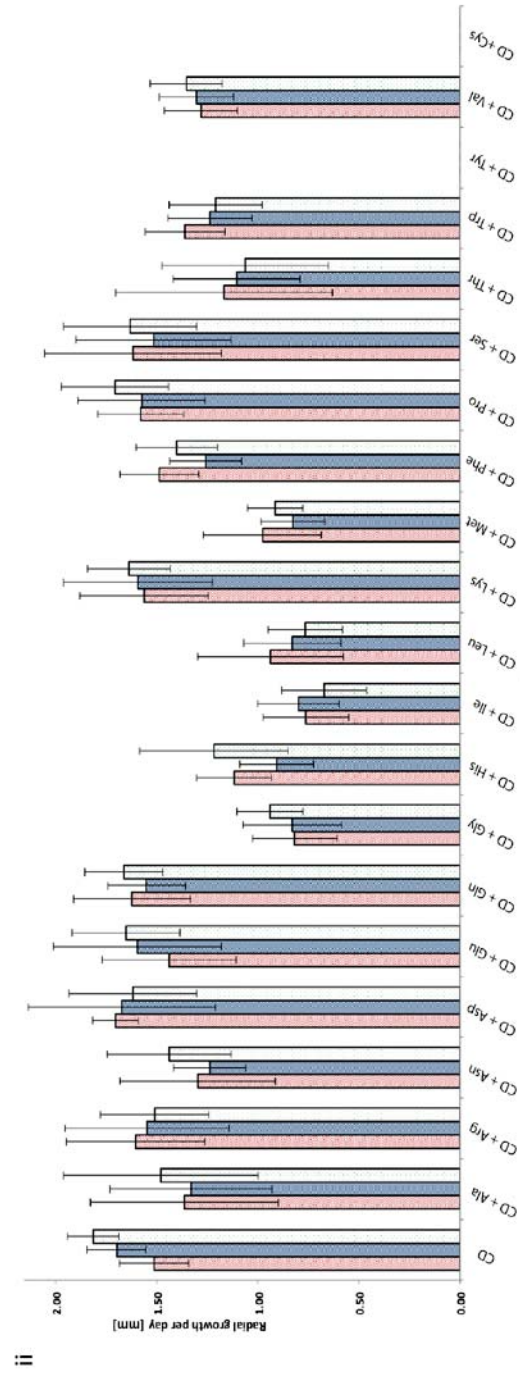
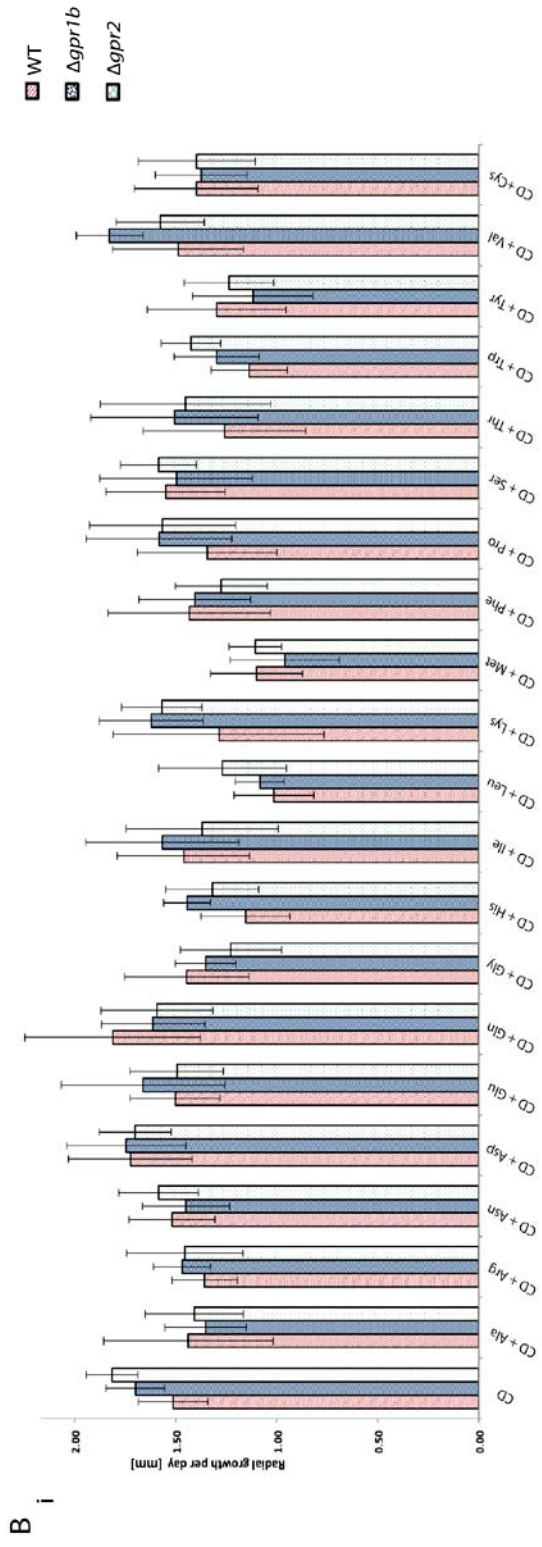
4.4.2 Gpr1b or Gpr2 may have an accessory role in sensing specific amino acids

To investigate if Gpr1b or Gpr2 is involved in sensing amino acids, in a series of preliminary experiments, hyphal growth in presence of individual amino acids was analysed (Fig. 4.24). While colony growth on PD medium containing individual amino acids was indistinguishable to that on PD medium, some differences in hyphal growth were observed on defined medium (CD) containing CD salts supplemented with the individual amino acids (Table 2.4). No noticeable effect or differences in colony growth and determined hyphal growth-rate per day was observed when the $\Delta gpr1b$ or $\Delta gpr2$ mutant strain and the wild-type were compared (Fig. 4.24). The hyphal growth rate in presence of glycine (Gly) or was significantly lower for the $\Delta gpr1b$ mutant strain compared to the wild-type ($p < 0.05$), while the $\Delta gpr2$ mutant strain showed a significantly higher hyphal growth-rate ($p < 0.05$) when histidine (His), proline (Pro), serine (Ser) or valine (Val) were present at a concentration of 1 mM (Fig. 24Ai). No additional effect was observed, when colonies were transferred onto the particular media (Fig. 4.24 B). It is noteworthy that some amino acids (e.g. Gly) did have a concentration-dependent inhibitory effect on the hyphal growth-rate, when growth of any strain was compared to that on the CD control medium (Fig. 4.24).

The absence of a distinct phenotype with alteration in hyphal growth compared to the wild-type in response to any amino acid, suggests that Gpr1b and Gpr2 are not involved in perception of extracellular amino acids.

Figure 4-24 Variation in hyphal growth-rate of the GPCR mutant strains in response to amino acids: *E. festucae* colony growth in axenic culture of the wild-type (WT), $\Delta gpr1b$ and $\Delta gpr2$ mutant strains, in the presence of individual amino acids (AA), (A) following a non-transfer experiment and (B) a transfer experiment. Radial growth on defined media containing CD salts (CD), supplemented with the respective amino acid in two concentrations (i) 1 mM and (ii) 10 mM¹, was measured after 7 days at 22°C on respective medium and hyphal growth-rate per day was determined. Data are represented as the Mean \pm SD. Significant differences in hyphal growth rate between the WT and the respective mutant strain, $\Delta gpr1b$ and $\Delta gpr2$ on each growth medium are denoted * $p < 0.05$ (*Student's t test*; n = 4 non-transfer experiment, n = 5 transfer experiment). ¹Note: strains on cysteine and tyrosine showed no growth and were therefore excluded from the graph. AA: Ala = alanine, Arg = arginine, Asn = asparagine, Asp = aspartic acid, Glu = glutamic acid, Gln = glutamine, Gly = glycine, His = histidine, Ile = isoleucine, Leu = leucine, Lys = lysine, Met = methionine, Phe = phenylalanine, Pro = proline, Ser = serine, Thr = threonine, Trp = tryptophan, Tyr = tyrosine, Val = valine, Cys = cysteine.





4.4.3 Deletion of *gpr1b* may increase sensitivity of *E. festucae* to oxidative stress

To test whether the loss of Gpr1b or Gpr2 resulted in an increased sensitivity to environmental stress, the *E. festucae* wild-type and the $\Delta gpr1b$ and $\Delta gpr2$ mutant strains were treated with various stress agents (2.4.3).

The $\Delta gpr1b$ and $\Delta gpr2$ mutant strain grew the same as the wild-type under high temperature stress conditions at 30°C, under osmotic stress conditions on PD medium containing various concentrations of sodium chloride (NaCl), potassium chloride (KCl) or sorbitol and under acidic or alkaline environmental conditions on medium with adjusted pH (Fig. 4.25 A, B). However, when transferred onto acidic medium (pH 4), the $\Delta gpr1b$ mutant strain exhibited a significantly reduced growth-rate to that of the wild-type strain ($p < 0.05$) (Fig. 4.25 Bii). The wild-type strain and the two mutant strains showed no difference in colony morphology in response to sodium dodecyl sulfate (SDS), a chemical known to readily lyse cells with membrane defects (Fig. 4.25 C). No significant differences between WT and mutants was exhibited when colonies were grown on media containing the cell-wall stress agents Calcofluor white (CFW), Congo red (CR) or caffeine (caff), known to trigger activation of the CWI pathway (Fig. 4.25 C). When tested for sensitivity to oxidative stress, the addition of 40 μ M menadione to the PD medium had no effect on the growth of the mutant strains compared to wild-type. On the other hand, growth on PD medium containing 7 mM hydrogen peroxide (H₂O₂) exhibited a stronger inhibition in hyphal growth for the $\Delta gpr1b$ mutant strain than for the wild-type strain (Fig. 4.25 C). This effect was more pronounced when culture plates were incubated for an additional 10 days at 4°C. The *gpr1b* complementation strains (*gpr1b*#24C-4, *gpr1b*#24C-5, *gpr1b*#24C-6, *gpr1b*#24C-10, *gpr1b*#222C-4, *gpr1b*#222C-5, *gpr1b*#222C-6, *gpr1b*#222C-13) showed similar inhibited growth as the wild-type strain. Treatment with 3,3'-diaminobenzidine (DAB), a chemical that detects fungal-produced hydrogen peroxide (reactive oxygen species) in culture, did not show a difference between wild-type and either of the two mutants (Fig. 4.25 C), when grown on PD or CD media. No difference in ROS production between the mutants and the wild-type strain was observed when cultures were grown on PD or CD media containing apoplastic fluid.

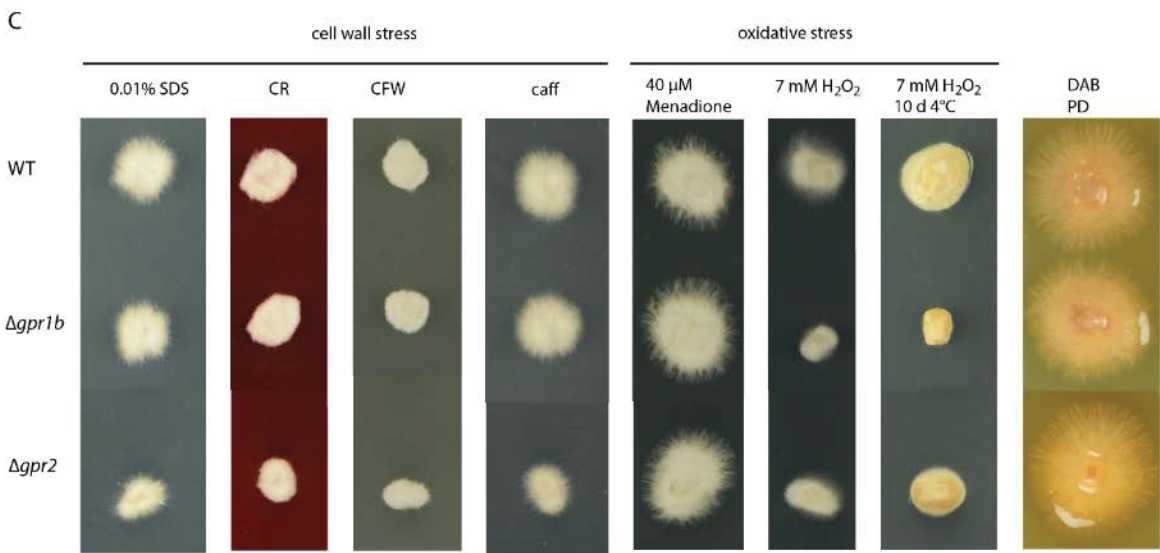
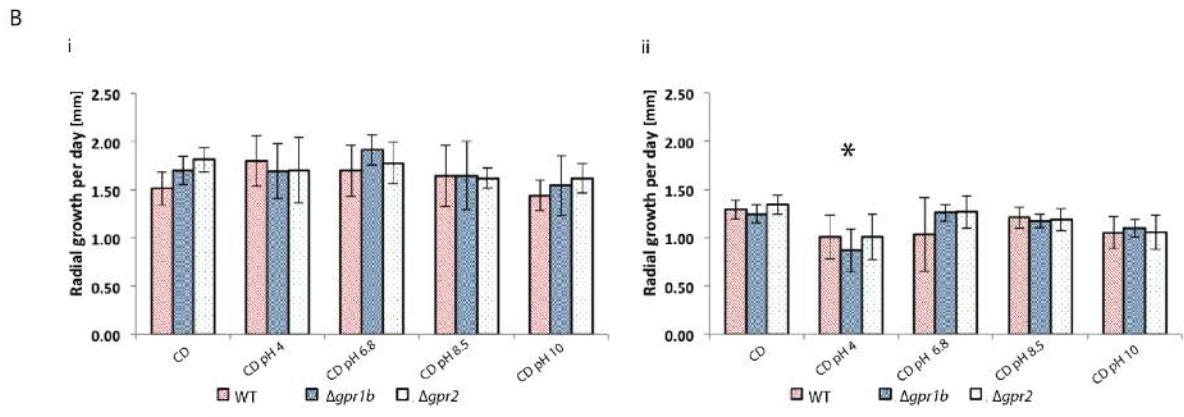
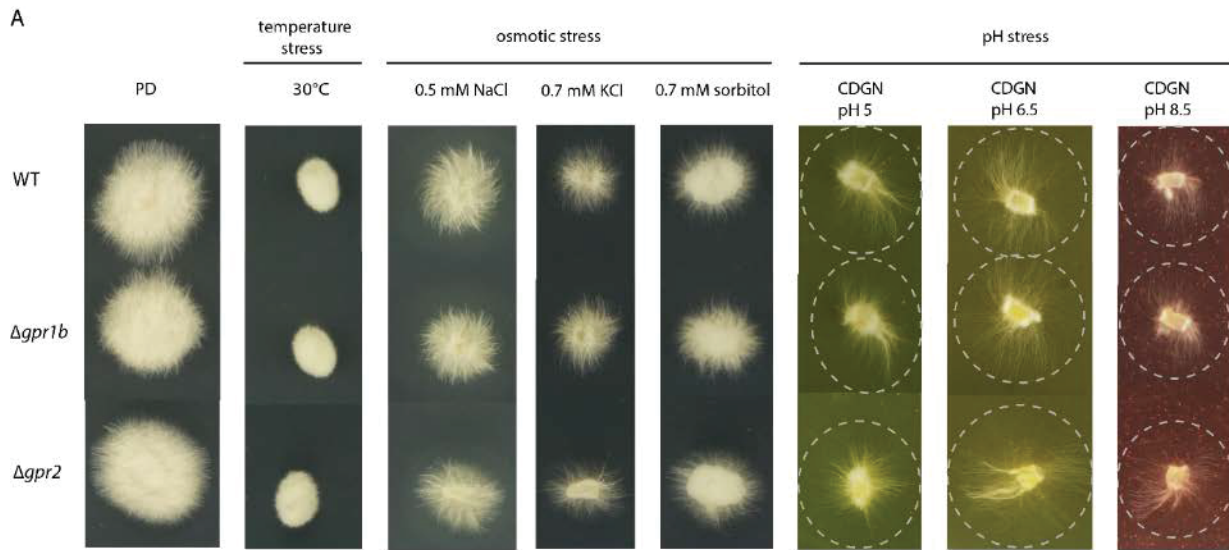


Figure 4-25 Variation in colony growth of the GPCR mutant strains under various stress conditions: *E. festucae* colony growth in axenic culture of the wild-type (WT), $\Delta gpr1b$ and $\Delta gpr2$ mutant strains in response to extracellular stimuli after 7 days at 22°C. (A) Fungal growth on PD agar. The fungal colonies were tested for sensitivity to temperature stress on PD agar incubated at 30°C and osmotic stress on PD agar containing 0.5 M NaCl, 0.7 M KCl and 0.7 M Sorbitol. Fungal colonies were tested for sensitivity to acidic and alkaline environment using defined medium containing CD salts supplemented with 100 mM glucose and 10 mM (NH₄)₂SO₄ (CDGN) adjusted to pH 5, 6.5 and 8.5 (buffered with 30 mM K₂HPO₄ and 30 mM KH₂PO₄) and (B) using CD media adjusted for pH (pH 4, pH 6.8, pH 8.5 and pH 10; medium with adjusted pH 10 changed to pH 8 after 7 days incubation). Radial growth in response to changing pH was measured after 7 days at 22°C and the hyphal growth-rate per day was determined, following a (i) non-transfer and a (ii) transfer experiment. Data are represented as the Mean \pm SD. Significant differences in hyphal growth rate between the WT and the respective mutant strain, $\Delta gpr1b$ and $\Delta gpr2$ on each growth medium are denoted * $p < 0.05$ (*Student's t test*; n = 4 non-transfer experiment, n = 5 transfer experiment). (C) Fungal colonies were tested for sensitivity to cell wall stress (0.01% sodium dodecyl sulphate (SDS), 25 μ g/ml Congo red (CR), 100 μ g/ml Calcofluor white (CFW), 3 mM caffeine (caff)) and to oxidative stress (40 μ M menadione, 7 mM hydrogen peroxide (H₂O₂)) on PD media containing the respective agent. Culture phenotype for $\Delta gpr1b$ and $\Delta gpr2$ mutant strains on 7 mM H₂O₂ was more pronounced after additional storage at 4°C for 10 days. Fungal colonies were treated with 3,3'-Diaminobenzidine (DAB) to test fungal production of hydrogen peroxide.

4.4.4 *E. festucae* Gpr1b is potentially involved in sensing of an unknown component in apoplastic fluid

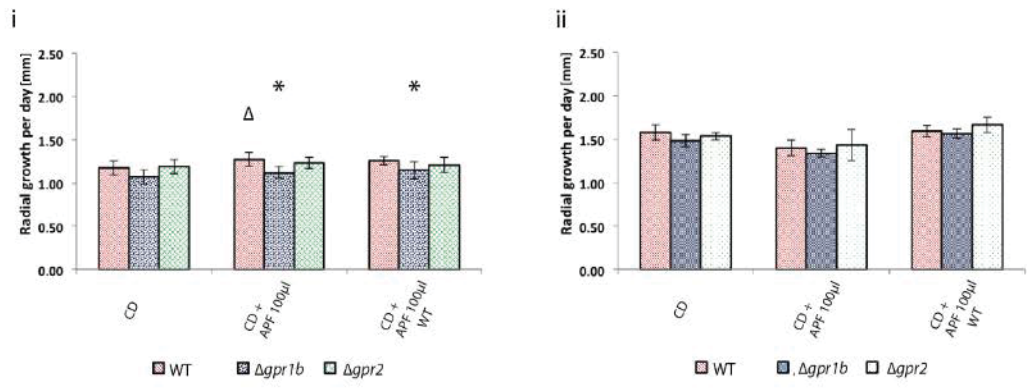
In order to mimic the *in planta* environment and to investigate if the cAMP signalling pathway is triggered through specific plant derived molecules perceived by Gpr1b or Gpr2, preliminarily hyphal growth in the presence of apoplastic fluid and linoleic acid was analysed in axenic culture (2.4.4). The hyphal radial growth was measured on defined medium containing CD salts and apoplastic fluid (APF) or various concentration of linoleic acid (LA) and the hyphal growth-rate per day was determined. When APF was present, the wild-type strain showed a statistically significant ($p < 0.05$) increase in hyphal growth compared to that on the control CD medium, while the $\Delta gpr1b$ mutant strain showed significantly reduced hyphal growth compared to the wild-type ($p < 0.05$) (Fig.4. 26 A). In the presence of linoleic acid (LA), colonies of the wild-type strain and the $\Delta gpr1b$ and $\Delta gpr2$ mutant strains showed a significantly reduced hyphal growth-rate likewise ($p < 0.05$) compared to growth on the control medium containing ethanol (Fig. 4.26 B). Hyphal growth on defined medium containing ethanol was reduced compared to that on CD control

medium, which was significantly inhibited further by linoleic acid ($p < 0.05$), similarly for all strains (Fig. 4.26 B, C).

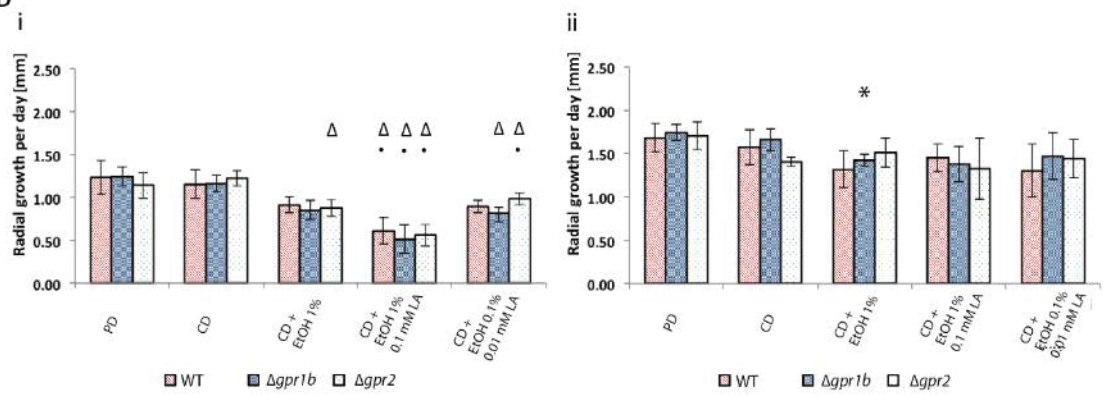
The alteration of hyphal growth in the presence of apoplastic fluid seems to suggest that Gpr1b may be involved in perceiving a yet to be identified molecule contained in the apoplastic fluid, which potentially increases fungal growth. Based on the indirect link that altered levels of intracellular cAMP negatively affects hyphal growth and colony morphology (Voisey et al., 2007), growth promoting or inhibitory factors could be mediated through the cAMP signalling pathway, initially perceived by specific GPCRs. This preliminary analysis could not identify a direct role for Gpr1b or Gpr2 in sensing the oxylipin precursor linoleic acid, which had an inhibitory effect on the hyphal growth overall.

Figure 4-26 Variation in hyphal growth rate of the GPCR mutants in response to plant extracts: *E. festucae* growth in axenic culture of the wild-type (WT), $\Delta gpr1b$ and $\Delta gpr2$ mutant strains in response to (A) plant derived apoplastic fluid (APF) and (B) the oxylipin-precursor linoleic acid (LA) in axenic culture. Radial growth was measured after 7 days at 22°C on respective medium and hyphal growth-rate per day was determined (A + B), following a (i) non-transfer and a (ii) transfer experiment. Growth was compared to that on defined media containing CD salts (CD) for 7 days at 22°C. (A) Hyphal growth rate per day was determined on defined media containing CD salts supplemented with APF, extracted from uninfected (APF) or wild-type infected (APF WT) *Lolium perenne* plants. (B) Hyphal growth rate per day was determined on defined media containing CD salts supplemented with LA, solubilised in ethanol (EtOH). Hyphal growth was compared to growth on defined media containing CD salts (CD) and CD salt media containing ethanol (EtOH). Data (A + B) are represented as the Mean \pm SD. Significant differences in hyphal growth rate between the WT and the respective mutant strain, $\Delta gpr1b$ and $\Delta gpr2$ on each growth medium are denoted * $p < 0.05$ (*Student's t test*); Δ = significant growth difference ($p < 0.05$) of particular strain compared to growth of respective strain on CD control media (*Student's t test*); • = significant growth difference ($p < 0.05$) of particular strain compared to growth of respective strain on CD + 1% EtOH control media (*Student's t test*). $n = 4$ non-transfer experiment, $n = 5$ transfer experiment (C) Fungal colonies grown on defined media containing CD salts (control media) and CD media containing 10% EtOH, 1% EtOH, 10% EtOH/1 mM LA, 1% EtOH/0.1 mM LA and 0.1% EtOH/0.01 mM LA for 7 days at 22°C. Circle (grey dashed line) indicates colony edge.

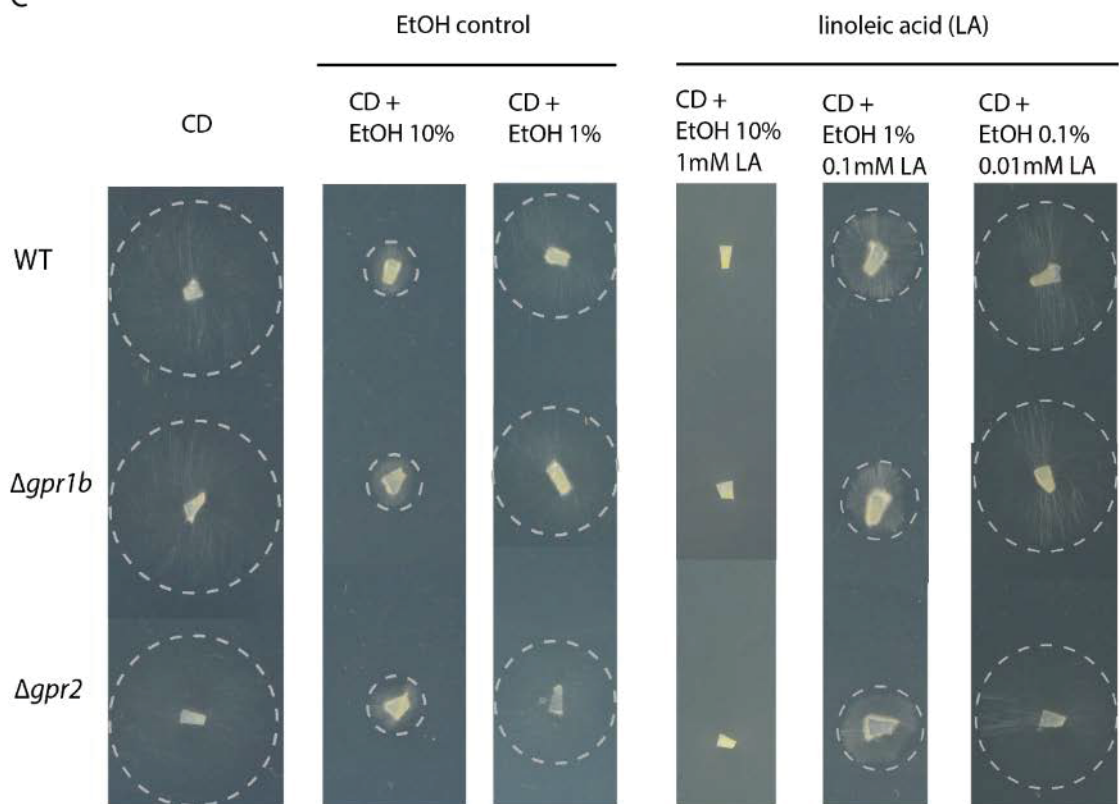
A



B



C



4.4.5 Gpr1b and Gpr2 are not directly involved in any processes in culture potentially mediated by the cAMP signalling pathway

To test whether an alteration of key-enzyme activity of the cAMP signalling pathway has an effect on hyphal growth and colony morphology and which role the Gpr1b or Gpr2 proteins play under these conditions, the fungal strains were treated with a variety of chemicals (2.4.5). Addition of apoplastic fluid (2.7.7) was also examined to see if hyphal growth in culture change in the presence of these activators and inhibitors.

No noticeable differences between wild-type strain and the $\Delta gpr1b$ or $\Delta gpr2$ mutant strains was observed when colonies were grown on PD medium containing histamine, a known cAMP signalling and phosphodiesterase activator, or quinine, a chemical known to inhibit adenylate cyclase activity (Scott and Solomon 1975). The addition of both chemicals in equal concentrations had no further effect on colony morphology and hyphal growth (Fig. 4.27 A). Treatment with methylated xanthines, such as caffeine (caff), theobromine (theo) and 3-isobutyl-1-methylxanthine (IMBX), chemicals known to inhibit PDE activity, showed a similar reduced colony growth for the wild-type and the two mutant strains (Fig. 4.27 B). No difference between wild-type and the $\Delta gpr1b$ or $\Delta gpr2$ mutant strains was observed when colonies were grown on PD medium containing histamine, quinine, caffeine or IMBX at higher concentrations in combination with apoplastic fluid.

Alterations of the cellular cAMP homeostasis caused a reduction in colony growth, demonstrating a crucial role for fungal growth to regulate this balance. However, chemical treatment could not identify a role for Gpr1b and Gpr2 in the cAMP signalling pathway for hyphal growth in culture, neither on nutrient rich medium (e.g. PD) nor in the presence of apoplastic fluid. The predicted beneficial effect of apoplastic fluid on hyphal growth could not be confirmed in this assay.

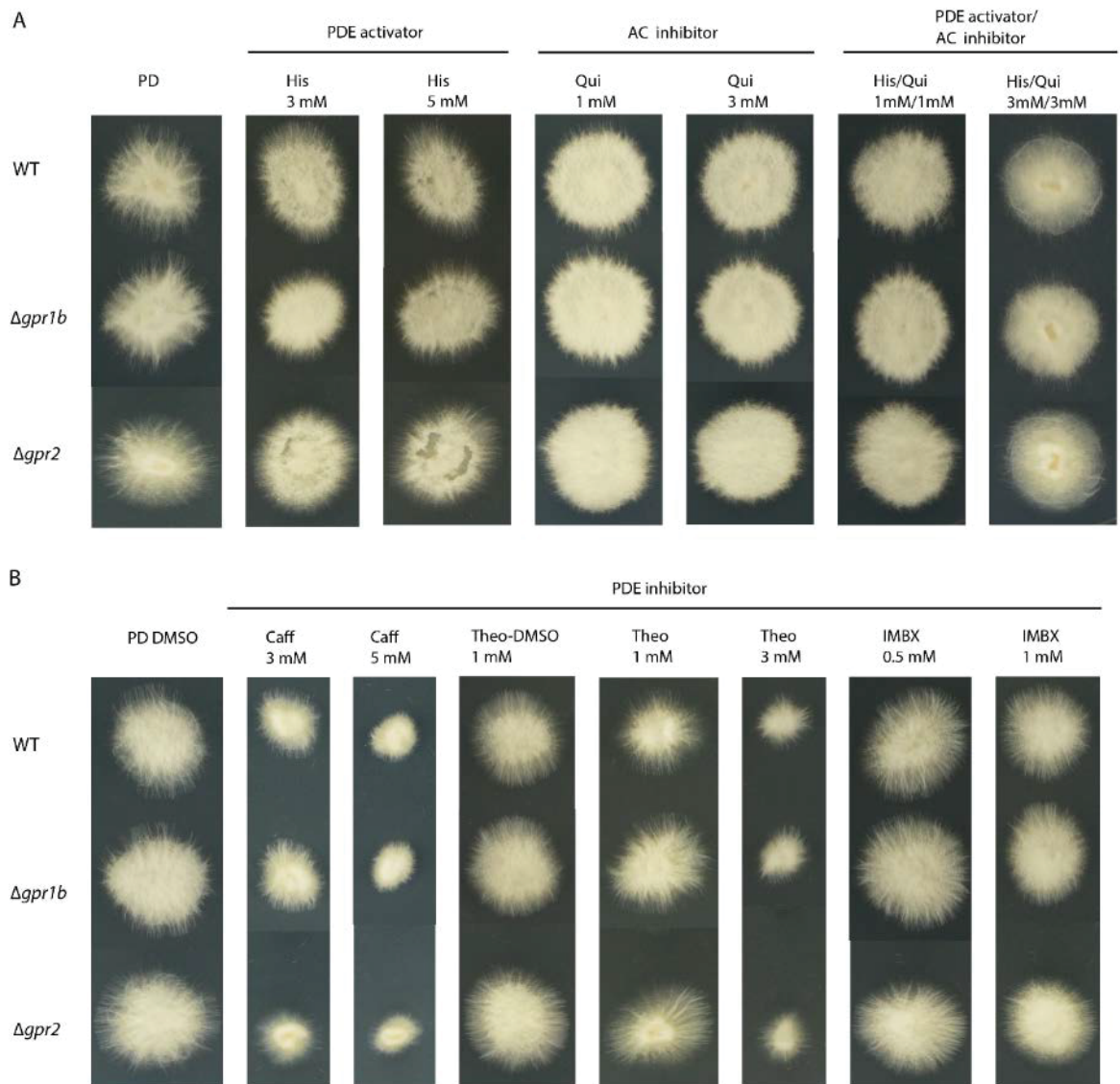


Figure 4-27 Effect of inhibition/activation of key enzymes in the cAMP signalling pathway on growth of wild-type and GPCR mutants: *E. festucae* colony growth of the wild-type (WT) and $\Delta gpr1b$ and $\Delta gpr2$ mutant strains in response to chemical inhibition of adenylate cyclase (AC) activity using quinine and activation or inhibition of phosphodiesterase (PDE) activity by treatment with histamine or methylated xanthines respectively. Fungal growth was analysed after a total of 7 days post-incubation at 22°C. (A) Colony growth on PD agar and PD agar containing histamine (His; 3 mM, 5 mM), quinine (Qui; 1 mM, 3 mM) or both (His/Qui; 1 mM/1 mM, 3 mM/3 mM). (B) Colony growth on PD agar containing DMSO (control) and PD agar containing caffeine (caff; 3mM, 5 mM), theobromine solubilised in DMSO (Theo-DMSO 1 mM), theobromine (Theo; 1 mM, 3 mM) and Iso-butyl-methylxanthine (IMBX; 0.5 mM, 1 mM).

4.4.6 Nutrient rich medium triggers increase in intracellular cAMP levels, but Gpr1b or Gpr2 are not directly responsible

The cAMP signalling cascade is triggered by G-protein coupled receptors, depending on the particular ligand, which increases the concentration of cAMP in the cell (reviewed in Li et al., 2007, Xue et al., 2008). To analyse whether the cAMP signalling pathway is involved in nutrient sensing in *E. festucae* and whether Gpr1b or Gpr2 are involved in the signal transduction, intracellular cAMP levels were measured (2.6) on nutrient-rich and nutrient-poor media. Following transfer experimental conditions (2.4.1.2), colonies were first grown on PD medium for 4 days and then transferred to either a fresh PD medium or a minimal or selective medium such as water agar (e.g. H₂O) and grown for further 3 days before measurement (2.4.2.2). Compared to the wild-type strain, the $\Delta gpr1b$ and $\Delta gpr2$ mutant strains showed similar levels of cAMP on nutrient rich medium (PD) and when transferred onto nutrient limiting medium (H₂O) (Fig. 4.28). Similar levels of cAMP for the $\Delta gpr1b$ or $\Delta gpr2$ mutants strains compared to the wild-type strain suggests that both receptors are not directly involved in sensing extracellular nutrient. Reduced accumulation of cAMP on nutrient rich medium would be expected when either GPCR was involved in nutrient sensing, due to reduced or missing pathway activation. Comparable levels of cAMP in all three strains similar for both conditions (transferred onto nutrient-rich and nutrient-poor), show that cAMP concentration increases in the presence of nutrients (PD), while decreases in its absence (H₂O) through termination of the cAMP signalling pathway via hydrolysis by PDEs. This preliminary experiment also showed that lysis of *E. festucae* cells and cAMP extraction was sufficient for quantitative analysis, following the manufacturer's protocol. However, validation of the cAMP assay was not reliable in later experiments and subsequent analysis did not provide reliable data for quantification of intracellular cAMP levels.

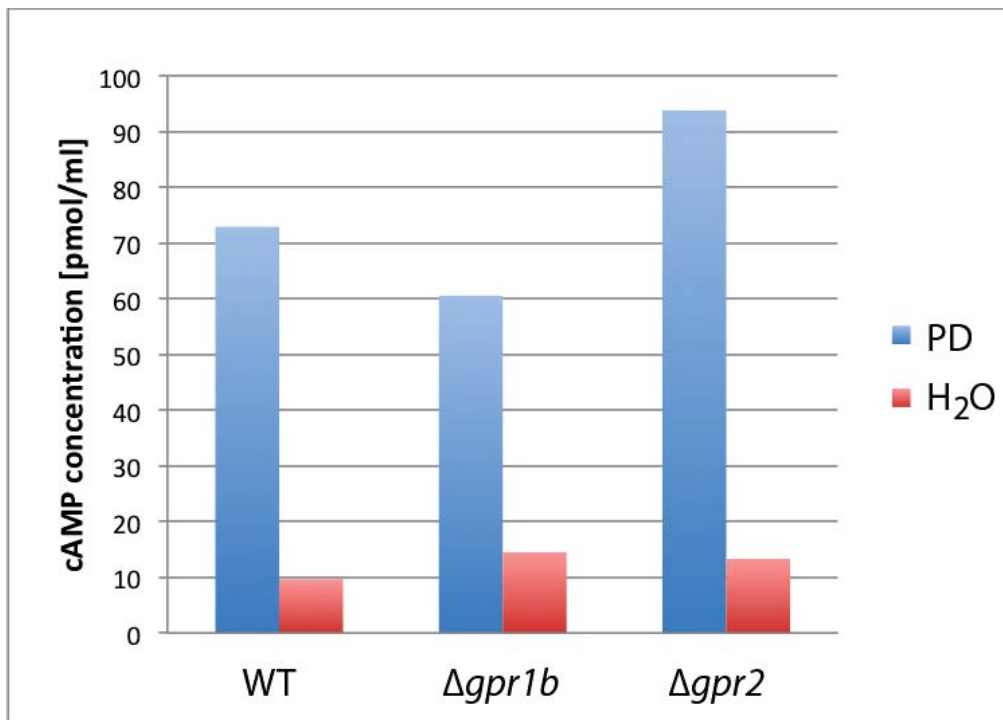


Figure 4-28 Quantification of the intracellular cAMP levels in the $\Delta gpr1b$ and $\Delta gpr2$ mutants under nutrient limitation: Quantification of intracellular cAMP levels in *E. festucae* colonies, grown on nutrient rich (PD) medium or transferred onto nutrient poor (H₂O) medium using the direct cyclic AMP ELISA kit under non-acetylated conditions (Enzo Life sciences).

Further testing conducted involved alteration of growth conditions for the GPCR strains and planned as follows: After the transfer experiment (2.4.1.2) colonies were grown on nutrient rich medium (PD) for 4 days, subsequently transferred onto nutrient poor medium (CD) for an additional 2 days and then finally transferred onto selective medium (e.g. minimal media (CD) containing Glucose, apoplastic fluid, linoleic acid or any amino acid that showed significant alteration in the hyphal growth-rate compared to the wild-type strain) for 24 hours. The rationale being that the ligands present in the selective medium would potentially trigger an increase in the intracellular cAMP concentrations. However, given that data obtained from validation assays of cAMP were not reliable the data from these sets of experiments were not included data interpretation in the thesis.

Chapter 5 Functional analysis of cAMP-phosphodiesterases

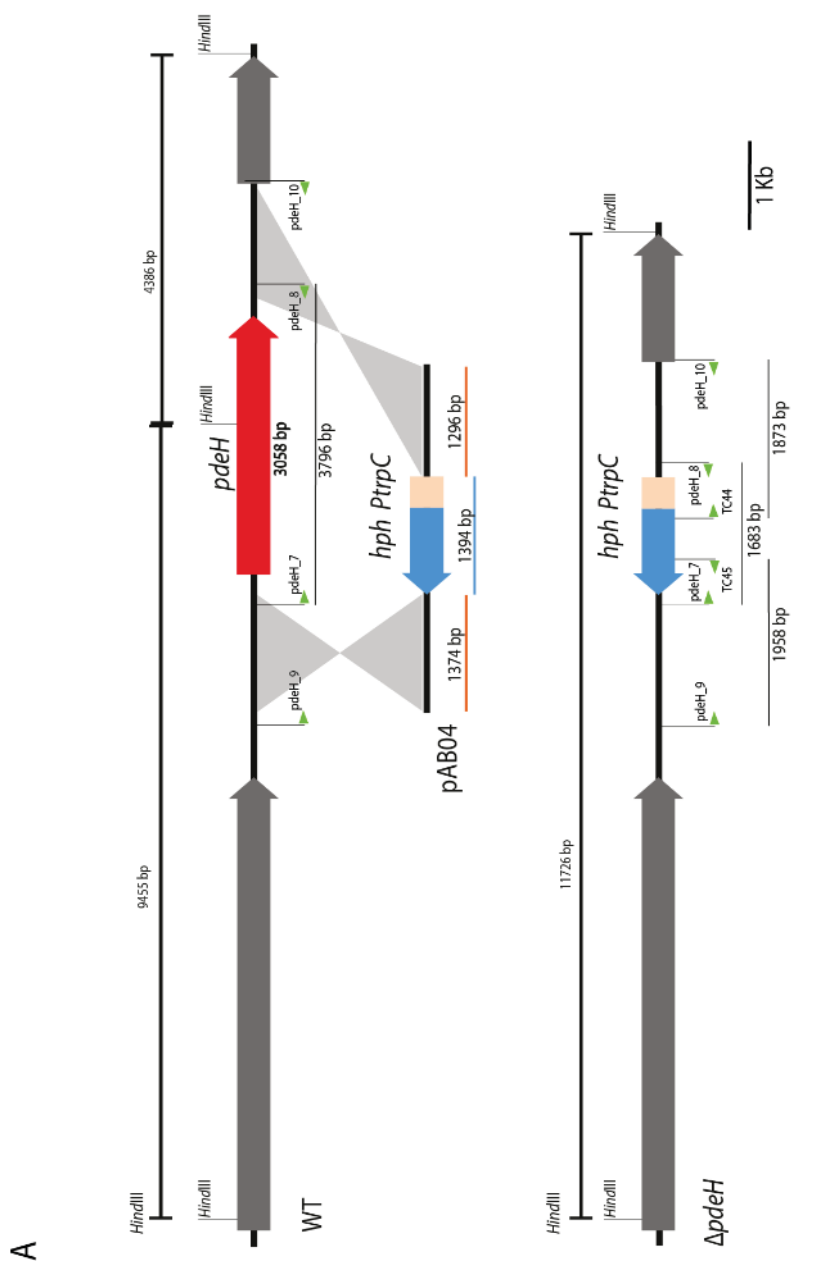
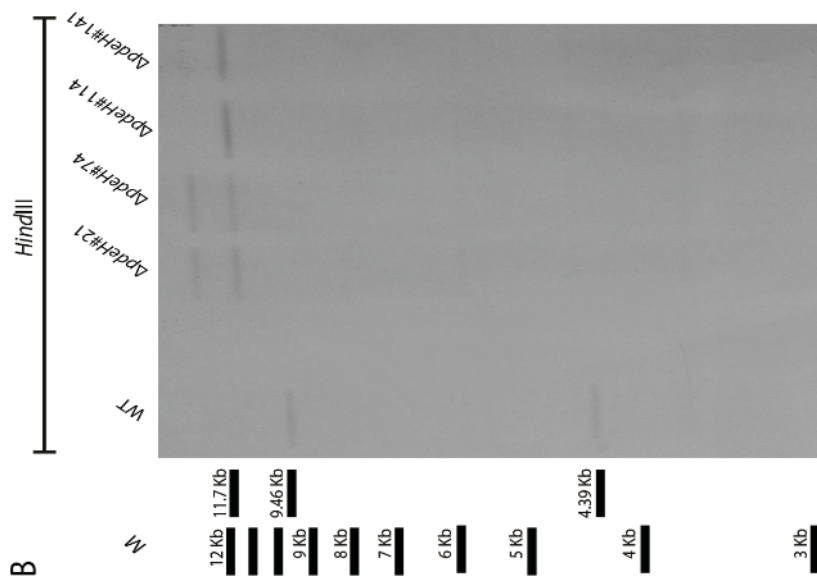
To investigate the role of the 3', 5'-cyclic AMP phosphodiesterases (PDEs) in *E. festucae*, a reverse genetic approach was taken to delete genes encoding the two putative PDEs, PdeH and PdeL and to determine their function in hyphal growth, and in regulating the association with its host *L. perenne*.

5.1 Functional analysis of PdeH

5.1.1 Deletion of the *E. festucae pdeH* gene

To functionally analyse the symbiotic role of the putative cAMP high-affinity PDE (PdeH) in *E. festucae*, a gene deletion mutant of *pdeH* was generated by replacing the *pdeH* gene with the hygromycin B phosphotransferase (*hph*) cassette using homologous recombination with the construct pAB04 (Fig. 5.1 A; Appendix 8; 2.5.10.4). A linear fragment containing the *hph* cassette and *pdeH* flanking regions was PCR-amplified from pAB04 plasmid DNA (2.5.7.2), purified (2.5.2), transformed into protoplasts of wild-type *E. festucae* (2.5.12), and screened for antibiotic resistance by growth on PD medium (2.3.3.1) containing hygromycin. PCR screening of an arbitrary selection of these transformants identified four putative $\Delta pdeH$ (#21, #74, #114, #141) mutants, where two (#114, #141) of these candidates were confirmed as clean 'knock-outs' by genomic DNA digest and Southern blot (2.5.14) analysis (Fig. 5.1 B). The two other candidates (#21, #74) were also confirmed as 'knock-outs' but additionally showed tandem copies of the gene replacement construct integrated into the genome (Fig. 5.1 B).

Figure 5-1 Strategy for deletion of *pdeH* and identification of $\Delta pdeH$ mutant strains: (A) Physical map of the *pdeH* genomic locus in wild-type *E. festucae* (WT), linear insert of the *pdeH* replacement construct (pAB04) and $\Delta pdeH$ mutant locus. Also shown are primers used to screen for *pdeH* replacement mutants (pdeH_7/pdeH_8, pdeH_9/TC45, TC44/pdeH_10) and restriction enzyme cutting sites for *Hind*III. Digestion with *Hind*III, followed by probing with pAB04 will produce diagnostic fragments of 9455 bp and 4386 bp for the wild-type strain and a single fragment of 11726 bp for $\Delta pdeH$. (B) Autoradiograph of Southern blot of *Hind*III genomic digest (1 μ g) of wild-type and $\Delta pdeH$ strains probed with DIG-labelled linear insert of the *pdeH* replacement construct (pAB04). Approximate fragment sizes in kilobase (kb).



5.1.2 Deletion of *pdeH* does not alter fungal development in axenic culture

In axenic culture, the colony size and morphology of the $\Delta pdeH$ strains were indistinguishable from wild-type (Fig. 5.2 A). Microscopic examination (2.8.1) of hyphal development and morphology was conducted in detail by bright field (BF) and inverted light microscopy (iLM) of stained hyphae, using Calcofluor white (CFW), which binds to fungal chitin in the cell wall and septa. The microscopic examination showed, that wild-type and $\Delta pdeH$ mutant strains similarly form bundles of hyphae (Fig. 5.2 B), undergo hyphal fusion at a similar frequency to wild-type (Fig. 5.2 B; Fig. 5.3) and also grow in coils of hyphae from which conidiophores arise (Fig. 5.2 C). Conidia formation and conidiophore development of the $\Delta pdeH$ mutant strain was similar to that observed for the wild-type strain. Conidia formation was quantified by counting colonies that arose from single-spore isolation (2.5.13), which was slightly reduced compared to the wild-type strain (Section 5.2.2).

Colony growth and morphology was further tested on different media including Blankenship (2.3.3.7), modified Czapek-DOX (2.3.3.6), CDGN (2.3.3.4), media facilitating nutrient starvation (CD (2.3.3.5), H₂O (2.3.3.3)) and defined media containing CD salts and various carbon and/or nitrogen sources as listed in Table 1 (2.3.3.8). No noticeable difference in growth of $\Delta pdeH$ mutant strains compared to the wild-type strain was observed on all media that were tested (Section 5.3.1).

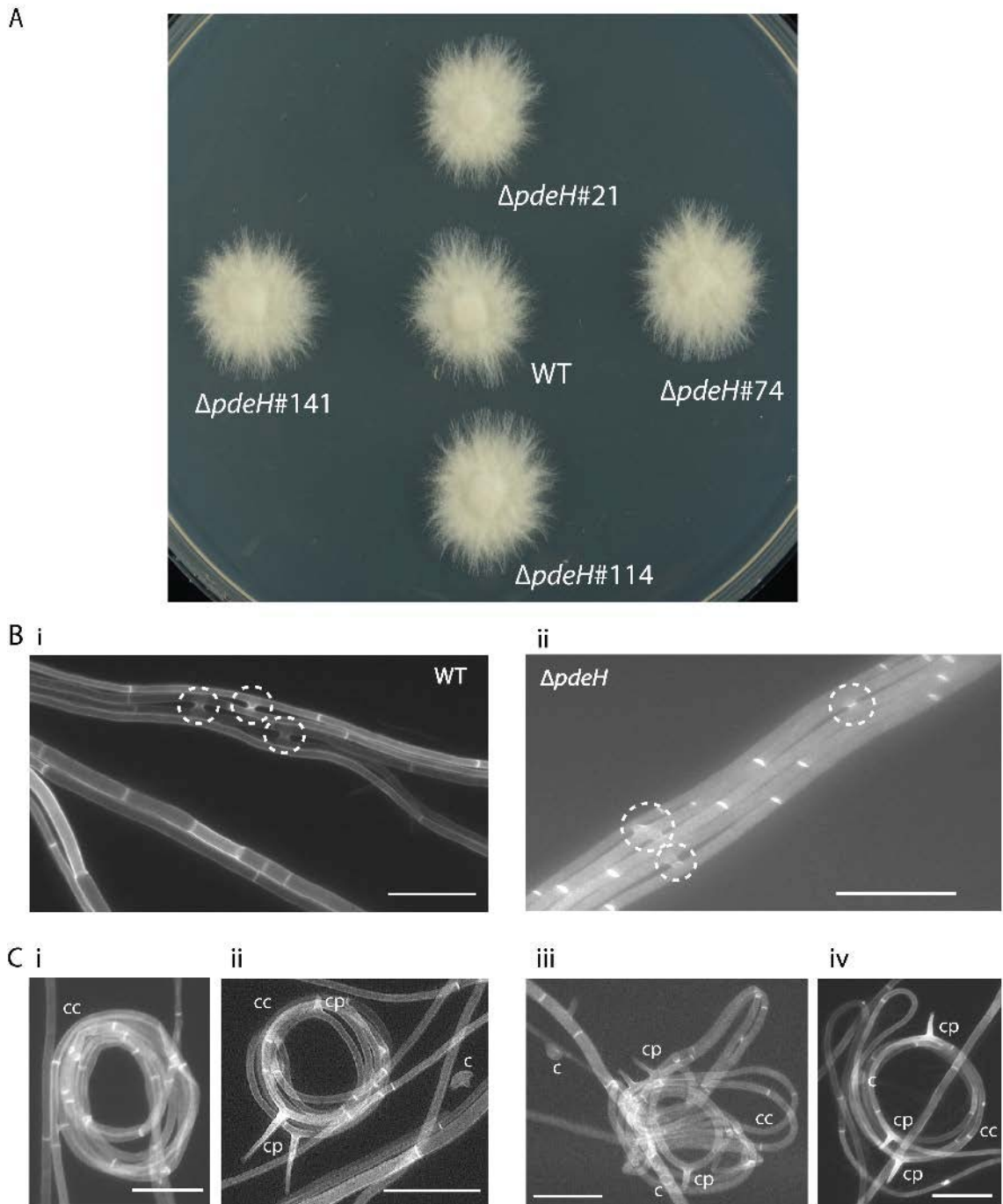


Figure 5-2 Culture phenotype analysis of $\Delta pdeH$ mutant strain: Phenotype analysis of the *E. festucae* $\Delta pdeH$ mutant compared to the wild-type strain in axenic culture. (A) growth on PD agar for 7 days. (B + C) Bright field (BF) light microscopy images of *E. festucae* $\Delta pdeH$ mutant and wild-type (WT) strains grown on 3% H₂O agar for 7-10 days. Hyphal cell wall and septa stained with Calcofluor white (CFW). (B) Hyphal growth of $\Delta pdeH$ mutant strain with frequent hyphal fusion (circles); (C) hyphae growing in coils (cc) to form conidophores (cp) and conidiospores (c). Bar = 20 μ m.

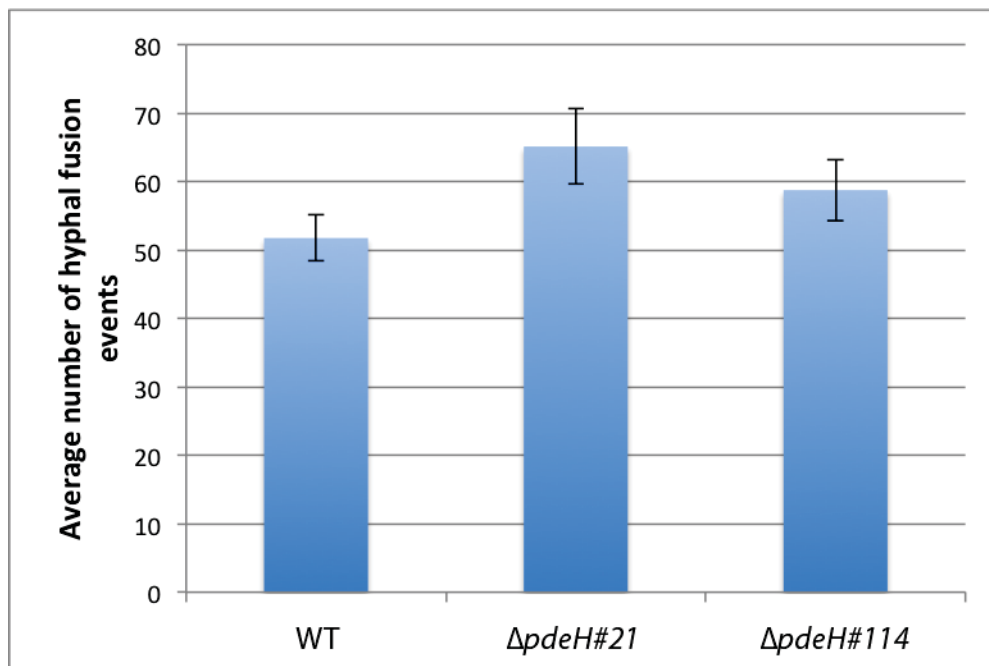


Figure 5-3 Hyphal fusion event in $\Delta pdeH$ mutant strains: Graph showing no significant differences (*Student's t-test*) in the average number of hyphal fusion events of the wild-type (WT) and the $\Delta pdeH$ mutant strains ($\Delta pdeH\#21$, $\Delta pdeH\#114$) in axenic culture, grown on 3% water agar (H₂O) for 10 days at 22°C. Hyphal fusion events were counted at 10 microscopic sites per strain in eight independent repeats. (Mean ± SD)

5.1.3 Deletion of *pdeH* caused a dramatic breakdown of the symbiotic interaction

5.1.3.1 Symbiotic interaction phenotype of $\Delta pdeH$ strains

To determine whether PdeH was required for establishment and maintenance of a mutualistic symbiotic interaction, seedlings of *L. perenne* were inoculated (2.7.3) with wild-type and all four $\Delta pdeH$ mutant strains individually. In contrast to wild-type, $\Delta pdeH$ infected plants showed a high plant mortality about 3-5 weeks post inoculation. From those plants that survived, single tillers were immunoblotted (2.7.6) at 10-12 weeks post inoculation, to identify which plants were infected. Plants infected with $\Delta pdeH$, were severely stunted with reduced tillering, exhibited premature senescence and had poorly developed root systems,

compared to plants infected with wild-type (Fig. 5.4). Infected plants were subsequently analysed by microscopy (2.8.2).

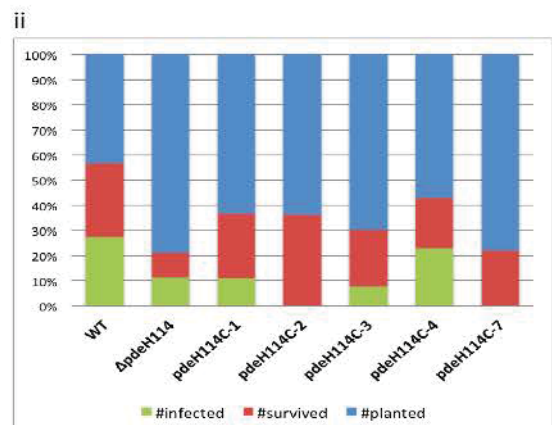
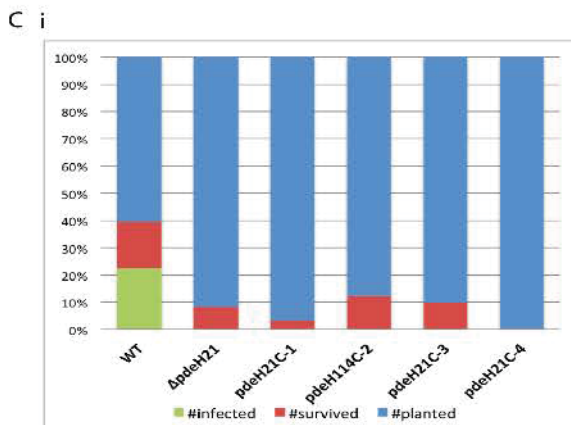
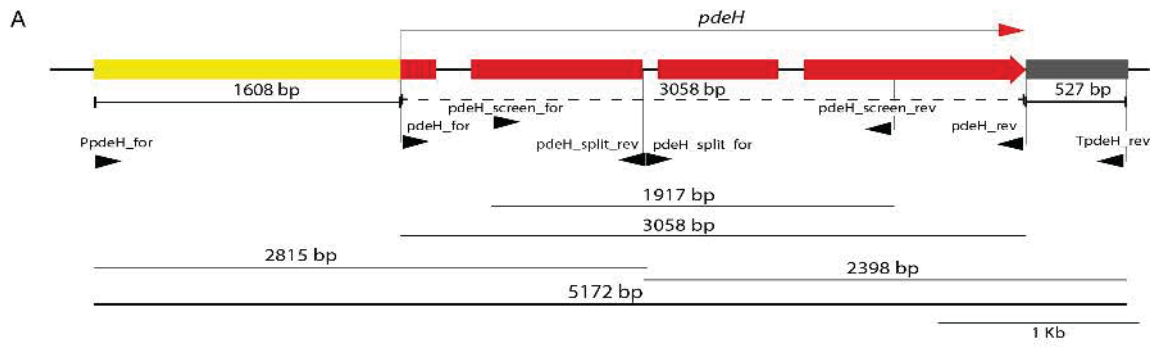


Figure 5-4 Symbiosis phenotype of *Lolium perenne* infected with $\Delta pdeH$ mutant strain: Phenotype of perennial ryegrass plants infected with *Epichloë festucae* wild-type (WT) and three independent $\Delta pdeH$ mutant strains $\Delta pdeH\#21$, $\Delta pdeH\#74$ and $\Delta pdeH\#114$. Dead leaves were removed for imaging. Photographs were taken 12 weeks post-inoculation.

To confirm the phenotype observed was due to deletion of *pdeH*, a DNA fragment (referred to as pAB07) of the *pdeH* wild-type copy (a linear 5172 bp fragment, directly amplified from *E. festucae* wild-type genomic DNA by PCR using PpdeH_for/TpdeH_rev) (2.5.10.7) was co-transformed (2.5.12.2) with pSF16.17 (Appendix 4) for selective screening, into the $\Delta pdeH$ mutant background to facilitate resistance against geneticin in addition to the hygromycin resistance of the $\Delta pdeH$ mutant strain (Fig. 5.5 A). The resulting transformants were screened for antibiotic resistance by growth on PD medium (2.3.3.1) containing geneticin and an arbitrary selection of transformants were screened by PCR (Fig. 5.5 A).

PCR using the primers pdeH_screen_for/pdeH_screen_rev, pdeH_for/pdeH_rev, PpdeH_for/pdeH_split_rev and pdeH_split_for/TpdeH_rev produced bands of 1917 bp, 3058 bp, 2815 bp and 2398 bp, respectively, if the construct was integrated. Of those positively identified strains, four for the $\Delta pdeH\#21$ mutant background (*pdeH21C-1*, *pdeH21C-2*, *pdeH21C-3*, *pdeH21C-4*) and five for the $\Delta pdeH\#114$ mutant background (*pdeH114C-1*, *pdeH114C-2*, *pdeH114C-3*, *pdeH114C-4*, *pdeH114C-7*), were inoculated into *L. perenne* plants for further analysis (2.7.3). Ectopic integration of the *pdeH* complementation construct fully restored the wild-type interaction phenotype for plants infected with the *pdeH114C-1* complementation strain (Fig. 5.5 B), while *pdeH114C-3* and *pdeH114C-4* displayed solely mutant-like interactions (Fig. 5.5 C). However, the survival and infection rate for the *pdeH114C-1* strain was still lower than for plants infected with the wild-type strain (Fig. 5.5 C). Further, infection with the *pdeH114C-1* complementation strain also displayed a single infected plant with a rather stunted interaction phenotype, potentially indicative for a plant genotype specific incompatibility or extracellular effects during plant growth.

Figure 5-5 Complementation of $\Delta pdeH$ mutant strain: (A) Physical map of the *pdeH* complementation (pAB07), containing 1608 bp of the promotor sequence (yellow), the wild-type copy of *pdeH* (red) and 527 bp of the terminator sequence (grey). Also shown are primers used for PCR-amplification (PpdeH_for/TpdeH_rev) and screening for integration of *pdeH* in the $\Delta pdeH\#114$ mutant background (pdeH_screen_for/pdeH_screen_rev; pdeH_for/pdeH_rev; PpdeH_for/pdeH_split_rev; pdeH_split_for/TpdeH_rev) and PCR product sizes. (B) Phenotype of perennial ryegrass plants infected with *E. festucae* wild-type (WT), the $\Delta pdeH\#114$ mutant strain and the complementation strain *pdeH114C-1*. Dead leaves were removed for imaging. Photographs were taken 12 weeks post-inoculation. (C) Graphs showing the proportion of plants, inoculated with the respective fungal strains in the (i) $\Delta pdeH\#21$ and (ii) $\Delta pdeH\#114$ mutant background, that were planted (blue), survived (red) and were infected (green), superimposed onto each other.



5.1.3.2 Microscopic analysis reveals unrestricted growth and increase of fungal biomass

To examine the cellular phenotype, plants infected with the $\Delta pdeH$ mutant strains were harvested and pseudostem tissue was analysed using light -, transmission electron (TEM; 2.8.2.2) and confocal laser scanning microscopy (CLSM; 2.8.2.1).

While wild-type infected plants typically showed one-two electron dense hyphae per intercellular space and no colonisation of the vascular bundles (Fig. 5.6; Fig. 5.7A, B and E; Fig. 5.8), plants infected with $\Delta pdeH$ revealed an unrestricted pattern of fungal growth, resulting in an increased fungal biomass (Fig. 5.6; Fig. 5.7). Multiple hyphae of $\Delta pdeH$ were observed in the intercellular space (Fig. 5.7 C and D; Fig. 5.8) and extensive colonisation of the plant vascular bundles was also seen (Fig. 5.6; Fig. 5.7 F). While hyphae in the vascular bundle tissue appeared to be more electron-dense, hyphae in other tissue were highly vacuolated and frequently formed intrahyphal hyphae (Fig. 5.7 C and D). Where the wild-type strains exhibited an electron dense darkly stained layer around the hyphae in the intracellular space (Fig. 5.7 A and B), hyphae of the $\Delta pdeH$ mutant strain seemed to often miss this outer layer (Fig. 5.7 C and D), suggesting a change in composition of the hyphal cell-wall. The complementation strain *pdeH114C-1* showed a fully restored wild-type phenotype *in planta*, including restricted fungal colonisation, absence of highly vacuolated hyphae or intra hyphal hyphae and the above mentioned electron-dense layer around the hyphal cell-wall. However, only plants infected with the *pdeHC-1* mutant strain with an fully restored symbiotic interaction plant phenotype were further analysed.

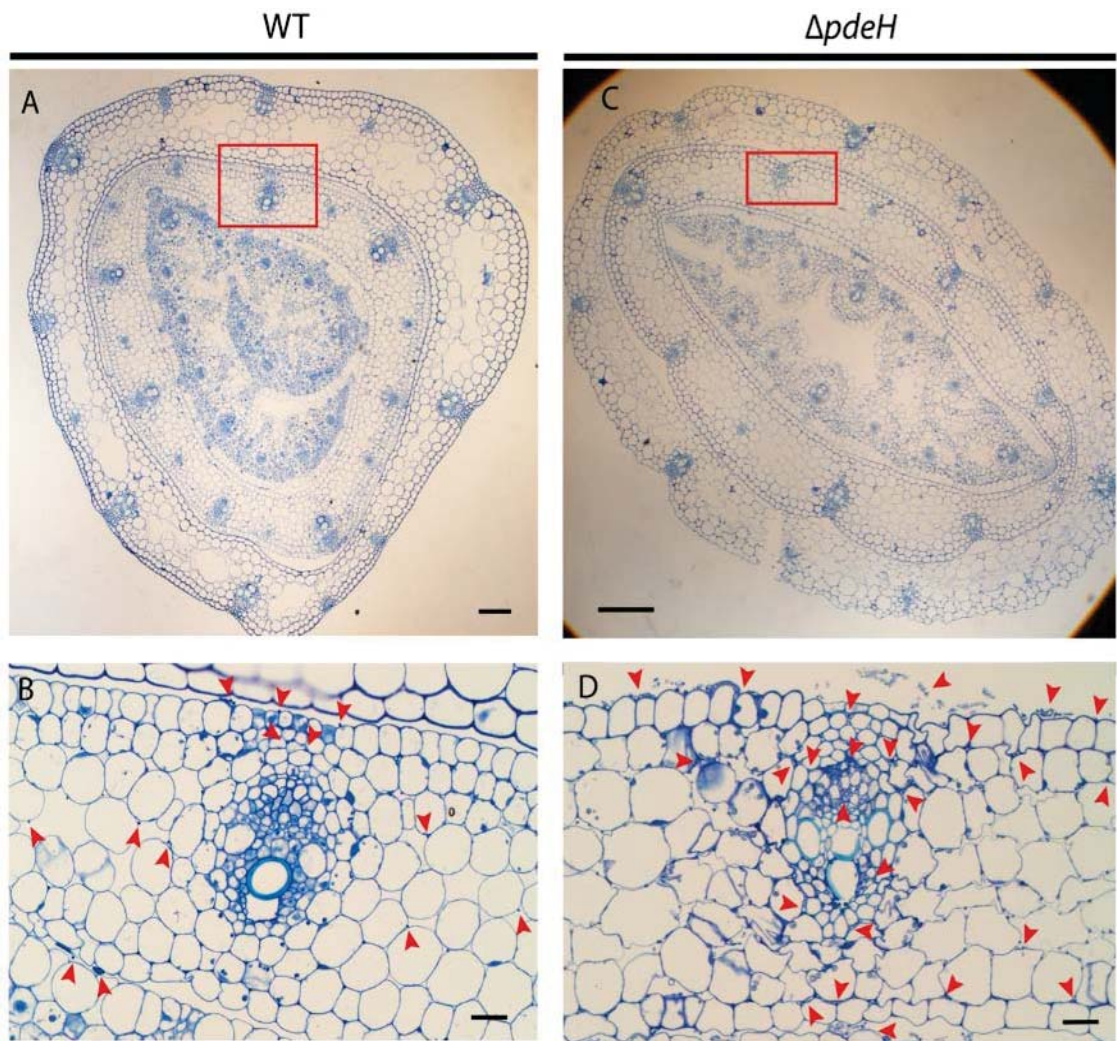


Figure 5-6 Light microscopy of the $\Delta pdeH$ mutant strain *in planta*: Microscopic analysis of ryegrass pseudostem tissue infected with the wild-type and $\Delta pdeH$ mutant strain using light microscopy (LM). Transverse sections of ryegrass pseudostem tissue infected with wild-type (A + B) and $\Delta pdeH$ mutant strain (C + D), stained with toluidine blue. Light micrograph shows increased fungal colonisation including colonisation of the host vascular bundles and epiphyllous hyphae for $\Delta pdeH$ (D). Arrow indicates hyphae position. Red box in A and C indicates the magnified area in B and D, respectively. Bar = 100 mm (A + C) and 20 mm (B +D).

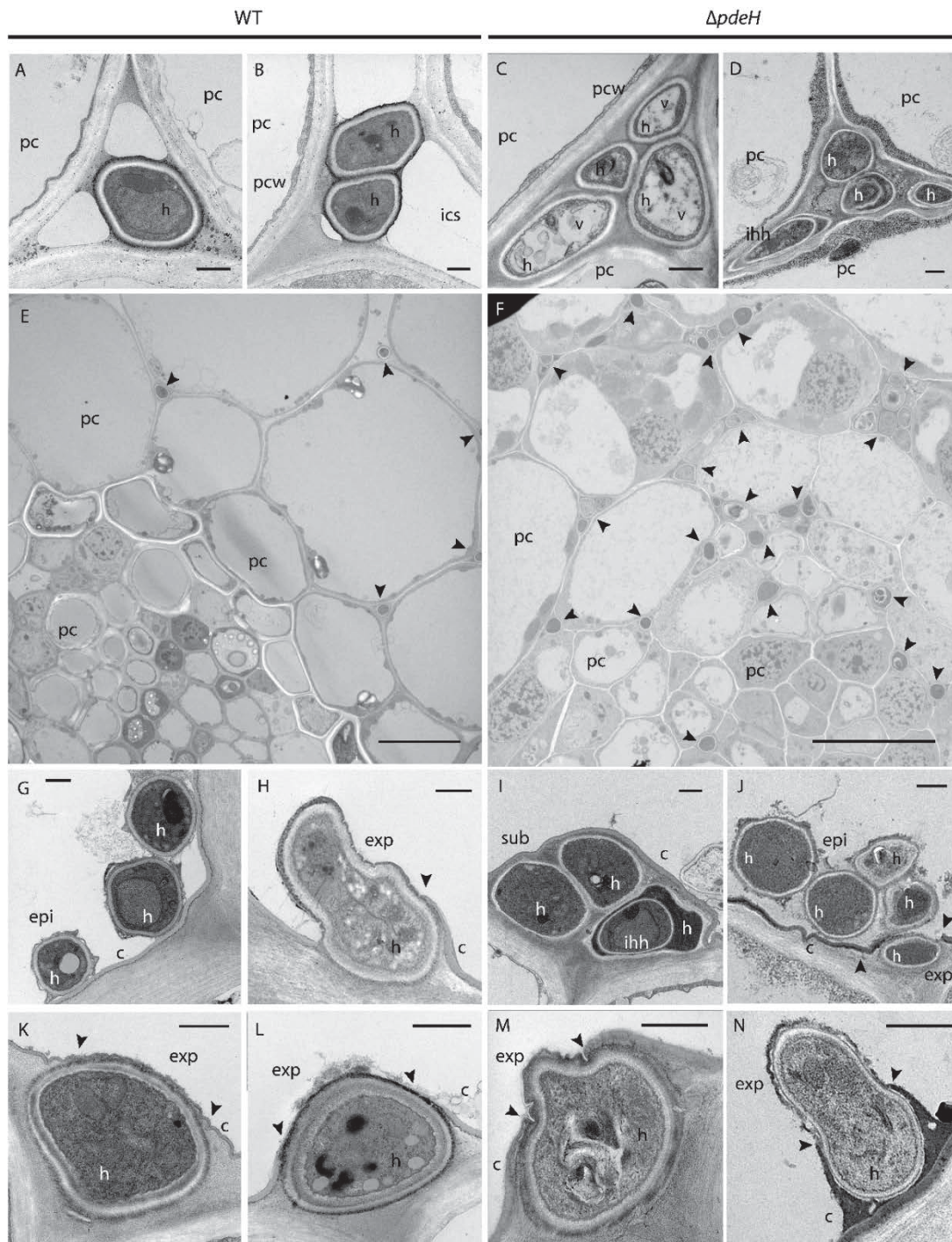


Figure 5-7 Transmission electron microscopy of the $\Delta pdeH$ mutant strain *in planta*: Microscopic analysis of ryegrass pseudostem tissue infected with the wild-type and $\Delta pdeH$ mutant strain using transmission electron microscopy (TEM). Micrographs of cross-sections show hyphal growth in host apoplast with multiple hyphae per intercellular space (ics) (C, D); colonisation of vascular bundles (F), highly vacuolated (v) hyphae (C), intra-hyphal hyphae (ihh) formed by $\Delta pdeH$ mutant strains (D, I), epiphyllous hyphae (epi) (G, J), sub-cuticular hyphae (sub) (I) and exessoria-like structure (exp) (H, J - N). Arrow indicates fungal hyphae in E and F, Arrows indicates hyphal breaching through plant cuticle in H, K - N. pc = plant cell; pcw = plant cell wall. Bar = 500nm (A-D, G - N), 10 μ m (E, F).

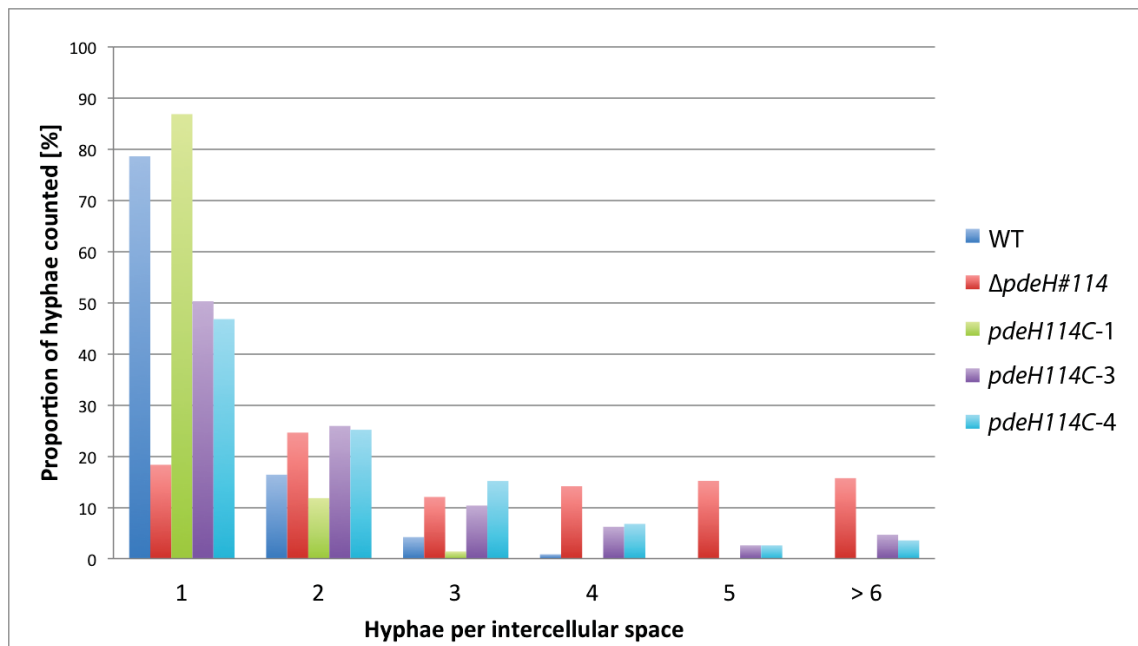
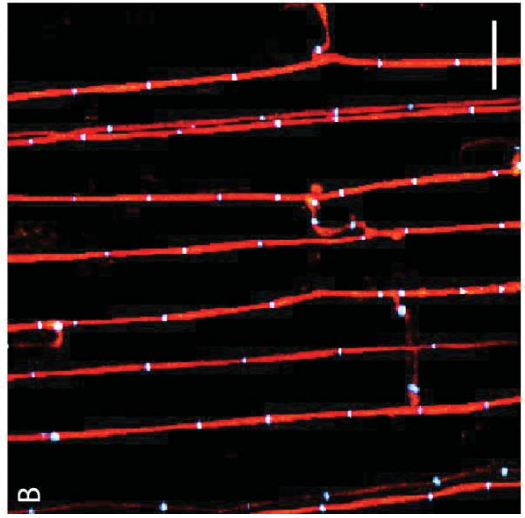
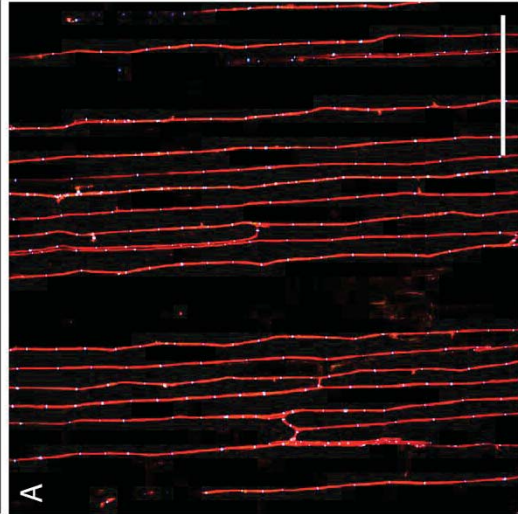


Figure 5-8 Hyphae per intercellular space of $\Delta pdeH$ mutant and complementation strains: Graph showing the proportion of hyphae per intercellular space in *L. perenne* tissue, infected with the wild-type (WT), the $\Delta pdeH\#114$ mutant strain and the complementation strains *pdeHC-1*, *pdeHC-3* and *pdeHC-4*.

The prolific growth of the $\Delta pdeH$ mutants in leaf tissue compared to the more restrictive growth of the wild-type infected plants was also evident using CLSM (Fig. 5.9). Longitudinal sections of pseudostem were stained (2.8.2.1) with aniline blue (red pseudocolour) and WGA-AlexaFlour488 (blue pseudocolour), which stain the fungal β -glucan and fungal chitin in cell walls and septa respectively (Ram and Klis 2006). Despite the increased number of hyphae, hyphal branching and fusion still occurred in $\Delta pdeH$ mutants similar to the wild-type (Fig. 5.9 D and B). Occasionally, large patches of WGA-AlexaFlour488 (blue pseudocolour) were visible alongside bundles of hyphae (Fig. 5.9 E), whereas in the wild-type only the hyphal septa were stained. This irregular labelling of the chitin by the fluorophore suggests increased accessibility of fungal chitin for the staining, potentially due to changes in the fungal cell-wall. A similar suggestion was made for the missing darkly stained outer layer found by TEM analysis. Irregular patterns of hyphal growth were observed infrequently, which occasionally formed highly convoluted structures (Fig. 5.9 F), indicating potential disorientation of polarised growth.

WT



$\Delta pdeH$

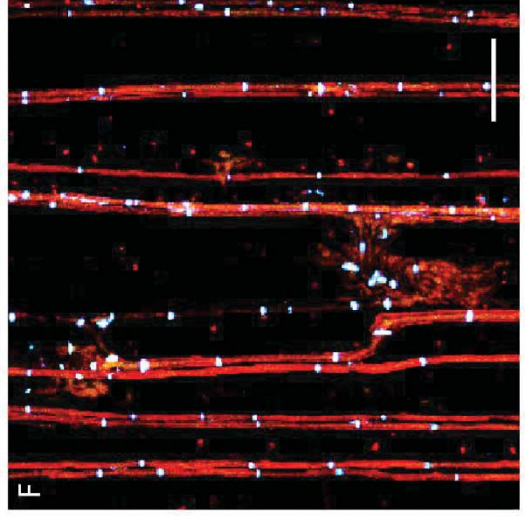
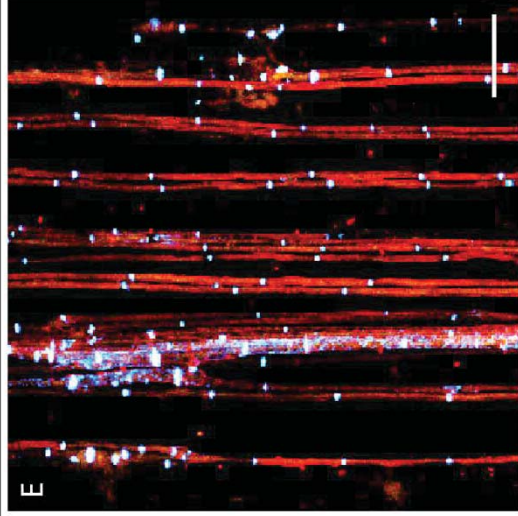
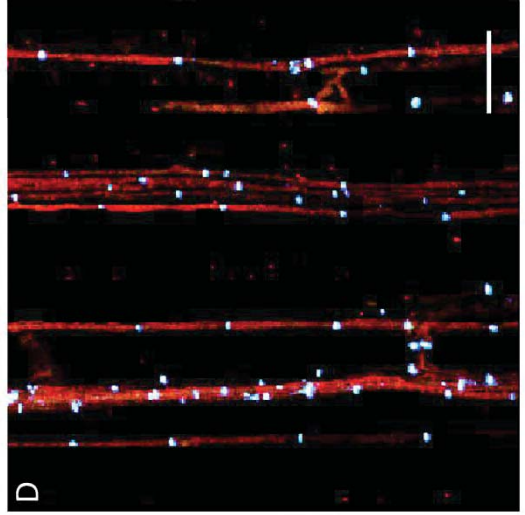
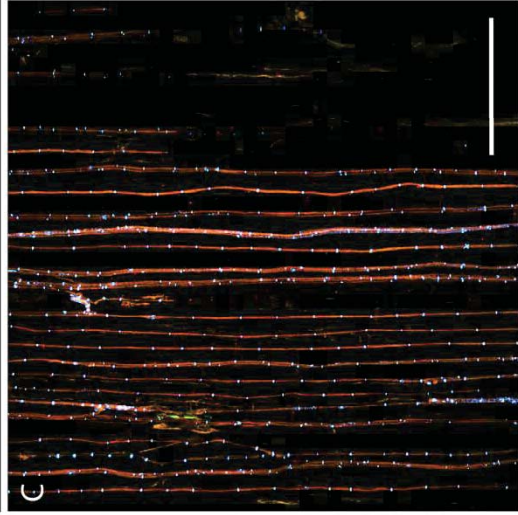


Figure 5-9 Confocal laser-scanning microscopy of the $\Delta pdeH$ mutant strain *in planta*: Microscopic analysis of ryegrass leaf pseudostem tissue infected with the wild-type (WT) and $\Delta pdeH$ mutant strains using confocal laser-scanning microscopy (CLSM) showing longitudinal section with hyphal growth parallel to the leaf axis. The $\Delta pdeH$ mutant strain (C - F) with increased fungal biomass compared to wild-type (A - B) infected plants. Plant tissue stained using aniline blue (red pseudocolour) and WGA-AlexaFluor488 (blue pseudocolour). Frequent hyphal fusion occurs in WT (B) and $\Delta pdeH$ mutant strain (D). Confocal depth series images generated by maximum intensity projection of 10 x 1 μm confocal Z-stacks. Bar = 100 μm A, C, D; Bar = 20 μm B, D, E, F.

5.1.3.3 Microscopic analysis of $\Delta pdeH$ revealed wild-type like fungal colonisation of host tissue

The formation of expressoria, a structure involved in allowing endophytic hyphae to exit the host plant to form an epiphytic hyphal network (Becker et al. 2016), were observed in various stages in plants infected with the wild-type or the $\Delta pdeH$ mutant strain (Fig. 5.7 H, K, L, M and N). Despite the increased number of hyphae, the formation of hyphal bundles underneath the cuticle layer (Fig. 5.7 I) and a massively increased number of epiphyllous hyphae (Fig. 5.6 D), expressoria formation appeared not to be impaired. The characteristic curling of the cuticle layer (Fig. 5.7 K and M), followed by a thinning and breaching of the cuticle layer by polarised growth at the point of contact (Fig. 5.7 H, L, M and N). To date, the actual mechanism by which the fungus generates the expressoria structures and how these hyphae exit the plant is not well understood (Becker et al. 2016). However, the large number of subcuticular hyphae potentially caused the cuticle layer to rupture at places where the formation of expressoria structures were not initiated and released the hyphae accumulating underneath, especially when multiple hyphae at the same point formed subcuticular hyphal bundles.

In summary, the unrestricted hyphal growth resulting in an increased fungal biomass *in planta*, that putatively caused the strong symbiotic interaction phenotype, indicates an essential role for PdeH for maintaining the mutualistic *E. festucae-L. perenne* association.

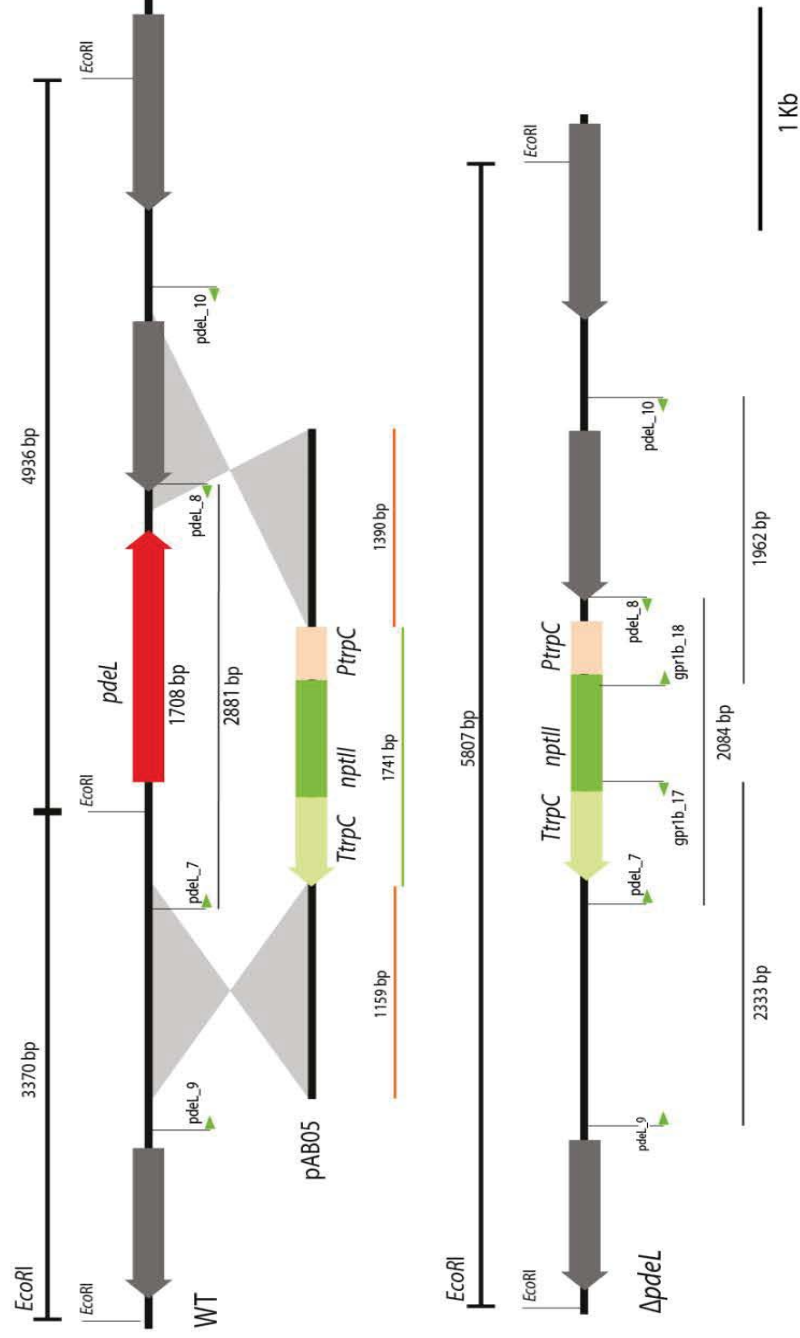
5.2 Functional analysis of PdeL

5.2.1 Deletion of the *E. festucae pdeL* gene

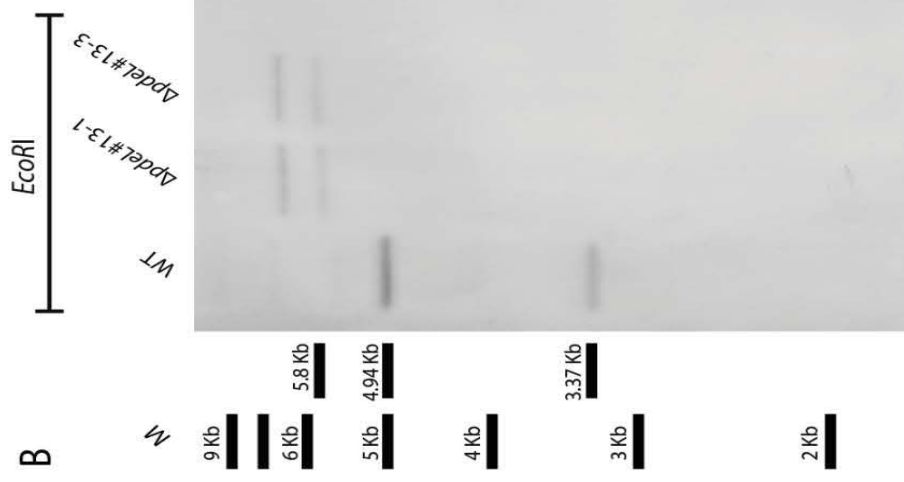
To functionally analyse the symbiotic role of the putative low-affinity PDE (PdeL) in *E. festucae*, a gene deletion mutant of *pdeL* was generated by replacing the *pdeL* gene with the neomycin phosphotransferase II (*nptII*) cassette using homologous recombination with the construct pAB05 (Fig. 5.10; Appendix 9; 2.5.10.5). A linear fragment containing the *nptII* cassette and the *pdeL* flanking regions was PCR-amplified from pAB05 plasmid DNA (2.5.7.2), purified (2.5.2), transformed into protoplasts of wild-type *E. festucae* (2.5.12), and screened for antibiotic resistance by growth on PD medium (2.3.3.1) containing geneticin. PCR screening of an arbitrary selection of these transformants identified only one putative $\Delta pdeL$ mutant strain ($\Delta pdeL\#13$), which was then confirmed as a 'knock-out' with tandem copy by genomic DNA digest and Southern blot (2.5.14) analysis (Fig. 5.10 B). When isolated first, the transformant $\Delta pdeL\#13$ grew in two colonies ($\Delta pdeL\#13-1$, $\Delta pdeL\#13-3$) and it was unclear whether both derived from a single origin or from two independent transformants. To test this, homokaryotic colonies were generated using single spore isolation (2.5.13), which were individually screened. PCR screening and Southern blot analysis confirmed that these colonies were genetically identical (Fig 5.10 B). Given that the two $\Delta pdeL$ mutant strains are highly likely to have the same origin, subsequent analysis was conducted using the mutant strain $\Delta pdeL\#13-1$.

Figure 5-10 Strategy for deletion of and identification of $\Delta pdeL$ mutant strains: (A) Physical map of the *pdeL* genomic locus in wild-type *E. festucae* (WT), linearised *pdeL* replacement fragment construct (pAB05) and $\Delta pdeL$ mutant locus. Also shown are primers used to screen for *pdeL* replacement mutants (pdeL_7/pdeL_8, pdeL_9/gpr1b_17, gpr1b_18/pdeL_10) and restriction enzyme cutting sites for *EcoRI*. Digestion with *EcoRI*, followed by probing with pAB05 will produce diagnostic fragments of 4936 bp and 3370 bp for wild-type strains and a single fragment of 5807 bp for $\Delta pdeL$. (B) Autoradiograph of Southern blot of *EcoRI* genomic digest (1 μ g) of wild-type and $\Delta pdeL$ strains probed with DIG-labelled linear insert of the *pdeL* replacement construct (pAB05). Approximate fragment sizes in kilobase (kb).

A



B



5.2.2 Deletion of *pdeL* resulted in a significant reduction in hyphal growth in axenic culture

In axenic culture, the $\Delta pdeL$ strain grew in smaller colonies that appeared to be morphologically more compact than the wild-type strain (Fig. 5.11 A). While radial growth was significantly reduced compared to the wild-type ($p < 0.05$), independent of the growth medium (5.3.1), aerial hyphae seemed to be increased on PD medium (Fig. 5.11 A).

Microscopic examination of hyphal development and morphology was conducted using bright field (BF) and inverted light microscopy (iLM) of stained hyphae, using calcofluor white (CFW) that binds to fungal chitin in the cell wall and septa (2.8.1). While colony density is dependent on the frequency of hyphal branching, no difference between the wild-type strain and the $\Delta pdeL$ mutant strain was observed when grown on water agar. Microscopy analysis showed that the wild-type and the $\Delta pdeL$ mutant strains form hyphal bundles (Fig. 5.11 B), underwent hyphal fusion at a similar frequency to wild-type (Fig. 5.11 B; Fig. 5.12) and form coils of hyphae from which conidiophores arise (Fig. 5.11 C). However, hyphal coil structures were less frequent in the $\Delta pdeL$ mutant strains and predominantly without developed conidiophores, while conidiophores also arose from vegetative hyphae (Fig. 5.11 Ciii). Conidiation of the $\Delta pdeL$ mutant strain was reduced compared to that of the wild-type or other mutant strains (Fig. 5.13), quantified by counting colonies that arose from single-spore isolation (2.5.13). Further analysis showed that the aerial hyphae seemed to be irregular shaped at older areas of the colony (Fig. 5.11 D). Intrahyphal hyphae were frequently observed at the centre or older areas of the colony, indicative of cellular stress (Fig. 5.11 E). To analyse whether the formation of coiled structures and development of conidiophores was altered or delayed, the wild-type and the $\Delta pdeL$ mutant strain, grown on PD medium, were examined using scanning electron microscopy (SEM). The $\Delta pdeL$ mutant strains formed coil structures and conidiophores in the aerial hyphal network similar to those observed for the wild-type strain (Fig. 5.14). Aerial hyphae of the wild-type and the $\Delta pdeL$ mutant strain were indistinguishable using SEM analysis.

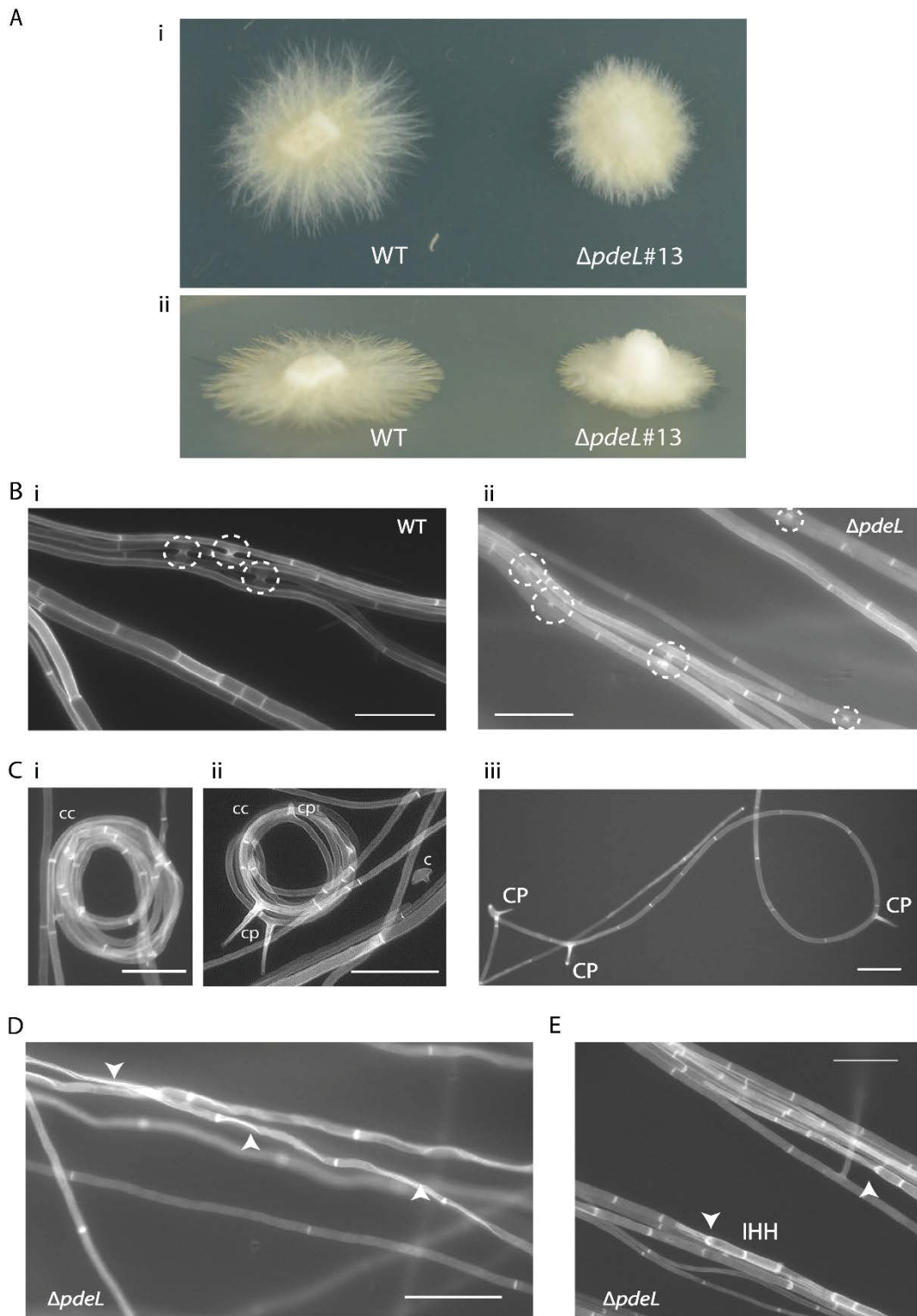


Figure 5-11 Culture phenotype analysis of $\Delta pdeL$ mutant strain: Phenotype analysis of the *E. festucae* $\Delta pdeL$ mutant compared to the wild-type strain in axenic culture. (A) Growth on PD agar for 7 days. (B) Bright field (BF) light microscopy images of *E. festucae* $\Delta pdeL$ mutant and wild-type (WT) strains grown on 3% H₂O agar for 7-10 days. Hyphal cell wall and septa stained with Calcofluor white (CFW); hyphal growth of $\Delta pdeL$ mutant strain with frequent hyphal fusion (circles); (C) hyphae growing in coils (cc) to form conidophores (cp) and conidiospores (c); (D) collapsed aerial hyphae (indicated by arrow) and (E) intra hyphal hyphae (ihh) in the $\Delta pdeL$ mutant strain. Bar = 20 μ m

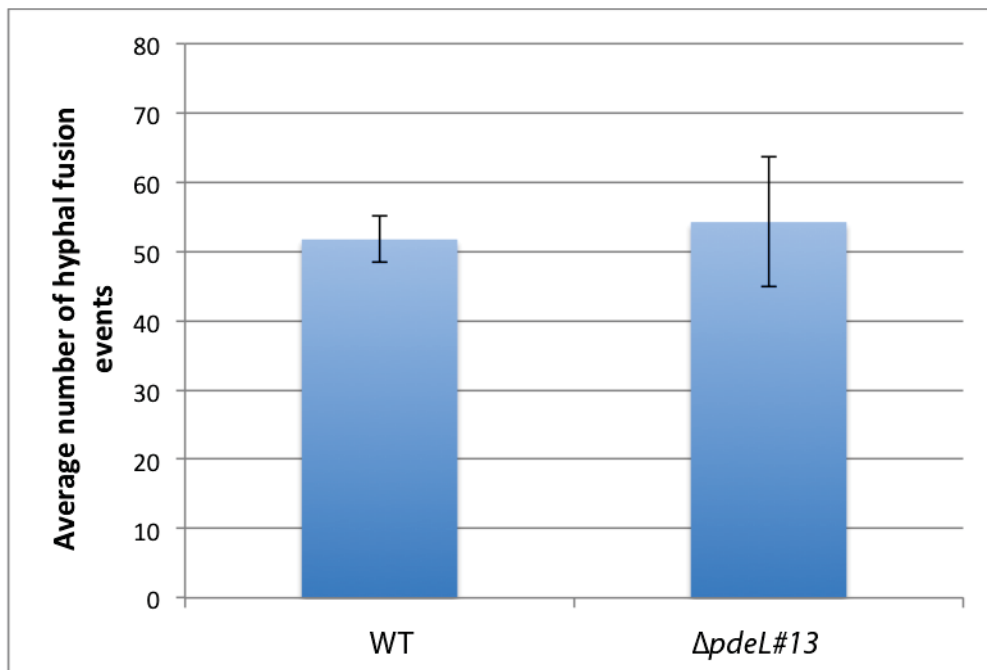


Figure 5-12 Hyphal fusion event in $\Delta pdeL$ mutant strains: Graph showing no significant differences (*Student's t-test*) in the average number of hyphal fusion events of the wild-type (WT) and the $\Delta pdeL$ mutant strains ($\Delta pdeL\#13-1$) in axenic culture, grown on 3% water agar (H₂O) for 10 days at 22°C. Hyphal fusion events were counted at 10 microscopic sites per strain in eight independent repeats (Data represented as Mean \pm SD).

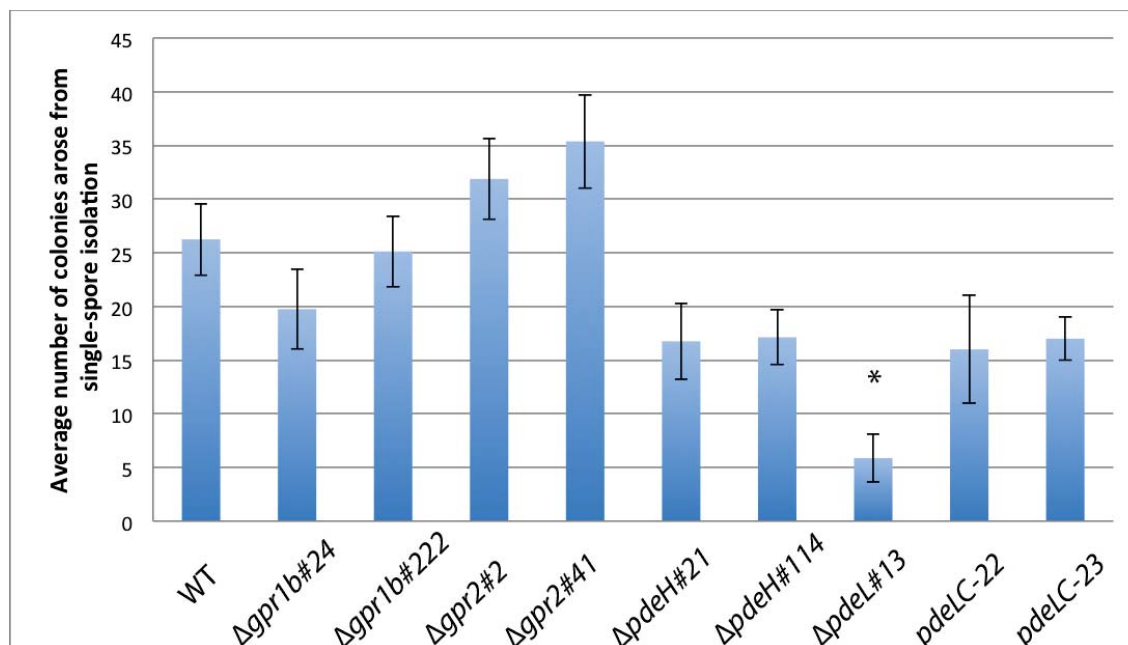


Figure 5-13 Sporulation assay for the $\Delta pdeL$ mutant strains: Graph showing the average number of colonies resulting from single-spore isolation for the wild-type (WT), the mutant strains $\Delta gpr1b\#24$, $\Delta gpr1b\#222$, $\Delta gpr2\#2$, $\Delta gpr2\#41$, $\Delta pdeH\#21$, $\Delta pdeH\#114$ (n = 8 respectively), $\Delta pdeL\#13$ (n = 6) and the complementation strains pdeLC-22 and pdeLC-23 (n = 2) grown on PD medium for 7 days at 22°C. Data represented as Mean \pm SE. Significantly (* $p < 0.05$) reduced number of colonies of the $\Delta pdeL$ mutant strain arose in comparison to the WT (*Student's t test*). Note: Complementation strains not included in statistical analysis.

Colony growth and morphology was further tested on different media including Blankenship (2.3.3.7), modified Czapek-DOX (2.3.3.6), CDGN (2.3.3.4), media facilitating nutrient starvation (CD (2.3.3.5), H₂O (2.3.3.3)) and defined media containing CD salts and various different carbon and/or nitrogen supplements as listed in Table 2.3. The reduced growth phenotype observed on PD medium was also observed when the mutant was grown on different media. While radial growth remained similar on all media, the fungal biomass was reduced on nutrient poor media where a total absence of aerial hyphae, was also observed, for the wild-type. Hyphal radial growth and the hyphal growth-rate per day was significantly reduced ($p < 0.05$), when compared to the wild-type strain on all media tested (Section 5.3.1).

To confirm the phenotype observed was due to deletion of *pdeL*, a construct containing a wild-type copy of *pdeL* (a linear 3503 bp fragment, amplified from *E. festucae* wild-type genomic DNA by PCR using PpdeL_for/TpdeL_rev) was prepared (pAB08; Appendix 11) (2.5.10.8). For selective screening, the pAB08 plasmid was co-transformed (2.5.12.2) with pSF15.15 (Appendix 3) into the $\Delta pdeL$ mutant background to facilitate antibiotic resistance against hygromycin resistance in addition to the geneticin resistance of the $\Delta pdeL$ mutant strain (Fig. 5.14 A). The resulting transformants were screened for antibiotic resistance by growth on selective PD medium (2.3.3.1) containing hygromycin and an arbitrary selection of transformants were screened by PCR (Fig. 5.14 A). Screening by PCR using the primers pdeL_screen_for/pdeL_screen_rev and PpdeL_for/TpdeL_rev produced bands of 1048 bp and 3503 bp, respectively, if the construct was integrated. Of those positively identified strains, five (*pdeL13C-4*, *pdeL13C-5*, *pdeL13C-6*, *pdeL13C-22* *pdeL13C-23*) were transformed into the $\Delta pdeL\#13$ mutant background. Introduction by ectopic integration of a *pdeL* wild-type copy fully restored the growth defect observed for the $\Delta pdeL$ mutants (Fig. 5.14 B) for all strains positively identified. Two strains (*pdeL13C-22*, *pdeL13C-23*) were randomly chosen for further analysis. Hyphal coil structures were observed in a similar frequency and structure for the wild-type, the $\Delta pdeL$ mutant strain and the *pdeLC-22* and *pdeLC-23* complementation strains (Fig. 5.14 C).

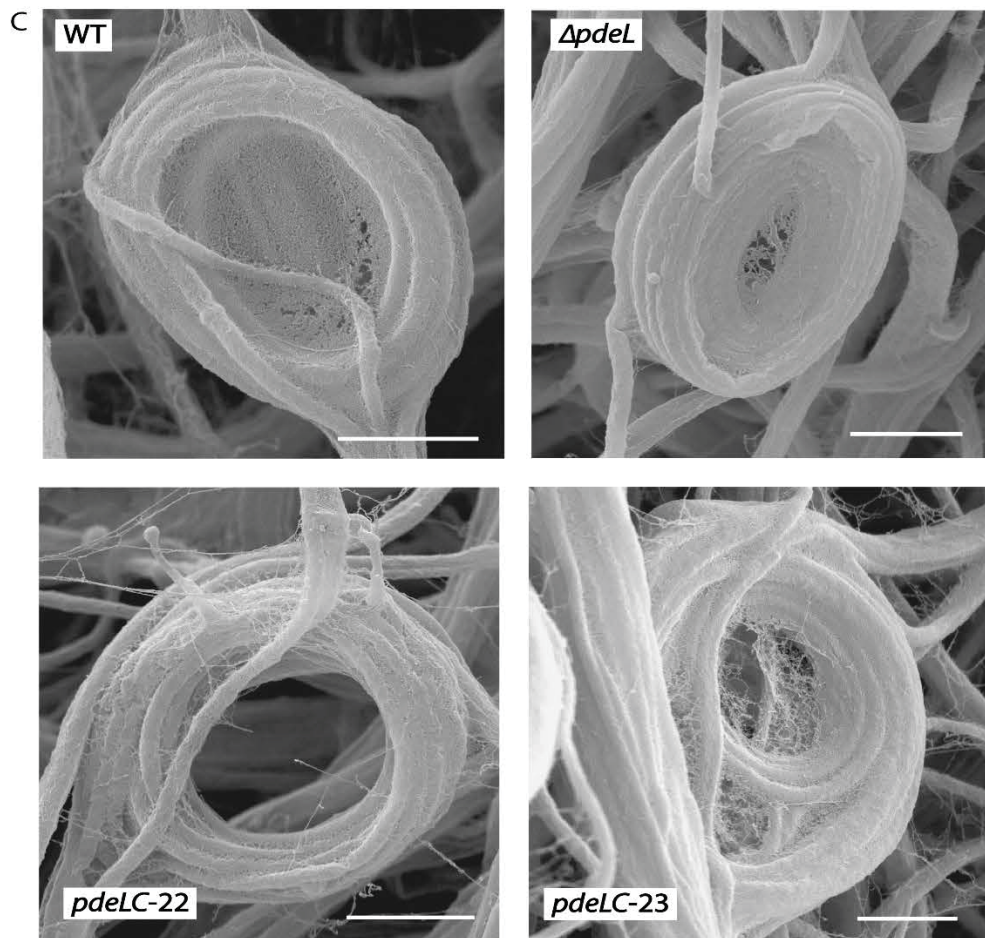
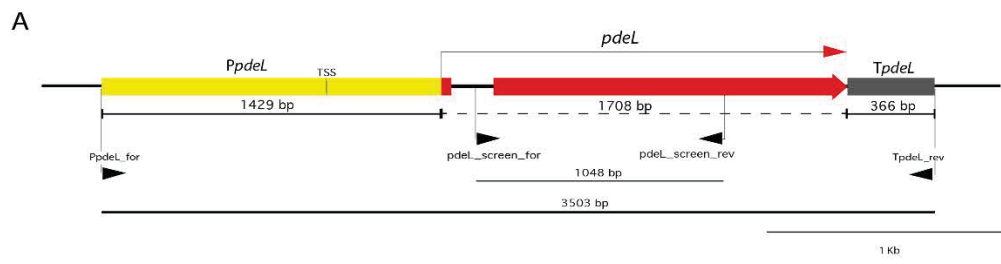


Figure 5-14 Complementation of $\Delta pdeL$ mutant strain: (A) Physical map of the *pdeL* complementation (pAB08), containing 1429 bp of the promoter sequence (yellow), the wild-type copy of *pdeL* (red) and 366 bp of the terminator sequence (grey). Also shown are primers used for PCR-amplification (PpdeL_for/TpdeL_rev) and screening for integration of *pdeL* in the $\Delta pdeL$ #13 mutant background (pdeL_screen_for/pdeL_screen_rev; PpdeL_for/TpdeL_rev) and PCR product sizes. (B) Phenotype of wild-type strain (WT), the $\Delta pdeL$ #13 mutant strain and the complementation strain *pdeLC*-22 and *pdeLC*-23 in axenic culture, grown on PD agar for 7 days at 22°C. (C) Analysis of coil structure and conidiophore formation in the wild-type strain (WT), the $\Delta pdeL$ mutant strain and the complementation strains *pdeL13C*-22 and *pdeL13C*-23 in axenic culture, grown on PD agar for 7 days at 22°C, using scanning electron microscopy (SEM).

5.2.3 PdeL does not show a functional role in the plant symbiotic interaction

5.2.3.1 Symbiotic interaction phenotype of the $\Delta pdeL$ strain

To determine whether PdeL was required for establishment and maintenance of a mutualistic symbiotic interaction, seedlings of *L. perenne* were inoculated (2.7.3) with wild-type and the $\Delta pdeL$ mutant strain ($\Delta pdeL$ #13-1). After 10-12 weeks post inoculation, single tillers were immunoblotted (2.7.6) to identify which plants were infected. The symbiosis phenotype of wild-type and $\Delta pdeL$ infected plants were indistinguishable (Fig. 5.15). Infected plants were subsequently analysed by microscopy (2.8.2). Due to the lack of an observable plant phenotype, the $\Delta pdeL$ complementation strains (*pdeLC*-22, *pdeLC*-23) were not inoculated into *L. perenne* plants.

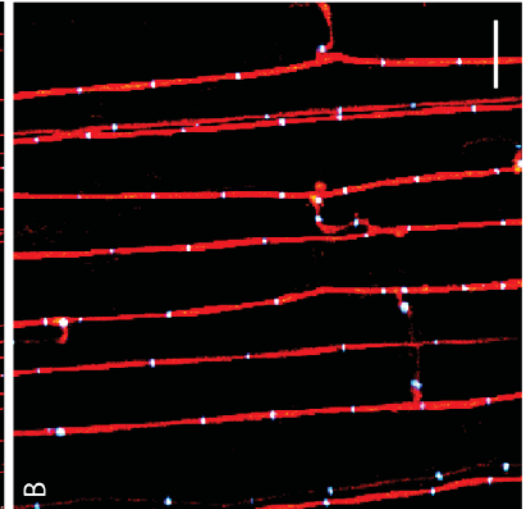
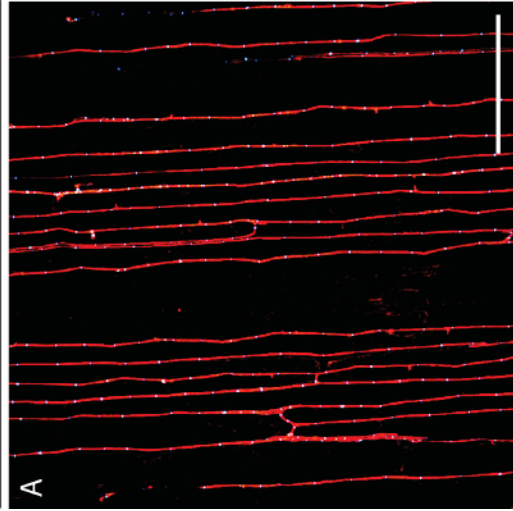


Figure 5-15 Symbiosis phenotype of *Lolium perenne* infected with $\Delta pdeL$ mutant strain: Phenotype of perennial ryegrass plants infected with *Epichloë festucae* wild-type (WT) and the $\Delta pdeL$ mutant strain $\Delta pdeL\#13$ ($\Delta pdeL\#13-1$). Dead leaves were removed for imaging. Photographs were taken 12 weeks post-inoculation.

5.2.3.2 Microscopic analysis of *ΔpdeL* revealed wild-type like fungal colonisation of host tissue

To examine the cellular phenotype, plants infected with the fungal *ΔpdeL* mutant strain were sampled and pseudostem tissue was analysed using confocal laser scanning microscopy (CLSM; 2.8.2.1) (Fig. 5.16). Longitudinal sections of pseudostem from plants infected with the wild-type or the *ΔpdeL* mutant strain, were stained (2.8.2.1) with aniline blue (red pseudocolour) and WGA-AlexaFluor488 (blue pseudocolour). Infected host tissue showed a similar fungal colonisation and distribution with hyphae aligned along the leaf axis, primarily with single hyphae per intercellular space. Frequent hyphal branching and fusion were indistinguishable between wild-type and *ΔpdeL* mutant strain (Fig. 5.16 B, D, E). Also observed were hyphae growing towards the leave surface (brighter orange colour) indicating exressoria formation (Fig. 5.16 C and D).

WT



$\Delta pdeL$

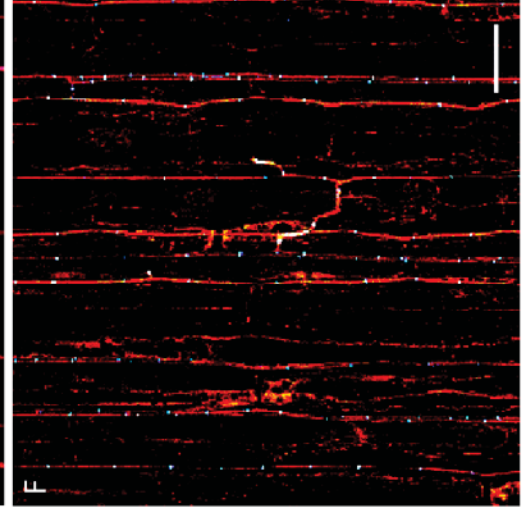
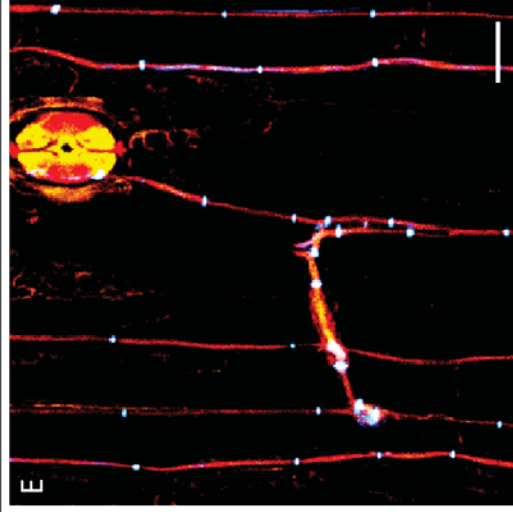
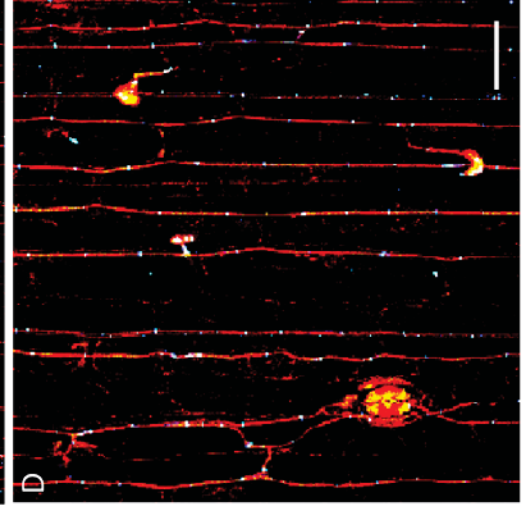
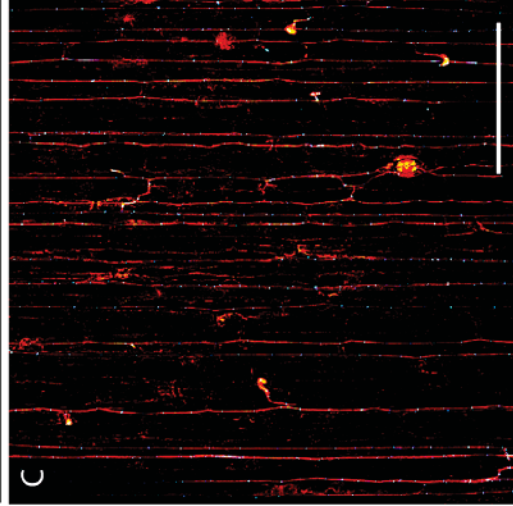


Figure 5-16 Confocal laser-scanning microscopy of the $\Delta pdeL$ mutant strain *in planta*: Microscopic analysis of ryegrass pseudostem tissue infected with the wild-type (WT) and $\Delta pdeL$ ($\Delta pdeL\#13$) mutant strains using confocal laser-scanning microscopy (CLSM) showing longitudinal section with hyphal growth parallel to the leaf axis. The $\Delta pdeL$ mutant strain (C - F) showing similar hyphae number and distribution to wild-type (A-B) infected plants. Plant tissue stained using aniline blue (red pseudocolour) and WGA-AlexaFluor488 (blue pseudocolour). Frequent hyphal fusion occurs in WT and $\Delta pdeL$ mutant strain. Confocal depth series images generated by maximum intensity projection of 10 x 1 μm confocal Z-stacks. Bar = 100 μm A, C; Bar = 20 μm B, D, E.

5.3 Analysis of hyphal growth for the $\Delta pdeH$ and $\Delta pdeL$ mutant strains

As described in section 4.3, hyphal growth-rate and colony morphology are cellular processes indirectly linked with the cAMP signalling pathway. To investigate whether the $\Delta pdeH$ and $\Delta pdeL$ mutant strains display a reduced hyphal growth-rate and therefore potentially altered levels of intracellular cAMP compared to the wild-type strain a series of preliminary analysis were conducted following the non-transfer (2.4.1.1) and transfer (2.4.1.2) experimental conditions. Growth media on which the $\Delta pdeH$ and $\Delta pdeL$ mutant strain showed a significant changes in hyphal growth-rate were then selected for sequential quantification of intracellular cAMP under these conditions. Hypothetically, activation of the cAMP signalling pathway results in an accumulation of intracellular cAMP in these mutants, which are putatively impaired or diminished in cAMP hydrolysis. This preliminary and sequential analysis could identify a direct link between cAMP signalling and hyphal growth.

5.3.1 *E. festucae* low affinity phosphodiesterase is important for hyphal growth especially on nutrient-rich media

To investigate whether PdeH or PdeL were involved in processing extracellular signals from molecules such as carbon sources (nutrient sensing), hyphal growth was analysed on various growth media including nutrient rich (e.g. PD, CZ, CDGN), nutrient poor (e.g. H₂O, CD) and defined media containing CD salts (CD) and various different C sources in the latter. Colonies of the wild-type and the

ΔpdeH and *ΔpdeL* mutant strains grew on nutrient rich medium with a solid fungal biomass similar to that observed on PD medium, but exhibited reduced biomass when grown on nutrient poor medium (Fig. 5.17), although colony diameter and hyphal growth-rate was similar to that observed on PD medium (Fig. 5.17, Fig. 5.18). The radial growth of the *ΔpdeH* and *ΔpdeL* mutant strains was measured and the hyphal growth-rate per day compared to that of the wild-type strain (2.4.1; 2.4.2; Fig. 5.18). The *ΔpdeH* mutant strain and the wild-type were indistinguishable on most growth media tested (Fig. 5.17). However, in the presence of glucose (Gluc) or sucrose (Suc) at a concentration of 100 mM or 10 mM respectively, the *ΔpdeH* mutant exhibited significantly reduced growth ($p < 0.05$) (Fig. 5.18). As previously described (5.2.2), the *ΔpdeL* mutant strain showed significantly reduced colony diameter and hyphal growth-rate per day compared to the wild-type strain on all media tested except in the presence of galactose (Gal) (Fig. 5.18). However, nutrient-limiting conditions reduce this effect. Both mutant strains showed significantly reduced growth on medium containing xylan (Xyl) as the sole carbon source ($p < 0.05$). The presence of the tested nutrients or specific carbon sources had no effect on the growth of the *ΔpdeH* or *ΔpdeL* mutant strains in comparison to the wild-type strain. These results suggest that PdeH has no obvious function in culture, while PdeL plays an important role in hyphal growth, independent of the available nutrient source. Colony density and aerial hyphae formation is dependent on hyphal branching frequency, a nutrient-dependent morphological differentiation, which leads to less dense colonies on nutrient-poor media. Despite, branching frequency was not analysed on nutrient-rich medium, the hyphal growth-rate and therefore colony size of the *ΔpdeL* mutant strains remains reduced compared to the wild-type strain. However, the reduced growth of the *ΔpdeL* mutant strains appeared less severe on nutrient-poor medium than observed on nutrient-rich medium, suggesting a potential alteration in hyphal branching under these conditions.

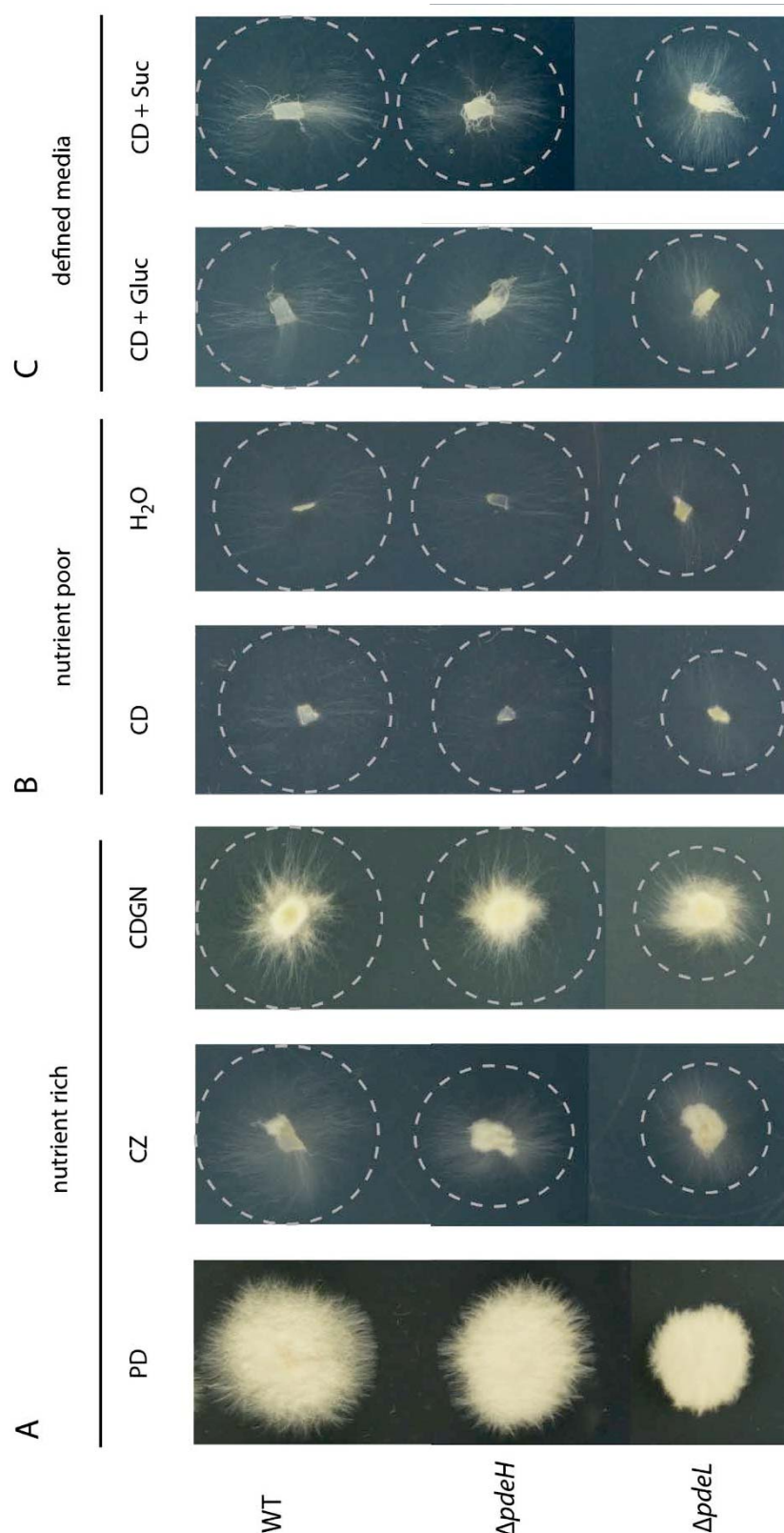


Figure 5-17 Colony morphology of the PDE mutant strains in response to nutrient limitation: *E. festucae* hyphal growth and colony morphology in axenic culture of the wild-type (WT), $\Delta pdeH$ and $\Delta pdeL$ mutant strains on nutrient rich and nutrient poor medium after 7 days at 22°C. Fungal growth on (A) nutrient rich media, PD agar, Czapek-Dox (CZ) and defined media containing CD salts (CD) supplemented with glucose and $(NH_4)_2SO_4$ (CDGN), (B) on nutrient poor medium, 3% water (H₂O) agar and defined medium containing CD salts (CD) for nutrient starvation conditions and (C) on defined medium containing CD salts and 100 mM glucose (CD + Gluc) or 100 mM sucrose (CD + Suc). Dashed circle indicates colony edge.

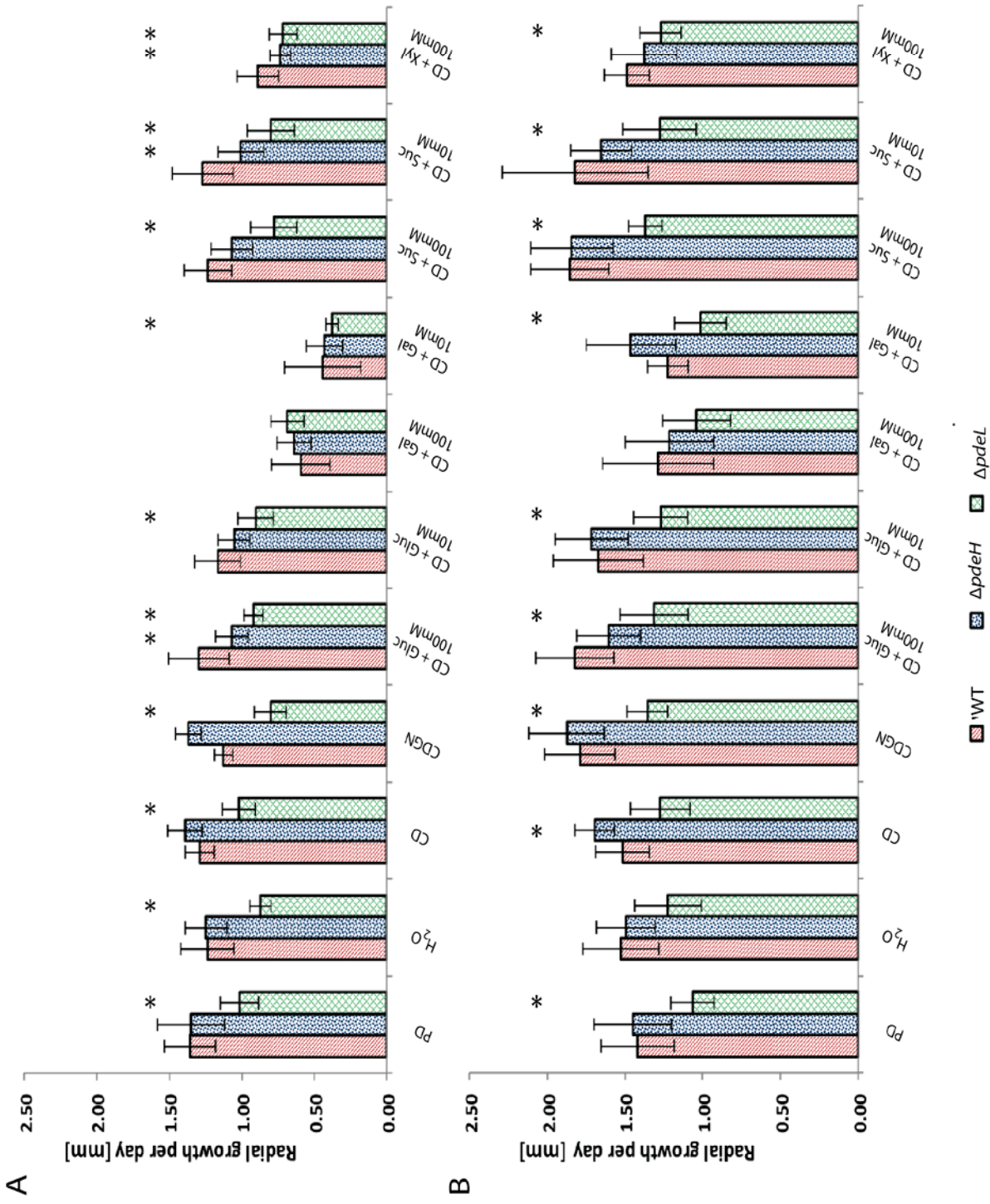


Figure 5-18 Variation in hyphal growth rate of the PDE mutant strains in response to nutrient starvation and to growth on various carbon sources: *E. festucae* colony growth in axenic culture of the wild-type (WT), $\Delta pdeH$ and $\Delta pdeL$ mutant strains in response to nutrient starvation or to various carbon sources, (A) following a non-transfer experiment and (B) a transfer experiment. Radial growth on nutrient rich media (PD and CDGN), nutrient poor media (H₂O and CD) and on defined media containing CD salts, supplemented with the particular carbon sources in two concentrations, 100 mM and 10 mM, was measured after 7 days at 22°C and hyphal growth-rate per day was determined. Data are represented as Mean \pm SD. Significant differences in hyphal growth rate between the WT and the respective mutant strain, $\Delta pdeH$ and $\Delta pdeL$ on each growth medium are denoted * $p < 0.05$ (Student's t test; n = 4 non-transfer experiment, n = 5 transfer experiment). Media contained 1.5% agar. PD = Potato Dextrose, CD = Czapek Dox salts media, CDGN = CD + 100 mM glucose + 10 mM (NH₄)₂SO₄, CD salts supplemented with individual carbon sources: Glu = glucose, Suc = sucrose, Gal = galactose, Xyl = xylan.

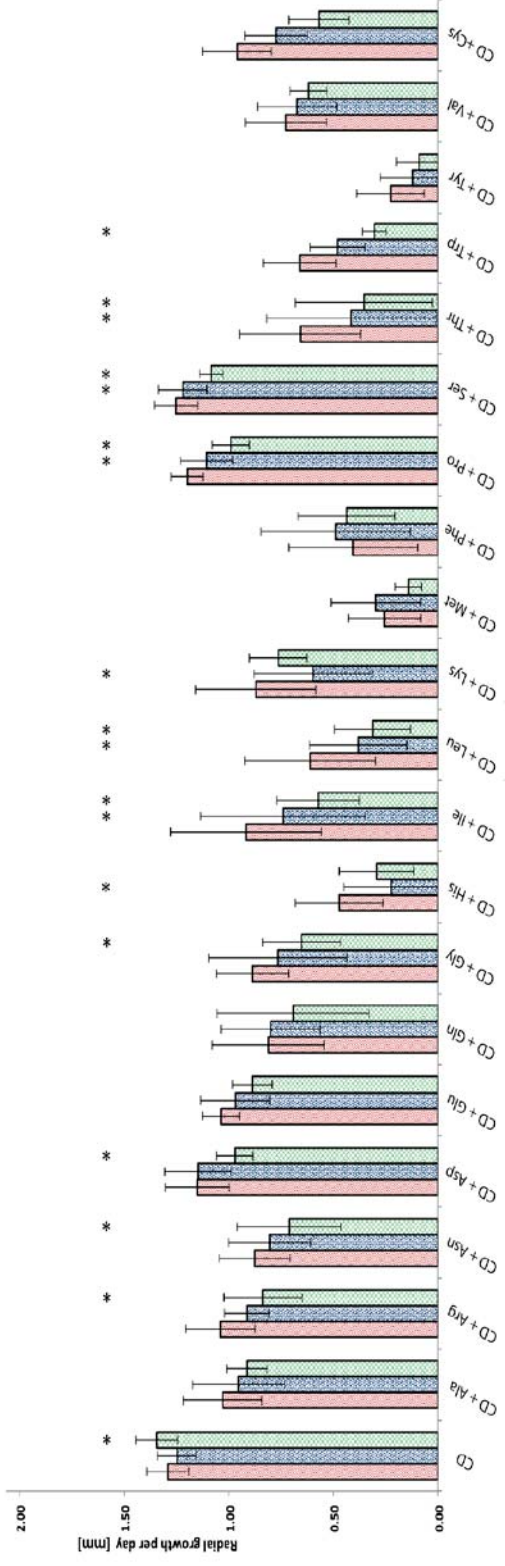
5.3.2 Hyphal growth is negatively affected by the presence of various amino acids when PdeH or PdeL are absent

The cAMP/PKA signalling pathway is associated with amino acid sensing and to investigate if PdeH or PdeL are involved in modulating intracellular cAMP levels after triggered signal transduction, hyphal growth in presence of individual amino acids was analysed as preliminary indicator. With the exception of the already described reduced growth of the $\Delta pdeL$ mutant strain (Fig. 5.19), no noticeable difference in colony morphology was observed when the $\Delta pdeH$ and $\Delta pdeL$ mutant strain were compared to the wild-type strain (Fig. 5.19). However, the hyphal growth-rate of the $\Delta pdeH$ mutant strain was significantly reduced compared to the wild-type ($p < 0.05$), when grown in the presence of isoleucine (Ile), leucine (Leu), proline (Pro), serine (Ser) and threonine (Thr) at a concentration of 10 mM or arginine (Arg), asparagine (Asn), glutamine (Gln), glycine (Gly), histidine (His), lysine (Lys), tryptophan (Trp), valine (Val) at a concentration of 1 mM (Fig. 5.19 A). When transferred onto these media a significant growth reduction was observed in the presence of histidine at a concentration of 10 mM and tryptophan (Trp) at a concentration of 1 mM and 10 mM (Fig. 5.19 B). The presence of alanine (Ala) at a concentration of 1 mM or glutamic acid (Glu), glutamine (Gln), methionine (Met), phenylalanine (Phe) at a concentration of 1 mM and 10 mM appeared to have a growth promoting effect for the $\Delta pdeL$ mutant strain (Fig. 5.19 A). This was also evident when colonies of the $\Delta pdeL$ mutant were transferred onto media containing

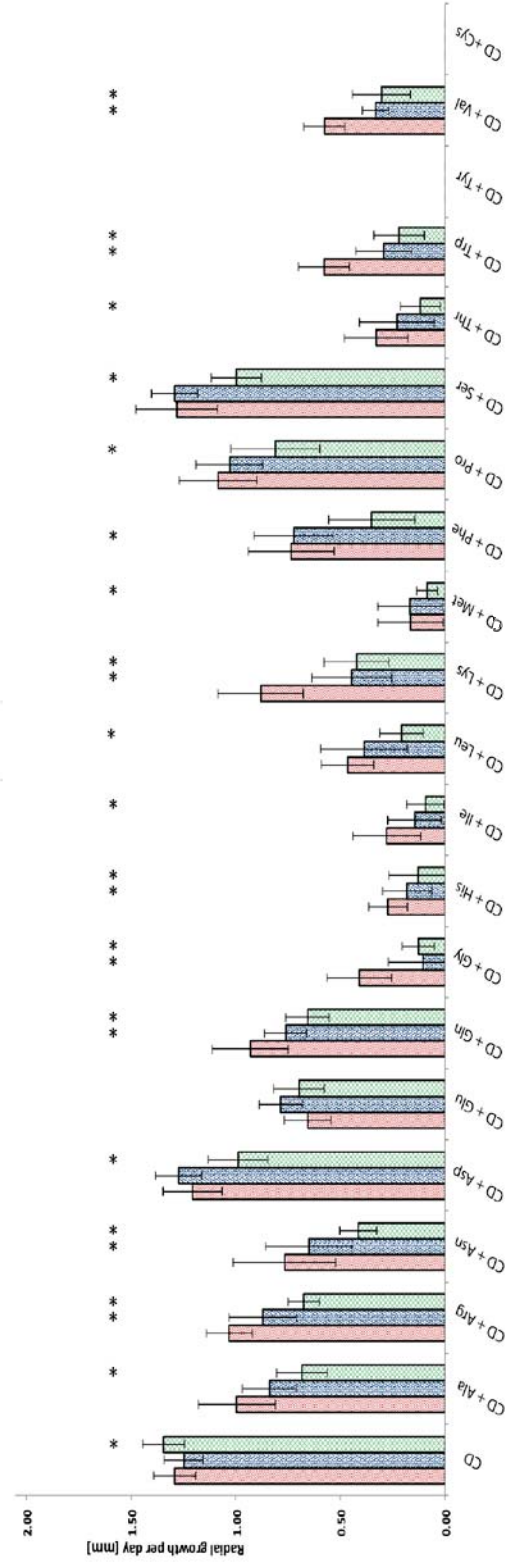
alanine, phenylalanine, lysine or valine (Fig. 5.19 B). For unknown reasons, the $\Delta pdeL$ mutant strain grew comparable to the wild-type strain on the control media containing CD salts in this particular experiment (Fig. 5.19 A). However, this was not the case when transferred onto this medium (Fig. 5.19 B).

Figure 5-19 Variation in hyphal growth-rate of the PDE mutant strains in response to amino acids: *E. festucae* colony growth in axenic culture of the wild-type (WT), $\Delta pdeH$ and $\Delta pdeL$ mutant strains, in the presence of individual amino acids (AA), (A) following a non-transfer experiment and (B) a transfer experiment. Radial growth on defined media containing CD salts (CD), supplemented with the respective amino acid in two concentrations (i) 1 mM and (ii) 10 mM¹, was measured after 7 days at 22°C on respective medium and hyphal growth-rate per day was determined. Data are represented as the Mean \pm SD. Significant differences in hyphal growth rate between the WT and the respective mutant strain, $\Delta pdeH$ and $\Delta pdeL$ on each growth medium are denoted * $p < 0.05$ (*Student's t test*; n = 4 non-transfer experiment, n = 5 transfer experiment). ¹Note: strains on cysteine and tyrosine showed no growth and were therefore excluded from the graph. AA: Ala = alanine, Arg = arginine, Asn = asparagine, Asp = aspartic acid, Glu = glutamic acid, Gln = glutamine, Gly = glycine, His = histidine, Ile = isoleucine, Leu = leucine, Lys = lysine, Met = methionine, Phe = phenylalanine, Pro = proline, Ser = serine, Thr = threonine, Trp = tryptophan, Tyr = tyrosine, Val = valine, Cys = cysteine.

WT
 $\Delta pdeH$
 $\Delta pdeL$

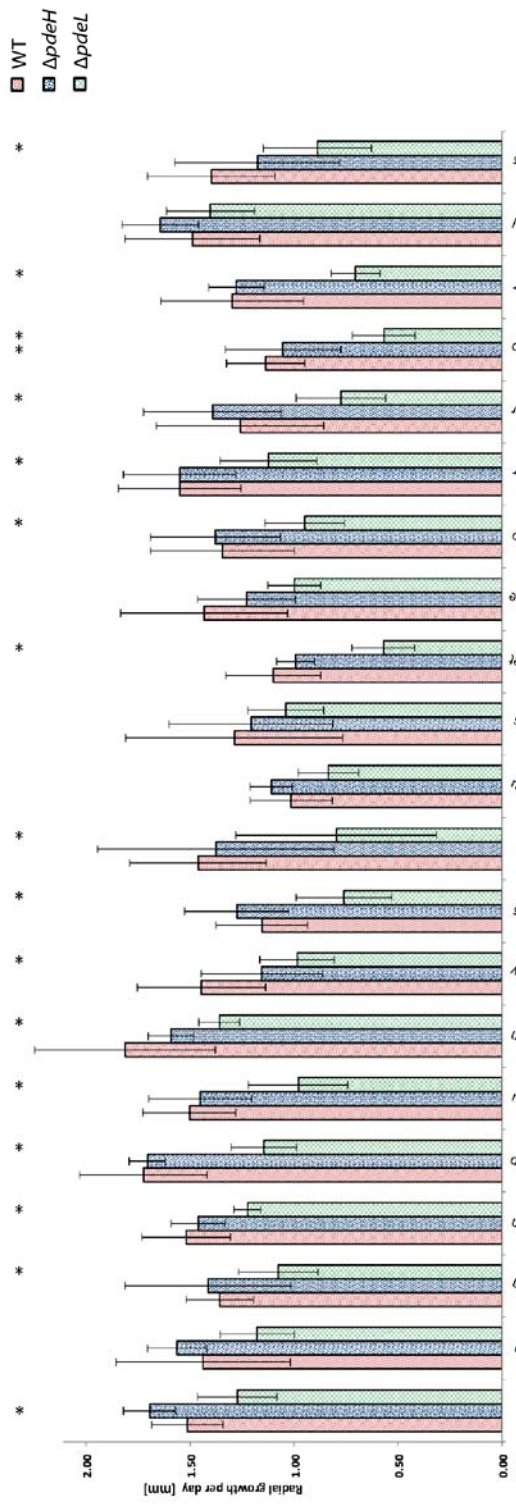


A i

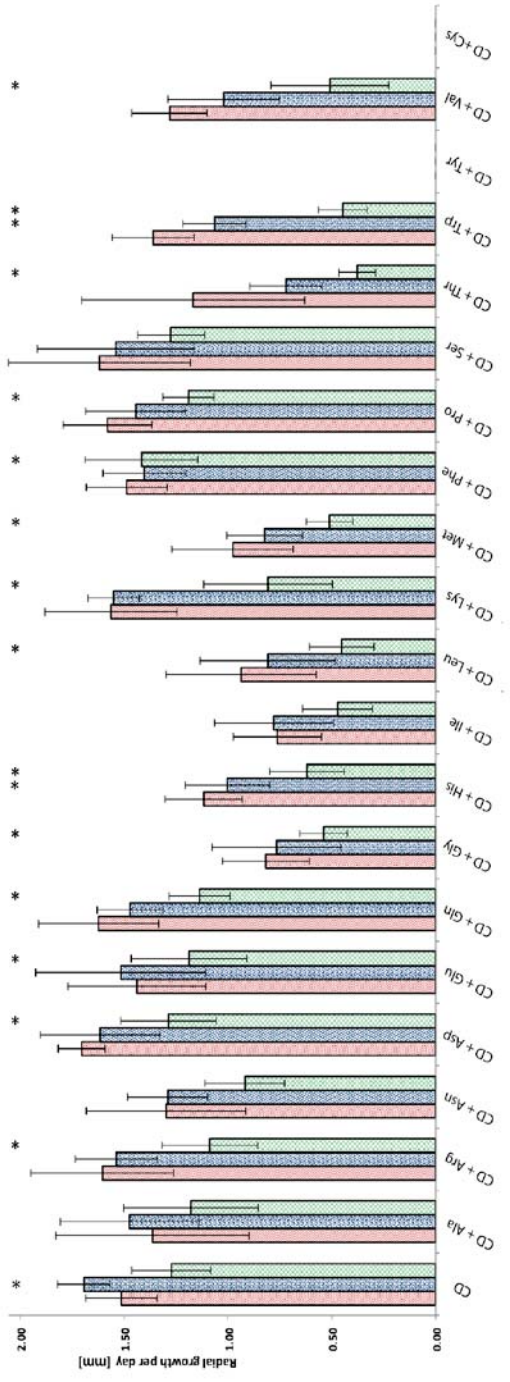


ii

B i



ii



5.3.3 Cell-wall stress and oxidative stress masks the hyphal growth defect of the $\Delta pdeL$ mutant strain in culture

To test whether the loss of the cAMP-phosphodiesterases PdeH or PdeL affected the ability of the fungus to cope with environmental stress, the *E. festucae* wild-type strain and the $\Delta pdeH$ and $\Delta pdeL$ mutant strains were treated with various stress agents (2.4.3). High temperature stress conditions (30°C), osmotic stress (NaCl, KCl, sorbitol) or acidic and alkaline environment (pH) had a similar effect on the colony morphology and hyphal growth of the two mutant strains as on the wild-type strain (Fig. 5.20). The hyphal growth of the $\Delta pdeL$ mutant strain remained reduced compared that of the wild-type. Aside from the characteristic reduced growth of the $\Delta pdeL$ mutant strain, colonies of the $\Delta pdeH$ and $\Delta pdeL$ mutant strain displayed a similar growth response to cell-wall stress or oxidative stress conditions as the wild-type strain (Fig. 5.20). Treatment with the cell-wall stress agents sodium dodecyl sulfate (SDS), Calcofluor white (CFW), Congo red (CR) or caffeine (caff) had no differing effects between the wild-type strain, $\Delta pdeH$ mutant and interestingly the $\Delta pdeL$ mutant strain. A similar effect was observed when these colonies grew on PD medium containing 40µM menadione or 7 mM hydrogen peroxide (H₂O₂). No noticeable difference between the wild-type strain and the $\Delta pdeH$ or $\Delta pdeL$ mutant strain was observed when colonies were treated with 3,3'-diaminobenzidine (DAB), indicating no alteration in the production of reactive oxygen species (ROS) (Fig. 5.20 C). It is hypothesised that the severe effect of cell-wall stress and oxidative stress on colony growth seems to mask or overcomes the reduced hyphal growth phenotype of the $\Delta pdeL$ mutant strain. However, no specific role for PdeH or PdeL in the cellular stress response was identified.

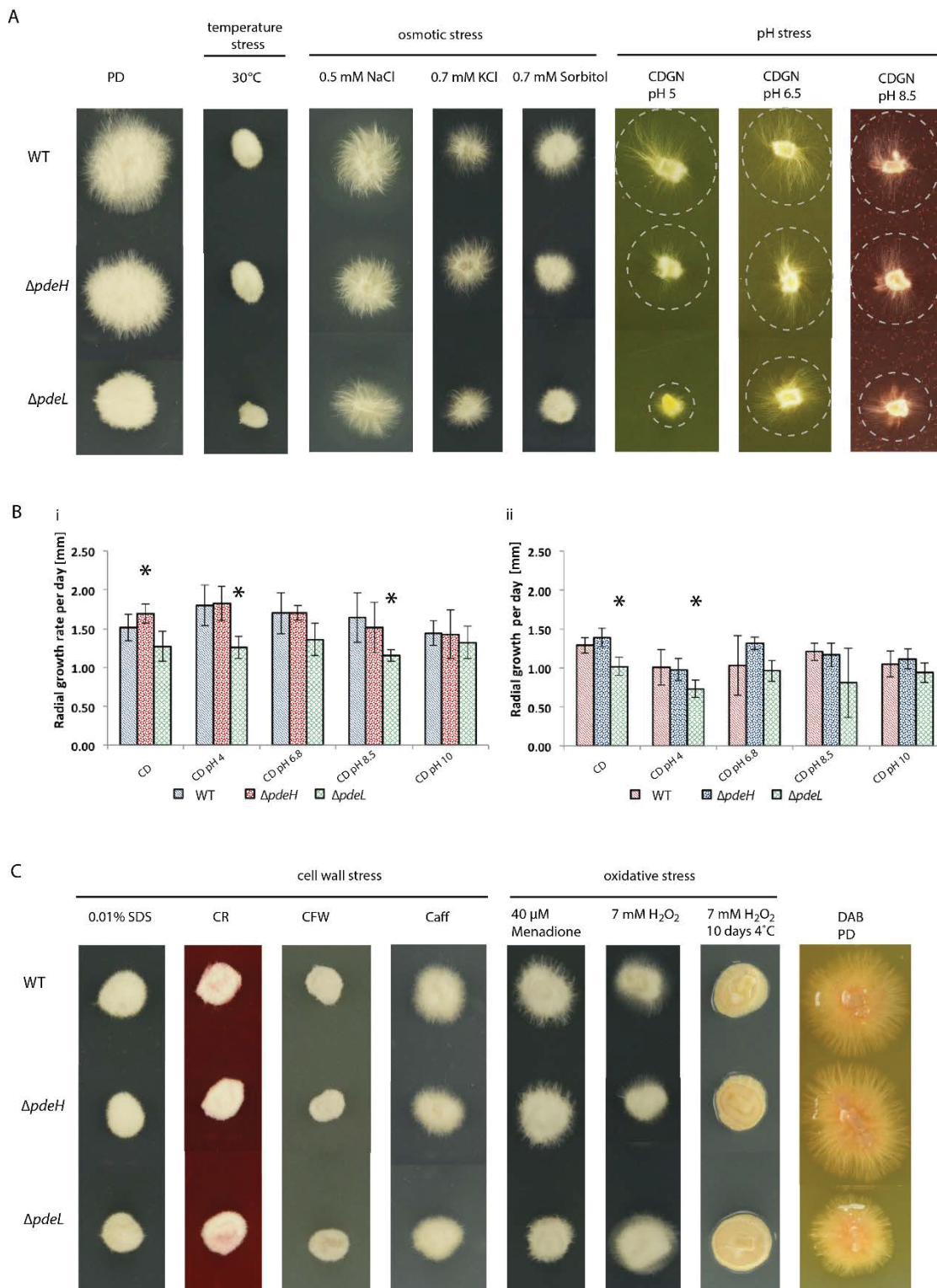


Figure 5-20 Variation in colony growth of the PDE mutant strains under various stress conditions: *E. festucae* colony growth in axenic culture of the wild-type (WT), $\Delta pdeH$ and $\Delta pdeL$ mutant strains in response to extracellular stimuli after 7 days at 22°C. (A) Fungal growth on PD agar. The fungal colonies were tested for sensitivity to temperature stress on PD agar incubated at 30°C and osmotic stress on PD agar containing 0.5 M NaCl, 0.7 M KCl and 0.7 M Sorbitol. Fungal colonies were tested for sensitivity to acidic and alkaline environment using defined medium containing CD salts supplemented with 100 mM glucose and 10 mM (NH₄)₂SO₄ (CDGN) adjusted to pH 5, 6.5 and 8.5 (buffered with 30 mM K₂HPO₄ and 30 mM KH₂PO₄) and (B) using CD media adjusted to pH (pH 4,

pH 6.8, pH 8.5 and pH 10; medium with adjusted pH 10 changed to pH 8 after 7 days incubation). Radial growth in response to changing pH was measured after 7 days at 22°C and the hyphal growth-rate per day was determined, following a (i) non-transfer and a (ii) transfer experiment. Significant differences in hyphal growth rate between the WT and the respective mutant strain, $\Delta pdeH$ and $\Delta pdeL$ on each growth medium are denoted * $p < 0.05$ (*Student's t test*; $n = 4$ non-transfer experiment, $n = 5$ transfer experiment). Data represented as Mean \pm SD (C) Fungal colonies were tested for sensitivity to cell wall stress (0.01% sodium dodecyl sulphate (SDS), 25 $\mu\text{g/ml}$ Congo red (CR), 100 $\mu\text{g/ml}$ Calcofluor white (CFW), 3 mM caffeine (caff)) and to oxidative stress (40 μM menadione, 7 mM hydrogen peroxide (H_2O_2)) on PD media containing the respective agent. Culture phenotype for $\Delta pdeH$ and $\Delta pdeL$ mutant strains on 7 mM H_2O_2 was more pronounced after additional storage at 4°C for 10 days. Fungal colonies were treated with 3,3'-Diaminobenzidine (DAB) to test fungal production of hydrogen peroxide.

5.3.4 Plant derived molecules have no obvious effect on the hyphal growth for the mutant strains, $\Delta pdeH$ and $\Delta pdeL$, in axenic culture

In order to mimic the *in planta* environment and to investigate if plant derived molecules activate the cAMP signalling pathway, regulated by PdeH or PdeL, hyphal growth and morphology in the presence of plant extracts were analysed in axenic culture. Fungal colonies were grown on defined medium containing CD salts and apoplastic fluid (APF) (2.7.7) or linoleic acid (LA). In the presence of APF, the colony morphology and hyphal growth of the $\Delta pdeH$ mutant strain and the wild-type strain were indistinguishable, whereas the $\Delta pdeL$ mutant strain grew with its characteristic reduced growth compared to the wild-type strain (Fig. 5.21 A). Colonies of the wild-type strain and the two mutant strains grew with a reduced hyphal growth-rate on defined media containing CD salts and ethanol, which was further inhibited by the addition of linoleic acid (LA) (Fig. 5.21 B and C). In the presence of low concentrations of LA, the $\Delta pdeH$ mutant strain exhibited a significant reduction in hyphal growth compared to the wild-type strain and compared to its growth on the CD control medium ($p < 0.05$) (Fig. 5.21 B).

These results demonstrate that the presence of apoplastic fluid has no growth promoting or inhibitory effect on the hyphal growth of the wild-type or the $\Delta pdeH$ and $\Delta pdeL$ mutants. Linoleic acid on the other hand inhibited hyphal growth, especially for the $\Delta pdeH$ mutant strain.

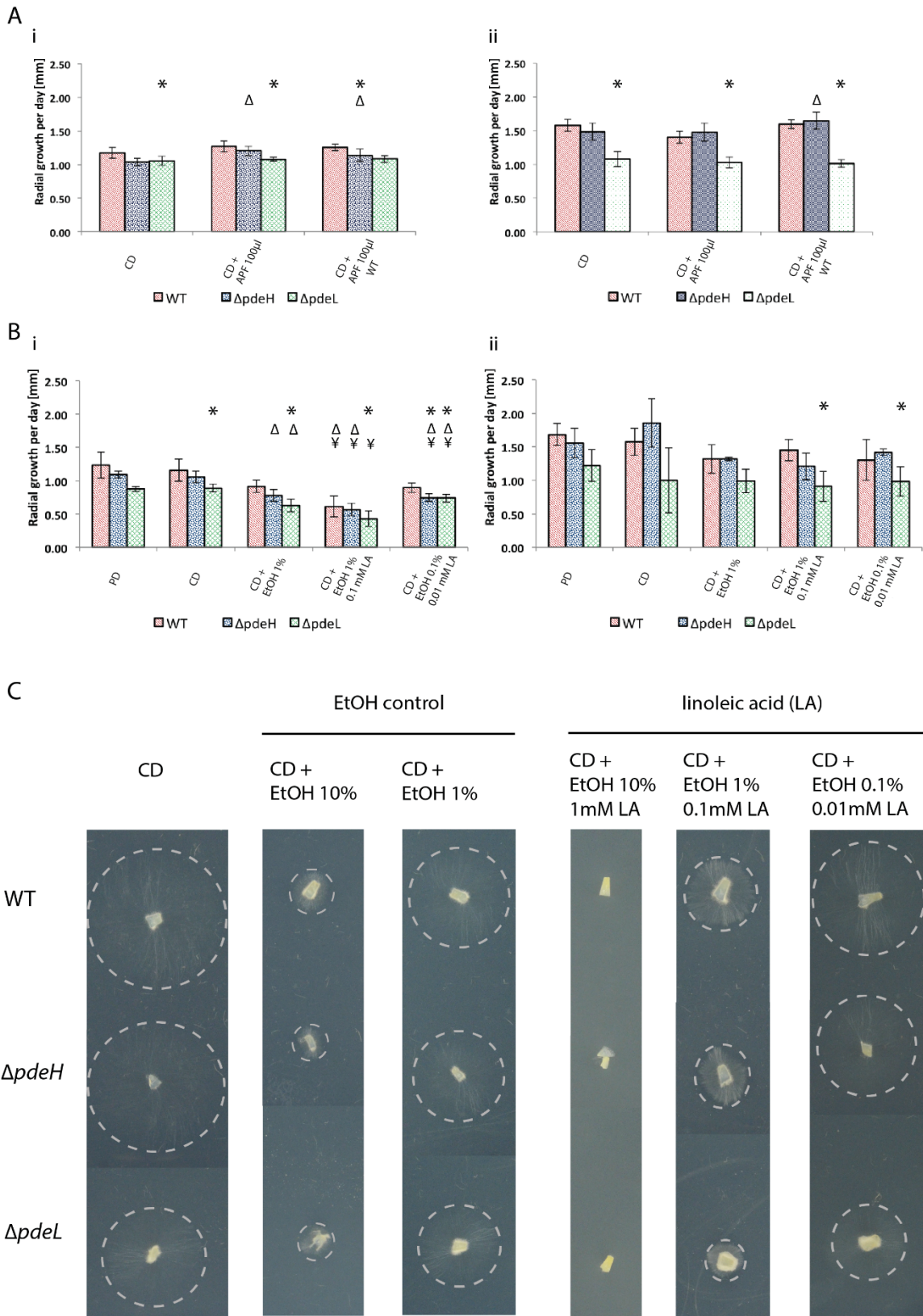


Figure 5-21 Variation in hyphal growth rate of the PDE mutants in response to plant extracts: *E. festucae* growth in axenic culture of the wild-type (WT), $\Delta pdeH$ and $\Delta pdeL$ mutant strains in response to (A) plant derived apoplastic fluid (APF) and (B) the oxylipin-precursor linoleic acid (LA) in axenic culture. Radial growth was measured after 7 days at 22°C on respective medium and hyphal growth-rate per day was determined (A + B), following a (i) non-transfer and a (ii) transfer experiment. Growth was compared to that on defined media containing CD salts (CD) for 7 days at 22°C. (A) Hyphal growth rate per day was determined on defined media containing CD salts supplemented with APF, extracted from uninfected (APF) or wild-type infected (APF WT) *Lolium perenne* plants. (B) Hyphal growth rate per day was determined on defined media containing CD salts supplemented with LA, solubilised in ethanol (EtOH). Hyphal growth was compared to growth on defined media containing CD salts (CD) and CD salt media containing ethanol (EtOH). Data (A + B) are represented as the Mean \pm SD, Significant differences in hyphal growth rate between the WT and the respective mutant strain, $\Delta gpr1b$ and $\Delta gpr2$ on each growth medium are denoted * $p < 0.05$ (*Student's t test*); Δ = significant growth difference ($p < 0.05$) of particular strain compared to growth of respective strain on CD control media (*Student's t test*); • = significant growth difference ($p < 0.05$) of particular strain compared to growth of respective strain on CD + 1% EtOH control media (*Student's t tes*). $n = 4$ non-transfer experiment, $n = 5$ transfer experiment (C) Fungal colonies grown on defined media containing CD salts (control media) and CD media containing 10% EtOH, 1 % EtOH, 10% EtOH/1 mM LA, 1% EtOH/0.1 mM LA and 0.1% EtOH/0.01 mM LA for 7 days at 22°C. Circle (grey dashed line) indicates colony edge.

5.3.5 Chemical alteration of activity for key-enzymes of the cAMP signalling pathway in the PDE mutants

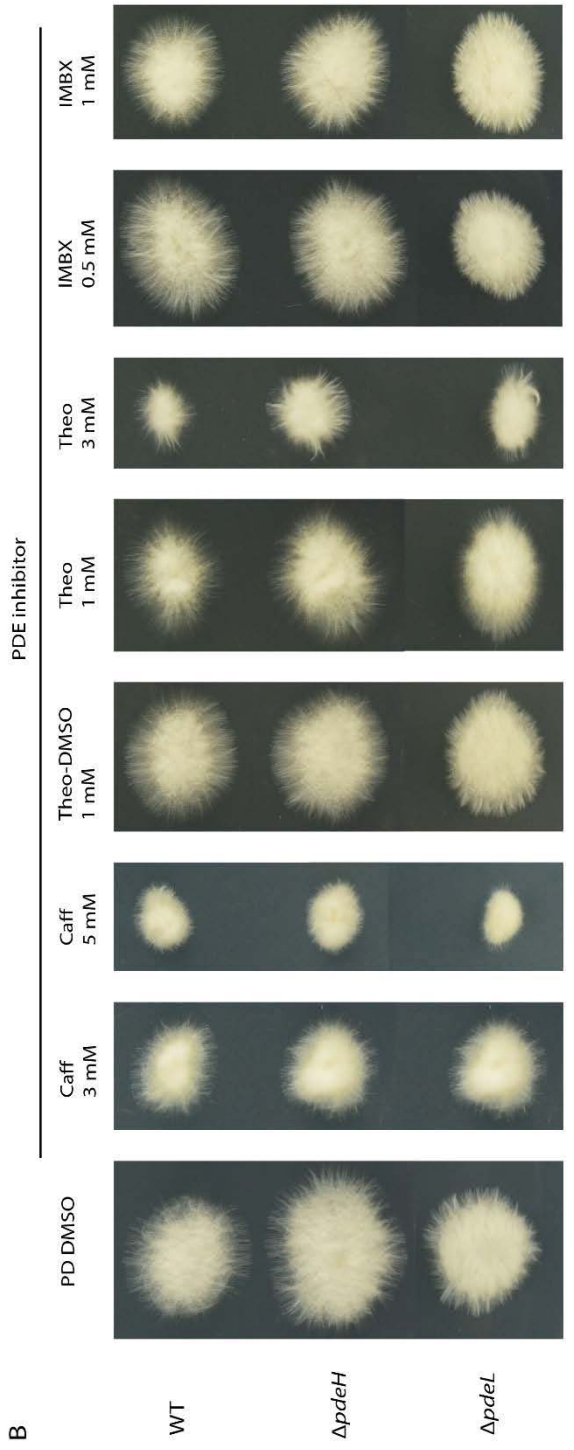
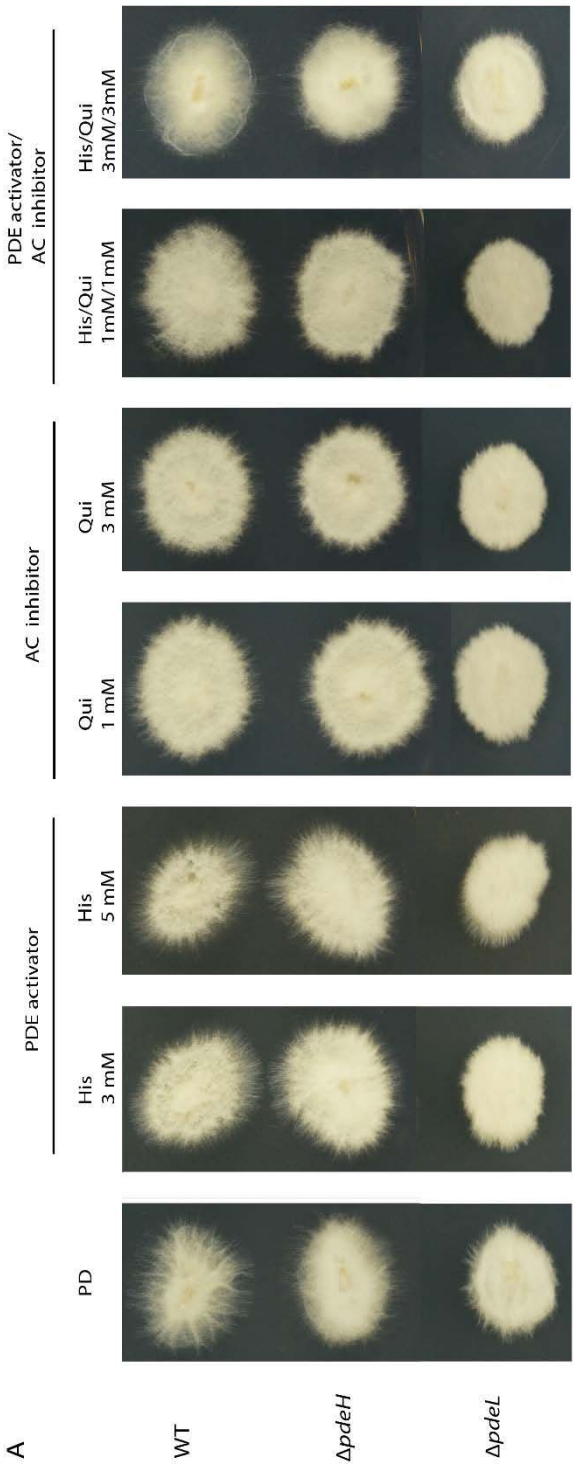
To analyse whether an alteration of cAMP synthesis and hydrolysis has an effect on hyphal growth and colony morphology in the $\Delta pdeH$ and $\Delta pdeL$ mutant strains, the fungal colonies were treated with a variety of chemicals. Addition of apoplastic fluid (2.7.7) was also examined to see if hyphal growth in culture changed in the presence of these activators and inhibitors. Further, the enzyme activity of the phosphodiesterases was inhibited using unspecific PDE inhibitors in the wild-type strain and the $\Delta pdeH$ and $\Delta pdeL$ mutant background which potentially mimics a PDE double deletion in the latter (Scott and Solomon 1975).

No difference in growth of the $\Delta pdeH$ and $\Delta pdeL$ mutant strains compared to the wild-type strain was observed when grown on PD medium containing histamine or quinine, chemicals known to activate the cAMP signalling pathway and so the phosphodiesterases activity or inhibit the adenylate cyclase activity, respectively (Fig.5.22 A)(Scott and Solomon 1975). The addition of histamine and quinine in equal amounts showed no further effect (Fig. 5.22 A). No difference was observed when the colonies of the wild-type and the two mutant strains were treated with

methylated xanthines, such as caffeine (caff), theobromine (theo) or 3-isobutyl-1-methylxanthine (IMBX), chemicals known to inhibit the phosphodiesterase activity (Fig. 5.22 B). At higher concentrations, colony growth and morphology of the wild-type and the $\Delta pdeL$ mutant strain were similar. No different effect on hyphal growth and colony morphology of all strains was observed when apoplastic fluid was added to the PD medium containing histamine, quinine, caffeine or IMBX at higher concentrations.

These results suggest that the regulation of cAMP is important for hyphal growth and PdeL likely plays a role in regulating the balance of cAMP levels in the cell.

Figure 5-22 Effect of inhibition/activation of key enzymes in the cAMP signalling pathway on growth of wild-type and GPCR mutants: *E. festucae* colony growth of the wild-type (WT) and $\Delta pdeH$ and $\Delta pdeL$ mutant strains in response to chemical inhibition of adenylate cyclase (AC) activity using quinine and activation or inhibition of phosphodiesterase (PDE) activity by treatment with histamine or methylated xanthines respectively. Fungal growth was analysed after a total of 7 days post-incubation at 22°C. (A) Colony growth on PD agar and PD agar containing histamine (His; 3 mM, 5 mM), quinine (Qui; 1 mM, 3 mM) or both (His/Qui; 1 mM/1 mM, 3 mM/3 mM). (B) Colony growth on PD agar containing DMSO (control) and PD agar containing caffeine (caff; 3 mM, 5 mM), theobromine solubilised in DMSO (Theo-DMSO 1 mM), theobromine (Theo; 1 mM, 3 mM) and Iso-butyl-methylxanthine (IMBX; 0.5 mM, 1 mM).



5.3.6 Nutrient-dependent increase of intracellular cAMP levels in culture is regulated mainly by the low affinity phosphodiesterase in culture

Cyclic AMP mediates extracellular signals depending on the intracellular concentration, regulated by its synthesis and hydrolysis. Phosphodiesterases terminate the cAMP-dependent signalling cascade by hydrolysing cAMP. To examine whether PdeH and PdeL are involved in the nutrient-triggered signal transduction, the levels of cAMP in the wild-type and the $\Delta pdeH$ and $\Delta pdeL$ mutant strains were measured on nutrient-rich (PD) and nutrient-poor (H₂O) media. Following transfer experimental conditions, colonies were first grown on PD medium for 4 days and then transferred to either a fresh PD medium or H₂O medium and grown for further 3 days before measurement. The $\Delta pdeL$ mutant strain showed significant elevation of the intracellular cAMP-concentration compared to the wild-type when grown on PD medium, whereas the $\Delta pdeH$ mutant showed lower or similar levels of cAMP compared to the wild-type strain under these conditions (Fig. 5.23). When transferred onto H₂O medium, a decreased level of cAMP for the wild-type strain and the $\Delta pdeH$ and $\Delta pdeL$ mutant strains was measured. However, in the two mutant strains compared to the wild-type higher levels of intracellular cAMP-concentration were detected, especially in the $\Delta pdeL$ mutant strain (Fig. 5.23). This indicates that PdeL modulates cAMP levels after nutrient-depending induction of the cAMP/PKA signalling pathway, whereas PdeH appears dispensable under these conditions. However, the reduced intracellular cAMP level in the $\Delta pdeL$ mutant strain after transfer onto H₂O medium indicates that cAMP hydrolysis takes place in reduced quantity, despite of the lack of PdeL. Because cAMP hydrolysis is not completely abolished, an additional enzyme partially complements hydrolysis-functions in the absence of PdeL, most likely PdeH. Functional complementation for PDEs is described in many fungi (Hicks et al., 2005, Ramanujam and Naqvi 2010, Zhang et al., 2011, Harren et al., 2013). Unfortunately, the attempted generation of the *E. festucae* $\Delta pdeH\Delta pdeL$ double-mutant strain that could demonstrate the potential complete abolished cAMP hydrolysis was unsuccessful and therefore not included in the analysis. The quantification of the intracellular cAMP levels in later

experiments was unreliable and additional tests, including *pdeL* complementation strains (*pdeLC-22*, *pdeLC-23*), under the above conditions were not analysed. It is noteworthy, that the $\Delta pdeH$ mutant strain showed similar levels of cAMP compared to the wild-type strain when transferred onto nutrient-rich medium and nutrient-limiting medium in later experiments. However, these later experiments showed unreliable results in the generated standard curve and therefore was not used in the data interpretation. The unsuccessful assay validation also prevented the final determination of cAMP per sample (pmol cAMP per mg of total protein), because the total protein concentration from which the sample concentration is determined, was above the detectable limit of the assay. Due to financial restrictions no further conditions and strains, or alternative cAMP quantification kits were tested.

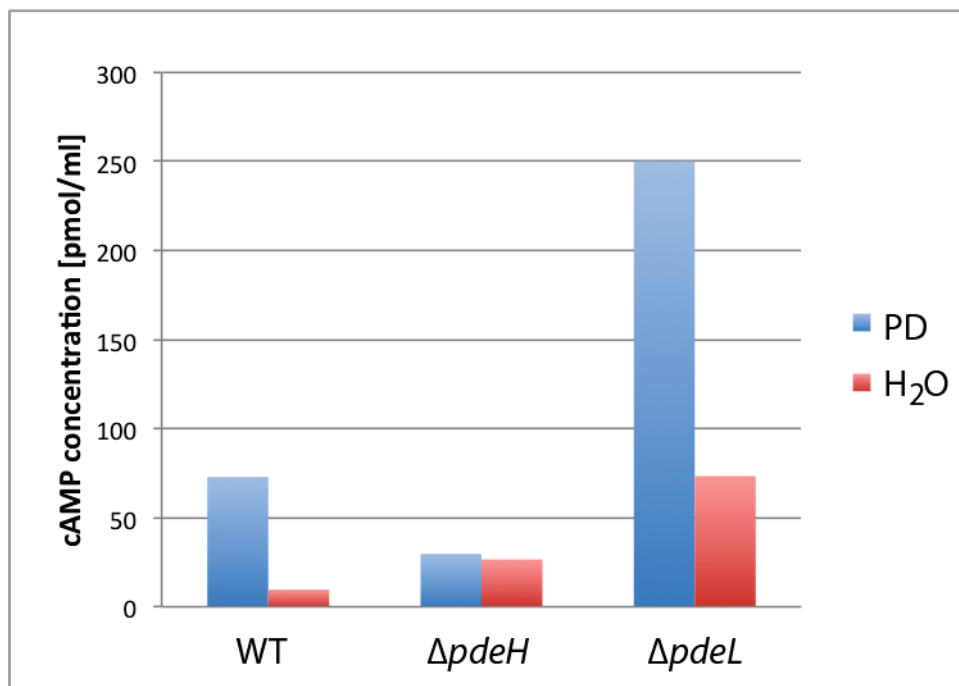


Figure 5-23 Quantification of intracellular cAMP concentration in $\Delta pdeH$ and $\Delta pdeL$ mutants under nutrient limitation: Quantification of intracellular cAMP levels in *E. festucae* colonies, grown on nutrient rich (PD) medium or transferred onto nutrient poor (H₂O) medium using the direct cyclic AMP ELISA kit under non-acetylated conditions (Enzo Life sciences).

**Chapter 6 Summary discussion and
conclusions with recommendations for
future work**

6.1 Fungal GPCRs and the role of cAMP receptor-like GPCRs in the mutualistic *E. festucae* – *L. perenne* association

The ability of organisms to live in and adapt to their environment is dependent on their capability to communicate with it, to sense their exterior and to be able to respond to changes (Xue et al. 2008). Filamentous fungi rely primarily on G protein-coupled receptors (GPCRs), which transmit extracellular signals predominantly via heterotrimeric G proteins to downstream pathways such as the cAMP/Protein Kinase A (PKA) signalling pathway (Li et al. 2007, Xue et al. 2008). Perception of environmental signals by GPCRs and transduction of the signal via G proteins has been shown in many species to be essential for vegetative growth, various developmental processes, primary and secondary cellular processes and survival under any conditions (Lafon et al. 2006, Gruber et al., 2013, Brunner et al., 2008, Cabrera et al., 2015).

GPCRs represent the largest group of cell-surface receptors in eukaryotic cells, and are responsible for sensing a wide range of extracellular signals, such as photons (light), pheromones, nutrients, amino acids, hormones, odours and specific molecules, that are crucial for survival (Oldham and Hamm 2006, Xue et al. 2008). In fungi, GPCRs are involved in various essential cellular processes like hyphal growth, mating, sexual and asexual development, morphogenesis, pathogenicity, secondary metabolite production and intra- and inter-species communication (Cottier 2011, Gruber et al., 2013). Functionally, GPCRs are a highly diverse protein family, even though they share a common seven-transmembrane spanning α -helix domain structure. Due to structural, topological and sequence differences with mammalian GPCRs fungal GPCRs have been categorized using a separate classification system, which has been recently revised. Better accessibility to genome sequence and transcriptomic data, with improved bioinformatics protein prediction tools and genome wide *in silico* analysis in a variety of different fungal species including *N. crassa*, *Aspergillus* spp.; *M. oryzae*, *Trichoderma* spp., *Verticillium* spp., *B. cinerea*, *Sclerotinia sclerotiorum*, *Cryptococcus neoformans*, has led to the identification of a large number of putative GPCRs (DeZwaan et al. 1999, Kulkarni et al. 2005, Lafon et al. 2006, Li et al. 2007, Brunner et al. 2008, Zheng et al. 2010, Amselem et al. 2011, Brakhage 2013, Gruber et al. 2013, Affeldt et al. 2014, Cabrera

et al. 2015). Despite the common structural feature of the seven-transmembrane domain-containing proteins, these studies revealed a high diversity among fungal GPCRs and a separation into 14 classes (Oldham and Hamm 2006, Gruber et al. 2013, Cabrera et al. 2015). Up to 40 putative GPCRs were identified in the genome of the endophyte *Epichloe festucae* strain Fl1, using a protein sequence homology based approach (Blast) with the recently predicted and partially characterised GPCRs, analysed in *N. crassa*, *M. oryzae* and *Trichoderma* spp. (Kulkarni et al. 2005, Gruber et al. 2013, Cabrera et al. 2015). The putative GPCRs in the genome of *E. festucae* fall into 13 of the proposed 14 classes (Gruber et al. 2013). A high conservation in number and structure of GPCRs within individual classes was described, with some classes containing one to two GPCRs (e.g. pheromone, carbon-source or microbial opsins), while other classes comprise a greater variety (e.g. cAMP receptor-like, PARQ, PTH11-like proteins) among all fungal species (Gruber et al. 2013). A high diversity of GPCRs, suggests a role in species-specific functions in adaptation to a particular life style or a biological niche (reviewed in Zeilinger et al. 2015, Steindorff et al. 2015). Variable numbers of cell-surface receptors within or between different classes might indicate specific events based on evolutionary selected gene duplication (reviewed in Steindorff et al. 2015). For example, the filamentous fungal-specific GPCR class of PTH11-like receptors comprise the highest number of GPCRs within any of the individual species, including 20 putative GPCRs in *E. festucae*, while also displaying the highest variety in number among filamentous fungi (Kulkarni et al. 2005, Amselem et al. 2011, Gruber et al. 2013, Affeldt et al. 2014, Cabrera et al. 2015). In the phytopathogen *M. oryzae*, the originally identified GPCR Pth11 fulfills an essential function in specific host surface recognition, initiation of appressoria formation and cellular differentiation leading to invasive growth, and is therefore crucial for interaction with the host (DeZwaan et al. 1999, Kulkarni et al. 2005). The Pth11 receptor acts upstream of the cAMP/PKA signalling pathway, which has been shown to be essential for various developmental and pathogenic processes in multiple fungi.

6.1.1 Phylogenetic diversity of cAMP receptor-like GPCRs

Another important class of GPCRs, displaying high diversity among species within the respective family or between fungal species, are the cAMP-receptor-like GPCRs (class V). The three receptors of this class in *N. crassa* (Gpr-1, Gpr-2, Gpr-3) are well characterised (Krystofova and Borkovich 2006, Cabrera et al. 2015). Using the *N. crassa* protein sequences as query, the three homologues of the cAMP-receptor like GPCRs, Gpr1a, Gpr1b and Gpr2, were identified in the genome of *E. festucae*. Interestingly, *N. crassa* Gpr-1 shows high sequence identity to the *E. festucae* Gpr1a and Gpr1b, indicating a gene duplication event for this ortholog. While a homolog of the *N. crassa* Gpr-2 was identified in *E. festucae* (Gpr2), no homolog of the *N. crassa* Gpr-3 was identified in the *E. festucae* genome. However, *N. crassa* Gpr3 shares high sequence identity to *E. festucae* Gpr2, suggesting a close phylogenetic relationship. The lack of a unique *N. crassa* Gpr3 homolog in other fungi suggests Gpr2 and Gpr3 are the result of a gene duplication event in the *N. crassa* genome, as is evident for Gpr1a and Gpr1b in *E. festucae*. In the cAMP-receptor like GPCRs (class V), multiple gene duplication events have occurred among a variety of fungal species including *N. crassa*, *F. graminearum*, *M. oryzae*, *Trichoderma* spp. and within the *Clavicipitaceae* family (Kulkarni et al. 2005, Gruber et al. 2013, Cabrera et al. 2015). The *Epichloë* endophytes and closely related species including *Metarhizium* spp. (*M. acridum*, *M. robertsii*) and *Claviceps* spp. share considerable variation in the number of homologues within these classes. While the gene duplication of Gpr1a and Gpr1b appears conserved within the *Epichloë* spp., some species contain a second Gpr2 ortholog. A similar event was observed within the *Metharhizium* spp., between *M. acridum* and *M. robertsii*. High diversity among the class V GPCRs also occurs in the genome of the *Claviceps* species, where *C. purpurea*, *C. fusiformis* and *C. paspali* contain one, two or three orthologs, respectively, grouping with their individual homologues in *E. festucae*. In *C. purpurea* only a Gpr2 homolog as member of the class V GPCRs was identified, similar to the distantly related *A. nidulans* GprH, suggesting an ancestral origin for Gpr2. *Trichoderma* spp. possess four class V GPCRs, with the *T. atroviride* Tagpr4, Tagpr3 and Tagpr2 were identified as homologous to the *E. festucae* Gpr1a, Gpr1b and Gpr2, respectively (Brunner et al. 2008, Gruber et al. 2013). A homolog for the Tagpr1 was not identified in the genome of *E. festucae*. Overall, the large variation of orthologs, that share sequence similarity among the members of the same class

within the species and between other fungi, suggest multiple evolutionary gene duplication events in order to adapt to the species-specific lifestyle (reviewed in Semyonov et al. 2008, Vaudry 2014, Steindorff et al. 2015, Galagan et al. 2005, Yun et al. 2015).

6.1.2 Role of class V GPCRs in *E. festucae* and other fungi

In this study, I focused on the identification and characterisation of cAMP receptor-like GPCRs (class V) in the genome of *E. festucae* with the goal of determining the role of cAMP/PKA signalling in maintaining and establishing a mutualistic association with the grass host.

Among the few functionally analysed GPCRs in fungi, the class V GPCRs of *N. crassa* (Gpr-1, Gpr-2, Gpr-3) are among the best-characterised ones. Gene deletion of the respective coding sequence ($\Delta gpr-1$, $\Delta gpr-2$, $\Delta gpr-3$) resulted in defective asexual and sexual development, however none of these mutants showed any strong vegetative growth phenotype (Krystofova and Borkovich 2006, Cabrera et al. 2015). Although, ascospore formation remained unaffected, all three mutant strains exhibited deformed perithecial beak structures that were impaired in proper ascospore discharge (Krystofova and Borkovich 2005, Krystofova and Borkovich 2006, Cabrera et al. 2015). Perithecial beaks are specific phototrophic structures at the tip of perithecia for ejection of mature ascospores via an ostiole (Harris et al. 1975, Harding and Melles 1983). While strains that lack Gpr-2 ($\Delta gpr-2$) or Gpr-3 ($\Delta gpr-3$) show fully developed but deformed beak structures, the $\Delta gpr-1$ mutant strains had impaired ostiole formation, resulting in a defective ejection mechanism, whereby ascospores exit the perithecial beak passively following rupture of this structure (Krystofova and Borkovich 2005, Krystofova and Borkovich 2006, Cabrera et al. 2015). In addition to the sexual development phenotype, the *N. crassa* $\Delta gpr-2$ and $\Delta gpr-3$ mutant strains were defective in proper aerial hyphae formation, conidiophore development and conida production from the tips of the aerial hyphae (Cabrera et al. 2015). Furthermore, localisation studies have shown that the cellular localization of Gpr-1 is predominantly in mature perithecia (Krystofova and Borkovich 2006). Transcriptome profiling in *N. crassa* showed highest expression of Gpr-1 in mature perithecia, while transcriptional abundance of Gpr-2 and Gpr-3 was high in protoperithecial and perithecial structures (Cabrera et al. 2015). These

results confirm the importance of the class V GPCRs Gpr-1, Gpr-2, Gpr-3 in *N. crassa* in proper perithecia development and ascospore release during sexual development.

Similar to their homologues in *N. crassa*, deletion of the genes encoding Gpr1b and Gpr2 in *E. festucae* had no effect on hyphal growth, colony morphology or the ability to adapt to various stresses compared to the wild-type strain. These mutations also had no effect on aerial hyphae formation or asexual development with conidiophore development the same as wild-type. Several attempts to delete the gene encoding Gpr1a by homologous recombination were unsuccessful. PCR-amplification of the 3'-flanking region adjacent to the *gpr1a* open reading frame could have failed because this region is GC rich. Local GC rich regions are known to readily form secondary structures in a single stranded stage, making these sequences difficult to amplify due to polymerase slippage (Mamedov et al. 2008, Strien et al. 2013).

Unlike in *N. crassa*, sexual development in the *Epichloë* endophytes require the association with the host plant and the formation of the pre-sexual "choke" structure on mature host leaves for horizontal transmission, including the developmental switch to reproduction of the plant (Scott and Schardl 1993, Schardl et al. 1997). Then, cellular differentiation occurs in multiple steps that includes endophytic hyphae exit from the plant to form a compact mycelial structure (stromata) around the developing plant inflorescence. For horizontal transmission, spermatia are produced in the stromata which are transferred to stromata of the opposite mating types by symbiotic *Botanophila* flies, that are attracted by fungal volatile organic compounds (Bultman and White 1988, Steinebrunner et al. 2008). The sexually derived ascospores, from fertilized stromata, are horizontally transferred to uninfected hosts, germinate and undergo immediate mycrocycle conidiogenesis to form large numbers of conidia. Conidia then germinate and infect the ovule of the developing plant inflorescence and subsequently the developing embryo of the grass seed (Rodriguez et al. 2009). Once grass seeds germinate the fungal colonisation of the host starts in the meristematic tissue reviewed in (Johnson et al. 2013, Tadych et al. 2014). Sexual species such as *E. festucae* can form choke and enter the sexual cycle on some grass hosts such as *Festuca rubra* but not in association with *Lolium perenne* (Schardl et al. 1997, Inda et al. 2008). *E. festucae* is predominantly transferred by vertical transmission through the seed. Some

Epichloë species such as *E. typhina* readily exhibit full sexual development, and are not vertically transmitted through the grass seeds, unlike *E. festucae* (Siegel et al. 1987, Scott and Schardl 1993, Schardl and Leuchtmann 2005). However, considering the importance of these class V GPCR in proper perithecia formation in *N. crassa*, their role in sexual development in the *Epichloë* endophytes would be of interest either in a compatible *E. festucae*-host association where sexual development occurs, or by analysing the respective Gpr1a, Gpr1b and Gpr2 homologues in a sexual species, such as *E. typhina*. Nonetheless, if the mutants stunt the growth of the host, they will never form stromata and enter full sexual development. Tissue specific transcriptome analysis of the wild-type association, cellular localisation studies with fully restored wild-type phenotypes or fluorescence-based protein-protein interaction studies can be used for functional analysis of these proteins.

The homologous cAMP receptor-like GPCRs in *T. atroviride*, TaGpr4, TaGpr3 and TaGpr2 had no specific function in sexual development (Brunner et al. 2008). However, gene silencing of *Tagpr1*, resulted in a phenotype that exhibit reduced vegetative and aerial hyphal growth, and hyperconidiation, although conidia germination is reduced (Brunner et al. 2008). Therefore, *Tagpr1* plays an important role during vegetative growth and for the regulation of asexual conidiation. High sensitive real-time PCR revealed transcriptional response for *Tagpr4* and *Tagpr3* to exogenous cAMP and changes in nutrient sources, while the latter also showed a decrease in gene expression during surface contact with an artificial membrane as with fungal hyphae during confrontation assays, suggesting for regulation after physical contact (Brunner et al. 2008). In *A. nidulans*, GprH, is involved in controlling the switch between asexual and sexual development and therefore negatively regulates sexual development (Han et al. 2004, Affeldt et al. 2014, Brown et al. 2015). Deletion of *gprH* results in the production of more cleistothecia and reduction of conidiophore development and formation of conidia (Brown et al. 2015). Carbon starvation has been shown to induce sexual development in *Aspergillus* spp. (Lafon et al. 2006, Krohn et al. 2014). Transcriptional profiling revealed that GprH is upregulated in long-term starvation, suggesting this protein has a key role in carbon source sensing, despite not being the main carbon sensor in *A. nidulans* (Krohn et al. 2014, Brown et al. 2015). Intracellular cAMP levels and PKA activity were increased after carbon starvation in the $\Delta gprH$ mutant strain as they

were in the wild-type (Krohn et al. 2014). No growth defect of the $\Delta gprH$ mutant strain compared to the wild-type strain was observed on a variety of carbon and nitrogen sources, although hyphal recovery and conidia germination after carbon starvation was delayed (Brown et al. 2015). This study showed that GprH mediates signals through the cAMP/PKA signalling pathway and functions as an alternative glucose sensor that acts in parallel to the main glucose sensor GprD in *A. nidulans* and *A. flavus* (Han et al. 2004, Affeldt et al. 2012, de Souza et al. 2013, Affeldt et al. 2014, Brown et al. 2015). Taken together, the class V GPCR GprH in *Aspergillus* spp. functions as an important regulator of sexual development and is involved in carbon source sensing in early hyphal recovery and germination after carbon starvation (Brown et al. 2015). These authors further showed that GprH is crucial for sensing the amino acid tryptophan, indicating these GPCRs are also involved in specific amino acid sensing (Xue et al. 2008, Brown et al. 2015). In *A. flavus*, the $\Delta gprH$ mutant strain showed suppressed secondary metabolism and reduced production of aflatoxin, which is also regulated by cAMP/PKA signalling (Affeldt et al. 2014). In the human pathogen *C. neoformans*, the class V GPCR Gpr4 is required for sensing the amino acid methionine, but is involved in carbon sensing (Xue et al. 2006). This methionine-triggered sensing is mediated through the cAMP/PKA signalling pathway resulting in stimulation of morphological differentiation to filamentous growth during mating and sexual development (Schweingruber et al. 1998, Xue et al. 2006). Production of secondary metabolites for capsule formation and melanin production, important virulence factors, is also regulated by cAMP-dependent signalling (Xue et al. 2006).

6.1.3 Role of cAMP receptor-like GPCRs in nutrient and amino acid sensing

Similar to their homologues in *N. crassa* and *A. nidulans*, deletion of the class V GPCR-encoding genes *gpr1b* or *gpr2* in *E. festucae* had no noticeable effect on vegetative growth compared to the wild-type strain. Preliminary growth experiments on nutrient-rich and nutrient-poor medium or in the presence of specific carbon sources or amino acids, did not indicate a role for these receptors in nutrient or amino-acid sensing. Although both mutant strains exhibited intracellular cAMP levels similar to the wild-type on nutrient-rich medium and when transferred

onto nutrient-poor medium. Intracellular cAMP levels were not quantified under conditions with defined carbon sources or individual amino acids. Given that the preliminary growth experiments showed no direct evidence that these GPCRs function in carbon source or amino acid sensing, a key role in nutrient sensing could not be assigned to Gpr1b or Gpr2. However, there are major differences in the fungal transcriptome of axenic culture compared to association with the host plant (Chujo et al., unpublished). Comparative transcriptomic analysis of the wild-type strain, grown in axenic culture and in association with the host plant, revealed that Gpr1b and Gpr2 are among the nine GPCRs significantly upregulated *in planta*, indicating a more specific role in the host environment.

6.1.4 Role in association with the host

Inoculation of ryegrass with the $\Delta gpr1b$ mutant strain caused a severe plant interaction phenotype, similar to that described for a number of other *E. festucae* mutant strains including $\Delta noxA$ and $\Delta noxR$ genes that encode components of the Nox complex (Kayano et al. 2013); $\Delta proA$, a gene encoding a Zn(II)₂Cys₆ transcription factor (Tanaka et al. 2013); Δso , $\Delta mkkA$ and $\Delta mpkA$, genes encoding components of the cell wall integrity (CWI) MAPK pathway (Charlton et al. 2012, Teichert et al. 2014, Becker et al. 2015) or $\Delta mobC$, encoding a component of the STRIPAK complex (Green et al. 2016). These mutant strains shared a defect in cell-cell fusion in axenic culture and *in planta*. Based on this research, hyphal fusion and the ability of the fungus to form an interconnected hyphal network is proposed to be a key factor for successful establishment and maintenance of a mutualistic fungal-plant interaction (Scott et al. 2012, Becker et al. 2015, Green et al. 2016). Further, these mutants are predicted to function in an interconnected signalling complex essential for the symbiotic interaction (Becker et al. 2015, Green et al. 2016). Despite the similar plant interaction phenotype, the $\Delta gpr1b$ mutant strain is not impaired in hyphal fusion and is therefore not likely to be a component of the conserved MAPK signalling pathway. The severe plant phenotype of the $\Delta gpr1b$ mutant strain indicates that the associated cAMP/PKA signalling pathway is essential for maintaining the mutualistic host-endophyte interaction, parallel to and independent of hyphal fusion. In contrast, the deletion of *E. festucae acyA*, a gene encoding the adenylate cyclase which synthesizes cAMP after antagonist-induction,

did not result in a severe plant phenotype as seen for the *Δgpr1b*-infected plants (Voisey et al. 2007). While the infection-rate of plants inoculated with the *ΔacyA* mutant strains was strongly reduced, growth of infected plants was indistinguishable to those infected with the wild-type strain. However the *ΔacyA* mutant strains had increased fungal colonisation of the host tissue including hyper-branching and unrestricted growth (Voisey et al. 2007). These results suggest a regulatory role for cAMP-dependent signalling in maintenance of restricted hyphal growth and systemic colonisation of the host (Voisey et al. 2007). Intracellular cAMP levels of the *ΔacyA* mutant strains have not been quantified in culture and an effect on the cAMP homeostasis is unclear (Voisey et al. 2007). Given the different plant interaction phenotypes of the *ΔacyA* and the *Δgpr1b* mutant strains, both associated with cAMP signalling, it would be of interest to investigate and compare the transcriptome of these mutants *in planta*. Other *E. festucae* mutant strains, with a severe plant interaction phenotype, such as *Δsaka*, encoding the MAPK of the high osmolarity glycerol (HOG) pathway and *ΔsidN*, encoding an iron siderophore, exhibited similar unrestricted growth in the host as observed for the *Δgpr1b*-plant association (Eaton et al. 2008, Eaton et al. 2010, Johnson et al. 2013). However hyphal fusion in these strains, including the *ΔacyA* mutant strain, was not analysed and it is unclear whether these strains are impaired in hyphal fusion or not.

Interestingly, when perennial ryegrass plants were infected with the *Δgpr1b* mutant strain, an accumulation of hyphal bundles underneath the plant cuticle along with an increased number of epiphyllous hyphae were observed by TEM analysis. This was not accompanied by the formation of exressorial structures, suggesting an impairment in differentiation of exressoria due to the lack of Gpr1b. Increased numbers of epiphyllous hyphae and subcuticular hyphae were also described for the *ΔsidN* mutant strain, although the *in planta* phenotype was not further analysed (Johnson et al. 2013). In mutant strains lacking components of the Nox complex, formation of exressoria were impaired, resulting in identical phenotypes (Becker et al. 2016). The production and detoxification of reactive oxygen species (ROS), dependent on the Nox complex and iron uptake, respectively, are associated with polarised growth and hyphal orientation within the plant tissue and are important for retaining the restricted endophytic growth and cellular differentiation processes (Johnson et al. 2013, Kayano et al. 2013, Becker et al. 2016). Impairment of exressoria development in the *Δgpr1b* mutant would suggest that Gpr1b has a

function in specific host signal and surface sensing, that is important in regulating cellular differentiation of expressoria. A similar role in host surface recognition and initiation of cellular differentiation has been proposed for the GPCR Pth11 in *M. oryzae* (DeZwaan et al. 1999, Kulkarni et al. 2003, Kulkarni et al. 2005). Germinated *M. oryzae* $\Delta pth11$ mutants grew as long hyphae on the surface of rice plant leaves and were impaired in appressoria formation and pathogenic development (DeZwaan et al. 1999). The Pth11 GPCR mediates host-specific signalling through both the cAMP/PKA signalling pathway and MAPK pathways (Choi and Dean 1997, DeZwaan et al. 1999, Kulkarni et al. 2005, Wilson and Talbot 2009). Functional analysis of components of the cAMP/PKA signalling pathway have shown that cAMP-dependent signalling initiates cellular differentiation for appressorium formation and invasive growth after penetration (Lee and Dean 1993, Mitchell and Dean 1995, Choi and Dean 1997). However, expressoria formation was not analysed in detail for the *E. festucae* $\Delta gpr1b$ mutants in association with perennial ryegrass, primarily because of the high plant mortality and resulting lack of infected plants to work with. By determining the cellular localisation of the class V GPCRs in *E. festucae*, using fluorescence-based localisation studies as done for Gpr-1 in *N. crassa*, specific cellular roles of the individual receptors can be identified, especially the potential role in hyphal tip growth and expressoria formation.

All *E. festucae* mutants with severe plant host phenotype share common symptoms of hyphal stress such as highly vacuolated endo- and epiphytic hyphae and the formation of intrahyphal hyphae, suggesting that nutrient starvation and a potential alteration of pH in the apoplast, due to the massive increase of fungal biomass in the host plant, leads to these hyphal stress symptoms (Eaton et al. 2010, Johnson et al. 2013, Kayano et al. 2013, Becker et al. 2015). Cellular adaptation to changes in environmental pH is regulated by the Pal pathway by activation of the PacC transcription factor (Lukito et al. 2015). A comparative transcriptome analysis of the *E. festucae* $\Delta sakA$, $\Delta proA$ and $\Delta noxA$ mutants, which have increased fungal biomass phenotypes *in planta*, revealed transcriptional upregulation of the PacC transcription factor, indicative of a change to an alkaline pH of the apoplast (Eaton et al. 2015). Further, mimicry of alkaline environmental conditions by dominant active *pacC* (*pacC^C*) resulted in an abnormal phenotype *in planta* (Lukito et al. 2015). The phenotype of intrahyphal hyphae, formed in *E. festucae* hyphae, was previously described for mutants of the CWI MAPK $\Delta mkkA$ and $\Delta mpkA$ (Becker et al. 2015). The

formation of intrahyphal hyphae was described for various ascomycetes, a naturally occurring phenomenon, formed under conditions of hyphal stress such as nutrient deficiency, hyperosmolarity or cell wall damage (Becker et al. 2015).

For unknown reasons, the ectopic insertion of the wild-type copy of *gpr1b* into each independent $\Delta gpr1b$ mutant strain background ($\Delta gpr1b\#24$, $\Delta gpr1b\#222$), did not restore a wild-type phenotype *in planta*, of those positively-identified complementation strains tested and inoculated into *L. perenne* plants. However, only five independent strains in each mutant background of those showing wild-type like construct integrity, were inoculated into *L. perenne* plants. A higher number of complementation strains might have identified one that may have restored the severe plant phenotype. The lack of an in culture phenotype for the $\Delta gpr1b$ mutant strains required the time consuming analysis in association with the host plant, and made it only possible to test a limited number of candidates. One possible reason for the lack of complementation might be poor expression of the *gpr1b* because it was integrated outside its native locus. Although 941 bp of the *gpr1b* 5' upstream sequence was included in the complementation construct, it is possible that additional regulatory domains such as activator and enhancer sequences, upstream of the core promoter sequence, were missing. Expression levels of *gpr1b* in wild-type and complementation strains were not tested, but the quantification of the *gpr1b* transcript by qRT-PCR would indicate functional integrity of *gpr1b* in the complementation strains and would provide an in culture test method prior to the *in planta* analysis. It is also possible that the integration of the *gpr1b* replacement construct (pAB02) inserted additional mutations, which were not complemented by the ectopic reinsertion of the *gpr1b* wild-type copy. Reinsertion of the *gpr1b* gene into the native locus by homologous recombination ("knock-in") could effectively complement the mutant phenotype or identify potential additional spurious alterations, caused by the insertion of the gene replacement construct.

Taken together, it appears that sensing through the class V GPCR Gpr1b, which putatively acts upstream of the cAMP/PKA signalling pathway, is crucial for establishment and maintenance of the mutualistic *E. festucae*-ryegrass association, independent of hyphal fusion. In addition to the CWI MAPK signalling complex, the cAMP/PKA cascade has the potential to be a sole or accessorially important for interaction with the host. Interestingly, similar plant interaction phenotypes in both

suggests crosstalk between the two pathways or a common breakdown in the signalling outcome.

In pathogenic fungi, different GPCRs have been shown to be essential for the interaction with the host and development of pathogenesis, especially those required for the cAMP/PKA signalling pathway. In the phytopathogen *M. oryzae*, recognition of the host plant surface depends on hydrophobin sensing and other unknown components, and is mediated by the GPCR Pth11 which transmits the signal through the cAMP/PKA signalling pathway (DeZwaan et al. 1999, Kulkarni et al. 2005). Loss of Pth11 or the adenylate cyclase MAC1 resulted in impaired formation of the appressorium penetration structure with absence of the pre-appresorial germ-tube swelling, indicative for defective initiation of the cellular differentiation process that resulted in avirulent phenotypes (Lee and Dean 1993, Choi and Dean 1997, DeZwaan et al. 1999). While exogenous cAMP restored the wild-type phenotype to $\Delta aycA$ mutants, formation of appressoria but not penetration of the plant cuticle was restored for the $\Delta pth11$ mutant background, which required additional diacylglycerol (DeZwaan et al. 1999). The impaired cellular differentiation leading to formation of appressoria and penetration of the plant cuticle, indicated the specific role for the receptor for inductive substrate cues (DeZwaan et al. 1999). The $\Delta pth11$ mutants failed to progress beyond the recognition phase of appressorium differentiation, that resulted in severe loss of pathogenicity (DeZwaan et al. 1999). Additional receptors might be required for initiation leading to appressoria differentiation, that also activate the cAMP/PKA signalling pathway, as the $\Delta mac1$ mutant completely failed to initiate this process (Lee and Dean 1993, Choi and Dean 1997). A similar phenotype with retarded appressoria development and an impaired penetration mechanism was described for the adenylate cyclase deletion strains in *B. cinerea*, Δbac (Klimpel et al. 2002). Host-specific sensing, initiation of the pathogenic development and invasive growth in *M. oryzae* is a complex mechanism that requires a highly coordinated cascade of cellular processes, orchestrated by various interlinked signalling pathways reviewed in (Wilson and Talbot 2009). Appressoria formation in *M. oryzae* indicated additional cAMP-independent functions for Pth11, necessary for full pathogenic development. While Pth11 activates the cAMP/PKA signalling pathway through the G protein α -subunit MagA, the β -subunit Mgb1 initiates the phosphorylation-cascade of the pheromone response pathway, also known as phytopathogenicity

MAPK (Pmk1) signalling pathway (reviewed in Wilson and Talbot 2009). The *M. oryzae* Pmk1 MAPK pathway includes the kinases Mst11, Mst7 and Pmk1, homologues to the *S. cerevisiae* pheromone response pathway Ste11 (MAPKKK), Ste7 (MAPKK) and Kss1/Fus3 (MAPKs), respectively (Xu and Hamer 1996, Zhao et al. 2005). In common with *M. oryzae*, the pheromone response pathway in *S. cerevisiae* is activated by the stimulated G β -subunit after pheromone-binding to the cell surface receptor (Rispaill and Di Pietro 2010). Activation by the G β -subunit, the Ste5 scaffold protein and the p21-activated kinase (PAK), Ste20, initiates the downstream phosphorylation of Ste11, Ste7, Fus3/Kss1 resulting cellular differentiation of mating and filamentation (Cherkasova et al. 2003; reviewed in Rispaill and Di Pietro 2010). This pathway is also involved in mating and in pathogenic development in phytopathogens such as *M. oryzae* as host surface recognition on hydrophobic surface or by addition of exogenous cAMP, that triggers appressorium formation, was impaired in the $\Delta pkm1$ mutant strains (Zhao et al. 2005). The $\Delta pkm1$ mutant phenotype exhibits initial appressoria formation with swollen germtube tips but is incapable of full appressoria development or invasive growth when artificially infected (Zhao et al. 2005). The G β -subunit Mgb1 interacts with the scaffold protein Mst50, therefore activates the Pmk1 MAPK which in turn activates various transcription factors such as Mst12 (Park et al. 2002, Nishimura et al. 2003, Park et al. 2006). Homologues to Ste12 in *S. cerevisiae*, Mst12 is indispensable for appressorium-mediated penetration and infectious growth, therefore coordinates the pathogenic development of *M. oryzae* alongside target enzymes of the cAMP-dependent catalytic PKA subunit (Mitchell and Dean 1995, Park et al. 2002, Park et al. 2004). Signalling through the Pth11 receptor demonstrates co-dependence of Pmk1 MAPK and cAMP/PKA signalling pathway for adaptation to the host (Xu and Hamer 1996, Wilson and Talbot 2009). In the mycoparasitic fungus *Trichoderma atroviridae*, recognition of the host fungus *Rhizoctonia solani* and initiation of pathogenic development and penetration is regulated by the cAMP/PKA signalling pathway (Zeilinger et al. 2005, Brunner et al. 2008, Omann et al. 2012). Silencing of *Tagpr1*, a gene encoding a class V GPCR upstream of the cAMP/PKA signalling pathway, resulted in impaired host recognition and cAMP-dependent mycoparasitism as well as expression of cell-wall degrading enzymes and other secondary metabolites (Zeilinger et al. 2005, Brunner et al. 2008, Omann and Zeilinger 2010, Omann et al. 2012). Exogenous cAMP

restored the fungal-host recognition and attachment phenotypes but the $\Delta Tagpr1$ mutant strain remained impaired in activation of secondary metabolism, host penetration and invasive growth (Zeilinger et al. 2005, Brunner et al. 2008, Omann et al. 2012). While this indicates that TaGpr1 mediates cellular differentiation and initiation of pathogenic development in contact with a host fungus, it also indicates cAMP-independent functions for TaGpr1 that are essential for the pathogenicity (Zeilinger et al. 2005, Brunner et al. 2008, Omann et al. 2012). Similar to the described function of Pth11 in *M. oryzae* above, activation of two or more downstream signalling pathways through TaGpr1 is likely. The homolog of the *M. oryzae* Pmk1 MAPK in *T. atroviride* is TmkA, which plays an important role in the initiation process of the mycopathogenic host penetration (Mukherjee et al. 2003). While $\Delta tmkA$ mutant strains were capable of host recognition, production of chitinolytic and proteolytic enzymes, invasive growth was impaired in a confrontation assay with *R. solani* or *B. cinerea* (Mukherjee et al. 2003; reviewed in Zeilinger and Omann 2007). While the pathogenic infection structures of *T. atroviride* differs fundamentally from appressoria in *M. oryzae*, the mechanism that triggers host penetration seems to be similar. Prior to pathogenic development and invasive growth, hyphae of *T. atroviride* coil around the host hyphae, attach firmly and initiate production of chitinase and antifungal metabolites for penetration (Reithner et al. 2007, Zeilinger and Omann 2007). This process was not impaired for the $\Delta tmkA$ mutant, unlike invasive mycoparasitic growth (Zeilinger and Omann 2007). Direct physical interaction with the host hyphae triggers the hyphal coiling, independently of specific host signals as shown for $\Delta tmkA$ or $\Delta Tagpr1$ mutants that extensively coiled around nylonfibres or host hyphae without penetration (Zeilinger and Omann 2007, Brunner et al. 2008). However, physical contact did not induce Tmk1-dependent mycoparasitic invasive growth or cAMP-dependent expression of pathogenicity-related secondary metabolites (Harman et al. 2004, Zeilinger and Omann 2007). Similar to *M. oryzae*, the Tmk1 MAPK pathway activates the Ste12 transcription factor in *T. atroviride*, that shares high sequence identity with Ste12 in *S. cerevisiae* (Gruber and Zeilinger 2014). Despite enhanced expression of cAMP-dependent lysing enzymes, the deletion of Ste12 resulted in a decreased mycoparasitism, impaired invasive growth and reduced hyphal fusion (Gruber and Zeilinger 2014). A similar correlation between functions of the cAMP-signalling and the pathogenicity MAPK in coordinating pathogenic development and host

penetration was described for the necrotrophic phytopathogen *B. cinerea* (Zheng et al. 2000, Doehlemann et al. 2006, Zhao et al. 2007, Zhang et al. 2011, Harren et al. 2013). This conserved mechanism among pathogenic fungi in host recognition and initiation of the respective pathogenic development, coordinated by the parallel action of these two signalling pathways, links the fungal pheromone response with cAMP-signalling pathway for a normal host interaction. Although no specific receptor was identified in *B. cinerea*, perception and signalling of chemoattractants through parallel pathways to initiate cellular differentiation and pathogenic development, specific to the individual organism, appears to be conserved and likely coordinated by GPCRs with adapted ligand-specificity to the individual host. Therefore it is likely that the GPCR TaGpr1 activates the cAMP/PKA signalling pathway and the pheromone response pathway (Tmk1) through the G α -subunit and the G β -subunit, respectively. Interestingly, while the pheromone response pathway in *E. festucae* has yet to be analysed, deletion of the Ste12 homolog in *E. festucae* resulted in a significant decreased in the plant infection rate (Kamiya S 2016). Of the four class V GPCRs in *T. atroviride*, TaGpr1 shares the least sequence similarity with Gpr1a, Gpr1b or Gpr2 in *E. festucae*, however, a similar function in host recognition and cellular differentiation is likely. The Gpr1b homolog in *T. atroviride* TaGpr3, shows increased mRNA levels in response to physical interaction with hyphae of the host fungus but also to hyphae from other *T. atroviride* colonies or to artificial cellulose membrane (Brunner et al. 2008). This was not further analysed and silencing of TaGpr3 failed, however a putative role similar to TaGpr1 or in combination with TaGpr1 is possible. Based on the phenotype analysis of the *E. festucae* Δ *gpr1b* strain, Gpr1b is required for a normal host interaction and is involved in regulation of the restricted endophytic growth, a putative equivalent for mutualistic endophytes to the invasive growth of pathogens. However, potential ligands for Gpr1b such as specific host-derived molecules remain unknown, that putatively regulate the mutualistic *E. festucae* - *L. perenne* association.

Taken together, cAMP/PKA signalling and the related GPCRs in *M. oryzae*, *T. atroviride* and *E. festucae*, play important roles in sensing host-specific signals (chemoattractants) that enable species-specific interaction with the host. Other signalling pathways such as the pheromone response pathway in pathogenic fungi have similar roles, which indicates signalling cross-talk with the cAMP/PKA signalling pathway for coordinated functions, which is mediated by the same

receptor. As Pth11 in *M. oryzae* functions as a mediator of multiple pathways for coordinated cellular and developmental processes leading to a normal host interaction, Gpr1b in *E. festucae* has the potential for a similar regulatory function. To support this hypothesis and to identify the potential involvement of Gpr1b in the pheromone response pathway or other signalling pathways parallel to cAMP-dependent signalling requires further research.

The specific molecules involved in the *E. festucae*-ryegrass interaction, that regulate the highly restricted and synchronised growth within the host plant, are yet to be identified. However it has been shown that oxylipins function as important signalling molecules for inter-species communication (reviewed in Brodhun and Feussner 2011). Oxylipins are oxygenated polyunsaturated fatty acids (PUFA), produced by mammals, plants and fungi alike. Synthesis occurs through enzymatic or non-enzymatic incorporation of molecular oxygen into the fatty acid backbone by oxygenases such as cyclooxygenases (COX), lipoxygenases (LOX) or monooxygenases, or free-radicals such as hydrogen peroxide, respectively (Brodhun and Feussner 2011, Barbosa et al. 2016). Bioactive oxylipins regulate biological responses and cellular development similarly in all kingdoms, while it has been shown that fungal-produced oxylipins are implicated in disease development and alternate plant defence response in phytopathogenic fungi (Fischer and Keller 2016). It has been shown that microbial oxylipins mimic endogenous plant signal molecules and plant hormones such as jasmonic acid (JA) and therefore manipulate the plant defence response as identified in *Pseudomonas syringae* (Wasternack and Kombrink 2010, Brodhun and Feussner 2011). In *M. oryzae*, the antibiotic biosynthesis monooxygenase (*abm*), modifies JA to hydroxylated 12-OH-JA, an essential molecule for successful infection of rice plants (Riemann et al. 2013, Patkar et al. 2015). Hypothetically, fungal generated 12-OH-JA binds to the plant receptor responding to JA, resulting in suppression of the plant pathogen response (Riemann et al. 2013, Patkar et al. 2015). Fungal-produced oxylipins were first described in *Aspergillus* spp. through their involvement in regulation of cellular differentiation of sexual and asexual development, therefore referred to as precocious sexual inducers (Psi-factors) (Tsitsigiannis et al. 2005, Horowitz Brown et al. 2008). Cyclooxygenases-like enzymes, the Psi factor-producing oxygenases (Ppo), oxygenate PUFAs that induce sexual development, while also have an impact on various cellular processes such as production of

secondary metabolites and hydrolyzing enzymes, that are essential for pathogenic development (Champe et al. 1987, Tsitsigiannis et al. 2004, Tsitsigiannis et al. 2005, Horowitz Brown et al. 2008, Brown et al. 2009, Brodhun and Feussner 2011, Affeldt et al. 2012). In many phytopathogenic fungi such as *A. flavus* or *Fusarium verticillioides*, expression of Ppo genes is essential for host infection and avoidance of the host defence, likely by mimicking plant hormones (Brodhagen et al. 2008, Scala et al. 2014, Scarpari et al. 2014). Pathogenic and non-pathogenic fungi possess Ppo genes, also known as linoleate diol synthases or linoleate dioxygenases (LDSs), however only a limited number are functionally characterised [reviewed in (Fischer and Keller 2016)]. In *Aspergillus* spp. and other fungi, linoleic acid (C₁₈ PUFA) is the primary substrate for oxylipin production, however α -linolenic acid, oleic acid or the C₂₀-PUFA arachidonic acid can serve as substrate for several specific oxylipins (Tsitsigiannis et al. 2005, Brown et al. 2009, Brodhun and Feussner 2011, Affeldt et al. 2012, reviewed in Fischer and Keller 2016). Several fungal-produced oxylipins manipulate host defense response in a host-fungal association, while plants use oxylipins as early pathogen recognition and defence mechanisms (Prost et al. 2005, Fischer and Keller 2016). Further, locally produced linoleic acid-derived oxylipins produced by plants can inhibit fungal growth, thereby preventing fungal colonisation (Hause et al. 2000, Noverr et al. 2003, Prost et al. 2005, Herrero-Garcia et al. 2011, Scala et al. 2014, Fischer and Keller 2016). Oxylipin production and signalling has not been analysed in the *E. festucae* - *L. perenne* association, however the genome of *E. festucae* contains a gene (EfM3.057040) encoding a Ppo homolog, based on sequence identity to the *A. nidulans* PpoA, PpoB, PpoC (Horowitz Brown et al. 2008). Interestingly, comparing gene expression between mycelia grown in culture expression and in association with the host revealed a 5.59 fold upregulated *in planta* for this Ppo homolog, indicative of a potential important role in the host-endophyte interaction [Chujo et al., unpublished]. *E. festucae* does not only affect plant metabolism to increase drought resistance, it can also produce plant hormones such as auxin to alter plant tissue development and generate other changes in plant metabolism besides the plant defense system (De Battista et al. 1990, Redman et al. 1999, Rodriguez et al. 2008, Rodriguez et al. 2009, Dupont et al. 2015). In addition to the highly synchronised endophytic growth to host development, this form of adaptation requires the exchange of signals between the

endophyte and the host, potentially mediated by certain oxylipins that mimic plant hormones for suppression of the plant response.

Oxylipins are perceived by various GPCRs in all kingdoms and affect secondary metabolite production in fungi, such as aflatoxin production in the *A. flavus* (reviewed in Brodhun and Feussner 2011, Obinata and Izumi 2009, Mukherjee et al. 2013, Affeldt et al. 2014, Brown et al. 2015). It has been shown that *Aspergillus* spp. respond to oxylipins and linoleic acid by changes in intracellular cAMP levels, which are perceived by various GPCRs including the class V GprH (Affeldt et al. 2012, Affeldt et al. 2014, Brown et al. 2015, Fischer and Keller 2016). Addition of the oxylipin precursor linoleic acid to colonies of *E. festucae* wild-type and the $\Delta gpr2$ mutant strains had a minor inhibitory effect but had no major effect on morphology or hyphal growth-rate between the two strains. The hyphal growth-rate of the $\Delta gpr1b$ mutant was slightly more reduced, indicating a role in linoleic acid sensing and cellular adaptation. However, with the limited data obtained in the preliminary growth experiment, it is not possible to hypothesize a specific role for Gpr1b or Gpr2 in oxylipin sensing despite the attractiveness of this hypothesis. Oxylipins may induce cellular changes in *E. festucae* or fungal-produced oxylipins induce changes in the host plant to favour the symbiotic interaction. The specific receptor mediating these signals has yet to be identified. To date, the biochemical composition of the grass apoplast is not known and the composition of lipids, saturated and unsaturated fatty acids or oxylipins, the apoplastic lipidosome, has not been analysed (Misra 2016). Considering the role of the apoplast in lipid signalling for plant development, stress and pathogen response, and as hub for pathogenic or mutualistic microbe-interaction, the identification of lipids and oxylipins in the plant apoplast by mass spectrometry could identify potential GPCR triggering-molecules. Given a key role for oxylipins in inter-kingdom communication, future work is required to elucidate if these molecules have a role in the mutualistic endophyte-grass association. Potential Gpr1b-binding ligands that trigger an increase in intracellular cAMP, as has been found for specific oxylipins in *Aspergillus* spp., require efficient detection methods for high-throughput biochemical screens. The hypothetical role of Gpr1b in sensing specific plant-derived oxylipins, to regulate the restricted endophytic growth or initiate differential processes such as expressoria development, requires future work.

To analyse the impact of individual gene deletion on the interaction with the host in *E. festucae*, common pathogenicity assays by spraying or injecting defined spore solutions on to or into the host as used in most phytopathogenic fungi, can't be used. Firstly, development of conidia in axenic cultures of *E. festucae* is rather sparse thereby making the analysis of conidiogenesis and conidia germination in axenic culture difficult, because of low number of conidia. Effects on conidiation are quantified by growing colonies from conidia obtained from single spore isolation. Unlike phytopathogens like *M. oryzae* or *B. cinerea*, which penetrate the plant cuticle after development of specific penetration structures followed by invasive growth, the route of host-infection in *Epichloë* species is different to that of pathogens. Plant infection by *Epichloë* endophytes naturally occurs by vertical transmission where plant ovule and embryo sac and subsequently the maturing seeds are infected by endophytic hyphae. For horizontal transmission during sexual development, the host plant has to enter inflorescence development, stromata have to be formed, spermatia have to be transmitted by symbiotic *Botanophila* flies, meiosis-derived ascospores have to be horizontally transferred to uninfected host inflorescence followed by asexual microcycle conidiogenesis where the resulting conidia then can infect the new host ovule (White and Bultman 1987, Rodriguez et al. 2008). Colonisation of the new host starts after germination of infected seeds. Because sexual development of *E. festucae* is rare and does not occur in the synthetic association with *L. perenne*, young ryegrass seedlings are artificially infected with fungal strains by inoculation of small pieces of vegetative hyphae, which then systemically infect the plant as the seedling grows and matures over a period of three to four months. Because of the severe plant phenotype caused by infection with the $\Delta gpr1b$ mutant strain, very few infected plants will survive, making this type of analysis a time-consuming process.

In summary, the deletion of *gpr1b*, encoding a cAMP-receptor like GPCR in *E. festucae*, resulted in disruption of the mutualistic endophyte-grass association and caused a severe plant-interaction phenotype. Sensing through Gpr1b appears to be plant-specific, given no obvious phenotype was observed in culture. While this hypothesis as to be confirmed by complementation of the mutant phenotype, it is supported by the higher expression of this gene *in planta* compared to that in culture. This study also shows that the cAMP/PKA signalling pathway is required in

addition to the CWI MAPK signalling complex for establishment and maintenance of the mutualistic *E. festucae*-*L. perenne* association. Disruption of either signalling pathway leads to a common host phenotype that is indicative of some common break down in inter-species communication. This may be due to a change in the physiological conditions in the apoplast such as increased pH that are brought about by the increased fungal biomass and unrestricted endophytic growth, associated with disruption of either signalling pathway. Alternatively, in response to impaired perception of plant-specific signals such as certain oxylipins through the loss of Gpr1b, which putatively regulates the restricted endophytic growth, no signalling cross-talk between the cAMP/PKA signalling pathway and other regulatory pathways occurs.

6.2 The role of the cAMP-phosphodiesterases in *E. festucae*

To further investigate the role of the cAMP signalling pathway in establishing and maintaining the mutualistic association of *E. festucae* and perennial ryegrass the function of the putative 5'-3' cyclic nucleotide phosphodiesterases were analysed. The cAMP phosphodiesterases (PDEs) regulate the intracellular balance between the basal levels of cAMP in the cell and the signal-dependent temporal and spatial accumulation of this secondary messenger. After the antagonist-induced synthesis of cAMP by the adenylate cyclase (AC) and sequential cAMP-dependent activation of the protein kinase A (PKA), the phosphodiesterases themselves are phosphorylated by the activated catalytic PKA subunit (cPKA) to initiate the regulatory negative feedback loop. Once activated, the phosphodiesterases hydrolyse cAMP into 5'-AMP, thereby decreasing the intracellular levels and terminating the cAMP-mediated signal. Fine-tuned regulation of the intracellular cAMP levels, coordinated by synthesis and hydrolysis, are crucial for various cellular processes in all eukaryotes.

In fungi, the transduction of extracellular signals through activation of the cAMP/PKA signalling pathway as well as the signal termination through PDE activity is important to maintain the cellular cAMP homeostasis (Fig. 6.1). This process is crucial for vegetative growth, sexual and asexual development,

pathogenic development and the production of secondary metabolites (Calvo et al. 2002, Houslay et al. 2007, Mukherjee et al. 2012, Conti et al. 2014, Guo et al. 2016).

6.2.1 PDEs in *E. festucae*

Like most fungi, the genome of *E. festucae* possesses two genes *pdeL* and *pdeH* encoding low and high affinity cAMP phosphodiesterases with the conserved characteristic class II and class I consensus signature motifs, respectively. Apart from the related function of modulating intracellular levels of cAMP, the two PDEs share no sequence or domain similarity, indicating distinct functions. Both proteins were identified by protein sequence identity to the characterized homologues MoPdeL and MoPdeH in *M. oryzae* using BLAST (Ramanujam and Naqvi 2010). Both group with the respective PDEs from other fungi. Among the fungal species, the individual PDE with low or high affinity towards cAMP have related but distinct cellular functions, which is species dependent. However, it has been shown, that the lack of one of the PDEs triggers at least partial complementation by the other (Hicks et al. 2005, Ramanujam and Naqvi 2010, Zhang et al. 2011, Harren et al. 2013).

In fungi, activity of the low affinity PDE is generally dependent on glucose-stimulated phosphorylation by the catalytic PKA subunit (cPKA). Similar to what has been found in this study for other fungi, including *S. cerevisiae*, *S. pombe*, *C. albicans*, *C. neoformans*, *A. nidulans* and *N. crassa* PdeL in *E. festucae* is predicted to have one PKA phosphorylation site, that could be activated by cPKA. Accumulation of intracellular cAMP after transfer from nutrient-rich to nutrient-poor media indicates nutrient-dependent activation. However, it has yet to be shown conclusively whether glucose-induction and cPKA activity leads to phosphorylation of PdeL. Using ExPasy prosite and a high sensitivity scan that includes motifs with a high probability of occurrence, two PKA phosphorylation sites within the common motif were predicted for PdeH in *E. festucae*. However so far no PKA phosphorylation sites have been functionally analysed in the high-affinity phosphodiesterase of fungi. Antagonist-induced PKA-dependent activation is likely, in addition to the possible PKA-independent allosteric activation directly by cAMP as shown for *Dictyostelium discoideum* (Lacombe et al. 1986, Krishnamurthy et al. 2015). Deletion of the gene encoding PdeL in *E. festucae* resulted in reduced hyphal growth and conidia formation but increased formation of aerial hyphae in axenic

culture. Further, preliminary analysis of the $\Delta pdeL$ mutant strain showed a higher intracellular cAMP concentration when transferred from nutrient-rich media to starved conditions, a result suggestive of a reduced hydrolysis efficiency and indicative of glucose-dependent activation and a role in the regulation of the cAMP/PKA signalling pathway in nutrient sensing. In ascomycetes including *E. festucae*, carbon-starvation triggers asexual development. Alteration in intracellular cAMP levels have been shown to affect vegetative growth and asexual conidiogenesis in *E. festucae* (Voisey et al. 2007). Deletion of the cAMP-synthesising adenylate cyclase enzyme *acyA*, resulted in reduced vegetative growth and increased production of conidia (Voisey et al. 2007). As reported for other fungi, the cAMP/PKA signalling pathway and the levels of intracellular cAMP regulate the morphological switch between asexual and sexual development (Gold et al. 1994, Adachi and Hamer 1998, Kays et al. 2000, Han et al. 2004, Li et al. 2007, Xue et al. 2008, Dyer and O'Gorman 2012, Park and Yu 2012, Krijgsheld et al. 2013). In *A. fumigatus*, *A. nidulans*, *B. cinerea* and *M. oryzae*, cAMP-dependent signalling negatively regulates sexual development as deletion mutants of the respective adenylate cyclase show increased sexual development and reduced conidiation (Choi and Dean 1997, Fillinger et al. 2002, Klimpel et al. 2002, Liebmann et al. 2003). In contrast, the hypersporulation phenotype of the *E. festucae* $\Delta acyA$ mutant strain indicates negative regulation of asexual development by the cAMP/PKA signalling pathway (Voisey et al. 2007). The reduced conidiation and lower levels of cAMP of the $\Delta pdeL$ mutant strain suggests the regulation is concentration-dependent. Low levels of intracellular cAMP cause a shift to conidia development, while high levels of cAMP represses asexual development, suggesting cAMP-homeostasis is required for the balance. Reduced conidiation was also shown for strains lacking the low affinity PDE MoPdeL and BcPde1 in *M. oryzae* and *B. cinerea*, respectively (Ramanujam and Naqvi 2010, Zhang et al. 2011, Harren et al. 2013). However, aerial and radial growth in these mutant strains was not affected (Ramanujam and Naqvi 2010, Zhang et al. 2011, Harren et al. 2013). As previously mentioned, asexual conidiation in *E. festucae* is rather sparse, resulting in low numbers of conidia, and sexual development only occurs in association with the host plant and only in compatible species. While sexual development of *E. festucae* in association with *L. perenne* does not occur and the endophyte is only transmitted vertically, it is not possible to analyse a potential impact of cAMP signalling on sexual development in

this interaction. Using *E. typhina* or *E. festucae* in association with *Festuca rubra*, *Epichloë* endophytes which are capable of inducing sexual development, could provide insights into this particular role of cAMP-dependent signalling. The increase in aerial hyphal formation in the $\Delta pdeL$ mutant strain, a necessary cellular differentiation for asexual development in ascomycetes, is indicative of a morphological shift to conidiogenesis given conidiophores and conidia arise from aerial hyphae in ascomycetes (Kües and Fischer 2006). In *N. crassa*, deletion of the adenylate cyclase *cr-1*, resulted in an increase in aerial hyphae formation, reduced vegetative growth and abundant conidia (Terenzi et al. 1979). The deletion of the high affinity PDE in *N. crassa*, Pde2, resulted in a lack of conidia formation, indicative of a role for this PDE in cellular differentiation from aerial growth to proconidial chain formation that is dependent on the intracellular cAMP concentration (Greenwald et al. 2010). In the dimorphic phytopathogen *U. maydis*, loss of the low affinity PDE UmPde1, resulted in a shift to asexual development with a multiple budding phenotype (Agarwal et al. 2010). Deletion of *uca1*, a gene encoding the adenylate cyclase in *U. maydis*, caused constitutive filamentation and therefore a shift to sexual development, despite the absence of a compatible mating type (Gold et al. 1994). A regulatory role for the cAMP/PKA signalling pathway mediating cellular differentiation and morphogenesis between asexual and sexual development appears to be consistent function of this pathway in fungi (Wilson and Talbot 2009, Ramanujam and Naqvi 2010, Harren et al. 2013). Based on the cellular phenotype, it can be concluded that the low affinity PDE PdeL in *E. festucae* modulates cellular cAMP levels during morphogenesis of aerial hyphae and conidia formation. The cellular phenotypes of the $\Delta pdeL$ and $\Delta acyA$ mutant strains in culture indicate that the cAMP/PKA signalling pathway is involved in cellular differentiation processes for asexual development in *E. festucae*.

The *E. festucae* $\Delta pdeH$ strain grew as well as the wild-type in axenic culture, similar to the saprophytic yeast-like growth of the $\Delta umpde2$ mutant strain, encoding the high affinity PDE in the dimorphic phytopathogen *U. maydis* (Agarwal et al. 2010). In contrast, deletion mutants lacking the high affinity PDEs in the phytopathogens *M. oryzae* $\Delta mopdeH$ and *B. cinerea* $\Delta Bcpde2$, which exhibited slightly reduced radial growth and aerial hyphae formation, but an increase in pigmentation compared to the wild-type strain (Ramanujam and Naqvi 2010, Harren et al. 2013). Deletion of BcPde2 in *B. cinerea* resulted in a more severe

phenotype in culture to that observed for $\Delta bcpde1$ mutants, regarding vegetative growth, conidiation and formation of misshapened conidia (Harren et al. 2013). Under osmotic stress conditions, conidia were completely absent, but under conditions that induce sexual development an abundance of conidia instead of sclerotia was observed, indicative of atypical cellular differentiation (Harren et al. 2013). Germination of conidia was reduced on inductive medium in the *M. oryzae* $\Delta MopdeH$ and *B. cinerea* $\Delta Bcpde2$ mutants (Ramanujam and Naqvi 2010, Zhang et al. 2011, Harren et al. 2013). In *E. festucae*, the $\Delta pdeL$ and the $\Delta pdeH$ mutant strains exhibited no difference to the wild-type in their growth under osmotic stress or any other stress conditions, apart from the general reduction in hyphal growth observed for the $\Delta pdeL$ mutant strain on all media tested. Although conidia germination was not analysed in detail, the $\Delta pdeL$ mutants exhibit slightly delayed growth after single spore isolation. This effect is likely to be correlated with the reduced vegetative growth that resulted in smaller colonies arising from isolated conidia. The increased aerial hyphae formation, visible early during colony formation, indicates a role for cAMP-dependent signalling for differentiation of aerial hyphae. PdeL is further involved in regulation of the cAMP homeostasis after nutrient-triggered activation of the cAMP/PKA signalling pathway and coordinates cellular differentiation processes in axenic culture, whereas PdeH shows no obvious function in axenic culture. As shown for other fungi, the two PDEs have distinct cellular functions, dependent on the specific life-style (Sass et al. 1986, Wera et al. 1997, Ma et al. 1999, Hicks et al. 2005, Agarwal et al. 2010, Ramanujam and Naqvi 2010, Zhang et al. 2011, Harren et al. 2013).

While PdeL seems to play an important role in axenic culture, in association with perennial ryegrass, no noticeable difference between plants inoculated with the wild-type or the $\Delta pdeL$ mutant strain was observed. On the other hand, loss of the high-affinity PDE PdeH resulted in a breakdown of the mutualistic association and a severe plant interaction phenotype, similar to that observed for the $\Delta gpr1b$ mutant strain. A comparison of gene expression levels, using a global transcriptome data set for wild-type strain grown in culture or in association with the host, revealed that PdeH is highly expressed *in planta*, while PdeL is downregulated [Chujo et al., unpublished]. The transcriptomic data and the phenotype analysis support a functional categorisation of the two PDEs, where PdeL predominantly regulates the intracellular cAMP level for signalling and cellular processes in culture,

such as asexual development and nutrient sensing, while PdeH is important for functions specifically in association with the host. Plants inoculated with the $\Delta pdeH$ mutant strain, were severely stunted, had poorly developed root systems and exhibited a high mortality rate. Similar to the $\Delta gpr1b$ mutant strain, infection with the $\Delta pdeH$ mutant strain led to unrestricted growth that resulted in colonisation of the vascular bundles and an increase in fungal biomass *in planta*. The highly vacuolated hyphae and the formation of intrahyphal hyphae are phenotypes indicative of poor nutrient access due to the numerous hyphae colonising the plant. Unlike other *E. festucae* mutant strains including $\Delta noxA$ and $\Delta noxR$, Δso , $\Delta proA$, $\Delta mkkA$, $\Delta mpkA$ and $\Delta mobC$ (Charlton et al. 2012, Kayano et al. 2013, Tanaka et al. 2013, Becker et al. 2015, Green et al. 2016) that had similar severe plant interaction phenotypes hyphal fusion was not impaired in the $\Delta pdeH$ mutant strain. This was also described for the $\Delta gpr1b$ mutant strain which exhibited a similar plant interaction phenotype. The pleiotropic phenotype observed for these mutants suggests that PdeH and Gpr1b function in the same signalling cascade. The severe phenotype of $\Delta pdeH$ -infected plants indicate an important role for cellular cAMP-homeostasis of the fungal hyphae in association with the host. Therefore cellular processes activated by the cAMP/PKA signalling pathway, to regulate the restricted growth in plant tissue, require that levels of intracellular cAMP are balanced.

While dispensable for growth in culture, PdeH is crucial for plant-endophyte interaction, similar to the role of the cAMP receptor-like GPCR Gpr1b. The pleiotropic phenotypes of the $\Delta pdeH$ and $\Delta gpr1b$ mutant strains in culture and *in planta*, are indicative that both act in the cAMP/PKA signalling, and specifically when in association with the host plant. These results demonstrate the importance of the cAMP/PKA signalling pathway and signal mediation for the regulation of the restricted endophytic growth and systemic host colonisation. In parallel to the important CWI MAPK signalling complex and independent of hyphal anastomosis, cAMP-dependent signalling is crucial for establishment and maintenance of the mutualistic *E. festucae* – ryegrass association.

In phytopathogenic fungi, the high affinity PDE plays the dominant role in modulating cAMP-dependent developmental processes in association with the host. The deletion of the low affinity PDE BcPde1 in *B. cinerea* showed no effect on growth and pathogenic development of the fungus, while the high affinity PDE BcPde2 had a major pathogenicity phenotype, in addition to its important role in development

and differentiation in culture (Harren et al. 2013). Conidia of the wild-type germinate on the host leave, form short germ-tubes, which initiate the formation of appressoria-like structures. These structures allow penetration of the host cuticle layer and invasive growth of the host cells (Harren et al. 2013). In the $\Delta bcpde2$ mutant germination of conidia is reduced, and the germ-tubes that do form grow as long hyphae with impaired formation of appressoria, resulting in an avirulence phenotype (Harren et al. 2013). Where appressoria do form they successfully penetrate the plant cells but are impaired in proper invasive hyphal growth and conidiogenesis in the host (Harren et al. 2013). *In vitro* studies have shown that BcPde2 functions in nutrient-induced and hydrophobic surface-induced conidia germination and cellular differentiation processes that lead to appressorium formation, mediated by the cAMP/PKA or the MAP kinase Bmp1 signalling pathway (Doehlemann et al. 2006, Schumacher et al. 2008, Harren et al. 2013). Surface recognition, conidia germination, induction of appressoria formation and host penetration follows a similar mechanism in *M. oryzae*, involving the Pth11 receptor, the cAMP/PKA and the Pmk1 MAPK signalling pathway as described above (reviewed in Wilson and Talbot 2009, Ding et al. 2009, Zhang et al. 2011). In *M. oryzae* the mutant strain lacking the high affinity PDE $\Delta MopdeH$ exhibited a similar phenotype to *B. cinerea*, with strongly reduced growth, delayed appressoria formation and impaired invasive growth, in association with the host plant (Ramanujam and Naqvi 2010, Zhang et al. 2011). In both phytopathogens, the high affinity PDEs are involved in surface sensing and cellular differentiation of appressoria and invasive hyphae (Ramanujam and Naqvi 2010, Zhang et al. 2011, Harren et al. 2013). The importance of the cAMP-dependent signalling and crosstalk to various MAPK pathways for interaction with and penetration of the host is well described in different fungi (reviewed in Mehrabi et al. 2009). Mutations in components of the cAMP/PKA signalling pathway, such as the adenylate cyclase in both *B. cinerea* (BAC) and *M. oryzae* (MAC1) exhibited a related effect in pathogenic development, showing retarded formation of appressoria and penetration pegs (Choi and Dean 1997, Klimpel et al. 2002). These results show that the cAMP/PKA signalling pathway regulates central functions in cellular differentiation for pathogenic development, a process highly dependent on balanced levels of intracellular cAMP that is modulated by phosphodiesterases that have high affinity towards cAMP. The interaction with and invasion of the particular host plant of

phytopathogenic fungi such as *M. oryzae*, *B. cinerea* or *U. maydis* are fundamentally different to that of the mutualistic *Epichloë* endophytes, which do not penetrate the host leaves and develop a different route of infection as described above.

A more severe host phenotype was observed in both *B. cinerea* and *M. oryzae*, when genes encoding both the low and high affinity PDE were deleted to those described for the particular single mutation (Ramanujam and Naqvi 2010, Zhang et al. 2011, Harren et al. 2013). It has been demonstrated that both PDEs regulate intracellular cAMP levels, and partially complement the function of the other when one is missing (Sass et al. 1986, Nikawa et al. 1987, Hicks et al. 2005, Park et al. 2005, Agarwal et al. 2010, Ramanujam and Naqvi 2010, Zhang et al. 2011, Agarwal et al. 2013, Harren et al. 2013). Generation of a double $\Delta pdeL\Delta pdeH$ mutant strain would be required to test a complementary function for either of the PDEs in *E. festucae*. Attempts to isolate a double mutant were unsuccessful, possibly because of a potential lethal effect or a strongly impaired vegetative growth phenotype that gave rise to very small colonies. For the latter, transformants of the $\Delta pdeL\Delta pdeH$ mutant strain could have been missed during primary selection or were not able to grow through the selective overlay medium due to reduced hyphal growth, as seen for the *E. festucae* $\Delta pdeL$ single mutant strain. The importance of a stable cAMP-homeostasis was shown for the *E. festucae* $\Delta cyaA$ mutant strain, which exhibited severely reduced vegetative growth (Voisey et al. 2007). The possibility of a severely reduced hyphal growth-rate was considered and potential transformants were diluted and were spread onto multiple plates to prevent overgrowth by transformants with ectopically integrated antibiotic resistance. Given mutants lacking the high affinity PDE or both PDEs in *M. oryzae* and *B. cinerea* were defective in hyphal stress-recovery and germination (Ramanujam and Naqvi 2010, Zhang et al. 2011, Harren et al. 2013), it is also possible that potential transformants of the *E. festucae* $\Delta pdeL\Delta pdeH$ mutant strain failed to regenerate after transformation. It may be possible to more readily isolate the *E. festucae* $\Delta pdeL\Delta pdeH$ double deletion mutant using alternative methods such as CRISPR-Cas technology (Nødvig et al. 2015). A $\Delta pdeL\Delta pdeH$ double deletion was mimicked by chemical inhibition of PDE activity in the wild-type and both single mutant strains, which showed an $\Delta pdeL$ mutant-like phenotype, with increasing reduced hyphal growth correlated to the concentration of PDE inhibitors used. However, levels of cAMP in the $\Delta pdeL$ mutant strain after transfer onto nutrient-poor medium were slightly reduced when

compared to the cAMP levels on nutrient-rich medium. This indicates that PdeH partially complements the function of PdeL in the $\Delta pdeL$ mutant background.

In summary, the two PDEs PdeL and PdeH fulfil distinct roles in modulating cellular cAMP levels in *E. festucae*, depending on the stage of hyphal growth and signals that activate the cAMP/PKA signalling pathway. While PdeL has an important role in regulating cAMP levels in cellular processes such as hyphal growth, nutrient sensing and cellular differentiation in asexual development, it seems to be dispensable for maintaining a symbiotic association with the host plant. This indicates that PdeL functions primarily in vegetative growth and nutrient-induced cAMP/PKA signalling in culture and regulation of the basal levels of intracellular cAMP in the cell. PdeL potentially has a more accessory role to PdeH or has a rather ancestral function for hyphal growth and development, because *E. festucae* exclusively growth in association with the host apart from laboratory conditions. However, gene expression or further analysis on epiphyllous hyphae or within stromata structures could identify an alternative role for PdeL. While dispensable for growth in culture, PdeH is crucial for maintenance of restricted endophytic growth *in planta*, highlighting the importance of the cAMP/PKA signalling pathway in this process.

Neither the $\Delta pdeL$ nor the $\Delta pdeH$ mutant strain exhibited increased sensitivity to extracellular stress in cultures. However, the cellular phenotype of the $\Delta pdeH$ mutant strain exhibited abnormal cell-wall structures *in planta*, which were also observed for the $\Delta gpr1b$ mutant, indicative of an alteration in the cell-wall composition. Biosynthesis and repair of the cell wall in response to environmental stress is regulated by the cell-wall integrity (CWI) mitogen-activated protein kinase (MAPK) pathway (reviewed in Fuchs and Mylonakis 2009). In *E. festucae*, mutants lacking components of the CWI MAPK, $\Delta mpkA$ and $\Delta mkkA$, exhibited a similar cellular phenotype in association with *L. perenne*, including unrestricted growth, colonisation of the vascular bundles, host stunting and a modified cell-wall structure (Becker et al. 2015). In *E. festucae*, it was shown that the CWI MAPK pathway is essential for establishment and maintenance of the mutualistic host-endophyte interaction (Becker et al. 2015, Green et al. 2016). Mutants in this pathway share common phenotypes including defects in hyphal anastomosis, an essential requirement for maintaining a mutualistic *E. festucae*-ryegrass association (Green et al. 2016). In filamentous fungi, the CWI MAPK pathway is involved in various

cellular processes such as conidiation, appressorium development, plant infection and pathogenic development, cell differentiation in sexual development and hyphal fusion (Birkaya et al. 2009, Fuchs and Mylonakis 2009, Malavazi et al. 2014, Zhang et al. 2015). In contrast to other fungi, the $\Delta mkkA$ and $\Delta mpkA$ mutant strains in *E. festucae* exhibit no increased sensitivity to extracellular stress in culture including the cell-wall stress agents Congo red and calcofluor white, similar to the $\Delta pdeH$ and $\Delta gpr1b$ mutants (Becker et al. 2015). The common phenotypes for mutants of the CWI MAPK and the cAMP/PKA signalling pathway, both equally important to maintain the mutualistic association, indicate both are required. The connection between CWI MAPK and cAMP/PKA signalling pathway has been described in a number of fungi including *C. neoformans*, *U. maydis*, *C. albicans* and *M. oryzae*, where changes in cell-wall composition for mutants of the CWI MAPK pathway as well as for strains lacking the high-affinity PDE of the cAMP/PKA signalling pathway was described (Hamel et al. 2012, Donlin et al. 2014, Zhang et al. 2015, Yin et al. 2016). Deletion of the high affinity PDE CaPde2 resulted in defects in the cell-wall and membrane, causing greater susceptibility to various extracellular stresses (Jung et al. 2005). In *C. neoformans* and *U. maydis*, transcriptional profiling showed downregulation of multiple components of cell-wall biosynthesis in mutants of both pathways (Donlin et al. 2014). In addition, these mutants showed reduced levels of cAMP and phenotypes could be partially restored after addition of exogenous cAMP (Donlin et al. 2014). More recently, physical and functional interaction between the high affinity PDE MoPdeH of the cAMP/PKA signalling pathway and the CWI pathway MAPK MoMckA in *M. oryzae* was shown, indicating conserved cross-talk between these two signalling pathways (Yin et al. 2016). This signalling cross-talk is also likely to occur in *E. festucae*, indicated by the overlapping phenotypes in association with the host (Becker et al. 2015). Protein interaction analysis and comparative global transcriptome profiling with overlapping target enzymes would be required to support a conserved connection between the CWI MAPK and cAMP/PKA signalling pathways.

6.2.2 The potential role of cAMP signalling in expressoria development

Although, development of expressoria of the $\Delta pdeH$ mutants have not been analysed in detail, preliminary analysis using TEM indicates that the ability to form expressoria was not impaired. However, the increased number of epiphyllous hyphae and the accumulation of hyphal bundles under the plant cuticle that occasionally rupture the cuticle layer correlated with the increased fungal biomass, suggests a reduction of expressoria structures or delayed formation. Observations made by TEM indicated an increased number of epiphyllous hyphae and hyphal accumulation underneath the cuticle layer for the $\Delta gpr1b$ and the $\Delta sidN$ mutant strains, although no expressoria structures were observed in this mutant (Johnson et al. 2013). Expressoria are cellular structures that endophytic hyphae develop to exit the host plant for epiphyllous growth (Becker et al. 2016). For signal and nutrient exchange, the epiphyllous hyphae stay connected to the endophytic hyphal network. The cellular differentiation processes to initiate expressoria formation and specific components involved in this have yet to be identified. A strong reduction in appressoria formation was described in *M. oryzae* and *B. cinerea* for mutants lacking the high affinity PDE (Ramanujam and Naqvi 2010, Zhang et al. 2011, Harren et al. 2013). In both organisms, a defective morphological switch led to reduced or impaired pathogenic development in two steps; formation of appressoria structures from germ tubes and differentiation of these structures to invasive hyphae after penetration. Involvement in specific host-surface sensing was found to be associated with the high affinity PDEs in *M. oryzae* and *B. cinerea* (Ramanujam and Naqvi 2010, Zhang et al. 2011, Harren et al. 2013). After perception of specific host-derived signals through the Pth11 receptor in *M. oryzae*, the cAMP/PKA signalling pathway mediates cellular differentiation that leads to the initiation of appressorium development, a process regulated by the high affinity PDE MoPdeH (DeZwaan et al. 1999, Kulkarni et al. 2005, Ramanujam and Naqvi 2010, Zhang et al. 2011). After host penetration, a second cellular differentiation process enables invasive growth, again mediated by cAMP/PKA signalling pathway and regulated by MoPdeH (Zhang et al. 2011). Similar cellular differentiation occurs in the pathogenic development and penetration process of *B. cinerea*, also mediated by cAMP/PKA signalling pathway and regulated by BcPde2 (Harren et al. 2013). Although,

appressoria and expressoria are fundamentally and functionally distinct cellular structures, both require cellular differentiation initiated by unknown factors, potentially from the plant host. Based on conserved functions in filamentous fungi and common phenotypes, it is likely that the cAMP/PKA signalling pathway, including Gpr1b and PdeH, is involved in the cellular differentiation process leading to expressoria formation in *E. festucae*. To support this hypothesis, a detailed microscopic analysis including determination of cellular localisation of the Gpr1b and PdeH is required.

Mutants of the NADPH oxidase (Nox) complex in *E. festucae* were analysed in detail for expressoria development and shown to form a hyphal network underneath the plant cuticle layer, impaired in formation of expressoria (Becker et al. 2016). In filamentous fungi, the production of reactive oxygen species (ROS) as signalling molecules by the Nox complex is essential for polarised growth and hyphal orientation (Tanaka et al. 2006, Eaton et al. 2010, Scott et al. 2012, Kayano et al. 2013, Becker et al. 2016). Apart from the impaired hyphal fusion phenotype, Nox mutants share common phenotypes *in planta* with $\Delta pdeH$ and $\Delta gpr1b$, indicative of connected functions between the two pathways. Further, ryegrass plants infected with the $\Delta sidN$ deletion mutant strain revealed a similar plant interaction phenotype (Johnson et al. 2013). The high-affinity siderophore synthetase (NRPS), SidN, mediates iron uptake and regulation of cellular iron homeostasis (Haas 2003, Johnson et al. 2013). Generation and the detoxification of ROS requires iron-containing heme as a cofactor for catalase and peroxidase-activity (Schrettl et al. 2007, Chung 2012). Cellular iron acquisition and the generation of ROS as signalling molecules are connected processes, both shown to be crucial for maintenance of the *E. festucae*-ryegrass interaction (Eaton et al. 2010, Scott et al. 2012, Johnson et al. 2013). Despite there being no direct evidence increased hyphal branching and the disorientation of hyphal growth of the $\Delta sidN$ mutant strains *in planta* connects fungal ROS-production with the high-affinity iron-uptake system (Scott and Eaton 2008, Johnson et al. 2013). Even though, expressoria formation was not analysed in $\Delta sidN$ mutants, the common plant interaction phenotype between mutants of the Nox complex, $\Delta sidN$, $\Delta gpr1b$ and $\Delta pdeH$ suggests signalling cross-talk (Johnson et al. 2013, Becker et al. 2016). In addition, a phenotype of unrestricted growth and increased lateral branching *in planta* was similarly described for $\Delta sidN$ and for the mutant strain lacking adenylate cyclase

activity, *ΔacyA*, which further exhibited alteration in ROS signalling (Voisey et al. 2007, Johnson et al. 2013, Voisey pers. com). The connection between ROS- and cAMP-dependent signalling is well described in fungi (reviewed in Fuller and Rhodes 2012, Chung 2012). Defects in restricted hyphal growth and vascular bundle colonisation of the *ΔnoxA*, *Δgpr1b* and *ΔpdeH* mutant suggests a functional connection (Tanaka et al. 2008, Scott et al. 2012). Common plant interaction phenotypes between mutants of the Nox complex, the *ΔsidN* mutant strain and components of the cAMP/PKA signalling pathway indicates cross-talk between these signalling pathways. However, further research is required to support this hypothesis. Cross-talk between iron acquisition and cAMP/PKA signalling was shown in the human pathogen *C. neoformans* and in the phytopathogen *U. maydis*, where overlapping target enzymes of both pathways were identified using comparative transcriptomic profiling (Kronstad et al. 2011, Choi et al. 2015, Jung et al. 2015, Maier et al. 2015). A similar approach is required to identify target enzymes specifically regulated by the cAMP/PKA signalling pathway as well as overlapping target enzymes shared with other pathways to determine signalling cross-talk.

6.3 Conclusion

The ability of organisms to adapt to changes in the environment depends on sensitive cellular responses, triggered through various signalling cascades. In filamentous fungi, perception of extracellular stimuli is primarily mediated through GPCRs and the G-protein signalling pathway. GPCRs are highly diverse, a necessary feature to provide high ligand-specificity of individual receptors that in turn provide for adaptation to specific environmental changes. This is especially so in symbiotic fungi whose life-style requires host interaction. In phytopathogenic or mutualistic fungi, evolutionary adaptation through gene duplication, including genes encoding GPCRs, enable adjustment to the host. In this study 40 GPCRs were identified in the genome of the mutualistic ryegrass-endophyte *E. festucae*, and these categorised into 13 of the 14 GPCR classes currently recognised by the fungal classification system. Among these GPCRs, only a few were transcriptionally upregulated in association with the host, a response indicative of a specific function within the host. Signalling through the cAMP/PKA signalling pathway, triggered through specific

GPCRs, is crucial for a normal interaction with the host, regulating various cellular and developmental processes. *E. festucae* possesses three cAMP-associated GPCRs Gpr1a, Gpr1b and Gpr2 of the cAMP receptor-like class, from which Gpr1b and Gpr2 are significantly upregulated *in planta*. Both Gpr1b and Gpr2 are dispensable in culture and, while the role of Gpr2 in association with the host remains unknown, the deletion of *gpr1b* resulted in a severe plant interaction phenotype. Gpr1b is crucial for perception of plant-specific signals involved in maintenance of the restricted endophytic growth. The cAMP-dependent signalling is regulated by phosphodiesterases that terminate the signalling cascade and maintain cellular cAMP-homeostasis. The *E. festucae* PDEs PdeL and PdeH, with low and high affinity towards cAMP, respectively, have distinct functions in the cell. While PdeL modulates cellular cAMP levels in processes like hyphal growth, cellular differentiation in asexual development and nutrient sensing in culture, it is dispensable *in planta*. In contrast, PdeH regulates the cellular cAMP levels in association with perennial ryegrass. Deletion of *pdeH*, causes unrestricted growth *in planta* and a severe plant interaction phenotype. Pleiotropic phenotypes suggest that Gpr1b and PdeH act both in the cAMP/PKA signalling pathway, triggered by signals to maintain restricted growth *in planta*. Unlike other *E. festucae* mutants with similar severe plant interaction phenotype, hyphae of the $\Delta gpr1b$ and $\Delta pdeH$ mutant strains are still capable of hyphal fusion. In parallel to the recently described CWI MAPK signalling complex, the cAMP/PKA signalling pathway also plays a crucial role in establishment and maintenance of the mutualistic *E. festucae* - *L. perenne* association.

Based on the key results obtained in this study, the following cascade of events are concluded (Fig. 6.1). Specific plant-derived molecules when perceived by the fungal GPCR Gpr1b triggers activation of the heterotrimeric G-protein from which the G-alpha subunit activates the adenylate cyclase to synthesise intracellular cAMP. Once a threshold level of cellular cAMP is reached, it binds to the regulatory subunit of protein kinase A (PKA) to release the catalytic subunits from the tetrameric holoenzyme. The catalytic PKA subunits subsequently phosphorylate various target enzymes and transcription factors.

These target enzymes, which are yet to be identified, initiate cellular processes that putatively result in restricted endophytic growth by either inhibiting processes that promote apical expansion or activating cellular differentiation leading to intercalary growth. The maintenance of this process is dependent on a balanced level of cAMP that is modulated through PdeH in a regulatory negative feedback loop. The balanced level of cAMP keeps this intrinsic signal active, while fluctuations alter the functional and transcriptomal outcome. Therefore, the cAMP/PKA signalling pathway in combination with other signalling pathways maintain the restricted hyphal growth within the plant.

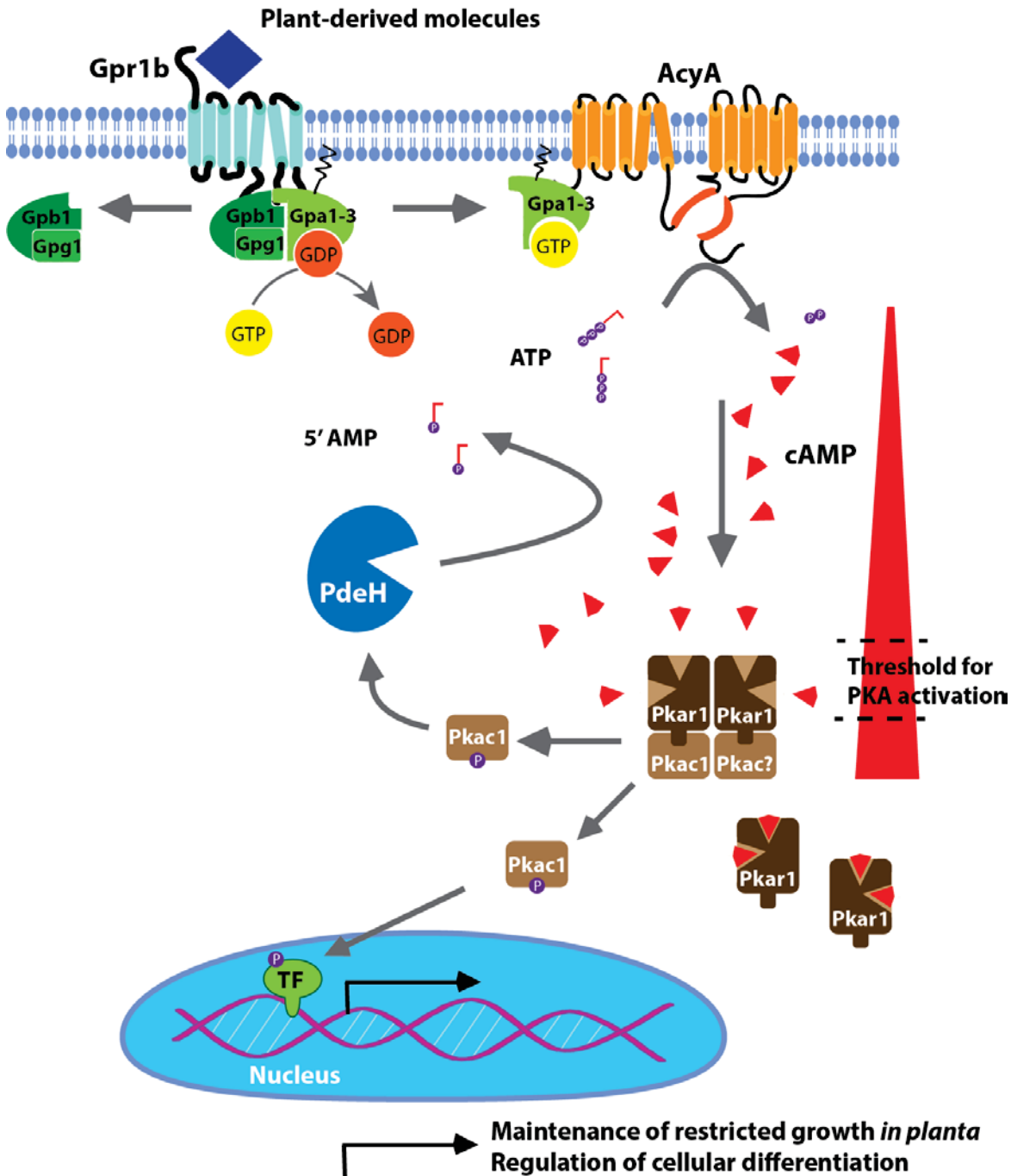


Figure 6-1 The fungal G protein and cAMP pathway in association with the host. The GPCR Gpr1b perceives extracellular molecules, putatively derived from the host plant and transmits this signal through a conformational change to the intracellular heterotrimeric G protein. GEF function of the receptor triggers the exchange of GDP to GTP in the Gα subunit (Gpa1, Gpa2 or Gpa3), which dissociates from the heterotrimer and activates the adenylate cyclase AcyA, while the Gpb1/Gpg1 (Gβ/Gγ)-dimer putatively activates other pathways. AcyA synthesises cAMP from ATP, which in turn binds to the regulatory PKA subunit (Pkar1) once a certain threshold is reached. Activation of the PKA tetramer triggers dissociation of the catalytic PKA subunits (Pkc1, Pkc?), that activates several downstream transcription factors (TF) which regulate the maintenance of the restricted hyphal growth *in planta*. Crucial for this process is the stable concentration of the intracellular levels of cAMP, which is modulated by the high affinity phosphodiesterase PdeH.

Further analysis is required to support this hypothesis and to determine the intracellular interaction with the particular G α - (Gpa1, Gpa2 or Gpa3) and the G β / γ -subunit (Gpr1b and Gpg1) of the heterotrimeric G protein, to determine target enzymes of the cAMP/PKA signalling pathway and functional cross-talk with other pathways. The analysis of the cellular localisation of Gpr1b, Gpr2, PdeH and PdeL, the functional characterisation of Gpr1a, protein-protein interaction studies of the individual components, identification of specific ligands for Gpr1b and transcriptional profiling of the individual mutant strains could provide more insight into the specific role of the cAMP/PKA signalling pathway in *E. festucae*.

Chapter 7 Appendices

Appendix 1: Table of genes used in this study

<i>Neurosopra crassa</i> (OR74A)			
	Name	Locus Identifier	GenBank accession number
Nc	<i>pre2</i>	NCU05758	XM_954640
Nc	<i>pre1</i>	NCU00138	XM_951098
Nc	<i>gpr4</i>	NCU06312	XM_957481
Nc	<i>gpr5</i>	NCU00300	XM_952678
Nc	<i>gpr6</i>	NCU09195	XM_954046
Nc	<i>gpr1</i>	NCU00786	XM_959849
Nc	<i>gpr2</i>	NCU04626	XM_952851
Nc	<i>gpr3</i>	NCU09427	XM_952894
Nc	<i>gpr7</i>	NCU09883	XM_953557
Nc	<i>gpr8</i>	NCU03253	XM_959313
Nc	<i>gpr9</i>	NCU03238	XM_011394820
Nc	<i>gpr10</i>	NCU04987	XM_952920
Nc	<i>nop1</i>	NCU10055	XM_954328
Nc	<i>orpA</i>	NCU01735	XM_011395195
Nc	<i>gpr11</i>	NCU00182	XM_951312
Nc	<i>gpr12</i>	NCU00005	XM_951899
Nc	<i>gpr13</i>	NCU06629	XM_956724
Nc	<i>gpr14</i>	NCU06987	XM_957534
Nc	<i>gpr15</i>	NCU00700	XM_011394517
Nc	<i>gpr16</i>	NCU02903	XM_960492
Nc	<i>gpr17</i>	NCU04106	XM_011396313
Nc	<i>gpr18</i>	NCU04931	XM_954286
Nc	<i>gpr19</i>	NCU05101	XM_951994
Nc	<i>gpr20</i>	NCU05187	XM_011395829
Nc	<i>gpr21</i>	NCU05189	XM_957095
Nc	<i>gpr22</i>	NCU05307	XM_956985
Nc	<i>gpr23</i>	NCU05829	XM_954996
Nc	<i>gpr24</i>	NCU05854	XM_011396911
Nc	<i>gpr25</i>	NCU06531	XM_956710
Nc	<i>gpr26</i>	NCU17171	XM_011397048
Nc	<i>gpr27</i>	NCU07538	XM_953958
Nc	<i>gpr28</i>	NCU16721	XM_011396050

Nc	<i>gpr29</i>	NCU07649	XM_957639
Nc	<i>gpr30</i>	NCU07769	XM_953170
Nc	<i>gpr31</i>	NCU08429	XM_958306
Nc	<i>gpr32</i>	NCU08431	XM_958308
Nc	<i>gpr33</i>	NCU08447	XM_958197
Nc	<i>gpr34</i>	NCU08624	XM_959739
Nc	<i>gpr35</i>	NCU08718	XM_958486
Nc	<i>gpr36</i>	NCU09022	XM_953876
Nc	<i>gpr37</i>	NCU09201	XM_954052
Nc	<i>gpr38</i>	NCU09796	XM_955101
Nc	<i>gpr9b</i>	NCU08283	XM_9567162
Nc	<i>gpr39</i>	NCU09823	XM_953429
Nc	<i>gpr9b</i>	NCU08283	XM_9567162
Nc	<i>gna-1</i>	NCU06493	XM_952040
Nc	<i>gna-2</i>	NCU06729	XM_011396408
Nc	<i>gna-3</i>	NCU05206	XM_957112
Nc	<i>gnb-1</i>	NCU00440	XM_951611
Nc	<i>gng-1</i>	NCU00041	XM_951059
Nc	<i>ric8</i>	NCU02788	XM_958851
Nc	<i>cr-1</i>	NCU08377	XM_011394895
Nc	<i>pkac1</i>	NCU06240	XM_957998
Nc	<i>pkar1</i>	NCU01166	XM_011396176
Nc	<i>pde2</i>	NCU00478	XP_011393859
Nc	<i>pde1</i>	NCU00237	XP_957708

***Magnaporthe oryzae* (70-15)**

	Name	Locus Identifier	GenBank accession number
Mo	<i>Ste2</i>	MGG_04711	XM_003710778
Mo	<i>Ste1</i>	MGG_06452	XM_003717066
Mo	<i>gpr4</i>	MGG_08803	XM_003719120
Mo	<i>gpr5</i>	MGG_04698	XM_003713629
Mo	<i>gpr6</i>	MGG_02855	XM_003720832
Mo	<i>gpr1</i>	MGG_11962	XM_003709032
Mo	<i>gpr2</i>	MGG_06738	XM_003709404
Mo	<i>gpr7a</i>	MGG_13926	XM_003713158
Mo	<i>gpr7b</i>	MGG_11693	XM_003719067

Mo	<i>gpr8</i>	MGG_00532	XM_003718476
Mo	<i>gpr9</i>	MGG_04679	XM_003710809
Mo	<i>gpr10</i>	MGG_16855	XM_003712539
Mo	<i>gpr10b</i>	MGG_09091	XM_003711150
Mo	<i>ops1</i>	MGG_09015	XM_003721277
Mo	<i>gpr11</i>	MGG_06418	XM_003717102
Mo	<i>gpr12</i>	MGG_05269	XM_003712779
Mo	<i>gpr13a</i>	MGG_07414	XM_003711251
Mo	<i>gpr13b</i>	MGG_06103	XM_003711920
Mo	<i>gpr14a</i>	MGG_01467	XM_003714376
Mo	<i>gpr14b</i>	MGG_15321	XM_003714689
Mo	<i>pth11</i>	MGG_05871	XP_003711700
	<i>pth11-like</i>	MGG_10473	XP_003713375
	<i>pth11-like</i>	MGG_06755	XP_003709469
	<i>pth11-like</i>	MGG_07553	XP_003711467
	<i>pth11-like</i>	MGG_09022	XP_003721317
	<i>pth1-like</i>	MGG_07565	XP_003711480
	<i>pth11-like</i>	MGG_11006	XP_003717718
	<i>pth11-like</i>	MGG_09070	XP_003711172
	<i>pth11-like</i>	MGG_07806	XP_003713023
	<i>pth11-like</i>	MGG_03584	XP_003716326
	<i>pth11-like</i>	MGG_05214	XP_003712761
	<i>pth11-like</i>	MGG_09863	XP_003720372
	<i>pth11-like</i>	MGG_10407	XP_003719425
	<i>pth11-like</i>	MGG_10571	XP_003721381
	<i>pth11-like</i>	MGG_01867	XP_003714888
	<i>pth11-like</i>	MGG_10050	XP_003717456
	<i>pth11-like</i>	MGG_09667	XP_003721422
	<i>pth11-like</i>	MGG_05352	XP_003710192
	<i>pth11-like</i>	MGG_07420	XP_003711305
	<i>pth11-like</i>	MGG_10442	XP_003713344
	<i>pth11-like</i>	MGG_02160	XP_003713344
	<i>pth11-like</i>	MGG_02160	XP_003708932
	<i>pth11-like</i>	MGG_02001	XP_003708744
	<i>pth11-like</i>	MGG_10257	XP_016846028
	<i>pth11-like</i>	MGG_01905	XP_003719354

<i>Pth11-like</i>	MGG_07987	XP_003714940
<i>pth11-like</i>	MGG_10438	XP_003713338
<i>pth11-like</i>	MGG_06171	XP_003712052
<i>pth11-like</i>	MGG_07851	XP_003713085
<i>pth11-like</i>	MGG_04935	XP_003712427
<i>pth11-like</i>	MGG_05386	XP_003710240
<i>pth11-like</i>	MGG_09865	XP_003720369
<i>pth11-like</i>	MGG_09061	XP_003721286
<i>pth11-like</i>	MGG_05514	XP_003710379
<i>pth11-like</i>	MGG_06535	XP_003717009
<i>pth11-like</i>	MGG_01190	XP_003714078
<i>pth11-like</i>	MGG_10581	XP_003721370
<i>pth11-like</i>	MGG_03009	XP_003720681
<i>pth11-like</i>	MGG_10747	XP_003713284
<i>pth11-like</i>	MGG_03935	XP_003719929
<i>pth11-like</i>	MGG_09416	XP_003720188
<i>pth11-like</i>	MGG_02692	XP_003721073
<i>pth11-like</i>	MGG_04682	XP_003710850
<i>pth11-like</i>	MGG_07857	XP_003713093
<i>pth11-like</i>	MGG_00826	XP_003718157
<i>pth11-like</i>	MGG_06624	XP_003716903
<i>pth11-like</i>	MGG_00435	XP_003718634
<i>pth11-like</i>	MGG_08653	XP_003711085
<i>pth11-like</i>	MGG_10706	XP_003720337
<i>pth11-like</i>	MGG_04170	XP_003719657
<i>pth11-like</i>	MGG_08525	XP_003716028
<i>pth11-like</i>	MGG_00277	XP_003718820
<i>pth11-like</i>	MGG_06595	XP_003716934
<i>pth11-like</i>	MGG_06084	XP_003711949
<i>pth11-like</i>	MGG_09437	XP_003720167
<i>pth11-like</i>	MGG_01890	XP_003714911
<i>pth11-like</i>	MGG_03794	XP_003720098
<i>pth11-like</i>	MGG_00532	XP_003718524
Mo <i>gpr9b</i>	MGG_01538	XM_003714463
Mo <i>mgpa1</i>	MGG_00365	XM_003718667
Mo <i>mgpa2</i>	MGG_04204	XM_003719569

Mo	<i>mgpa3</i>	MGG_01818	XM_003714783
Mo	<i>mgbp1</i>	MGG_05201	XM_003712698
Mo	<i>mgpg1</i>	MGG_10193	XM_003713775
Mo	<i>ric8</i>	MGG_14008	XM_003716081
Mo	<i>mac</i>	MGG_09898	XM_003709944
Mo	<i>pkac1</i>	MGG_06368	XM_003717158
Mo	<i>sum1</i>	MGG_07335	XM_003715524
Mo	<i>pdeH</i>	MGG_05664	XP_003710562
Mo	<i>pdeL</i>	MGG_07707	XP_003712910

***Fusarium graminearum* (PH-1)**

	Name	Locus Identifier	GenBank accession number
Fg	<i>pre2</i>	FGSG_02655	XM_011320304
Fg	<i>pre1</i>	FGSG_07270	XM_011328706
Fg	<i>gprC</i>	FGSG_05006	XM_011325185
Fg	<i>gpr5</i>	FGSG_05579	XM_011325830
Fg	<i>gpr6</i>	FGSG_08496	XM_011321964
Fg	<i>gpr1</i>	FGSG_09693	XM_011329710
Fg	<i>gpr2</i>	FGSG_05239	XM_011325448
Fg	<i>gpr3</i>	FGSG_01861	XM_011319407
Fg	<i>gpr4</i>	FGSG_07716	XM_011329216
Fg	<i>gpr5</i>	FGSG_03023	XM_011324461
Fg	<i>gpr7a</i>	FGSG_04628	XM_011322643
Fg	<i>gpr7b</i>	FGSG_05425	XM_011325659
Fg	<i>gpr8</i>	FGSG_00527	XM_011317901
Fg	<i>gpr9</i>	FGSG_01064	XM_011318519
Fg	<i>gpr10</i>	FGSG_04051	XM_011323300
Fg	<i>ops1</i>	FGSG_03064	XM_011324414
Fg	<i>ops2</i>	FGSG_01440	XM_011318943
Fg	<i>ops3</i>	FGSG_07554	XM_011329031
Fg	<i>gpr11a</i>	FGSG_05404	XM_011325633
Fg	<i>gpr11b</i>	FGSG_07166	XM_011328582
Fg	<i>gpr13</i>	FGSG_09814	XM_011329570
Fg	<i>gpr14a</i>	FGSG_09576	XM_011329833
Fg	<i>gpr14b</i>	FGSG_03059	XM_011324420
Fg	<i>gpr9b</i>	FGSG09798	XM_011329588

Fg <i>fga1</i>	FGSG_05535	XM_011325781
Fg <i>fga2</i>	FGSG_09988	XM_011320598
Fg <i>fga3</i>	FGSG_09614	XM_011329792
Fg <i>fgb1</i>	FGSG_04104	XM_011323230
Fg <i>fgg1</i>	FGSG_07235	XM_011328668
Fg <i>ric8</i>	FGSG_01511	XM_011319018
Fg <i>fgac</i>	FGSG_01234	XM_011318707
Fg <i>pkac1</i>	FGSG_07251	XM_011328687
Fg <i>pkar1</i>	FGSG_09908	XM_011320512
Fg <i>pdeH</i>	FGSG_06914	XP_011326581
Fg <i>pdeL</i>	FGSG_06633	XP_011326256

***Trichoderma atroviride* (IMI 206040)**

	Name	Locus Identifier	GenBank accession number
Ta	<i>pre2</i>	TRIATDRAFT_147894	XM_014086371
Ta	<i>pre1</i>	TRIATDRAFT_147894	XM_014084086
Ta	<i>gprC</i>	TRIATDRAFT_246916	XM_014085678
Ta	<i>gpr5</i>	TRIATDRAFT_238619	XM_014090304
Ta	<i>gpr6</i>	TRIATDRAFT_300620	XM_014087116
Ta	<i>gpr1</i>	TRIATDRAFT_160995	XM_014082089
Ta	<i>gpr2</i>	TRIATDRAFT_50902	XM_014092365
Ta	<i>gpr3</i>	TRIATDRAFT_83166	XM_014092499
Ta	<i>gpr4</i>	TRIATDRAFT_81233	XM_014093068
Ta	<i>gpr7a</i>	TRIATDRAFT_40423	XM_014088266
Ta	<i>gpr7b</i>	TRIATDRAFT_293686	XM_014087181
Ta	<i>gpr7c</i>	TRIATDRAFT_210761	XM_014093622
Ta	<i>gpr8</i>	TRIATDRAFT_133045	XM_014090803
Ta	<i>gpr9</i>	TRIATDRAFT_136196	XM_014085001
Ta	<i>gpr10a</i>	TRIATDRAFT_290047	XM_014091966
Ta	<i>gpr10b</i>	TRIATDRAFT_210209	XM_014093824
Ta	<i>gpr10c</i>	TRIATDRAFT_142943	XM_014091042
Ta	<i>gpr10d</i>	TRIATDRAFT_46847	XM_014090582
Ta	<i>gpr10e</i>	TRIATDRAFT_142946	XM_014091043
Ta	<i>gpr10f</i>	TRIATDRAFT_152366	XM_014088889
Ta	<i>ops1</i>	TRIATDRAFT_210598	XM_014093534
Ta	<i>gpr11</i>	TRIATDRAFT_210445	XM_014093707

Ta	<i>gpr12</i>	TRIATDRAFT_93659	XM_014091330
Ta	<i>gpr13</i>	TRIATDRAFT_130836	XM_014086080
Ta	<i>gpr14a</i>	TRIATDRAFT_152316	XM_014088888
Ta	<i>gpr14b</i>	TRIATDRAFT_296436	XM_014083164
Ta	<i>gpr14c</i>	TRIATDRAFT_136442	XM_014086178
Ta	<i>gpr9b</i>	TRIATDRAFT_161784	XM_014085821
Ta	<i>gpa1</i>	TRIATDRAFT_299359	XM_014088485
Ta	<i>gpa2</i>	TRIATDRAFT_301492	XM_014083671
Ta	<i>gpa3</i>	TRIATDRAFT_34532	XM_014085191
Ta	<i>gpb1</i>	TRIATDRAFT_42956	XM_014088918
Ta	<i>gpg1</i>	TRIATDRAFT_259183	XM_014084118
Ta	<i>ric8</i>	TRIATDRAFT_89180	XM_014082703
Ta	<i>ac</i>	TRIATDRAFT_318748	XM_014087939
Ta	<i>pkac1</i>	TRIATDRAFT_164264	XM_014084103
Ta	<i>pkar1</i>	TRIATDRAFT_29552	XM_014083323
Ta	<i>pdeH</i>	TRIATDRAFT_315287	XM_014091596
Ta	<i>pdeL</i>	TRIATDRAFT_31692	XM_014083460

***Aspergillus nidulans* (FGSC A4)**

	Name	Locus Identifier	GenBank accession number
An	<i>gprH</i>	AN8262	XM_676439
An	<i>pdeH</i>	AN2740	XP_660344
An	<i>pdeL</i>	AN0829	XP_658433

***Saccharomyces cerevisiae* (S288c)**

	Name	Locus Identifier	GenBank accession number
Sc	<i>pde2</i>	PDE2p	CAA99689
Sc	<i>pde1</i>	PDE1p	CAA64139; NM_001181114

***Schizosacchomyces pombe* (972h)**

	Name	Locus Identifier	GenBank accession number
Sp	<i>pde1</i>	Cgs2	NM_001023328

***Candida albicans* (SC5314)**

	Name	Locus Identifier	GenBank accession number
Ca	<i>pde2</i>	PDE2	AAM89252
Ca	<i>pde1</i>	PDE1	XP_720545

Cryptococcus neoformans var. grubii

	Name	Locus Identifier	GenBank accession number
Cn	<i>pde2</i>	PDE2	AY874131
Cn	<i>pde1</i>	PDE1	AY864841

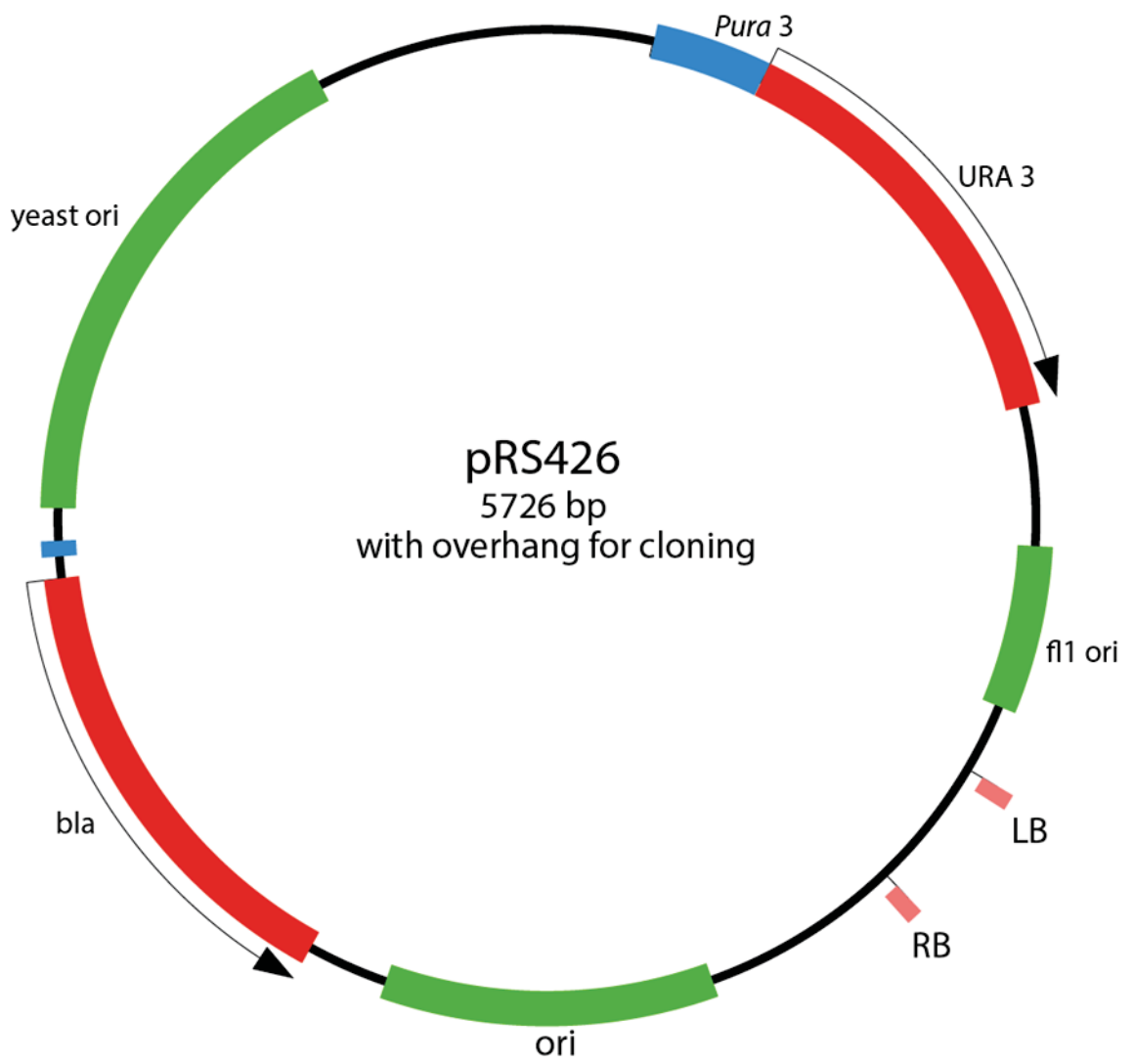
***Metarhizium acridum* (CQMa 102)**

	Name	Locus Identifier	GenBank accession number
Mac	<i>gpr1a</i>	MAC_03969	XM_007812118
Mac	<i>gpr1b</i>	MAC_01277	XM_007809426
Mac	<i>gpr2a</i>	MAC_08590	XM_007816739
Mac	<i>gpr2b</i>	MAC_02892	XM_007811041
Mac	<i>gpr3</i>	MAC_08966	XM_007817115

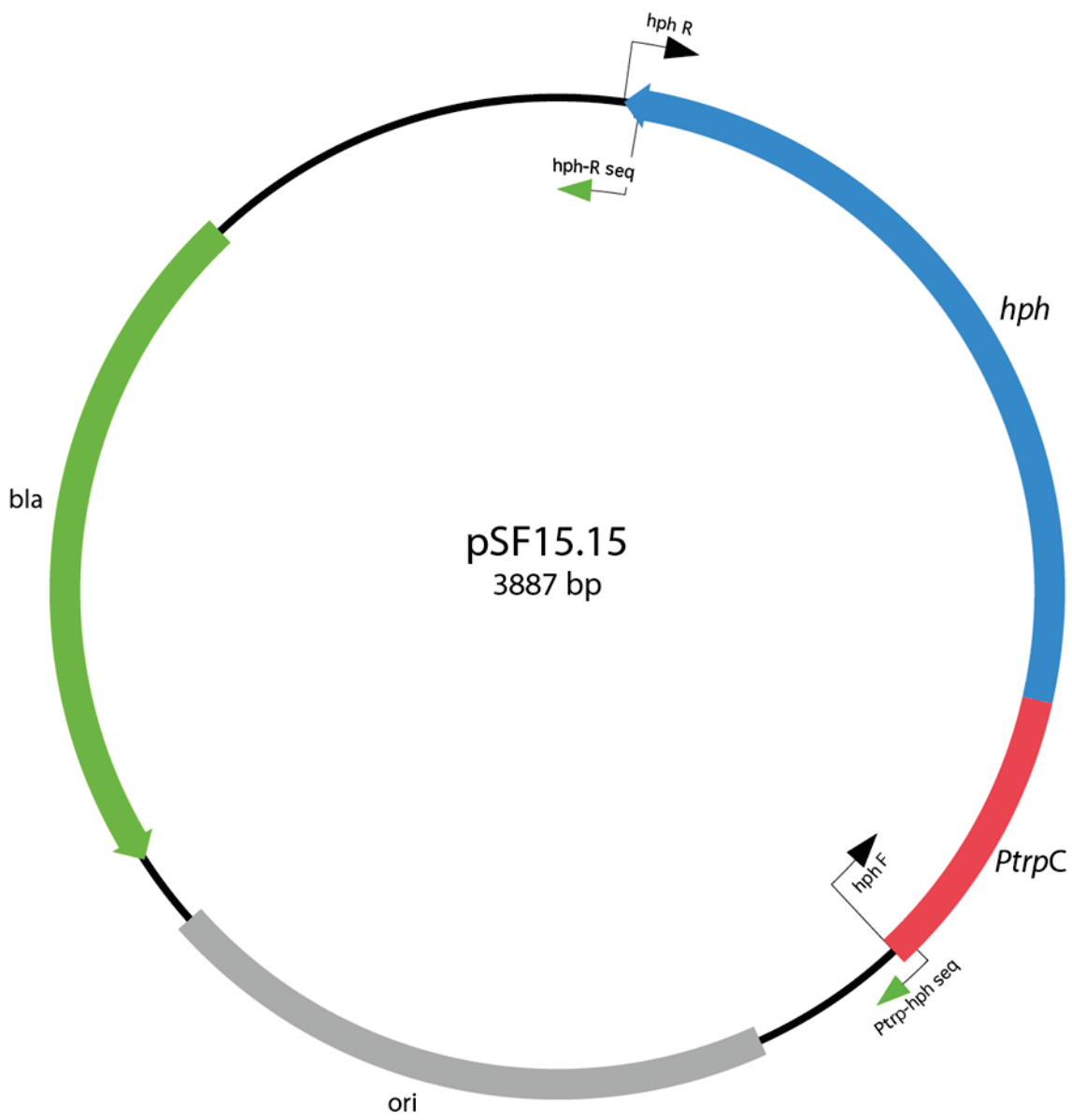
***Metarhizium robertsii* (ARSEF 23)**

	Name	Locus Identifier	GenBank accession number
Mrob	<i>gpr1a</i>	MAA_07004	XM_007825002
Mrob	<i>gpr1b</i>	MAA_06299	XM_007824297
Mrob	<i>gpr2a</i>	MAA_10964	XM_011412909
Mrob	<i>gpr2b</i>	MAA_01664	XM_007819662
Mrob	<i>gpr3</i>	MAA_09921	XM_007827919

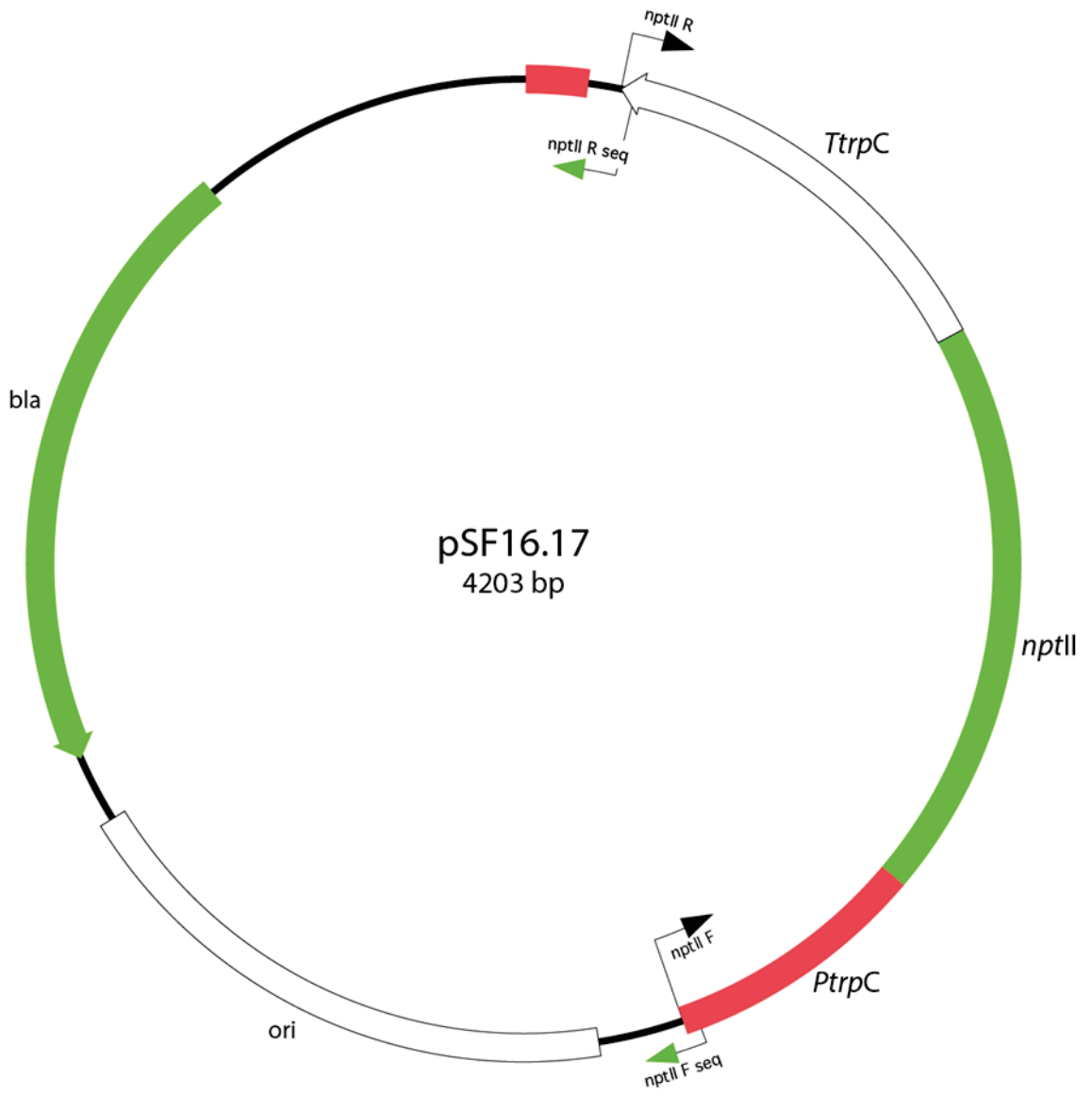
Appendix 2: Plasmid map of pRS426



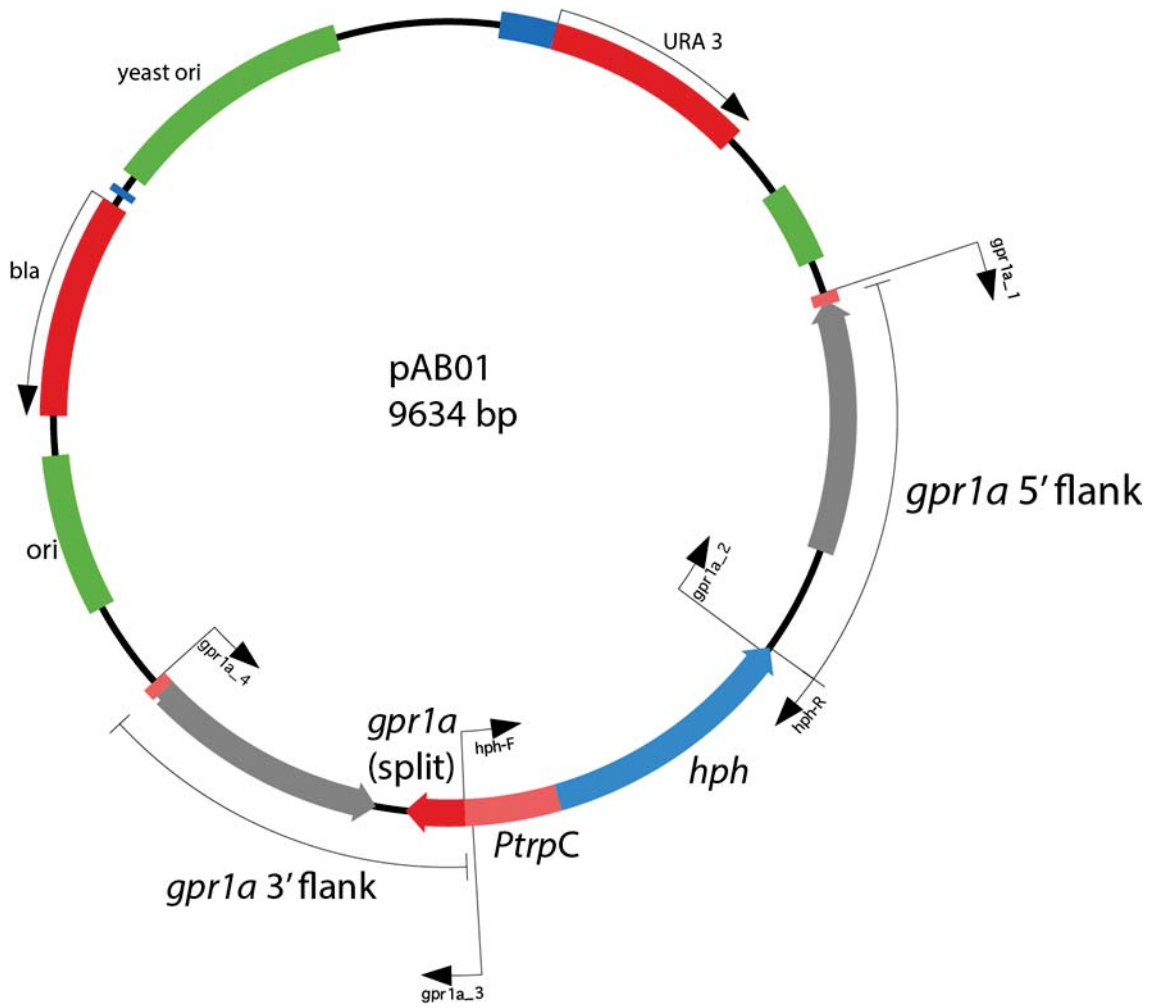
Appendix 3: Plasmid map of pSF15.15



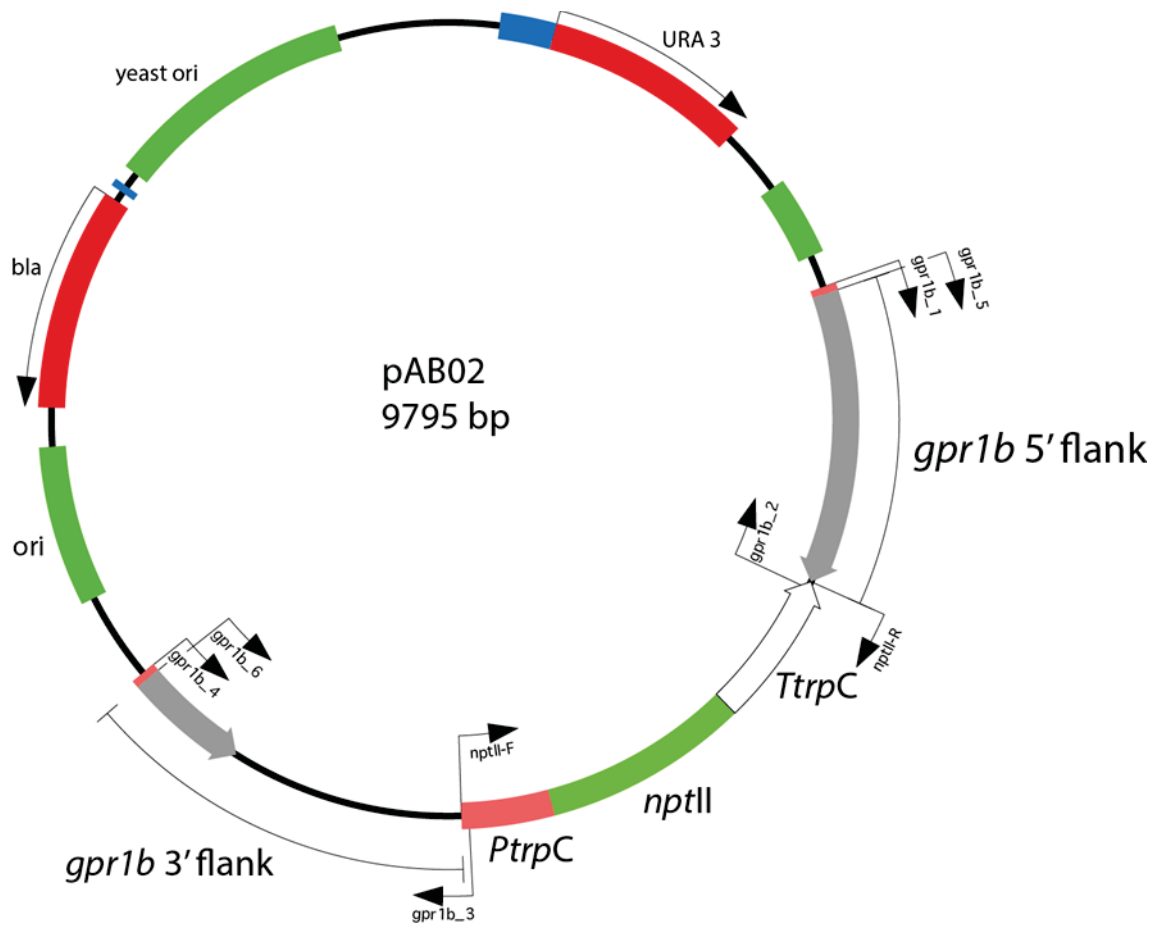
Appendix 4: Plasmid map of pSF16.17



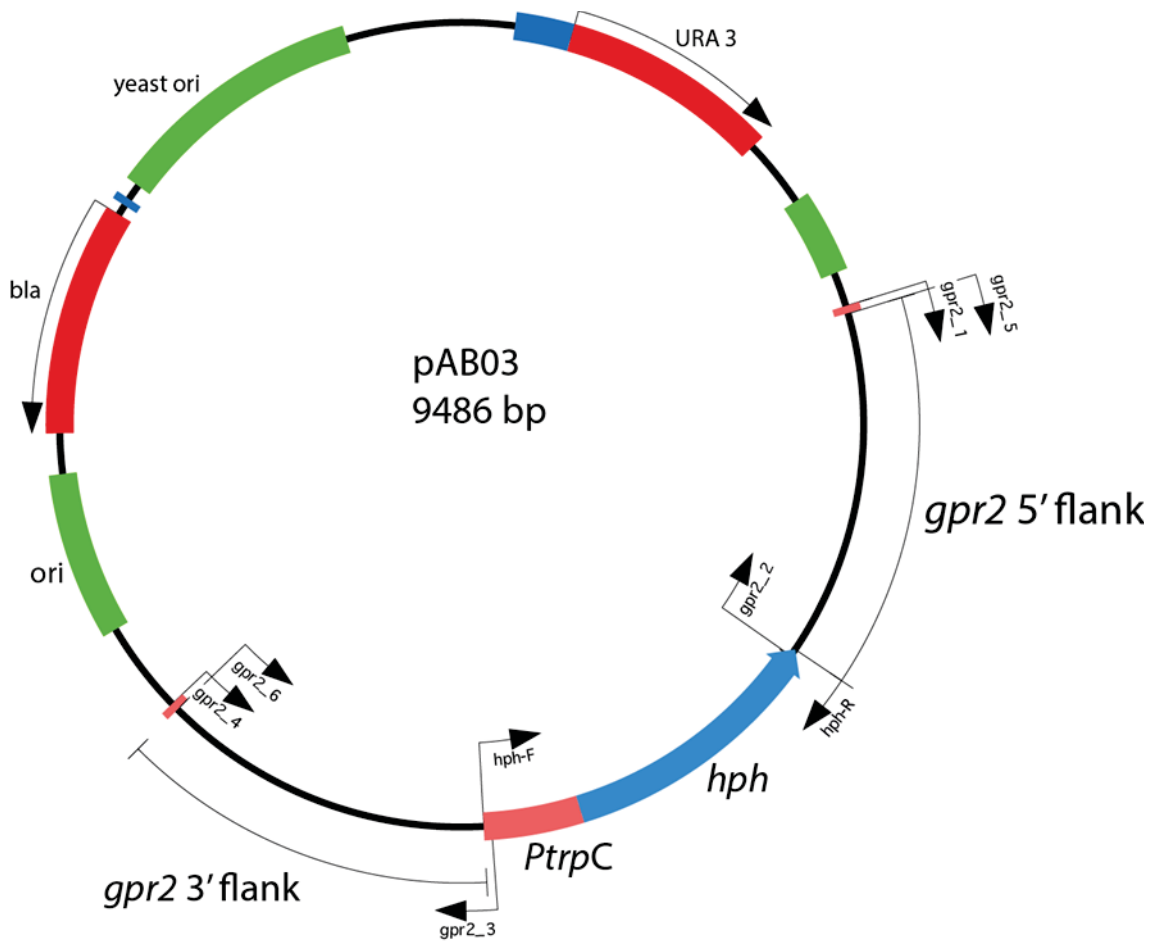
Appendix 5: Plasmid map of pAB01



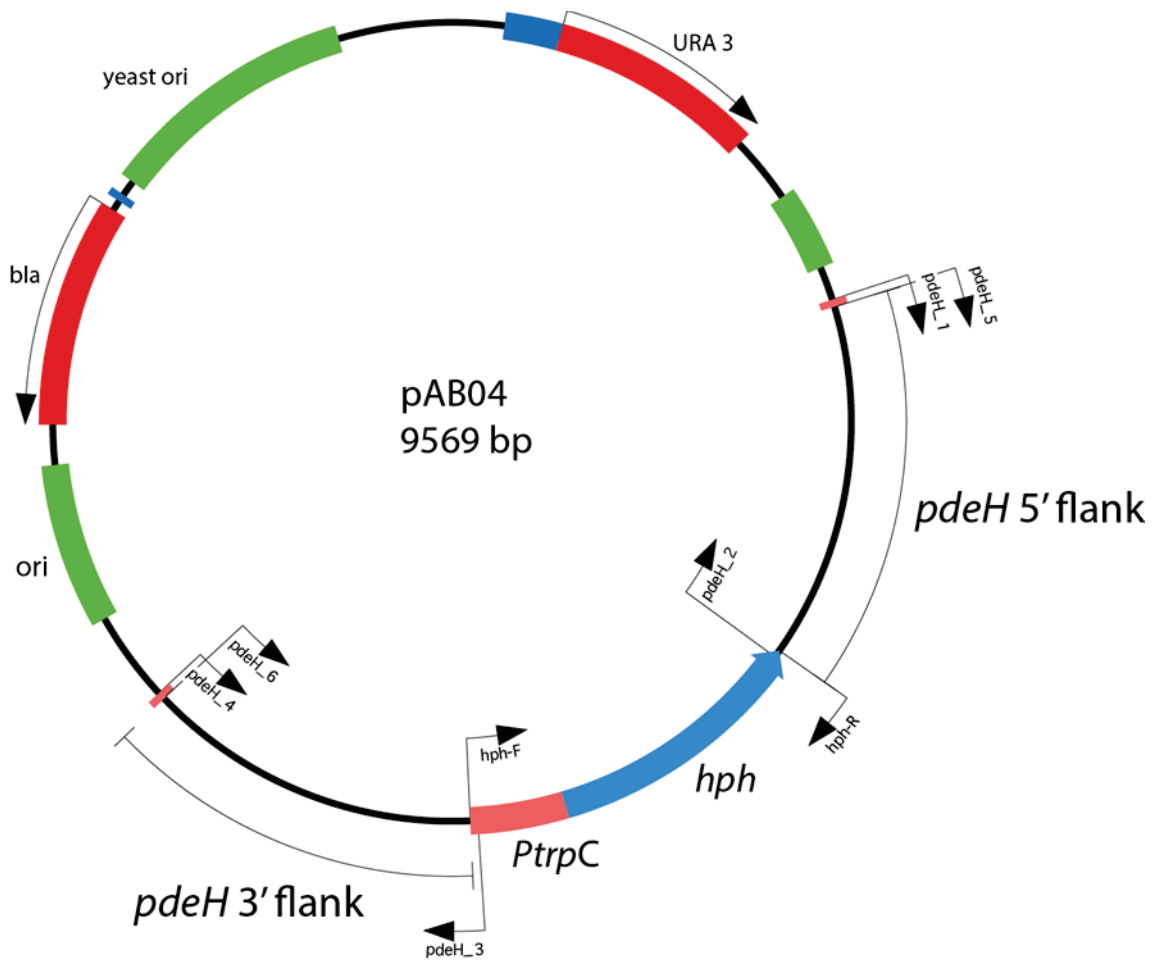
Appendix 6: Plasmid map of pAB02



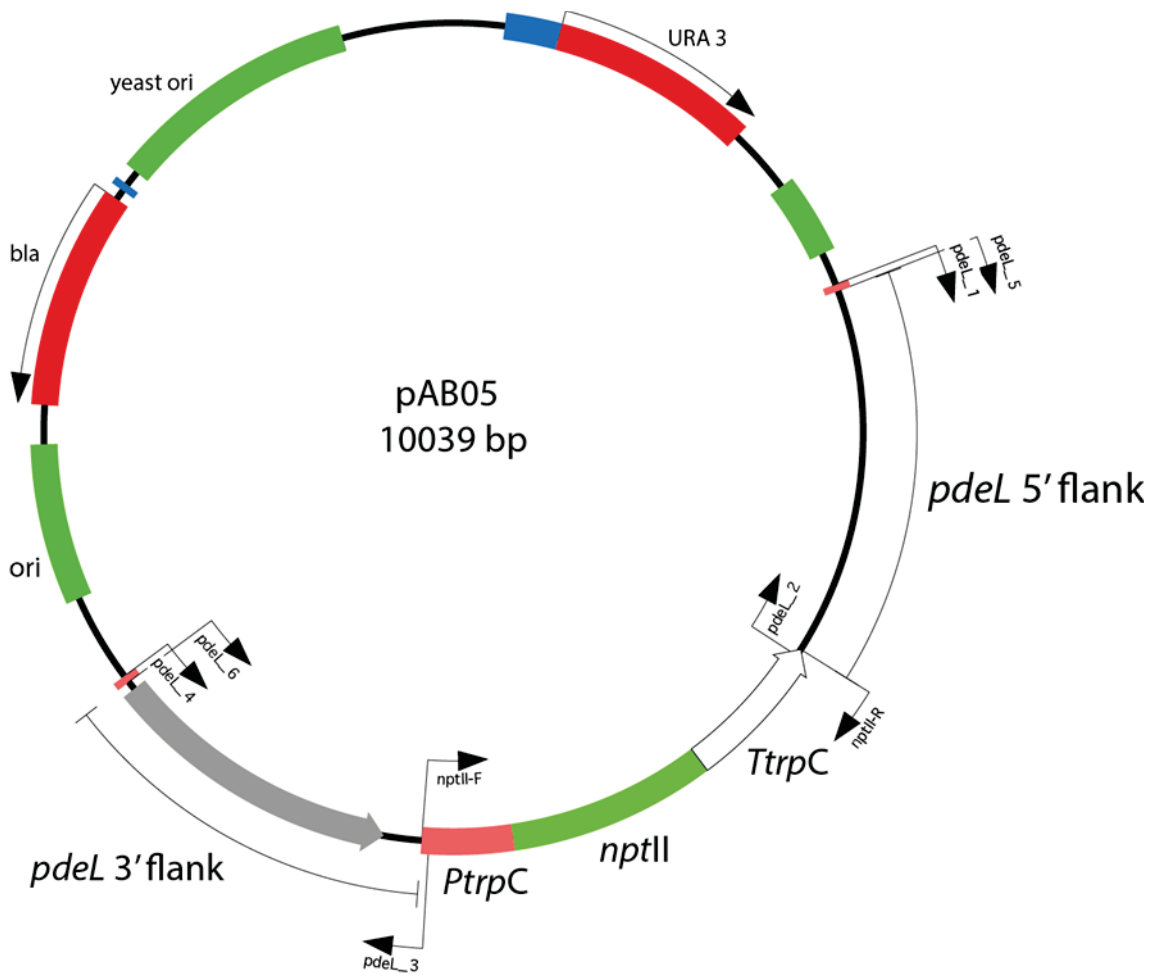
Appendix 7: Plasmid map of pAB03



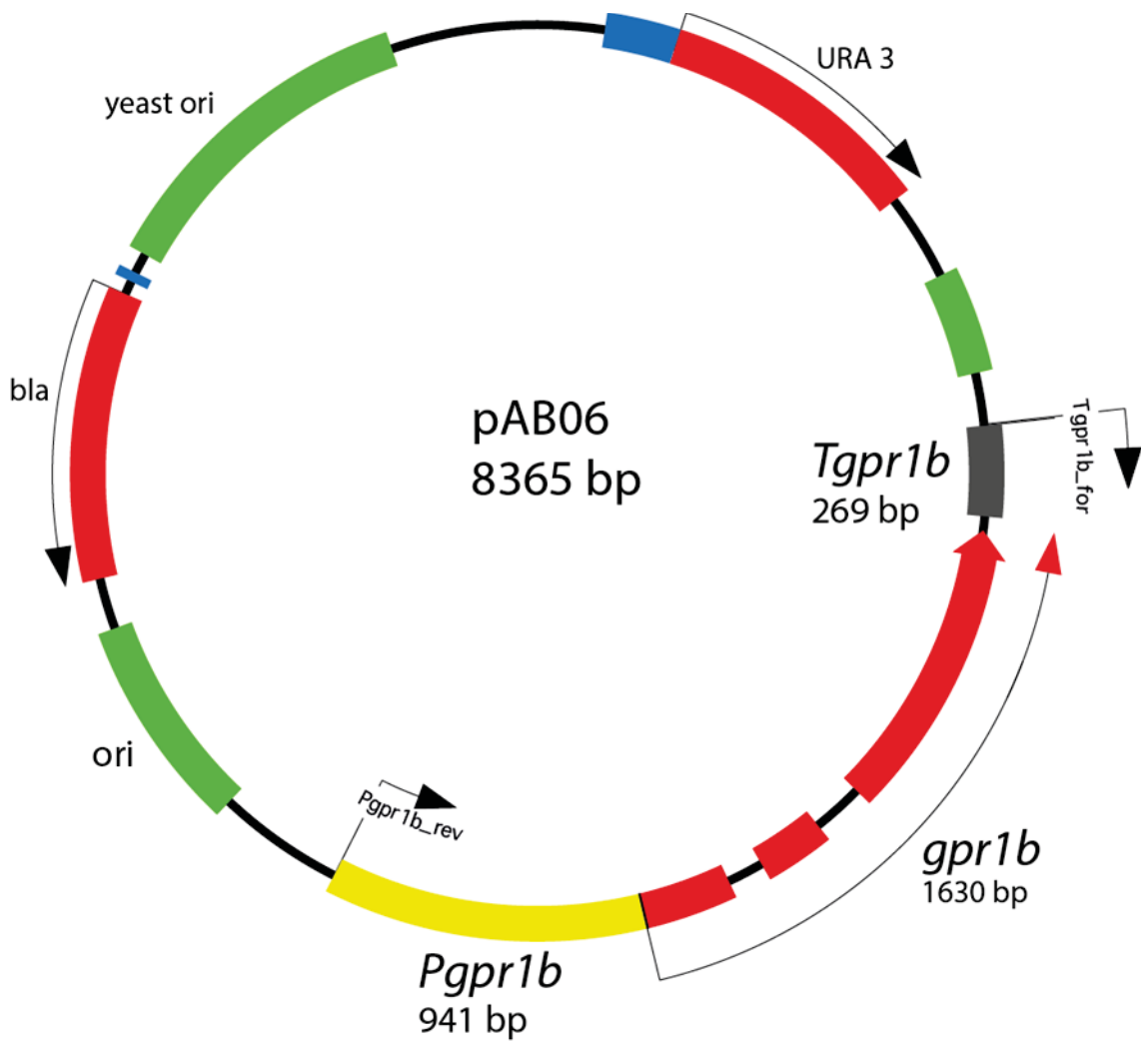
Appendix 8: Plasmid map of pAB04



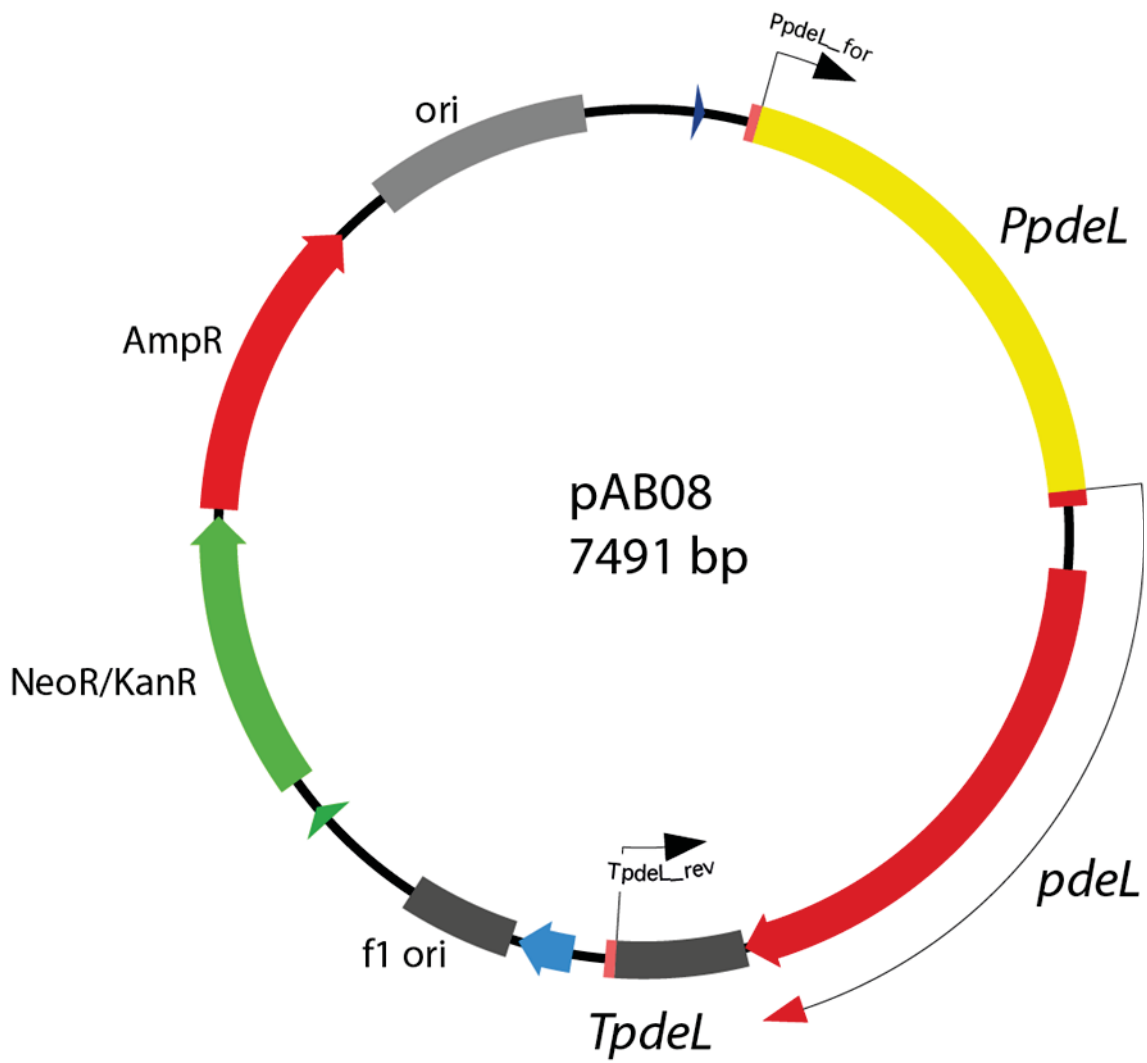
Appendix 9: Plasmid map of pAB05



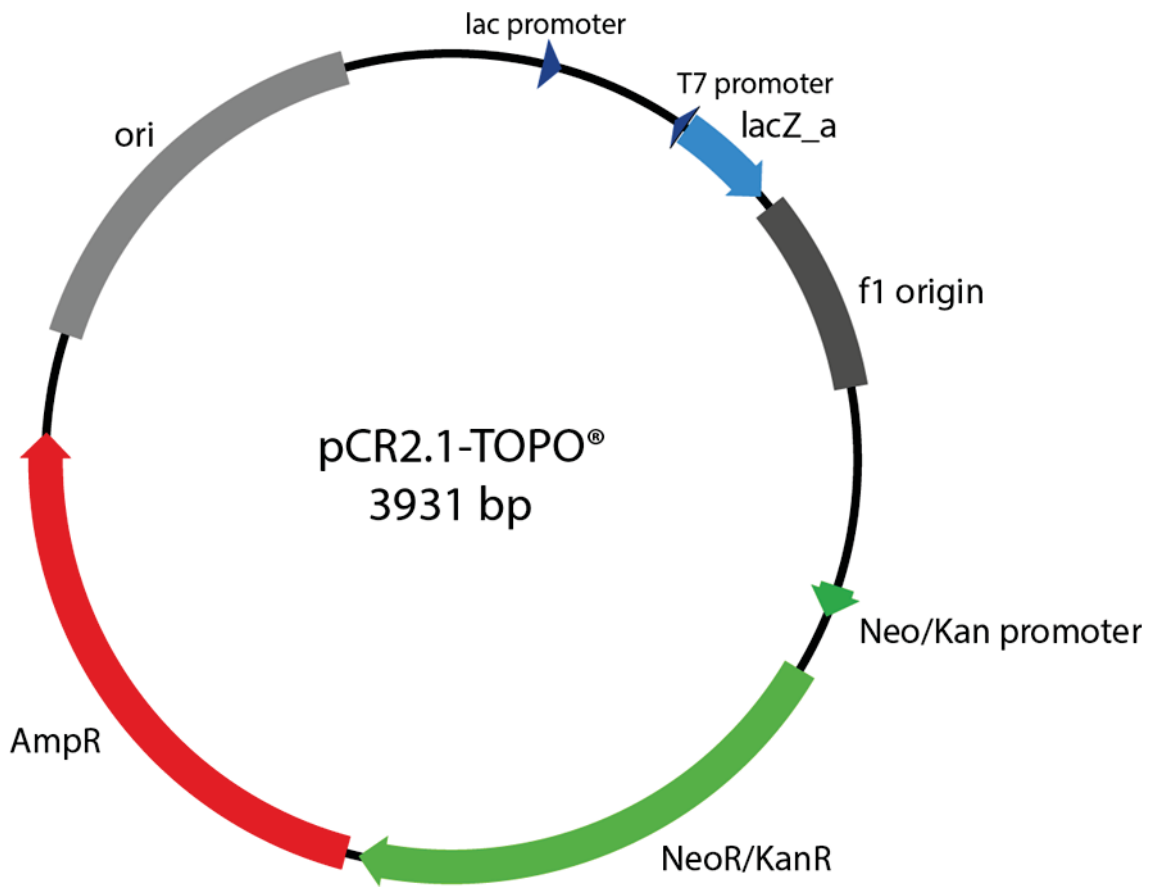
Appendix 10: Plasmid map of pAB06



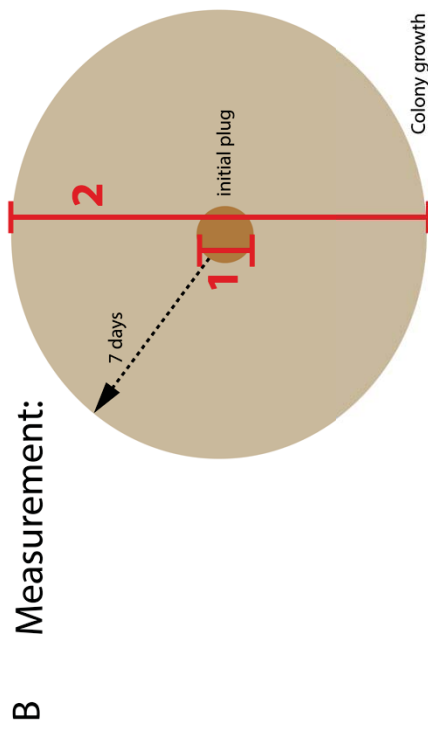
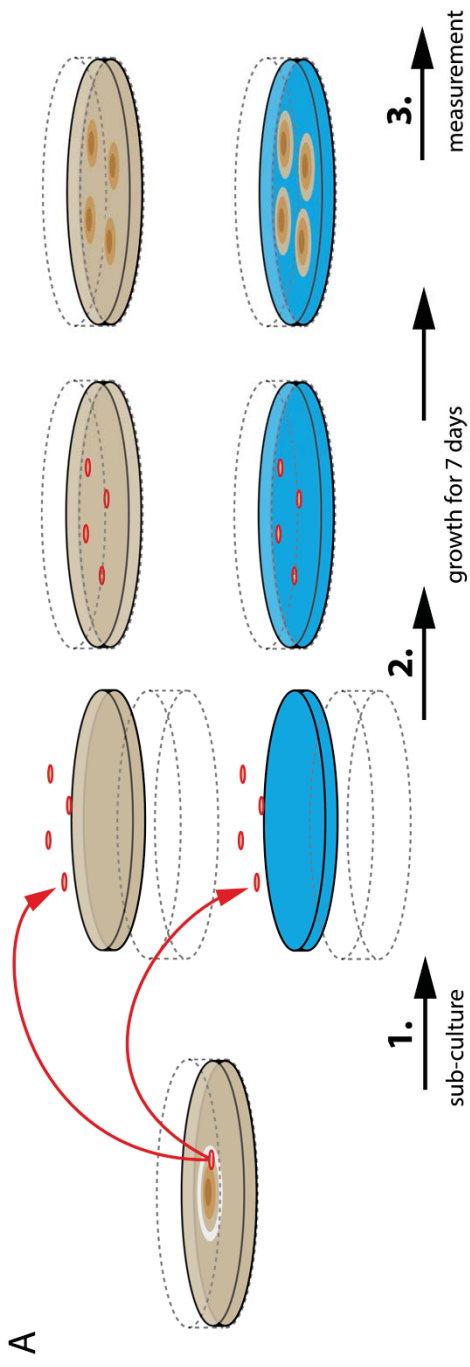
Appendix 11: Plasmid map of pAB08



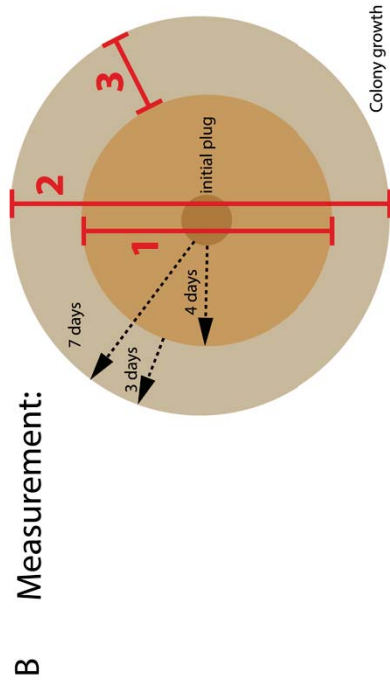
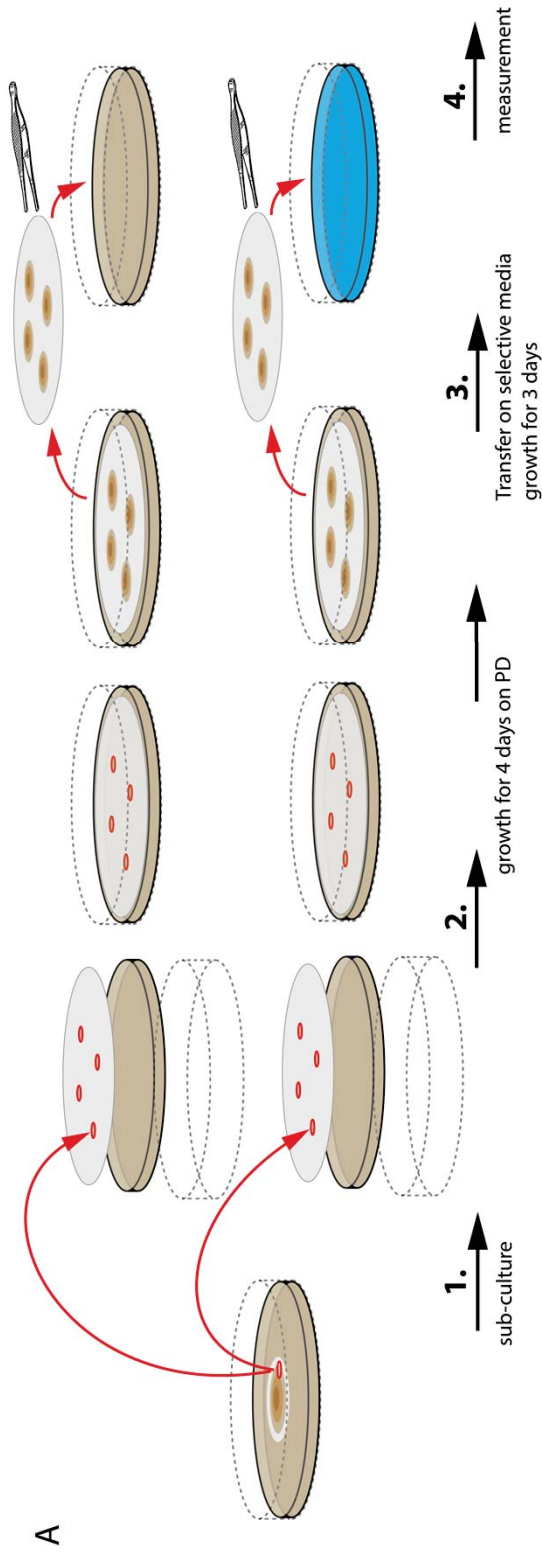
Appendix 12: Plasmid map of pCR2.1-TOPO®



Appendix 13: Non-transfer experiment design (A) and measurement (B)



Appendix 14: Transfer experiment design (A) and measurement (B)



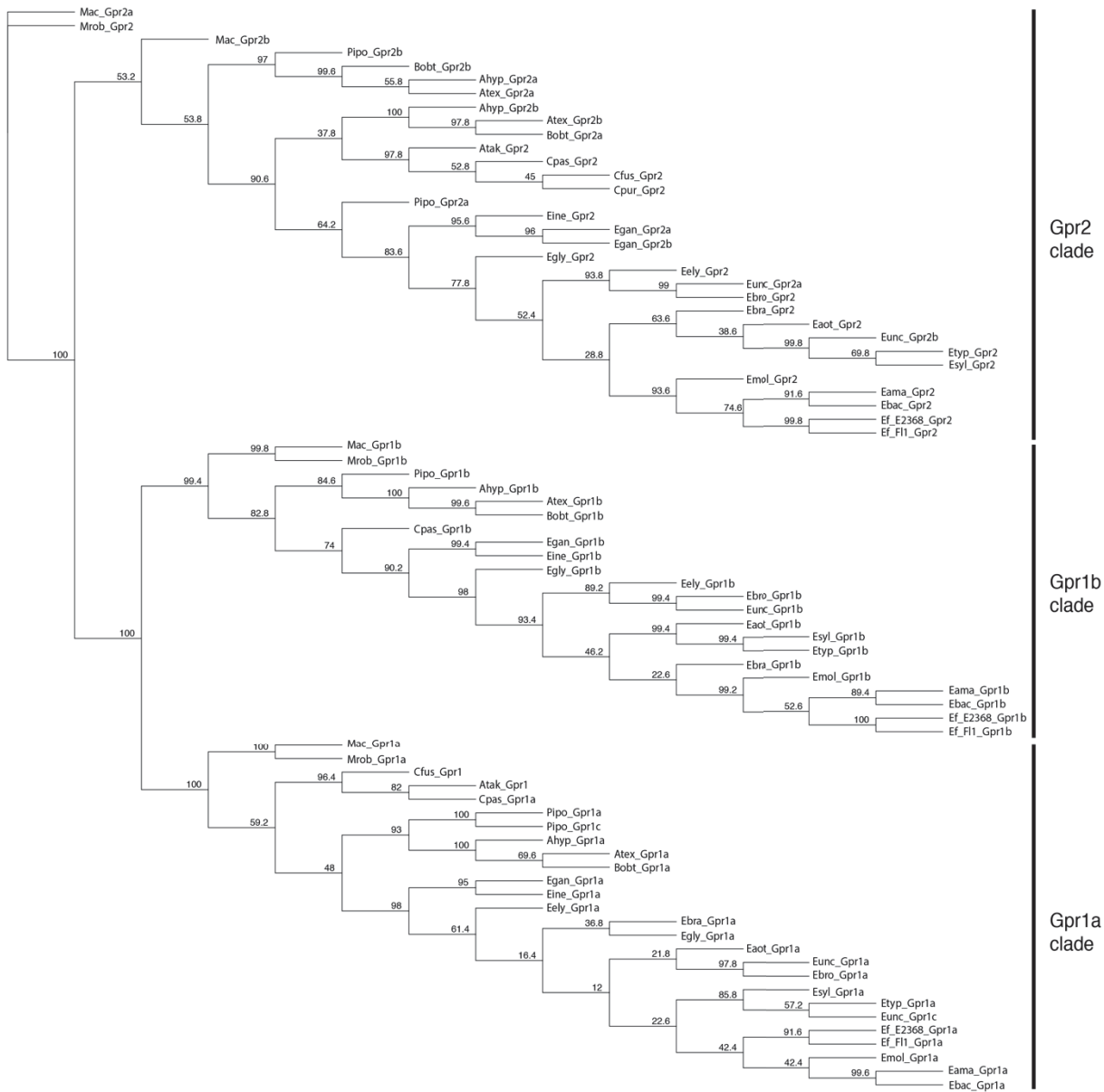
Appendix 15: Table of *E. festucae* GPCR homologues

Class	<i>Epichloe festucae</i>			<i>Neurospora crassa</i>			<i>Magnaporthe oryzae</i>			<i>Fusarium graminearum</i>			<i>Trichoderma atroviride</i>		
	Locus (EfM3)	Locus (NCU)	Identity (%)	E value	Locus (MGG)	Identity (%)	E value	Locus (FGSG)	Identity (%)	E value	Locus (TRIAT)	Identity (%)	E value		
I	<i>pre2</i>	072620	05758	25.1	6.e ⁻³³	04711	33.5	e ⁻⁴¹	02655	42.9	4e ⁻⁵⁵	36032	39.5	3e ⁻⁶¹	
II	<i>pre1</i>	016320	00138	25.3	e ⁻⁵⁰	06452	26.3	8e ⁻⁵⁵	07270	48	e ⁻¹¹³	147894	53	e ⁻¹⁰⁹	
III	<i>gpr4</i>	044840	06312	26.3	6.e ⁻³⁸	08803	19.6	3e ⁻²⁴	05006	30.6	5e ⁻⁶⁷	246916	6.7		
IV	<i>gpr5</i>	042760	00300	35.1	e ⁻⁴¹	04698	50.1	7e ⁻⁸⁷	05579	63	4e ⁻⁸²	238619	60.2	2e ⁻⁹⁰	
	<i>gpr6</i>	019030	09195	54.6	4e ⁻⁴⁹	03051	53.1	3e ⁻⁵³	08496	57	3e ⁻⁷⁴	300620	47.3	e ⁻⁵¹	
V	<i>gpr1a</i>	049190	00786	27	6e ⁻⁵³	11962	28.9	2e ⁻⁵¹	09693	45.2	8e ⁻⁸⁶	81233	56.8	8e ⁻⁵³	
	<i>gpr1b</i>	080640		25.1	7e ⁻⁴⁰		30.3	e ⁻³⁷	05239	48.6	3e ⁻⁶⁴	83166	52.7	2e ⁻⁶⁶	
	<i>gpr2</i>	066920	04626	40.4	5e ⁻⁹³	06738	45.1	e ⁻¹⁰⁶	01861	60.2	e ⁻¹¹⁹	50902	57.8	e ⁻¹²⁶	
			09427	35.7	2e ⁻⁸⁵				7716	42.4	2e ⁻⁸⁷	160995	46.1	e ⁻¹⁰⁴	
									3023	41.1	5e ⁻⁶⁷				
VI	<i>gpr-7a</i>	007810	09883	43.6	e ⁻¹³⁶	13926	45.5	e ⁻¹⁴⁹	04628	46.1	e ⁻¹⁰⁸	40423	63	e ⁻¹⁷⁸	
	<i>gpr-7b</i>	040610		44.7	e ⁻¹²⁷		46.3	e ⁻¹³⁰		50	9e ⁻⁶³	293686	54.2	e ⁻¹⁶⁹	
	<i>gpr-7c</i>	059600		34.5	4e ⁻⁶²		39.1	4e ⁻⁶⁹		38.7	2e ⁻⁴⁷	210761	49.3	2e ⁻⁶⁶	
VII	<i>gpr8</i>	118420	03253	53.7	e ⁻¹²⁸	00532	51.3	e ⁻¹⁰⁹	00527	47.5	2e ⁻⁸⁰	133045	68	e ⁻¹⁴²	
VIII	<i>gpr9</i>	063600	03238	63.1	e ⁻¹⁷⁰	04679	66.4	e ⁻¹⁷⁷	1064	67.9	0.0	136196	77.5	0.0	
	<i>gpr10</i>	029580	04986	57.1	e ⁻¹⁰³	16855	60.1	2e ⁻⁸³	04051	63.7	2e ⁻⁹⁴	290047	68	e ⁻¹²¹	
												210209	65	e ⁻¹¹⁸	

	<i>gpr10b</i>	021530	32.4	5e ⁻³⁷	9091	30.8	3e ⁻⁸⁴		152366	33.2	9e ⁻⁴⁷
									142946	79.9	e ⁻¹³⁸
									46847	68.4	e ⁻¹¹⁸
									142943	36	2.e ⁻⁴⁴
IX	<i>ops-1</i>	031650	33.3	2e ⁻³⁸	09015	37	2e ⁻³⁴	03064	210598	29	8e ⁻¹⁹
		10055	31.4	6e ⁻³²				1440		33	2e ⁻³⁴
								7554		23.4	3e ⁻²⁶
X	<i>gpr11</i>	071470	60.3	e ⁻¹⁵⁹	06418	58.9	4e ⁻⁸⁴	05404	210445	68.3	0.0
XI	<i>gpr12</i>	00005			5269				93659		
XII	<i>gpr13</i>	38560	23.1	6e ⁻²³	07414	32.4	e ⁻⁷⁰	09814	130836	25	2.e ⁻³³
					06103	22.2	2e ⁻²⁶				
XIII	<i>gpr14a</i>	040570	44.1	e ⁻¹²⁸	01467	50.9	e ⁻¹²⁴	09576	152316	59.7	e ⁻¹⁶⁸
									296436	23.5	e ⁻¹⁴
	<i>gpr14b</i>	021230	16.6	4e ⁻²⁶	15321	54.3	7e ⁻¹⁹	03059	136442	69.4	0.0
XIV		19	25			61				106	38

Appendix 15: Rooted phylogenetic dendrogram of class V GPCRs among *Epichloë* species

B



Appendix 17: Table of *E. festucae* homologues for components of the G protein and cAMP/PKA signalling pathway

<i>Epichloe festucae</i>		<i>Neurospora crassa</i>		<i>Magnaporthe oryzae</i>		<i>Fusarium graminearum</i>		<i>Trichoderma atroviride</i>					
Name	Locus (EfM3.)	Locus (NCU)	Identity (%)	E value	Locus (MGG)	Identity (%)	E value	Locus (FGSG)	Identity (%)	TRIAT	Identity (%)	E value	
Gpa1	062630	06493	98.9	e ⁻¹⁵⁷	00365	99.7	e ⁻¹⁶⁰	5535	99.2	e ⁻¹⁶⁰	299359	98.3	e ⁻¹⁶⁰
Gpa2	045200	06729	87.9	e ⁻¹³⁴	04204	87.9	e ⁻¹³⁴	9988	80.8	e ⁻¹³⁹	301492	81.9	e ⁻¹⁴⁴
Gpa3	073950	05206	91.6	e ⁻⁷⁵	01818	95.2	8e ⁻⁸⁰	9614	91.6	6e ⁻⁶⁷	34532	89	2e ⁻⁷³
Gpb1	013730	00440	98.9	e ⁻¹⁶⁵	05201	95.5	e ⁻¹⁸⁰	4104	97.5	e ⁻¹⁷³	42956	96.7	0.0
Gpg1	015250	00041	93.5	2e ⁻²⁴	10193	95.7	8e ⁻³⁹	7235	96.8	9e ⁻²⁹	259183	94.6	3e ⁻³¹
Ric8	064840	02788	65.8	e ⁻¹²⁸	14008	61.2	e ⁻⁹⁹	1511	50.4	e ⁻¹¹³	89180	59.4	e ⁻¹⁴¹
AcyA	022460	08377	71.4	0	09898	72.6	0	1234	70.2	e ⁻¹¹³	318748	74.6	e ⁻¹⁴¹
Pkac1	015410	06240	73.9	e ⁻¹⁶³	06368	71.7	e ⁻¹⁵⁵	7251	68.1	e ⁻¹⁶⁵	164264	66.5	e ⁻¹⁶⁴
Pkar1	071930	01166	77	e ⁻¹³¹	07335	79.1	e ⁻¹⁴⁵	9908	74.7	e ⁻¹⁶²	29552	75.4	e ⁻¹⁵⁸
PdeH	026670	00478	35.8	e ⁻¹¹³	05664	48.7	e ⁻¹⁵⁵	6914	60.5	0.0	315287	58.8	0.0
PdeL	002980	00237	37.9	e ⁻¹¹³	07707	48.1	e ⁻¹⁴¹	6633	60.8	e ⁻¹⁵⁴	31692	60.6	e ⁻¹⁵⁶

Appendix 18: Table of transcriptional difference of *E. festucae* wild-type growth in culture and in association with the host

Name	Gene locus	Culture (RPMK)	<i>In planta</i> (RPMK)	Regulation	FoldDiff	Log2 FoldDiff
GPCR						
<i>pre1</i>	EfM3.072620	2.6895	0.7393	-	3.64	1.86
<i>pre2</i>	EfM3.016320	2.6221	1.4349	-	1.83	0.87
<i>gpr4</i>	EfM3.044840	31.0324	35.4336	+	1.14	0.19
<i>gpr5</i>	EfM3.042760	48.4957	47.6621	-	1.02	0.03
<i>gpr6</i>	EfM3.019030	36.7566	34.7777	-	1.06	0.08
<i>gpr1a</i>	EfM3.049190	6.9227	5.5091	-	1.26	0.33
<i>gpr1b</i>	EfM3.080640	3.7571	21.5789	+	5.74	2.52
<i>gpr2</i>	EfM3.066920	55.6357	134.9953	+	2.43	1.28
<i>gpr7a</i>	EfM3.007810	21.6291	28.6578	+	1.32	0.41
<i>gpr7b</i>	EfM3.040610	26.9247	42.5810	+	1.58	0.66
<i>gpr7c</i>	EfM3.059600	11.6061	12.9814	+	1.12	0.16
<i>gpr8</i>	EfM3.118420					
<i>gpr9</i>	EfM3.063600	31.4923	32.8537	+	1.04	0.06
<i>gpr10</i>	EfM3.029580	16.5103	21.0528	+	1.28	0.35
<i>gpr10b</i>	EfM3.021530	70.4203	49.4645	-	1.42	0.51
<i>ops1</i>	EfM3.031650	100.8601	44.1508	-	2.28	1.19
<i>gpr11</i>	EfM3.071470	85.0577	97.9548	+	1.15	0.20
<i>gpr13</i>	EfM3.038560	12.7687	10.2675	-	1.24	0.31
<i>gpr14a</i>	EfM3.040570	36.0359	41.1699	+	1.14	0.19
<i>gpr14b</i>	EfM3.021230	119.9884	44.7734	-	2.68	1.42
<i>pth11-1</i>	EfM3.055430	13.7977	7.0038	-	1.97	0.98
<i>pth11-2</i>	EfM3.012710	29.9543	14.5739	-	2.06	1.04
<i>pth11-3</i>	EfM3.031700	47.4558	26.2612	-	1.81	0.85
<i>pth11-4</i>	EfM3.041190	50.6470	69.7658	+	1.38	0.46
<i>pth11-5</i>	EfM3.079370	3.9061	37.3050	+	9.55	3.26
<i>pth11-6</i>	EfM3.008620	4.0260	10.7699	+	2.68	1.42
<i>pth11-7</i>	EfM3.056870	28.2176	23.1141	-	1.22	0.29
<i>pth11-8</i>	EfM3.042570	16.4656	37.4483	+	2.27	1.19
<i>pth11-9</i>	EfM3.028870	83.6917	40.2583	-	2.08	1.06

<i>pth11-10</i>	EfM3.008360	64624	14.8374	+	2.30	1.20
<i>pth11-11</i>	EfM3.001250	0.8536	2.5855	+	3.03	1.60
<i>pth11-12</i>	EfM3.048960	4.1626	18.3561	+	4.41	2.14
<i>pth11-13</i>	EfM3.032250	58.7659	45.4230	-	1.29	0.37
<i>pth11-14</i>	EfM3.012500	10.8919	13.8800	+	1.27	0.35
<i>pth11-15</i>	EfM3.025720	21.3107	21.4548	+	1.01	0.01
<i>pth11-16</i>	EfM3.047160	23.9733	547.5212	+	22.84	4.51
<i>pth11-17</i>	EfM3.062190	103.7546	32.7725	-	3.17	1.66
<i>pth11-18</i>	EfM3.000460	23.9683	32.8783	+	1.37	0.46
<i>pth11-19</i>	EfM3.159360					
<i>gpr9b</i>	EfM3.064650	31.4808	76.5649	-	1.76	0.82

Components of the G protein and cAMP/PKA signalling pathway

<i>gpa1</i>	EfM3.062630	33.6797	72.5160	+	2.15	1.11
<i>gpa2</i>	EfM3.045200	39.7263	51.0584	+	1.29	0.36
<i>gpa3</i>	EfM3.073950	18.7600	52.2067	+	2.78	1.48
<i>gpb1</i>	EfM3.013730	31.4297	112.0883	+	3.57	1.83
<i>gpg1</i>	EfM3.015250	107.6077	249.9004	+	2.32	1.22
<i>ric8</i>	EfM3.064840	37.9119	46.3760	+	1.22	0.29
<i>acyA</i>	EfM3.022460	9.1677	17.6461	+	1.92	0.94
<i>pkac1</i>	EfM3.015410	41.0679	38.0701	-	1.08	0.11
<i>pkar1</i>	EfM3.071930	100.8058	168.1944	+	1.67	0.74
<i>pdeH</i>	EfM3.026670	18.0875	26.5002	+	1.47	0.55
<i>pdeL</i>	EfM3.002980	28.4128	10.0801	-	2.82	1.50

Chapter 8 Supplementary data files in accompanying digital media

Supplementary 1: Multiple sequence alignment of *E. festucae* Pre2 homologues

Supplementary 2: Predicted protein topology of *E. festucae* Pre2

Supplementary 3: Multiple sequence alignment of *E. festucae* Pre1 homologues

Supplementary 4: Predicted protein topology of *E. festucae* Pre1

Supplementary 5: Multiple sequence alignment of *E. festucae* Gpr4 homologues

Supplementary 6: Predicted protein topology of *E. festucae* Gpr4

Supplementary 7: Multiple sequence alignment of *E. festucae* Gpr5 homologues

Supplementary 8: Predicted protein topology of *E. festucae* Gpr5

Supplementary 9: Multiple sequence alignment of *E. festucae* Gpr6 homologues

Supplementary 10: Predicted protein topology of *E. festucae* Gpr6

Supplementary 11: Multiple sequence alignment of *E. festucae* Gpr7a homologues

Supplementary 12: Predicted protein topology of *E. festucae* Gpr7a

Supplementary 13: Multiple sequence alignment of *E. festucae* Gpr7b homologues

Supplementary 14: Predicted protein topology of *E. festucae* Gpr7b

Supplementary 15: Multiple sequence alignment of *E. festucae* Gpr7c homologues

Supplementary 16: Predicted protein topology of *E. festucae* Gpr7c

Supplementary 17: Multiple sequence alignment of *E. festucae* Gpr8 homologues

Supplementary 18: Predicted protein topology of *E. festucae* Gpr8

Supplementary 19: Multiple sequence alignment of *E. festucae* Gpr9 homologues

Supplementary 20: Predicted protein topology of *E. festucae* Gpr9

Supplementary 21: Multiple sequence alignment of *E. festucae* Gpr10 homologues

Supplementary 22: Predicted protein topology of *E. festucae* Gpr10

Supplementary 23: Multiple sequence alignment of *E. festucae* Gpr10b homologues

Supplementary 24: Predicted protein topology of *E. festucae* Gpr10b

Supplementary 25: Multiple sequence alignment of *E. festucae* Gpr9b homologues

Supplementary 26: Predicted protein topology of *E. festucae* Gpr9b

Supplementary 27: Multiple sequence alignment of *E. festucae* Ops1 homologues

Supplementary 28: Predicted protein topology of *E. festucae* Ops1

Supplementary 29: Multiple sequence alignment of *E. festucae* Gpr11 homologues

Supplementary 30: Predicted protein topology of *E. festucae* Gpr11

Supplementary 31: Multiple sequence alignment of *E. festucae* Gpr13 homologues

Supplementary 32: Predicted protein topology of *E. festucae* Gpr13

Supplementary 33: Multiple sequence alignment of *E. festucae* Gpr14a homologues

Supplementary 34: Predicted protein topology of *E. festucae* Gpr14a

Supplementary 35: Multiple sequence alignment of *E. festucae* Gpr14b homologues

Supplementary 36: Predicted protein topology of *E. festucae* Gpr14b

Supplementary 37: Predicted protein topology of *E. festucae* Pth11-1

Supplementary 38: Predicted protein topology of *E. festucae* Pth11-2

Supplementary 39: Predicted protein topology of *E. festucae* Pth11-3

Supplementary 40: Predicted protein topology of *E. festucae* Pth11-4

Supplementary 41: Predicted protein topology of *E. festucae* Pth11-5

Supplementary 42: Predicted protein topology of *E. festucae* Pth11-6

Supplementary 43: Predicted protein topology of *E. festucae* Pth11-7

Supplementary 44: Predicted protein topology of *E. festucae* Pth11-8

Supplementary 45: Predicted protein topology of *E. festucae* Pth11-9

Supplementary 46: Predicted protein topology of *E. festucae* Pth11-10

Supplementary 47: Predicted protein topology of *E. festucae* Pth11-11

Supplementary 48: Predicted protein topology of *E. festucae* Pth11-12

Supplementary 49: Predicted protein topology of *E. festucae* Pth11-13

Supplementary 50: Predicted protein topology of *E. festucae* Pth11-14

Supplementary 51: Predicted protein topology of *E. festucae* Pth11-15

Supplementary 52: Predicted protein topology of *E. festucae* Pth11-16

Supplementary 53: Predicted protein topology of *E. festucae* Pth11-17

Supplementary 54: Predicted protein topology of *E. festucae* Pth11-18

Supplementary 55: Predicted protein topology of *E. festucae* Pth11-19

Supplementary 56: Multiple sequence alignment of *E. festucae* Gpa1 homologues

Supplementary 57: Multiple sequence alignment of *E. festucae* Gpa2 homologues

Supplementary 58: Multiple sequence alignment of *E. festucae* Gpa3 homologues

Supplementary 59: Multiple sequence alignment of *E. festucae* Gpb1 homologues

Supplementary 60: Multiple sequence alignment of *E. festucae* Gpg1 homologues

Supplementary 61: Multiple sequence alignment of *E. festucae* Ric8 homologues

Supplementary 62: Multiple sequence alignment of *E. festucae* AcyA homologues

Supplementary 63: Multiple sequence alignment of *E. festucae* Pkac1 homologues

Supplementary 64: Multiple sequence alignment of *E. festucae* Pkar1 homologues

Chapter 9 References

Adachi, K. and Hamer, J. E. (1998). Divergent cAMP signalling pathways regulate growth and pathogenesis in the rice blast fungus *Magnaporthe grisea*. *The Plant Cell* **10**(8): 1361-1374.

Affeldt, K. J., Brodhagen, M. and Keller, N. P. (2012). *Aspergillus* oxylipin signaling and quorum sensing pathways depend on G protein-coupled receptors. *Toxins* **4**(9): 695-717.

Affeldt, K. J., Carrig, J., Amare, M. and Keller, N. P. (2014). Global survey of canonical *Aspergillus flavus* G protein-coupled receptors. *MBio* **5**(5): e01501-01514.

Agarwal, C., Aulakh, K. B., Edelen, K., Cooper, M., Wallen, R. M., et al. (2013). *Ustilago maydis* phosphodiesterases play a role in the dimorphic switch and in pathogenicity. *Microbiology* **159**(5): 857-868.

Agarwal, C., Schultz, D. J. and Perlin, M. H. (2010). Two phosphodiesterases from *Ustilago maydis* share structural and biochemical properties with non-fungal phosphodiesterases. *Frontiers Microbiology* **1**: 127.

Alspaugh, J. A., Pukkila-Worley, R., Harashima, T., Cavallo, L. M., Funnell, D., et al. (2002). Adenylyl cyclase functions downstream of the G α protein Gpa1 and controls mating and pathogenicity of *Cryptococcus neoformans*. *Eukaryotic Cell* **1**(1): 75-84.

Amselem, J., Cuomo, C. A., van Kan, J. A., Viaud, M., Benito, E. P., et al. (2011). Genomic analysis of the necrotrophic fungal pathogens *Sclerotinia sclerotiorum* and *Botrytis cinerea*. *PLoS Genetics* **7**(8): e1002230.

Ariyawansa, K. G. S. (2015). Sensing and signalling mechanical stress during intercalary growth in *Epichloë* grass endophytes. Doctor of Philosophy (PhD) in Genetics Massey University.

Attwood, T. and Findlay, J. (1994). Fingerprinting G-protein-coupled receptors. *Protein Engineering* **7**(2): 195-203.

- Bacon, C. W. and Hinton, D. M. (1991). Microcyclic conidiation cycles in *Epichloë typhina*. *Mycologia* **83**(6): 743-751.
- Banuett, F. (1998). Signaling in the yeasts: an informational cascade with links to filamentous fungi. *Microbiology & Molecular Biology Reviews* **62**: 249-274.
- Barbosa, M., Valentao, P. and Andrade, P. B. (2016). Biologically active oxylipins from enzymatic and nonenzymatic routes in macroalgae. *Marine Drugs* **14**(1): 23.
- Becker, M., Becker, Y., Green, K. and Scott, B. (2016). The endophytic symbiont *Epichloë festucae* establishes an epiphyllous net on the surface of *Lolium perenne* leaves by development of an expressorium, an appressorium-like leaf exit structure. *New Phytologist* **211**: 240-254.
- Becker, Y., Eaton, C. J., Brasell, E., May, K. J., Becker, M., et al. (2015). The fungal cell wall integrity MAPK cascade is crucial for hyphal network formation and maintenance of restrictive growth of *Epichloë festucae* in symbiosis with *Lolium perenne*. *Molecular Plant-Microbe Interactions* **28**: 69-85.
- Bergman, L. W. (2001). Growth and maintenance of yeast. *Methods in Molecular Biology* **177**: 9-14.
- Bhattacharya, S., Hall, S. E. and Vaidehi, N. (2008). Agonist-induced conformational changes in bovine rhodopsin: insight into activation of G-protein-coupled receptors. *Journal of Molecular Biology* **382**(2): 539-555.
- Birkaya, B., Maddi, A., Joshi, J., Free, S. J. and Cullen, P. J. (2009). Role of the cell wall integrity and filamentous growth mitogen-activated protein kinase pathways in cell wall remodeling during filamentous growth. *Eukaryotic Cell* **8**(8): 1118-1133.
- Blankenship, J. D., Spiering, M. J., Wilkinson, H. H., Fannin, F. F., Bush, L. P., et al. (2001). Production of loline alkaloids by the grass endophyte, *Neotyphodium uncinatum*, in defined media. *Phytochemistry* **58**(3): 395-401.

Borroto-Escuela, D. O., Brito, I., Romero-Fernandez, W., Di Palma, M., Oflijan, J., et al. (2014). The G protein-coupled receptor heterodimer network (GPCR-HetNet) and its hub components. *International Journal of Molecular Sciences* **15**(5): 8570-8590.

Brakhage, A. A. (2013). Regulation of fungal secondary metabolism. *Nature Reviews Microbiology* **11**(1): 21-32.

Brand, A. and Gow, N. A. (2009). Mechanisms of hypha orientation of fungi. *Current Opinion in Microbiology* **12**(4): 350-357.

Brefort, T., Doehlemann, G., Mendoza-Mendoza, A., Reissmann, S., Djamei, A., et al. (2009). *Ustilago maydis* as a pathogen. *Annual Reviews Phytopathology* **47**: 423-445.

Brewster, J. L., de Valoir, T., Dwyer, N. D., Winter, E. and Gustin, M. C. (1993). An osmosensing signal transduction pathway in yeast. *Science* **259**(5102): 1760-1763.

Brodhagen, M., Tsitsigiannis, D. I., Hornung, E., Goebel, C., Feussner, I., et al. (2008). Reciprocal oxylipin-mediated cross-talk in the *Aspergillus*-seed pathosystem. *Molecular Microbiology* **67**(2): 378-391.

Brodhun, F. and Feussner, I. (2011). Oxylipins in fungi. *FEBS Journal* **278**(7): 1047-1063.

Brown, N. A., dos Reis, T. F., Ries, L. N. A., Caldana, C., Mah, J. H., et al. (2015). G-protein coupled receptor-mediated nutrient sensing and developmental control in *Aspergillus nidulans*. *Molecular Microbiology* **98**(3): 420-439.

Brown, S. H., Scott, J. B., Bhaheetharan, J., Sharpee, W. C., Milde, L., et al. (2009). Oxygenase coordination is required for morphological transition and the host-fungus interaction of *Aspergillus flavus*. *Molecular Plant-Microbe Interactions* **22**(7): 882-894.

Brunner, K., Omann, M., Pucher, M. E., Delic, M., Lehner, S. M., et al. (2008). *Trichoderma* G protein-coupled receptors: functional characterisation of a cAMP

receptor-like protein from *Trichoderma atroviride*. *Current Genetics* **54**(6): 283-299.

Bultman, T. L. and White, J. F. (1988). Pollination of fungus by a fly. *Oecologia* **75**(2): 317-319.

Bultman, T. L., White, J. F., Jr., Bowdish, T. I. and Welch, A. M. (1998). A new kind of mutualism between fungi and insects. *Mycological Research* **102**(2): 235-238.

Byrd, A. D., Schardl, C. L., Songlin, P. J., Mogen, K. L. and Siegel, M. R. (1990). The β -tubulin gene of *Epichloë typhina* from perennial ryegrass (*Lolium perenne*). *Current Genetics* **18**(4): 347-354.

Cabrera, I. E., Pacentine, I. V., Lim, A., Guerrero, N., Krystofova, S., et al. (2015). Global analysis of predicted G protein-coupled receptor genes in the filamentous fungus, *Neurospora crassa*. *G3 (Bethesda)* **5**(12): 2729-2743.

Calvo, A. M., Wilson, R. A., Bok, J. W. and Keller, N. P. (2002). Relationship between secondary metabolism and fungal development. *Microbiology & Molecular Biology Reviews* **66**(3): 447-459.

Cartwright, G.M., Tanaka, A., Eaton, C.J., and Scott, B. (2014). Formation of arthroconidia during regeneration and selection of transformed *Epichloë festucae* protoplasts. *Fungal Biology* **118**: 462-471.

Champe, S. P., Rao, P. and Chang, A. (1987). An endogenous inducer of sexual development in *Aspergillus nidulans*. *Journal of General Microbiology* **133**(5): 1383-1387.

Charbonneau, H., Beier, N., Walsh, K. A. and Beavo, J. A. (1986). Identification of a conserved domain among cyclic nucleotide phosphodiesterases from diverse species. *Proceedings of the National Academy of Sciences* **83**(24): 9308-9312.

Charlton, N. D., Shoji, J. Y., Ghimire, S. R., Nakashima, J. and Craven, K. D. (2012). Deletion of the fungal gene *soft* disrupts mutualistic symbiosis between the grass endophyte *Epichloë festucae* and the host plant. *Eukaryotic Cell* **11**(12): 1463-1471.

Chattopadhyay, A. (2014). GPCRs: lipid-dependent membrane receptors that act as drug targets. *Advances in Biology* **2014**.

Cherkasova, V. A., McCully, R., Wang, Y., Hinnebusch, A. and Elion, E. A. (2003). A novel functional link between MAP kinase cascades and the Ras/cAMP pathway that regulates survival. *Current Biology* **13**(14): 1220-1226.

Choi, J., Jung, W. H. and Kronstad, J. W. (2015). The cAMP/protein kinase A signaling pathway in pathogenic basidiomycete fungi: Connections with iron homeostasis. *Journal of Microbiology* **53**(9): 579-587.

Choi, W. and Dean, R. A. (1997). The adenylate cyclase gene MAC1 of *Magnaporthe grisea* controls appressorium formation and other aspects of growth and development. *The Plant Cell* **9**(11): 1973-1983.

Christensen, M. J., Ball, O. J.-P., Bennett, R. J. and Schardl, C. L. (1997). Fungal and host genotype effects on compatibility and vascular colonization by *Epichloë festucae*. *Mycological Research* **101**(4): 493-501.

Christensen, M. J., Bennett, R. J., Ansari, H. A., Koga, H., Johnson, R. D., et al. (2008). *Epichloë* endophytes grow by intercalary hyphal extension in elongating grass leaves. *Fungal Genetics & Biology* **45**: 84-93.

Christensen, M. J., Bennett, R. J. and Schmid, J. (2001). Vascular bundle colonisation by *Neotyphodium* endophytes in natural and novel associations with grasses. *Mycological Research* **105**(10): 1239-1245.

Christensen, M. J., Bennett, R. J. and Schmid, J. (2002). Growth of *Epichloë/Neotyphodium* and p-endophytes in leaves of *Lolium* and *Festuca* grasses. *Mycological Research* **106**: 93-106.

Christensen, M. J., Leuchtman, A., Rowan, D. D. and Tapper, B. A. (1993). Taxonomy of *Acremonium* endophytes of tall fescue (*Festuca arundinacea*), meadow fescue (*F. pratensis*) and perennial rye-grass (*Lolium perenne*). *Mycological Research* **97**(9): 1083-1092.

Christianson, T. W., Sikorski, R. S., Dante, M., Shero, J. H. and Hieter, P. (1992). Multifunctional yeast high-copy-number shuttle vectors. *Gene* **110**(1): 119-122.

Chung, K.-R. (2012). Stress response and pathogenicity of the necrotrophic fungal pathogen *Alternaria alternata*. *Scientifica* **2012**.

Chung, K.-R. and Schardl, C. L. (1997). Sexual cycle and horizontal transmission of the grass symbiont, *Epichloë typhina*. *Mycological Research* **101**(3): 295-301.

Clay, K. and Schardl, C. (2002). Evolutionary origins and ecological consequences of endophyte symbiosis with grasses. *The American Naturalist* **160**: S99-S127.

Colot, H. V., Park, G., Turner, G. E., Ringelberg, C., Crew, C. M., et al. (2006). A high-throughput gene knockout procedure for *Neurospora* reveals functions for multiple transcription factors. *Proceedings National Academy of Sciences USA* **103**(27): 10352-10357.

Conti, M. and Beavo, J. (2007). Biochemistry and physiology of cyclic nucleotide phosphodiesterases: essential components in cyclic nucleotide signaling. *Annual Review of Biochemistry* **76**: 481-511.

Conti, M., Mika, D. and Richter, W. (2014). Cyclic AMP compartments and signaling specificity: role of cyclic nucleotide phosphodiesterases. *The Journal General Physiology* **143**(1): 29-38.

Cullen, P. J. and Sprague, G. F. (2012). The regulation of filamentous growth in yeast. *Genetics* **190**(1): 23-49.

D'Souza, C. A., Alspaugh, J. A., Yue, C., Harashima, T., Cox, G. M., et al. (2001). Cyclic AMP-dependent protein kinase controls virulence of the fungal pathogen *Cryptococcus neoformans*. *Molecular & Cellular Biology* **21**(9): 3179-3191.

D'Souza, C. A. and Heitman, J. (2001). Conserved cAMP signaling cascades regulate fungal development and virulence. *FEMS Microbiology Reviews* **25**(3): 349-364.

De Battista, J. P., Bacon, C. W., Severson, R., Plattner, R. D. and Bouton, J. H. (1990). Indole acetic acid production by the fungal endophyte of tall fescue. *Agronomy Journal* **82**: 878-880.

de Souza, W. R., Morais, E. R., Krohn, N. G., Savoldi, M., Goldman, M. H., et al. (2013). Identification of metabolic pathways influenced by the G-protein coupled receptors GprB and GprD in *Aspergillus nidulans*. *PLoS One* **8**(5): e62088.

Deupi, X. and Kobilka, B. K. (2010). Energy landscapes as a tool to integrate GPCR structure, dynamics, and function. *Physiology* **25**(5): 293-303.

DeZwaan, T. M., Carroll, A. M., Valent, B. and Sweigard, J. A. (1999). *Magnaporthe grisea* Pth11p is a novel plasma membrane protein that mediates appressorium differentiation in response to inductive substrate cues. *The Plant Cell* **11**(10): 2013-2030.

Ding, S., Zhou, X., Zhao, X. and Xu, J.-R. (2009). The PMK1 MAP kinase pathway and infection-related morphogenesis. In: *Advances in Genetics, Genomics and Control of Rice Blast Disease*, Springer (Netherlands): 13-21.

Dobson, L., Remenyi, I. and Tusnady, G. E. (2015). CCTOP: a Consensus Constrained TOPology prediction web server. *Nucleic Acids Research* **43**(W1): W408-412.

Doehlemann, G., Berndt, P. and Hahn, M. (2006). Different signalling pathways involving a Galpha protein, cAMP and a MAP kinase control germination of *Botrytis cinerea* conidia. *Molecular Microbiology* **59**(3): 821-835.

Dohlman, H. G., Thorner, J., Caron, M. G. and Lefkowitz, R. J. (1991). Model systems for the study of seven-transmembrane-segment receptors. *Annual Review of Biochemistry* **60**(1): 653-688.

Donlin, M. J., Upadhyaya, R., Gerik, K. J., Lam, W., VanArendonk, L. G., et al. (2014). Cross talk between the cell wall integrity and cyclic AMP/protein kinase A pathways in *Cryptococcus neoformans*. *MBio* **5**(4): e01573-01514.

Dower, W. J., Miller, J. F. and Ragsdale, C. W. (1988). High efficiency transformation of *E. coli* by high voltage electroporation. *Nucleic Acids Research* **16**(13): 6127-6145.

Dupont, P. Y., Eaton, C. J., Wargent, J. J., Fechtner, S., Solomon, P., et al. (2015). Fungal endophyte infection of ryegrass reprograms host metabolism and alters development. *New Phytologist* **208**(4): 1227-1240.

Dyer, P. S. and O'Gorman, C. M. (2012). Sexual development and cryptic sexuality in fungi: insights from *Aspergillus* species. *FEMS Microbiology Reviews* **36**(1): 165-192.

Eaton, C., Mitic, M. and Scott, B. (2011). Signalling in the *Epichloë festucae*-perennial ryegrass mutualistic symbiotic interaction. In: *Signaling and Communication in Plant Symbiosis*. Springer-Verlag (Heidelberg),. **11**: 143-181.

Eaton, C. J., Cox, M. P., Ambrose, B., Becker, M., Hesse, U., et al. (2010). Disruption of signaling in a fungal-grass symbiosis leads to pathogenesis. *Plant Physiology* **153**(4): 1780-1794.

Eaton, C. J., Dupont, P.-Y., Solomon, P. S., Clayton, W., Scott, B., et al. (2015). A core gene set describes the molecular basis of mutualism and antagonism in *Epichloë* species. *Molecular Plant-Microbe Interactions* **28**: 218-231.

Eaton, C. J., Jourdain, I., Foster, S. J., Hyams, J. S. and Scott, B. (2008). Functional analysis of a fungal endophyte stress-activated MAP kinase. *Current Genetics* **53**(3): 163-174.

Fillinger, S., Chaverroche, M. K., Shimizu, K., Keller, N. and d'Enfert, C. (2002). cAMP and ras signalling independently control spore germination in the filamentous fungus *Aspergillus nidulans*. *Molecular Microbiology* **44**(4): 1001-1016.

Fischer, G. J. and Keller, N. P. (2016). Production of cross-kingdom oxylipins by pathogenic fungi: An update on their role in development and pathogenicity. *Journal Microbiology* **54**(3): 254-264.

Fleetwood, D. J., Scott, B., Lane, G. A., Tanaka, A. and Johnson, R. D. (2007). A complex ergovaline gene cluster in *Epichloë* endophytes of grasses. *Applied and Environmental Microbiology* **73**(8): 2571-2579.

Fredriksson, R., Lagerström, M. C., Lundin, L.-G. and Schiöth, H. B. (2003). The G-protein-coupled receptors in the human genome form five main families. Phylogenetic analysis, paralogon groups, and fingerprints. *Molecular Pharmacology* **63**(6): 1256-1272.

Fuchs, B. B. and Mylonakis, E. (2009). Our paths might cross: the role of the fungal cell wall integrity pathway in stress response and cross talk with other stress response pathways. *Eukaryotic Cell* **8**(11): 1616-1625.

Fuller, K. K. and Rhodes, J. C. (2012). Protein kinase A and fungal virulence: a sinister side to a conserved nutrient sensing pathway. *Virulence* **3**(2): 109-121.

Galagan, J. E., Henn, M. R., Ma, L.-J., Cuomo, C. A. and Birren, B. (2005). Genomics of the fungal kingdom: insights into eukaryotic biology. *Genome Research* **15**(12): 1620-1631.

Gao, F. and Zhang, C. T. (2006). GC-Profile: a web-based tool for visualizing and analyzing the variation of GC content in genomic sequences. *Nucleic Acids Research* **34**(2): W686-691.

Gehret, A. U., Bajaj, A., Naider, F. and Dumont, M. E. (2006). Oligomerization of the yeast α -factor receptor: implications for dominant negative effects of mutant receptors. *Journal of Biological Chemistry* **281**(30): 20698-20714.

Gehrke, A., Heinekamp, T., Jacobsen, I. D. and Brakhage, A. A. (2010). Heptahelical receptors GprC and GprD of *Aspergillus fumigatus* are essential regulators of colony growth, hyphal morphogenesis, and virulence. *Applied Environmental Microbiology* **76**(12): 3989-3998.

Girard, V., Fèvre, M., and Bruel, C. (2004). Involvement of cyclic AMP in the production of the acid protease Acp1 by *Sclerotinia sclerotiorum*. *FEMS Microbiology Letters* **237**: 227-233.

Gold, S., Duncan, G., Barrett, K. and Kronstad, J. (1994). cAMP regulates morphogenesis in the fungal pathogen *Ustilago maydis*. *Genes and Development* **8**(23): 2805-2816.

Green, K. A., Becker, Y., Fitzsimons, H. L. and Scott, B. (2016). An *Epichloë festucae* homolog of MOB3, a component of the STRIPAK complex, is required for establishment of a mutualistic symbiotic interaction with *Lolium perenne*. *Molecular Plant Pathology*. doi: 10.1111/mpp,12443.

Greenwald, C. J., Kasuga, T., Glass, N. L., Shaw, B. D., Ebbole, D. J., et al. (2010). Temporal and spatial regulation of gene expression during asexual development of *Neurospora crassa*. *Genetics* **186**(4): 1217-1230.

Grice, C. M., Bertuzzi, M. and Bignell, E. M. (2013). Receptor-mediated signaling in *Aspergillus fumigatus*. *Frontiers Microbiology* **4**: 26.

Gronover, C. S., Kasulke, D., Tudzynski, P. and Tudzynski, B. (2001). The role of G protein alpha subunits in the infection process of the gray mold fungus *Botrytis cinerea*. *Molecular Plant-Microbe Interactions* **14**(11): 1293-1302.

Gruber, S., Omann, M. and Zeilinger, S. (2013). Comparative analysis of the repertoire of G protein-coupled receptors of three species of the fungal genus *Trichoderma*. *BMC Microbiology* **13**: 108.

Gruber, S. and Zeilinger, S. (2014). The transcription factor Ste12 mediates the regulatory role of the Tmk1 MAP kinase in mycoparasitism and vegetative hyphal fusion in the filamentous fungus *Trichoderma atroviride*. PLoS One **9**(10): e111636.

Guindon, S., Dufayard, J. F., Lefort, V., Anisimova, M., Hordijk, W., et al. (2010). New algorithms and methods to estimate maximum-likelihood phylogenies: assessing the performance of PhyML 3.0. Systematic Biology **59**(3): 307-321.

Gummer, J. P., Trengove, R. D., Oliver, R. P. and Solomon, P. S. (2012). A comparative analysis of the heterotrimeric G-protein G α , G β and G γ subunits in the wheat pathogen *Stagonospora nodorum*. BMC Microbiology **12**: 131.

Guo, L., Breakspear, A., Zhao, G., Gao, L., Kistler, H. C., et al. (2016). Conservation and divergence of the cyclic adenosine monophosphate-protein kinase A (cAMP-PKA) pathway in two plant-pathogenic fungi: *Fusarium graminearum* and *F. verticillioides*. Molecular Plant Pathology **17**(2): 196-209.

Haas, H. (2003). Molecular genetics of fungal siderophore biosynthesis and uptake: the role of siderophores in iron uptake and storage. Applied Microbiology & Biotechnology **62**(4): 316-330.

Hamel, L.-P., Nicole, M.-C., Duplessis, S. and Ellis, B. E. (2012). Mitogen-activated protein kinase signaling in plant-interacting fungi: distinct messages from conserved messengers. The Plant Cell **24**(4): 1327-1351.

Han, K. H., Seo, J. A. and Yu, J. H. (2004). A putative G protein-coupled receptor negatively controls sexual development in *Aspergillus nidulans*. Molecular Microbiology **51**(5): 1333-1345.

Harding, R. W. and Melles, S. (1983). Genetic analysis of phototropism of *Neurospora crassa* perithecial beaks using white collar and albino mutants. Plant Physiology **72**(4): 996-1000.

Harman, G. E., Howell, C. R., Viterbo, A., Chet, I. and Lorito, M. (2004). *Trichoderma* species-opportunistic, avirulent plant symbionts. *Nature Reviews Microbiology* **2**(1): 43-56.

Harren, K., Brandhoff, B., Knodler, M. and Tudzynski, B. (2013). The high-affinity phosphodiesterase BcPde2 has impact on growth, differentiation and virulence of the phytopathogenic ascomycete *Botrytis cinerea*. *PLoS One* **8**(11): e78525.

Harris, J. L., Howe, H. B., Jr. and Roth, I. L. (1975). Scanning electron microscopy of surface and internal features of developing perithecia of *Neurospora crassa*. *Journal Bacteriology* **122**(3): 1239-1246.

Hause, B., Stenzel, I., Miersch, O., Maucher, H., Kramell, R., et al. (2000). Tissue-specific oxylipin signature of tomato flowers: allene oxide cyclase is highly expressed in distinct flower organs and vascular bundles. *The Plant Journal* **24**(1): 113-126.

Herrero-Garcia, E., Garzia, A., Cordobes, S., Espeso, E. A. and Ugalde, U. (2011). 8-carbon oxylipins inhibit germination and growth, and stimulate aerial conidiation in *Aspergillus nidulans*. *Fungal Biology* **115**(4-5): 393-400.

Hicks, J. K., Bahn, Y.-S. and Heitman, J. (2005). Pde1 phosphodiesterase modulates cyclic AMP levels through a protein kinase A-mediated negative feedback loop in *Cryptococcus neoformans*. *Eukaryotic Cell* **4**(12): 1971-1981.

Hofmann, K. and Stoffel, W. (1993). TMbase - A database of membrane spanning protein segments. *Biological Chemistry Hoppe-Seyler* **347**: 166.

Horowitz Brown, S., Zarnowski, R., Sharpee, W. C. and Keller, N. P. (2008). Morphological transition governed by density dependence and lipoxygenase activity in *Aspergillus flavus*. *Applied Environmental Microbiology* **74**(18): 5674-5685.

Houslay, M. D., Baillie, G. S. and Maurice, D. H. (2007). cAMP-specific phosphodiesterase-4 enzymes in the cardiovascular system a molecular toolbox for

generating compartmentalized cAMP signaling. *Circulation Research* **100**(7): 950-966.

Inda, L. A., Segarra-Moragues, J. G., Müller, J., Peterson, P. M. and Catalán, P. (2008). Dated historical biogeography of the temperate Loliinae (Poaceae, Pooideae) grasses in the northern and southern hemispheres. *Molecular Phylogenetics & Evolution* **46**(3): 932-957.

Jain, S., Akiyama, K., Kan, T., Ohguchi, T. and Takata, R. (2003). The G protein β -subunit FGB1 regulates development and pathogenicity in *Fusarium oxysporum*. *Current Genetics* **43**(2): 79-86.

Jain, S., Akiyama, K., Mae, K., Ohguchi, T. and Takata, R. (2002). Targeted disruption of a G protein α subunit gene results in reduced pathogenicity in *Fusarium oxysporum*. *Current Genetics* **41**(6): 407-413.

Jeraj, N., Lenasi, H. and Breskvar, K. (2005). The involvement of cAMP in the growth inhibition of filamentous fungus *Rhizopus nigricans* by steroids. *FEMS Microbiology Letters* **242**(1): 147-154.

Johnson, L. J., de Bonth, A. C., Briggs, L. R., Caradus, J. R., Finch, S. C., et al. (2013). The exploitation of *Epichloë* endophytes for agricultural benefit. *Fungal Diversity* **60**(1): 171-188.

Jung, K.-W., Yang, D.-H., Maeng, S., Lee, K.-T., So, Y.-S., et al. (2015). Systematic functional profiling of transcription factor networks in *Cryptococcus neoformans*. *Nature Communications* **6**: 6757.

Jung, W. H., Warn, P., Ragni, E., Popolo, L., Nunn, C. D., et al. (2005). Deletion of *PDE2*, the gene encoding the high-affinity cAMP phosphodiesterase, results in changes of the cell wall and membrane in *Candida albicans*. *Yeast* **22**(4): 285-294.

Kahmann, R., Basse, C. and Feldbrugge, M. (1999). Fungal-plant signalling in the *Ustilago maydis*-maize pathosystem. *Current Opinion Microbiology* **2**(6): 647-650.

Kahmann, R., Romeis, T., Bölker, M. and Kämper, J. (1995). Control of mating and development in *Ustilago maydis*. *Current Opinion in Genetics & Development* **5**(5): 559-564.

Kall, L., Krogh, A. and Sonnhammer, E. L. (2004). A combined transmembrane topology and signal peptide prediction method. *Journal Molecular Biology* **338**(5): 1027-1036.

Kamiya S, O. Y., Okamura A, Kameoka S, Kayano Y, Sanjay S., et al. (2016). Novel nuclear protein, NsiA, and its interacting transcription factor Ste12 and MAP kinase Mak2 mediate balanced symbiotic infection of endophytic fungus *Epichloë festucae* in perennial ryegrass. International Society for Molecular Plant-Microbe Interactions, Congress Abstracts. Portland, Oregon, USA.

Katoh, K., Misawa, K., Kuma, K. and Miyata, T. (2002). MAFFT: a novel method for rapid multiple sequence alignment based on fast Fourier transform. *Nucleic Acids Research* **30**(14): 3059-3066.

Katoh, K. and Standley, D. M. (2013). MAFFT multiple sequence alignment software version 7: improvements in performance and usability. *Molecular Biology and Evolution* **30**(4): 772-780.

Kayano, Y., Tanaka, A., Akano, F., Scott, B. and Takemoto, D. (2013). Differential roles of NADPH oxidases and associated regulators in polarized growth, conidiation and hyphal fusion in the symbiotic fungus *Epichloë festucae*. *Fungal Genetics & Biology* **56**: 87-97.

Kays, A. M., Rowley, P. S., Baasiri, R. A. and Borkovich, K. A. (2000). Regulation of conidiation and adenylyl cyclase levels by the Galpha protein GNA-3 in *Neurospora crassa*. *Molecular Cell Biology* **20**(20): 7693-7705.

Kelley, L. A., Mezulis, S., Yates, C. M., Wass, M. N. and Sternberg, M. J. (2015). The Phyre2 web portal for protein modeling, prediction and analysis. *Nature Protocols* **10**(6): 845-858.

Klimpel, A., Gronover, C. S., Williamson, B., Stewart, J. A. and Tudzynski, B. (2002). The adenylate cyclase (BAC) in *Botrytis cinerea* is required for full pathogenicity. *Molecular Plant Pathology* **3**(6): 439-450.

Krijgsheld, P., Bleichrodt, R., van Veluw, G. J., Wang, F., Muller, W. H., et al. (2013). Development in *Aspergillus*. *Studies in Mycology* **74**(1): 1-29.

Krishnamurthy, S., Tulsian, N. K., Chandramohan, A. and Anand, G. S. (2015). Parallel allostery by cAMP and PDE coordinates activation and termination phases in cAMP signaling. *Biophysical Journal* **109**(6): 1251-1263.

Krishnan, A., Almén, M. S., Fredriksson, R. and Schiöth, H. B. (2012). The origin of GPCRs: identification of mammalian like rhodopsin, adhesion, glutamate and frizzled GPCRs in fungi. *PLoS One* **7**(1): e29817.

Krogh, A., Larsson, B., von Heijne, G. and Sonnhammer, E. L. (2001). Predicting transmembrane protein topology with a hidden Markov model: application to complete genomes. *Journal Molecular Biology* **305**(3): 567-580.

Krohn, N. G., Brown, N. A., Colabardini, A. C., Reis, T., Savoldi, M., et al. (2014). The *Aspergillus nidulans* ATM kinase regulates mitochondrial function, glucose uptake and the carbon starvation response. *G3 (Bethesda)* **4**(1): 49-62.

Kronstad, J., De Maria, A., Funnell, D., Laidlaw, R. D., Lee, N., et al. (1998). Signaling via cAMP in fungi: interconnections with mitogen-activated protein kinase pathways. *Archives of Microbiology* **170**(6): 395-404.

Kronstad, J. W., Hu, G. and Choi, J. (2011). The cAMP/Protein Kinase A pathway and virulence in *Cryptococcus neoformans*. *Mycobiology* **39**(3): 143-150.

Krystofova, S. and Borkovich, K. A. (2005). The heterotrimeric G-protein subunits GNG-1 and GNB-1 form a G $\beta\gamma$ dimer required for normal female fertility, asexual development, and G α protein levels in *Neurospora crassa*. *Eukaryotic Cell* **4**(2): 365-378.

Krystofova, S. and Borkovich, K. A. (2006). The predicted G-protein-coupled receptor GPR-1 is required for female sexual development in the multicellular fungus *Neurospora crassa*. *Eukaryotic Cell* **5**(9): 1503-1516.

Kües, U. and Fischer, R. (2006). *The Mycota I: Growth, differentiation and sexuality*, Springer (Berlin, Heidelberg). 263-292.

Kuldau, G. and Bacon, C. (2008). *Clavicipitaceous* endophytes: Their ability to enhance resistance of grasses to multiple stresses. *Biological Control* **46**(1): 57-71.

Kulkarni, R. D., Kelkar, H. S. and Dean, R. A. (2003). An eight-cysteine-containing CFEM domain unique to a group of fungal membrane proteins. *Trends in Biochemical Sciences* **28**(3): 118-121.

Kulkarni, R. D., Thon, M. R., Pan, H. and Dean, R. A. (2005). Novel G-protein-coupled receptor-like proteins in the plant pathogenic fungus *Magnaporthe grisea*. *Genome Biology* **6**(3): R24.

Lacombe, M.-L., Podgorski, G., Franke, J. and Kessin, R. (1986). Molecular cloning and developmental expression of the cyclic nucleotide phosphodiesterase gene of *Dictyostelium discoideum*. *Journal of Biological Chemistry* **261**(36): 16811-16817.

Ladds, G., Davis, K., Das, A. and Davey, J. (2005). A constitutively active GPCR retains its G protein specificity and the ability to form dimers. *Molecular Microbiology* **55**(2): 482-497.

Lafon, A., Han, K. H., Seo, J. A., Yu, J. H. and d'Enfert, C. (2006). G-protein and cAMP-mediated signaling in *Aspergilli*: a genomic perspective. *Fungal Genetics & Biology* **43**(7): 490-502.

Larkin, M. A., Blackshields, G., Brown, N. P., Chenna, R., McGettigan, P. A., et al. (2007). Clustal W and Clustal X version 2.0. *Bioinformatics* **23**(21): 2947-2948.

Latch, G. C. M. and Christensen, M. J. (1985). Artificial infection of grasses with endophytes. *Annals of Applied Biology* **107**(1): 17-24.

Lee, Y. H. and Dean, R. A. (1993). cAMP regulates infection structure formation in the plant pathogenic fungus *Magnaporthe grisea*. *The Plant Cell* **5**(6): 693-700.

Letunic, I., Doerks, T. and Bork, P. (2015). SMART: recent updates, new developments and status in 2015. *Nucleic Acids Research* **43**(1): D257-260.

Leuchtman, A., Bacon, C. W., Schardl, C. L., White, J. F., Jr. and Tadych, M. (2014). Nomenclatural realignment of *Neotyphodium* species with genus *Epichloë*. *Mycologia* **106**(2): 202-215.

Levin, D. E. (2005). Cell wall integrity signaling in *Saccharomyces cerevisiae*. *Microbiology Molecular Biology Reviews* **69**(2): 262-291.

Levin, D. E. (2011). Regulation of cell wall biogenesis in *Saccharomyces cerevisiae*: the cell wall integrity signaling pathway. *Genetics* **189**(4): 1145-1175.

Li, L., Wright, S. J., Krystofova, S., Park, G. and Borkovich, K. A. (2007). Heterotrimeric G protein signaling in filamentous fungi. *Annual Reviews Microbiology* **61**: 423-452.

Lichius, A. and Lord, K. M. (2014). Chemoattractive mechanisms in filamentous fungi. *The Open Mycology Journal* **8**(1): 28-57.

Liebmann, B., Gattung, S., Jahn, B. and Brakhage, A. (2003). cAMP signaling in *Aspergillus fumigatus* is involved in the regulation of the virulence gene *pksP* and in defense against killing by macrophages. *Molecular Genetics and Genomics* **269**(3): 420-435.

Liu, S. and Dean, R. A. (1997). G protein α subunit genes control growth, development, and pathogenicity of *Magnaporthe grisea*. *Molecular Plant-Microbe Interactions* **10**(9): 1075-1086.

Lukito, Y., Chujo, T. and Scott, B. (2015). Molecular and cellular analysis of the pH response transcription factor PacC in the fungal symbiont *Epichloë festucae*. *Fungal Genetics & Biology* **85**: 25-37.

Ma, P., Wera, S., Van Dijck, P. and Thevelein, J. M. (1999). The PDE1-encoded low-affinity phosphodiesterase in the yeast *Saccharomyces cerevisiae* has a specific function in controlling agonist-induced cAMP signaling." *Molecular Biology of the Cell* **10**(1): 91-104.

Maier, E. J., Haynes, B. C., Gish, S. R., Wang, Z. A., Skowrya, M. L., et al. (2015). Model-driven mapping of transcriptional networks reveals the circuitry and dynamics of virulence regulation. *Genome Research* **25**(5): 690-700.

Malavazi, I., Goldman, G. H. and Brown, N. A. (2014). The importance of connections between the cell wall integrity pathway and the unfolded protein response in filamentous fungi. *Briefings in Functional Genomics*: elu027. doi: 10.1093/bfpg/elu027

Mamedov, T., Pienaar, E., Whitney, S. E., TerMaat, J. R., Carvill, G., et al. (2008). A fundamental study of the PCR amplification of GC-rich DNA templates. *Computational Biology and Chemistry* **32**(6): 452-457.

Martín, J. P. and Di Pietro, A. (2012). *Morphogenesis and pathogenicity in fungi*, Springer (Berlin, Heidelberg).

Masloff, S., Pöggeler, S. and Kück, U. (1999). The *pro1(+)* gene from *Sordaria macrospora* encodes a C6 zinc finger transcription factor required for fruiting body development. *Genetics* **152**(1): 191-199.

Mehrabi, R., Ben M'Barek, S., van der Lee, T. A., Waalwijk, C., de Wit, P. J., et al. (2009). G α and G β proteins regulate the cyclic AMP pathway that is required for development and pathogenicity of the phytopathogen *Mycosphaerella graminicola*. *Eukaryotic Cell* **8**(7): 1001-1013.

Mey, G., Oeser, B., Lebrun, M. H. and Tudzynski, P. (2002). The biotrophic, non-appressorium-forming grass pathogen *Claviceps purpurea* needs a Fus3/Pmk1 homologous mitogen-activated protein kinase for colonization of rye ovarian tissue. *Molecular Plant-Microbe Interactions* **15**(4): 303-312.

Miller, J. H. (1972). Experiments in molecular genetics. New York, Cold Spring Harbor Laboratory Press.

Misra, B. B. (2016). The black-box of plant apoplast lipidomes. *Frontiers Plant Science* **7**: 323.

Mitchell, T. K. and Dean, R. A. (1995). The cAMP-dependent protein kinase catalytic subunit is required for appressorium formation and pathogenesis by the rice blast pathogen *Magnaporthe grisea*. *The Plant Cell* **7**: 1869-1978.

Moon, C. D., Craven, K. D., Leuchtmann, A., Clement, S. L. and Schardl, C. L. (2004). Prevalence of interspecific hybrids amongst asexual fungal endophytes of grasses. *Molecular Ecology* **13**: 1455-1467.

Mukherjee, P. K., Horwitz, B. A., Herrera-Estrella, A., Schmoll, M. and Kenerley, C. M. (2013). *Trichoderma* research in the genome era. *Annual Reviews Phytopathology* **51**: 105-129.

Mukherjee, P. K., Horwitz, B. A. and Kenerley, C. M. (2012). Secondary metabolism in *Trichoderma* - a genomic perspective. *Microbiology* **158**(Pt 1): 35-45.

Mukherjee, P. K., Latha, J., Hadar, R. and Horwitz, B. A. (2003). TmkA, a mitogen-activated protein kinase of *Trichoderma virens*, is involved in biocontrol properties and repression of conidiation in the dark. *Eukaryotic Cell* **2**(3): 446-455.

Narasimhan, M. L., Coca, M. a. A., Jin, J., Yamauchi, T., Ito, Y., et al. (2005). Osmotin is a homolog of mammalian adiponectin and controls apoptosis in yeast through a homolog of mammalian adiponectin receptor. *Molecular Cell* **17**(2): 171-180.

Neer, E. J. (1995). Heterotrimeric G proteins: organizers of transmembrane signals. *Cell* **80**(2): 249-257.

Nikawa, J.-L., Sass, P. and Wigler, M. (1987). Cloning and characterization of the low-affinity cyclic AMP phosphodiesterase gene of *Saccharomyces cerevisiae*. *Molecular & Cellular Biology* **7**(10): 3629-3636.

Nishimura, M., Park, G. and Xu, J. R. (2003). The G- β subunit MGB1 is involved in regulating multiple steps of infection-related morphogenesis in *Magnaporthe grisea*. *Molecular Microbiology* **50**(1): 231-243.

Nødvig, C. S., Nielsen, J. B., Kogle, M. E. and Mortensen, U. H. (2015). A CRISPR-Cas9 system for genetic engineering of filamentous fungi. *PLoS One* **10**(7): e0133085.

Noverr, M. C., Erb-Downward, J. R. and Huffnagle, G. B. (2003). Production of eicosanoids and other oxylipins by pathogenic eukaryotic microbes. *Clinical Microbiology Reviews* **16**(3): 517-533.

Oberhofer, M. and Leuchtman, A. (2012). Genetic diversity in epichloid endophytes of *Hordelymus europaeus* suggests repeated host jumps and interspecific hybridizations. *Molecular Ecology* **21**(11): 2713-2726.

Obinata, H. and Izumi, T. (2009). G2A as a receptor for oxidized free fatty acids. *Prostaglandins & Other Lipid Mediators* **89**(3): 66-72.

Oldham, W. M. and Hamm, H. E. (2006). Structural basis of function in heterotrimeric G proteins. *Quarterly Reviews Biophysics* **39**(2): 117-166.

Oldham, W. M. and Hamm, H. E. (2008). Heterotrimeric G protein activation by G-protein-coupled receptors. *Nature Reviews Molecular Cell Biology* **9**(1): 60-71.

Oliver, R. P., Roberts, I. N., Harling, R., Kenyon, L., Punt, P. J., et al. (1987). Transformation of *Fulvia fulva*, a fungal pathogen of tomato, to hygromycin B resistance. *Current Genetics* **12**: 231-233.

Omann, M. and Zeilinger, S. (2010). How a mycoparasite employs G-protein signaling: using the example of *Trichoderma*. *Journal of Signal Transduction* **2010**:123126.

Omann, M. R., Lehner, S., Escobar Rodriguez, C., Brunner, K. and Zeilinger, S. (2012). The seven-transmembrane receptor Gpr1 governs processes relevant for the

antagonistic interaction of *Trichoderma atroviride* with its host. *Microbiology* **158**(1): 107-118.

Omasits, U., Ahrens, C. H., Muller, S. and Wollscheid, B. (2014). Protter: interactive protein feature visualization and integration with experimental proteomic data. *Bioinformatics* **30**(6): 884-886.

Park, G., Bruno, K. S., Staiger, C. J., Talbot, N. J. and Xu, J. R. (2004). Independent genetic mechanisms mediate turgor generation and penetration peg formation during plant infection in the rice blast fungus. *Molecular Microbiology* **53**(6): 1695-1707.

Park, G., Xue, C., Zhao, X., Kim, Y., Orbach, M., et al. (2006). Multiple upstream signals converge on the adaptor protein Mst50 in *Magnaporthe grisea*. *The Plant Cell* **18**(10): 2822-2835.

Park, G., Xue, C., Zheng, L., Lam, S. and Xu, J. R. (2002). MST12 regulates infectious growth but not appressorium formation in the rice blast fungus *Magnaporthe grisea*. *Molecular Plant-Microbe Interactions* **15**(3): 183-192.

Park, H. S. and Yu, J. H. (2012). Genetic control of asexual sporulation in filamentous fungi. *Current Opinion Microbiology* **15**(6): 669-677.

Park, J.-I., Grant, C. M. and Dawes, I. W. (2005). The high-affinity cAMP phosphodiesterase of *Saccharomyces cerevisiae* is the major determinant of cAMP levels in stationary phase: involvement of different branches of the Ras-cyclic AMP pathway in stress responses. *Biochemical & Biophysical Research Communications* **327**(1): 311-319.

Patkar, R. N., Benke, P. I., Qu, Z., Chen, Y. Y. C., Yang, F., et al. (2015). A fungal monooxygenase-derived jasmonate attenuates host innate immunity. *Nature Chemical Biology* **11**(9): 733-740.

Philipson, M. N. and Christey, M. C. (1986). The relationship of host and endophyte during flowering, seed formation, and germination of *Lolium perenne*. *New Zealand Journal of Botany* **24**: 125-134.

Pinto, C., Hübner, M., Gille, A., Richter, M., Mou, T.-C., et al. (2009). Differential interactions of the catalytic subunits of adenylyl cyclase with forskolin analogs. *Biochemical Pharmacology* **78**(1): 62-69.

Pinto, C., Papa, D., Hübner, M., Mou, T.-C., Lushington, G. H., et al. (2008). Activation and inhibition of adenylyl cyclase isoforms by forskolin analogs. *Journal of Pharmacology & Experimental Therapeutics* **325**(1): 27-36.

Prost, I., Dhondt, S., Rothe, G., Vicente, J., Rodriguez, M. J., et al. (2005). Evaluation of the antimicrobial activities of plant oxylipins supports their involvement in defense against pathogens. *Plant Physiology* **139**(4): 1902-1913.

Quevillon, E., Silventoinen, V., Pillai, S., Harte, N., Mulder, N., et al. (2005). InterProScan: protein domains identifier. *Nucleic Acids Research* **33**(2): W116-120.

Ram, A. F. and Klis, F. M. (2006). Identification of fungal cell wall mutants using susceptibility assays based on Calcofluor white and Congo red. *Nature Protocols* **1**(5): 2253-2256.

Ramanujam, R. and Naqvi, N. I. (2010). PdeH, a high-affinity cAMP phosphodiesterase, is a key regulator of asexual and pathogenic differentiation in *Magnaporthe oryzae*. *PLoS Pathology* **6**(5): e1000897.

Rasmussen, S., Parsons, A. J., Fraser, K., Xue, H. and Newman, J. A. (2008). Metabolic profiles of *Lolium perenne* are differentially affected by nitrogen supply, carbohydrate content, and fungal endophyte infection. *Plant Physiology* **146**(3): 1440-1453.

Rasmussen, S. G., DeVree, B. T., Zou, Y., Kruse, A. C., Chung, K. Y., et al. (2011). Crystal structure of the [bgr] 2 adrenergic receptor-Gs protein complex. *Nature* **477**(7366): 549-555.

Redman, R. S., Freeman, S., Clifton, D. R., Morrel, J., Brown, G., et al. (1999). Biochemical analysis of plant protection afforded by a nonpathogenic endophytic mutant of *Colletotrichum magna*. *Plant Physiology* **119**(2): 795-804.

Regenfelder, E., Spellig, T., Hartmann, A., Lauenstein, S., Bolker, M., et al. (1997). G proteins in *Ustilago maydis*: transmission of multiple signals? *European Molecular Biology Organization Journal* **16**(8): 1934-1942.

Reithner, B., Schuhmacher, R., Stoppacher, N., Pucher, M., Brunner, K., et al. (2007). Signaling via the *Trichoderma atroviride* mitogen-activated protein kinase Tmk1 differentially affects mycoparasitism and plant protection. *Fungal Genetics & Biology* **44**(11): 1123-1133.

Riemann, M., Haga, K., Shimizu, T., Okada, K., Ando, S., et al. (2013). Identification of rice allene oxide cyclase mutants and the function of jasmonate for defence against *Magnaporthe oryzae*. *The Plant Journal* **74**(2): 226-238.

Rispail, N. and Di Pietro, A. (2009). *Fusarium oxysporum* Ste12 controls invasive growth and virulence downstream of the Fmk1 MAPK cascade. *Molecular Plant-Microbe Interactions* **22**(7): 830-839.

Rispail, N. and Di Pietro, A. (2010). The homeodomain transcription factor Ste12: Connecting fungal MAPK signalling to plant pathogenicity. *Communicative & Integrative Biology* **3**(4): 327-332.

Rispail, N., Soanes, D. M., Ant, C., Czajkowski, R., Grunler, A., et al. (2009). Comparative genomics of MAP kinase and calcium-calcineurin signalling components in plant and human pathogenic fungi. *Fungal Genetics & Biology* **46**(4): 287-298.

Rodriguez, R. J., Henson, J., Van Volkenburgh, E., Hoy, M., Wright, L., et al. (2008). Stress tolerance in plants via habitat-adapted symbiosis. *The ISME Journal* **2**(4): 404-416.

- Rodriguez, R. J., White, J. F., Jr., Arnold, A. E. and Redman, R. S. (2009). Fungal endophytes: diversity and functional roles. *New Phytologist* **182**(2): 314-330.
- Sass, P., Field, J., Nikawa, J., Toda, T. and Wigler, M. (1986). Cloning and characterization of the high-affinity cAMP phosphodiesterase of *Saccharomyces cerevisiae*. *Proceedings of the National Academy of Sciences* **83**(24): 9303-9307.
- Scala, V., Giorni, P., Cirlini, M., Ludovici, M., Visentin, I., et al. (2014). LDS1-produced oxylipins are negative regulators of growth, conidiation and fumonisin synthesis in the fungal maize pathogen *Fusarium verticillioides*. *Frontiers Microbiology* **5**: 669.
- Scarpari, M., Punelli, M., Scala, V., Zaccaria, M., Nobili, C., et al. (2014). Lipids in *Aspergillus flavus*-maize interaction. *Frontiers Microbiology* **5**: 74.
- Schardl, C. L. (1996). *Epichloë* species: fungal symbionts of grasses. *Annual Review of Phytopathology* **34**: 109-130.
- Schardl, C. L. (2010). The *Epichloë*, symbionts of the grass subfamily Poöideae. *Annals of the Missouri Botanical Garden* **97**: 646-665.
- Schardl, C. L. and Leuchtman, A. (2005). The *Epichloë* endophytes of grasses and the symbiotic continuum. *Mycology Series* **23**: 475.
- Schardl, C. L., Leuchtman, A., Chung, K.-R., Penny, D. and Siegel, M. R. (1997). Coevolution by common descent of fungal symbionts (*Epichloë* spp.) and grass hosts. *Molecular Biology & Evolution* **14**(2): 133-143.
- Schardl, C. L., Leuchtman, A. and Spiering, M. J. (2004). Symbioses of grasses with seedborne fungal endophytes. *Annual Review of Plant Biology* **55**: 315-340.
- Schardl, C. L., Leuchtman, A., Tsai, H.-F., Collett, M. A., Watt, D. M., et al. (1994). Origin of a fungal symbiont of perennial ryegrass by interspecific hybridization of a mutualist with the ryegrass choke pathogen, *Epichloë typhina*. *Genetics* **136**: 1307-1317.

Schardl, C. L., Young, C. A., Faulkner, J. R., Florea, S. and Pan, J. (2012). Chemotypic diversity of epichloae, fungal symbionts of grasses. *Fungal Ecology* **5**: 331-344.

Schardl, C. L., Young, C. A., Hesse, U., Amyotte, S. G., Andreeva, K., et al. (2013). Plant-symbiotic fungi as chemical engineers: multi-genome analysis of the *Clavicipitaceae* reveals dynamics of alkaloid loci. *PLoS Genetics* **9**(2): e1003323.

Schardl, C. L., Young, C. A., Pan, J., Florea, S., Takach, J. E., et al. (2013). Currencies of mutualisms: sources of alkaloid genes in vertically transmitted epichloae. *Toxins (Basel)* **5**(6): 1064-1088.

Schrettl, M., Bignell, E., Kragl, C., Sabiha, Y., Loss, O., et al. (2007). Distinct roles for intra- and extracellular siderophores during *Aspergillus fumigatus* infection. *PLoS Pathology* **3**(9): e128.

Schultz, J., Milpetz, F., Bork, P. and Ponting, C. P. (1998). SMART, a simple modular architecture research tool: identification of signaling domains. *Proceedings National Academy Science* **95**(11): 5857-5864.

Schumacher, J., Kokkelink, L., Huesmann, C., Jimenez-Teja, D., Collado, I. G., et al. (2008). The cAMP-dependent signaling pathway and its role in conidial germination, growth, and virulence of the gray mold *Botrytis cinerea*. *Molecular Plant-Microbe Interactions* **21**(11): 1443-1459.

Schweingruber, A. M., Hilti, N., Edenharter, E. and Schweingruber, M. E. (1998). Methionine induces sexual development in the fission yeast *Schizosaccharomyces pombe* via an *ste11*-dependent signalling pathway. *Journal Bacteriology* **180**(23): 6338-6341.

Scott, B., Becker, Y., Becker, M. and Cartwright, G. (2012). Morphogenesis, growth and development of the grass symbiont *Epichloë festucae*. In: *Morphogenesis and pathogenicity in fungi*. Springer-Verlag (Berlin, Heidelberg),: 243-264.

Scott, B. and Eaton, C. J. (2008). Role of reactive oxygen species in fungal cellular differentiations. *Current Opinion in Microbiology* **11**(6): 488-493.

- Scott, B. and Schardl, C. (1993). Fungal symbionts of grasses: evolutionary insights and agricultural potential. *Trends in Microbiology* **1**(5): 196-200.
- Scott, B., Takemoto, D. and Tanaka, A. (2007). Fungal endophyte production of reactive oxygen species is critical for maintaining the mutualistic symbiotic interaction between *Epichloë festucae* and perennial ryegrass. *Plant Signaling & Behavior* **2**(3): 170-172.
- Scott, W. A. and Solomon, B. (1975). Adenosine 3',5'-cyclic monophosphate and morphology in *Neurospora crassa*: drug-induced alterations. *Journal of Bacteriology* **122**(2): 454-463.
- Semighini, C. P. and Harris, S. D. (2008). Regulation of apical dominance in *Aspergillus nidulans* hyphae by reactive oxygen species. *Genetics* **179**(4): 1919-1932.
- Semyonov, J., Park, J. I., Chang, C. L. and Hsu, S. Y. (2008). GPCR genes are preferentially retained after whole genome duplication. *PLoS One* **3**(4): e1903.
- Siegel, M. R., Jarlfors, U., Latch, G. C. M. and Johnson, M. C. (1987). Ultrastructure of *Acremonium coenophialum*, *Acremonium lolii*, and *Epichloe typhina* endophytes in host and nonhost *Festuca* and *Lolium* species of grasses. *Canadian Journal of Botany* **65**(11): 2357-2367.
- Solomon, P. S., Tan, K. C., Sanchez, P., Cooper, R. M. and Oliver, R. P. (2004). The disruption of a G α subunit sheds new light on the pathogenicity of *Stagonospora nodorum* on wheat. *Molecular Plant-Microbe Interactions* **17**(5): 456-466.
- Sonnhammer, E. L., von Heijne, G. and Krogh, A. (1998). A hidden Markov model for predicting transmembrane helices in protein sequences. *Proceedings of the International Conference on Intelligent Systems for Molecular Biology; ISMB*. (6): 175-182.
- Southern, E. M. (1975). Detection of specific sequences among DNA fragments separated by gel electrophoresis. *Journal of Molecular Biology* **98**: 503-517.

Spiers, A. G. and Hopcroft, D. H. (1993). Black canker and leaf spot of *Salix* in New Zealand caused by *Glomerella miyabeana* (*Colletotrichum gloeosporioides*). *European Journal of Forest Pathology* **23**: 92-102.

Steindorff, A. S., Persinoti, G. F., Monteiro, V. N. and Silva, R. N. (2015). *Fungal metabolic diversity*, John Wiley & Sons Ltd. Chichester, UK

Steinebrunner, F., Schiestl, F. P. and Leuchtman, A. (2008). Ecological role of volatiles produced by *Epichloë*: differences in antifungal toxicity. *FEMS Microbiology & Ecology* **64**(2): 307-316.

Steinebrunner, F., Twele, R., Francke, W., Leuchtman, A. and Schiestl, F. P. (2008). Role of odour compounds in the attraction of gamete vectors in endophytic *Epichloë* fungi. *New Phytologist* **178**(2): 401-411.

Strien, J., Sanft, J. and Mall, G. (2013). Enhancement of PCR amplification of moderate GC-containing and highly GC-rich DNA sequences. *Molecular Biotechnology* **54**(3): 1048-1054.

Tadych, M., Bergen, M. S. and White, J. F., Jr. (2014). *Epichloë* spp. associated with grasses: new insights on life cycles, dissemination and evolution. *Mycologia* **106**(2): 181-201.

Takemoto, D., Tanaka, A. and Scott, B. (2006). A p67(Phox)-like regulator is recruited to control hyphal branching in a fungal-grass mutualistic symbiosis. *The Plant Cell* **18**(10): 2807-2821.

Tan, Y. Y., Spiering, M. J., Scott, V., Lane, G. A., Christensen, M. J., et al. (2001). In planta regulation of extension of an endophytic fungus and maintenance of high metabolic rates in its mycelium in the absence of apical extension. *Applied Environmental Microbiology* **67**(12): 5377-5383.

Tanaka, A., Cartwright, G. M., Saikia, S., Kayano, Y., Takemoto, D., et al. (2013). ProA, a transcriptional regulator of fungal fruiting body development, regulates leaf

hyphal network development in the *Epichloë festucae-Lolium perenne* symbiosis. *Molecular Microbiology* **90**(3): 551-568.

Tanaka, A., Christensen, M. J., Takemoto, D., Park, P. and Scott, B. (2006). Reactive oxygen species play a role in regulating a fungus-perennial ryegrass mutualistic association. *The Plant Cell* **18**: 1052-1066.

Tanaka, A., Takemoto, D., Chujo, T. and Scott, B. (2012). Fungal endophytes of grasses. *Current Opinion Plant Biology* **15**(4): 462-468.

Tanaka, A., Takemoto, D., Hyon, G. S., Park, P. and Scott, B. (2008). NoxA activation by the small GTPase RacA is required to maintain a mutualistic symbiotic association between *Epichloë festucae* and perennial ryegrass. *Molecular Microbiology* **68**(5): 1165-1178.

Tanaka, A., Tapper, B. A., Popay, A., Parker, E. J. and Scott, B. (2005). A symbiosis expressed non-ribosomal peptide synthetase from a mutualistic fungal endophyte of perennial ryegrass confers protection to the symbiotum from insect herbivory. *Molecular Microbiology* **57**(4): 1036-1050.

Tang, Y. T., Hu, T., Arterburn, M., Boyle, B., Bright, J. M., et al. (2005). PAQR proteins: a novel membrane receptor family defined by an ancient 7-transmembrane pass motif. *Journal of Molecular Evolution* **61**(3): 372-380.

Teichert, I., Steffens, E. K., Schnass, N., Franzel, B., Krisp, C., et al. (2014). PRO40 is a scaffold protein of the cell wall integrity pathway, linking the MAP kinase module to the upstream activator protein kinase C. *PLoS Genetics* **10**(9): e1004582.

Terenzi, H. F., Jorge, J. A., Roselino, J. E. and Migliorini, R. H. (1979). Adenylyl cyclase deficient *cr-1* (Crisp) mutant of *Neurospora crassa*: cyclic AMP-dependent nutritional deficiencies. *Archives of Microbiology* **123**(3): 251-258.

Thompson, J. D., Higgins, D. G. and Gibson, T. J. (1994). CLUSTAL W: improving the sensitivity of progressive multiple sequence alignment through sequence weighting,

position-specific gap penalties and weight matrix choice. *Nucleic Acids Research* **22**(22): 4673-4680.

Tsitsigiannis, D. I., Kowieski, T. M., Zarnowski, R. and Keller, N. P. (2005). Three putative oxylipin biosynthetic genes integrate sexual and asexual development in *Aspergillus nidulans*. *Microbiology* **151**(6): 1809-1821.

Tsitsigiannis, D. I., Kunze, S., Willis, D. K., Feussner, I. and Keller, N. P. (2005). *Aspergillus* infection inhibits the expression of peanut 13S-HPODE-forming seed lipoxygenases. *Molecular Plant-Microbe Interactions* **18**(10): 1081-1089.

Tsitsigiannis, D. I., Zarnowski, R. and Keller, N. P. (2004). The lipid body protein, PpoA, coordinates sexual and asexual sporulation in *Aspergillus nidulans*. *Journal of Biological Chemistry* **279**(12): 11344-11353.

Turner, G. E. and Borkovich, K. A. (1993). Identification of a G protein alpha subunit from *Neurospora crassa* that is a member of the Gi family. *The Journal of Biological Chemistry* **268**(20): 14805-14811.

Turrà, D., El Ghalid, M., Rossi, F. and Di Pietro, A. (2015). Fungal pathogen uses sex pheromone receptor for chemotropic sensing of host plant signals. *Nature* **527**(7579): 521-524.

Tusnady, G. E. and Simon, I. (2001). The HMMTOP transmembrane topology prediction server. *Bioinformatics* **17**(9): 849-850.

Tuteja, N. (2009). Signaling through G protein coupled receptors. *Plant Signaling & Behavior* **4**(10): 942-947.

van Hove, L. W. A., Heeres, P. and Bossen, M. E. (2002). The annual variation in stomatal ammonia compensation point of rye grass (*Lolium perenne* L.) leaves in an intensively managed grassland. *Atmospheric Environment* **36**: 2965-2977.

Vaudry, H. (2014). Molecular evolution of GPCRs: What we know and what the future holds. *Journal Molecular Endocrinology* **52**(3): E1-2.

Vienken, K. and Fischer, R. (2006). The Zn(II)₂Cys₆ putative transcription factor NosA controls fruiting body formation in *Aspergillus nidulans*. *Molecular Microbiology* **61**(2): 544-554.

Voisey, C. R. (2010). Intercalary growth in hyphae of filamentous fungi. *Fungal Biology Reviews* **24**: 123-131.

Voisey, C. R., Christensen, M. J., Johnson, R. D., Johnson, L. J., Khan, A. K., et al. (2007). The role of cAMP signalling in the symbiosis between *Epichloë festucae* and *Lolium perenne*. Proceedings of the 6th International Symposium on Fungal Endophytes of Grasses. Grasslands Research and Practice Series No. 13, Christchurch, New Zealand, New Zealand Grassland Association.

Wang, Y., Geng, Z., Jiang, D., Long, F., Zhao, Y., et al. (2013). Characterizations and functions of regulator of G protein signaling (RGS) in fungi. *Applied Microbiology & Biotechnology* **97**(18): 7977-7987.

Wang, Y., Li, A., Wang, X., Zhang, X., Zhao, W., et al. (2010). GPR11, a putative seven-transmembrane G protein-coupled receptor, controls zoospore development and virulence of *Phytophthora sojae*. *Eukaryotic Cell* **9**(2): 242-250.

Wasternack, C. and Kombrink, E. (2010). Jasmonates: structural requirements for lipid-derived signals active in plant stress responses and development. *ACS Chemical Biology* **5**(1): 63-77.

Wera, S., Ma, P. and Thevelein, J. M. (1997). Glucose exerts opposite effects on mRNA versus protein and activity levels of Pde1, the low-affinity cAMP phosphodiesterase from budding yeast, *Saccharomyces cerevisiae*. *FEBS Letters* **420**(2-3): 147-150.

White, J., Jr. and Chambless, D. A. (1991). Endophyte-host associations in forage grasses XV. Clustering of stromata-bearing individuals of *Agrostis hiemalis* infected by *Epichloë typhina*. *American Journal of Botany* **78**(4): 527-533.

White, J. F., Jr., Bacon, C. W. and Hinton, D. M. (1997). Modifications of host cells and tissues by the biotrophic endophyte *Epichloë amarillans* (Clavicipitaceae; Ascomycotina). *Canadian Journal of Botany* **75**: 1061-1069.

White, J. F., Jr. and Bultman, T. L. (1987). Endophyte-host associations in forage grasses. VIII. Heterothallism in *Epichloë typhina*. *American Journal of Botany* **74**(11): 1716-1721.

Wilkinson, L. (2010). SYSTAT. Wiley Interdisciplinary Reviews: Computational Statistics **2**(2): 256-257.

Wilson, R. A. and Talbot, N. J. (2009). Under pressure: investigating the biology of plant infection by *Magnaporthe oryzae*. *Nature Reviews Microbiology* **7**(3): 185-195.

Won, S., Michkov, A. V., Krystofova, S., Garud, A. V. and Borkovich, K. A. (2012). Genetic and physical interactions between G α subunits and components of the G $\beta\gamma$ dimer of heterotrimeric G proteins in *Neurospora crassa*. *Eukaryotic Cell* **11**(10): 1239-1248.

Wright, S. J., Inchausti, R., Eaton, C. J., Krystofova, S. and Borkovich, K. A. (2011). RIC8 is a guanine-nucleotide exchange factor for G α subunits that regulates growth and development in *Neurospora crassa*. *Genetics* **189**(1): 165-176.

Xu, J. R. and Hamer, J. E. (1996). MAP kinase and cAMP signaling regulate infection structure formation and pathogenic growth in the rice blast fungus *Magnaporthe grisea*. *Genes and Development* **10**(21): 2696-2706.

Xue, C., Bahn, Y. S., Cox, G. M. and Heitman, J. (2006). G protein-coupled receptor Gpr4 senses amino acids and activates the cAMP-PKA pathway in *Cryptococcus neoformans*. *Molecular Biology of the Cell* **17**(2): 667-679.

Xue, C., Hsueh, Y. P. and Heitman, J. (2008). Magnificent seven: roles of G protein-coupled receptors in extracellular sensing in fungi. *FEMS Microbiology Reviews* **32**(6): 1010-1032.

Yang, Q. and Borkovich, K. A. (1999). Mutational activation of a G α i causes uncontrolled proliferation of aerial hyphae and increased sensitivity to heat and oxidative stress in *Neurospora crassa*. *Genetics* **151**(1): 107-117.

Yang, Z. (2002). Small GTPases: versatile signaling switches in plants. *The Plant Cell* **14**: S375-S388.

Yelton, M. M., Hamer, J. E. and Timberlake, W. E. (1984). Transformation of *Aspergillus nidulans* by using a *trpC* plasmid. *Proceedings of the National Academy of Science USA* **81**: 1470-1474.

Yin, Z., Tang, W., Wang, J., Liu, X., Yang, L., et al. (2016). Phosphodiesterase MoPdeH targets MoMck1 of the conserved mitogen-activated protein (MAP) kinase signalling pathway to regulate cell wall integrity in rice blast fungus *Magnaporthe oryzae*. *Molecular Plant Pathology*. **17**: 654-668.

Young, C. A., Bryant, M. K., Christensen, M. J., Tapper, B. A., Bryan, G. T., et al. (2005). Molecular cloning and genetic analysis of a symbiosis-expressed gene cluster for lolitrem biosynthesis from a mutualistic endophyte of perennial ryegrass. *Molecular Genetics and Genomics* **274**: 13-29.

Yun, S., Furlong, M., Sim, M., Cho, M., Park, S., et al. (2015). Pre-vertebrate local gene duplication facilitated expansion of the neuropeptide GPCR superfamily." *Molecular Biology and Evolution*: msv179. doi: 10.1093/molbev/msv179

Zdobnov, E. M. and Apweiler, R. (2001). InterProScan - an integration platform for the signature-recognition methods in InterPro. *Bioinformatics* **17**(9): 847-848.

Zeilinger, S., Gupta, V. K., Dahms, T. E., Silva, R. N., Singh, H. B., et al. (2015). Friends or foes? Emerging insights from fungal interactions with plants. *FEMS Microbiology Reviews*(40): 182-207.

Zeilinger, S. and Omann, M. (2007). *Trichoderma* biocontrol: signal transduction pathways involved in host sensing and mycoparasitism. *Gene Regulation & Systems Biology* **1**: 227.

Zeilinger, S., Reithner, B., Scala, V., Peissl, I., Lorito, M., et al. (2005). Signal transduction by Tga3, a novel G protein α subunit of *Trichoderma atroviride*. *Applied & Environmental Microbiology* **71**(3): 1591-1597.

Zhang, C., Wang, J., Tao, H., Dang, X., Wang, Y., et al. (2015). FvBck1, a component of cell wall integrity MAP kinase pathway, is required for virulence and oxidative stress response in sugarcane Pokkah Boeng pathogen. *Frontiers Microbiology* **6**: 1096. doi 10.3389/fmicb.2015.01096.

Zhang, D., Zhao, Q. and Wu, B. (2015). Structural studies of G protein-coupled receptors. *Molecules & Cells* **38**(10): 836.

Zhang, D. X., Nagabhyru, P. and Schardl, C. L. (2009). Regulation of a chemical defense against herbivory produced by symbiotic fungi in grass plants. *Plant Physiology* **150**(2): 1072-1082.

Zhang, H., Liu, K., Zhang, X., Tang, W., Wang, J., et al. (2011). Two phosphodiesterase genes, *PDEL* and *PDEH*, regulate development and pathogenicity by modulating intracellular cyclic AMP levels in *Magnaporthe oryzae*. *PLoS One* **6**(2): e17241.

Zhang, H., Xue, C., Kong, L., Li, G. and Xu, J. R. (2011). A Pmk1-interacting gene is involved in appressorium differentiation and plant infection in *Magnaporthe oryzae*. *Eukaryotic Cell* **10**(8): 1062-1070.

Zhao, X., Kim, Y., Park, G. and Xu, J. R. (2005). A mitogen-activated protein kinase cascade regulating infection-related morphogenesis in *Magnaporthe grisea*. *The Plant Cell* **17**(4): 1317-1329.

Zhao, X., Mehrabi, R. and Xu, J. R. (2007). Mitogen-activated protein kinase pathways and fungal pathogenesis. *Eukaryotic Cell* **6**(10): 1701-1714.

Zheng, H., Zhou, L., Dou, T., Han, X., Cai, Y., et al. (2010). Genome-wide prediction of G protein-coupled receptors in *Verticillium* spp. *Fungal Biology* **114**(4): 359-368.

Zheng, L., Campbell, M., Murphy, J., Lam, S. and Xu, J.-R. (2000). The BMP1 gene is essential for pathogenicity in the gray mold fungus *Botrytis cinerea*. *Molecular Plant-Microbe Interactions* **13**(7): 724-732.

